



## **A surface topographical analysis of explanted knee prostheses**

**Emma Ritchie**

This thesis is submitted to the School of Engineering, Newcastle University in partial fulfilment of the requirements for the Degree of Doctor of Philosophy

**Newcastle University**

**School of Engineering**

**February 2020**



**Abstract**

In 2017 there were 106,334 primary and 6,502 revision knee replacement surgeries reported in England, Wales, Northern Ireland and the Isle of Man. Annual increases of both procedures are predicted. Analyses of explanted orthopaedic prostheses enables greater understanding of their true clinical performance and can lead to design improvements, increased longevity and enhanced patient safety and benefit. This thesis provides a thorough investigation into the surface topographical analysis of explanted knee prostheses and the relationship between *in vivo* surface topographical changes and patient and implant demographics. This is the largest surface topographical analysis of explanted knee prostheses to date within the United Kingdom. This work is the first to report the surface roughness of explanted Unicondylar Knee Replacement (UKR) prostheses. Within this thesis, 135 knee prostheses were retrieved from revision surgery, processed for analysis and catalogued with patient data. Non-contacting profilometry and semi-quantitative damage scoring were used to analyse the surface topography of explanted and reference Total Knee Replacements (TKRs) and UKRs with cobalt chromium alloy (CoCr) and oxidised zirconium (OxZr) femoral components. All explanted femoral components showed an increase in surface roughness between 33% and 263% after time *in vivo*. There were no correlations found between the surface roughness and the damage scores recorded on the explanted prostheses or between the surface topography measurements and the duration *in vivo*, side of implantation or patient age, BMI or gender. No differences were found between *in vivo* surface topographical changes recorded on retrieved TKR compared with retrieved UKR components. No differences were found between *in vivo* surface topographical changes recorded on retrieved CoCr components compared with retrieved OxZr components. This work provides valuable data concerning the true *in vivo* performance of knee replacement prostheses and contributes to furthering the understanding of the mechanisms of failure of these prostheses.

*Blank page*



## Dedication

This work is dedicated to my family as you are the reason for everything. To my patient, supportive, and always encouraging husband Leigh Ritchie, who has shared this long journey with me, I owe you everything. To my beautiful babies Miriam and Zach, I hope you are proud of your engineering mummy. To my mother and father, Valerie and Harry Kennard. My incredible Mum over the course of me working towards this thesis has bravely undergone four orthopaedic surgeries, two emergency trauma hip procedures, one which resulted in a revision to Total Hip Replacement, and one elective Total Knee Replacement. Mum, you inspire me every day and are a constant reminder to me of the importance of ensuring the safety and efficacy of medical devices. I also couldn't have completed this thesis without the help and support from my gorgeous sister Claire Kennard and my lovely friends Anna Little, Emily Surash, Kate Riley, Rowena Ward and Shona McCreedy. Thank you, ladies, for your friendship and kindness, you are amazing.

“Not everything that can be counted counts, and not everything that counts can be counted” William Bruce Cameron 1963 *Informal Sociology: A Causal Introduction to Sociological Thinking*.

*Blank page*

## **Acknowledgements**

I would like to thank my supervisors Professor Tom Joyce, Dr Susan Scholes and Dr Philip Hyde, and my co-author Dr Simon Smith. From proposing my name for a PhD, securing funding and supervising me throughout this time, Tom you have continually encouraged, challenged and motivated me, thank you. Susan, thank you for all you have done for me, you have taught and inspired me. I respect your engineering professionalism and value your friendship and kindness. Thank you to Phil and Simon for your help, advice and feedback. Without all of your support and guidance this thesis would not have been possible.

I must also acknowledge and extend my gratitude to the surgeons who have provided the explants for analysis and who have provided me with guidance throughout this project: Professor David Deehan, Mr Raj Ganadarahan, Mr James Holland and Mr David Weir. Particularly I would like to give a special thanks to Mr Raj Gangadarahan who worked hard to help me collect the patient and implant details. Finally, I wish to thank the School of Engineering (specifically the members of the former School of Mechanical Engineering) for funding my PhD studies and providing me with the scholarship to enable me to complete this work.

*Blank page*

## Table of Contents

CHAPTER 1 INTRODUCTION.....	1
1.1    BACKGROUND .....	1
1.2    AIM AND OBJECTIVES .....	3
1.3    THESIS STRUCTURE .....	4
CHAPTER 2 LITERATURE REVIEW .....	7
2.1    THE KNEE .....	7
2.1.1 <i>Anatomy of the Knee</i> .....	8
2.1.2 <i>Biomechanics of the Knee</i> .....	10
2.1.3 <i>Osteoarthritis</i> .....	14
2.2    TRIBOLOGY AND SURFACE TOPOGRAPHY .....	18
2.2.1 <i>Surface Topography</i> .....	19
2.2.2 <i>Surface Roughness Parameters</i> .....	19
2.2.3 <i>Surface Roughness Measurement</i> .....	23
2.2.4 <i>Friction</i> .....	28
2.2.5 <i>Lubrication</i> .....	30
2.2.6 <i>Wear</i> .....	31
2.3    KNEE ARTHROPLASTY .....	34
2.3.1 <i>Materials in Knee Replacement</i> .....	37
2.3.2 <i>Demographics of Knee Replacements</i> .....	40
2.3.3 <i>Revision Knee Replacement</i> .....	42
2.3.4 <i>PE Wear in Knee Replacements</i> .....	44
2.3.5 <i>Knee Replacement Retrieval Studies</i> .....	48
2.3.6 <i>TKR Component Surface Roughness</i> .....	56
CHAPTER 3 MATERIALS AND METHODS .....	73
3.1    MATERIALS .....	73
3.1.1 <i>Patient and Implant Variables</i> .....	79
3.2    QUALITATIVE AND SEMI-QUANTITATIVE DAMAGE ASSESSMENT .....	80
3.2.1 <i>Femoral Damage Scoring (FDS)</i> .....	80
3.2.2 <i>PE Articular Surface Damage Scoring (PE ADS)</i> .....	82
3.2.3 <i>PE Backside Damage Scoring (PE BDS)</i> .....	83
3.3    SURFACE ROUGHNESS MEASUREMENT .....	88
3.3.1 <i>Roughness Parameters</i> .....	90
3.3.2 <i>Measurement Controls</i> .....	90
3.3.3 <i>Analysis Controls</i> .....	91

3.3.4	<i>Challenges of Performing Non-contacting Profilometry on Knee Replacement Prostheses.</i>	91
3.4	STATISTICAL ANALYSIS	92
3.5	PRESENTATION OF RESULTS	93
CHAPTER 4 SURFACE TOPOGRAPHICAL ANALYSIS OF EXPLANTED TOTAL KNEE REPLACEMENTS WITH COBALT CHROMIUM ALLOY FEMORAL COMPONENTS		
4.1	IMPLANT AND PATIENT VARIABLES	97
4.2	MACROSCOPIC VISUAL ASSESSMENT AND SEMI-QUANTITATIVE DAMAGE SCORING	100
4.2.1	<i>Femoral Components</i>	102
4.2.2	<i>PE Components Articular Surface</i>	104
4.2.3	<i>PE Components Backside Surface and Tibial Components</i>	107
4.3	NON-CONTACTING PROFILOMETRY	110
4.3.1	<i>Femoral Component</i>	110
4.3.2	<i>PE Component Backside Surface</i>	119
4.3.3	<i>Tibial Component</i>	124
4.4	RESULTS SUMMARY	130
4.4.1	<i>Damage Scoring</i>	130
4.4.2	<i>Surface Profilometry</i>	132
CHAPTER 5 SURFACE TOPOGRAPHICAL ANALYSIS OF EXPLANTED UNICONDYLAR KNEE REPLACEMENTS WITH COBALT CHROMIUM ALLOY FEMORAL COMPONENTS		
5.1	IMPLANT AND PATIENT VARIABLES	139
5.2	MACROSCOPIC VISUAL ASSESSMENT AND SEMI-QUANTITATIVE DAMAGE SCORING	141
5.3	NON-CONTACTING PROFILOMETRY	145
5.4	RESULTS SUMMARY	150
CHAPTER 6 SURFACE TOPOGRAPHICAL ANALYSIS OF EXPLANTED KNEE REPLACEMENT PROSTHESES WITH OXIDISED ZIRCONIUM FEMORAL COMPONENTS		
6.1	IMPLANT AND PATIENT VARIABLES	153
6.2	MACROSCOPIC VISUAL ASSESSMENT AND DAMAGE SCORING	157
6.2.1	<i>Femoral Components</i>	157
6.2.2	<i>PE Components Articular Surface</i>	160
6.2.3	<i>PE Components Backside Surface and Tibial Trays</i>	162
6.3	NON-CONTACTING PROFILOMETRY	164
6.4	RESULTS SUMMARY	172
CHAPTER 7 DISCUSSION		
7.1	SURFACE TOPOGRAPHICAL ANALYSIS OF EXPLANTED TKRS WITH COCr FEMORAL COMPONENTS	176

7.2	SURFACE TOPOGRAPHICAL ANALYSIS OF EXPLANTED UKRS WITH CoCr FEMORAL COMPONENTS	185
7.3	SURFACE TOPOGRAPHICAL ANALYSIS OF EXPLANTED KNEE PROSTHESES WITH OXZR FEMORAL COMPONENTS .....	186
7.4	LIMITATIONS AND PRACTICAL CONSTRAINTS .....	193
7.4.1	<i>Patient and Implant Variables</i> .....	194
7.4.2	<i>Damage Scoring</i> .....	195
7.4.3	<i>Surface Roughness Measurement</i> .....	197
7.4.4	<i>Approximation of a Reference Surface</i> .....	204
7.5	SUMMARY .....	205
CHAPTER 8 CONCLUSIONS.....		209
8.1	SUMMARY .....	209
8.2	FUTURE WORK.....	212
8.3	CONTRIBUTION TO THE LITERATURE .....	214
CHAPTER 9 REFERENCES.....		217
APPENDIX A: KNEE EXPLANT RETRIEVAL PROTOCOL .....		239
APPENDIX B: KNEE EXPLANT CATALOGUE .....		253
APPENDIX C: SURFACE TOPOGRAPHICAL ANALYSIS OF EXPLANTED TKRS RESULTS.....		281
APPENDIX D: SURFACE TOPOGRAPHICAL ANALYSIS OF EXPLANTED UKRS RESULTS .....		299
APPENDIX E: SURFACE TOPOGRAPHICAL ANALYSIS OF EXPLANTED KNEE PROSTHESES WITH OXZR FEMORAL COMPONENTS .....		309
APPENDIX F: SMITH, S., KENNARD E. AND JOYCE T.J. BIOTRIBOLOGY 2018 .....		321
APPENDIX G: KENNARD ET AL MEP 2018 .....		343
APPENDIX H: SCHOLES ET AL JMATSCI:MATMED 2018 .....		363

## List of Figures

FIGURE 2.1	ANATOMICAL CARDINAL PLANES AND DIRECTIONAL TERMINOLOGY [33] ...	7
FIGURE 2.2	THE ANATOMY OF THE KNEE JOINT [34] .....	8
FIGURE 2.3	THE ANATOMICAL AND MECHANICAL AXES OF THE FEMUR [36] .....	9
FIGURE 2.4	THE FLEXION AND EXTENSION OF THE KNEE [44].....	11
FIGURE 2.5	FLEXION AND EXTENSION OF THE KNEE DURING THE GAIT CYCLE [53]....	13

FIGURE 2.6	TYPICAL KNEE JOINT CONTACT FORCE, AS A MULTIPLE OF BODY WEIGHT (BW) DURING A GAIT CYCLE [54] .....	14
FIGURE 2.7	SCHEMATIC OF A NORMAL JOINT (LEFT) AND A JOINT WITH OSTEOARTHRITIS (RIGHT) [55] .....	16
FIGURE 2.8	A: MILD OA GRADE 1 B: MODERATE OA GRADE2 [63]. .....	17
FIGURE 2.9	A: MODERATE TO SEVERE OA GRADE 3 B SEVERE OA GRADE 4 [63]. .....	17
FIGURE 2.10	REPRESENTATION OF $R_A$ AND $R_Q$ : $S_A$ AND $S_Q$ ARE THE AREAL EXTENSIONS OF THESE PARAMETERS RESPECTIVELY.....	20
FIGURE 2.11	REPRESENTATION OF SKEWNESS.....	21
FIGURE 2.12	REPRESENTATION OF KURTOSIS.....	22
FIGURE 2.13	A STYLUS-TYPE PROFILOMETER [80].....	24
FIGURE 2.14	CSI INSTRUMENT OPERATION [79] .....	25
FIGURE 2.15	SCHEMATIC OF A ZYGO NEWVIEW 5000 PROFILOMETER [82] .....	25
FIGURE 2.16	THE CREATION OF (A) BRIGHT INTERFERENCE FRINGES AND (B) DARK INTERFERENCE FRINGES [79].....	26
FIGURE 2.17	(A) TWO-BODY ABRASIVE WEAR (B) THREE-BODY ABRASIVE WEAR .....	33
FIGURE 2.18	TOTAL KNEE REPLACEMENT AND UNICONDYLAR KNEE REPLACEMENT [95] .....	35
FIGURE 2.19	DIFFERENT BEARINGS SHOWN ON UKRS [96] .....	35
FIGURE 2.20	A CR AND A PS ROTATING PLATFORM TKR [97] .....	36
FIGURE 2.21	DIAGRAM REPRESENTING HOOD DAMAGE SCORE AREAS ON THE ARTICULAR SURFACE OF A PE COMPONENT [194] .....	49
FIGURE 2.22	DIAGRAM REPRESENTING THE 8 FEMORAL COMPONENT DAMAGE SCORE AREAS AS PER THE METHOD DESCRIBE BY BRANDT ET AL [180] .....	55
FIGURE 3.1	KNEE PROSTHESES CATALOGUE BREAKDOWN.....	74
FIGURE 3.2	EXAMPLE EXPLANTED AGC, K+ AND PFC TKRS .....	76
FIGURE 3.3	EXAMPLE EXPLANTED HFZ, OB, SL AND OTH UKRS.....	77
FIGURE 3.4	EXPLANTED TKRS AND UKRS WITH OXZR FEMORAL COMPONENTS .....	78
FIGURE 3.5	DAMAGE AREAS ON A CRUCIATE RETAINING TKR FEMORAL COMPONENT [180] .....	81



FIGURE 3.6	DAMAGE AREAS ON THE ARTICULAR SURFACE OF A CRUCIATE RETAINING TKR PE COMPONENT .....	83
FIGURE 3.7	DAMAGE AREAS ON THE BACKSIDE SURFACE OF A TKR AND UKR PE COMPONENT .....	84
FIGURE 3.8	SCHEMATIC OF A ZYGO NEWVIEW 5000 PROFILOMETER [82].....	89
FIGURE 3.9	OXZR AND COCR FEMORAL COMPONENT POSITIONED ON THE ZYGO NEWVIEW 5000 PLATFORM .....	92
FIGURE 3.10	EXAMPLE OF A SURFACE TOPOGRAPHY PLOT FROM THE METROPRO SOFTWARE .....	94
FIGURE 4.1	RETRIEVED AGC, K+ AND PFC TKR COMPONENTS .....	98
FIGURE 4.2	RETRIEVED AGC, K+ AND PFC FEMORAL COMPONENTS.....	102
FIGURE 4.3	FDS & DFS FOR RETRIEVED AGC, PFC & K+ FEMORAL COMPONENTS ....	103
FIGURE 4.4	ARTICULAR SURFACE OF RETRIEVED AGC, PFC AND K+ PE COMPONENTS .....	105
FIGURE 4.5	PE ADS & DFS FOR RETRIEVED AGC, PFC AND K+ PE COMPONENTS.....	106
FIGURE 4.6	TIBIAL TRAYS AND PE BACKSIDE SURFACES OF RETRIEVED PFC TKRS WITH NON-POLISHED AND POLISHED TRAYS AND K+ TKRS WITH NO PE WEAR THROUGH (W/T) AND WITH PE WEAR THROUGH (W/T).....	107
FIGURE 4.7	PE BDS FOR RETRIEVED PFC & K+ PE COMPONENTS.....	109
FIGURE 4.8	SURFACE TOPOGRAPHY PLOTS FOR A MEASUREMENT AREA ON A REFERENCE PFC FEMORAL COMPONENT $S_Q = 0.033\mu\text{M}$ , $S_Z = 0.321\mu\text{M}$ .....	112
FIGURE 4.9	SURFACE TOPOGRAPHY PLOTS FOR A MEASUREMENT AREA ON A REFERENCE K+ FEMORAL COMPONENT $S_Q = 0.038\mu\text{M}$ , $S_Z = 0.196\mu\text{M}$ .....	112
FIGURE 4.10	SURFACE TOPOGRAPHY PLOTS FOR A MEASUREMENT AREA ON A REFERENCE PCF FEMORAL COMPONENT $S_Q = 0.150\mu\text{M}$ , $S_Z = 0.880\mu\text{M}$ .....	113
FIGURE 4.11	SURFACE TOPOGRAPHY PLOTS FOR A MEASUREMENT AREA ON A REFERENCE K+ FEMORAL COMPONENT $S_Q = 0.260\mu\text{M}$ , $S_Z = 2.784\mu\text{M}$ .....	113
FIGURE 4.12	SURFACE TOPOGRAPHY PLOTS FOR A MEASUREMENT AREA ON A REFERENCE K+ FEMORAL COMPONENT $S_Q = 0.086\mu\text{M}$ , $S_Z = 0.803\mu\text{M}$ .....	114
FIGURE 4.13	FEMORAL COMPONENT RMS SURFACE ROUGHNESS, $S_Q$ .....	117
FIGURE 4.14	FEMORAL COMPONENT 10-POINT HEIGHT, $S_Z$ .....	117

FIGURE 4.15	SURFACE TOPOGRAPHY PLOTS FOR A MEASUREMENT AREA ON A RETRIEVED AGC FEMORAL COMPONENT $S_Q = 0.110\mu\text{M}$ , $S_Z = 0.398\mu\text{M}$ .....	118
FIGURE 4.16	SURFACE TOPOGRAPHY PLOTS FOR A MEASUREMENT AREA ON A RETRIEVED PCF FEMORAL COMPONENT $S_Q = 0.120\mu\text{M}$ , $S_Z = 0.725\mu\text{M}$ .....	118
FIGURE 4.17	SURFACE TOPOGRAPHY PLOTS FOR A MEASUREMENT AREA ON A RETRIEVED K+ FEMORAL COMPONENT $S_Q = 0.197\mu\text{M}$ , $S_Z = 1.367\mu\text{M}$ .....	119
FIGURE 4.18	PE COMPONENT BACKSIDE SURFACE RMS SURFACE ROUGHNESS, $S_Q$ .	121
FIGURE 4.19	SURFACE TOPOGRAPHY PLOTS FOR A MEASUREMENT AREA ON THE REFERENCE K+ PE COMPONENT BACKSIDE SURFACE $S_Q = 1.303\mu\text{M}$ , $S_Z = 5.512\mu\text{M}$ .....	122
FIGURE 4.20	SURFACE TOPOGRAPHY PLOTS FOR A MEASUREMENT AREA ON THE BACKSIDE OF A RETRIEVED K+ PE COMPONENT FROM A TKR WITH NO PE WEAR THROUGH $S_Q = 1.426\mu\text{M}$ , $S_Z = 5.512\mu\text{M}$ .....	122
FIGURE 4.21	SURFACE TOPOGRAPHY PLOTS FOR A MEASUREMENT AREA ON THE BACKSIDE OF A RETRIEVED K+ PE COMPONENT FROM A TKR WITH PE WEAR THROUGH $S_Q = 1.102\mu\text{M}$ , $S_Z = 3.967\mu\text{M}$ .....	123
FIGURE 4.22	SURFACE TOPOGRAPHY PLOTS FOR A MEASUREMENT AREA ON THE BACKSIDE OF A RETRIEVED PFC PE COMPONENT MATED WITH A NON-POLISHED TIBIAL TRAY $S_Q = 0.842\mu\text{M}$ , $S_Z = 4.636\mu\text{M}$ .....	123
FIGURE 4.23	SURFACE TOPOGRAPHY PLOTS FOR A MEASUREMENT AREA ON THE BACKSIDE OF A RETRIEVED PFC PE COMPONENT MATED WITH A POLISHED TIBIAL TRAY $S_Q = 1.202\mu\text{M}$ , $S_Z = 5.002\mu\text{M}$ .....	124
FIGURE 4.24	TIBIAL COMPONENT SURFACE RMS SURFACE ROUGHNESS, $S_Q$ .....	125
FIGURE 4.25	SURFACE TOPOGRAPHY PLOTS FOR A MEASUREMENT AREA ON THE REFERENCE K+ TIBIAL COMPONENT $S_Q = 3.635\mu\text{M}$ , $S_Z = 7.153\mu\text{M}$ .....	127
FIGURE 4.26	SURFACE TOPOGRAPHY PLOTS FOR A MEASUREMENT AREA ON A RETRIEVED K+ TIBIAL COMPONENT FROM A TKR WITH NO PE WEAR THROUGH $S_Q = 3.272\mu\text{M}$ , $S_Z = 10.643\mu\text{M}$ .....	128
FIGURE 4.27	SURFACE TOPOGRAPHY PLOTS FOR A MEASUREMENT AREA ON A POLISHED AREA OF A RETRIEVED K+ TIBIAL COMPONENT FROM A TKR WITH PE WEAR THROUGH $S_Q = 0.075\mu\text{M}$ , $S_Z = 1.073\mu\text{M}$ .....	128
FIGURE 4.28	SURFACE TOPOGRAPHY PLOTS FOR A MEASUREMENT AREA ON A RETRIEVED NON-POLISHED PCF TIBIAL COMPONENT $S_Q = 0.922\mu\text{M}$ , $S_Z = 7.666\mu\text{M}$ .....	129
FIGURE 4.29	SURFACE TOPOGRAPHY PLOTS FOR A MEASUREMENT AREA ON A RETRIEVED POLISHED PFC TIBIAL COMPONENT $S_Q = 0.045\mu\text{M}$ , $S_Z = 0.609\mu\text{M}$ .....	129

FIGURE 4.30	MEAN FDS AGAINST MEAN PE ADS .....	130
FIGURE 4.31	MEAN PE BDS AGAINST MEAN PE ADS .....	131
FIGURE 4.32	MEAN FDS AND MEAN PE ADS AGAINST TIME <i>IN VIVO</i> .....	132
FIGURE 4.33	RETRIEVED FEMORAL COMPONENT $S_Q$ AGAINST LENGTH OF TIME <i>IN VIVO</i> . .....	133
FIGURE 4.34	RETRIEVED FEMORAL COMPONENT $S_{SK}$ AGAINST LENGTH OF TIME <i>IN VIVO</i> .....	134
FIGURE 4.35	RETRIEVED TIBIAL COMPONENT $S_Q$ AGAINST LENGTH OF TIME <i>IN VIVO</i> .	134
FIGURE 4.36	RETRIEVED FEMORAL COMPONENT $S_Q$ AGAINST PE ADS .....	135
FIGURE 4.37	PE COMPONENT BACKSIDE SURFACE $S_Q$ AGAINST TIBIAL COMPONENT $S_Q$ . .....	136
FIGURE 4.38	TIBIAL COMPONENT SURFACE $S_Q$ AGAINST PE COMPONENT BDS.....	137
FIGURE 5.1	(A) RETRIEVED HFZ (B) OB (C) SL AND (D) OTH UKR COMPONENTS .....	140
FIGURE 5.2	FDS, PE ADS AND PE BDS FOR RETRIEVED UKRS .....	143
FIGURE 5.3	FDS AND DFS VALUES FOR RETRIEVED HFZ AND OB UKRS .....	144
FIGURE 5.4	PE ADS AND DFS VALUES FOR RETRIEVED HFZ AND OB UKRS .....	145
FIGURE 5.5	RETRIEVED VS REFERENCE UKR FEMORAL COMPONENT SURFACE ROUGHNESS PARAMETERS .....	147
FIGURE 5.6	SURFACE TOPOGRAPHY PLOTS FOR A MEASUREMENT AREA ON A RETRIEVED HFZ FEMORAL COMPONENT $S_Q = 0.082\mu\text{M}$ , $S_Z = 0.672\mu\text{M}$ .....	148
FIGURE 5.7	SURFACE TOPOGRAPHY PLOTS FOR A MEASUREMENT AREA ON A RETRIEVED OB FEMORAL COMPONENT $S_Q = 0.074\mu\text{M}$ , $S_Z = 0.423\mu\text{M}$ .....	149
FIGURE 5.8	SURFACE TOPOGRAPHY PLOTS FOR A MEASUREMENT AREA ON THE RETRIEVED SL FEMORAL COMPONENT $S_Q = 0.649\mu\text{M}$ , $S_Z = 2.186\mu\text{M}$ .....	149
FIGURE 5.9	SURFACE TOPOGRAPHY PLOTS FOR A MEASUREMENT AREA ON THE RETRIEVED OTH FEMORAL COMPONENT $S_Q = 0.073\mu\text{M}$ , $S_Z = 0.483\mu\text{M}$ .....	150
FIGURE 5.10	UKR FDS AGAINST PE ADS .....	151
FIGURE 5.11	UKR PE ADS AGAINST PE BDS .....	151
FIGURE 6.1	RETRIEVED OXZR TKRS AND RETRIEVED OXZR UKRS .....	156
FIGURE 6.2	FDS AND DFS VALUES FOR RETRIEVED OXZR AND COCR TKRS AND UKRS. .....	159

FIGURE 6.3	PE ADS AND DFS FOR RETRIEVED OXZR AND COCR TKRS AND UKRS ....	161
FIGURE 6.4	PE BDS AND DFS FOR RETRIEVED OXZR AND COCR TKRS AND UKRS ....	163
FIGURE 6.5	OXZR AND COCR RETRIEVED AND REFERENCE TKR AND UKR FEMORAL COMPONENT SURFACE ROUGHNESS PARMETERS $S_Q$ , $S_Z$ AND $S_{SK}$ .....	167
FIGURE 6.6	OXZR AND COCR RETRIEVED AND REFERENCE TKR AND UKR FEMORAL COMPONENT SURFACE ROUGHNESS PARMETERS $S_P$ , $S_V$ AND $P$ .....	168
FIGURE 6.7	SURFACE TOPOGRAPHY PLOTS FOR A MEASUREMENT AREA ON THE REFERENCE OXZR FEMORAL COMPONENT $S_Q = 0.098\mu\text{M}$ , $S_Z = 0.546\mu\text{M}$ .....	169
FIGURE 6.8	SURFACE TOPOGRAPHY PLOTS FOR A MEASUREMENT AREA ON A RETRIEVED OXZR TKR FEMORAL COMPONENT $S_Q = 0.236\mu\text{M}$ , $S_Z = 1.392\mu\text{M}$ .....	169
FIGURE 6.9	SURFACE TOPOGRAPHY PLOTS FOR A MEASUREMENT AREA ON A RETRIEVED OXZR UKR FEMORAL COMPONENT $S_Q = 0.134\mu\text{M}$ , $S_Z = 0.854\mu\text{M}$ .....	170
FIGURE 6.10	SURFACE TOPOGRAPHY PLOTS FOR A MEASUREMENT AREA ON A REFERENCE COCR FEMORAL COMPONENT $S_Q = 0.061\mu\text{M}$ , $S_Z = 0.922\mu\text{M}$ .....	170
FIGURE 6.11	SURFACE TOPOGRAPHY PLOTS FOR A MEASUREMENT AREA ON A RETRIEVED COCR TKR FEMORAL COMPONENT $S_Q = 0.099\mu\text{M}$ , $S_Z = 0.267\mu\text{M}$ .....	171
FIGURE 6.12	SURFACE TOPOGRAPHY PLOTS FOR A MEASUREMENT AREA ON A RETRIEVED COCR UKR FEMORAL COMPONENT $S_Q = 0.082\mu\text{M}$ , $S_Z = 0.672\mu\text{M}$ .....	171
FIGURE 6.13	OXZR AND COCR TKR AND UKR FDS AGAINST PE ADS VALUES .....	172
FIGURE 6.14	OXZR AND COCR TKR AND UKR FEMORAL COMPONENT $S_Q$ AGAINST PE ADS VALUES .....	173
FIGURE 7.1	SURFACE TOPOGRAPHY PLOTS FOR A MEASUREMENT AREA ON A RETRIEVED COCR FEMORAL COMPONENT SHOWING AN INDENTATION, $S_Q = 0.250\mu\text{M}$ , $S_Z = 0.957\mu\text{M}$ .....	181
FIGURE 7.2	SURFACE TOPOGRAPHY PLOTS FOR A MEASUREMENT AREA ON A RETRIEVED COCR FEMORAL COMPONENT SHOWING DEFINED SCRATCHING, $S_Q = 0.110\mu\text{M}$ , $S_Z = 0.539\mu\text{M}$ .....	182
FIGURE 7.3	SURFACE TOPOGRAPHY PLOTS FOR A MEASUREMENT AREA ON A RETRIEVED COCR FEMORAL COMPONENT SHOWING THE EDGE OF A BURNISHED AREA AND A SCRATCH, $S_Q = 0.120\mu\text{M}$ , $S_Z = 0.725\mu\text{M}$ .....	182
FIGURE 7.4	SURFACE TOPOGRAPHY PLOTS FOR A MEASUREMENT AREA ON A RETRIEVED COCR FEMORAL COMPONENT SHOWING A BURNISHED AREA, $S_Q = 0.065\mu\text{M}$ , $S_Z = 0.533\mu\text{M}$ .....	183

FIGURE 7.5	SURFACE TOPOGRAPHY PLOTS AND PROFILOMETER LENS VIEW FOR A MEASUREMENT AREA ON A RETRIEVED COCR FEMORAL COMPONENT SHOWING WAVINESS, $S_Q = 0.127\mu\text{M}$ , $S_Z = 0.635\mu\text{M}$ .....	183
FIGURE 7.6	SURFACE TOPOGRAPHY PLOTS AND PROFILOMETER LENS VIEW FOR A MEASUREMENT AREA ON A RETRIEVED COCR FEMORAL COMPONENT SHOWING WAVINESS, $S_Q = 0.169\mu\text{M}$ , (THERE IS NOT ENOUGH DATA TO CALCULATE $S_Z$ ) .....	184
FIGURE 7.7	(A) FIXATION OF JOURNEY UKR FEMORAL COMPONENT (B) FIXATION OF GENESIS II TKR FEMORAL COMPONENT. (IMAGES FROM SMITH & NEPHEW SURGICAL TECHNIQUES) [229, 230].....	188
FIGURE 7.8	SURFACE TOPOGRAPHY PLOTS FROM MEASUREMENT AREAS ON FEMORAL COMPONENTS (A) COCR REFERENCE ( $S_Q = 0.063$ , $S_Z = 0.403$ ) (B) COCR RETREIVED ( $S_Q = 0.099$ , $S_Z = 0.267$ ) (C) OXZR REFERENCE ( $S_Q = 0.099$ , $S_Z = 0.433$ ) AND (D) OXZR RETRIEVED ( $S_Q = 0.123$ , $S_Z = 0.799$ ) .....	190
FIGURE 7.9	IMAGES FROM HEYSE ET AL [217] .....	191
FIGURE 7.10	IMAGES TAKEN FROM BRANDT ET AL [180] ON THE LEFT ARE SEM IMAGES. SHOWING NEW (TOP) AND RETRIEVED (BOTTOM) COCR (LEFT) AND OXZR (RIGHT). ON THE RIGHT ARE CONTACT PROFILOMETRY PLOTS FOR COCR (TOP) AND OXZR (BOTTOM).....	192
FIGURE 7.11	POSITIONING OF AN OXZR TKR FEMORAL COMPONENT FOR MEASUREMENT UTILISING A POSITIONING BLOCK .....	200

## List of Tables

TABLE 2.1	SUMMARY OF AVERAGE KNEE JOINT LOADING FOR ACTIVITIES OF DAILY LIVING [45] .....	12
TABLE 2.2	MECHANICAL PROPERTIES OF MATERIALS USED IN FEMORAL COMPONENTS OF KNEE REPLACEMENTS [128, 129] .....	37
TABLE 2.3	SUMMARY OF MEAN ( $\pm$ STANDARD DEVIATION) PHYSICAL AND TENSILE MECHANICAL PROPERTIES OF EXTRUDED AND MOULDED UHMWPE [140] .....	39
TABLE 2.4	PE ARTICULAR SURFACE AND BACKSIDE SURFACE DAMAGE MODE DESCRIPTIONS AND IDENTIFICATION. IMAGES SHOWING 1MM SCALE. IMAGES FROM HARMAN ET AL 2011 [195] .....	50
TABLE 2.5	REVIEW OF PUBLISHED LITERATURE REGARDING SURFACE PROFILOMETRIC MEASUREMENT OF KNEE REPLACEMENT COMPONENTS .....	60
TABLE 3.1	PE ARTICULAR SURFACE AND BACKSIDE SURFACE DAMAGE MODE DESCRIPTIONS AND IDENTIFICATION. IMAGES SHOWING 1MM SCALE. IMAGES FROM HARMAN ET AL 2011 [195] .....	85
TABLE 4.1	TKR IMPLANT AND PATIENT VARIABLES .....	99

TABLE 4.2	FDS, PE ADS AND PE BDS FOR RETRIEVED TKRS .....	101
TABLE 4.3	REFERENCE PFC AND K+ FEMORAL COMPONENT SURFACE ROUGHNESS PARAMETERS .....	110
TABLE 4.4	AGC, PFC AND K+ FEMORAL COMPONENT SURFACE ROUGHNESS PARAMETERS .....	115
TABLE 4.5	REFERENCE K+ AND RETRIEVED K+ AND PFC PE COMPONENT BACKSIDE SURFACE ROUGHNESS PARAMETERS .....	120
TABLE 4.6	REFERENCE K+ AND RETRIEVED K+ AND PFC TIBIAL COMPONENT SURFACE ROUGHNESS PARAMETERS .....	126
TABLE 5.1	FDS PE ADS AND PE BDS FOR RETRIEVED UKRS .....	142
TABLE 5.2	UKR FEMORAL COMPONENT SURFACE ROUGHNESS PARAMETERS.....	147
TABLE 6.1	OXZR TKR AND CoCr TKR PATIENT AND IMPLANT VARIABLES.....	155
TABLE 6.2	OXZR AND CoCr TKR AND UKR FDS, PE ADS AND PE BDS VALUES.....	158
TABLE 6.3	OXZR TKR AND UKR SURFACE ROUGHNESS VALUES.....	164
TABLE 6.4	CoCr TKR AND UKR SURFACE ROUGHNESS VALUES .....	165
TABLE 7.1	SURFACE ROUGHNESS MEASUREMENT RESULTS FOR THE SAME LOCATION ON A CoCr FEMORAL COMPONENT AT DIFFERENT OPTICAL ZOOMS .....	201
TABLE 7.2	SURFACE ROUGHNESS MEASUREMENT RESULTS FOR THE SAME LOCATION ON AN OXZR FEMORAL COMPONENT AT DIFFERENT OPTICAL ZOOMS .....	202
TABLE 7.3	SURFACE ROUGHNESS PARAMETERS VARIATION DEPENDENT ON ANALYSIS CONTROL REMOVE SPIKES AND DATA FILL FILTERS.....	203

## List of Abbreviations

ACL	Anterior Cruciate Ligament
AGC	AGC ® Zimmer Biomet, Warsaw, IN, US
AOAJRR	Australian Orthopaedic Association Joint Replacement Registry
AP	Anterior / Posterior
BMI	Body Mass Index
BS	British Standards
BW	Body Weight
CMM	Coordinate Measurement Machine
CoCr	Cobalt Chromium alloy
CR	Cruciate Retaining
CSI	Coherence Scanning Interferometry
CT	Computer Topography
DFS	Damage Feature Score
EHL	ElastoHydrodynamic Lubrication
FDS	Femoral Damage Score
GDT	Geometric Design and Tolerancing
HD	Hydrodynamic
HFZ	High Flexion Unicompartmental Knees Zimmer Biomet, Warsaw, IN, US
IKDC	International Knee Document Committee
ISO	International Organisation for Standardisation
JOxZr	Oxinium Journey Unicondylar Knee Replacement ® Smith & Nephew, London, UK
K+	Kinemax Plus ® Stryker, Mahwah, NJ, US
MC	million cycles
MgPSZ	Magnesia-Stabilised Zirconia
ML	Medial / Lateral
NHS	National Health Service
NICE	National Institute for Clinical Excellence
NJR	National Joint Register
OA	Osteoarthritis
OB	Oxford ® UKR Zimmer Biomet, Warsaw, IN, US
OBJ	Objective
OC	Outcome
Oth	Unidentified Unicondylar Knee Replacement
OxZr	Oxidised Zirconium
PCA	Porous Coated Anatomic

PCL	Posterior Cruciate Ligament
PE	Polyethylene
PE ADS	Polyethylene Articular surface Damage Score
PE BDS	Polyethylene Backside surface Damage Score
PFC	PFC Sigma ® DePuy, Warsaw, IN, US
PS	Posterior Stabilising
PV	Max Peak to Valley Height
RMN	Representative Measurement Number
$S_a$	Mean Surface Roughness
$S_k$	Kurtosis
$S_p$	Max Peak Height
$S_q$	Root Mean Square Surface Roughness
$S_{sk}$	Skewness
$S_v$	Max Valley Depth
$S_z$	10 – point Height Average
SI	Superior / Inferior
SL	Sled ® Unicondylar Knee Replacement Link, Hamburg, Germany
THR	Total Hip Replacement
TKR	Total Knee Replacement
Ti	Titanium
TiN	Titanium Nitride
TIV	Time <i>In Vivo</i>
TKR	Total Knee Replacement
TSRM	True Surface Roughness Mean
UHMWPE	Ultra-High Molecular Weight Polyethylene
UKR	Unicondylar Knee Replacement
WOMAC	Western Ontario & McMaster University Osteoarthritis Index
XLPE	Cross-Linked Polyethylene



## Chapter 1 Introduction

### 1.1 Background

Knee replacement surgery is a successful medical procedure that offers pain relief and improved mobility for many people suffering with debilitating diseases such as osteoarthritis [1]. Published in September 2018, the 15<sup>th</sup> Annual National Joint Registry (NJR) report for England, Wales, Northern Ireland and the Isle of Man recorded that 112,836 knee replacement procedures were performed in 2017 [1]. This represents a 3.8% increase in the number of procedures performed in the previous year. Excellent functional outcomes for knee replacement procedures and long-term survivorship of ten years and more are currently reported worldwide with some knee replacement prostheses reported to have lasted over twenty years [2-7]. However, despite these successes, failures of the prostheses do occur. When this happens a revision surgery is necessary to remove and replace the failed prosthesis to relieve patients of pain and prevent further harm. In England, Wales, Northern Ireland and the Isle of Man 6,502 revision knee procedures were performed in 2017 [1]. This is a 5% increase from the previous year. At a mean cost of approximately £16,000 per revision knee procedure the total annual cost of revision knee procedures may be estimated at just over £104 million for England, Wales, Northern Ireland and the Isle of Man [8]. In addition to the financial cost of revision surgery, there is the increased risk to the patient of an additional surgery and hospital stay with the associated increased social burden.

The following statement from the British Orthopaedic Association illustrates the responsibility of the orthopaedic community, including medical practitioners, device manufacturers and academic researchers, to continually strive towards the goal of improving the performance of the implants and the surgical procedures and to work collaboratively to reduce failure rates and increase the time to revision to the benefit and safety of the patient.

*“Trauma and Orthopaedic Surgery is a highly cost-effective form of treatment which aims to restore pain free mobility for patients. By restoring mobility, Trauma and*

*Orthopaedic surgery can not only help people stay active for longer but deliver major economic savings enabling people to return to work or live more independently.*

*Given the growing musculoskeletal disease burden, and the transformative impact surgery can have for the right patients, we believe surgeons, commissioners and colleagues across the NHS should work together to increase surgical capacity.” [9]*

Analyses and testing of orthopaedic prostheses enable greater understanding of their performance and function and can lead to design improvements, increased longevity and ultimately enhanced patient safety and benefit. Laboratory simulation studies are an essential part of pre-clinical testing of prostheses and provide useful information on the predicted performance and function of orthopaedic prostheses [10-13].

However it is the analysis of retrieved explanted prostheses that provides evidence and information of the actual performance of the prostheses within the *in vivo* environment [14-17]. The analysis of retrieved explanted prostheses that have undergone the truest test of all through time *in vivo* is invaluable in furthering the understanding of the true prosthesis performance.

The main indication for revision of knee replacement prostheses after ten years *in vivo* is aseptic loosening of the femoral and tibial components of the prostheses resulting from osteolysis [1]. Osteolysis is the resorption of bone triggered by an auto-immune response to polyethylene (PE) wear debris particles generated from wear of the PE component of the prostheses [1, 18-23]. PE wear debris generation, osteolysis and the associated aseptic loosening of the femoral and tibial components of knee replacement prostheses are widely acknowledged as multifaceted problems [24-27]. An increased surface roughness of the femoral component has been identified as one of the causative mechanisms of PE wear leading to PE wear debris generation [11, 28-31]. However, the extent of the importance of an *in vivo* increase in the surface roughness of the femoral component is not well defined or quantified within the existing body of knowledge. There is also limited understanding of the influence of patient variables on a potential *in vivo* increase of the surface roughness of the femoral component.

The work contained within this thesis provides a thorough investigation into the surface topographical analysis of explanted knee prostheses and the relationship between *in vivo* surface topographical changes and patient and implant demographics. This is the largest surface topographical analysis of explanted knee prostheses to be conducted to date within the United Kingdom and is the first to report the surface roughness of explanted Unicondylar Knee Replacement (UKR) prostheses. Within this thesis one hundred and thirty-five explanted knee prostheses were retrieved from revision surgery and were processed and catalogued with the associated patient and implant data. This catalogue of explants and data developed within this thesis is available for future research use at Newcastle University. Ethical approval for this work is granted via REC reference 09/H0906/72. Non-contacting profilometry and semi-quantitative damage scoring were used to provide quantifiable surface topographical analyses of the retrieved explanted and reference Total Knee Replacement (TKR) and UKR prostheses with both cobalt chromium alloy (CoCr) and oxidised zirconium (OxZr) femoral components.

## **1.2 Aim and Objectives**

The aim of this research was to use engineering techniques to quantify the surface topography of retrieved explanted knee replacement prostheses and to investigate relationships between *in vivo* surface topographical changes and patient and implant demographics. The results from this work contribute to the body of knowledge within the field of orthopaedic knee prosthesis retrieval studies and offer a standardised protocol for the surface topographical analysis for explanted knee replacement prostheses.

The following research questions were posed:

**Q1** - Do the quantified *in vivo* surface topographical changes correlate with patient and implant variables?

**Q2** - Are there any correlations between the femoral component *in vivo* topographical changes and the PE articular surface *in vivo* topographical changes?

**Q3** - Are there any correlations between the PE backside surface *in vivo* topographical changes and the tibia tray *in vivo* topographical changes?

To fulfil the specific aim and answer the above research questions, the following objectives (OBJ) were set:

- **OBJ1:** to develop a protocol for the collection of explanted knee prostheses, and for the analysis and quantification of *in vivo* surface topographical changes observed in explanted knee prostheses.
- **OBJ2:** to establish a physical collection of explanted knee prostheses and a written knee prosthesis explant catalogue at Newcastle University.
- **OBJ3:** to use surface topographical measurement techniques to investigate *in vivo* surface changes of explanted knee components.
- **OBJ4:** to correlate surface topographical analysis results with patient and implant variables.
- **OBJ5:** to discuss the limitations and constraints and significance of the results.
- **OBJ6:** to provide suggestions for future studies of explanted knee replacement prostheses.

### 1.3 Thesis Structure

This thesis is divided into nine chapters.

The current **Chapter 1** provides the background and introduction to the work, defines the aim, sets the specific objectives and illustrates the thesis structure.

**Chapter 2** presents a review of the literature pertaining to this thesis. Included is an overview of the anatomy and kinematics of the natural knee joint, a discussion on tribology and surface topography and a review of knee arthroplasty. Within the review of knee arthroplasty, a critical review of the current literature on knee replacement retrieval analyses is provided.

**Chapter 3** contains the methods and materials used for realising the thesis objectives. The protocol that was developed within this PhD to enable the collection, processing, storage and analysis of explanted knee prostheses is presented. The details of the knee explant catalogue which was established as part of this PhD are given. The knee explant catalogue is a physical collection of explanted knee prostheses and a database of the associated patient and implant data that was collected. The details of the surface topographical analysis techniques used to collect the results presented in this thesis are described within this chapter. The statistical methods applied to the data are described. Also provided within this chapter is a description of the method of presentation of the results.

Within **Chapter 4** the results of the surface topographical analysis of forty explanted TKRs with CoCr femoral components are presented. The surface topographical analysis results of forty explanted TKRs are analysed and compared to those taken on un-used, as-manufactured TKRs which were considered as references. The surface topographical analysis results are correlated with patient and impact variables.

Within **Chapter 5** the results of the surface topographical analysis of seventeen explanted UKRs with CoCr femoral components are presented. Comparisons are made between the analyses of UKRs and TKRs and where available, comparisons are made with reference components. Correlations between the patient and implant variables and the surface topographical results are made. This is the first time the surface roughness measurement data of explanted UKRs has been presented.

Within **Chapter 6** the results of the surface topographical analysis of explanted TKRs and UKRs with OxZr femoral components are presented. Comparisons are made with explanted knee prostheses with CoCr femoral components and with reference components. The results presented in this section are published and the manuscript is included in Appendix G.

**Chapter 7** provides a discussion of the results presented in Chapters 4, 5 and 6. The discussion is separated into subsections which include a discussion of the surface topographical analysis results of explanted TKRs with CoCr femoral components, a

discussion of the surface topographical analysis results of explanted UKRs with CoCr femoral components and a discussion of the surface topographical analysis results of explanted knee prostheses with OxZr femoral components. There is a discussion specifically on the limitations and practical constraints and the clinical impact of the results.

In **Chapter 8**, the conclusions and outcomes of the work are detailed and recommendations for future work are made. A subsection of this chapter includes details of the contributions made to the literature that have resulted from this PhD work. Three publications resulting from the work done within this PhD are referenced in this chapter and the manuscripts are included in Appendices F, G and H.

**Chapter 9** includes the references used within this thesis.

A point to note is that this thesis is submitted in my legal married name Emma Ritchie however my authored publications are written in my maiden name Emma Kennard. This is relevant to references Smith, Kennard and Joyce [32], Kennard et al [14] and Scholes and Kennard et al [15].

Appendix A contains the Knee Explant Retrieval Protocol that I wrote to enable the explanted prostheses to be collected, processed and stored. This contains details of the analysis methods. Appendix B provides the details of the patient and implant information of the 135 explanted prostheses that I collected from revision surgeries, processed and catalogued. A large part of this PhD work has been in writing the protocol, establishing the surface topographical analysis methods and in collecting and processing of both the physical explants and the patient and implant data. At the start of this PhD project the collection of explanted knee prostheses did not exist and there was no protocol for the analysis. These are now available for use for future research at Newcastle University.

Appendices C, D and E provide the detailed results for each of the chapters, Chapter 4, 5 and 6. Appendix F, G and H contain the manuscripts of three publications that have been the result of the work done within this PhD (Smith, Kennard and Joyce [32], Kennard et al [14] and Scholes and Kennard et al [15]).

## Chapter 2 Literature Review

Within this chapter a review of the current literature pertaining to this thesis is presented. The chapter is divided into three sections, The Knee, Surface Roughness and Tribology, and Knee Arthroplasty.

### 2.1 The Knee

The knee functions in conjunction with the hip and ankle joints to support the body's weight during static erect posture. Dynamically, the knee is responsible for moving and supporting the body during a range of routine activities (e.g. walking, sitting or moving into a lying position) and more challenging activities (e.g. dancing and participating in sports). The structure of the knee allows it to fulfil both stability and mobility functions. The anatomical reference planes (sagittal, coronal and transverse) and directional terminology (superior/ inferior (SI), anterior/posterior (AP) and medial/lateral (ML)) are shown in Figure 2.1.

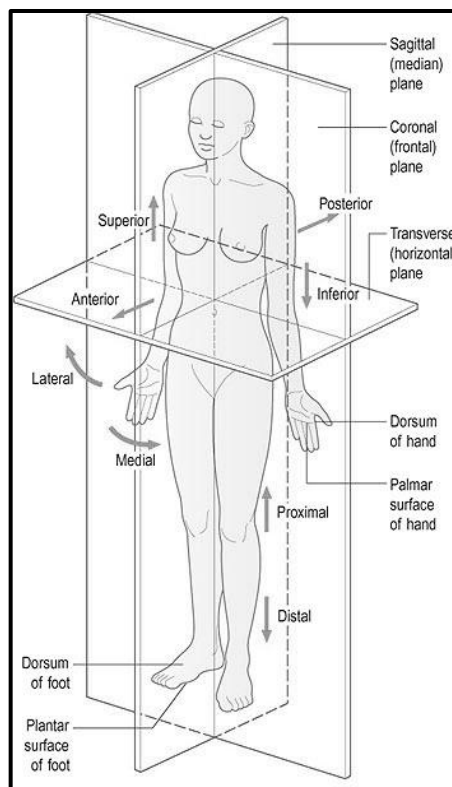


Figure 2.1 Anatomical cardinal planes and directional terminology [33]

### 2.1.1 *Anatomy of the Knee*

The knee joint is a synovial bi-condylar joint [34, 35]. The non-conforming articulation between the condyles of the femur and the tibial plateau forms the weight-bearing tibiofemoral joint. The articulation between the patella and the femoral condyles forms the patellofemoral joint. Figure 2.2 shows the anatomy of the knee joint and the main anatomical features are labelled including the anterior cruciate ligament, the posterior cruciate ligament and the medial and lateral condyles.

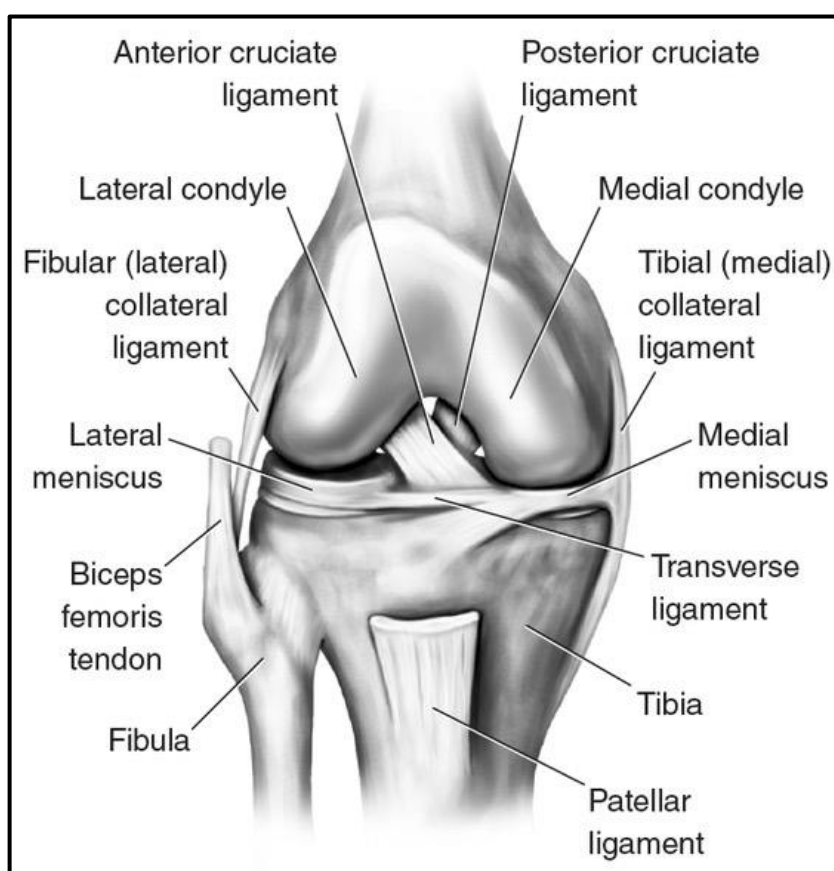


Figure 2.2 The anatomy of the knee joint [34]

A synovial joint is one in which the ends of the bones are freely moveable in relation to each other and are contained within a joint capsule. The ends of the bones contained within the joint capsule are covered in articular cartilage and separated by a synovial cavity which contains synovial fluid. Synovial fluid provides lubrication to the knee joint [33, 35].



The medial femoral condyle of the knee joint is larger, has a greater radius of curvature, and projects further from femur than the lateral condyle [33, 35]. However, due to the anatomical axis of the femur being a medially oblique angle, the distal end of the femur remains horizontal. The centre of the knee joint aligns with the centre of the hip and ankle joints to create a vertical mechanical axis of the femur and tibia. The mechanical axis and anatomic axis and the tibiofemoral angle are labelled in Figure 2.3 below [36].

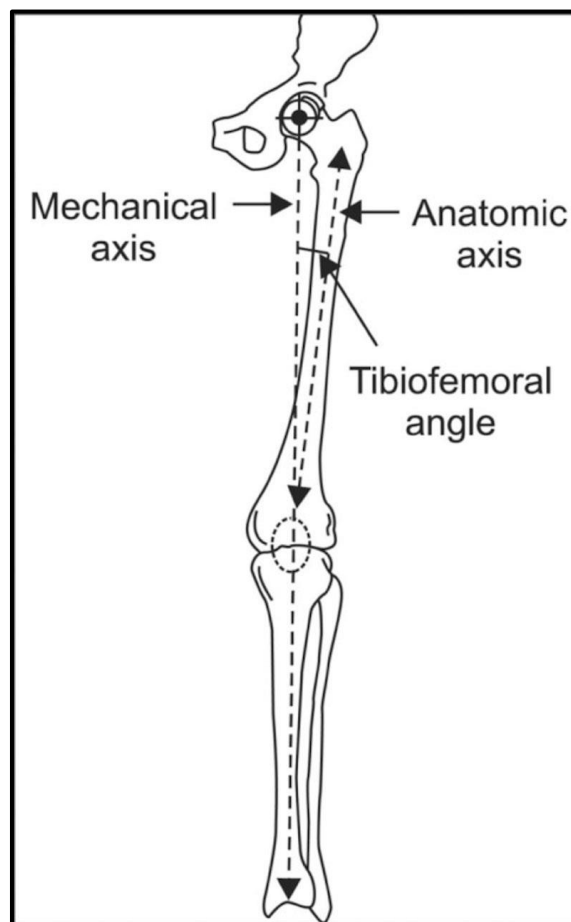


Figure 2.3 The anatomical and mechanical axes of the femur [36]

The quadriceps extensor muscle works to provide extension to the knee and is comprised of the rectus femoris muscle and three vasti muscles, vastus medialis, intermedius and lateralis. The popliteus is a posterior muscle which aids in flexion and provides a lateral rotation of the femur over the tibia [37].

The tibial collateral ligament (on the medial side of the joint), the fibular collateral ligament (on the lateral side of the joint), and the intracapsular ligaments of the anterior cruciate ligament (ACL) and the posterior cruciate ligament (PCL), compensate for the inherent instability of the non-conforming articulation between the femoral condyles and the tibial plateau [33]. The ligaments provide stability to the joint. In Figure 2.2 the fibular collateral ligament and the ACL and PCL are shown. The ACL attaches to the tibia on the anterior medial part of tibia and passes superiorly, posteriorly and laterally to attach to the posterior lateral intercondylar fossa of the femur. The PCL attaches to the posterior medial aspect of the intercondylar area of the tibia and passes superiorly and anteriorly to attach to the anterior medial intercondylar fossa of the femur [34]. The function of the ACL is to prevent anterior displacement of the tibia relative to the femur and the function of the PCL is to restrict posterior displacement.

The articulating joint surfaces of the knee are covered with articular cartilage, which is a load bearing, connective tissue within synovial joints. The mechanical functions of the articular cartilage are to provide a surface over which motion under applied load can be performed and to reduce the localized stresses located in the subchondral bone by improving the congruence between the joint surfaces. Articular cartilage is able to undergo high cyclic loads with minimal damage or degeneration [38].

Between the femoral and tibial condyles of the knee joint are the crescent-shaped menisci. The menisci function to improve the congruence between the articular surfaces of the femur of the tibia and to distribute the loads in weight bearing at the tibiofemoral joint over a broader area and thus reduce the magnitude of the compressive joint stress. The menisci also assist with impact force absorption at the knee acting as shock absorbers. [39, 40]

### **2.1.2 Biomechanics of the Knee**

The primary movement of the knee joint is the hinge-like movement of flexion and extension of the tibiofemoral joint in the sagittal plane. Internal and external rotation

occurs in the transverse plane about the longitudinal axis and abduction and adduction occur in the frontal plane around an anterior-posterior axis [35, 41-43]. During flexion of the knee joint the movement of the femoral condyles is achieved by a combination of rolling and sliding actions. Starting in full extension the femoral condyles roll against the menisci and as the flexion angle increases towards the end of flexion the motion becomes a slide without rolling. On the medial condyle rolling only occurs during the first 10-15° of flexion and on the lateral condyle this continues to around 20° of flexion. This change in motion from rolling to sliding is due to the change in radius of the femoral condyles [33]. Figure 2.4 below shows the rolling and sliding that occurs during tibial femoral extension [44].

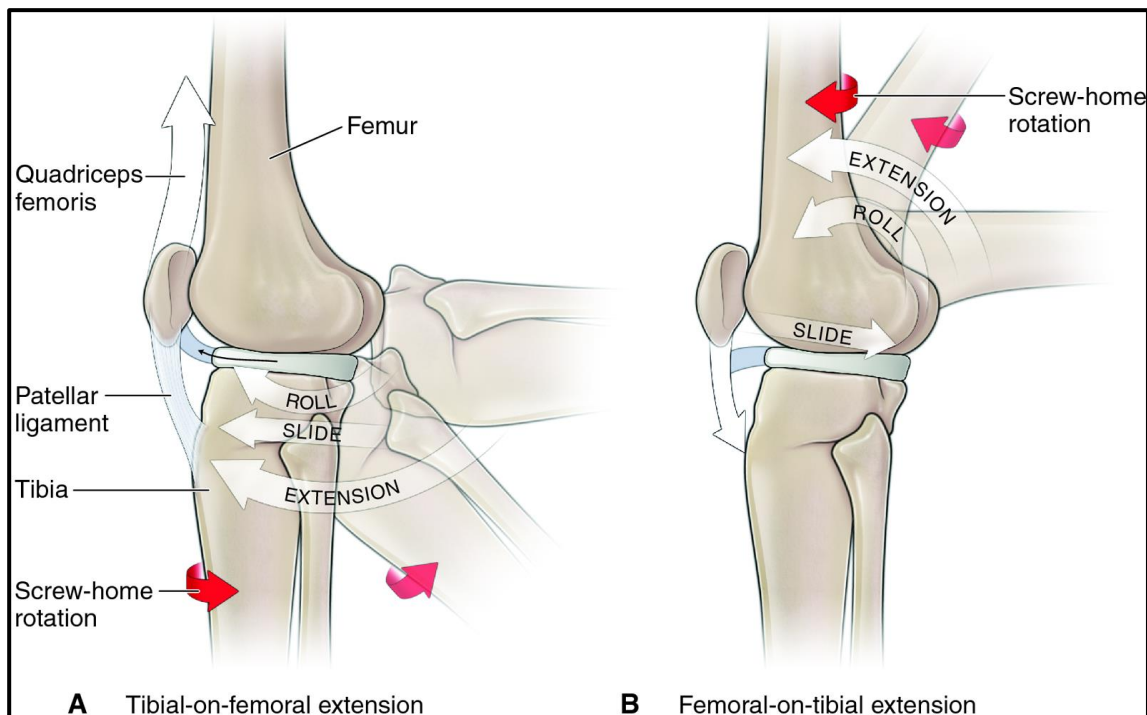


Figure 2.4 The flexion and extension of the knee [44]

The tibiofemoral joint is loaded in both compression and shear during daily activities such as walking, stair climbing, squatting and rising from a chair. Weight bearing and tension development in the muscles across the knee contribute to these forces, with compression dominating when the knee is fully extended and weight-bearing. By making simplified assumptions about the muscle groups working on the knee joint reasonable estimates of joint reaction forces have been obtained which are

consistent with the conclusions made using much more complex biomechanical models as well as by *in vivo* force measurement techniques. Table 2.1 is a version of a table in The UHMWPE Biomaterial Handbook by Kurtz 2016 and summarises knee joint loading forces and flexion / extension angle in the sagittal plane during different everyday activities [45]. Within Table 2.1 the force factor is a dimensionless factor that is a multiple of the force exerted by body weight which is measured in Newtons.

Table 2.1 Summary of Average Knee Joint Loading for Activities of Daily Living [45]

Activity	Reference	Patellofemoral joint		Tibiofemoral joint (compression)		Tibiofemoral joint (anterior shear)	
		Knee angle (°)	Force factor (-)	Knee angle (°)	Force factor (-)	Knee angle (°)	Force factor (-)
<b>Walking</b>	[46-49]	10	0.5	15	3.0-3.5	5	0.4
<b>Squatting</b>	[50]	140	4.7-7.6	140	4.7-5.6	140	2.9-3.5
<b>Rising from a chair</b>	[46, 51]	85-110	3-7	85-110	3-5	85-110	1.5-3.5
<b>Stair climbing / descent</b>	[46, 49]	60	3.3	45-60	3.8-4.3	5	0.6

\* The force factor is a dimensionless factor that is a multiple of body weight

Knee joint forces during activities such as walking, or stair climbing have typically been determined through measurement using force plates to determine the ground reaction force and calculated using musculoskeletal analysis techniques. The compressive force at the tibiofemoral joint has been reported to be slightly greater than three times body weight during the stance phase of gait and increasing up to approximately four times body weight during stair climbing [46-49]. The medial tibial plateau bears most of this load during the stance phase when the knee is extended, with the lateral tibial plateau bearing more of the much smaller loads imposed during

the swing phase of walking [47]. The medial tibial plateau has a surface area roughly 60% larger than that of the lateral tibial plateau and the articular cartilage on the medial plateau is approximately three times thicker than that on the lateral plateau. The larger surface area of the medial tibial plateau means that the stress acting on the joint is less than if peak loads were distributed laterally [52]. As flexion occurs and the angle at the knee joint increases to  $90^\circ$ , the shear component of joint force produced by weight bearing increases. Shear at the knee joint causes a tendency for the femur to displace anteriorly on the tibial plateau and is resisted by the ligaments supporting the knee.

The tibiofemoral joint flexion and extension during the gait cycle is shown in Figure 2.5 where the y-axis is the knee joint flexion and the x-axis describes the gait cycle in percentages corresponding to heel strike, the opposite foot (contralateral) heel strike and toe off. The two phases of the gait cycle, the stance phase where there is contact with the ground and the swing phase where there is no contact with the ground are indicated.

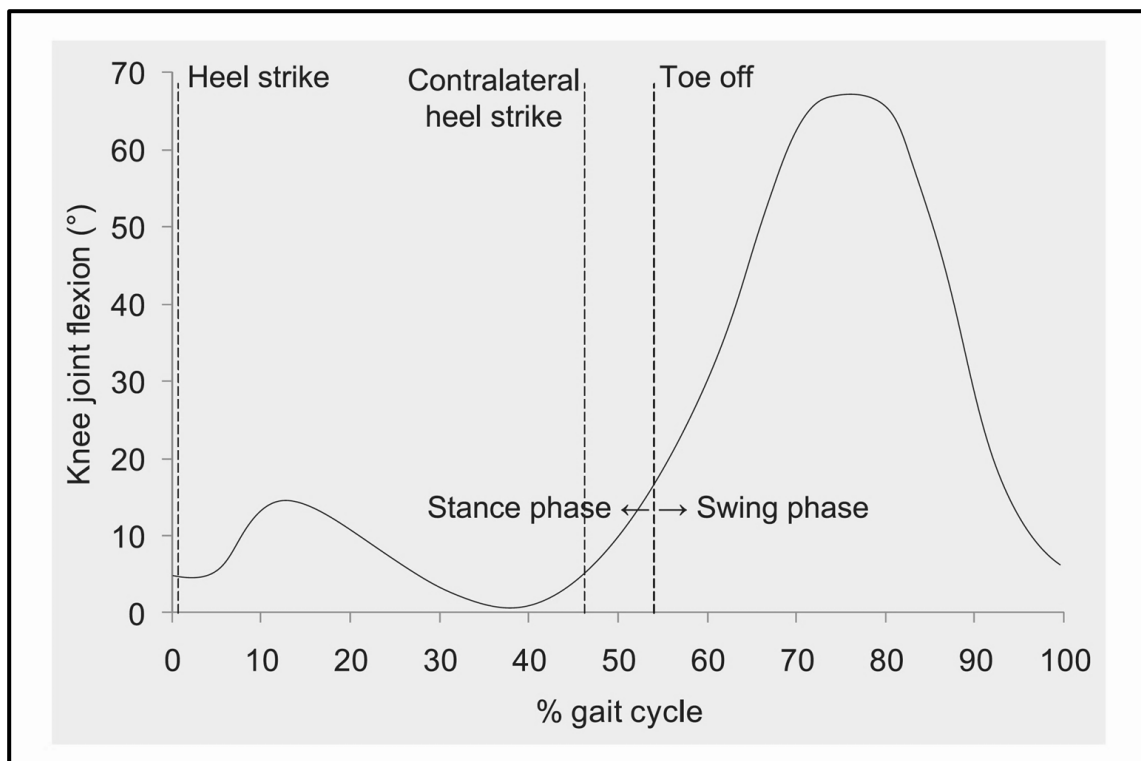


Figure 2.5 Flexion and extension of the knee during the gait cycle [53]

The forces within the tibiofemoral joint (shown as “Knee joint force (x BW)” in the y-axis in Figure 2.6) also vary during the gait cycle. Figure 2.6 is based on data from ISO 14243-3:2014 Implants for surgery where the loading and displacement parameters for wear-testing of total knee joint prostheses are described. This is shown for an individual weighing 750N.

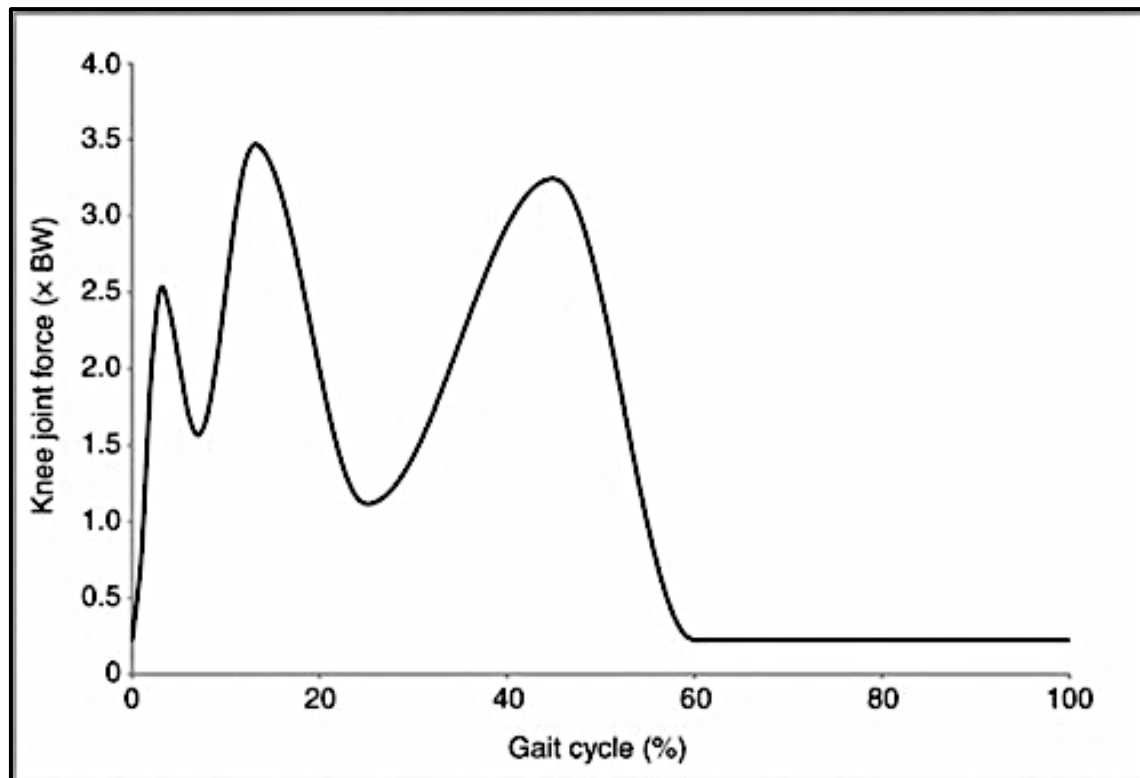


Figure 2.6 Typical knee joint contact force, as a multiple of body weight (BW) during a gait cycle [54]

### 2.1.3 Osteoarthritis

Arthritis is the term used to describe over two hundred different inflammatory and non-inflammatory musculoskeletal conditions. Osteoarthritis (OA) is the most common type of arthritis and is reported to affect nearly eight million people in the United Kingdom [55-57]. Osteoarthritis of the knee is the indication for 98% of all primary knee replacement procedures in England, Wales, Northern Ireland and the Isle of Man [1] and for 97.6% of all the primary TKRs recorded in the Australian Orthopaedic Association Joint Registry Record (AOAJRR) [58]. It is estimated that

within the UK, 4.71 million people have osteoarthritis of the knee and over 1.37 million people are affected by the most severe form of the condition which indicates knee replacement surgery [55].

Osteoarthritis may be defined clinically, pathologically and radiographically [56] and osteoarthritis of the knee joint can affect both medial and lateral sides of the tibiofemoral joint as well as the patellofemoral joint.

Clinically, osteoarthritis can be described by the following statement from the 2017 Joint Commissioning Guide from the British Orthopaedic Association and the Royal College of Surgeons: “Osteoarthritis...describes a clinical syndrome of joint damage resulting in pain accompanied by varying degrees of functional limitation and reduced quality of life” [59]. There are many patient-reported scoring systems used in the clinical assessment and definition of osteoarthritis. The WOMAC (Western Ontario and McMaster Universities Osteoarthritis Index) system and the Oxford Knee Scoring system are probably the most widely used and show the best correlation with radiological assessments and findings from investigatory arthroscopy [60].

The National Institute for Health and Care Excellence (NICE) “Clinical Guideline for Osteoarthritis: Care and Management” [57] characterises osteoarthritis pathologically as a “localised loss of cartilage, remodelling of adjacent bone and associated inflammation”. This may be more simply described as the processes of inflammation and repair following trauma to the joint. While osteoarthritis is closely associated with age, it is not caused by aging directly or simply “wear and tear” of the joint as was previously thought. It is now understood that osteoarthritis is the result of the complex interactions of multiple factors [61]. These include but are not limited to, joint integrity, genetics, mechanical forces at the joint and the biological process of inflammation and tissue repair. Figure 2.7 shows a simple diagrammatical representation of a healthy joint and the changes resulting from osteoarthritis.

In the knee joint, meniscal injury or joint malalignment often precede the onset of osteoarthritis. If in the case of injury, the trauma is severe or repetitive and / or the ability to repair the trauma is compromised, eventually symptomatic osteoarthritis is presented [57, 62]. It is identified pathologically by articular cartilage damage, bony

osteophyte formation, sclerosis of the subchondral bone and in more severe cases subchondral cysts may form [63].

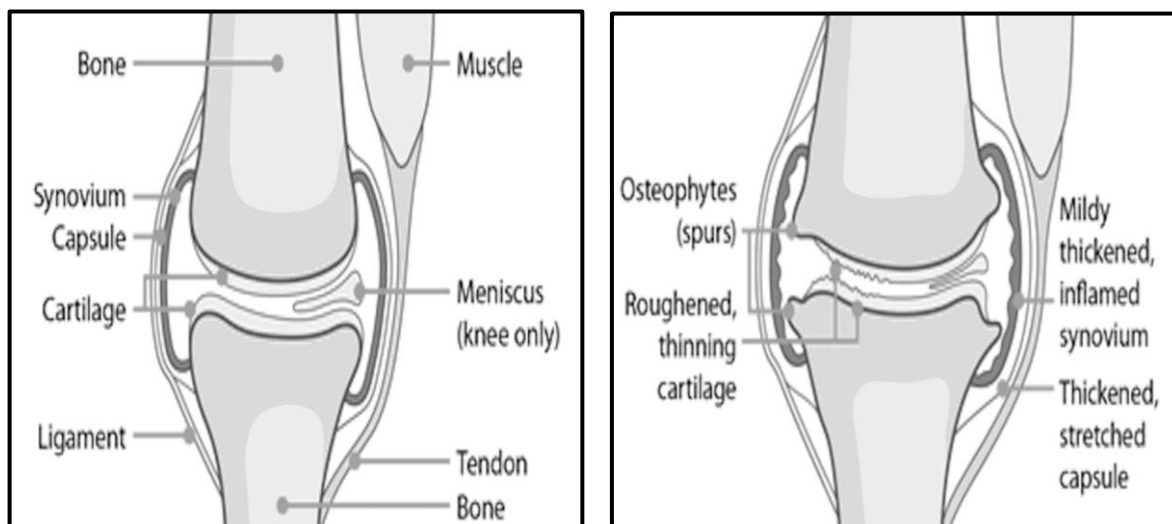


Figure 2.7 Schematic of a normal joint (left) and a joint with osteoarthritis (right) [55]

Radiologically, osteoarthritis of the knee is graded using a variety of systems. Of these systems the International Knee Documentation Committee (IKDC) system and the Ahlback system are reported to have the best interobserver precision and correlation to knee arthroscopy investigations [64]. Although the Kellgren and Lawrence Grading System is also very frequently used. Figure 2.8 (A) and (B) and Figure 2.9 (A) and (B) show four radiographs of knee joints with osteoarthritis with Kellgren and Lawrence grades one through to four [63]. Figure 2.8 (A) shows the AP radiograph of a left knee with mild OA which is a Kellgren and Lawrence Grade 1. The arrow indicates doubtful joint space narrowing and possible osteophytic lipping. Figure 2.8 (B) shows the AP radiograph of a left knee with moderate OA which is a Kellgren and Lawrence Grade 2. The arrow indicates definite osteophytes and possible joint space narrowing [63]. Figure 2.9 (A) shows the AP radiograph of a left knee with moderate to severe OA which is Kellgren and Lawrence Grade 3. The arrows indicate multiple osteophytes, definite joint space narrowing, sclerosis, and possible bony deformity. Figure 2.9 (B) shows the AP radiograph of a left knee with severe OA which is Kellgren and Lawrence Grade 4, showing large osteophytes



(downward arrow at right), marked joint space narrowing (upward arrow at left), severe bone sclerosis (asterisk), and definite bony deformity in medial tibial plateau [63].

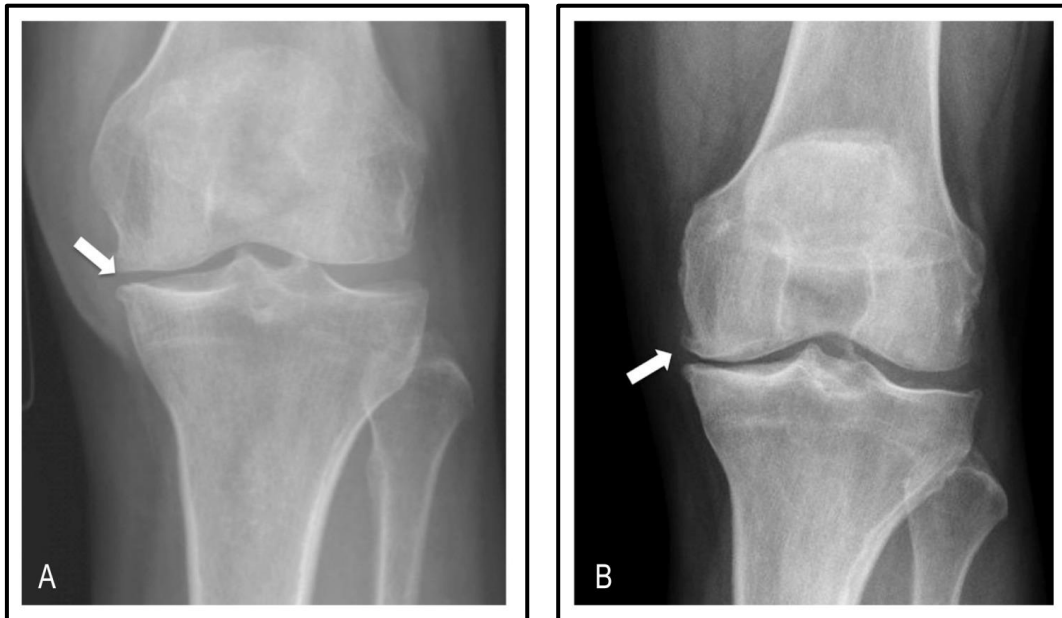


Figure 2.8 A: Mild OA Grade 1 B: Moderate OA Grade2 [63].

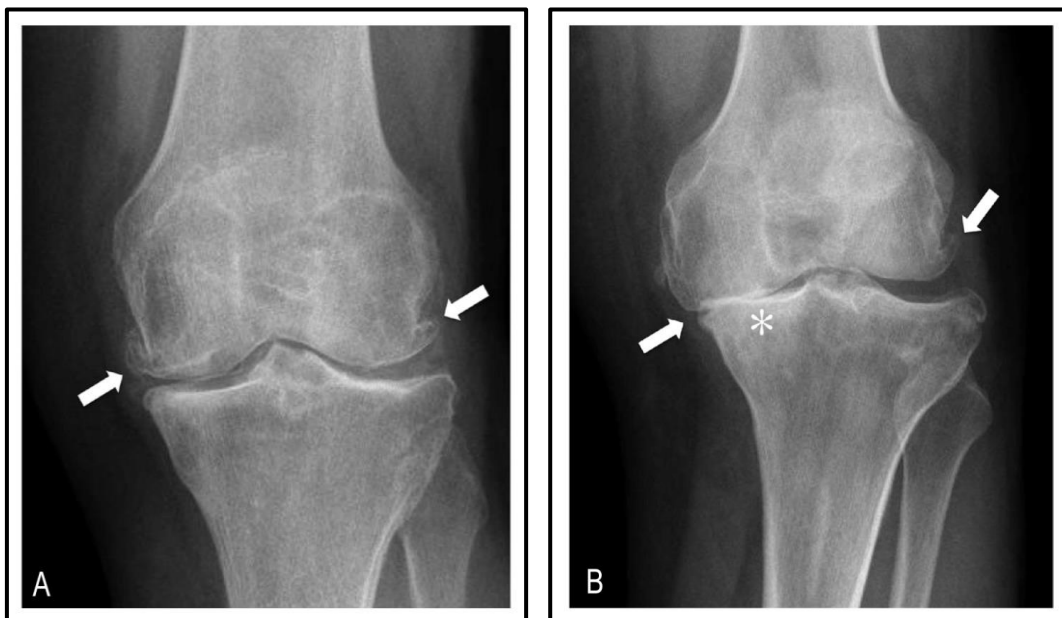


Figure 2.9 A: Moderate to severe OA Grade 3 B Severe OA Grade 4 [63].

The risk factors associated with knee osteoarthritis can be considered as non-modifiable and modifiable. The non-modifiable risk factors include genetic and congenital factors as well as gender. Women have a greater prevalence than men towards osteoarthritis and while the reasons are not entirely clear, research suggests that this is due to hormonal differences influencing the inflammation and repair pathways and anatomical differences resulting in different joint biomechanics [63, 65-67]. Of the modifiable risk factors, obesity is the main contributing factor as increased body weight increases the loading of the joint [68].

## **2.2 Tribology and Surface Topography**

The word “tribology” comes from the Greek word “*tribos*” which means rubbing or attrition. The Oxford English Dictionary defines tribology as “the branch of science and technology concerned with interacting surfaces in relative motion and with associated matters (as friction, wear, lubrication, and the design of bearings)” [69]. The term “tribology” was first used in the 1966 “Jost Report” which was presented to the United Kingdom Parliament Ministry for Science and Education by a steering group chaired by Dr Peter Jost [70]. However, Leonard DaVinci’s work on friction and ball bearings in the 15<sup>th</sup> Century may be considered the first recorded study of tribology [71]. Tribology has applications within all aspects of engineering where there are surfaces that move against each other. This includes anything from transport and heavy engineering to medical engineering and bioengineering. Biotribology specifically, is concerned with the tribology of biological systems and involves the study of natural joints and artificial joint replacements.

Friction in a basic description is the resistance to motion experienced when one solid body moves against another. Whenever two solid surfaces are in moving contact, wear, or damage, to one or both surfaces will occur. Wear is defined by the British Standard ISO 14243 as “material loss... due to combine movement and loading” [72]. Wear may be in the loss of material of either surface, or the transfer of material between the surfaces, or in the change in the topography of the surface. One of the most effective means of reducing friction and wear is through lubrication. Hence it can be seen that the study of friction, wear, lubrication and surface topography are

intrinsically linked. The tribological behaviour of interfaces is dependent on the surface topography, surface material, shape and operating environment [70]. More detailed discussions of the topics of surface topography, friction, wear and lubrication are provided in the following subsections of this chapter.

### **2.2.1 *Surface Topography***

All solid surfaces contain irregularities and deviations from the ideal required geometrical form on some scale. No machined or polished engineered component can be produced that is a molecularly flat surface. On the finest scale, the surface irregularities are at the level of the individual atoms and molecules that form the surface. [70].

When discussing surface topography differentiation needs to be made between surface roughness or texture, which includes micro- and nanoscale irregularities, and other deviations from the nominal surface which include form error and waviness. Form error is a measure of the deviation of the shape of the surface from its intended ideal (for example, a plane, sphere or cylinder) on a macroscopic level. Waviness is a periodic surface undulation observed on a scale between form error and surface roughness [70]. Lower frequencies refer to primary form, medium frequencies refer to waviness and higher frequencies refer to roughness [73]. The tribological function of an engineering component is related to its surface topography [74].

### **2.2.2 *Surface Roughness Parameters***

The following definitions and statistical equations for surface roughness parameters have been taken from BS ISO 25178-2:2012 which is the latest published version however it is currently under review by the standard committee [75]. When describing a linear profile, the prefix *R* is used and when describing an areal profile, the prefix *S* is used. For the purposes of this thesis the areal parameters, *S*, shall be defined here. No surface roughness parameter alone can define the topography of a surface. It is through the consideration of the parameters in combination that an assessment of the texture can be made [74].

The **Mean Surface Roughness,  $S_a$** , of a surface is the arithmetic mean height of a profile above the centre line of over an area,  $A$ . See Equation 1 and Figure 2.10. In the figures the linear profile prefix,  $R$ , is shown as it is simpler to illustrate graphically than the areal profile  $S$ .  $R_a$  is the linear mean surface roughness.

$$S_a = \frac{1}{A} \iint_A |z(x, y)| dx dy \quad \text{Equation 1 [76]}$$

The **Root Mean Square Surface Roughness,  $S_q$** , of a surface is the root mean square value over the area,  $A$ . See Equation 2 and Figure 2.10. In Figure 2.10,  $R_q$  is the linear root mean square surface roughness.

$$S_q = \sqrt{\frac{1}{A} \iint_A |z(x, y)|^2 dx dy} \quad \text{Equation 2 [76]}$$

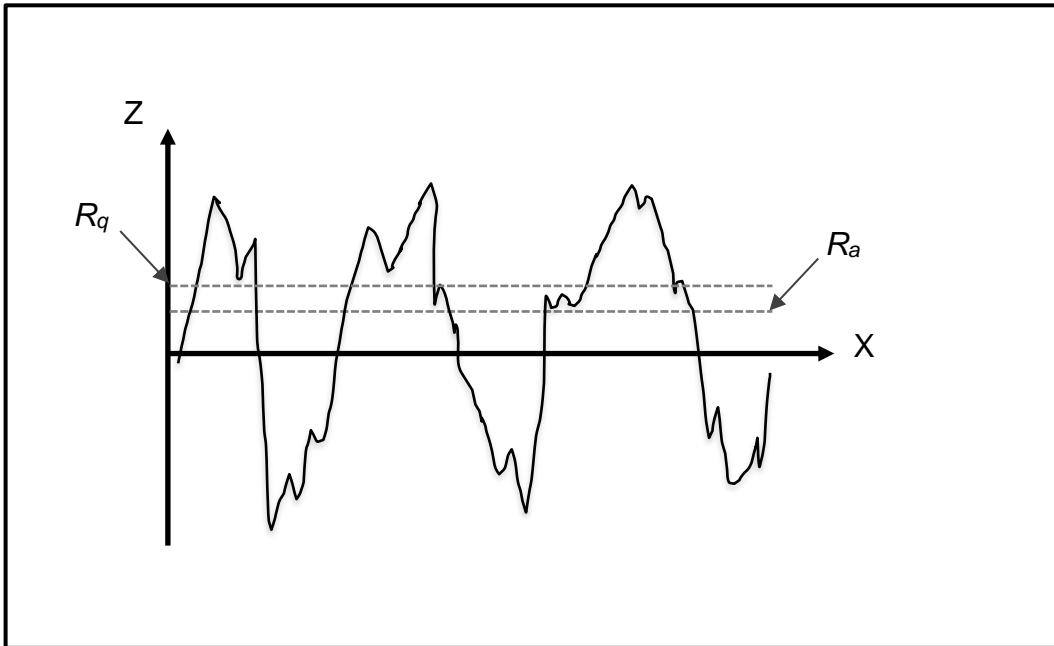


Figure 2.10 Representation of  $R_a$  and  $R_q$ :  $S_a$  and  $S_q$  are the areal extensions of these parameters respectively

The **Skewness,  $S_{sk}$** , of a surface is a measure of symmetry of the profile about the mean line over an area,  $A$ . A positively skewed surface has a predominance of peaks

and a negatively skewed surface has more valleys. A normally distributed profile has a skewness value of zero. See Equation 3 and Figure 2.11. Figure 2.11 shows two profiles one with a negative skewness and one with a positive skewness. Although not depicted graphically it can be inferred that a profile with no skewness falls within a normal distribution curve and is neither negative nor positive.

$$S_{sk} = \frac{1}{S_q^3} \left( \frac{1}{A} \iint_A z^3(x, y) dx dy \right) \quad \text{Equation 3 [76]}$$

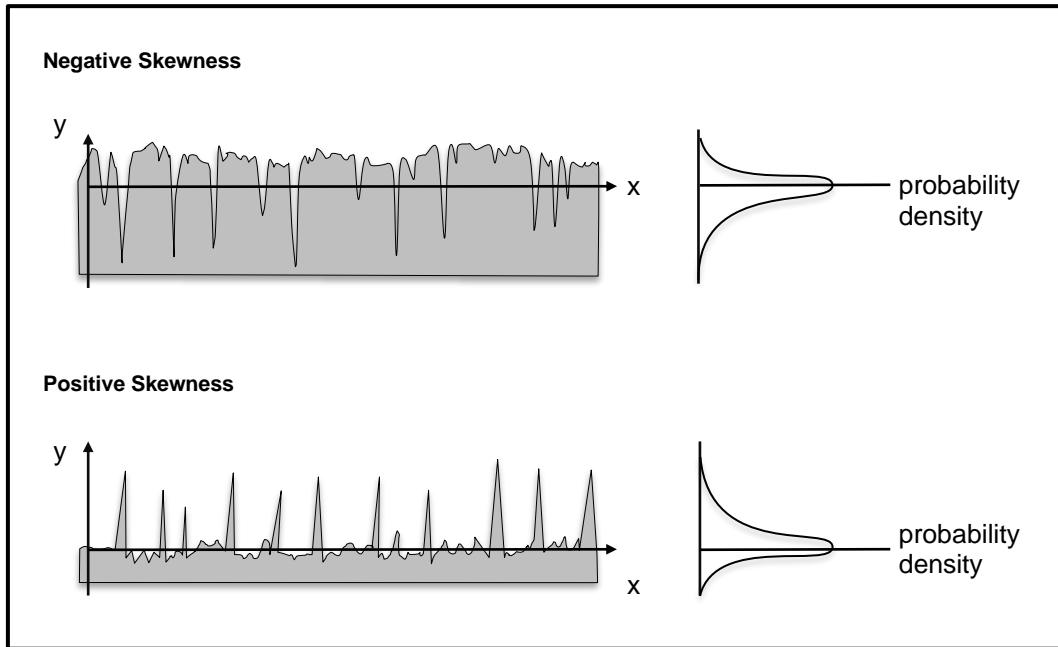


Figure 2.11 Representation of skewness

**Kurtosis,  $S_{ku}$ ,** like skewness, is a measure of the shape of the profile about the mean line over an area, A. However, Kurtosis not only describes how evenly spaced the profile peaks are but also how spiked those peaks are. A profile with a normal Gaussian height distribution will have a kurtosis value of 3. A profile with a kurtosis value of less than 3 represents a rounded, flat surface with less peaks and valleys and a profile with a kurtosis value of greater than 3 represents a surface with more, sharper spiked peaks and valleys. See Equation 4 and Figure 2.12. Figure 2.12 shows two profiles one with a Kurtosis value of greater than 3 and one with a

Kurtosis value of less than 3. Although not depicted graphically a profile with a normal Gaussian height distribution will have a kurtosis value of 3 and would be depicted as between the two profiles shown in Figure 2.12.

$$S_{ku} = \frac{1}{S_q^4} \left( \frac{1}{A} \iint_A z^4(x, y) dx dy \right) \quad \text{Equation 4 [76]}$$

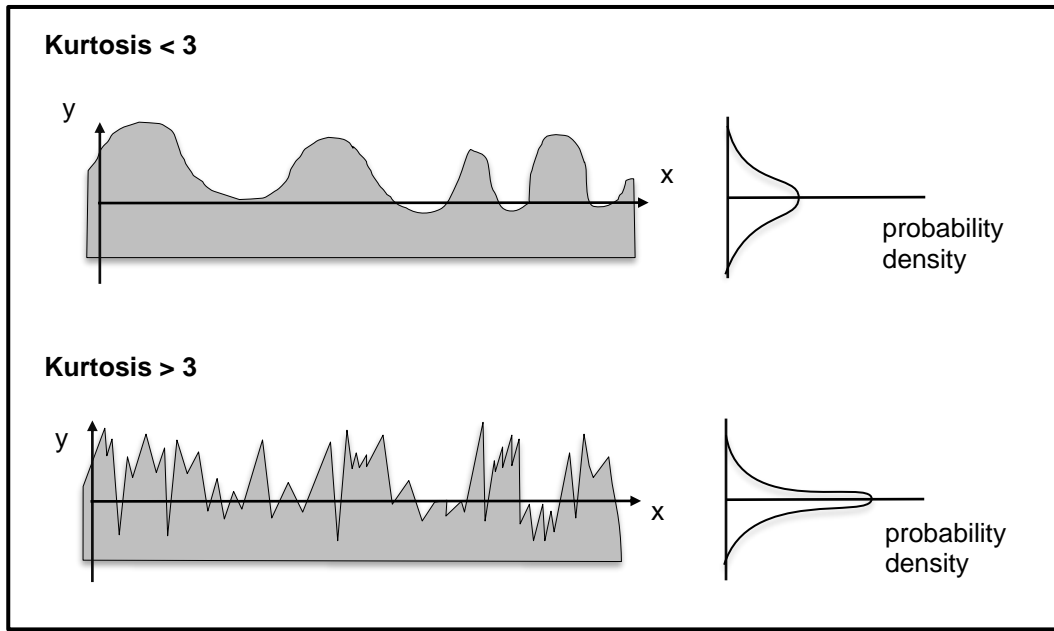


Figure 2.12 Representation of kurtosis

Both skewness and kurtosis are less mathematically stable than the other surface roughness parameters as they use higher order differentiations in defining equations (see Equations 3 and 4). This can lead to errors in the calculation of the parameters [74].

The **Maximum Peak Height,  $S_p$** , of a surface is the largest peak height value within the defined area. The **Maximum Valley Depth,  $S_v$** , of a surface is the largest valley depth within the defined area. The 10-point height is defined as the average distance between the five highest peaks and the five deepest valleys within the evaluation area measured. The peak to valley height,  $S_z$ , is the sum of the maximum peak height value and the maximum valley depth within a defined area. (It is important to note that in the yet un-published draft amendments to BS ISO 25178-2,  $S_z$  is defined

as the 10-point height average and the Peak to Valley height is given the nomenclature “PV”. This is the nomenclature that shall be used throughout this thesis.)

### **2.2.3 Surface Roughness Measurement**

British Standard BS ISO 25178-6:2010 classifies methods for measuring surface texture into line-profiling and areal-topography methods which produce linear topographic profiles ( $z(x)$ ) and areal topographic images ( $z(x, y)$ ) respectively [77]. Within line-profiling and areal-topography, the methodologies can further be classified as contacting or non-contacting methods.

Contact stylus scanning is one type of profilometry technique where the coordinates of points on a surface are measured by a fine stylus which is dragged smoothly and steadily across the surface [78]. Figure 2.13 shows a diagrammatical representation of a contact stylus profilometer. The position of the stylus in the plane of the surface is recorded and the vertical position of the stylus is monitored via a transducer.

Within contact stylus profilometry, there are limitations associated with damage to the sample from dragging a stylus across the surface and there are limitations resulting from the finite dimensions of the stylus [79]. The finite stylus tip radius may prevent the tip from being able to take measurements in deep and narrow profiles and there will always be an element of smoothing that occurs. In addition, although measurements along multiple lines can be taken to extrapolate areal surface roughness parameters it still remains that the roughness parameters calculated from single line traces would vary depending on the direction and orientation of the sweep. Contact stylus scanning can also be a laborious and time-consuming process.

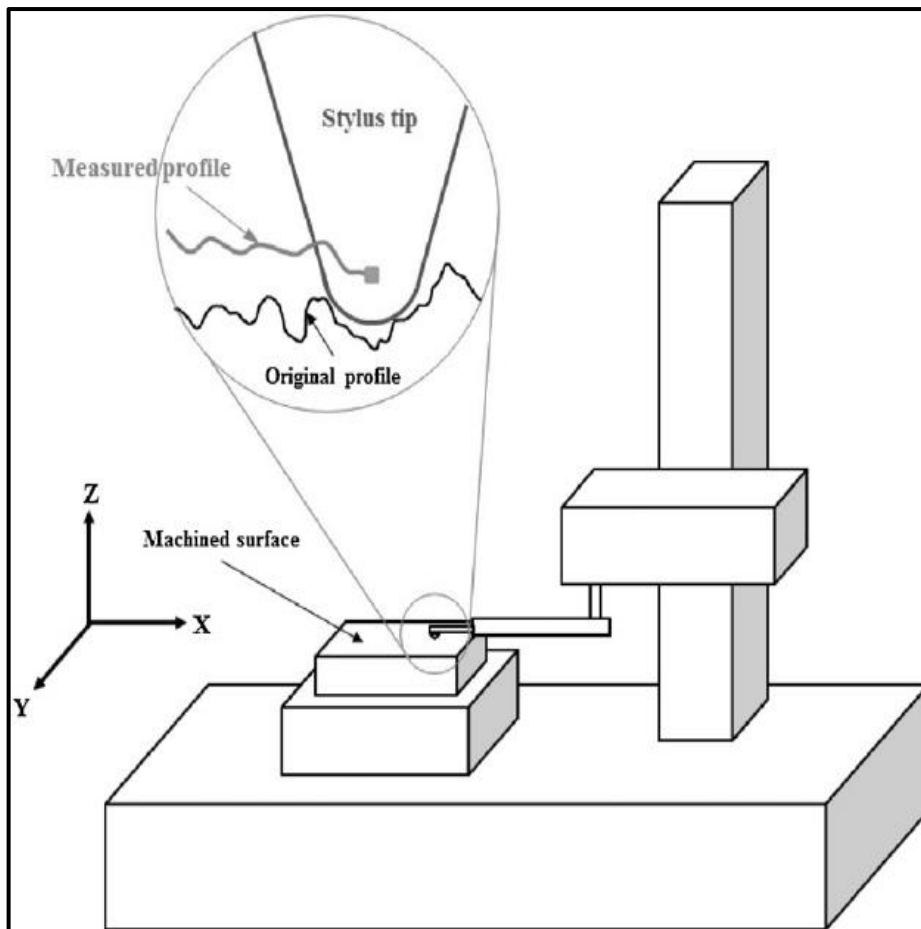


Figure 2.13 A stylus-type profilometer [80]

Optical profilometry is a microscope-based technique which uses interferometry to provide a non-contacting method of acquiring three-dimensional areal surface roughness measurements. Coherence scanning interferometry (CSI) is a form of optical profilometry where the modulation of interference fringes generated following amplitude division and recombination of a common light source reflected from a sample surface and a reference surface is measured [79, 81]. Figure 2.14 shows a diagrammatic illustration of the method of operation of a CSI instrument.

Figure 2.15 shows a diagram of a NewView 5000 (ZYGO, Middlefield, Connecticut, USA) non-contacting white light interferometric profilometer which was used for the surface roughness measurements taken for this thesis. The main controls and details are labelled.



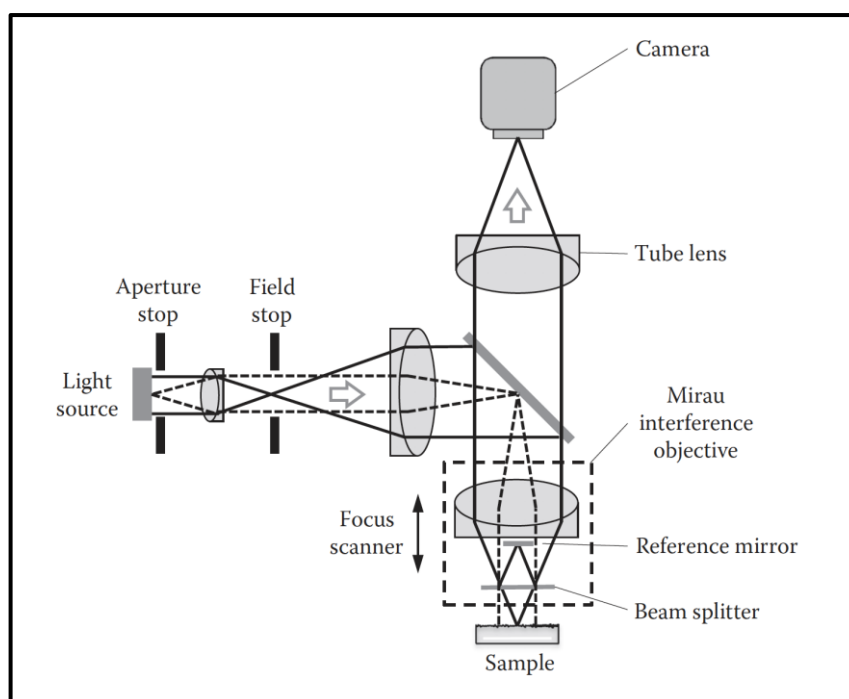


Figure 2.14 CSI instrument operation [79]

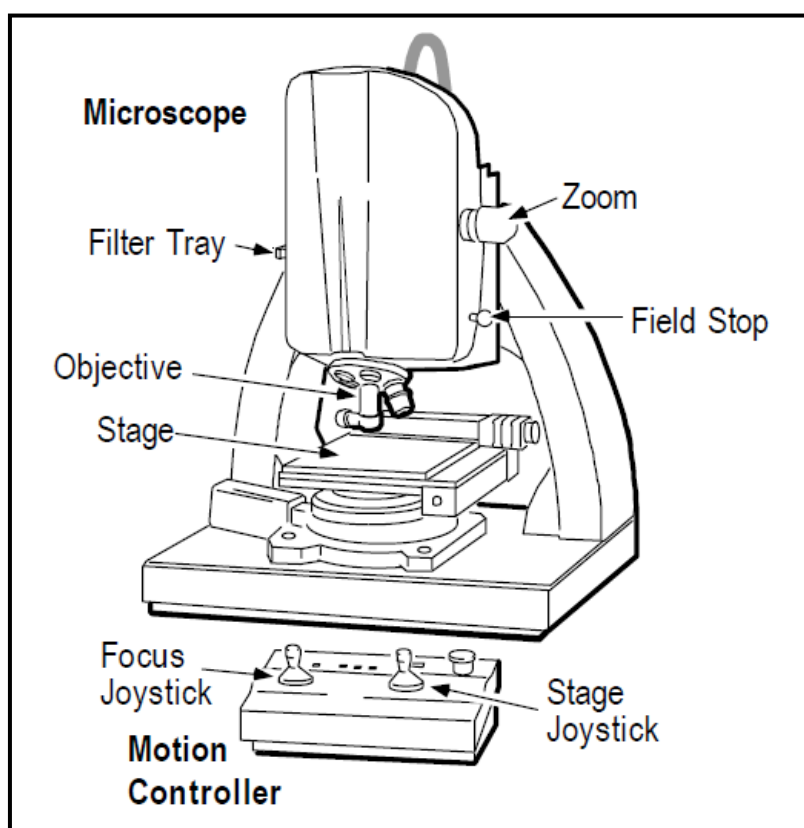


Figure 2.15 Schematic of a Zygo NewView 5000 profilometer [82]

Within white light CSI, a monochromatic beam of white light is split into two. One beam is reflected to an acquisition camera from the sample surface and the other beam is reflected to the acquisition camera via a reference surface. The reference surface is a mirror that effects a  $180^\circ$  phase change of the light source beam. The reference mirror is labelled in Figure 2.14. The modulation of the two beams of light enables the calculation of the surface topographical differences between the two surfaces [70]. When the two beams are in phase the result is constructive interference and a bright fringe is observed. When the beams are out of phase there is destructive interference and a dark fringe is observed. The nominal characteristic of non-contact CSI instruments are detailed in BS ISO 25178-604:2013 [81]. Figure 2.16 illustrates the creation of bright and dark interference fringes.

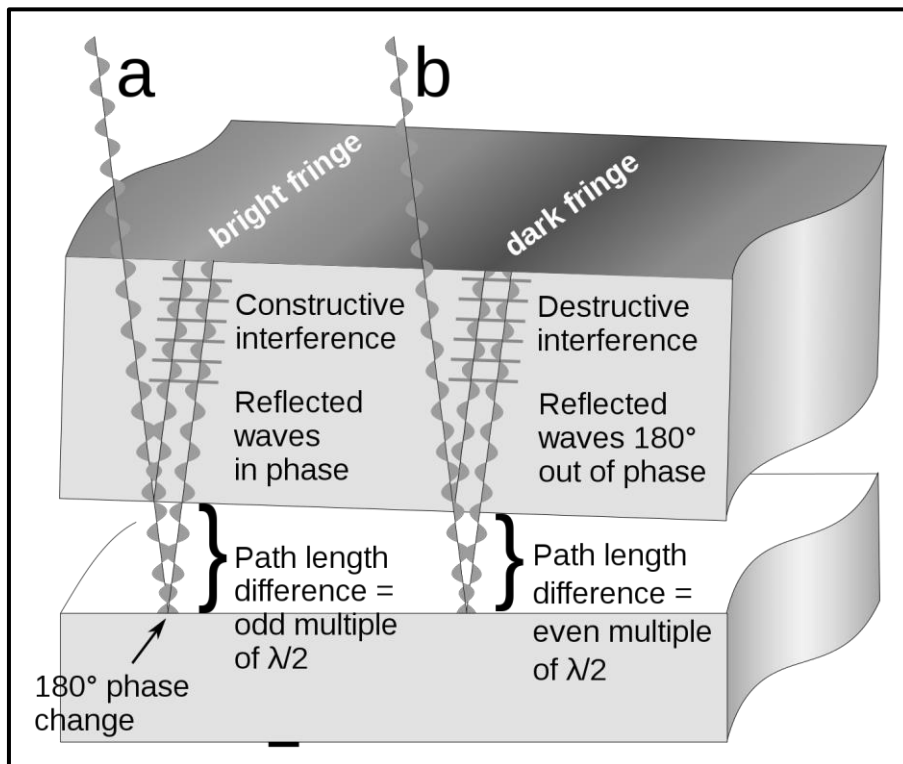


Figure 2.16 The creation of (a) bright interference fringes and (b) dark Interference fringes [79]

There are limitations associated with optical methods of profilometry that are more complex to define and consider than the limitations associated with contact scanning interferometry [83]. Gao et al wrote about errors and performance of commercially

available white light CSI machines [84]. The work concluded that most, if not all, CSI instruments report errors when used to measure surfaces with discontinuities and when sub-wavelength accuracy is required. Errors identified by Gao et al [84] include an edge or “bat wing” effect where the instrument over reports the peak and trough associated with a step discontinuity in the surface at the edge of a scratch for example. Another error may also be introduced by a full wavelength shift recorded by the instrument that is not actually present and these are referred to as “ghost steps”. There are also errors associated with the material optical properties of the sample as different materials will have a different phase change on reflection when compared with the reference surface. A further error may be introduced by the measurement of slope of the sample and the multiple scattering of the incident wave. An instrument’s ability to measure sloped surfaces will be determined by its numerical aperture and ability to capture the scattered sample data [83, 84]. CSI instruments are also limited by the physical positioning of the sample, specifically the tilt and curvature of the sample [81, 85]. Two separate studies evaluated errors in CSI introduced due to the measurement of concave and convex surfaces [85, 86]. Both recommended careful positioning of such samples can assist in reducing errors. This is a very important consideration to be aware of during the surface topographical analysis conducted throughout this thesis.

When using an optical profilometer, the measurement parameters must be appropriately selected. The strength of the objective lens and the magnification of the optical zoom will determine the area of view. The user can also select parameters such as the minimum modulation percentage and the scan length that are specific to the measurement taken. The minimum modulation percentage is the minimum percentage change of wavelength that the user determines that the software should consider as true roughness and not noise. The value is linked to the reflectivity and the roughness of the sample. [87]. The scan length determines the profilometer’s ability to measure surfaces with deep valleys and high peaks. A longer scan length can capture more data, however can also be more time consuming [87].

As well as careful positioning and the selection of the appropriate measurement parameters for the properties of the sample, filters must be used in the analysis of

the data to ensure accurate surface texture characterisation is achieved [74]. Guidance on the appropriate filters can be found within ISO 25178:2, which as noted above is currently under review by the standards committee [75] and in ISO 16610:61 [88]. A surface can be described as the superposition of geometric structures with different scales. When considering curved surfaces, a form filter is used to remove the nominal curvature form and the texture, or roughness can be defined [74, 83, 85, 86]. The application of filters to remove errors such as the edge effect errors and the “ghost step” errors need to be applied with caution as there is a chance of filtering true data [83, 84, 89].

#### **2.2.4 Friction**

The term friction describes the resistance to motion during sliding or rolling that is experienced when one solid body moves tangentially over another with which it is in contact. Hertzian contact theory of elastic deformation describes that when a sphere of elastic material is pressed against a plane under a normal load, contact will occur in a circular radius. Within this circular apparent contact area, the true contact area is the sum of the contact areas of the surface asperities. It is through these asperities that the normal load is distributed and Hertzian elastic deformation applies [70, 90]. If the normal load is increased further, plastic deformation may occur and the number of asperities in contact, and the areas of contact of these asperities will increase. It is the contact of the asperities that influences the frictional force during sliding.

The study of friction dates back to da Vinci in the 1500s and work by Amontons (1699) and Coulomb (1785). Between them, da Vinci, Amontons and Coulomb describe three laws of friction [70, 90]. The first two initially described by da Vinci and then subsequently confirmed by Amontons, state that the friction force is directly proportional to the normal load and that it is independent of the apparent area of loading. This may be shown in Equation 5 where  $F$  is the frictional force in Newtons (N)  $\mu$  is the coefficient of friction, and  $W$  is the applied load in Newtons (N).

$$F = \mu W \quad \text{Equation 5}$$

The third law of friction is said to have been introduced by Coulomb and suggests that the frictional force is independent of the sliding velocity. The first two laws of friction are generally obeyed by most metals for dry, or unlubricated, sliding however polymers do not obey the laws [70, 90].

Focusing specifically on sliding friction, a model suggested by Bowden and Taylor makes the assumption that the friction force is made up from an adhesive friction force,  $F_{adh}$ , and a deformational friction force,  $F_{def}$  (see Equation 6). The adhesive friction force is from adhesive interfacial bonds across asperity junctions which occur when two surfaces come together. The deformation friction force is the force required to plough the harder asperities through the softer material. [70].

$$F = F_{adh} + F_{def} \quad \text{Equation 6}$$

A coefficient of friction is a dimensionless value that relates the resulting frictional force and the normal applied load between two bodies in contact but these can vary depending on the environmental conditions. Coefficients of friction for metals self-mated in air typically range between 0.4 and 2 [70]. Ceramics have a lower adhesive coefficient of friction which is due to the difference in the interatomic forces, these being ionic or covalent in ceramics as opposed to metallic bonding. For ceramic against ceramic coefficients of friction are typically between 0.25 – 0.8, while the values for “engineered ceramics” which included examples such as silicon nitride ( $\text{Si}_3\text{N}_4$ ), alumina ( $\text{Al}_2\text{O}_3$ ) and zirconia ( $\text{ZrO}_2$ ) are strongly influenced by environmental factors and can vary widely [70].

Polymers do not obey the laws of friction. The reason being that the contact between polymers and between polymers and metals are predominantly elastic and most polymers are viscoelastic. Coefficients of friction between polymers against polymers range between 0.1 to 0.5 however, the coefficient of friction can vary widely with normal load, sliding speed and temperature that quoting specific values is not appropriate [70]. Coefficients of friction for mixed material combinations can vary widely and have a vast range also being influenced by environmental factors.

Understanding of the friction between two moving bodies can be related to the friction between the joint surfaces within the natural knee joint and also between the components of a knee replacement prosthesis. The friction between the surfaces of knee prosthesis components *in vivo*, specifically the femoral and PE bearing components has an influence on the adhesive and abrasive wear and the generation of PE wear debris particles.

### **2.2.5 Lubrication**

An effective way of reducing friction and wear in a system is via the introduction of a lubricant. A lubricant can provide a layer of material between the sliding surfaces that has a lower shear strength than the surfaces and can therefore act to lower the coefficient of friction. Depending on the system, the lubricant may not prevent asperity contact completely but just reduce it and it may also reduce the adhesive forces between the surfaces [70, 90]. Lubrication can be provided either through fluid or a solid lubricant. Within healthy, natural knee joints synovial fluid is generally present as a lubricant. After a knee joint replacement, a pseudo-periprosthetic synovial fluid is often found which is similar to that in patients with osteoarthritis [91].

Hydrodynamic (HD) lubrication, is a form of fluid-film lubrication and is also called full fluid-film lubrication. In hydrodynamic lubrication the two surfaces are separated by a fluid film which is thicker than the asperity height of the sum of both surfaces ensuring asperity contact does not occur [70, 90]. As the two solid surfaces slide against each other, the hydrodynamic pressure in the fluid film increases and the fluid film bears the normal load. The elastic deformation of the two surfaces can be assumed to be negligible and so the two surfaces can be approximated to rigid bodies. For hydrodynamic lubrication, the two surfaces must be conformal and must be converging to enable the viscous flow of the fluid film and the generation of hydrodynamic pressure. The relationship between the varying hydrodynamic pressure in a lubricant and the bearing geometry and the independent variables of applied load, sliding speed and lubricant viscosity was first defined by Reynolds in the late 1800s and was the first definition of full fluid-film lubrication [92].

ElastoHydrodynamic lubrication (EHL) is another form of fluid-film lubrication and occurs when the pressure in the fluid film increases and/or the fluid film becomes too thin and the fluid film can no longer bear normal load and elastic deformation of the two surfaces occurs [70, 90, 92]. However, despite elastic deformation of the surfaces occurring there is still no surface contact [70]. If the normal load increases, or the relative speed of sliding motion between the two surfaces decreases, or the viscosity of the lubricant decreases, the hydrodynamic forces in the lubricant may become insufficient to maintain even a thin EHL fluid film. This is when boundary lubrication can occur. In boundary lubrication, the surfaces become so close that they are only separated by molecular films of lubricant and asperity contact with adhesion and deformation due to junction growth can occur [70, 90]. The transition between the two distinct lubrication regimes of boundary and fluid-film lubrication is not a distinct cut-off but a gradual process. Moving from boundary through to elastohydrodynamic and hydrodynamic lubrication it can be that two lubrication mechanisms function at the same time. This is called “mixed lubrication” [70, 90, 92].

Within knee replacement prostheses functioning *in vivo* the lubrication regime between the femoral condyles and the PE bearing is usually considered to be boundary lubrication. This leads to contact between the components and wear of the components and generation of PE wear debris particles.

#### **2.2.6 Wear**

Wear is defined by the British Standard ISO 14243 as “material loss... due to combined movement and loading” [72]. Wear may be in the loss of material of either surface, or the transfer of material between the surfaces, or in the change in the topography of the surface.

There are five defined mechanisms of wear; adhesive, abrasive, fatigue, erosion and corrosive. In real systems such as a knee replacement prosthesis multiple wear mechanisms may occur at the same time [70, 90].

Adhesive wear is also sometimes called sliding wear and occurs when two solid surfaces slide against each other. This may be in the presence of a lubricant or not. Adhesion occurs at the asperity contacts of the interface and as the two surfaces move against each other these contacts are broken. This can result in a fragment attaching from one surface to the other by means of chemical bonding or it can result in loose wear particles being formed. These loose wear particles may lead to third body abrasive wear. This can happen between articulation of the femoral component and the PE bearing component of a knee replacement prosthesis.

A simple theory of adhesive or sliding wear can be described by the Archard wear equation (Equation 15) which was derived by Archard in 1953 based on original work by Holm and discussed by Hutchings and Bhushan [70, 90]. The derivation makes two main assumptions that the contact between two surfaces will occur where asperities touch and that the true area of contact will be equal to the sum of the individual asperity contact areas. This results in Equation 7, the Archard Wear Equation, where  $Q$  is the wear volume,  $W$  is the normal load,  $L$  is the distance slid,  $H$  is the indentation hardness of the softer contacting surface and  $K$  is the dimensionless wear coefficient.

$$Q = \frac{KWL}{H} \quad \text{Equation 7 [70].}$$

The Archard Wear Equation has been used to calculate volumetric wear in orthopaedic joint replacement prostheses. The complex geometries of knee replacement prostheses makes for a complicated theoretical calculation.

Abrasive wear involves hard particles being forced or slid against one or both of the surfaces and can involve plastic flow and or brittle fracture [70]. Material is removed or displaced by asperities of the harder surface (two-body abrasive wear) or loose particles (three-body abrasive wear) rolling and sliding between the surfaces. The particle properties of hardness, shape and size will have an influence on these



mechanisms of wear. Figure 2.17 shows a simple illustration of two-body and three-body abrasion.

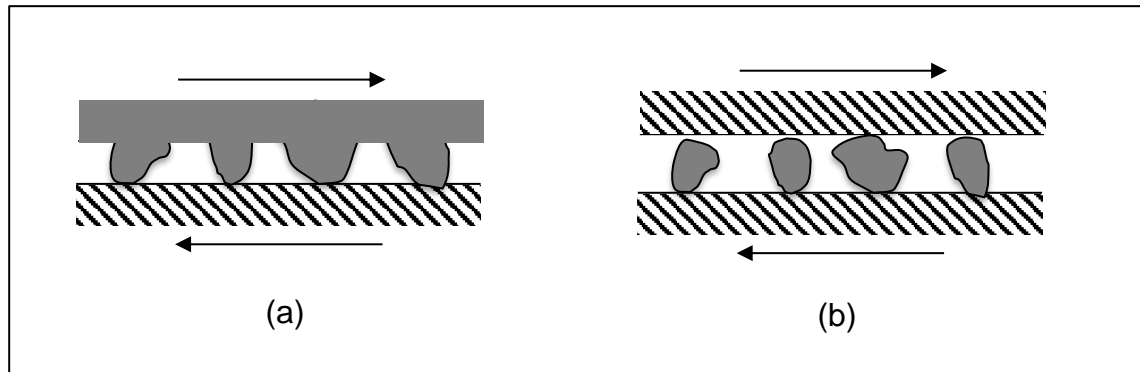


Figure 2.17 (a) Two-body abrasive wear (b) Three-body abrasive wear

Fatigue wear occurs due to surface and subsurface cracking and delamination under repeated cyclic loading (rolling and sliding) and can lead to large pieces of material being lost in one go. Fatigue wear is a sudden failure of the material in contrast to the gradual deterioration of adhesive and abrasive wear [70, 90].

Erosive wear is a form of third-body abrasive wear and occurs due to hard particles flowing over or between two surfaces in a fluid [70, 90]. The hard particle acts much like an asperity of material in abrasive wear, removing material in its path and causing surface deformation.

Corrosive or chemical wear occurs when sliding takes place in a corrosive environment. The chemical products of corrosion are removed during sliding which allows additional corrosion and provides corrosive debris to act as an abrasive third body [70].

Within knee replacement prostheses, wear can occur at any of the surfaces of the prostheses. This includes surfaces that are intended for articulation (for example the femoral condyles and the PE bearing) but also surfaces that are not intended for articulation (for example the backside of the PE bearing and the Tibial tray). Multiple wear mechanism can occur at any of the surfaces.

## **2.3 Knee Arthroplasty**

Arthroplasty is an elective orthopaedic surgical procedure where the articular surface of a joint is replaced or resurfaced with the aim of restoring function and relieving the patient of pain [1]. Joint replacement is the end-stage surgical treatment for painful and debilitating osteoarthritis. Knee arthroplasty or knee joint replacement, refers to the orthopaedic surgical reconstruction of the knee joint using a prosthesis [55]. The word “primary” is used to describe the initial replacement surgery performed. While osteoarthritis is the indication for the overwhelming majority of primary knee replacement surgeries, other conditions such as rheumatoid arthritis, previous trauma, inflammatory arthropathy, avascular necrosis and infections also can necessitate treatment through knee replacement surgery [1, 58]. If failure of the joint replacement system occurs a subsequent surgical procedure is required to replace a failed prosthesis and this is termed a revision procedure [1].

Reports of attempted knee joint replacement date back to as early as the 1890s when an orthopaedic surgeon Gluck, from the Charité Hospital, Berlin described a design of a fixed-hinged knee replacement with ivory components [93]. Ultra-High Molecular Weight Polyethylene (UHMWPE) was first recorded as being used in knee replacements in the late 1960s by a Canadian orthopaedic surgeon Frank Guston who was on a travelling fellowship at Wrightington Hospital, United Kingdom with Sir John Charnley. On his return to Canada, Guston continued to develop prostheses for knee arthroplasty [93].

Due to the complexity of the anatomy of the knee, there are many different designs of historical and contemporary knee replacement prostheses [1, 58]. A Total Knee Replacement (TKR) is when both condyles of the tibiofemoral joint are replaced [94]. If a single condyle is replaced, the term Unicondylar Knee Replacement (UKR) is used (see Figure 2.18). The patella-femoral joint may also be replaced either at the same time or independently of a total knee replacement. In some cases the patella-femoral joint may be removed altogether and not replaced [1].

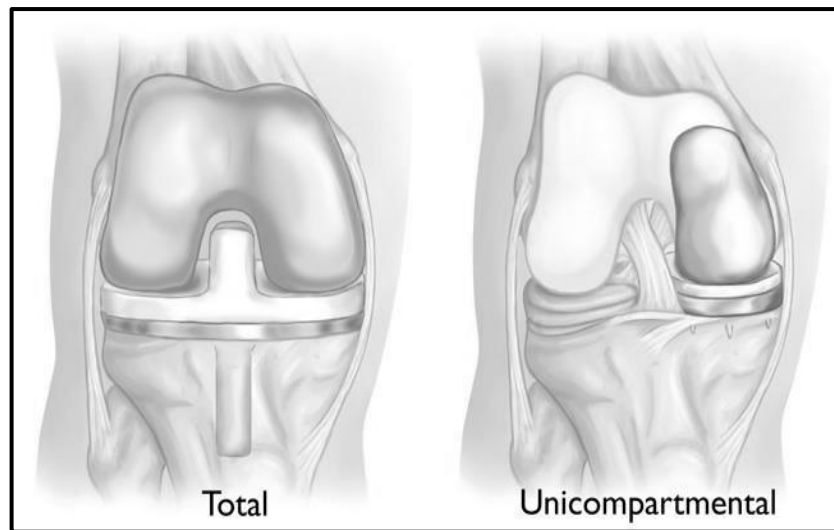


Figure 2.18 Total Knee Replacement and Unicompartmental Knee Replacement [95]

As shown in Figure 2.18, a TKR prostheses consists of a femoral component that resurfaces the medial and lateral femoral condyles and a tibial component. The tibial component may be modular with a metallic tibial tray and a polyethylene (PE) insert, or non-modular with a single all-PE tibial component. In modular tibial components, the PE insert may be mobile, semi-constrained (also known as medial pivot or rotating platform) or fixed into the metallic tibial tray. These definitions are also applicable to UKR prostheses [94]. Figure 2.19 shows different bearings as applied to UKRs.

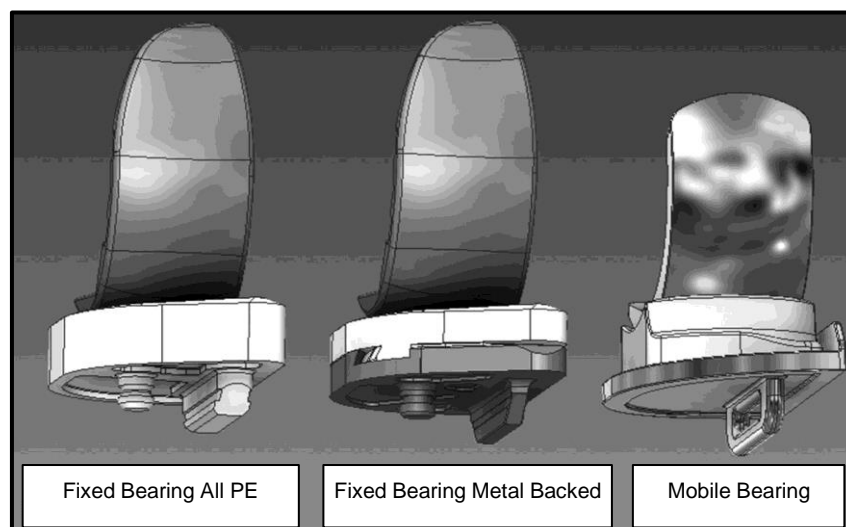


Figure 2.19 Different bearings shown on UKRs [96]

TKRs are designed either to preserve the cruciate ligaments (cruciate retaining, CR) or sacrifice the cruciate ligaments (posterior-stabilised, PS). A PS TKR is designed with a tibial insert and femoral component that provides constraint on the movement of the femoral component to prevent it sliding anteriorly over the tibia or femoral “roll back”. The constraint is typically in the form of a posterior post on the PE component with either a posterior bar or box on the femoral component. [94]. Figure 2.20 shows a CR and a PS TKR which uses a box on the femoral component to provide the restraint. The TKRs shown have a semi-constrained bearing that is neither fully fixed into the tibial tray or fully mobile.

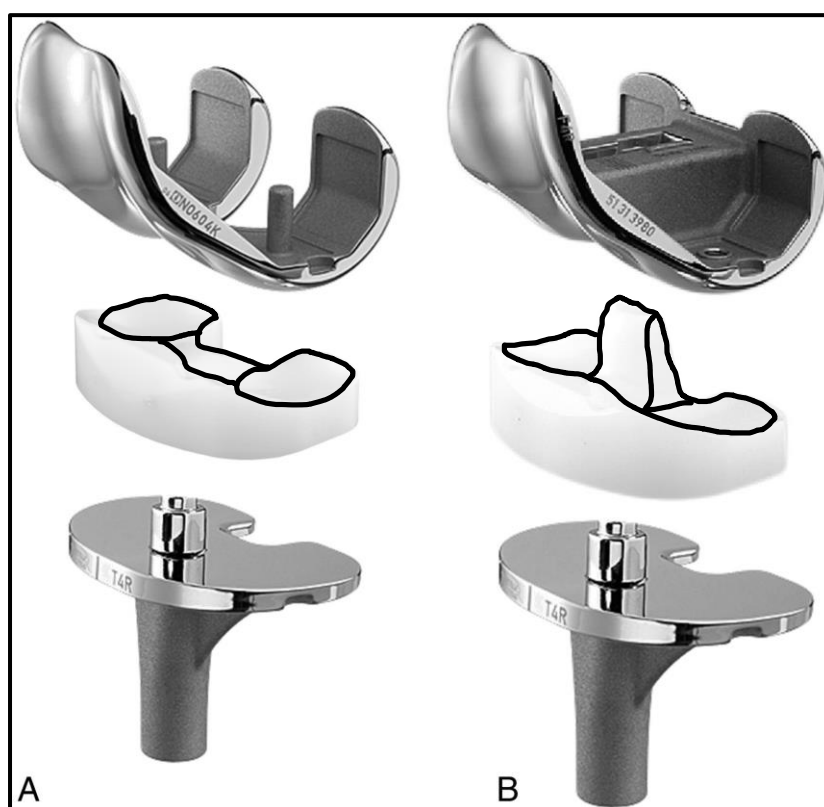


Figure 2.20 A CR and a PS rotating platform TKR [97]

Prostheses may be fixed in position with or without the use of bone cement. Some knee replacement prostheses use a combination where either one of the femoral or tibial components use cement and the other does not. Hybrid fixation is when the tibial component is cemented in place and the femoral component is un-cemented; reverse hybrid is opposite.

### 2.3.1 *Materials in Knee Replacement*

Typically, the femoral components of knee replacement prostheses are manufactured from medical grade cobalt-chromium (Co-28Cr-6Mo) alloy (CoCr). Ceramics and modified ceramic surfaces such as oxidised zirconium (OxZr) are also used for femoral components [98]. Tibial tray base plates are manufactured from either CoCr alloy or a titanium alloy (Ti-6Al-4V). Titanium alloy can also be used for femoral components although it is less common. Table 2.2 shows the material properties of some knee replacement femoral and tibial component materials including the Rockwell Hardness and the Fracture toughness.

Table 2.2 Mechanical Properties of Materials used in Femoral Components of Knee Replacements [99, 100]

Material	Rockwell Hardness number, A ( <i>dimensionless</i> )	Fracture toughness (MPa/m <sup>1/2</sup> )
Co-28Cr-6Mo	18-25	75
OxZr (monoclinic ZrO <sub>2</sub> )	35-40	2.6
OxZr substrate (Zr-2.5Nb)	10-15	15-75
Ti-6Al-4V	15-20	54-91

CoCr alloy is used in knee prostheses due to its biocompatibility, corrosion resistance, hardness and fracture toughness as well as a long history of wear simulation testing against PE. Titanium alloy is also biocompatible, corrosion resistant with good hardness and fracture toughness properties. Titanium alloys have a lower density compared to other metals used in knee prostheses and have a more elastic nature. These properties make titanium alloy more often selected as a tibial tray material to attempt to prevent stress shielding of the tibia and reduce the risk of implant failure due to bone resorption and atrophy.

The manufacture of the metallic components involves casting, machining and surface finishing processes. Many of these processes are proprietary and not in the public domain however limited information can be found in the manufacturers' product brochures [101-105]. BS ISO standard 7207-2 [106] describes surface finish requirements for articulating surfaces of metallic or ceramic knee replacement components: "When measured in accordance with ISO 4288, all articulating surfaces of a metallic or ceramic femoral component shall all be measured across the full articulating surface at locations in an approximate square grid of locations no more than 10mm apart. The component shall have a  $R_{a\max}$  value  $\leq 0.1 \mu\text{m}$ , using a cut-off value of 0.25 mm." It is important for the purposes of this thesis to note that this is a profile surface roughness parameter and that ISO 4288 [107] is for profile not areal methods of surface texture assessment.

Oxidised zirconium (OxZr) was introduced clinically in 2004 as an alternative femoral and patellafemoral component material [108, 109]. OxZr components consist of a bulk zirconium niobium alloy (Zr-2.5Nb) metallic structure and a  $5\mu\text{m}$  surface-hardened layer of ceramic monoclinic zirconia ( $\text{ZrO}_2$ ). The bulk metallic zirconium niobium alloy is oxidised in air in temperatures greater than  $500^\circ\text{C}$  to form a uniform black ceramic zirconia surface which has a gradual transition from the ceramic oxide to the substrate alloy. This gradual transition makes the ceramic oxide layer resistant to de-bonding, chipping or delamination. An OxZr component claims high scratch resistance due to the hardness of the ceramic surface and high fatigue strength and fracture resistance in the bulk metallic structure.

UHMWPE has been used as a bearing material in orthopaedic knee replacements for over 50 years [45, 110]. It is a linear polymer of ethylene ( $\text{C}_2\text{H}_4$ ) in which there are approximately 200,000 ethylene repeats in the molecular chain [111]. There are three types of medical grade UHMWPE powder described in the ISO Standard 5834-1 [111]. Types 1 and 2 are produced by the company Celanese (Oberhausen, Germany) and are given the trade names GUR1020 and GUR1050. They have average molecular weights of 3.5 and  $5.5\text{--}6 \times 10^6 \text{ g/mol}$  respectively (calculated using the ASTM standard) [112]. Up until 2002, Basel Polyolefins (Wilmington, Delaware, USA) produced type 3 resin with the trade name 1900H which has an average molecular

weight of  $>4.9 \times 10^6$  g/mol. Production was stopped in 2002 but many orthopaedic companies stock piled the product and so it is still currently in use [112].

The mechanical properties of UHMWPE are not only affected by the average molecular weight but also by the conversion process used to convert the powder to the consolidated bulk form [112]. Table 2.3 shows the mechanical properties of type 1 and 2 UHMWPEs that have been compression moulded and extruded.

Table 2.3 Summary of Mean ( $\pm$  standard deviation) Physical and Tensile Mechanical Properties of Extruded and Moulded UHMWPE [112]

Material		Density (kg/m <sup>3</sup> )	Tensile Yield (MPa)	Ultimate Tensile Strength (MPa)	Elongation to Failure (%)
GUR1020	Extruded	935 $\pm$ 1	22.3 $\pm$ 0.5	53.7 $\pm$ 4.4	452 $\pm$ 19
	Moulded	935 $\pm$ 1	21.9 $\pm$ 0.7	51.1 $\pm$ 7.7	440 $\pm$ 32
GUR1050	Extruded	931 $\pm$ 1	21.5 $\pm$ 0.5	50.7 $\pm$ 4.2	395 $\pm$ 23
	Moulded	930 $\pm$ 2	21.0 $\pm$ 0.7	46.8 $\pm$ 6.4	373 $\pm$ 29

The choice of packaging and sterilisation of UHMWPE orthopaedic components has historically been, and continues to be, a much debated issue as it can have an effect on the mechanical properties of the UHMWPE [113]. There is still no clear consensus as to the best packaging and sterilisation method. Prior to the mid-1990s, UHMWPE orthopaedic components were sterilised by gamma irradiation in the presence of air and stored in air-permeable packaging. It was discovered that gamma irradiation of UHMWPE can lead to the formation of microradicals which subsequently oxidise on contact with oxygen in air during the shelf-life of the component or on contact oxygen in bodily fluids *in vivo* [114, 115]. The resultant oxidative chain scission within the UHMWPE can lead to an increase in density and crystallinity of the polymer and a loss of mechanical properties. This can lead to *in vivo* fatigue damage including subsurface cracking and delamination of the UHMWPE component [113]. Current sterilisation and packaging methods include gamma irradiation in an oxygen reduced environment and the use of oxygen barrier packaging, and gas plasma and ethylene oxide sterilisation and the use of gas permeable packaging [113].

XLPE (Crosslinked polyethylene) is UHMWPE that has been irradiated with a high dose of radiation (>50kGy) to create free radicals and then thermally treated to result in the crosslinking of the polymeric chains. Antioxidants are often added in order to stabilise the material. This process improves the wear resistance and XLPE bearing inserts were introduced in the mid-2000s in knee arthroplasty to reduce volumetric wear rates [116]. Laboratory simulations and experimental studies indicate improved wear performance for XLPE compared with conventional UHMWPE [117-119] and clinical studies have indicated a comparable or improved performance [2, 120]. However, there are still concerns around the use of XLPE within TKR based on the decreased mechanical properties associated fracture resistance and fatigue crack propagation [121, 122]. Orthopaedic implant manufacturers use various modified UHMWPEs that include different amounts of crosslinking and different antioxidants to stabilize and enhance the material properties. As with the details of the conversion processes, manufacturing, packaging, and sterilization methods, details of crosslinking and antioxidant additives remain proprietary and information is not readily available in the public domain [101-105].

### **2.3.2 *Demographics of Knee Replacements***

There were 112,836 knee replacement procedures recorded by the 15<sup>th</sup> Annual Report of the National Joint Registry (NJR) for England, Wales, Northern Ireland and the Isle of Man for the year 2017 [1]. This is an increase of 3.8% from 2016. Of the procedures record in 2017, 106,334 (94%) were primary procedures (i.e. first surgical interventions) which included 94,420 (89%) primary TKRs, 10,750 (10%) primary UKRs and 1164 (1%) primary patellofemoral replacements. There were 6502 (6%) revision procedures including the revisions of total and partial (unicondylar and patellofemoral) replacements. Within the NJR, osteoarthritis is the main indication for 98% of all primary knee procedures with knee replacement surgery being the end-stage treatment for the disease. In 2017 over half the knee procedures (56%) were performed on women. The average ages were 69.2 years for men and 69.4 years for women. The average Body Mass Index (BMI) was 30.9, which is classed as “obese”.



The 2018 Australian Orthopaedic Association Joint Replacement Registry (AOAJRR) [58] recorded 63,854 knee replacement procedures where 59,129 (92.6%) were primary procedures which included 55,170 (86.4%) primary TKRs and 3,959 (6.2%) primary partial procedures (both UKRs and patellofemoral replacements). There were 4,725 (7.4%) revision procedures recorded.

In England, Wales, Northern Ireland and the Isle of Man in 2017 there were sixty-seven brands of TKR prostheses used in primary procedures, forty-six brands used in revision procedures. There were nineteen brands of UKR prostheses, nine brands of patellofemoral prostheses and seventeen brands of hinged prostheses used. [1]. The five most used TKR prostheses in England, Wales, Northern Ireland and the Isle of Man in 2017 were DePuy PFC® (27%), Stryker Triathlon (17%), Zimmer Biomet Nexgen® (16%), Zimmer Biomet Vanguard (10%) and Smith & Nephew Genesis 2 (8%). The majority of TKRs are cemented (86%) with a fixed bearing (94%) and a 71% have an unconstrained fixed bearing [1]. The Zimmer Biomet Oxford Partial Knee is the most used UKR prosthesis (57%) followed by the Physica ZUK (acquired from Zimmer in 2015 by the Lima Corporation in the United Kingdom and by Smith & Nephew in the US) (20%), the DePuy Sigma® HP Uni (14%) and the Smith & Nephew Journey Uni Oxinium®, the Zimmer Biomet Persona Partial Knee and the Stryker Triathlon Uni (all 2%) [1].

Details of the PE used in knee replacements within England, Wales, Northern Ireland and the Isle of Man, including the conversion from powder to bulk, sterilisation and modifications (i.e. crosslinking and addition of antioxidants) are not available from the NJR Annual Report [1]. The 2018 AOAJRR [58] does report that the use of cross-linked polyethylene (XLPE) in primary TKR increased from 7.1% in 2003 to 60.9% in 2017. In addition, the 2018 AOAJRR also includes the rate of revision of XLPE and showed that prostheses using XLPE have a cumulative percent revision rate of 5.00% at 15 years compared to 7.9% for non-XLPE. The reason for this difference was a reduction in the cumulative incidence for loosening (0.8% at fifteen years for XLPE compared with 2.0% for non-XLPE). In the United States, it has been estimated that XLPE components is now used for the majority of primary TKRs and all of the major orthopaedic implant manufacturers offer modified (XLPE and XLPE

+antioxidant) bearing components [116]. However, in Norway, XLPE is rarely used (8% between 2013-2015) [123].

The increases in the annual number of knee replacement procedures reported by the NJR [1] and the AOAJRR [58] are reflected worldwide [7, 124-128]. These increases are predicted to continue well into the mid-21<sup>st</sup> Century. The reported and predicted incidence rates are unique to each country and are influenced by the socioeconomic environment. Patel et al [129] analysed NJR and Office for National Statistics data and predicted that the volume of primary TKR in England and Wales will have increased by 117% from 2012 to 2030. This is comparable to an estimate made by Culliford et al of around 118,600 TKRs being performed in the United Kingdom in 2035 [128]. Using a conservative approach based on that developed by Nemes et al [126] for predictions in Sweden, Inacio et al [124] predicted that by 2050 the number of TKRs performed annually in the United States will reach 1.5 million cases per year compared with the current volume of 700,000. The incidence rates, and predicted increases in incidence rates, have been suggested to be influenced by multiple factors including an increasing aging population [124], an increase in obesity [130], an increase in the prevalence of osteoarthritis (which is linked to an aging population and an increase in obesity) [63], an expansion of surgical indications including to younger patients [131], and changes in patient behaviour and expectations of the quality of life [125].

### **2.3.3 Revision Knee Replacement**

Current TKR survivorship is reported as 90 - 96% at ten years for many TKR systems across joint registry reports and published series worldwide with some reporting up to 96% at fifteen years and 90% at twenty years [1, 6, 7, 58, 123, 132, 133]. UKR survivorship is lower at around 80% - 85% at ten years [123, 132, 134]. The lower UKR survivorship rates are thought to be due to the fact that progression of osteoarthritis in the other joint compartments and conversion to a TKR is an indication for UKR revision [123]. Even though the survivorship rates are very high particular for TKRs, when revision surgery is required it is costly, carries an increased risk to the patient, and has a lower level of patient satisfaction [135, 136]. Hence the

requirement to strive for further reductions in number of revisions and an increased time to revision.

As the numbers of primary knee replacement procedures increase, it is also predicted that the number of revision knee replacement procedures will increase. In the United Kingdom Patel et al [129] predicts that by 2030 the number of revision TKR procedures will have increased by 332% and similar cumulative percentage increases are predicted for the United States in the same time frame [127]. The increase in revision surgery is thought to be due not only to the increase in the number of primary procedures, but also to an increased life expectancy, an increase in obesity and the extension of the indication of primary procedures to younger patients with higher expectations [123, 131].

The current paradigm is that aseptic loosening of the femoral and tibial components is the result of periprosthetic osteolysis [26, 137-141]. Osteolysis is an inflammatory response to wear debris particles which results in the resorption of bone. The intended articulation of the femoral and PE component as well as articulation between the PE component and the tibial component (intended in the case of mobile bearing and unintended in the case of fixed bearings) results in wear of the PE component and the release of PE wear debris into the joint space. A further source of PE wear debris can also be from the post of posterior stabilised designs. The wear debris elicits a macrophage response and promotes osteoclasts which act to resorb bone. This bone resorption or osteolysis, leads to aseptic loosening or loss of fixation of the components.

In a comprehensive review, Gallo et al presents a summary of the pathogenetic mechanisms of osteolysis around total knee arthroplasty [26]. The overview describes the multifaceted implant, surgery and patient factors and the complex relationships between these factors that can cause and influence the development and progression of periprosthetic osteolysis, aseptic loosening and eventual prosthesis failure. Specifically, the volume of PE wear debris and the size and morphology of the PE wear debris has a major influence in the pathogenesis of

osteolysis. A larger volume of sub-micron sized particles with an elongated shape all stimulate increased macrophage response [142, 143].

Prior to the mid-1990s the main cause of TKR failure and indication for revision was the fatigue damage of the PE component leading to gross delamination and fracture [27, 144, 145]. Subsequent advancements in the material development, the sterilisation and packaging processes, and implant design led to significant improvements [110]. Currently, for TKR revisions performed before ten years *in vivo* the main indications are infection, instability and problems associated with pain of the patellofemoral. After ten years *in vivo*, and when all revisions are considered together regardless of time *in vivo*, despite advances in biomaterials, implant design and surgical techniques, aseptic loosening is still the most prevalent indication for TKR revision [1, 18, 19, 21, 58, 123, 132, 146-148]. For UKR prostheses the most prevalent indications are aseptic loosening and the progression of osteoarthritis or unexplained pain [1, 58, 123, 132].

A review of the NJR, AOAJRR and the Swedish Registry showed that numbers of revisions performed due to aseptic loosening reduced over the period 2004 – 2014 while the number of revisions performed due to septic infection increased over the same period [149]. Dyrhovden et al [123] conducted a review of the Norwegian Joint Registry and compared revisions performed between 1994 – 2004 with revisions performed between 2005 – 2015. They reported a similar reduction of revisions indicated for aseptic loosening and increase in revisions indicated for infection. A limitation in this discussion is that there is no consensus or consistency within surgeons as to the terminology and diagnosis regarding revision indications [148]. Registries can only report the data provided and published series often have classifications that are not standardised [149].

#### **2.3.4 PE Wear in Knee Replacements**

Wear of the PE component and the generation of PE wear debris in knee replacements is widely acknowledged as a multifaceted problem influenced by a combination of patient, surgeon and implant factors [24, 25, 27, 150, 151]. It is

challenging to differentiate the effect of each of these influences on the wear of the PE and determine their individual contribution on the mechanism of failure and reason for revision of a knee prosthesis. A holistic approach must be taken when considering the influencing factors involved in PE wear, aseptic loosening and knee replacement revision.

The BMI of the patient has been shown to impact on the PE wear, as has the selection of the size of the implant. Smaller implants in patients with higher BMIs results in high wear rates than larger implants. [152-154]. Component mal-positioning and limb mal-alignment can also have a detrimental impact on the wear and damage of the PE component. High contact stresses and increased wear and damage can occur in the PE component if the coronal plane limb alignment is in varus\* or the ligaments are not balanced appropriately [24, 27, 155-159].

The geometry of the implant design will impact on the wear of the PE component. Historically, more congruous bearing designs were favourable as they reduced contact stresses and the incidence of fatigue damage and delamination [160]. Congruous bearings have lower linear penetration rates than flat bearings [161]. However, congruous bearing designs have been identified as over-constraining the joint and limiting the range of motion causing additional stresses and resulting in increased wear and damage [162]. Increased articular surface conformity has also been shown to lead to increased backside wear of the PE component in both mobile, semi-constrained and fixed bearing designs [163-166]. Furthermore, higher surface damage has also been reported in congruous designs due to third body debris being trapped in the “dish” of the component [162]. However, a recent study comparing the clinical survivorship of mobile and fixed bearing UKRs at a minimum ten years follow-up showed that survival and functional outcomes were similar [167].

---

\* Varus is when the distal part of the bone is deviated toward the centre of the body; in the case of the knee joint also called “bowlegged”. The opposite being valgus which in the case of the knee joint is also commonly described as “knock-knees”.

---

A recent knee simulator study by Brockett et al [168] investigated the influence of bearing conformity on modern moderately crosslinked fixed bearing TKRs and reported a significant reduction in volumetric wear rate with decreasing conformity. Brockett et al commented however, that with reduced bearing conformity there is a greater need for ensuring correct component positioning, alignment and soft tissue balancing *in vivo* to enable this reduced wear rate to be reproduced clinically.

The topography of the counterface surface of the femoral component has long been identified as a factor that influences the rate of PE wear. *In vitro* wear simulation and fundamental tribological studies have shown that a rougher femoral component can result in greater PE wear, specifically transverse scratches in the femoral component with an increased peak height can result in increased ploughing in the softer PE component [11, 28-31, 169-176]. Experimental studies from the 1990s report that a threefold increase in the femoral component surface roughness can result in at least a tenfold increase in the rate of PE component wear and transvers scratches of 2 $\mu$ m can result in a 30% increase in PE wear [175, 177, 178].

A key recent simulation study using pin-on-disc simulations looked at the effect of roughened CoCr on PE wear and compared XLPE and non-XLPE. Against polished counterfaces, the XLPE showed negligible wear. However against roughened counterfaces, the XLPE wear was close to that of non-XLPE against polished counterfaces [11].

Retrieval studies have shown the femoral component to roughen *in vivo* [14, 15, 17, 179, 180]. But retrieval studies of both TKRs and total hip replacements (THRs) have failed to show evidence of a correlation between the extent of *in vivo* PE wear and the measured counterface femoral component surface roughness [15, 181, 182]. This may be attributed to the measurement and quantification methods used to determine the extent of *in vivo* PE wear and the femoral component surface roughness.

The roughness of the tibial tray of both mobile and fixed bearing components has also been identified as a possible factor influencing the rate of PE wear on the backside of the component with rougher components showing more PE backside

damage [163, 183, 184]. Due to this some manufacturers have opted for a polished tray with a comparatively lower surface roughness [101] and some have made modifications to the locking mechanism of the PE component into the tibial tray to try to reduce backside wear [102, 103].

As described in the previous section, XLPE was introduced clinically in knee arthroplasty in the mid-2000s with the aim of reducing volumetric PE wear [116]. Laboratory simulations and experimental studies indicate improved wear performance for XLPE compared with conventional UHMWPE [117-119]. Published clinical series and review analyses of registry data are not unanimous in reporting a significantly improved clinical outcome. Clinical performance of replacements with XLPE is comparable and in some cases improved when compared to replacements using non-XLPE [2, 120, 146, 185]. There are still concerns around the use of XLPE within TKR based on the decreased mechanical properties associated fracture resistance and fatigue crack propagation [121, 122]. These concerns and a lack of evidence of significant improvements in clinical performance of XLPE has led some to question the cost effectiveness of using XLPE and call for future studies evaluate the outcomes of XLPE versus non-XLPE [146, 186].

Also as described in the previous section, Oxidised Zirconium (OxZr) was introduced as an alternative bearing material for knee replacement femoral components. This was in an attempt to optimise the high scratch resistance of a ceramic bearing surface and high fatigue strength and fracture resistance of a bulk metallic structure and thereby reduce PE wear and PE wear debris generation [108, 109]. While *in vitro* wear simulation testing of OxZr TKRs has shown significant wear reduction when compared to CoCr TKRs [171, 172, 187], the ten-year clinical follow-up reviews report no difference in survivorship or patient-reported outcome measures [188-191]. The revision rates reported by both the 2018 NJR [1] and the 2018 AOAJRR [58] for Smith & Nephew's Genesis II ® Oxinium ® TKRs that utilises an OxZr femoral component are higher than that of Smith & Nephew's Genesis II ® TKRs that utilise a CoCr alloy femoral component. However, it is also reported that the OxZr TKRs are implanted into younger patients [1, 58]. Vertullo et al [192] analysed the data presented in the AOAJRR and concluded that OxZr femoral components did not

reduce revision rates compared with the same CoCr femoral components. The current research concludes that further analysis of the clinical outcomes and revised OxZr knee replacements is needed to realise the benefits and possible limitations in the longer term at fifteen years *in vivo* and beyond [14].

### **2.3.5 Knee Replacement Retrieval Studies**

While simulation studies and laboratory testing can provide information on the predicted performance of knee replacement systems, their efficacy in being able to truly represent the *in vivo* performance of prostheses has been questioned [150, 169]. Measurement of *in vivo* PE wear in knee replacement prostheses is challenging due to the geometry of the components and there is currently no standard procedure to do this [193]. There are also no standardised methods available for the quantifiable *in vivo* assessment of damage to the femoral component.

Retrieval studies of explanted components from revision surgery or autopsy, although not without limitations, can enable an analysis of the *in vivo* performance of joint replacement prostheses and the materials. Retrieval studies of knee replacement components have used a wide variety of different methodologies to provide quantitative and semi-quantitative analyses of the wear and damage of the components. The methodologies relevant to this thesis are discussed in this section. The methods are all limited by inherent inter- and intra-user variability.

The Hood PE Damage Scoring method was introduced in 1983 as a semi-quantitative method of assessing damage observed on the articular surface of PE components [194]. The original Hood method involves dividing the articular surface of the PE component into ten sections as shown in Figure 2.21.

Within each of the ten sections, 0-9, seven damage modes (surface deformation, pitting, embedded debris, scratching, burnishing, abrasion and delamination) are assigned a grade of 0, 1, 2 or 3. Table 2.4 gives further detail to the damage modes.



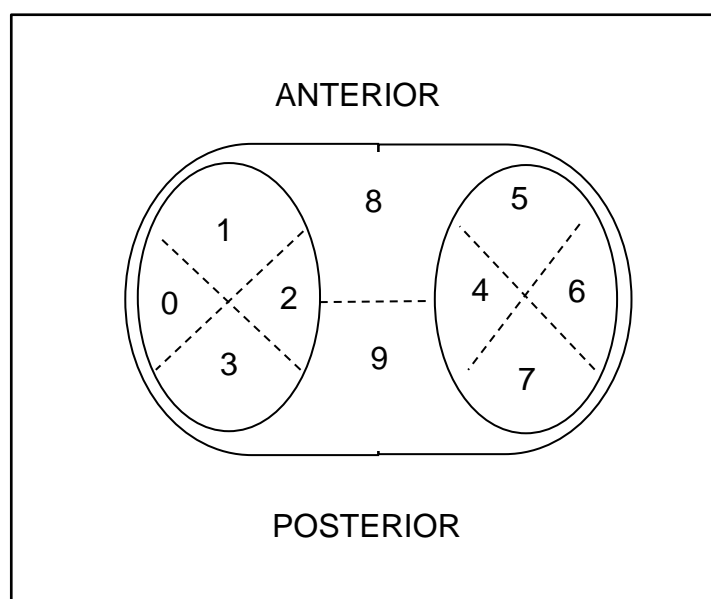
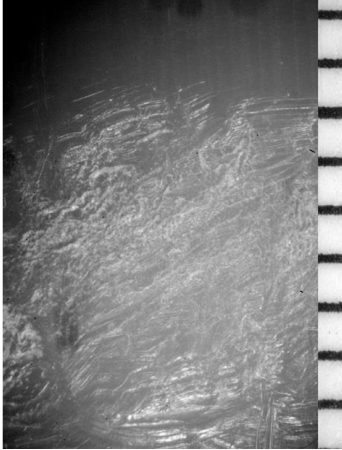
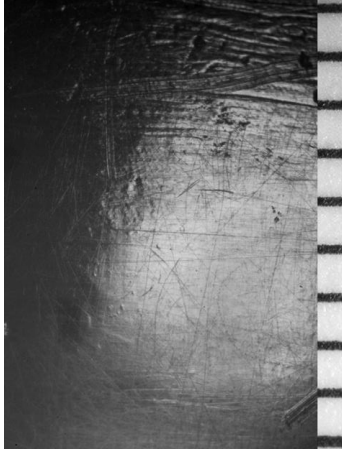
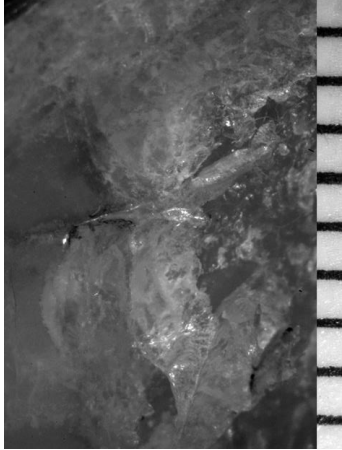


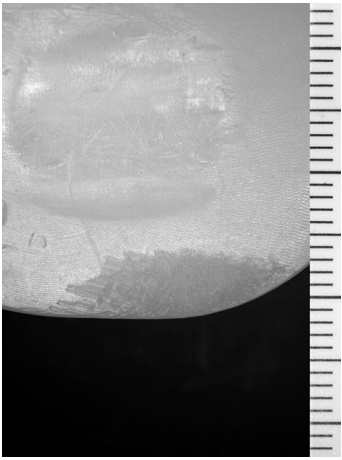
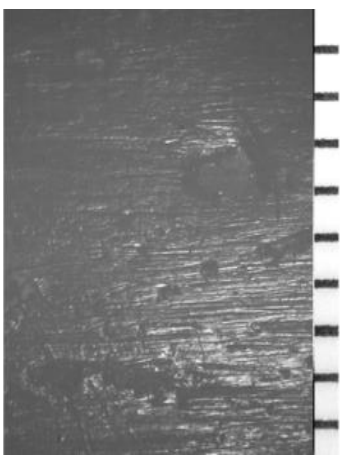
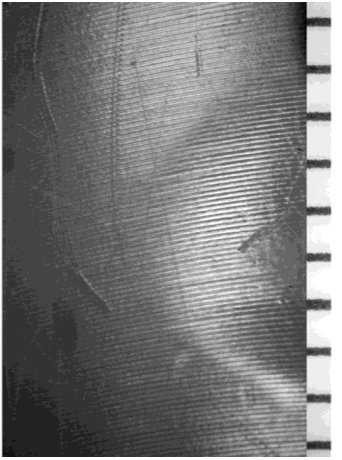
Figure 2.21 Diagram representing Hood damage score areas on the articular surface of a PE component [194]

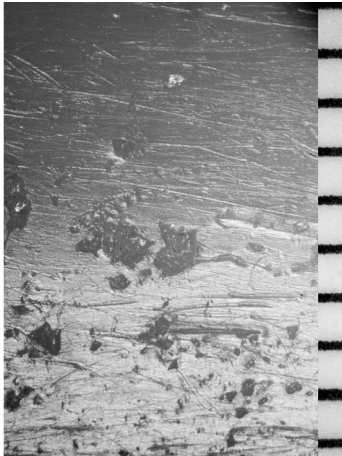
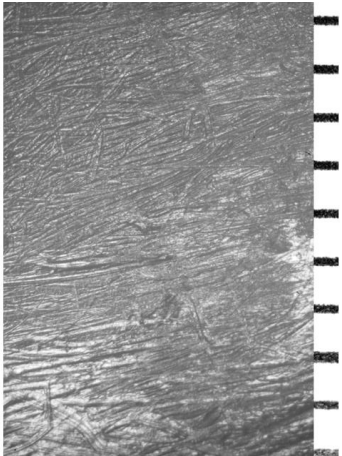
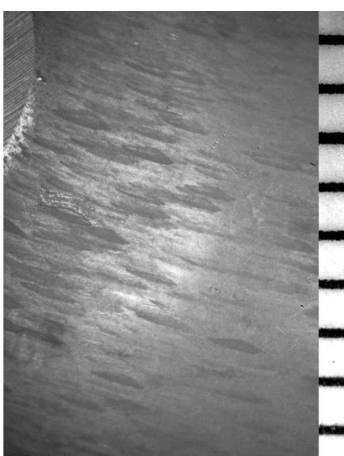
The grade assigned corresponds to the percentage area of the section the observed damage mode covers. If the damage mode is estimated to cover less than 10% of the section a grade 1 is given, if the damage mode is estimated to cover between 10 and 50% of the section a grade 2 is given, and if more than 50% of the section is covered by the identified damage mode a grade 3 is given. The sum of the grades for each damage mode in each section gives the PE Damage Score with the maximum possible being 210.

Since it was first used, the original Hood PE damage scoring method and variations of the method, have been used by many different researchers to provide a semi-quantitative analysis of the damage observed on explanted knee replacement prostheses [15, 24, 155, 156, 162-164, 166, 183, 184, 186, 188, 195-204]. It has been adapted for use not only on the articular PE surface but also on the PE backside surface [163, 164, 183, 184, 195, 198, 199, 205]. The Hood method and its variants have also been used for the analysis of the PE components of UKRs [164, 202].

Table 2.4 PE articular surface and backside surface damage mode descriptions and identification. Images showing 1mm scale. Images from Harman et al 2011[206],

Damage Mode	Description	Identification (1mm scale)
<u>Abrasion</u>	Abrasion is identified as areas where the PE has a rough, shredded or tufted appearance with limited directionality and with a change in colour of the PE from white to yellow.	
<u>Burnishing</u>	Burnishing is characterised by the observation of highly polished areas with a visibly increased reflectivity in comparison to the surrounding PE material.	
<u>Delamination / Subsurface cracking</u>	Delamination is observed where layers of PE material are separated and removed from the original surface, leaving an exposed surface. It may appear as a peeling of the PE. Subsurface cracking is where fatigue occurs to the PE below the original surface and is observed as a change in colour of the PE from white to yellow. Subsurface cracking often precedes delamination.	

Damage Mode (cont.)	Description (cont.)	Identification (cont.)
<u><b>Deformation</b></u>	<p>Surface deformation is observed as permanent deformation resulting in a change in the surface geometry. It is sometimes referred to as “plastic deformation” or “creep”. There is no material removal just a change in geometry. It is observed macroscopically and not typically associated with a change in colour of the PE. On the PE backside surface this can be the impression of screw holes from the tibial tray.</p>	
<u><b>Embedded Debris</b></u>	<p>Embedded debris are identified by areas that differ in colour and / or relative texture to the surrounding PE surface consistent with embedded third-body particles of suspected bone, cement or possibly metal.</p>	
<u><b>Indentations</b></u>	<p>Indentations are defined as non-uniform more pronounced scratches suspected to be the result of trapped third-body abrasions. Identified on the distal PE backside surface. Subsurface cracking often precedes delamination.</p>	

Damage Mode (cont.)	Description (cont.)	Identification (cont.)
<b><u>Pitting</u></b>	Pitting is visualised as depressions in the PE surface. Typically, the pits are between 1-2 mm in diameter, but they may be much larger with 20-30mm diameters. Within the pits the surface of the PE is burnished and very reflective.	
<b><u>Scratching</u></b>	Scratching is identified as thin indented lines which may be either ordered in the anterior / posterior direction or may be irregular in direction.	
<b><u>Stippling</u></b>	Stippling is uniquely identified on the distal PE backside surface and is visualised as short (approximately 1-2mm) unidirectional scratches often in a circumferential pattern.	

Damage scoring systems like the original Hood method and modified methods are subjective and dependent on the observer's classification of damage and also estimation of the area covered. In 2011, Harman et al [206] reviewed the PE damage scoring methods utilised within the literature at the time and provided a pictographic atlas to classifying damage modes on the articular and backside surfaces of the PE bearing. In 2012 Brandt et al [200] developed a modified semi-quantitative method for analysing the backside surfaces that incorporated a severity rating and further attempted to define the damage modes. These publications go some way towards standardising the terminology, however, the assignment of a grade based on percentage area covered and the estimation of the severity of a damage mode is still user dependent and subjective.

To provide a quantitative measure of volumetric *in vivo* PE wear research groups have more recently within the last ten years, developed methods using laser scanning [16, 157, 186, 195, 207], microCT scanning [163, 164, 183, 188, 208-210] and Co-ordinate Measuring Machines (CMM) [211, 212]. However, these techniques are not without limitations. They require specialist equipment which can be costly and are time consuming to employ. All of which mean the techniques are often not feasible for many research groups [205]. Additionally these techniques all require the definition of an original reference surface. Within THR, the femoral head and acetabulum cup of a THR are spherical, each with a defined radius with a defined tolerance. This enables an original reference surface to be estimated relatively easily [213]. The PE and femoral components of knee replacement prostheses can have complex geometries with multiple radii in both the anterior posterior and medial lateral direction and also multiple centres of rotation. The geometries not only differ within design but also within implant sizes of the same design. The geometric design and tolerancing (GDT) of the components is proprietary to the implant manufacturers [101-105]. In addition, there can also be variances in geometry of new unused PE components of different manufacturing lots. This may be due to the manufacturing tolerance dimensions on the design drawings but could also be due to concessions that can be made within the manufacturing process [214].

Recent studies have attempted to correlate a semi-quantitative PE damage score with volumetric wear derived using microCT scanning methods. The studies concluded that damage score did not correlate to a wear rates or penetration depth [164, 188]. This is in agreement with previous studies [156], that further concluded that damage scoring is not a good predictor of PE wear.

While it is accepted that damaging scoring methods cannot provide a fully quantitative measure or prediction of PE volumetric wear or linear penetration, they can still provide a non-destructive semi-quantitative method of describing *in vivo* damage to the PE. Damage scoring methods are useful as they can be employed without the use of expensive specialist equipment or skilled technicians [205].

The damage scores of retrieved PE components have been used to infer conclusions between cohorts with differences in fixed-bearing and rotating platform knee replacements [166, 201, 203], differences in high flexion and posterior stabilised TKRs [195, 196], differences in TKRs and UKRs with polished and non-polished tibial components [163, 184], differences in TKRs with varus / valgus alignment [24, 155], differences in TKRs and UKRs utilising OxZr or CoCr [188] and differences in the utilisation of XLPE and non-XLPE [186, 215].

Damage scoring methods have been modified to provide a semi-quantitative analysis of the damage observed on retrieved femoral components [17, 180] and also the trochlear region of the femoral component [216]. The method defined by Brandt et al [180] for analysing surface damage on femoral components divides the surface into 8 sections (defined in Figure 2.22).

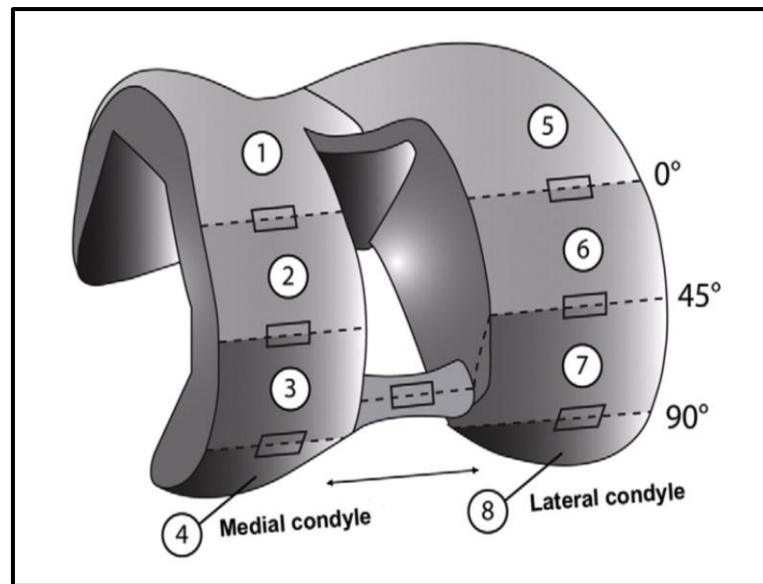


Figure 2.22 Diagram representing the 8 femoral component damage score areas as per the method describe by Brandt et al [180]

In each of the 8 sections a damage feature score (DFS) is calculated as the product of an area score and a severity score for three specific damage modes (grooving, indentation and gouging). The area score is classified 0 through to 10 and corresponds to the percentage estimated area of the section that the damage mode is identified. An area score of 0 corresponds to 0%, 1 corresponds to between 0 and 10%, 2 corresponds to between 10 and 20% and so on. The severity score for each damage mode was 0 (no damage), 0.33 (mild damage / just visible), 0.66 (moderate damage) or 1 (severe damage). The sum of the 8 DFSs give a total femoral damage score (FDS) with the maximum possible being 240 ( $8 \times 3 \times 10 \times 1$ ) [180].

Fabry et al [17] modified the femoral damage scoring method established by Brandt et al [180] for analysis of retrieved titanium nitride (TiN) coated femoral components. The severity and area scores were recorded for four damage modes (scratching, coating breakthrough, indentations and notches). The subtle differences in the scoring methods employed by Fabry et al [17] and Brandt et al [180] make direct comparisons between the two sets of results meaningless and highlight the need for standardisation.

### **2.3.6 TKR Component Surface Roughness**

As discussed in the preceding sections, an increased femoral component surface roughness has been identified as one of the causative mechanisms of accelerated PE wear [11, 28-30]. The measurement of the surface roughness of the femoral component of retrieved knee replacement prostheses has been reported as a method of providing a quantitative analysis of the *in vivo* damage to the component [15, 17, 153, 154, 180, 217-220]. The surface roughness analysis of the trochlear region of the femoral component [216] and of the tibial tray have also been reported [198, 221]. Two studies [198, 221] reported on the roughness of the PE component and Smith et al [32] reported on the surface roughness of glenoid PE components after wear simulation testing. The PE components all showed the loss of machining marks and a decrease in roughness parameters of mean surface roughness and peak height [32, 198, 221].

Table 2.5 gives an overview of the literature regarding the profilometry methods used for measuring the surface topography of the different component surfaces of knee replacements prostheses. The different measurement techniques and reported parameters are detailed, as are the published results.

The wide range in methodologies and reported parameters presented in Table 2.5 make meaningful comparisons between the quantitative published results very difficult to achieve and often impractical. There are also significant limitations in the methodologies used within all the studies which lead to questioning the significance of the results and the subsequent interpretations. In general, the existing literature does not cover the limitations in the actual methods of acquiring surface roughness data. It is evident that when using both contacting and non-contact profilometry the results are dependent on the measurement point or area selected by the assessor as well as all the other parameters that can be change. This only adds to the challenge of validating results between and within studies.

Taking into consideration the differences in methodologies and reported parameters and the associated limitations an attempt to summarise and critically review the findings is made in the following paragraphs.



There is general agreement that the articulating femoral condyles and the trochlear region of CoCr femoral components roughen after time *in vivo*, however no correlation has been found between the roughness of retrieved components and the length of time *in vivo* [15, 17, 153, 180, 216, 217, 220, 222]. Femoral components coated with TiN have been shown to roughen *in vivo* [17], however there is not agreement that OxZr femoral components roughen after time *in vivo* [180, 217, 218]. Polished tibial trays roughen after a time *in vivo*, however non-polished tibial trays reduce in roughness following period of time *in vivo* [198].

Scholes & Kennard et al [15] (manuscript included in Appendix H) and Que et al [220] found no correlation between retrieved femoral component roughness and patient age, BMI, PE Hood Damage Score or side of implantation. Scholes & Kennard et al showed higher roughness and more negative skewness seen with male patients, however this was not found by Que et al. Additionally, there is not agreement as to whether the medial or lateral femoral condyles show greater roughening with Fabry et al [17] and Brandt et al [180] reporting medial roughness being greater than lateral and Scholes & Kennard et al [15] reporting lateral roughness greater than medial.

Within this discussion regarding the *in vivo* surface roughness changes of TKR femoral components and influence of an increase femoral component surface roughness on the wear of the PE component, it is important to consider research done in this area relating to THRs. It is appreciably difficult to apply the conclusions reached from studying THRs to TKRs due to the differences in geometry, kinematics and tribology of the joints. However, knowledge regarding the fundamental influences of counterface surface roughness on PE wear can be shared.

In 1987 a laboratory study by Dowson et al [31] reported that a single scratch on the femoral counterface could increase the wear of the PE component by “a remarkable extent”. An increased PE wear factor of 11 times greater with a roughened counterface has been quoted [31]. Lancaster et al [223] carried out a further laboratory study in 1997 and concluded that although an increased counterface

roughness still had an impact on the PE wear, it was to a much lesser extent than reported by Dowson et al.

In 1997, Hall et al [142] used a Rodenstock RM 600 non-contacting profilometer to measure the surface roughness of thirty-five retrieved THR femoral heads. The roughness parameters were used to calculate a theoretical wear value which was compared to a clinical wear value that was measured on the retrieved PE acetabular components using a shadowgraph technique. The correlation between the measured clinical wear value and the calculated theoretical wear value was much less than found in laboratory results. In conclusion, further investigation was recommended.

In 1999 Elfick et al [182] assessed forty-two retrieved PCA THRs using optical profilometry (NewView 100, Zygo). Four measurements were taken on the periphery as reference values and ten measurements were taken in the defined contact region. A scan area of 180mm x 135mm was used with a remove spherical form filter applied. The roughness of the retrieved femoral heads increased, and the measured roughness parameters were used in a theoretical wear model to attempt to predict volumetric wear rate per cycle based on the average surface roughness. There was no evidence of a relationship between the topography of the worn region of the femoral head and that of the acetabular liner. Furthermore, as in Hall et al's retrieval study [142], the strength of the association between the surface roughness and the clinical wear factor was much lower than had been found in laboratory simulations. Elfick et al [182] concluded that their study failed to provide clinical evidence to substantiate the relationship between surface finish and wear rate in THRs. Due to the complexity of the geometries and the different designs of TKRs it has not been possible to carry out work similar that done by Hall et al [118] and Elfick et al [182].

This literature review has identified a definite need for a thorough investigation into the standardised quantification of the surface topography of explanted TKR components. Within the literature there is very little information on the influence and importance of *in vivo* TKR femoral component roughening and the impact of an increased femoral component surface roughness on the corresponding PE component wear and PE wear debris generation and subsequent osteolysis and

prosthesis failure due to aseptic loosening. There is a need for the standardised of measurement parameters and methodologies so that future surface profilometry studies can provide comparable surface roughness data. There is confusion regarding the *in vivo* roughening of OxZr components. There is limited understanding of the influence of patient and implant factors on the *in vivo* roughening of TKRs components. And finally, there no published literature available regarding the surface roughness measurement of retrieved UKR components.

The work done in this thesis aims to address the above questions and research gaps by presenting a thorough investigation into the surface topographical analysis of explanted knee prostheses. The protocols and methodologies used offer standardisation for future comparisons and the limitations and constraints of the work are fully investigated. This work is the first to report the surface roughness of explanted UKR prostheses and one of the few studies to provide further analysis of TKR and UKR explanted components that utilise OxZr.

Within orthopaedic bioengineering there is great value in reporting analysis data of explanted prostheses that have undergone the truest test of all, time *in vivo*. This was demonstrated most recently with the analysis of explanted Metal-on Metal hip replacement components whereby it was only through the reporting of large sets of data that patterns emerged that highlighted catastrophic problems. Specifically when considering OxZr knee replacement prostheses, the numbers of explanted components available for analysis in the United Kingdom are currently so very small that any results that contributes to the further understanding of their clinical performance is of great importance. Analyses of any explanted orthopaedic prostheses are extremely challenging and have inherent limitations and constraints however they should be pursued as they are invaluable in providing further information regarding the true working performance of these components.

Table 2.5 Review of published literature regarding surface profilometric measurement of knee replacement components

Reference & Profilometry measurement equipment	Materials	Methodology	Parameters reported	Results
<b>Fabry et al 2017 [17]</b>				
Contact profilometry (Hommel Tester T8000 Wave, Jenoptik Wedel, Germany)	25 retrieved TKR femoral components with titanium nitride (TiN) coating  3 reference TKR femoral components with TiN coating	3 linear transverse scans made on the <b>femoral component</b> at 0°, 45° and 90° flexion giving 9 measurements per condyle, 18 per component  Stylus tip radius - 2µm; Transverse length 1mm; Measurement speed 0.15 mm/s <sup>-1</sup>	Ra – arithmetical mean surface roughness Rq – root-mean-square deviation of the roughness profile Rp – maximum profile peak height of the roughness profile Rt – total height of the roughness profile	<b>Femoral components:</b> Ra, Rq and Rt: Retrieved > Reference Rp Retrieved < Reference Correlation Ra vs Time <i>in vivo</i> (TIV) very low Correlation Rp vs TIV low A direct correlation between surface roughness and TIV could be excluded. Medial > Lateral for BOTH retrieved and reference
<b>Matz et al 2017 [216]</b>				
White light optical profilometry (NT1100, WYKO Co, Tucson, Arizona, USA)	18 retrieved CoCr TKR femoral components (6 of 3 different models Stryker Triathlon, DePuy Sigma, Smith &	The <b>trochlear region</b> of the femoral component was divided into 6 zones and between 1 and 2 measurements were taken in each zone =	Ra – arithmetical mean surface roughness Rq – root mean square average of the profile height	<b>Trochlear region:</b> Triathlon and Sigma retrieved components were significantly rougher than reference components.

	Nephew Genesis II)  3 reference CoCr TKR femoral components (1 of each of the 3 models)	between 6-12 measurements per component  10x objective lens Reading length of 238nm	Rp – maximum peak height Rsk – skewness (*these are profile parameters, yet an areal method of surface topography measurement is described)	Genesis II components were not.
<b><u>Roy et al 2015 [169]</u></b>				
Optical profilometry – red light phase shifting except white light interferometry was used <i>“when deep scratches prohibited the use of red light phase shifting”</i>  ZoomSurf 3D Fogale Nanotech, Nimes, France	3 CoCr 3 MgPSZ (Magnesia-Stabilised Zirconia) Initial and post-15 million cycles (MC) wear simulation testing	1 areal scan at 0°, 15°, 30° and 45° flexion = 4 measurements per condyle / 8 per <b>femoral component</b>  10x magnification lens 1x zoom Scan area = 632µm x 475µm	Sa – average roughness Sq – root-mean-square roughness Sp – peak roughness Sv – valley roughness Ssk – skewness Sku – Kurtosis Polarity ratio 3*Ssk/Sku Sk – core roughness depth Spk – average height of peaks about the core roughness Svk average valley depth below the core roughness	<b><u>Femoral components:</u></b> <b><u>Pre-test:</u></b> CoCr characterised by positive features (mainly carbides) 20-30µm in diameter and 100-200nm tall. MgPSZ characterised by negative features up to 1000nm deep with most of the order 200-400nm deep Pre-test CoCr and MgPSZ have similar Sa, Sq and Sp values but different Sv and opposite polarities (Ssk and polarity ratio) <b><u>Post-test</u></b>

			(ASME B461-2009)	<u>9MC</u> CoCr had deep scratches 7 $\mu$ m MgPSZ no change. <u>15MC</u> CoCr deep scratches Sa, Sq, Sv 15MC>Pre-test by a factor of 5 Spk, Svk 15MC>Pre-test by a factor of 1.6 Spk 15MC >pre-test MgPSZ Only Sk changed from 25.3nm to 30.8nm
<b><u>Holleyman et al 2015 [198]</u></b>				
White light optical profilometry (NewView 5000, ZYGO, Middlefield, Connecticut, USA)	30 non-homogeneous retrieved TKR (9 designs) including CoCr, Ti and Stainless Steel tibial baseplates  4 control tibial baseplate components and PE components (2 DePuy PFC 2 Stryker Kinemax)	The <b>tibial baseplates</b> and the <b>backside of the PE components</b> were divided into a grid of 16 zones and 1 measurement was taken in each zone on each component.  10x magnification lens with 2x zoom Scan area = 317 $\mu$ m x 238 $\mu$ m	Sa – mean area surface roughness Ssk – surface skewness	<b><u>Tibial Baseplates and PE Backside:</u></b> DePuy PFC Sa: Retrieved > Reference Stryker Kinemax Sa: Retrieved < Reference  The use of a polished tibial tray can help reduce backside PE wear.

<b><u>Heyse et al 2014 [217]</u></b>				
White light optical profilometry (MicroXAM, Optical Profiler; ADE PhaseShift, Tuscon, Arizona, USA)	10 retrieved PS Smith & Nephew Genesis II TKRs with OxZr femoral components and 10 retrieved Smith & Nephew Genesis II TKRs with CoCr femoral component that were matched for duration <i>in vivo</i> , patient age and BMI  2 reference Smith & Nephew Genesis II TKR femoral components (1 x OxZr and 1 x CoCr)	60 measurements on each femoral condyle taken in 4 rows of 15 points at approximately 30° flexion / 120 measurements per <b>femoral component</b>  Scan area = 600µm x 800µm  <i>“Before calculation of surface roughness parameters, a global plane correction algorithm was used to subtract the macroscopic curvature from each scan”</i>	Sa – average surface roughness Sy – maximum peak to peak height Sz – 10-point height Ssk – surface skewness  *In the methods section the authors state median values were reported but in the results section the values are labelled as mean values.	<b><u>Femoral components:</u></b> Reference CoCr Sa, Sy, Sz < Reference OxZr Sa, Sy, Sz Reference CoCr Ssk +ve Reference OxZr Ssk -ve  Retrieved OxZr and retrieved CoCr roughness > Reference OxZr and CoCr  Retrieved CoCr Sa, Sy, Sz > Retrieved OxZr Sa, Sy, Sz Retrieved CoCr Ssk less +ve than reference CoCr Ssk Retrieved OxZr Ssk less -ve than reference OxZr Ssk  Retrieved CoCr medial condyle roughness > lateral condyle. No difference for OxZr condyles.
<b><u>Battaglia et al 2014 (1) [154]</u></b>				
Contact profilometry	6 Genesis mobile bearing TKRs (Ala	The <b>femoral components</b> and <b>tibial</b>	Ra – arithmetic average	After 4MC: <b><u>Femoral components:</u></b>

(Hommel Tester T8000, Hommel Werke, Germany)	ORTHO, Milan Italy) 3 of each size 2 (small) and size 6 (large)  Measurements taken at 2MC and post-4MC wear simulation	<b>baseplates</b> were scanned  Sampling length: 1.5mm Cut-off: 0.25mm	value of the deviations of the roughness profile filtered from the mean line into the sampling length Rsk – skewness of the profile	Ra Size 2 > Ra Size 6  <b><u>Tibial components:</u></b> Ra Size 2 < Ra Size 6
<b><u>Battaglia et al 2014 (2) [153]</u></b>				
Contact profilometry (Hommel Tester T800, Hommel Werke, Germany)	12 retrieved TKR (Nexgen, Zimmer)	30 measurements per femoral condyle / (60 per <b>femoral component</b> ) taken along the axial plane in a rectangular area (27mm x 22mm) chosen where the femoral components articulated against the PE component  Sampling length: 4.8mm Cut-off: 0.08mm	Ra – mean roughness Rsk – skewness	<b><u>Femoral components:</u></b> Time <i>in vivo</i> does not influence Ra or Rsk  No statistical difference was found between Ra of TKRs revised for aseptic and septic loosening. Revisions indicated for aseptic loosening
<b><u>Scholes &amp; Kennard et al 2013 [15] (manuscript included in Appendix H)</u></b>				
White light optical profilometry	19 non-homogeneous retrieved CoCr TKRs (Biomet	5 measurements per femoral condyle	Sq – Root mean squared	<b><u>Femoral components:</u></b> Sq increased between 2%



(NewView 5000, ZYGO, Middlefield, Connecticut, USA)	AGC, Biomet Dual Articular 2000, DePuy PFC Sigma, Stryker Kinematic and Stryker Kinemax)	<p>performed on an “unworn” area / 10 per <b>femoral component</b> 10 measurements per femoral condyle performed on a “worn” area / 20 per femoral component</p> <p>10x objective lens and 2x zoom Area of view = 317µm x 238µm</p>	<p>surface roughness</p> <p>Ssk – skewness</p>	<p>and 11% unworn to worn for all components. Ssk moved towards a more -ve value unworn to worn for 95% of components.</p> <p>Sq and Ssk were not correlated to length of time <i>in vivo</i>, patient age, BMI, PE Hood Damage Score or side of implantation of TKR. Higher Sq values and more -ve Ssk values were seen with male patients.</p> <p>Increased roughness was greater on the lateral condyle as opposed to the medial condyle</p>
<b><u>Brandt et al 2013 [180]</u></b>				
Contact profilometry (Surfcom 2900-SD2, Carl Zeiss GmbH, Oberkochen, Germany)	26 retrieved PS TKRs with OxZr femoral components and 26 retrieved PS TKRs with CoCr femoral components	3 surface roughness measurements performed at 0°, 45° and 90° flexion giving 9 measurements per condyle,	<p>Ra – mean height roughness</p> <p>Rq – Root mean square roughness</p> <p>Rp- Maximum</p>	<p><b><u>Femoral components:</u></b></p> <p>Reference CoCr Ra, Rq, Rp &lt; Reference OxZr Ra, Rq, Rp</p> <p>But no difference seen between</p>

	<p>matched for implantation period, BMI, patient gender, implant types and PE thickness. (Smith &amp; Nephew Genesis II, Legion and Journey TKRs)</p> <p>2 reference Smith &amp; Nephew Genesis II TKR femoral components (1 x OxZr and 1 x CoCr)</p>	<p>18 per <b>femoral component</b></p> <p>Stylus tip radius = 2µm Resolution = 0.1nm Max force = 0.75mN Measurement length = 1mm Cut-off wavelength = 0.08mm Measurement speed 60µm/s <i>"A tilt correction suing least squares-fit used to compensate for the condyle curvature"</i></p>	<p>height of peaks Rpm – Mean height of peaks (average of 5 highest peaks) Rpk – Reduced peak height (measure of surface profile that is worn away during the run-in period) Rsk – surface skewness</p>	<p>reference CoCr Rpm and Rpk and reference OxZr Rpm and Rpk</p> <p>CoCr: Retrieved &gt; Reference Medial &gt; lateral OxZr: No significant difference between Retrieved and Reference; no significant difference between medial and lateral</p> <p>CoCr: Rsk +ve for reference and retrieved and reduced with increased implantation time</p> <p>OxZr: Rsk -ve for both reference and retrieved and no change with implantation time</p>
--	---	---	---	---

#### **Burnell et al 2011 [218]**

Contact profilometry (Surfcom 1800D, Carl Zeiss, Oberkochen, Germany)	22 retrieved TKRs (3 designs: Zimmer Nexgen, Smith & Nephew Genesis II, Stryker Duracon).	Surface damage features were identified on the <b>femoral components</b> and classified as contact between femoral and	Seven roughness parameters were determined for each case  Ra, Rpm, Rsk, Rpk,	Femoral components: OxZr / Ti roughness parameters > CoCr / Ti roughness parameters
---	---	--	--	---

		<p>tibial component depending on component materials with the femoral component material detailed first (e.g. OxZr/Ti, CoCr/ Ti and CoCr/CoCr) Between 3-10 measurements were taken and the mean calculated.</p> <p>Traces were obtained starting from the visually non-damaged area through the damaged and ending in the visible non-damaged area. The evaluation length was different for each scratch.</p> <p>Stylus tip radius = 2<math>\mu</math>m Cut-off wavelength = 0.25mm Least square curve fit</p>	Rvk, Rp and Rv	<p>CoCr / Ti roughness parameters no different to CoCr / CoCr roughness parameters</p> <p>OxZr / Ti roughness parameters no different to CoCr / CoCr roughness parameters</p>
<b><u>Lakdawala et al 2005 [219]</u></b>				
Contact profilometry (Surftest)	22 retrieved TKRs with CoCr femoral	Damaged areas on the condyles	Ra – arithmetical mean of the	<b><u>Femoral components:</u></b>

SV400, Mitutoyo, Japan)	components (Freeman- Samuelson, Sulzer, Baar, Switzerland)	<p>within the articulating arc were measured.</p> <p>Measurements of surface roughness from the sides of the patellar groove at the apex of the femoral flange, an area which does not articulate with either the patella or tibia, were taken as controls.</p> <p>Stylus tip diameter = 0.0005mm Resolution = <math>0.01 \times 10^{-6}\text{m}</math> Max measurement length = 0.8mm</p>	absolute values of the measured deviation of height taken within the area evaluated	Articulating Ra not different to reference Ra
<b><u>Muratoglu et al 2004 [222]</u></b>				
Contact profilometry (Surftest 501, Mitutoyo, Japan)	<p>4 retrieved TKRS femoral components (Natural Knee-II, Zimmer) with visible 3<sup>rd</sup> body damage used in wear simulation</p> <p>1 reference femoral component</p>	5 roughness measurements taken on the <b>femoral condyles</b> in the mediolateral direction in the neutral position (0°) and 45° flexion.	Rp – peak roughness Ra – average roughness	<p><b><u>Femoral components:</u></b> Ra and Rp Retrieved &gt; Reference</p> <p><b><u>Post-test</u></b> Ra and RP 2MC&lt;pre-test 4MC&gt;pre-test</p>

	(Natural Knee-II, Zimmer)	Roughness measurements were taken pre-test, at 2MC and 4MC after articulation with different PE components  Stroke length = 2.4mm		
<b><u>Puloski et al 2003 [29]</u></b>				
Optical white light profilometry (NT-2000, WYCO, Tuscon, Arizona, USA)	9 “new” PS CoCr TKR <b>femoral components</b> (DePuy AMK, Smith & Nephew Genesis II, DePuy PFC, Sulzer Natural Knee, Wright Medical Advance Total Knee, Zimmer Nexgen, Howmedica Duracon, Biomet Maxim)	12 scans were taken per component (3 on each <b>femoral condyle</b> , 3 in the <b>trochlear groove</b> and 3 on the <b>posterior stabilising cam</b> )  Scan area = 1.3mm x 0.9mm	Ra – roughness average Rq – root mean square roughness Rsk – peak / valley skewness (*these are profile parameters, yet an areal method of surface topography measurement is described)	<b><u>Femoral condyles</u></b> No significant differences in the surface roughness of the femoral condyles were seen between implant designs  <b><u>Trochlear groove</u></b> 2 components Ra Trochlear groove > Ra femoral condyles 1 component Ra trochlear groove < Ra femoral condyles  <b><u>Posterior stabilising cam</u></b> Ra PS cam > Ra femoral condyles

<b>Chapman-Sheath et al 2002 [224]</b>				
Contact profilometry (Surfanalyser EMD-5400, Federal Products Co. Tokyo, Japan)	8 “new” mobile bearing CoCr TKRs (Zimmer MRK, Sulzer SAL, DePuy LCS Rotating Platform, Corin Rotaglide, Biomet Trac, Howmedica Interax, Smith & Nephew Profix, Smith & Nephew Genesis II)	10 measurements taken on the <b>femoral component, proximal PE surface, distal PE surface</b> and <b>tibial tray</b> taken in the AP and ML directions at 10 randomly selected locations  Scan length = 1mm Probe tip diameter = 2µm Travel speed = 0.5mm/s	Ra – mean deviation from the smooth surface line Rp – mean peak to smooth surface line	<b><u>Femoral component</u></b> and <b><u>Tibial Tray</u></b> No differences in AP and ML directions or between TKR design <b><u>Proximal PE component and distal PE component</u></b> Ra and Rp AP direction > ML direction  Distal PE component > proximal PE component.  Differences seen between implant designs
<b>Que et al 2000 [220]</b>				
Optical white light profilometry (NewView 100, Zygo, Connecticut, USA)	27 retrieved PCA (porous coated anatomic) TKRs	40 measurements were taken in an area 20mm x 10mm on each femoral condyle / 80 measurement per <b>femoral component</b>  Where metal on metal articulation was observed 15 further measurements	Ra – average surface roughness RMS – root mean square roughness PV – roughness total peak-to-valley roughness Rz – 10-point height parameter H - Swedish Height	<b><u>Femoral components:</u></b> All surface roughness increased (* reference was not defined)  No correlation between surface roughness (Ra and PV) and time of implantation, patient age or patient weight.

		<p>were taken in this area</p> <p>A best-fit cylinder removal filter was used</p> <p>Software filters were applied to mask surface features that were not considered of interest.</p>		<p>No difference in surface roughness between younger (&lt;70 yrs) and older (&gt;70 yrs) patients, heavier (&gt;200lbs) and lighter (&lt;200lbs) patients, longer (&gt;100 months) and shorter (&lt;100 months) implantation time, male and female or fixation with and without bone cement.</p> <p>However embedded debris in the PE caused increased femoral component surface roughness as did metal on metal articulation.</p>
--	--	---	--	---

**Que et al 1999 [225]**

Optical white light profilometry (NewView 100, Zygo, Connecticut, USA)	4 retrieved PCA (porous coated anatomic) TKRs	200 measurements were taken in a grid 20mm x 10mm per femoral condyle to calculate a True Surface Roughness Mean (TSRM)	$R_a$ – roughness average RMS – root mean square roughness	<p><b><u>Femoral components:</u></b></p> <p>For the retrieved femoral components, the RMN was 20 for a 10 x 10 mm<sup>2</sup> area</p>
--	---	---	---	--

		<p>3 sets of 30 measurements were made taken within the same grid at random points.</p> <p>The representative measurement number (RMN) was defined as the largest number of measurements required for the combined average of the randomly tested data to converge to within 10% of the TSRM.</p>		
--	--	---	--	--

As detailed in Chapter 1, the specific aim of this research is to use engineering techniques to quantify the surface topography of retrieved explanted knee replacement prostheses and to investigate relationships between *in vivo* surface topographical changes and patient and implant demographics. The results from this work will contribute to the body of knowledge within the field of orthopaedic knee prosthesis retrieval studies and will offer a standardised protocol for the surface topographical analysis for explanted knee replacement prostheses.



## **Chapter 3 Materials and Methods**

In this chapter the materials and methods used to realise the specific objectives detailed in Chapter 1 Introduction and address the questions posed by the literature reviewed in Chapter 2 Literature Review are presented.

As part of the work for this PhD a protocol for the collection and analysis of explanted knee replacement prostheses was developed and written and this is provided in Appendix A 'E. Ritchie Newcastle University: Knee Explant Retrieval Protocol'. Knee prostheses were explanted during revision surgery by a team of collaborating surgeons at the Freeman Hospital and the explanted prostheses were collected and processed according to the protocol. Within this PhD I collected, processed and catalogued a total of one hundred and thirty-five explanted knee prostheses for analysis. Any associated patient data that was available was also collected and correlated with the explant. The explants and data sets were de-identified by the allocation of a unique explant number in the format KXXX. The details of the explanted knee replacement prostheses and any available implant and patient data are recorded in a Knee Explant Catalogue which I developed and produced for the purposes of this thesis. This Knee Explant Catalogue is provided in Appendix B. This collection at Newcastle University represents the largest collection of catalogued explanted knee prostheses to date in the United Kingdom and provides a valuable resource for future studies.

### **3.1 Materials**

Ethical approval was obtained for the retrieval of explanted knee replacement prostheses from the Freeman Hospital, Newcastle upon Tyne, UK (REC Reference 09/H0906/72). Between 2011 and 2016, a total of one hundred and thirty-five explanted knee prostheses and any associated patient and implant data, were retrieved from revision surgery and catalogued by the author ER (see Figure 3.1).

Prostheses were immersed in formaldehyde solution immediately following surgery and left for a minimum of forty-eight hours before being rinsed with water and left to

air-dry. Prostheses that were sterilised using alternative methods such as steam sterilisation at the retrieval hospital's sterilisation services were included in the catalogue but excluded from study within this thesis. This was because it could not be confirmed that the surfaces had not been damaged during the cleaning and sterilisation process; six explanted prostheses were excluded for this reason. A further nine explanted TKR prostheses were excluded as there was no accompanying identifying data and no means of access to any of the patient and implant data. There were eight explanted prostheses excluded as they were incomplete and had missing components.

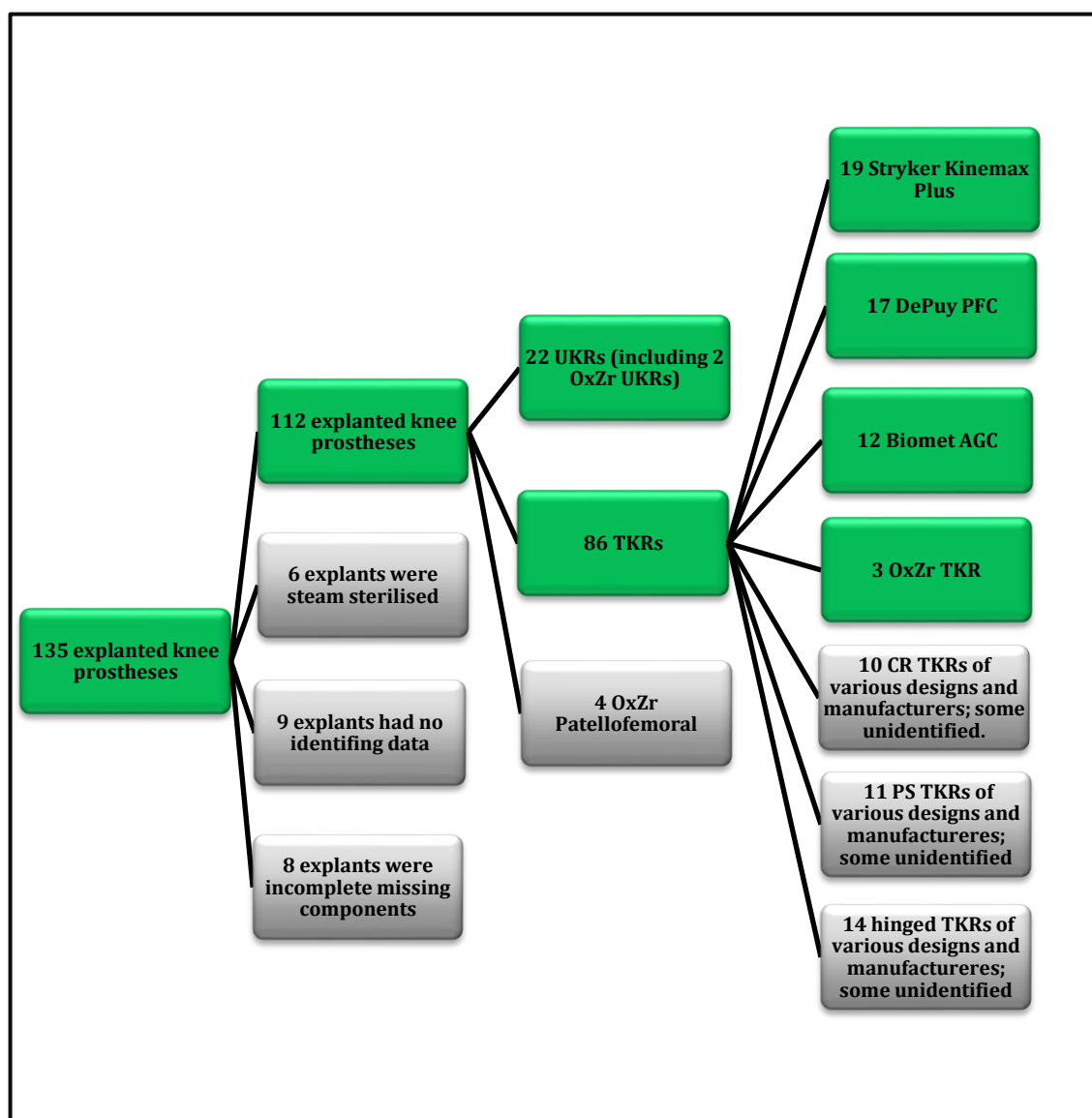


Figure 3.1 Knee prostheses catalogue breakdown

Of the remaining one hundred and twelve retrieved explanted knee prostheses there were eighty-six TKRs, twenty-two UKRs and four Patellofemoral prostheses. To enable the effective analysis and comparison of results, the retrievals were placed in homogenous groups according to prosthesis model, femoral component material and manufacturer.

This ordering of the prostheses resulted in a group of forty-eight TKR retrievals with cobalt-chromium alloy (CoCr) femoral components which included twelve AGC ® (AGC) (Zimmer Biomet, Warsaw, IN, US), seventeen PFC Sigma ® (PFC) (DePuy, Warsaw, IN, US) and nineteen Kinemax Plus (K+) ® (Stryker, Mahwah, NJ, US). These retrievals were further assessed for suitability in inclusion in this surface topography study. Two AGC TKR retrievals were excluded as they were of an older model of femoral component compared to the other ten retrieved AGC TKRs. Two PFC TKR retrievals were excluded as they were of an older model of femoral component compared to the other fifteen retrieved PFC TRKs. Two K+ TKR retrievals were excluded as it was found that the PE components did not have the same time *in vivo* as the femoral components due to a prior isolated PE component revision surgery having been performed. One K+ TKR retrieval was excluded as the PE component was a single unit which is different from all the others and one K+ TKR retrieval was excluded as there was no PE component available with the retrieved components. The remaining forty retrieved TKRs were of three designs, all with CoCr femoral components and modular fixed bearing PE components. All used cemented fixation of the femoral or tibial components or both. The PFC retrievals (n=15) and K+ retrievals (n=15) all were of cruciate retaining (CR) designs; the AGC retrievals (n=10) contained one posterior stabilised (PS), two partially stabilised designs and seven CR designs. The results of the surface topographical analysis of these forty retrieved prostheses are presented in Chapter 4. Figure 3.2 shows typical examples of the retrieved AGC, a K+ and a PFC, TKR prostheses. These are representative of a typical retrieved prosthesis within each design.

Included within the catalogue were a further ten cruciate retaining (CR) TKRs, eleven posterior-stabilised (PS) TKRs and fourteen hinged TKRs all of various designs and manufacturers and model versions (Biomet Maxim, Biomet Dual Articular 2000,

Endolink, Exactech Optrak, DePuy Noiles, DePuy SRom, DePuy TC3, Plus Orthopaedics TC Plus, Smith & Nephew Genesis, Smith & Nephew Triathlon, Zimmer). These retrieved components have been processed and catalogued as part of this project but the results of the analysis of these components are not included within this thesis.

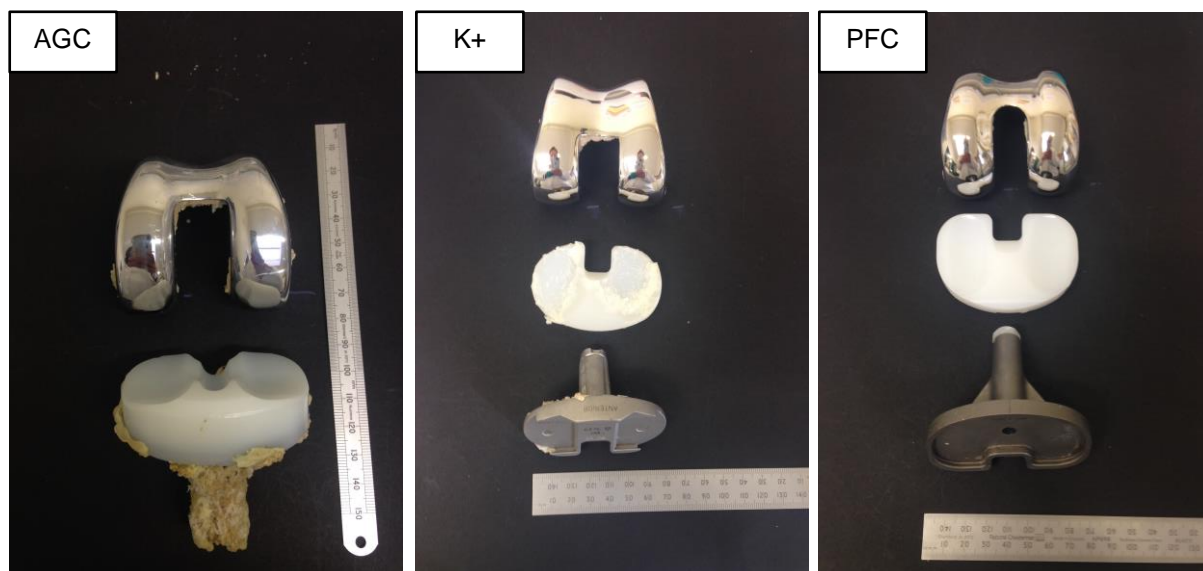


Figure 3.2 Example explanted AGC, K+ and PFC TKRs

Of the twenty-two UKR retrievals included in the catalogue there were ten High Flexion Unicompartmental Knees (HFZ) (Zimmer Biomet, Warsaw, IN, US), eight Oxford® UKRs (OB) (Zimmer Biomet, Warsaw, IN, US), two Oxinium Journey UKRs® (JOxZr) (Smith & Nephew, London, UK), one Sled® (SL) UKR (Link, Hamburg, Germany) and one other unidentified UKR (Oth). One of the retrieved OB UKRs was excluded from analysis as the retrieval only consisted of the PE component and a further two retrieved OB UKRs were excluded as there was no accompanying data with the prostheses and no means of accessing this data. Seventeen retrieved UKRs, the ten HFZs, the five OBs, the SL and the one Oth, all had CoCr alloy femoral components. The HFZs, and the SL UKRs were both fixed bearing designs whereas the OBs and the one Oth UKRs were mobile bearing designs; all used cemented fixation. The results of the surface topographical analysis of these seventeen retrieved UKRs with CoCr femoral components are included in Chapter 5.

There was very limited access to patient and implant data for fifteen UKR explants as some of the explanted prostheses were from retrieval surgeries at hospitals other than the Freeman Hospital. This meant that the patient data was not able to be accessed due to restrictions of data sharing between hospital trusts. These restrictions are in place to protect personal data and while unfortunate for this particular project have to be respected and must be adhered to. Figure 3.3 shows four examples of typical retrieved UKR with CoCr femoral components from within the catalogue.

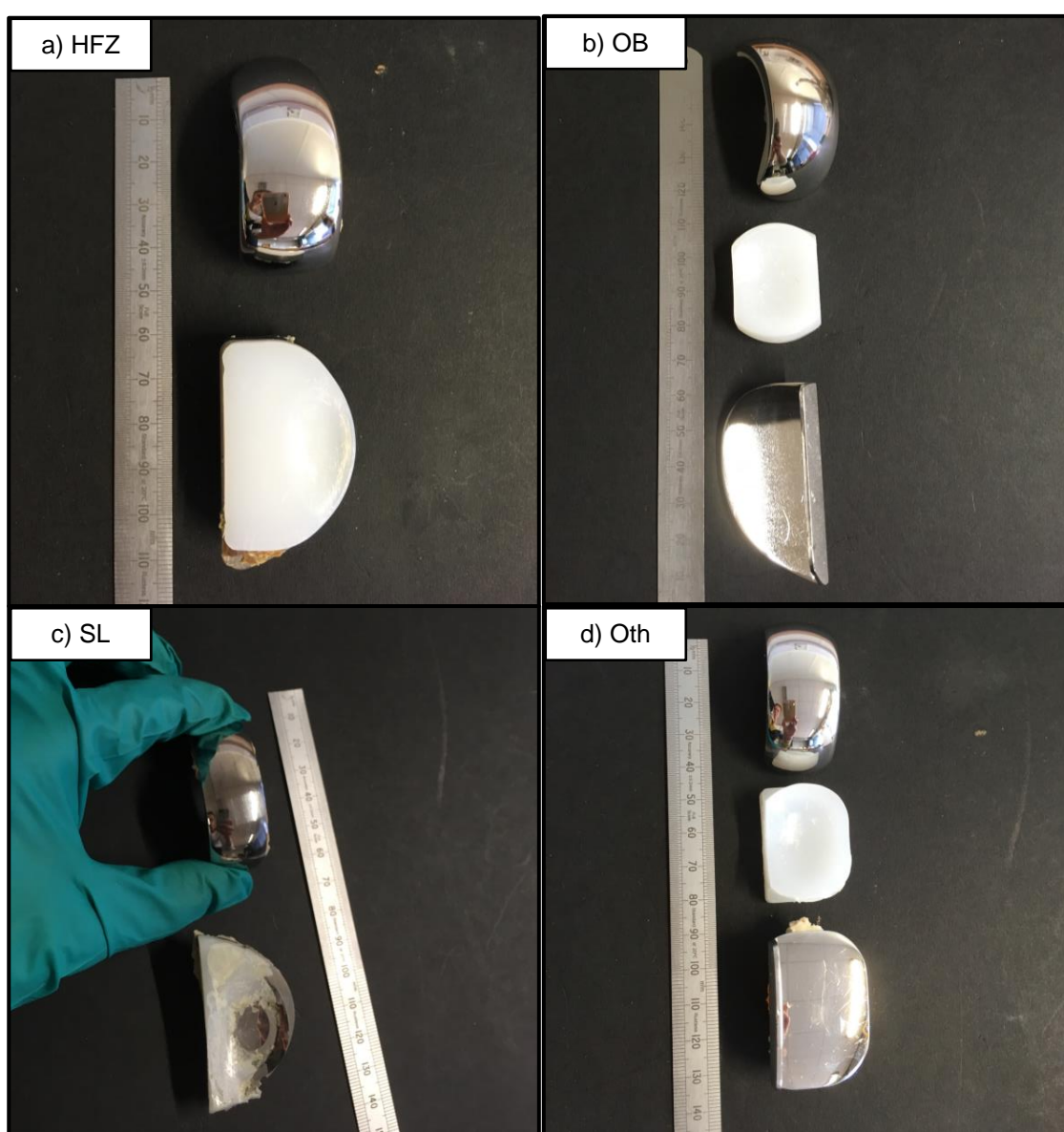


Figure 3.3 Example explanted HFZ, OB, SL and Oth UKRs

Five retrieved knee replacement prostheses with OxZr femoral components were identified within the catalogue and these are all shown in Figure 3.4. These included three Oxinium® (Smith & Nephew, Warsaw, London, UK) TKRs, two Genesis II and one Legion TKR, and two Oxinium® Journey UKRs. The results of the surface topographical analysis of these retrieved TKRs and UKRs are included in Chapter 6. The results of selected retrieved TKRs and UKRs with CoCr femoral components are also included in Chapter 6 for comparison.

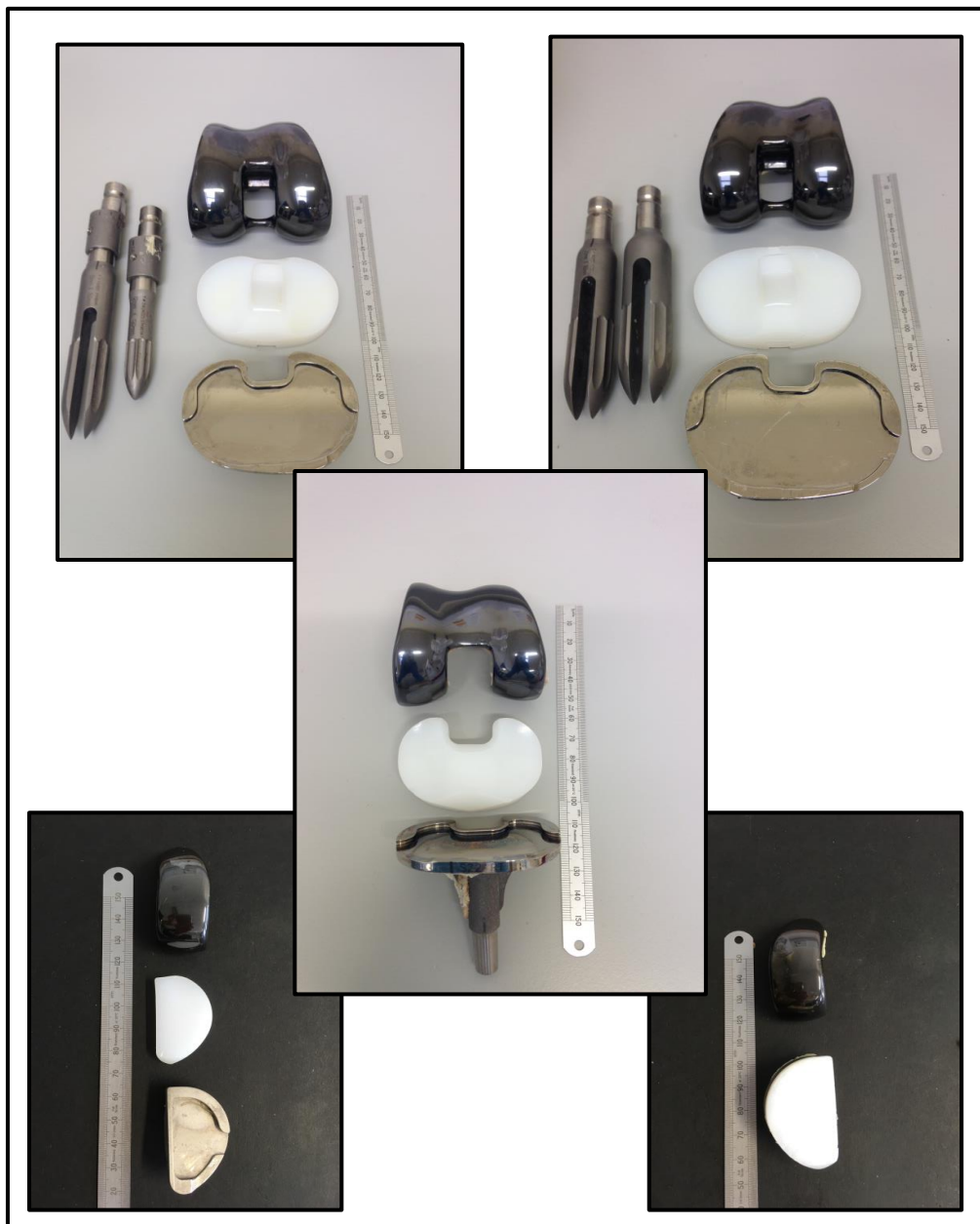


Figure 3.4 Explanted TKRs and UKRs with OxZr femoral components

There were four retrieved explanted OxZr patellofemoral components that have been retrieved, processed and catalogued as part of this project but not analysed within the scope of this thesis.

There was very limited information regarding the exact models or sizes for any of the explanted prosthesis. This meant that sizes of the implants could only be assumed based on limited manufacturer's markings on the explanted prostheses and analyses of surface roughness results could not be compared with size of prosthesis. This did impact the analysis of results but again is not an issue that can be addresses within the scope of this thesis.

### **3.1.1 *Patient and Implant Variables***

Within the bounds of the ethical approval for this project, patient and implant data was sought and where available included in the Knee Explant Catalogue (See Appendix B). Of the one hundred and thirty-five explants collected between 2011 and 2016, 91% are TKRs, 6% are UKRs and 3% are patellofemoral revisions. Of the TKRs, 60% are cruciate retaining, 24% are posterior stabilised and 16% are of a hinged design. For the explants where information regarding the primary surgery indication was available, 86% were indicated for osteoarthritis, 4% for rheumatoid arthritis, 3% psoriatic arthritis, 3% ankylosing spondylitis, 1% fracture from trauma, 1% Still's Disease, 1% septic arthritis.

For the TKRs explants where the information regarding the indication for revision surgery was available the cited indications for revision were as follows: aseptic loosening 23%, instability 18%, PE component wear 17%, infection 16%, pain 15%, malalignment 3%, arthrofibrosis 3%, hypermobility 1%, fixed flexion / tight anterior compartment 1%, oversized implants / no range of motion 1%, periprosthetic fracture 1%.

As detailed above, there was limited patient information available for the UKRs explants (only 33% had patient and implant data). However, where it was available,

the cited indications for revision were pain 33%, and PE wear, tibial shelf collapse, metallosis, aseptic loosening and lack of extension (each 11%).

For the revisions where the data was available, 54% of the TKR revision patients and 41% of the UKR patients were male. For both TKRs and UKRs, 54% were performed on the right side of the body. The median BMI for the TKR patients was 30 (range 22 - 40). For the TKRs 97% were fixed using bone cement either on both or one of the femoral and the tibial component; all of the UKRs were fixed using bone cemented. The median age at primary surgery for TKR was 61 years (range 33.5 years – 84.25 years) and for UKR was 62 years (range 49.2 years – 73.6 years). The median time *in vivo* was 119 months (range 10 months – 264 months) for the TKRs and 125 months (range 25 months – 175 months) for UKRs.

### **3.2 Qualitative and Semi-quantitative Damage Assessment**

A macroscopic visual assessment of damage was performed for each component and the location and extent of any macroscopically visible damage was recorded in a written description.

#### **3.2.1 Femoral Damage Scoring (FDS)**

Following the principles of the methodology presented by Brandt et al [180] damage scoring was performed for the femoral components of the TKRs and UKRs to calculate femoral damage scores (FDS). The Brandt et al [180] method was chosen in an attempt to allow comparisons to be made between the results within this work and that already in the field.

The femoral components were divided into eight sections for TKRs (Figure 3.5) and four sections for UKRs (sections 1-4 shown in Figure 3.5). For each section, three damage features, gouging, burnishing and indentations were assessed and three Damage Feature Scores (DFS) were calculated. As per Brandt et al [180] gouging was defined as deep scratches caused by third-body wear. Burnishing was defined as an area in the anterior- posterior direction of fine scratches and was identified by a



macroscopically visible change in reflectivity, these areas are also described as “damage tracks” in the macroscopic visual assessment. Burnishing was also used to describe the areas of damage from unintended metal on metal articulation of the femoral component with the tibial component resulting from PE wear through. Indentations or small pits caused by third body debris and light scratching also caused by third body debris were classed together as the same Damage Feature as defined in Brandt et al [180].

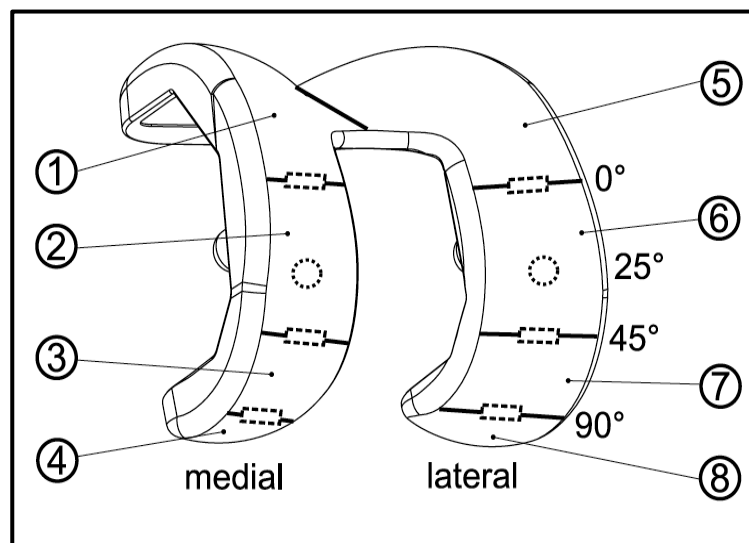


Figure 3.5 Damage areas on a cruciate retaining TKR femoral component [180]

The DFS is calculated as the product of an area score and a severity score. The area score is a numeric 0 – 10 assigned based on the percentage area within the section that the damage feature covers. The area scores are 0 for no coverage, 1 for under 10% coverage, 2 for above 10% and up to 20%, 3 is for above 20% and up to 30% so on until 10 is above 90% and up to 100%. The severity score is also a numerical value assigned based on how visible the damage feature is. If the damage feature is not visible the severity score of 0 is assigned, if it is just visible the severity score assigned is 0.33, clearly visible and a severity score of 0.66 is assigned and severe damage visible is assigned a severity score of 1. It is very important to note that the arbitrary severity scores of 0.33 and 0.66 have nothing to do with accuracy or precision but are purely an assigned value according to the methodology selected.

When the results are reported for the FDS and DFS they will have data to 2 decimal places but only because of this scoring system. As noted earlier, these methods were selected in an attempt to try to allow comparisons to be made between the results within this thesis and the existing literature.

The total FDS is the sum of the three DFS in each of the eight areas. The maximum FDS for a TKR femoral component is 240 (i.e.  $10 \times 3 \times 8$ ) and for a UKR femoral component is 120 (i.e.  $10 \times 3 \times 4$ ).

### **3.2.2 PE Articular Surface Damage Scoring (PE ADS)**

The semi-quantitative Hood technique [194] is considered to be the most widely used scoring system and the most easily comparable with published literature [15, 164, 195, 196]. The Hood damage scoring method was applied to the articulating surface of the PE component to determine a PE Articular Surface Damage Score (PE ADS). The Hood damage scoring method was chosen to be used to allow comparisons to be made between the results within this thesis and the existing literature.

In the Hood technique[194], the articulating surface of a TKR PE component is divided into ten sections as shown in Figure 3.6. For UKR PE components the articulating surface was divided into just four sections (sections 0 – 3 as shown in Figure 3.6). Within each section, for each of seven damage features (deformation, pitting, embedded debris, scratching, burnishing, abrasion and delamination/subsurface cracking), a Damage Feature Score (DFS) of 0, 1, 2 or 3 is assigned corresponding to the percentage area of the section the damage feature covers. The definitions of the damage features are detailed in Table 3.1.

If the damage feature is estimated to cover less than 10% of the section a damage feature score (DFS) of 1 is recorded, if the damage feature is estimated to cover between 10 and 50% of the section a DFS of 2 is recorded and if more than 50% of the section is covered by the identified damage feature a DFS of 3 is recorded. The sum of the grades for each damage feature in each section gives the PE ADS. For

TKR PE components the maximum possible PE ADS would be 210 and for UKR PE component the maximum possible PE ADS would be 84.

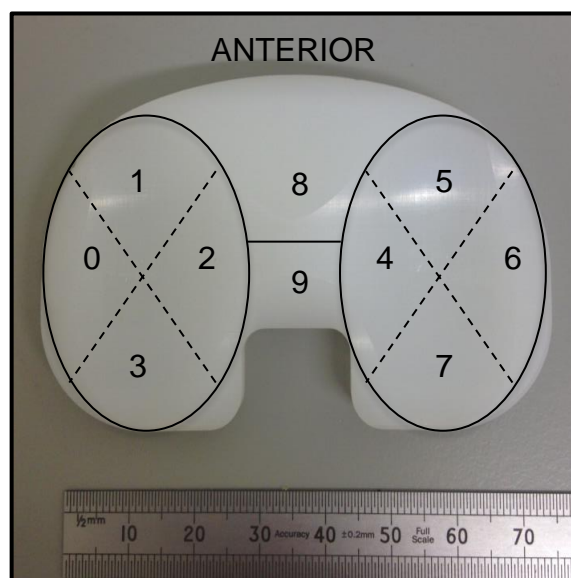


Figure 3.6 Damage areas on the articular surface of a cruciate retaining TKR PE component

### 3.2.3 PE Backside Damage Scoring (PE BDS)

A modified version of the method described by Brandt et al [200] was used to calculate a PE Backside Damage Score (PE BDS) for the distal surface of the PE component.

The backside surface of the PE component was divided into six sections for TKR PE components and four sections for UKR PE (see Figure 3.7). Within each section, six damage features, burnishing, scratching, indentations, surface deformation, pitting and stippling, were assessed and six Damage Feature Scores (DFS) were calculated. The definitions of the damage features are given in Table 3.1.

As for the femoral damage scoring method described above, a DFS is calculated as the product of an area score and a severity score. The area score is a numeric 0 – 10 assigned based on the percentage area within the section that the damage feature covers. The area scores are 0 for no coverage, 1 for under 10% coverage, 2 for

above 10% and up to 20%, 2 is for above 20% and up to 30% so on until 10 is above 90% and up to 100%. The severity score is also a numerical value assigned based on how visible the damage feature is. If the damage feature is not visible the severity score is 0, if it is just visible, the severity score is 0.33, clearly visible is assigned 0.66 and severe damage visible is assigned a severity score of 1. In a similar manner to the FDS, the PE BDS uses the arbitrarily assigned severity scores of 0.33 and 0.66. When the results are reported they will have data to 2 decimal places but only because of this scoring system.

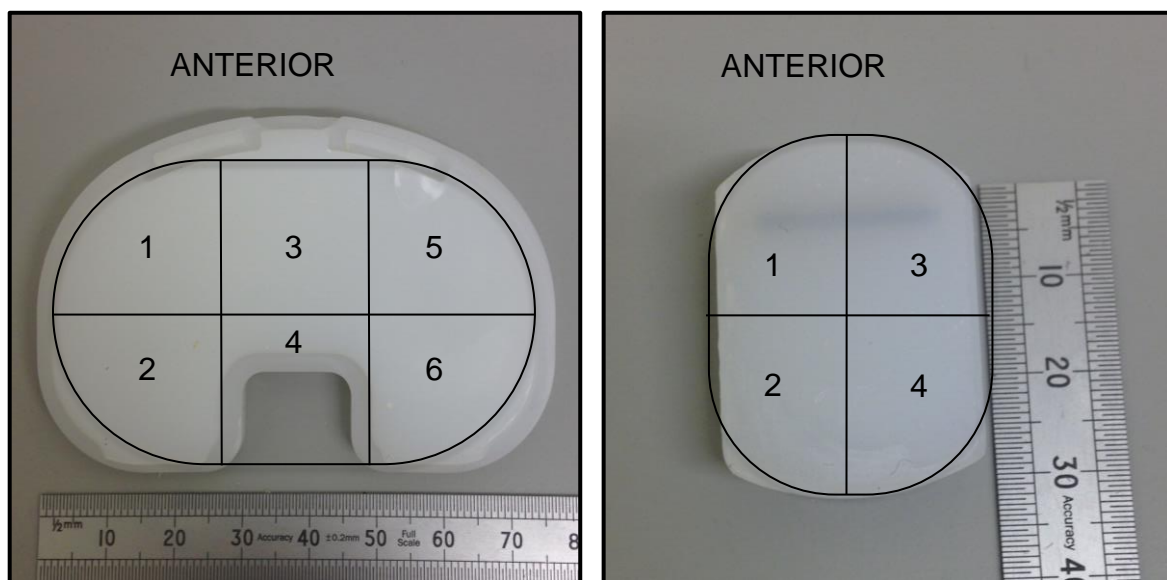
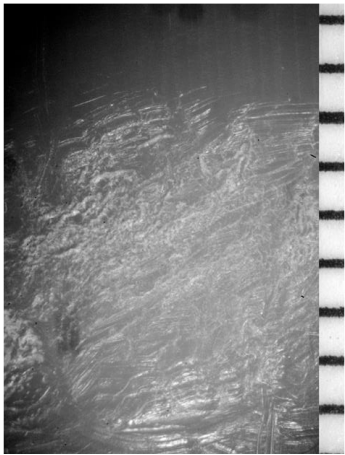
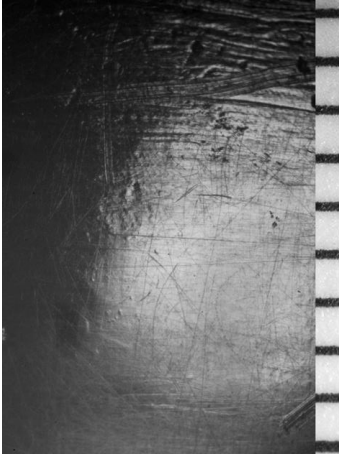
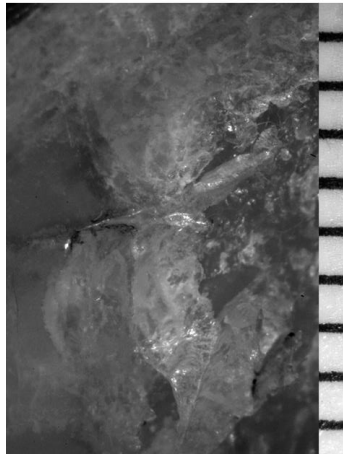
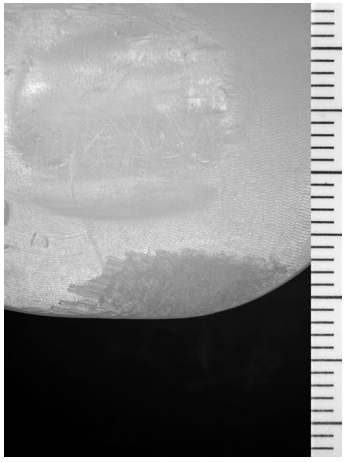
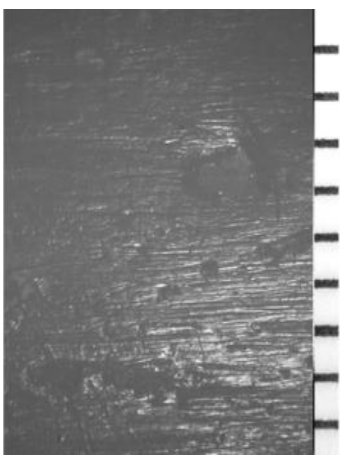



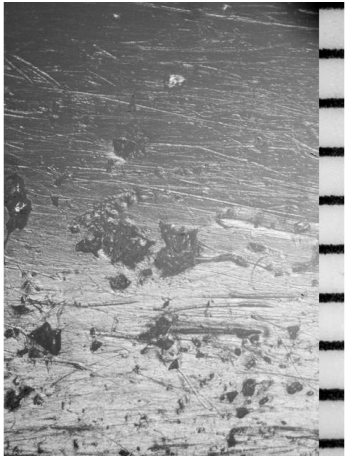
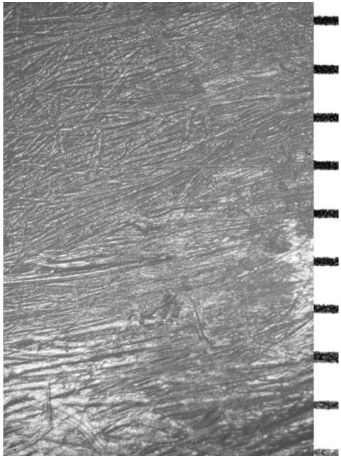
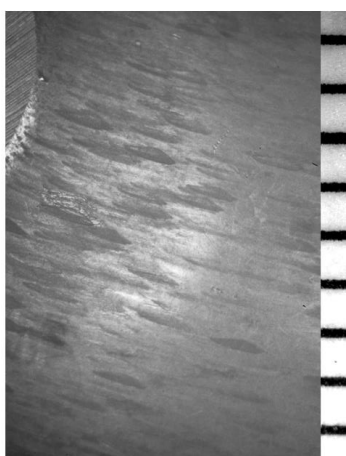
Figure 3.7 Damage areas on the backside surface of a TKR and UKR PE component

The total PE BDS is the sum of the six DFS values in each of the six areas for TKRs and four areas for UKRs. The maximum PE BDS for a TKR PE component is 360 (i.e.  $10 \times 6 \times 6$ ) and for a UKR femoral component is 240 (i.e.  $10 \times 6 \times 4$ ).

Table 3.1 PE articular surface and backside surface damage mode descriptions and identification. Images show 1mm scale. Images from Harman et al 2011 [206]

Damage Mode	Description	Identification (Scale 1mm)
<u>Abrasion</u>	Abrasion is identified as areas where the PE has a rough, shredded or tufted appearance with limited directionality and with a change in colour of the PE from white to yellow.	
<u>Burnishing</u>	Burnishing is characterised by the observation of highly polished areas with a visibly increased reflectivity in comparison to the surrounding PE material.	
<u>Delamination / Subsurface cracking</u>	Delamination is observed where layers of PE material are separated and removed from the original surface, leaving an exposed surface. It may appear as a peeling of the PE. Subsurface cracking is where fatigue occurs to the PE below the original surface and is observed as a change in colour of the PE from white to yellow. Subsurface cracking often precedes delamination.	

Damage Mode (cont.)	Description (cont.)	Identification (cont.)
<u>Deformation</u>	<p>Surface deformation is observed as permanent deformation resulting in a change in the surface geometry. It is sometimes referred to as “plastic deformation” or “creep”. There is no material removal just a change in geometry. It is observed macroscopically and not typically associated with a change in colour of the PE. On the PE backside surface this can be the impression of screw holes from the tibial tray.</p>	
<u>Embedded Debris</u>	<p>Embedded debris are identified by areas that differ in colour and / or relative texture to the surrounding PE surface consistent with embedded third-body particles of suspected bone, cement or possibly metal.</p>	
<u>Indentations</u>	<p>Indentations are defined as non-uniform more pronounced scratches suspected to be the result of trapped third-body abrasions. Identified on the distal PE backside surface. Subsurface cracking often precedes delamination.</p>	

Damage Mode (cont.)	Description (cont.)	Identification (cont.)
<u><b>Pitting</b></u>	Pitting is visualised as depressions in the PE surface. Typically, the pits are between 1-2 mm in diameter, but they may be much larger with 20-30mm diameters. Within the pits the surface of the PE is burnished and very reflective.	
<u><b>Scratching</b></u>	Scratching is identified as thin indented lines which may be either ordered in the anterior / posterior direction or may be irregular in direction.	
<u><b>Stippling</b></u>	Stippling is uniquely identified on the distal PE backside surface and is visualised as short (approximately 1-2mm) unidirectional scratches often in a circumferential pattern.	

It is acknowledged that semi-quantitative damage scoring methods have inherent inter- and intra-user variabilities. During the preparation of the data for the publication Scholes et al 2012 (Appendix H) [15] the semi-quantitative damage scoring method was used by two authors Scholes & Kennard for over thirty explanted prostheses. Comparisons of the results of the two authors were made in an attempt to assess the differences and validate the method. The guidance provided in “A pictographic atlas for classifying damage modes on polyethylene bearings” by Harman et al (2011) [206] was used to help minimise the differences between the assessors and to try to reduce the intra and inter-user variability of the application of this method. The output of this attempt at a validation exercise was that the most important aspect was a clear definition of the damage modes as in Table 3.1.

This said however, it was not possible to create a table similar to Table 3.1 with images of the femoral damage modes used in the FDS method. This was because the images were not of a high enough quality to capture the damage mode appropriately. The CoCr femoral components were highly reflective and the black appearance of the OxZr femoral components made it not possible to capture the damage modes on images. In this situation a written description had to be relied on to convey the detail of the damage mode. This is not a wholly satisfactory situation but could not be helped given the constraints of the imaging capabilities.

The specific limitations of semi-quantitative damage scoring methods are discussed in more detail in Section 7.4 Limitations and Practical Constraints sub-section 7.4.2 Damage Scoring.

### **3.3 Surface Roughness Measurement**

Surface roughness measurements were taken using a NewView 5000 (ZYGO, Middlefield, Connecticut, USA) non-contacting white light interferometric profilometer as used in previous published studies [14, 15, 32, 198, 226, 227] (See Figure 3.8).

Measurements were taken on the femoral condyles, proximal tibial tray surface, and the distal backside surface of the PE components of retrieved prostheses.



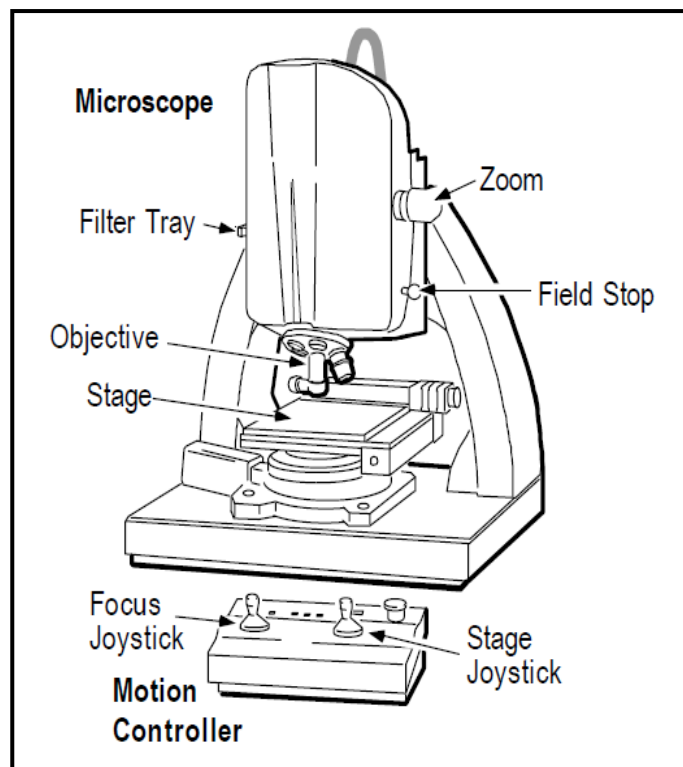


Figure 3.8 Schematic of a Zygo NewView 5000 profilometer [82]

On each retrieved femoral condyle fifteen measurements were taken on the most macroscopically visually damaged areas that were considered to have been *in vivo* damage. This resulted in thirty measurements taken per component for TKRs and fifteen measurements per component for UKRs [15]. The femoral components were macroscopically assessed with the corresponding PE components to determine whether damage was considered *in vivo* damage or retrieval damage. Damage on the femoral component that did not have any macroscopically visible resulting damage on the PE component and that was not consistent with the articulation of the component was considered to be retrieval or handling damage and was not included in the assessment. New, unopened as-manufactured femoral components were used as reference components; thirty measurements were taken on each reference femoral component [14].

On the retrieved tibial tray components where the proximal surface was able to be accessed, six measurements were taken per retrieved component. Six measurements were also taken on the distal backside surface of the PE components.

The measurements were taken in the areas that corresponded to the sections defined in the PE backside damage scoring method described above.

### **3.3.1 Roughness Parameters**

Based on the BS EN ISO 25178:2 [75] guidelines and the definitions within MetroPro Reference Guide Version 9.0 OMP-0347M [87] the following roughness parameters were recorded from the MetroPro Software Version 8.0.3:

Root-mean-square surface roughness  $S_q$ ; maximum peak height  $S_p$ ; maximum valley depth  $S_v$ ; peak to valley height PV; 10-point height average  $S_z$ ; surface kurtosis  $S_{ku}$ ; and surface skewness  $S_{sk}$ . These roughness parameters are defined in Section 2.2.2 Surface Roughness Parameters.

### **3.3.2 Measurement Controls**

Based on previous published studies [15, 226, 227] and the MetroPro software guidelines [87], measurement controls were selected. A 10X objective lens with a x2 optical zoom was used to give an area of view of 317 x 238 mm. A scan length of 100  $\mu\text{m}$  used for the CoCr femoral components and the tibial trays while for the PE components a scan length of 150  $\mu\text{m}$  was selected. For the measurement of CoCr and OxZr femoral components and polished tibial trays, a minimum modulation percentage (Min Mod%) of 15% was selected, however this was reduced to 4% when measuring non-polished tibial trays and as low as 2% when attempting to measure the PE component surfaces. These are the measurement controls used within the published studies, Scholes et al [15], Kennard et al [14] and Smith et al [32].

As explained in Section 2.2.3 Surface Roughness Measurement the minimum modulation percentage is the minimum percentage change of wavelength that the user determines that the measurement software should consider as true roughness and not noise. The value is linked to the reflectivity and roughness of the sample [87]. The scan length determines the profilometer's ability to measure surfaces with deep

valleys and high peaks. A longer scan length can capture more data however its use can be considerably more time consuming.

### **3.3.3 Analysis Controls**

For the curved surfaces of the femoral condyles a form filter of “remove cylinder” was applied to filter the effects of the curvature of the sample. For the measurement of the proximal surface of the tibial tray components and the distal backside surface of the PE components that were non-curved, a “remove plane” form filter was applied to filter the effects of the sample not being positioned perfectly perpendicular to the lens. Again, these are the analysis controls used within the published studies, Scholes et al [15], Kennard et al [14] and Smith et al [32].

For the CoCr and the OxZr femoral components and the polished tibial tray components a “remove spike” filter was applied, as was a “data fill filter” was also applied.

### **3.3.4 Challenges of Performing Non-contacting Profilometry on Knee Replacement Prostheses.**

There are numerous practical considerations that make performing non-contacting profilometry on knee replacement prostheses challenging and are important to consider within the context of this thesis. In addition to the appropriate selection of the measurement and analysis controls of the profilometer and the profilometer software, the physical positioning of the components for analysis by the Zygo poses a challenge simply due to the size and the changing radii of the knee prostheses femoral and PE bearing components. The length of time that each measurement takes due to the set up must be noted as it is a time-consuming and laborious process. The limitations and practical considerations associated with using the Zygo NewView 5000 for measurement of knee replacement prostheses are discussed in more detail in Section 7.4 Limitations and Practical Constraints sub-section 7.4.3 Surface Roughness Measurement. Figure 3.9 shows the Zygo NewView being used to take a surface roughness measurement on an OxZr femoral component (left

image) and on a CoCr femoral component (right image). The varying radii of these components can be seen in both images.

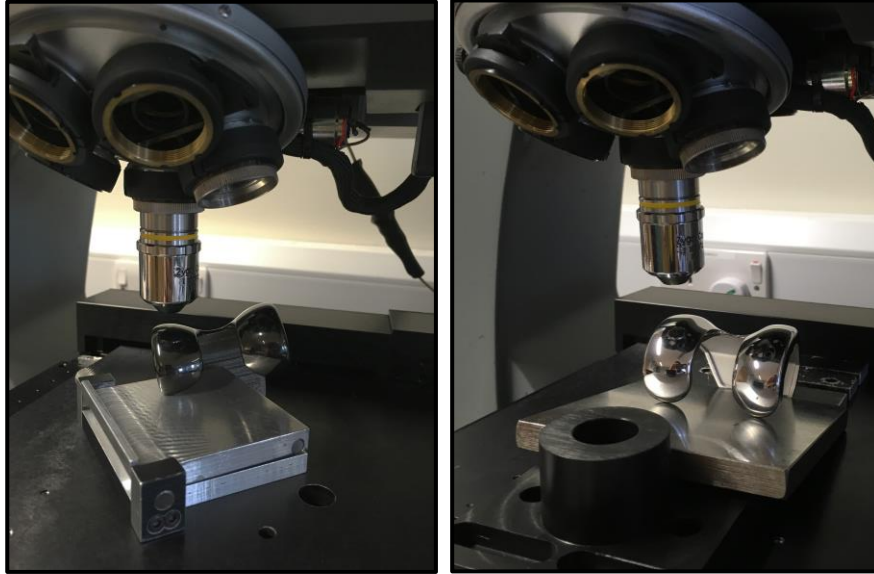


Figure 3.9 OxZr and CoCr femoral component positioned on the Zygo NewView 5000 platform

### 3.4 Statistical Analysis

The surface roughness data collected was analysed using statistical software programme Minitab® 18. For the non-contacting profilometry results, the mean values were calculated and cited with standard error (SE) for the following surface roughness parameters (as defined in Section 2.2.2 Surface Roughness Parameters):

- Root-mean-square surface roughness  $S_q$
- Maximum peak height  $S_p$
- Maximum valley depth  $S_v$
- Peak to valley height PV
- 10-point height average  $S_z$
- Surface kurtosis  $S_{ku}$
- Surface skewness  $S_{sk}$

An Anderson-Darling normality test was used to identify non-parametric data and Mann-Whitney tests were applied to detect significant differences between the surface roughness parameters of retrieved and reference components and also

between the surface roughness parameters of different groups of retrieved components. The level of statistical significance was considered at  $p < 0.05$ . Should a p-value of less than 0.05 be identified this would indicate that the two considered parameters were statistically significantly different.

Simple regression analysis was used to determine any correlations between results. An  $r^2$  value was quoted to provide an indication of the strength of the relationship.

The statistical analysis is limited as the data was identified as non-normal. There were also in some cases low numbers of data measurement points for analysis. This is acknowledged as a limitation and must be taken into consideration when reporting whether the differences are considered significant or not and when considering any relationships identified.

### **3.5 Presentation of Results**

As described above in Section 3.1, the explanted prostheses were grouped into three collections and the analysis results are presented in the three results chapters. The results chapters are Chapter 4 Surface Topographical Analysis of Explanted Total Knee Replacements with Cobalt Chromium Alloy Femoral Components, Chapter 5 Surface Topographical Analysis of Explanted Unicondylar Knee Replacements with Cobalt Chromium Alloy Femoral Components and Chapter 6 Surface Topographical Analysis of Explanted Knee Replacement Prostheses with Oxidised Zirconium Femoral Components.

Within each of these chapters the implants that are analysed and the associated patient variables are detailed. A written description of the macroscopic visual assessment and the Semi-Quantitative Damage Scoring results are provided in a tabulated form including the FDS, PE ADS and PE BDS for each component. Within the tabulated damage scoring results the FDS and PE BDS scores are provided as numbers with two decimal places. As detailed above the FDS and PE BDS both methods use arbitrarily selected severity scores of 0.33 and 0.66. These are purely

assigned values according to the methodologies selected and have no bearing on the precision and accuracy of the results.

The non-contacting profilometry results are presented in tabulated form and examples of the surface topography plots provided by the Zygo user interfacing software, MetroPro are used to illustrate the results. The reported resolution of the Zygo NewView 5000 is greater than 1 nanometre (nm) and hence throughout this thesis the surface roughness parameter measurement results are recorded as microns ( $\mu\text{m}$ ) to 3 decimal places, e.g.  $S_q = 0.341 \mu\text{m}$ .

Figure 3.10 shows the example surface topography plots that are the visual outputs from the Zygo NewView 5000 non-contacting white light profilometer.

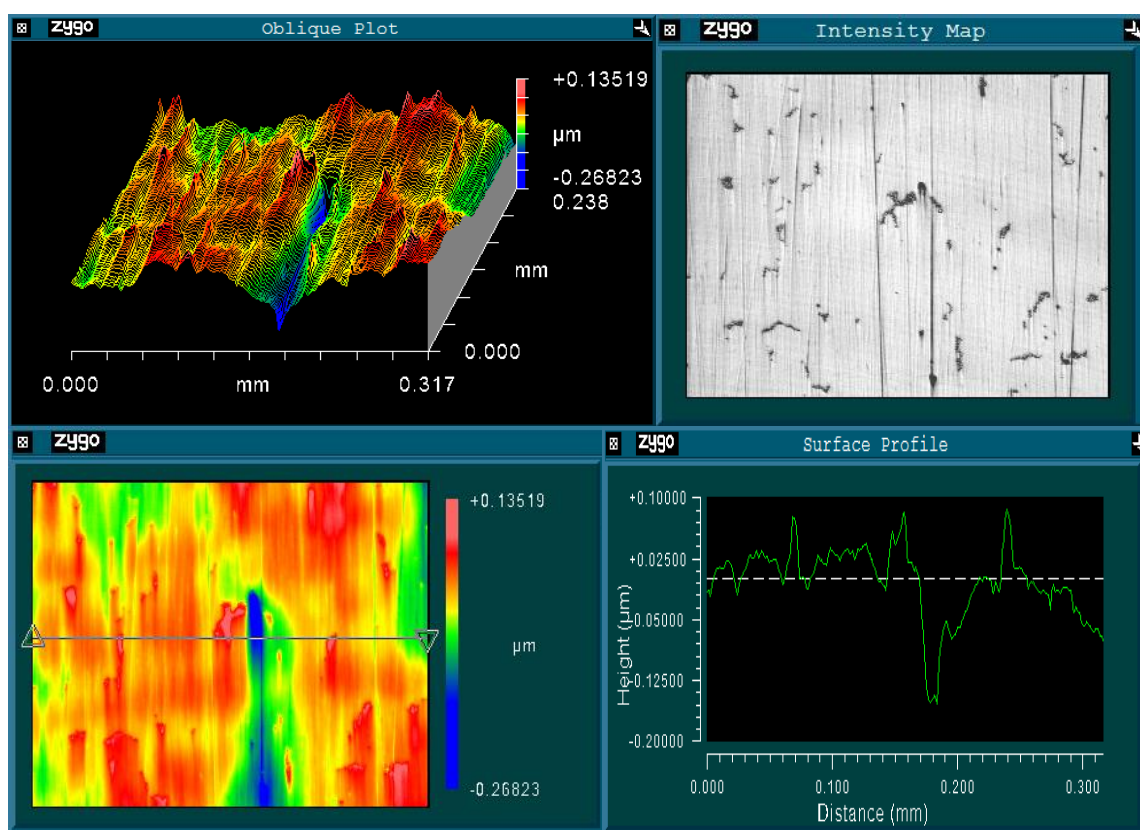


Figure 3.10 Example of a surface topography plot from the MetroPro software

Within Figure 3.10 there are four images which include in the top left a 3D oblique plot of the area of view (typically, this area is  $317 \mu\text{m} \times 238 \mu\text{m}$  but this is determined by the magnification and zoom setting selected). This 3D oblique plot is colour coded

along the scale on the right. In the top right there is 2D greyscale intensity map of the area of view. In the bottom left is a 2D 'heat map' of the area of view which is also colour coding against the scale to the right there is a line of interest crossing this plot. The graphical representation shown in the bottom right is the cross-sectional surface profile where that line of interest intersects the area of view.

Within each of the three results chapters the semi-quantitative results of the FDS, PE ADS, and PE BDS are compared with the patient and implant variables and the non-contacting profilometry results. And any relationships are illustrated in graph format.

*Blank page*



## **Chapter 4 Surface Topographical Analysis of Explanted Total Knee Replacements with Cobalt Chromium Alloy Femoral Components**

The surface topographical analysis results of retrieved explanted Total Knee Replacement (TKRs) prostheses with cobalt chromium alloy (CoCr) femoral components are presented in this chapter. The methods described in Chapter 3 Materials and Methods were used to collect the results. The patient and implant variables of the retrieved explanted TKRs analysed are detailed. The macroscopic observations, damage scoring results, and surface roughness measurements for the femoral components, the PE components and the tibial components of the selected explanted TKRs are included. A comparison between the surface roughness measurements of retrieved explanted components and reference components is made. The damage scoring results, surface roughness measurements and patient and implant variables are correlated and where applicable relationships between results are identified. The retrieved explanted components shall hereby be known as “retrievals” or “retrieved components”.

### **4.1 Implant and Patient Variables**

The results of the analysis of forty retrieved TKRs are presented within this chapter. The selection criteria of the retrieved explanted TKRs analysed is detailed in Chapter 3. The group of forty retrieved TKRs includes ten AGC ® (AGC) (Zimmer Biomet, Warsaw, IN, US), fifteen PFC Sigma ® (PFC) (DePuy, Warsaw, IN, US) and fifteen Kinemax Plus (K+) ® (Stryker, Mahwah, NJ, US). These retrieved TKRs all have CoCr femoral components and modular fixed bearing PE components. All were implanted using cemented fixation of the femoral or tibial component or both. The PFC retrievals (n=15) and K+ retrievals (n=15) were all of cruciate retaining (CR) designs; the AGC retrievals (n=10) contained one posterior stabilised (PS), two partially stabilised designs and seven CR designs.

Four new, unopened boxed femoral components, two DePuy PFC ® and two Stryker Kinemax ®, were available to be used as references. Two new as-manufactured,

unopened PE component (Stryker Kinemax ®) and one new as-manufactured, unopened tibial component (Stryker Kinemax ®) were available to be used as reference components. These components shall hereby be known as “reference components”.

Figure 4.1 shows one of each of the models of retrieved TKRs, these are typical of each of the designs.

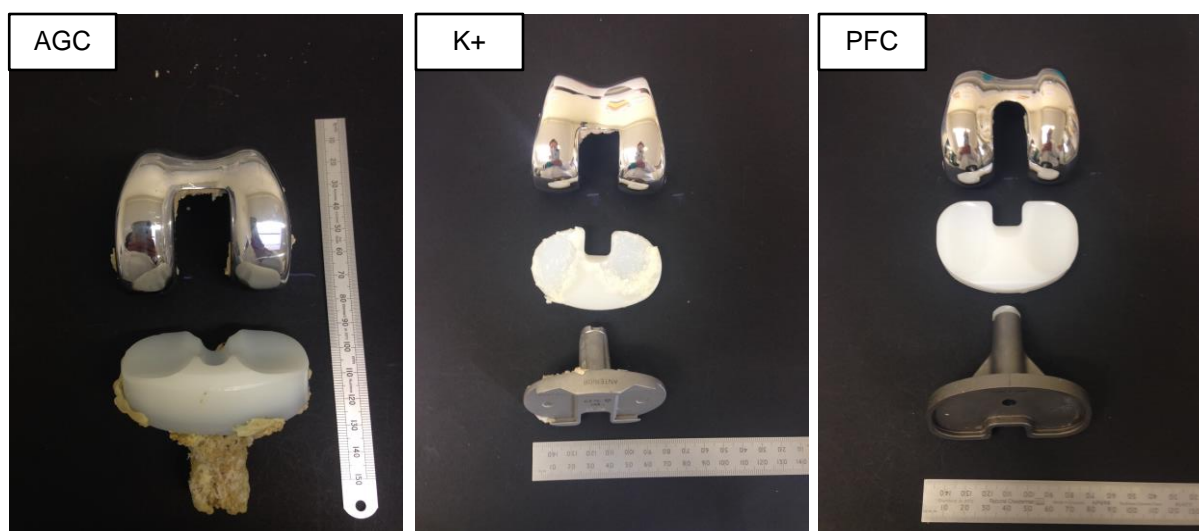


Figure 4.1 Retrieved AGC, K+ and PFC TKR components

The patient and implant variables for the retrieved TKRs are detailed in Table 4.1. The mean date of implantation was separated by ten years with the K+ prostheses being implanted between 1991 and 2005 (mean = 1998), the AGC prostheses being implanted between 1991 and 2009 (mean = 2002) and the PFC prostheses being implanted between 2000 and 2014 (mean 2008).

The details of the PE component material properties (i.e. use of XLPE and stabilising additives) and the details of the sterilisation and packaging of the PE components are not available. Components implanted prior to the mid-1990s may have been gamma sterilised in air and therefore may have been affected by *in vivo* or pre-implantation oxidation of the PE. Components implanted after the mid-2000s may be manufactured using XLPE and may contain stabilising additives.

Table 4.1 TKR Implant and Patient Variables

	<b>AGC ® (n = 10)</b>	<b>PFC Sigma ® (n = 15)</b>	<b>Kinemax + ® (n = 15)</b>
<b>Side of implantation</b>	6 Right 4 Left	8 Right 7 Left	8 Right 7 Left
<b>Patient gender</b>	5 Female 5 Male	8 Female 7 Male	6 Female 9 Male
<b>Mean patient BMI</b>	Data not available	33.9 (27.5 – 43.6) kg/m <sup>2</sup>	29.4 (21.5 – 41.1) kg/m <sup>2</sup>
<b>Mean year of implantation</b>	2002 (1991 – 2009)	2008 (2000 – 2014)	1998 (1991 – 2005)
<b>Mean patient age at primary surgery</b>	58 (50 – 79) years	66 (50 – 82) years	57 (38 – 71) years
<b>Mean Patient age at revision surgery</b>	69 (56 – 81) years	71 (54 – 85) years	72 (54 – 86) years
<b>Mean time <i>in vivo</i></b>	135 (16 – 241) months	67 (11 – 163) months	181 (110 – 240) months
<b>Indication for implantation</b>	Osteoarthritis = 10	Osteoarthritis = 13 Rheumatoid Arthritis = 1 Trauma = 1	Osteoarthritis = 9 Rheumatoid Arthritis = 2 Psoriatic Arthritis = 2 Ankylosing Spondylitis = 1 Still's Disease = 1
<b>Indication for revision (multiple reasons cited for some cases)</b>	Aseptic loosening = 7 Instability = 4 Pain = 4	Instability = 4 Component malalignment = 3 Aseptic loosening = 3 Arthrofibrosis = 2 Pain = 2 Infection = 2 Fixed flexion / tight anterior compartment = 1 PE wear = 1	PE Wear = 11 Aseptic loosening = 4 Instability = 5 Pain = 2 Infection = 1

The mean time *in vivo* for the AGC and K+ prostheses was fifteen years and eleven years respectively which are both greater than the mean time *in vivo* for the PFC prostheses which was five and a half years. All revisions of K+ prostheses except two, and all revisions of AGC prostheses except three, cited PE wear and/or aseptic loosening as an indication for revision. Only three of the PFC revisions cited PE wear and / or aseptic loosening as an indication for revision. The mean BMI for PFC patients (33.9) was greater than the BMI of K+ patients (29.4), There was no data available for the BMI values for AGC patients.

## **4.2 Macroscopic Visual Assessment and Semi-quantitative Damage Scoring**

Macroscopic visual assessments of the surfaces of the femoral condyles and articulating and backside surfaces of the PE components and the tibial trays were performed. The AGC components are designed so that the PE component is moulded to the tibial component and therefore for these components the PE backside and tibial tray were not able to be assessed. A summary of the assessments is given in the subsections below and the full assessments are tabulated in Table C1, Appendix C.

Femoral component damage scoring and PE articular surface damage scoring was performed for all the retrieved TKRs prostheses as per the methods described in Chapter 3. PE backside damage scoring was performed for the K+ and the PFC retrieved prostheses. The results are summarised in Table 4.2 where the FDS, PE ADS and PE BDS are provided for each component and the mean and median values are calculated. The results are described in more detail in the subsections below. In Table 4.2 it is important to note that the two decimal places of the FDS and PE BDS have no bearing on the level of precision and accuracy of the methodologies. In both the FDS and PE BDS methods, the arbitrary values of 0.33 and 0.66 are used to provide quantification of the severity score. Where the damage mode being just visible is assigned the numeric 0.33, the damage mode clearly visible is assigned 0.66 and where there is severe damage visible a numeric 1 is assigned.

Table 4.2 FDS, PE ADS and PE BDS for Retrieved TKRs

AGC	FDS	PE ADS	PFC	FDS	PE ADS	PE BDS	K+	FDS	PE ADS	PE BDS
AGC 1	22.45	24	PFC 1	3.33	27	28.38	K+1	8.27	71	28.74
AGC 2	27.09	26	PFC 2	3.96	16	2.64	K+2	36.52	86	19.80
AGC 3	6.60	77	PFC 3	2.97	35	18.81	K+3	12.61	86	20.87
AGC 4	13.25	58	PFC 4	7.31	24	0.33	K+4	27.21	62	17.18
AGC 5	27.52	46	PFC 5	2.98	25	1.32	K+5	12.26	53	15.20
AGC 6	30.60	62	PFC 6	3.99	26	1.65	K+6	6.66	61*	11.22*
AGC 7	29.07	50	PFC 7	9.00	26	34.32	K+7	26.97	90	14.52
AGC 8	24.90	69	PFC 8	6.99	15	2.64	K+8	4.95	74	16.17
AGC 9	9.24	55	PFC 9	2.31	12	2.64	K+9	36.17	72	15.21
AGC 10	27.84	28	PFC 10	2.97	12	0.00	K+10	8.31	65	16.21
			PFC 11	2.64	23	11.55	K+11	50.46	85*	20.81*
			PFC 12	4.62	24	3.30	K+12	27.88	69	16.51
			PFC 13	4.98	34	2.97	K+13	7.92	36	13.89
			PFC 14	2.31	26	17.16	K+14	7.27	37	13.88
			PFC 15	4.62	33	8.25	K+15	16.62	79	18.89
Mean	21.86	50	Mean	4.33	24	9.06	Mean	19.34	68	17.27
Median	26.00	53	Median	3.96	25	2.97	Median	12.61	71	16.21

\* The PE ADS and BDS for these two components may not be a true representation as part of the PE component was missing in some sections and could not be analysed.

### 4.2.1 Femoral Components

Damage considered to have occurred *in vivo* was observed on all of the retrieved femoral components. There was a noticeable difference in the macroscopic visual assessment of the three different designs and there is also a difference in the mean Femoral Damage Scores (FDS). The mean PFC FDS are lower than the means of the AGC and K+ FDSs. There was no observed difference between the FDS values on medial and lateral condyles. Figure 4.2 shows a typical component of each of the models of retrieved femoral components.

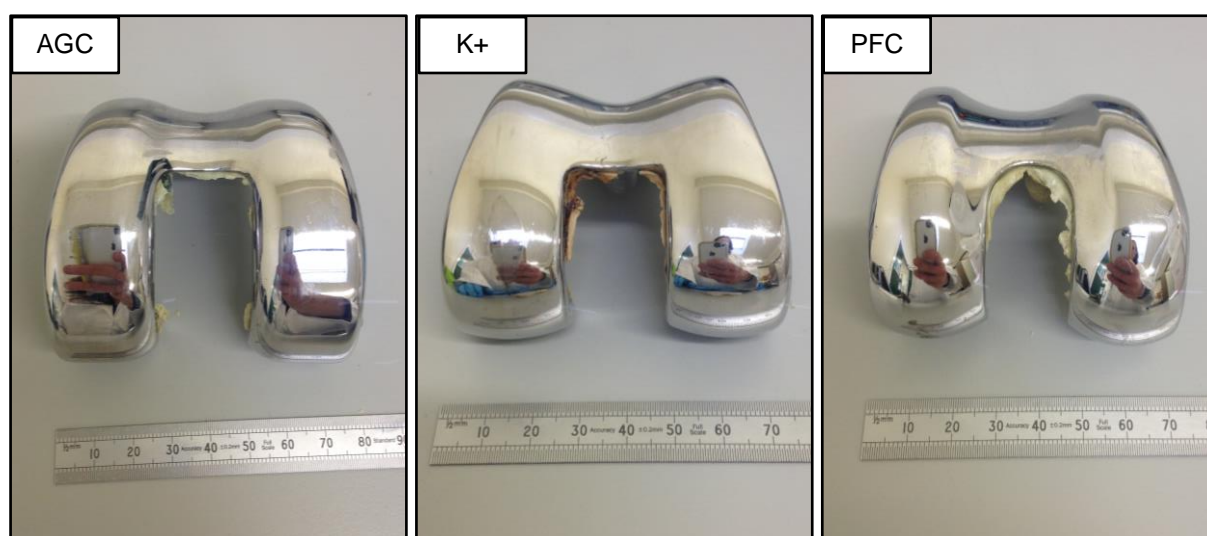


Figure 4.2 Retrieved AGC, K+ and PFC femoral components

The FDS and DFS median, maximum, minimum and inter-quartile ranges for femoral components of the retrieved AGC, PFC and K+ TKRs are shown in Figure 4.3 which is discussed in more detail below. Where there are less than three components the individual values are recorded in the place of the box and whisker plot.

The retrieved AGC femoral components showed the most damage with a mean FDS of 21.86 (range 6.60 – 30.9). All three damage features were identified on all AGC components with burnishing being the most prevalent, followed by gouging and then indentations and light scratching. The burnishing was observed as definite damage tracks on all AGC components. Three of the AGC components were observed to have deep scratches that are characterised as “wavy” which can be seen as the

outliers in Figure 4.3. The mean FDS for the retrieved K+ femoral components (mean 19.34 range 4.94 – 50.46) is not considered to be different from that of the AGC components however the distribution over the three damage features was different. Burnishing and gouging were the highest scoring damage features on the retrieved K+ femoral components, although not recorded on all components. Indentations and scratching gave a lower DFS but were seen on all components. High burnishing and gouging DFSs were assigned to five of the K+ components for damage that resulted from the articulation between the femoral and tibial components following complete PE component wear through. This can be seen as the outliers in Figure 4.3.

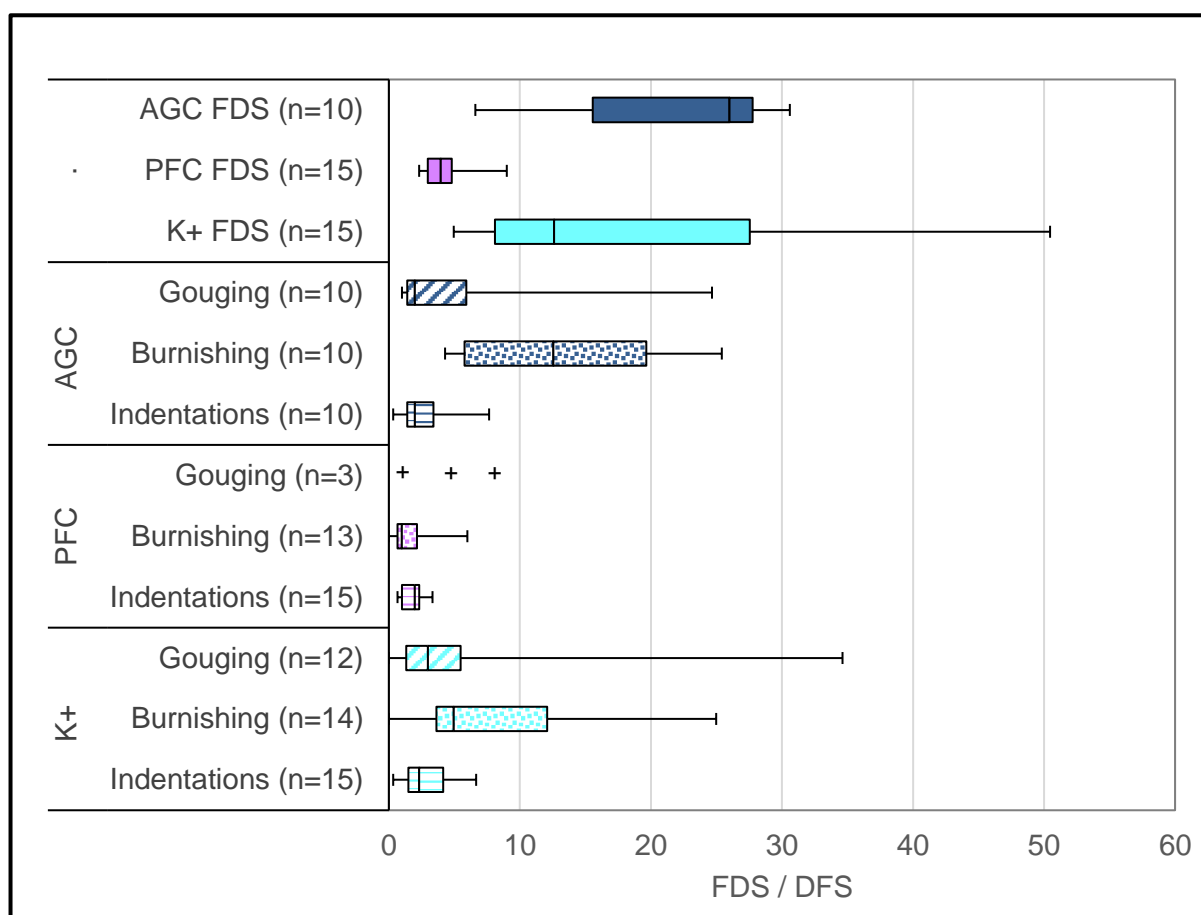


Figure 4.3 FDS & DFS for retrieved AGC, PFC & K+ femoral components

Three of the retrieved K+ components showed burnished damage tracks and two K+ components were observed to have deep scratches that gave a wavy appearance as seen on the AGC components. On two retrieved K+ components there was damage

identified posteriorly in high flexion that initially was thought to be retrieval damage however there is corresponding PE damage and is therefore is considered to have been on the component during the prosthesis time *in vivo*.

The retrieved PFC femoral components were observed to have the least damage with a mean FDS of 4.33 (range 2.13 – 9) which is lower than the FDS values for both the AGC and K+ components. All fifteen retrieved PFC femoral components were observed to have light scratches and indentations and thirteen were observed to have burnished damage tracks, although these were less severe than those observed on the AGC and K+ components. Only three PFC components were observed to have deep scratches defined as gouging.

#### **4.2.2 PE Components Articular Surface**

Damage considered to have occurred *in vivo* was observed on all the articular surface of all the retrieved PE components. There was a noticeable difference in the macroscopic visual assessment of the articular surfaces of the PE component of the three different designs of retrieved TKRs. The mean PE articular surface damage scores (ADSs) are different for all three models with the lowest scores being for the PFC PE components and the highest scores being for the K+ components. Figure 4.4 shows three of the retrieved PE components, one of each design and these are representative of a typical PE component for each of the designs.

The retrieved AGC PE components showed greater macroscopic damage than the PFC components but less than the K+ components. For the AGC PE components the mean ADS was 50 (range 24 – 77). The retrieved PFC PE components showed the least macroscopic damage and have the lowest mean ADS of 24 (range 12 - 35). The retrieved K+ PE components showed the greatest macroscopic damage and have the highest mean ADS of 68 (range 36 - 90). There is no difference between the ADS for the medial condyles and the lateral condyles for any of the three designs.



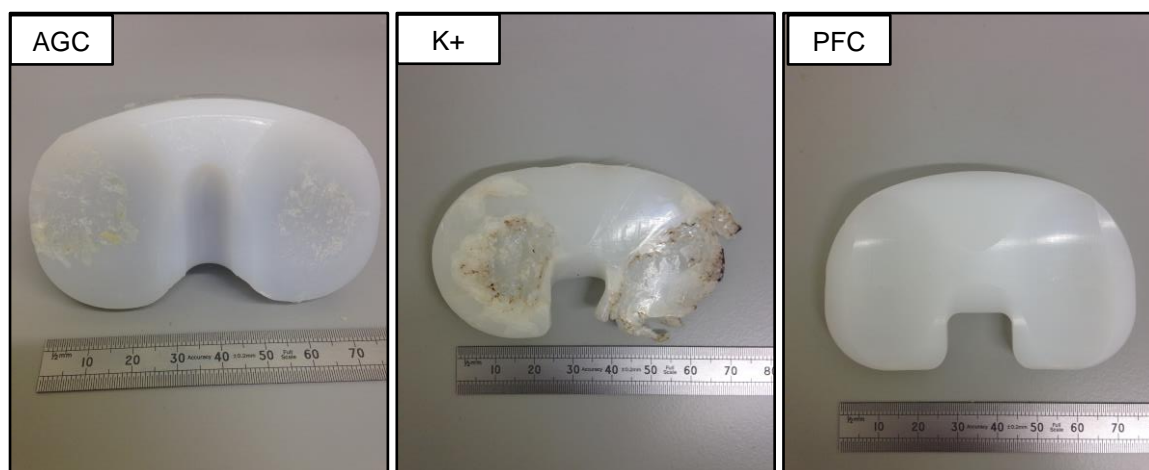
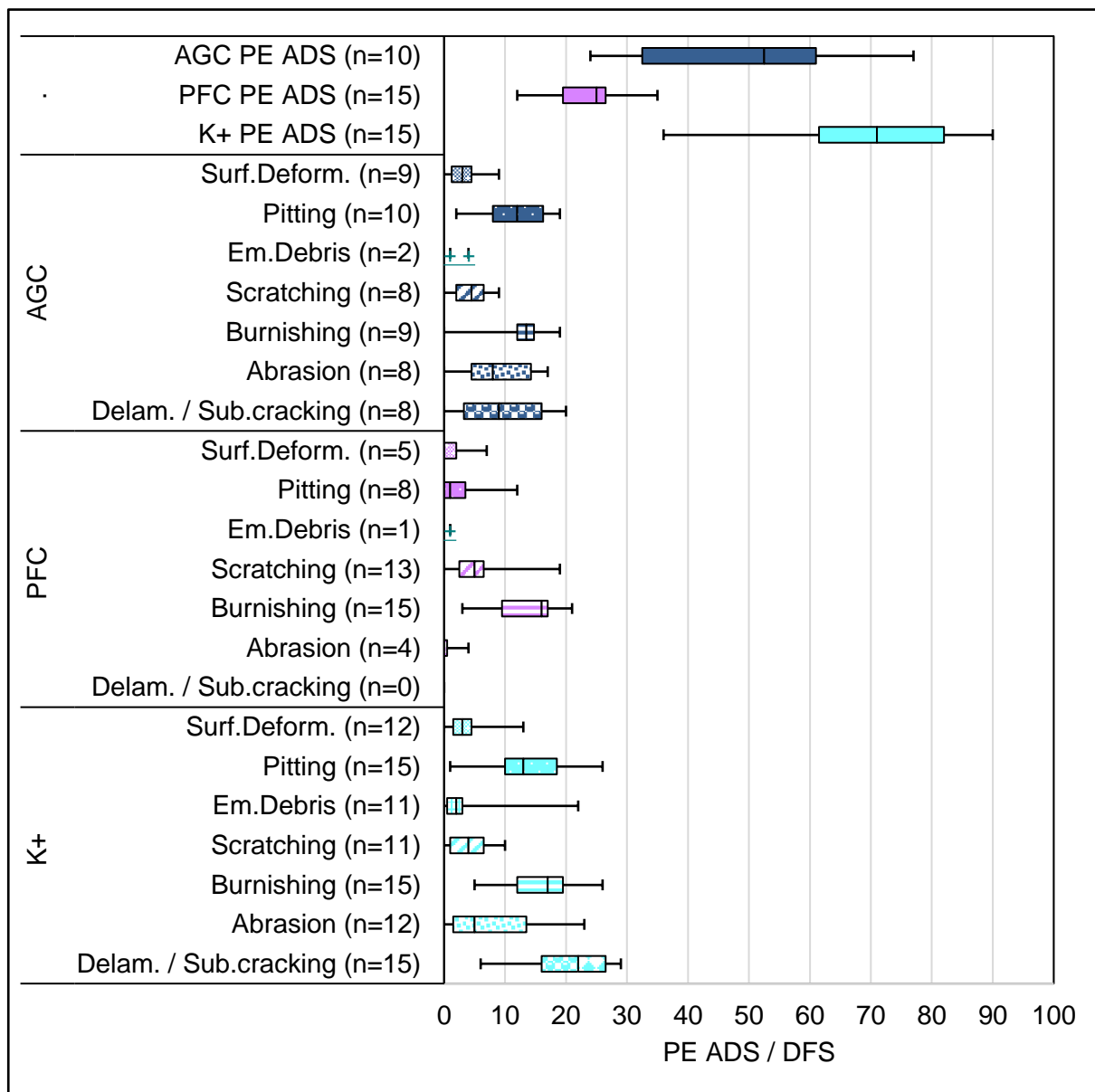


Figure 4.4 Articular surface of retrieved AGC, PFC and K+ PE components

Burnishing was the most prevalent damage feature observed for the retrieved AGC PE components, and this was closely followed by pitting and delamination / subsurface cracking which was seen on eight of the ten retrieved AGC PE components. Embedded debris were recorded on two retrieved AGC PE components. For the retrieved PFC PE components burnishing was also the most prevalent damage feature and was seen on all fifteen components. Scratching was the second highest scoring damage feature and was seen on thirteen of the fifteen retrieved PFC PE components. An embedded debris was observed only in one PFC PE component. Delamination / subsurface cracking was not recorded on any of the retrieved PFC PE components.

The highest scoring damage feature for the retrieved K+ PE components was delamination / subsurface cracking, and this was recorded on all fifteen retrieved K+ PE components. Burnishing and pitting were the next most prevalent damage features and were also seen on all fifteen retrieved K+ PE components. Embedded debris was recorded on eleven of the fifteen K+ PE components. Five of the K+ PE components were observed to have completely worn away and areas of material loss was evident. The damage scores for these PE components may not be truly representative as a DFS could not be assigned to the missing areas and therefore the descriptive statistical values for the ADS for the K+ group may not be accurate. The PE ADS and DFS median, maximum, minimum and inter-quartile ranges for the

articular surface of the PE components of the retrieved AGC, PFC and K+ TKRs are shown in Figure 4.5. Only two AGC and one PFC PE components were recorded as having embedded debris. These are shown as single data points on the graph in Figure 4.5.



\* Surf. Deform = Surface Deformation; Em.Debris = Embedded Debris; Delam. / Sub.cracking = Delamination / Subsurface cracking

Figure 4.5 PE ADS & DFS for retrieved AGC, PFC and K+ PE components

### 4.2.3 PE Components Backside Surface and Tibial Components

The backside of the PE components and the proximal surface of the tibial components of the retrieved PFC and K+ TKRs were macroscopically visually assessed. One retrieved K+ TKR did not have the tibial component available for analysis. Damage scoring was performed on the backside surface of the PE components of all the retrieved PFC and K+ TKRs. Figure 4.6 shows the backside surface of the PE component and proximal surface of the tibial trays for retrieved PFC TKRs with non-polished and polished tibial trays and retrieved K+ TKRs with and without PE wear through.

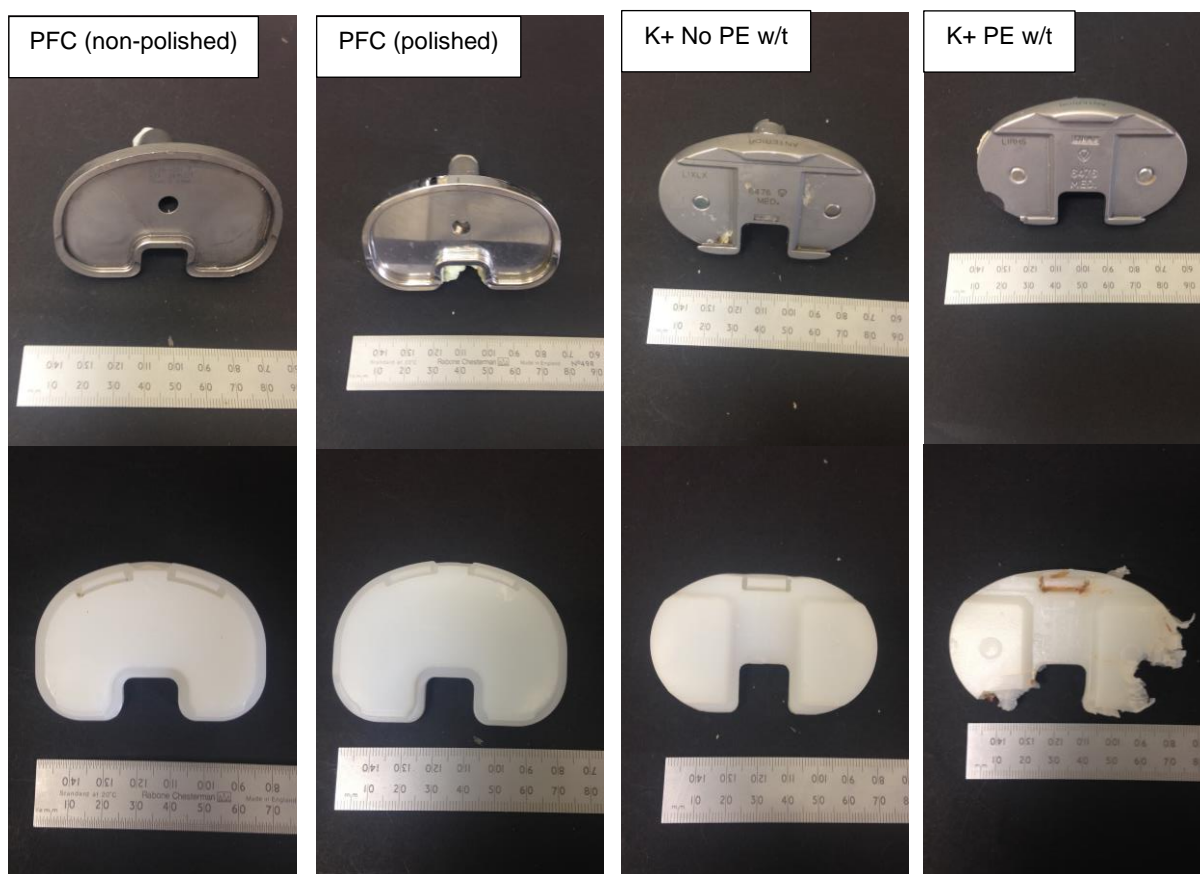


Figure 4.6 Tibial trays and PE backside surfaces of retrieved PFC TKRs with non-polished and polished trays and K+ TKRs with no PE wear through (w/t) and with PE wear through (w/t)

There were ten non-polished and five polished retrieved PFC tibial components. Four of the five polished PFC tibial components and two of the ten non-polished PFC tibial

components were observed to have very minimal if any *in vivo* damage. Burnishing, stippling and debris trapped in the locking mechanism were observed on eight non-polished PFC tibial components and scratching and trapped debris were observed on one polished PFC tibial component. The fourteen retrieved K+ tibial components are all non-polished. Very minimal if any *in vivo* damage was observed for six of the fourteen tibial components. Burnishing was observed on all eight of the damaged K+ tibial components, fracture or cracks were observed on three, stippling was observed on two and scratching on one. Five of the eight tibial components where burnishing was observed had experienced articulation between the femoral component and the tibial component due to complete wear through of the PE.

The median, maximum, minimum and inter-quartile ranges for the backside damage score of the PE components (PE BDS) of the retrieved PFC and K+ TKRs are shown in Figure 4.7. The PFC PE components are grouped according to the tibial component (i.e. polished or non-polished). The K+ PE components are grouped according to whether there was PE wear through (w/t) leading to articulation between the femoral and tibial components or no PE wear through (w/t).

Macroscopic visual assessment showed that the backsides of the PFC PE components were less damaged than those of the K+ PE components. The mean BDS for the PFC PE components was 9.06 (range 0 – 34.2). When divided into PFC PE components articulating against polished and non-polished PFC tibial components the mean BDS values were 3.04 (range 0 – 8.25) and 12.08 (range 0.33 – 34.2) respectively. The mean BDS for the K+ PE components (17.27 (range 11.22 – 28.74)) is greater than that of the polished PFC PE components but not than that of the non-polished PFC components. When divided into K+ PE components where there was complete PE wear through and those where the PE surface was intact the mean BDS values are 17.22 (range 11.22 – 28.74) and 17.38 (range 14.52 – 19.80) respectively.

Burnishing was observed on three of the five PFC PE components articulating with polished tibial components and a minimal amount of pitting was observed on one. One of the PFC PE components articulating with a polished tibial component was not

considered to have any damage resulting from the time *in vivo*. All of the ten PFC PE components articulating with non-polished tibial components were observed to have some damage although one had very minimal light burnishing. Burnishing was observed on five of the ten PE components, stippling was observed on four, deformations caused by the indentation of the screws on the tibial component were observed on three and pitting was observed on two components. None of the damage observed was considered severe.

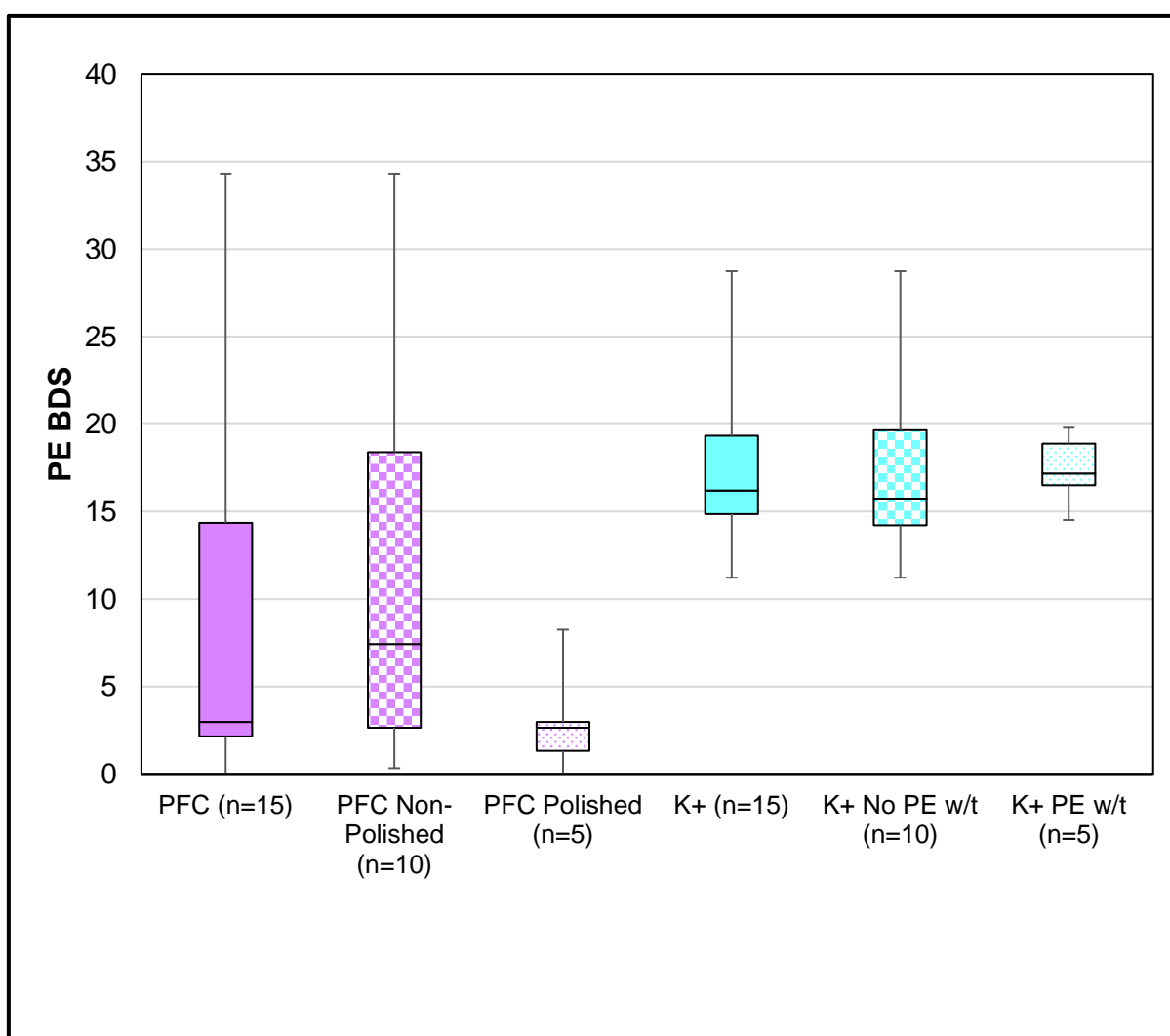


Figure 4.7 PE BDS for retrieved PFC & K+ PE components

All of the retrieved K+ PE components were observed to have backside damage. Furthermore, all were observed to have some amount of stippling. Deformations, mainly due to the indentation of the screw holes on the tibial components, were

recorded on the backside of fourteen of the K+ PE components. Burnishing was observed on the backside of nine of the fifteen components and pitting was observed on four. Only minimal scratching was observed on the backside of one of the retrieved K+ PE components and no indentations observed on the backside of any of the retrieved PE components. As per the ADS, the BDS for the five K+ PE components that were completely worn away and missing may not be truly representative and may not be accurate.

### 4.3 Non-contacting Profilometry

#### 4.3.1 Femoral Component

The mean and standard error for the surface roughness measurements for the reference components are recorded in Table 4.3. For each component thirty measurement points were taken, fifteen on each condyle.

Table 4.3 Reference PFC and K+ Femoral Component Surface Roughness Parameters

	Reference PFC1	Reference PFC2	Reference K+1	Reference K+2
<b>S<sub>q</sub> (μm)</b>	0.069 (±0.009)	0.051 (±0.003)	0.059 (±0.009)	0.043 (±0.004)
<b>S<sub>p</sub> (μm)</b>	0.294 (±0.017)	0.269 (±0.020)	0.523 (±0.114)	0.313 (±0.023)
<b>S<sub>v</sub> (μm)</b>	-0.497 (±0.110)	-0.596 (±0.161)	-0.732 (±0.200)	-0.287 (±0.028)
<b>PV (μm)</b>	0.790 (±0.122)	0.865 (±0.159)	1.255 (±0.302)	0.599 (±0.045)
<b>S<sub>z</sub> (μm)</b>	0.386 (±0.042)	0.371 (±0.038)	0.580 (±0.113)	0.437 (±0.035)
<b>S<sub>sk</sub> (-)</b>	-0.101 (±0.399)	-1.189 (±0.822)	-1.310 (±0.527)	0.071 (±0.209)
<b>S<sub>Ku</sub> (-)</b>	11.474 (±2.746)	66.582 (±39.258)	23.026 (±5.700)	9.584 (±1.238)

\*Mean value ± standard error is given for each parameter

No statistically significant differences were determined between the mean values of any of the roughness parameters between the reference components (A p-value of less than 0.05 is considered significant).

Figures 4.8 to 4.12 show some of the surface topography plots that are the visual outputs from the Zygo NewView 5000 for specific measurement points. As described in Chapter 3, within each of these figures there are four images which include in the top left a 3D oblique plot of the area of view (typically, this area is  $317\ \mu\text{m} \times 238\ \mu\text{m}$  but this is determined by the magnification and zoom setting selected). This 3D oblique plot is colour coded along the scale on the right. In the top right there is a 2D greyscale intensity map of the area of view. In the bottom left is a 2D 'heat map' of the area of view which is also colour coding against the scale to the right there is a line of interest crossing this plot. The graphical representation shown in the bottom right is the cross-sectional surface profile where that line of interest intersects the area of view.

The femoral components for both reference PFC and K+ were mainly characterised by areas similar to those in the surface topography plots shown in Figures 4.8 and 4.9. These are comparatively regular surfaces with no major distinguishing features. In contrast Figures 4.10 and 4.11 are measurements taken on reference PFC and K+ components. These figures are for measurement areas where pits were observed gave unusually high surface roughness measurements. This was unexpected for the reference components which were previously unopened as manufactured components that were only opened for measurement within this project. Figure 4.12 shows distinct scratching on one of the reference K+ components. The RMS surface roughness,  $S_q$ , and the ten-point height average,  $S_z$ , values for the measurement area are detailed in the figure title.

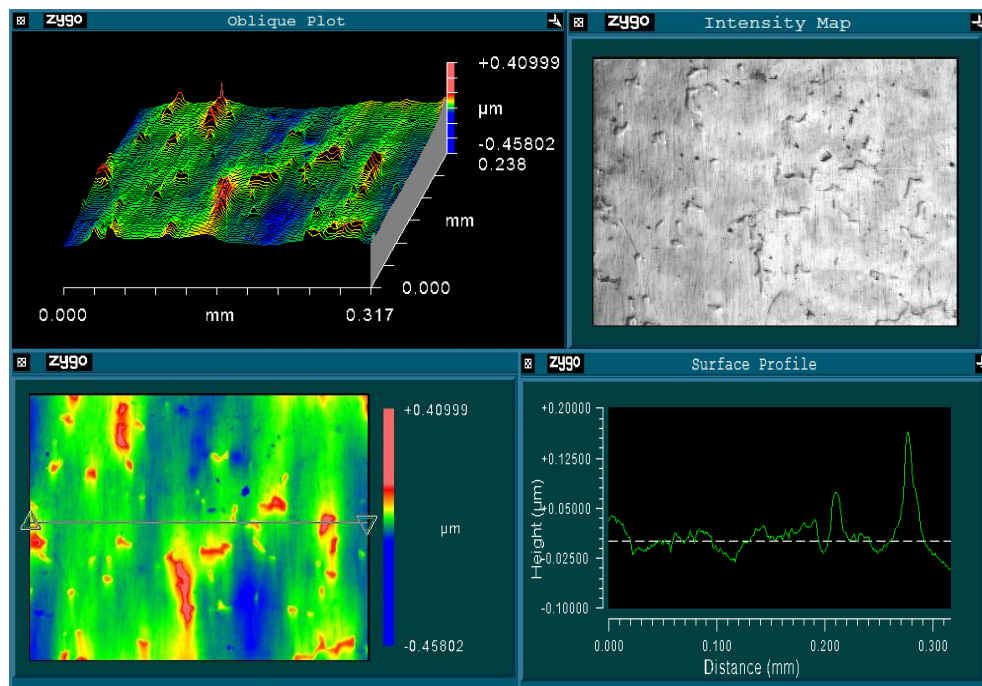


Figure 4.8 Surface topography plots for a measurement area on a reference PFC femoral component  $S_q = 0.033\mu\text{m}$ ,  $S_z = 0.321\mu\text{m}$

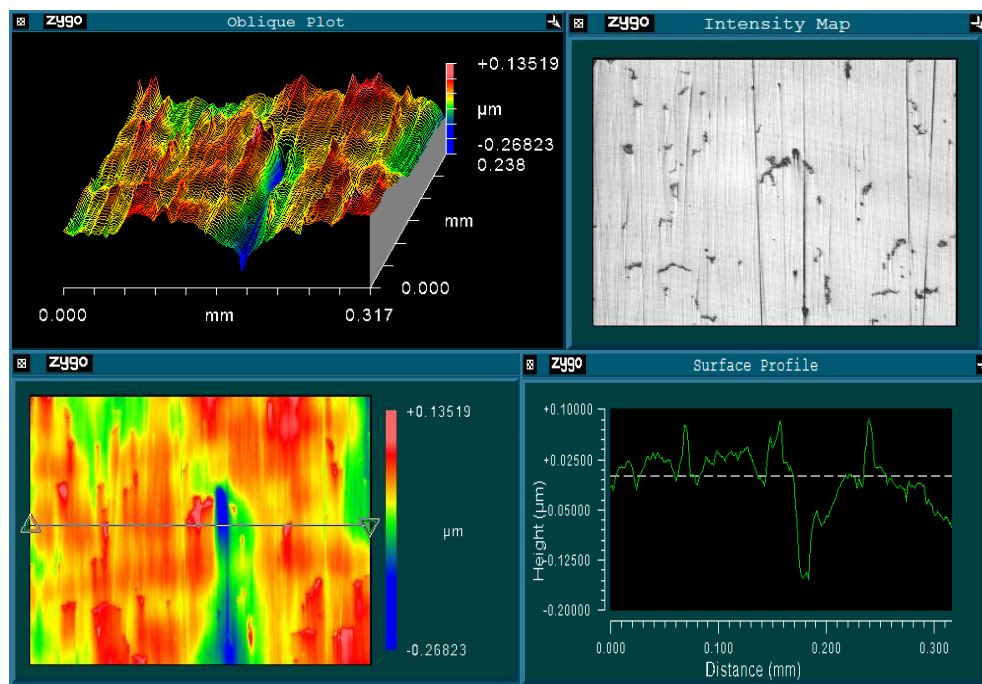


Figure 4.9 Surface topography plots for a measurement area on a reference K+ femoral component  $S_q = 0.038\mu\text{m}$ ,  $S_z = 0.196\mu\text{m}$



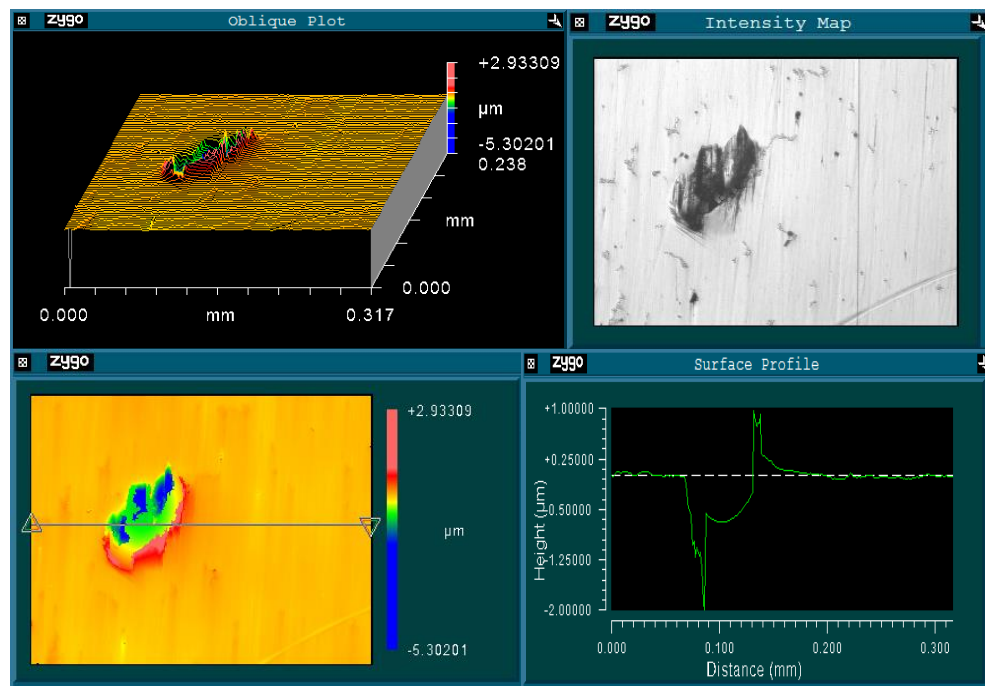


Figure 4.10 Surface topography plots for a measurement area on a reference PCF femoral component  $S_q = 0.150\mu\text{m}$ ,  $S_z = 0.880\mu\text{m}$

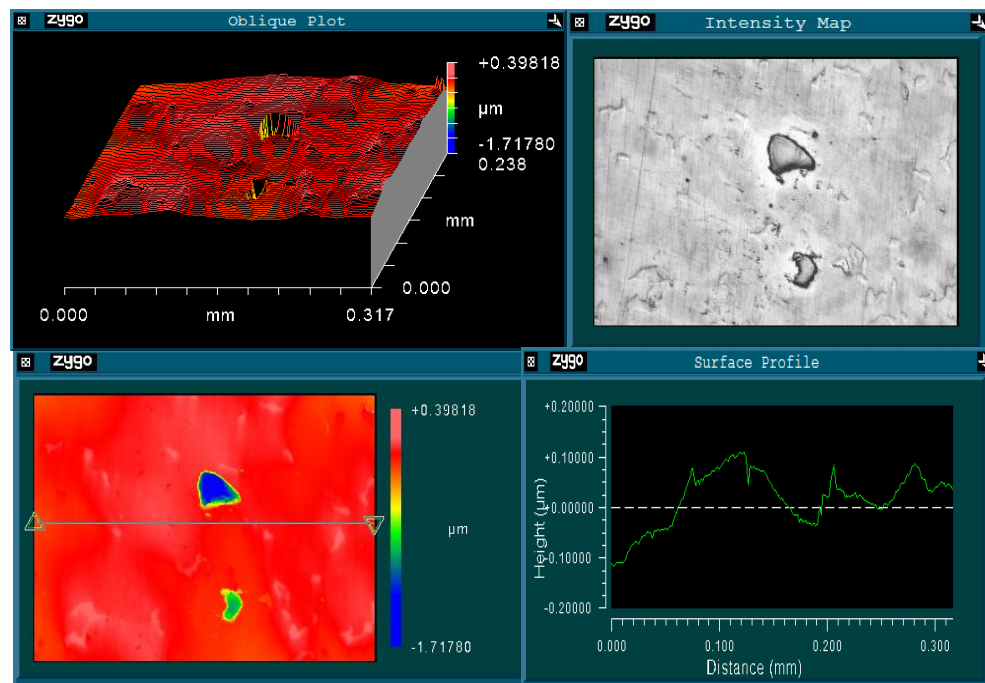


Figure 4.11 Surface topography plots for a measurement area on a reference K+ femoral component  $S_q = 0.260\mu\text{m}$ ,  $S_z = 2.784\mu\text{m}$

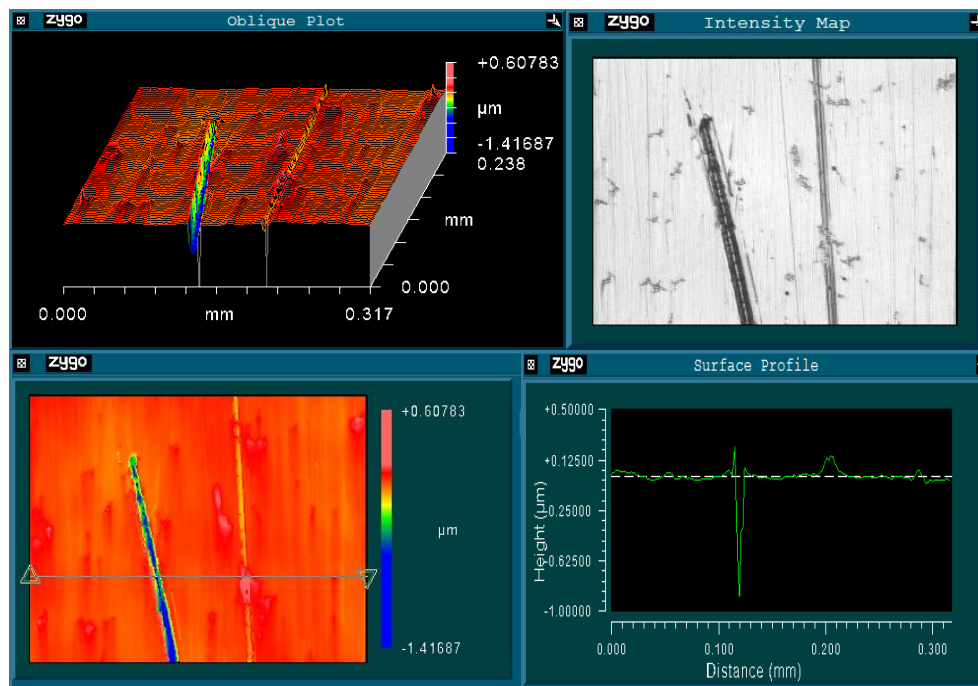


Figure 4.12 Surface topography plots for a measurement area on a reference K+ femoral component  $S_q = 0.086\mu\text{m}$ ,  $S_z = 0.803\mu\text{m}$

Table 4.4 shows the mean and standard errors of the measured femoral component surface roughness parameters for the reference PFC and K+ femoral components and the retrieved AGC, PFC and K+ femoral components. The number of components is the “n” value and for each component thirty measurement points were taken on each femoral component, fifteen on each condyle.

On average, the RMS surface roughness,  $S_q$  measured on the retrieved PFC femoral components increased by 67% when compared with the  $S_q$  of the reference PFC femoral components (range 9 – 167%), The  $S_q$  for the retrieved K+ femoral component increased on average 263% (range 35 – 837%) when compared with the reference K+ femoral component. No reference AGC femoral component was available and so the minimum mean  $S_q$  value ( $0.040\mu\text{m}$ ) of the retrieved AGC femoral components was selected as the reference value. The mean  $S_q$  values of the other 9 AGC components were on average 100% greater than this reference value (range 46% - 188%).

Table 4.4 AGC, PFC and K+ Femoral Component Surface Roughness Parameters

	Reference PFC (n = 2)	Retrieved PFC (n = 15)	
$S_q$ ( $\mu\text{m}$ )	0.060 ( $\pm$ 0.009)	0.100 ( $\pm$ 0.007)	
$S_p$ ( $\mu\text{m}$ )	0.281 ( $\pm$ 0.013)	0.432 ( $\pm$ 0.022)	
$S_v$ ( $\mu\text{m}$ )	-0.546 ( $\pm$ 0.050)	-0.692 ( $\pm$ 0.048)	
PV ( $\mu\text{m}$ )	0.828 ( $\pm$ 0.037)	1.124 ( $\pm$ 0.066)	
$S_z$ ( $\mu\text{m}$ )	0.379 ( $\pm$ 0.007)	0.595 ( $\pm$ 0.033)	
$S_{sk}$ (-)	-0.645 ( $\pm$ 0.544)	-0.740 ( $\pm$ 0.145)	
$S_{ku}$ (-)	39.028 ( $\pm$ 27.554)	11.868 ( $\pm$ 2.033)	
	Reference K+ (n = 2)	Retrieved K+ (n = 15)	Retrieved AGC (n = 10)
$S_q$ ( $\mu\text{m}$ )	0.051 ( $\pm$ 0.008)	0.185 ( $\pm$ 0.032)	0.080 ( $\pm$ 0.007)
$S_p$ ( $\mu\text{m}$ )	0.418 ( $\pm$ 0.105)	0.844 ( $\pm$ 0.120)	0.358 ( $\pm$ 0.029)
$S_v$ ( $\mu\text{m}$ )	-0.509 ( $\pm$ 0.223)	-1.232 ( $\pm$ 0.158)	-0.495 ( $\pm$ 0.063)
PV ( $\mu\text{m}$ )	0.927 ( $\pm$ 0.328)	2.077 ( $\pm$ 0.271)	0.853 ( $\pm$ 0.088)
$S_z$ ( $\mu\text{m}$ )	0.508 ( $\pm$ 0.072)	1.127 ( $\pm$ 0.159)	0.422 ( $\pm$ 0.046)
$S_{sk}$ (-)	-0.620 ( $\pm$ 0.690)	-1.654 ( $\pm$ 0.266)	-0.300 ( $\pm$ 0.205)
$S_{ku}$ (-)	16.305 ( $\pm$ 6.721)	35.030 ( $\pm$ 7.272)	10.925 ( $\pm$ 2.226)

\*Mean value  $\pm$  standard error is given for each parameter

A Mann-Whitney test was applied to compare the surface roughness parameters of the retrieved and reference femoral components. A p-value of less than 0.05 was considered to indicate a significant difference.

All the surface roughness parameters were significantly greater numerically ( $S_q$ ,  $S_p$ ,  $S_v$ , PV and  $S_z$ ) or significantly more negative ( $S_{sk}$ ) for the retrieved K+ femoral components when compared to the surface roughness parameters for the reference K+ femoral components. The same was true when comparing the surface roughness parameters of the retrieved PFC femoral components to the surface roughness

parameters of the reference PFC components. (p-values all <0.001). This result was as expected.

All the surface roughness parameters were significantly greater numerically ( $S_q$ ,  $S_p$ ,  $S_v$ , PV and  $S_z$ ) or significantly more negative ( $S_{sk}$ ) for the retrieved K+ femoral components when compared with the PFC femoral components and the AGG femoral components (p-values all <0.001). In turn all the surface roughness parameters were significantly greater numerically ( $S_q$ ,  $S_p$ ,  $S_v$ , PV and  $S_z$ ) or significantly more negative ( $S_{sk}$ ) for the retrieved PFC femoral components when compared with the retrieved AGG femoral components (p-values all <0.001).

There were no significant differences found between the medial and lateral surface roughness parameters of any of reference or retrieved femoral components for any of the different models of prosthesis. Figures 4.13 and 4.14 show  $S_q$  and  $S_z$  for the reference PFC and K+ and retrieved AGC, PFC and K+ femoral components. The 'n-value' shown is the number of prostheses. On each component there were thirty measurement points taken, fifteen on each condyle. The large range in values seen on the K+ femoral components are representative of the large variation in damage across the cohort. It can be seen that the surface roughness of the reference components was comparatively uniform. The difference between the median values for the retrieved AGC, PFC and K+ femoral components can be seen

Figures 4.15 – 4.17 show surface topography plots for measurement areas taken on the retrieved AGC, PFC and K+ components. These are representative of the damage observed on these retrieved components. Figure 4.15 shows a stippled area on an AGC component, Figure 4.16 shows fine high-density AP scratching and one larger scratch on a PFC component. Figure 4.17 shows heavy scratching on a K+ component.

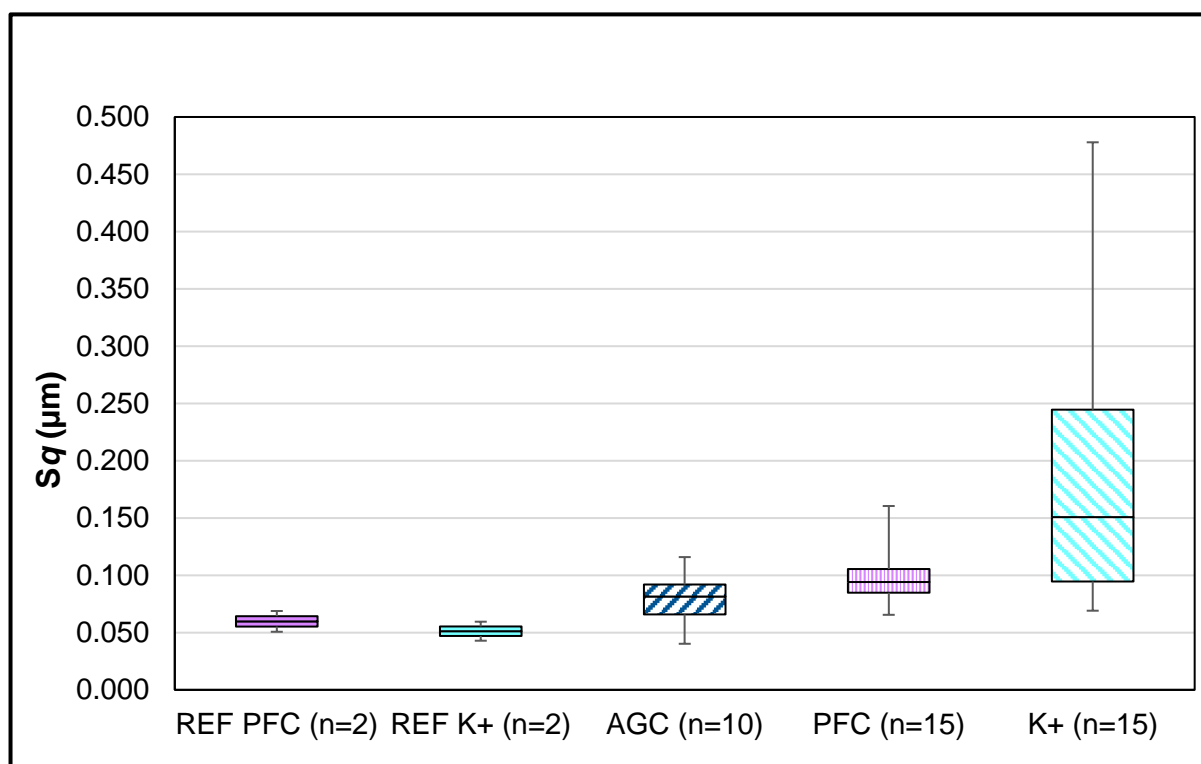


Figure 4.13 Femoral component RMS surface roughness,  $S_q$

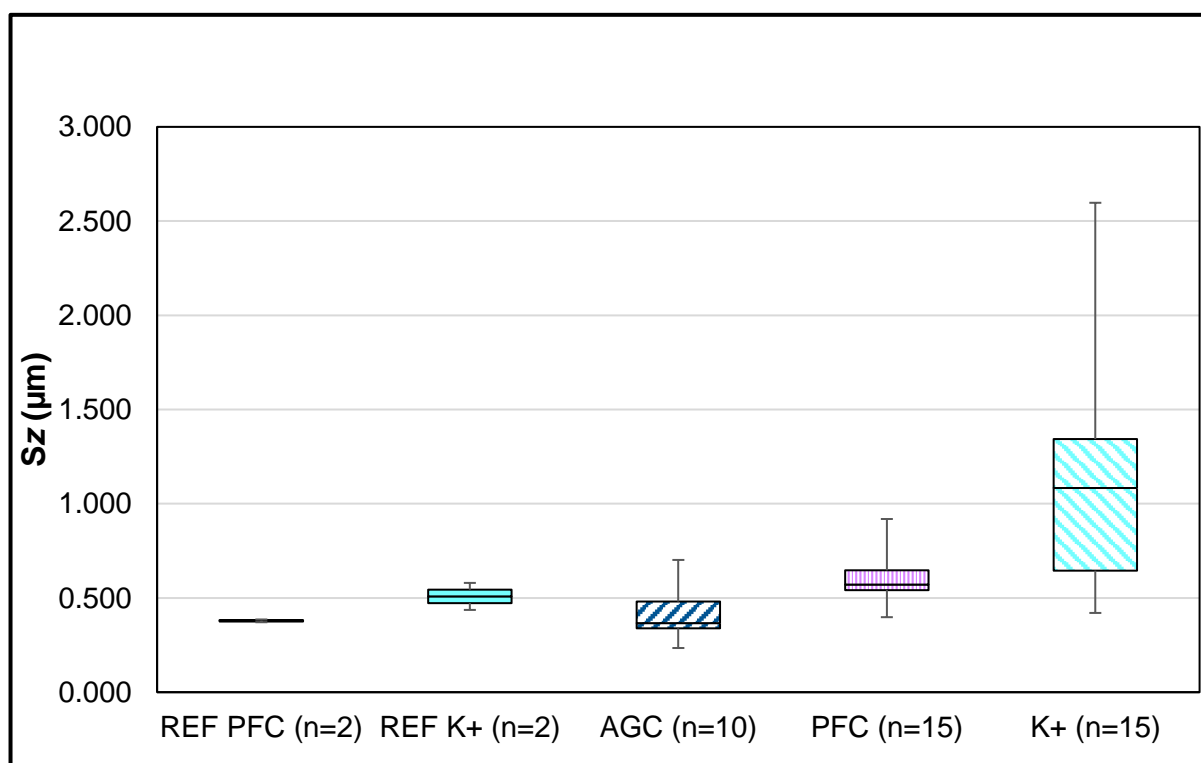


Figure 4.14 Femoral component 10-point height,  $S_z$

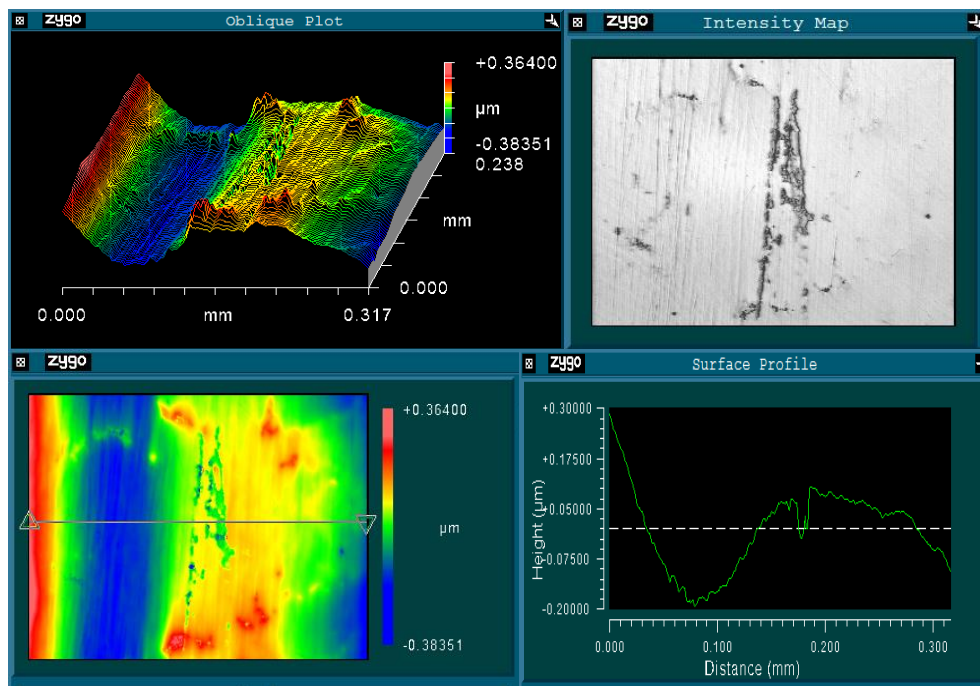


Figure 4.15 Surface topography plots for a measurement area on a retrieved AGC femoral component  $S_q = 0.110\mu\text{m}$ ,  $S_z = 0.398\mu\text{m}$

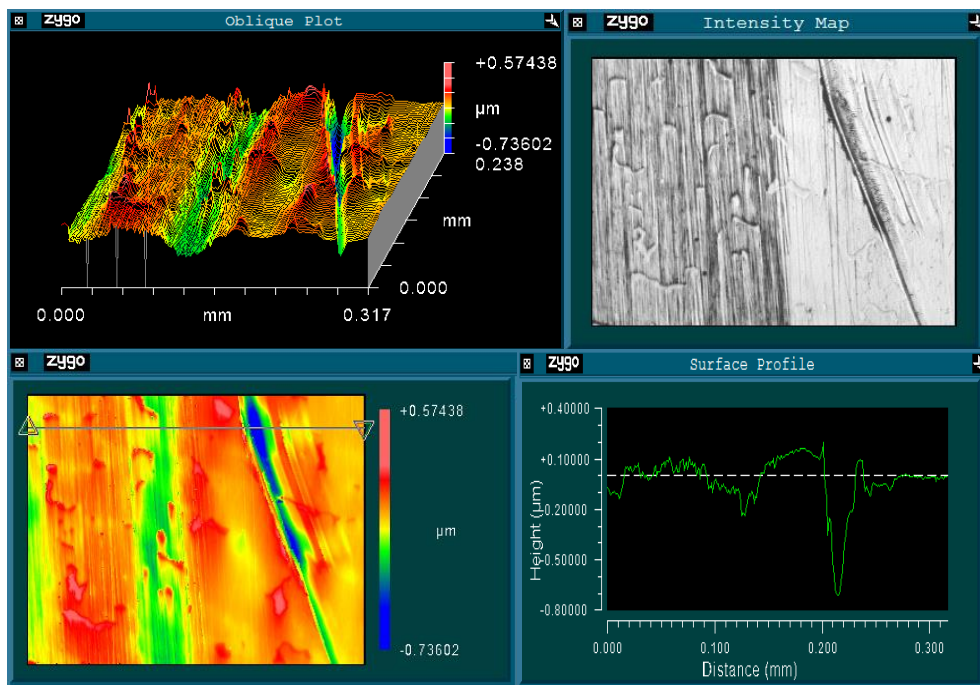


Figure 4.16 Surface topography plots for a measurement area on a retrieved PCF femoral component  $S_q = 0.120\mu\text{m}$ ,  $S_z = 0.725\mu\text{m}$

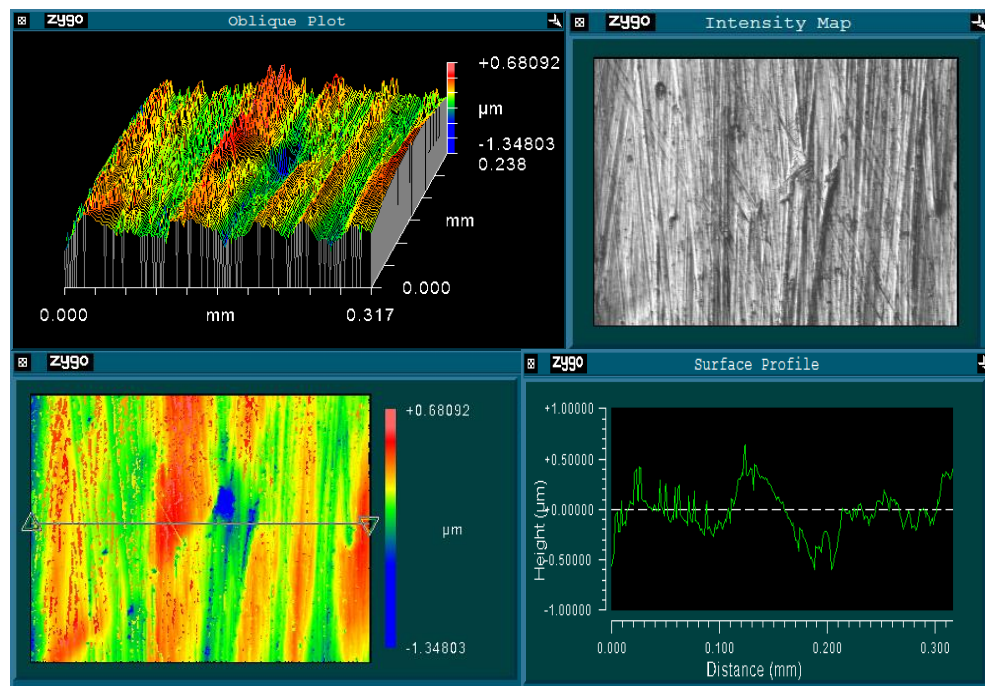


Figure 4.17 Surface topography plots for a measurement area on a retrieved K+ femoral component  $S_q = 0.197\mu\text{m}$ ,  $S_z = 1.367\mu\text{m}$

#### 4.3.2 PE Component Backside Surface

The retrieved PE components have been grouped according to whether the tibial tray is polished or non-polished and whether the PE component has completely worn through or not as detailed in the PE BDS results above. For each component six measurement points were taken. No significant differences between any of the surface roughness parameters measured on the reference and retrieved PE backside surfaces could be reliably reported. The mean and standard errors for the surface roughness measurements taken on the backside of the reference K+ PE component and the retrieved PFC and K+ PE components are recorded in Table 4.5.

Figure 4.18 shows the median, maximum, minimum and inter-quartile ranges for the  $S_q$  values of reference and retrieved PE components backside surfaces. The 'n-value' is the number of components, for each component 6 measurement points were taken as detailed in Chapter 3 Methods and Materials.

Table 4.5 Reference K+ and Retrieved K+ and PFC PE Component Backside Surface Roughness Parameters

\*Mean value  $\pm$  standard error is given for each parameter. w/t – wear through

	Reference K+ PE (n = 2)		
<b>Sq (<math>\mu\text{m}</math>)</b>	1.317 ( $\pm$ 0.033)		
<b>Sp (<math>\mu\text{m}</math>)</b>	4.707 ( $\pm$ 0.615)		
<b>Sv (<math>\mu\text{m}</math>)</b>	-4.515 ( $\pm$ 908)		
<b>PV (<math>\mu\text{m}</math>)</b>	9.222 ( $\pm$ 1.162)		
<b>Sz (<math>\mu\text{m}</math>)</b>	6.322 ( $\pm$ 0.442)		
<b>S<sub>sk</sub> (-)</b>	0.133 ( $\pm$ 0.040)		
<b>S<sub>ku</sub> (-)</b>	1.869 ( $\pm$ 0.055)		
	Retrieved K+ PE (n = 15)	Retrieved K+ PE No w/t (n = 10)	Retrieved K+ PE w/t (n = 5)
<b>Sq (<math>\mu\text{m}</math>)</b>	1.326 ( $\pm$ 0.158)	1.477 ( $\pm$ 0.208)	1.025 ( $\pm$ 0.180)
<b>Sp (<math>\mu\text{m}</math>)</b>	8.244 ( $\pm$ 1.619)	8.312 ( $\pm$ 2.220)	8.107 ( $\pm$ 2.309)
<b>Sv (<math>\mu\text{m}</math>)</b>	-8.780 ( $\pm$ 2.365)	-8.401 ( $\pm$ 2.521)	-9.536 ( $\pm$ 5.469)
<b>PV (<math>\mu\text{m}</math>)</b>	17.024 ( $\pm$ 3.568)	16.714 ( $\pm$ 4.313)	17.643 ( $\pm$ 7.057)
<b>Sz (<math>\mu\text{m}</math>)</b>	9.591 ( $\pm$ 2.051)	9.385 ( $\pm$ 2.508)	10.004 ( $\pm$ 3.976)
<b>S<sub>sk</sub> (-)</b>	0.090 ( $\pm$ 0.231)	-0.038 ( $\pm$ 0.168)	0.346 ( $\pm$ 0.641)
<b>S<sub>ku</sub> (-)</b>	11.171 ( $\pm$ 3.079)	8.500 ( $\pm$ 3.007)	16.513 ( $\pm$ 6.941)
	Retrieved PFC PE (n = 15)	Retrieved PFC PE Non-polished (n = 10)	Retrieved PFC PE Polished (n = 5)
<b>Sq (<math>\mu\text{m}</math>)</b>	1.141 ( $\pm$ 0.192)	1.042 ( $\pm$ 0.255)	1.338 ( $\pm$ 0.285)
<b>Sp (<math>\mu\text{m}</math>)</b>	4.640 ( $\pm$ 0.944)	4.719 ( $\pm$ 1.375)	4.483 ( $\pm$ 0.918)
<b>Sv (<math>\mu\text{m}</math>)</b>	-5.090 ( $\pm$ 1.636)	-5.709 ( $\pm$ 2.433)	-3.851 ( $\pm$ 0.946)
<b>PV (<math>\mu\text{m}</math>)</b>	9.730 ( $\pm$ 2.544)	10.428 ( $\pm$ 3.772)	8.334 ( $\pm$ 1.778)
<b>Sz (<math>\mu\text{m}</math>)</b>	6.972 ( $\pm$ 2.084)	7.455 ( $\pm$ 3.116)	6.005 ( $\pm$ 1.247)
<b>S<sub>sk</sub> (-)</b>	-0.330 ( $\pm$ 0.300)	-0.523 ( $\pm$ 0.435)	0.057 ( $\pm$ 0.182)
<b>S<sub>ku</sub> (-)</b>	8.694 ( $\pm$ 4.054)	11.722 ( $\pm$ 5.939)	2.637 ( $\pm$ 0.284))



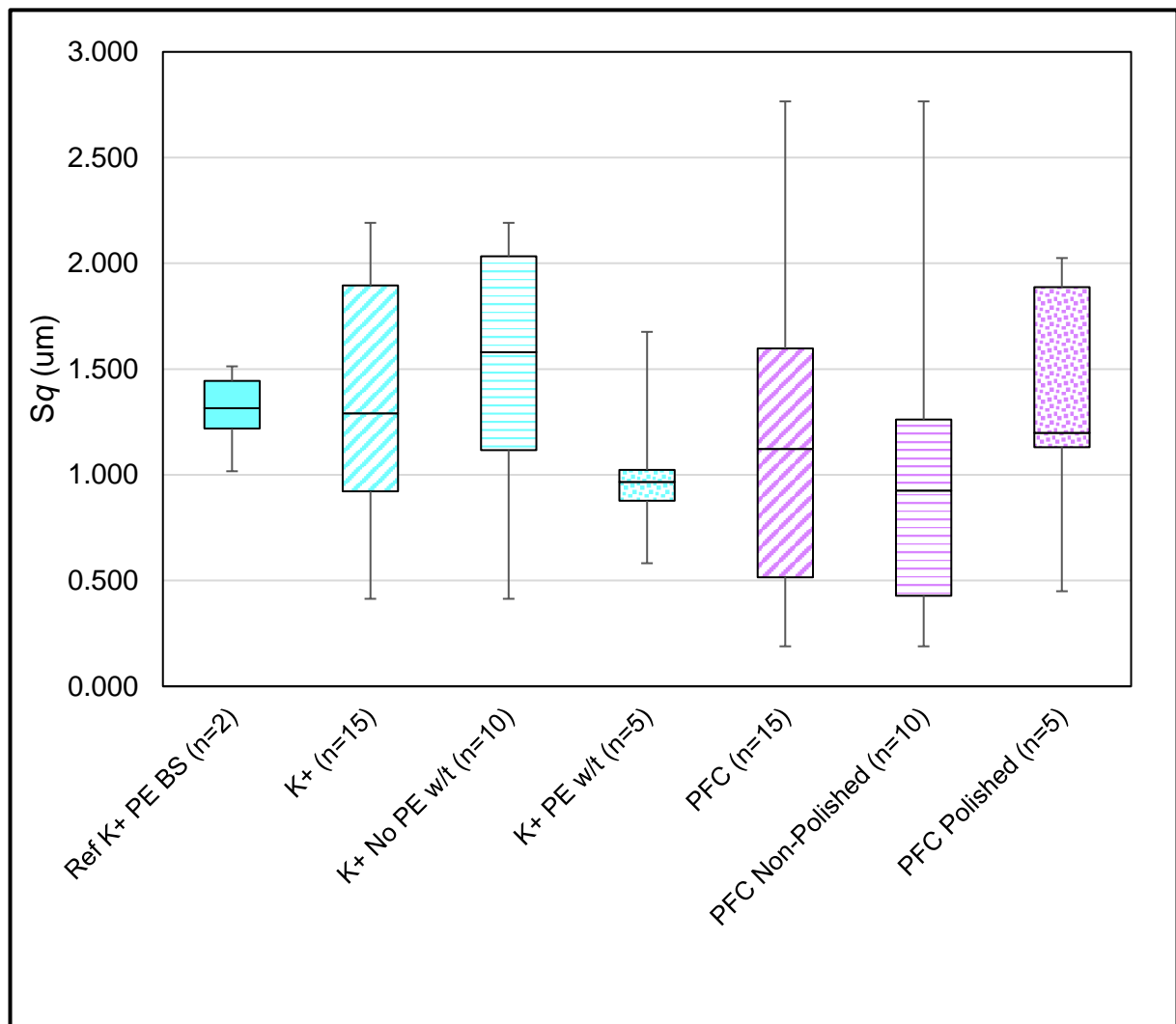


Figure 4.18 PE component backside surface RMS surface roughness,  $S_q$

Figures 4.19 – 4.23 show surface topography plots for measurement areas taken on the reference K+ and retrieved PFC and K+ PE component backside surfaces. In Figure 4.19 the machine markings can be observed clearly on the reference K+ PE component backside. In Figures 4.20 – 4.22 these machine marks are not observed, and a more mottled appearance is represented in the surface topography plots. In Figure 4.22 a defined scratch is observed on the backside of a retrieved PFC PE component that was mated with a non-polished tibial tray. In Figure 4.23 it is interesting that the original machine markings are observed on the backside of a retrieved PFC PE component that was mated with a polished tibial tray.

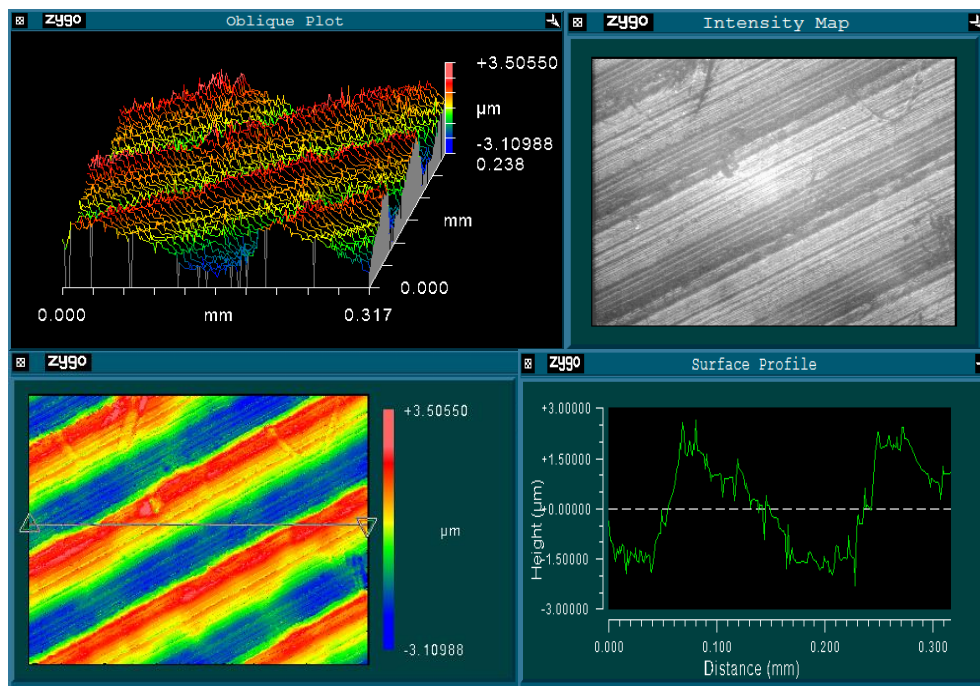


Figure 4.19 Surface topography plots for a measurement area on the reference K+ PE component backside surface  $S_q = 1.303\mu\text{m}$ ,  $S_z = 5.512\mu\text{m}$

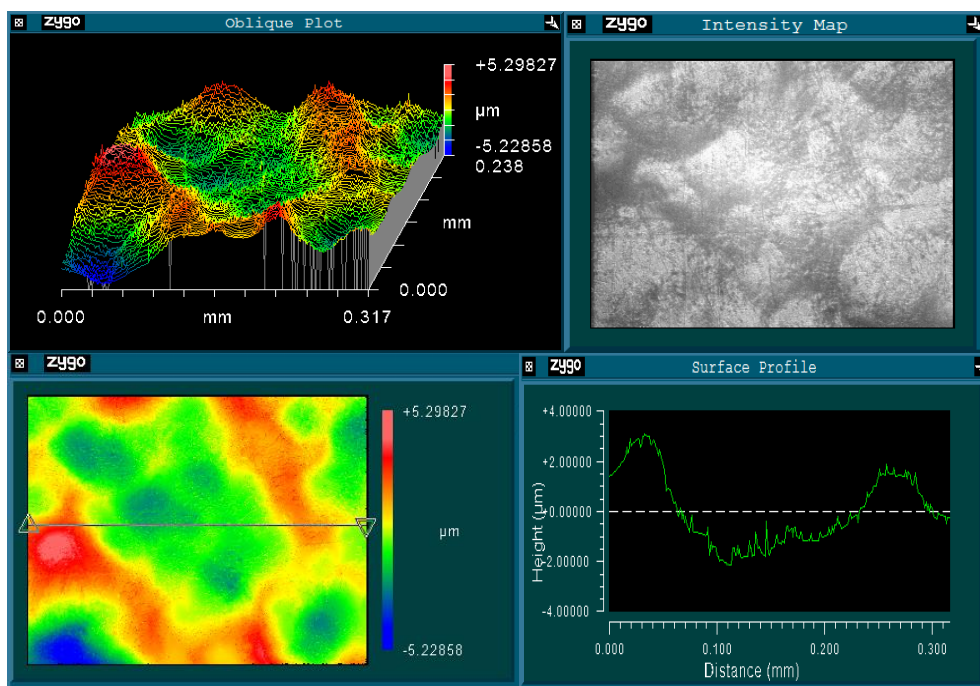


Figure 4.20 Surface topography plots for a measurement area on the backside of a retrieved K+ PE component from a TKR with no PE wear through  $S_q = 1.426\mu\text{m}$ ,  $S_z = 5.512\mu\text{m}$

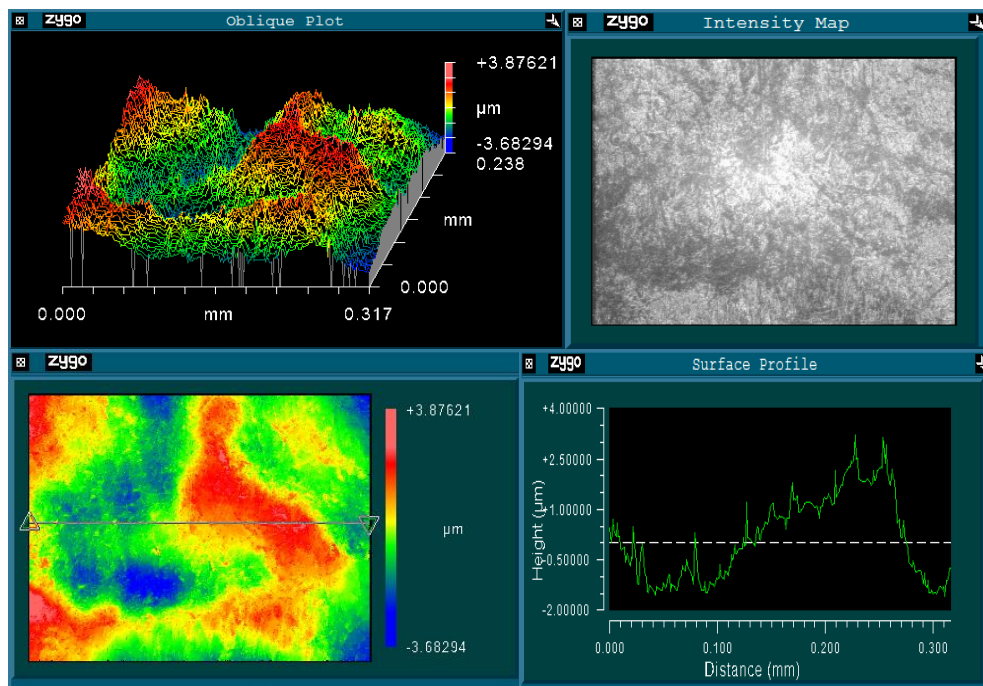


Figure 4.21 Surface topography plots for a measurement area on the backside of a retrieved K+ PE component from a TKR with PE wear through  $S_q = 1.102\mu\text{m}$ ,  $S_z = 3.967\mu\text{m}$

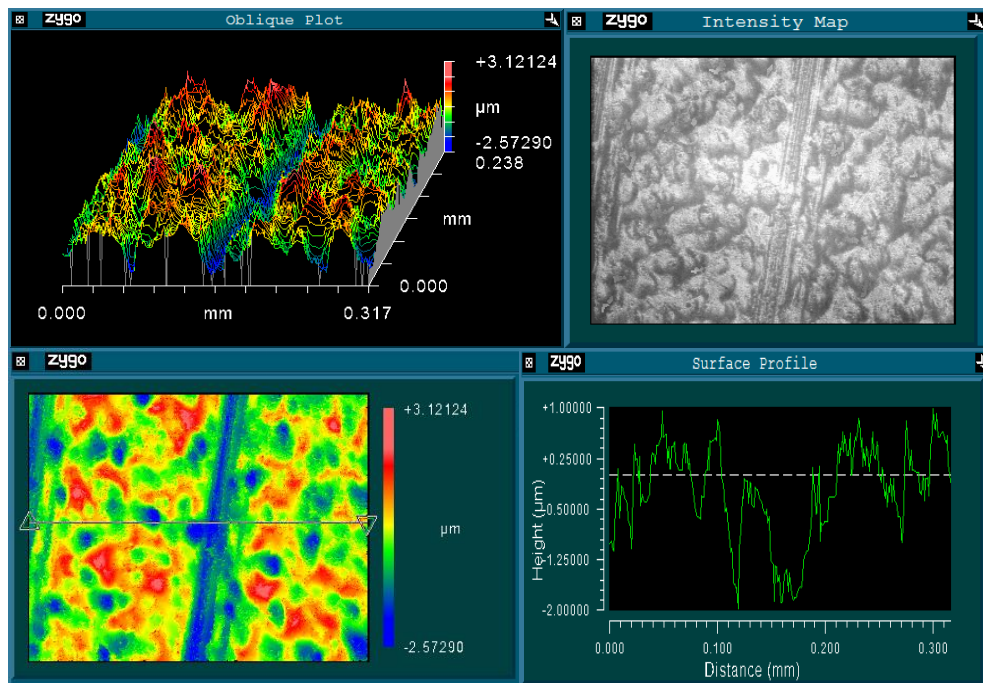


Figure 4.22 Surface topography plots for a measurement area on the backside of a retrieved PFC PE component mated with a non-polished tibial tray  $S_q = 0.842\mu\text{m}$ ,  $S_z = 4.636\mu\text{m}$

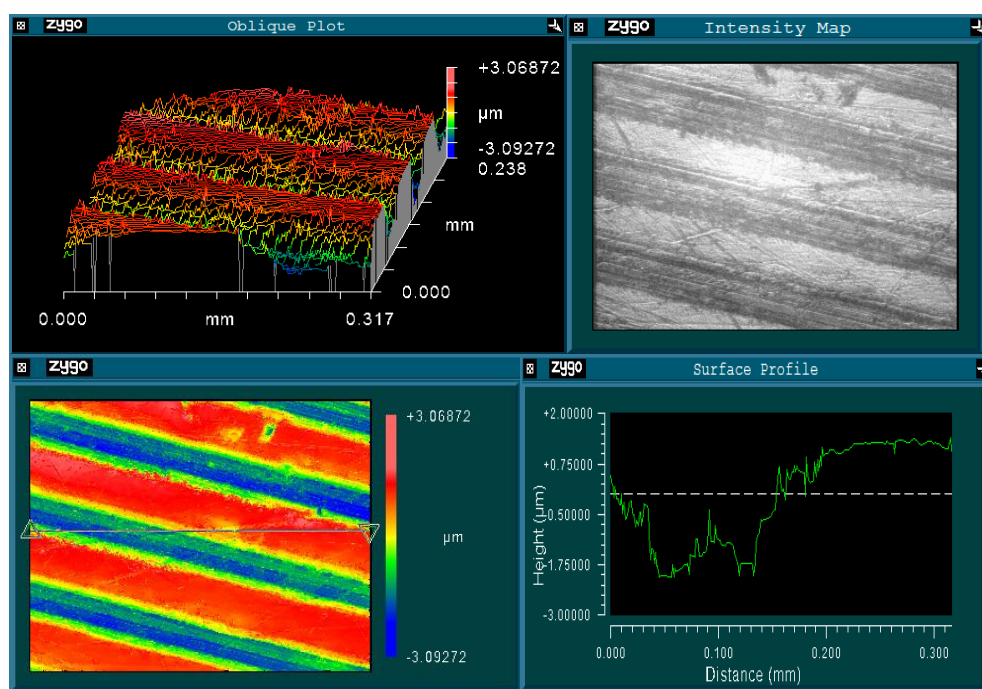


Figure 4.23 Surface topography plots for a measurement area on the backside of a retrieved PFC PE component mated with a polished tibial tray  $S_q = 1.202\mu\text{m}$ ,  $S_z = 5.002\mu\text{m}$

### 4.3.3 Tibial Component

The mean and standard errors for the surface roughness measurements taken on the tibial tray of the reference K+ tibial component and the retrieved PFC and K+ tibial components are recorded in Table 4.6. The 'n-value' indicates the number of prostheses in each group and six measurements were taken per prosthesis. Figure 4.24 shows the median, maximum, minimum and inter-quartile ranges for the  $S_q$  values of reference and retrieved tibial tray proximal surfaces. The results have been grouped according to whether the tibial component is polished or non-polished and whether the PE component had undergone complete wear through or not. One retrieved K+ TKR did not have a tibial component available for analysis.

There was only one K+ tibial component available to be used as a reference. Figure 4.24 clearly illustrates that the surface roughness measurements of the retrieved PFC tibial components, both polished and non-polished were significantly lower than those recorded for the reference K+ tibial component ( $p < 0.05$ ). No significant

different could be determined between the surface roughness parameters of the reference K+ tibial component compared with the retrieved K+ tibial components. The surface roughness parameters measured on the non-polished PFC tibial components were all significantly different to those measured on the polished PFC components ( $p < 0.05$ ). This illustrated in Figure 4.24.

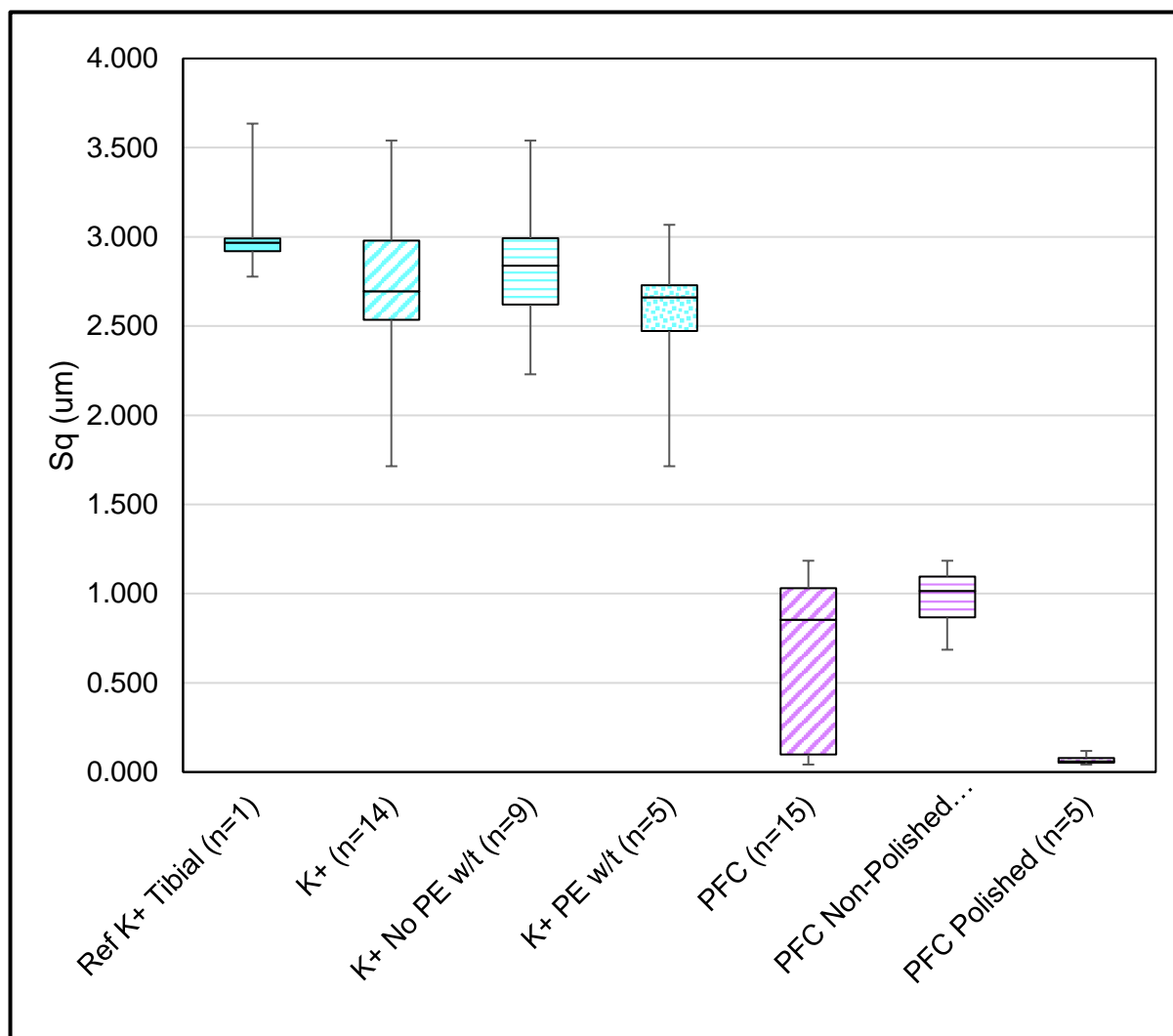


Figure 4.24 Tibial component surface RMS surface roughness,  $S_q$

Table 4.6 Reference K+ and Retrieved K+ and PFC Tibial Component Surface Roughness Parameters

\*Mean value  $\pm$  standard error is given for each parameter. w/t – wear through

	Reference K+ Tibial (n = 1)		
$S_q$ ( $\mu\text{m}$ )	3.042 ( $\pm$ 0.123)		
$S_p$ ( $\mu\text{m}$ )	8.859 ( $\pm$ 0.871)		
$S_v$ ( $\mu\text{m}$ )	-15.838 ( $\pm$ 1.334)		
PV ( $\mu\text{m}$ )	24.697 ( $\pm$ 1.163)		
$S_z$ ( $\mu\text{m}$ )	17.798 ( $\pm$ 1.227)		
$S_{sk}$ (-)	-0.627 ( $\pm$ 0.114)		
$S_{ku}$ (-)	3.571 ( $\pm$ 0.321)		
	Retrieved K+ Tibial (n = 14)	Retrieved K+ Tibial No w/t (n = 9)	Retrieved K+ Tibial w/t (n = 5)
$S_q$ ( $\mu\text{m}$ )	2.730 ( $\pm$ 0.119)	2.841 ( $\pm$ 0.133)	2.529 ( $\pm$ 0.225)
$S_p$ ( $\mu\text{m}$ )	8.274 ( $\pm$ 0.309)	8.419 ( $\pm$ 0.326)	8.015 ( $\pm$ 0.679)
$S_v$ ( $\mu\text{m}$ )	-15.491 ( $\pm$ 0.622)	-16.083 ( $\pm$ 0.672)	-14.426 ( $\pm$ 1.205)
PV ( $\mu\text{m}$ )	23.766 ( $\pm$ 0.876)	24.502 ( $\pm$ 0.883)	22.440 ( $\pm$ 1.868)
$S_z$ ( $\mu\text{m}$ )	16.418 ( $\pm$ 0.643)	16.700 ( $\pm$ 0.713)	15.910 ( $\pm$ 1.352)
$S_{sk}$ (-)	-0.727 ( $\pm$ 0.036)	-0.728 ( $\pm$ 0.054)	-0.727 ( $\pm$ 0.034)
$S_{ku}$ (-)	3.908 ( $\pm$ 0.114)	3.875 ( $\pm$ 0.127)	3.967 ( $\pm$ 0.243)
	Retrieved PFC Tibial (n = 15)	Retrieved PFC Tibial Non-polished (n = 10)	Retrieved PFC Tibial Polished (n = 5)
$S_q$ ( $\mu\text{m}$ )	0.671 ( $\pm$ 0.119)	0.972 ( $\pm$ 0.056)	0.070 ( $\pm$ 0.013)
$S_p$ ( $\mu\text{m}$ )	3.324 ( $\pm$ 0.585)	4.806 ( $\pm$ 0.257)	0.359 ( $\pm$ 0.048)
$S_v$ ( $\mu\text{m}$ )	-4.478 ( $\pm$ 0.749)	-6.339 ( $\pm$ 0.391)	-0.755 ( $\pm$ 0.081)
PV ( $\mu\text{m}$ )	7.801 ( $\pm$ 1.297)	11.145 ( $\pm$ 0.440)	1.114 ( $\pm$ 0.123)
$S_z$ ( $\mu\text{m}$ )	5.840 ( $\pm$ 0.963)	8.354 ( $\pm$ 0.235)	0.812 ( $\pm$ 0.100)
$S_{sk}$ (-)	-0.594 ( $\pm$ 0.162)	-0.233 ( $\pm$ 0.050)	-1.317 ( $\pm$ 0.262)
$S_{ku}$ (-)	7.630 ( $\pm$ 1.400)	5.073 ( $\pm$ 1.341)	12.743 ( $\pm$ 1.641)



Figures 4.25 – 4.29 show surface topography plots for measurement areas taken on the reference K+ and the retrieved K+ and PFC tibial components. Figures 4.25 and 4.26 show little difference in appearance and surface topography when comparing reference K+ tibial components to retrieved K+ tibial components. However, there is a difference between Figure 4.25 and Figure 4.27 which shows the surface topography plots for a polished area on a retrieved K+ tibial component where the PE had worn through and the femoral condyles were articulating with the tibial component. These images in Figure 2.7 are comparable to those in Figure 2.9 which are representative of a retrieved PFC polished tibial component. Figure 2.8 shows the surface topographical plots for a retrieved non-polished PFC tibial component and these are comparable to Figures 4.25 and 4.26 for the non-polished K+ tibial components.

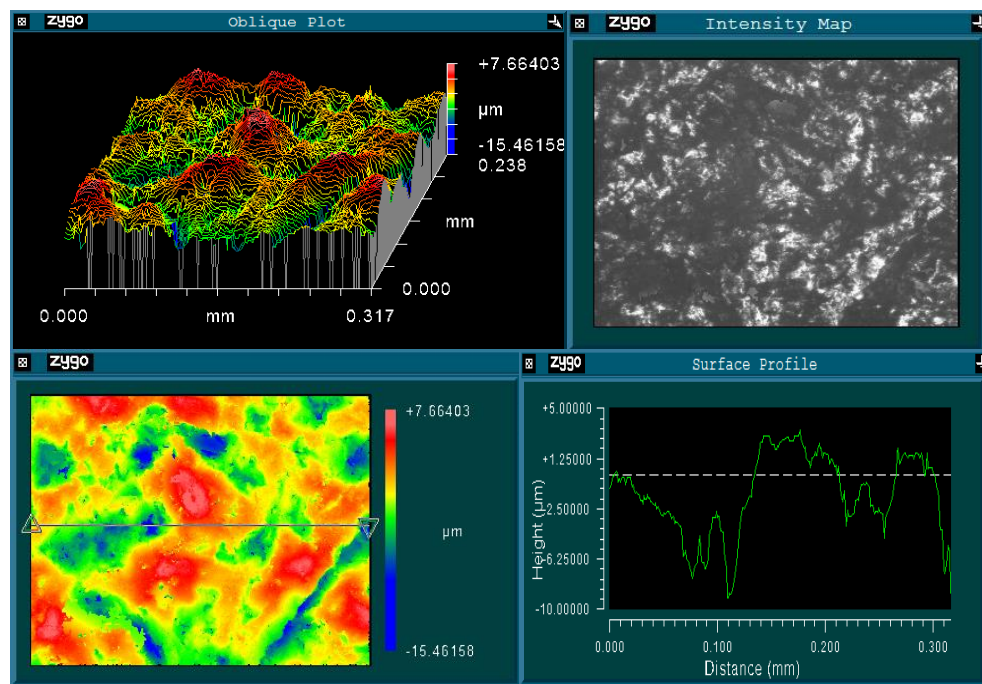


Figure 4.25 Surface topography plots for a measurement area on the reference K+ tibial component  $S_q = 3.635\mu\text{m}$ ,  $S_z = 7.153\mu\text{m}$

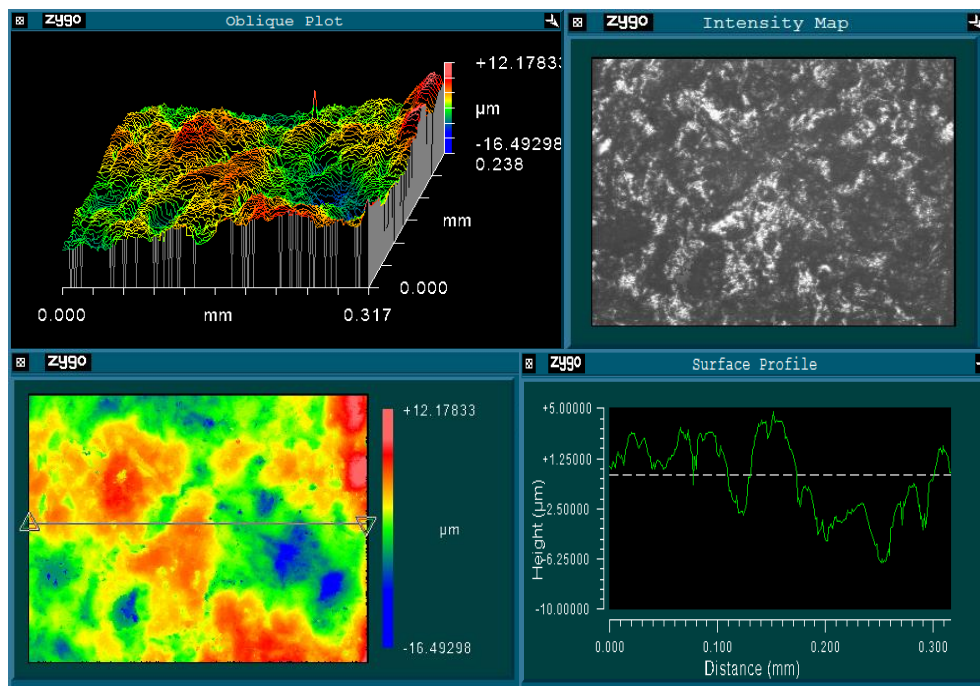


Figure 4.26 Surface topography plots for a measurement area on a retrieved K+ tibial component from a TKR with no PE wear through  $S_q = 3.272\mu\text{m}$ ,  $S_z = 10.643\mu\text{m}$

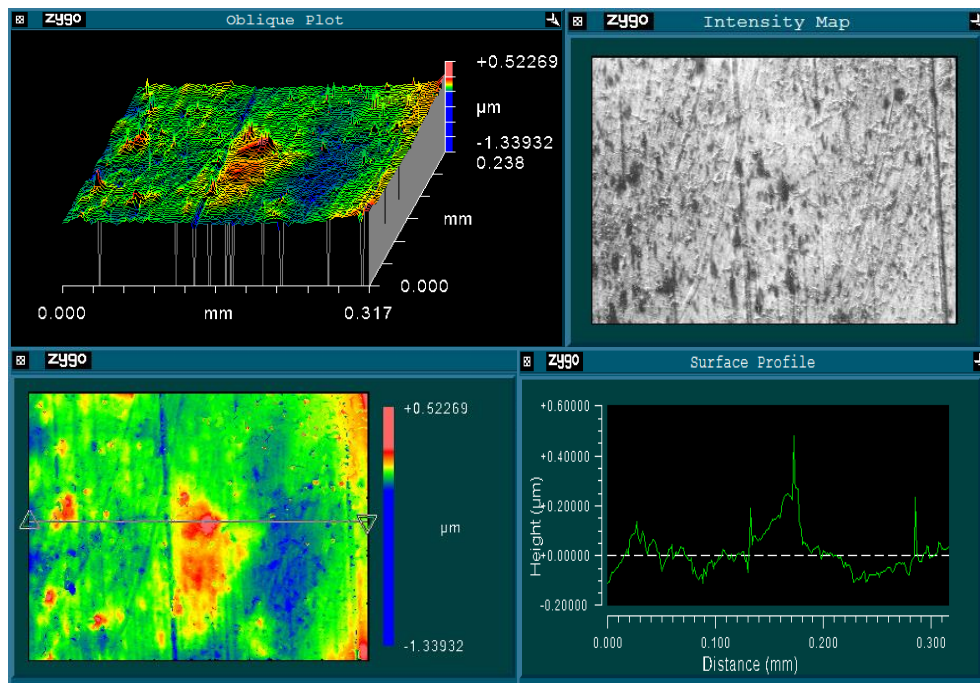


Figure 4.27 Surface topography plots for a measurement area on a polished area of a retrieved K+ tibial component from a TKR with PE wear through  $S_q = 0.075\mu\text{m}$ ,  $S_z = 1.073\mu\text{m}$



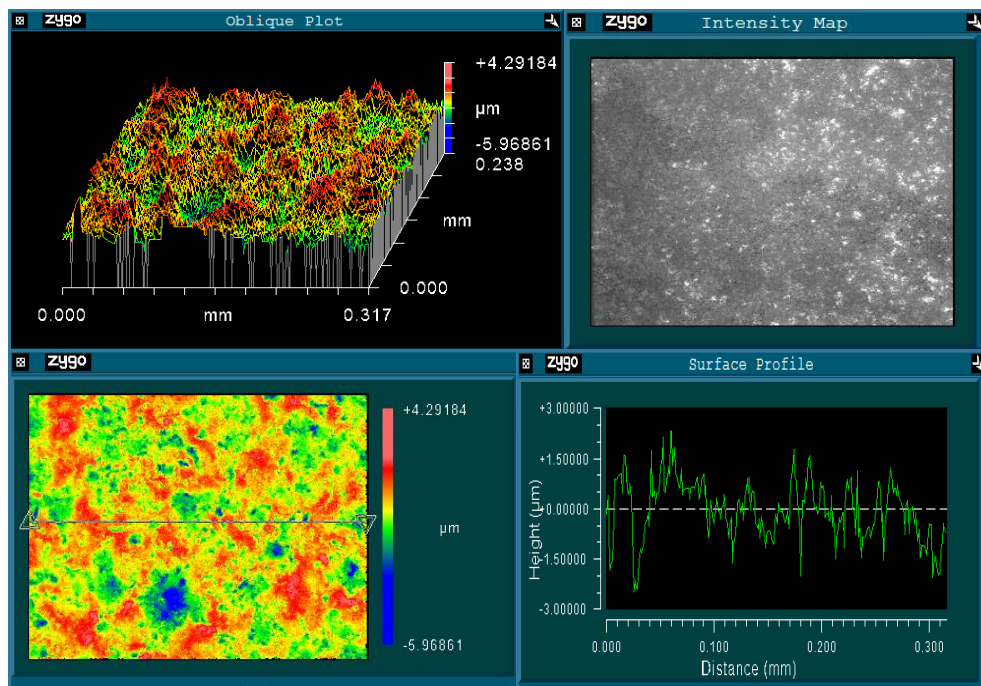


Figure 4.28 Surface topography plots for a measurement area on a retrieved non-polished PCF tibial component  $S_q = 0.922\mu\text{m}$ ,  $S_z = 7.666\mu\text{m}$

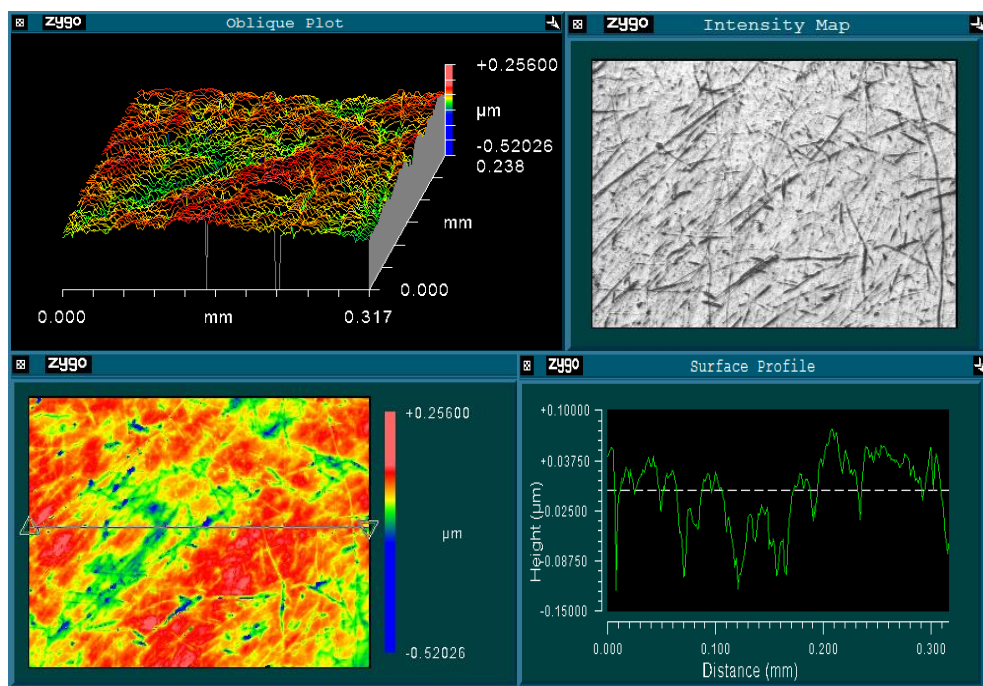


Figure 4.29 Surface topography plots for a measurement area on a retrieved polished PFC tibial component  $S_q = 0.045\mu\text{m}$ ,  $S_z = 0.609\mu\text{m}$

## 4.4 Results Summary

### 4.4.1 Damage Scoring

The data provided in Table 4.2 FDS, PE ADS and PE BDS for retrieved TKRs is represented graphically in Figures 4.30 and 4.31. There is no correlation to be found between the FDS values for the retrieved femoral components and the PE ADS values for the retrieved PE components ( $r^2 = 0.30$ ). Neither can it be said that there is any correlation between the PE ADS values for the retrieved PE components and the PE BDS values for the retrieved PE components ( $r^2 = 0.29$ ). The results for each group of retrieved components, AGC, PFC and K+ are grouped and show in colour ovals.

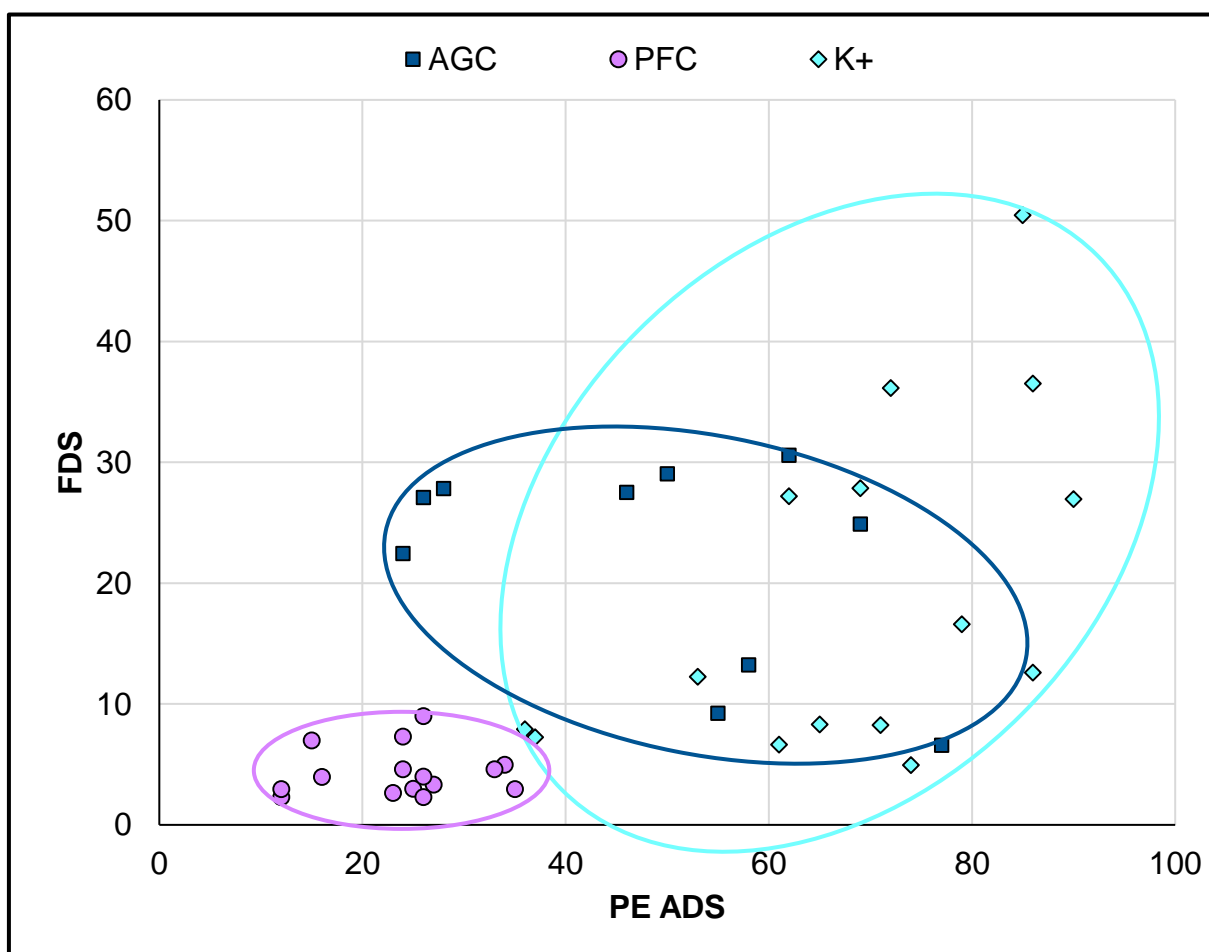


Figure 4.30 Mean FDS against mean PE ADS

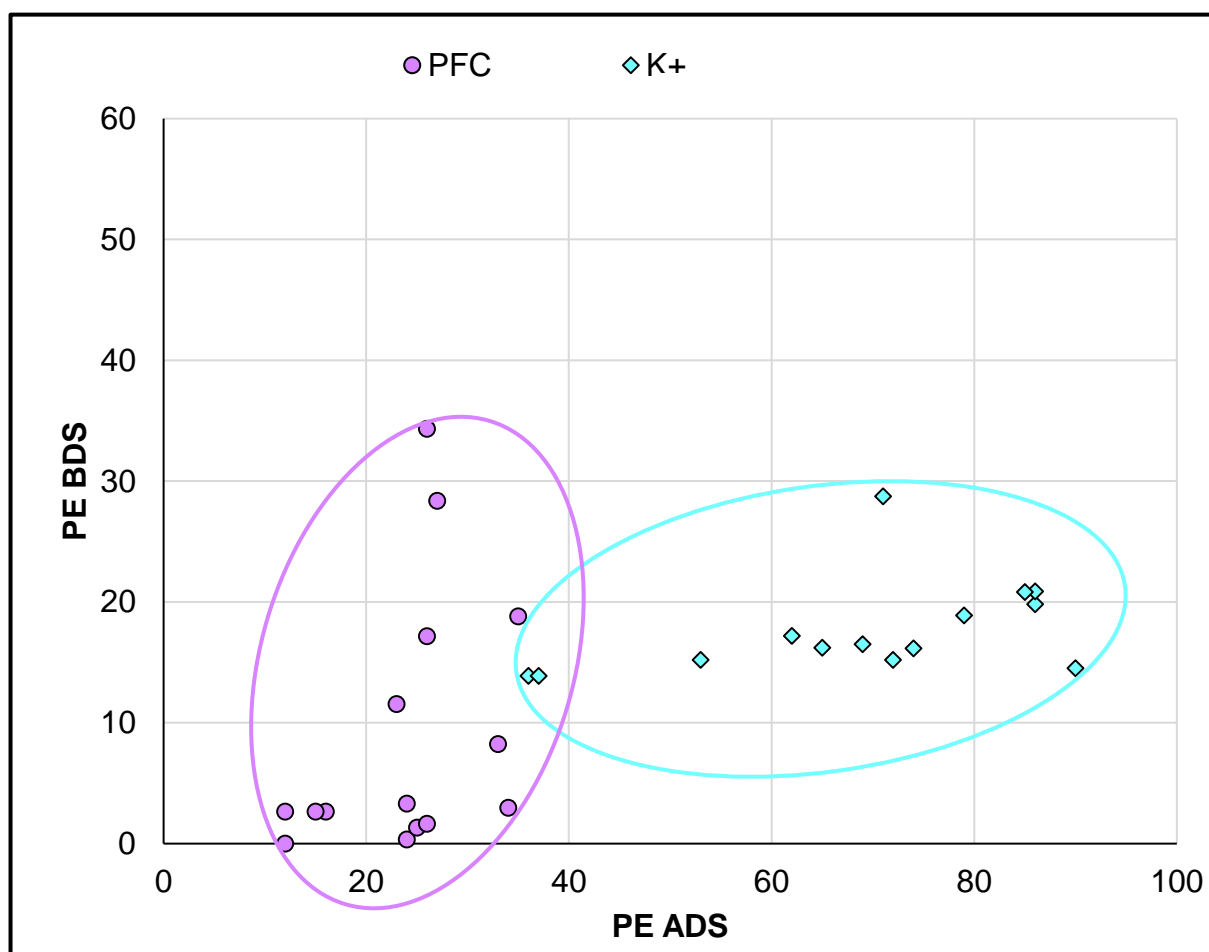


Figure 4.31 Mean PE BDS against mean PE ADS

The data provided in Tables 4.1 and 4.2 is shown graphically in Figure 4.32. There are no correlations found between the FDS, PE ADS and PE BDS values and the length of time *in vivo* ( $r^2 = 0.14$ ;  $r^2 = 0.50$ , and  $r^2 = 0.12$  respectively). Figure 4.32 shows the FDS and PE ADS plotted against time *in vivo*, to avoid cluttering the graph the PE BDS values are not shown. There are no correlations between the FDS, PE ADS or PE BDS and the patient BMI. There is no difference between the FDS, PE ADS or PE BDS values of retrieved components that were implanted into the right or left side of the body. There is no difference between the FDS, PE ADS or PE BDS values of retrieved components that had been implanted in female patients compared to male patients.

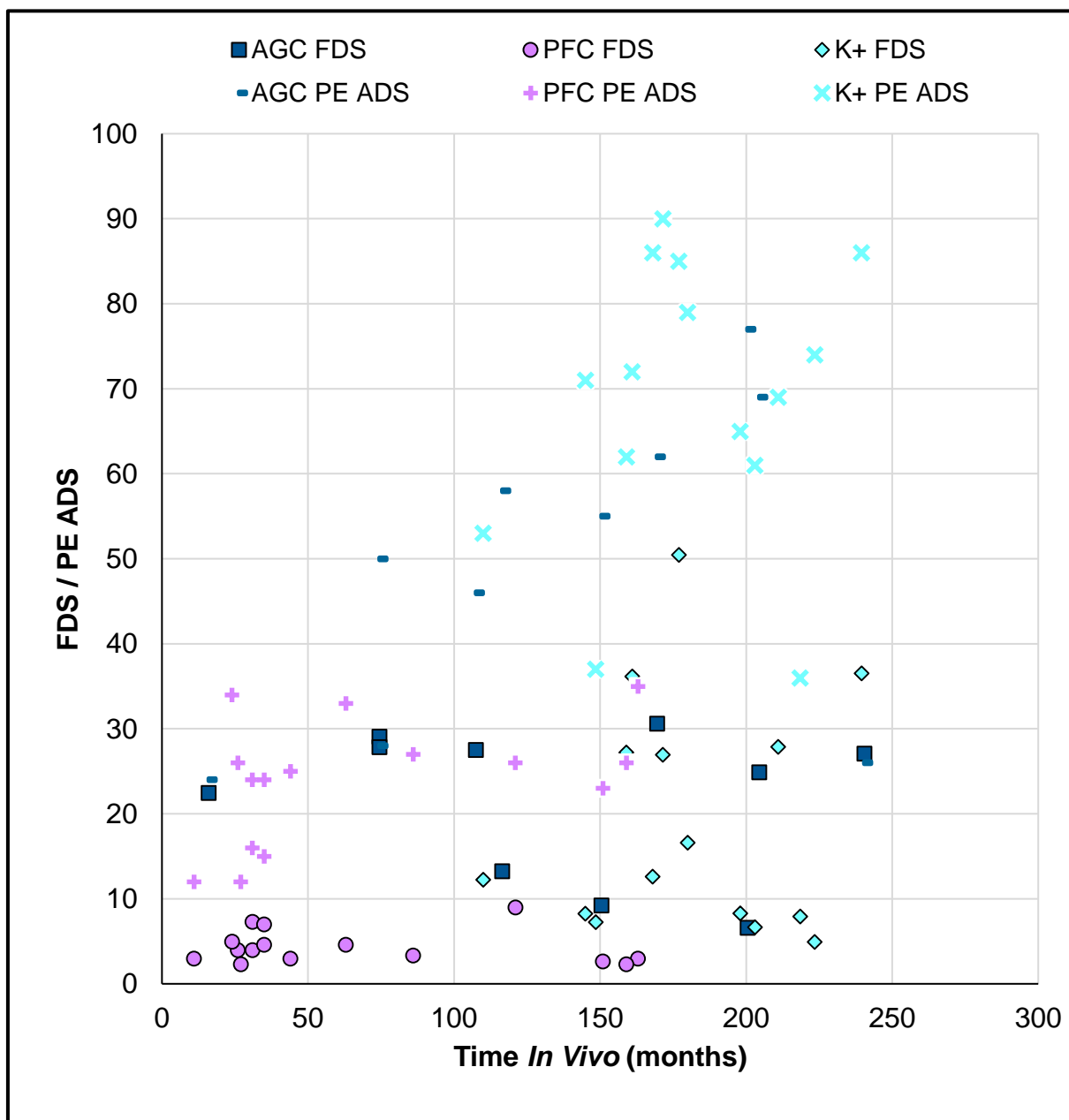


Figure 4.32 Mean FDS and mean PE ADS against time *in vivo*

#### 4.4.2 Surface Profilometry

None of the surface roughness parameters measured on the retrieved femoral components correlated with the length of time *in vivo*. None of the surface roughness parameters measured on retrieved tibial components correlated with the length of time *in vivo*. None of the surface roughness parameters measured on the backside surface of the retrieved PE components correlated with length of time *in vivo*.

Figures 4.33 and 4.34 show retrieved femoral component  $S_q$  and retrieved femoral component  $S_{sk}$  plotted against time *in vivo*. the respective  $R^2$  values for these graphs are 0.10 and 0.11 and show no correlation. Figure 4.35 shows retrieved tibial component  $S_q$  against time *in vivo*. In each of these three figures the groups are identified by coloured ovals. In Figure 4.35 it can be seen that there is no overlap between the different groups of retrieved tibial components, the polished PFC, non-polished PFC and K+ tibial components.

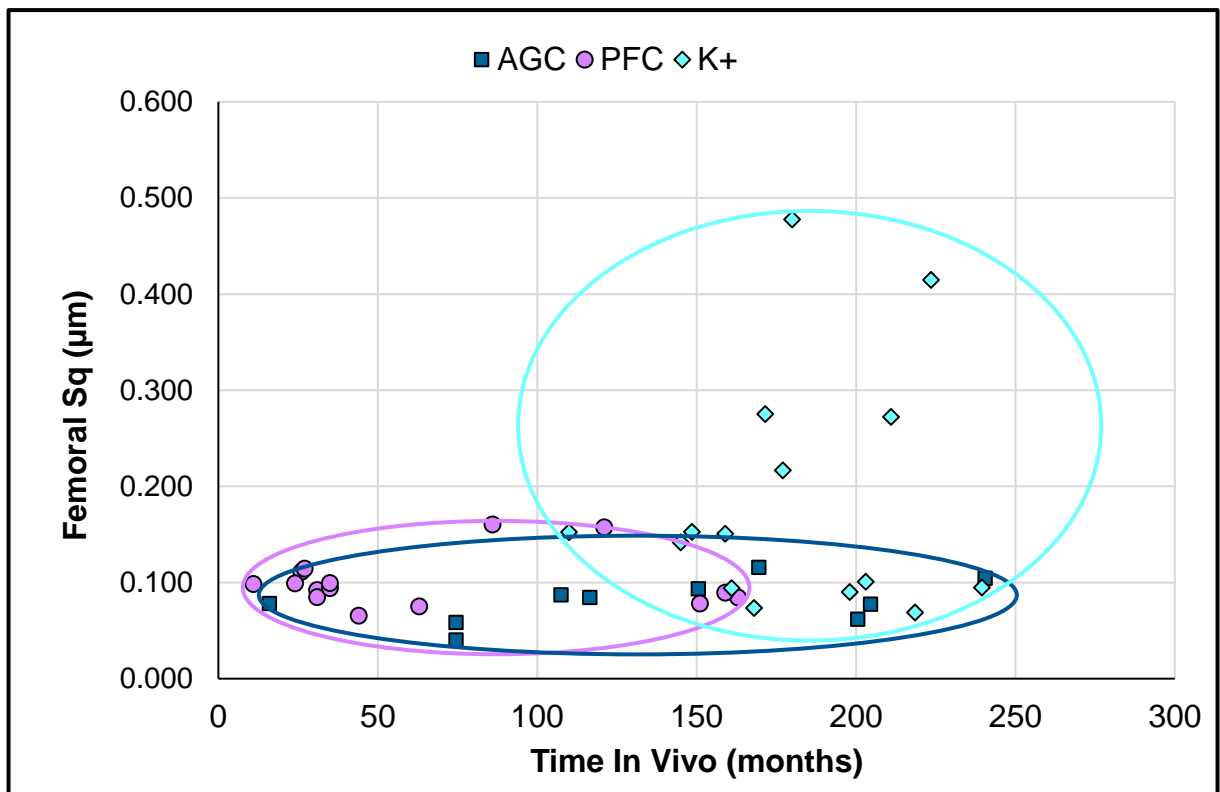


Figure 4.33 Retrieved femoral component  $S_q$  against length of time *in vivo*

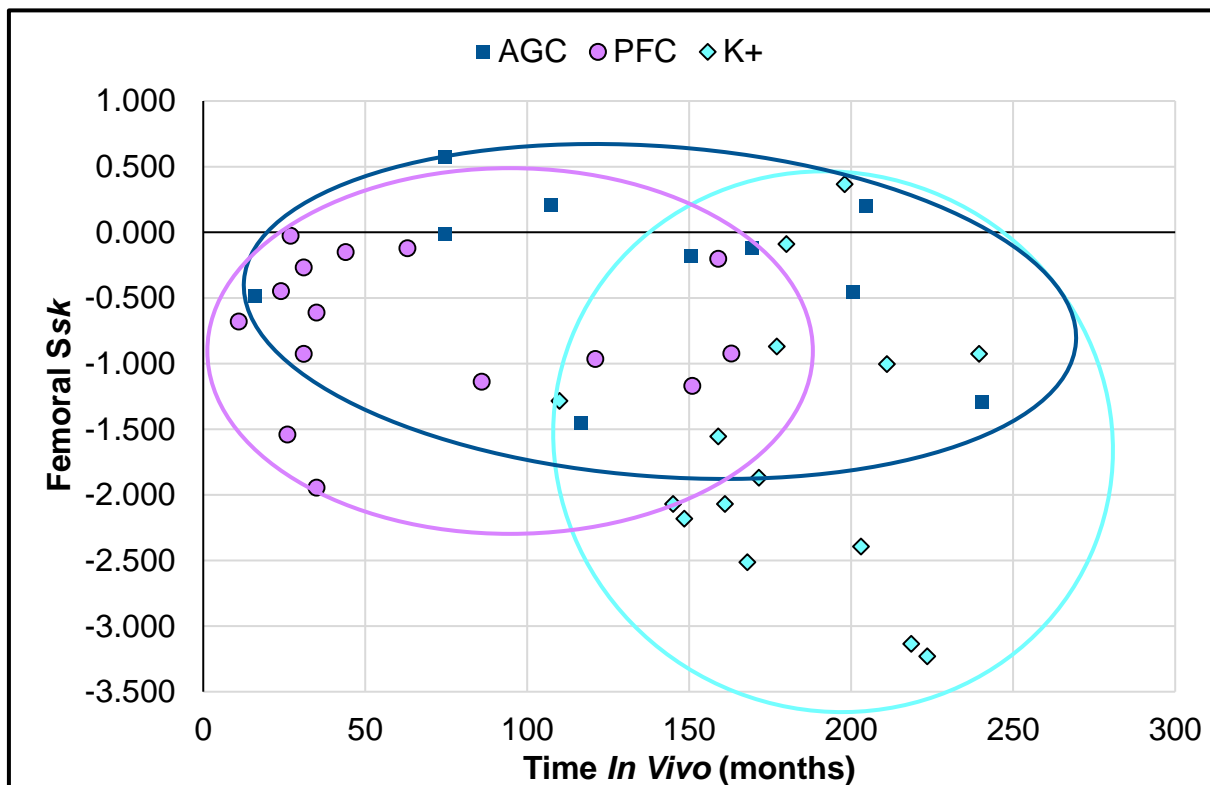


Figure 4.34 Retrieved femoral component  $S_{sk}$  against length of time *in vivo*

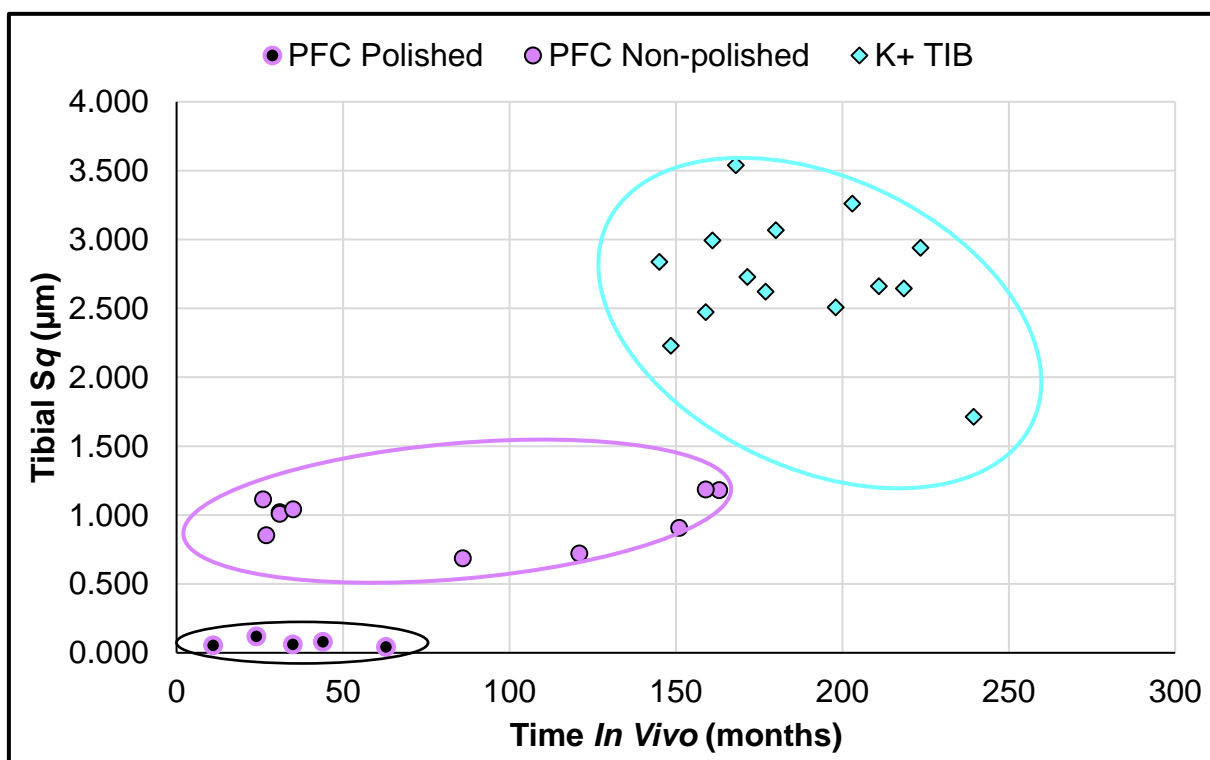


Figure 4.35 Retrieved tibial component  $S_q$  against length of time *in vivo*

There is no correlation between the surface roughness parameters measured on the retrieved femoral components, retrieved tibial components or the backside surface of the retrieved PE components and the patient age at primary surgery or the patient BMI. There is no difference between the surface roughness parameters measured on the retrieved components that were implanted into the right or left side of the body. There is no difference between the surface roughness parameters measured on retrieved component that had been implanted in female patients compared to male patients.

The retrieved femoral component surface roughness parameters do not correlate with the FDS for the retrieved components. And the retrieved femoral component surface roughness parameters do not correlate with the PE ADS. Figure 4.36 shows retrieved femoral component  $S_q$  plotted against PE ADS

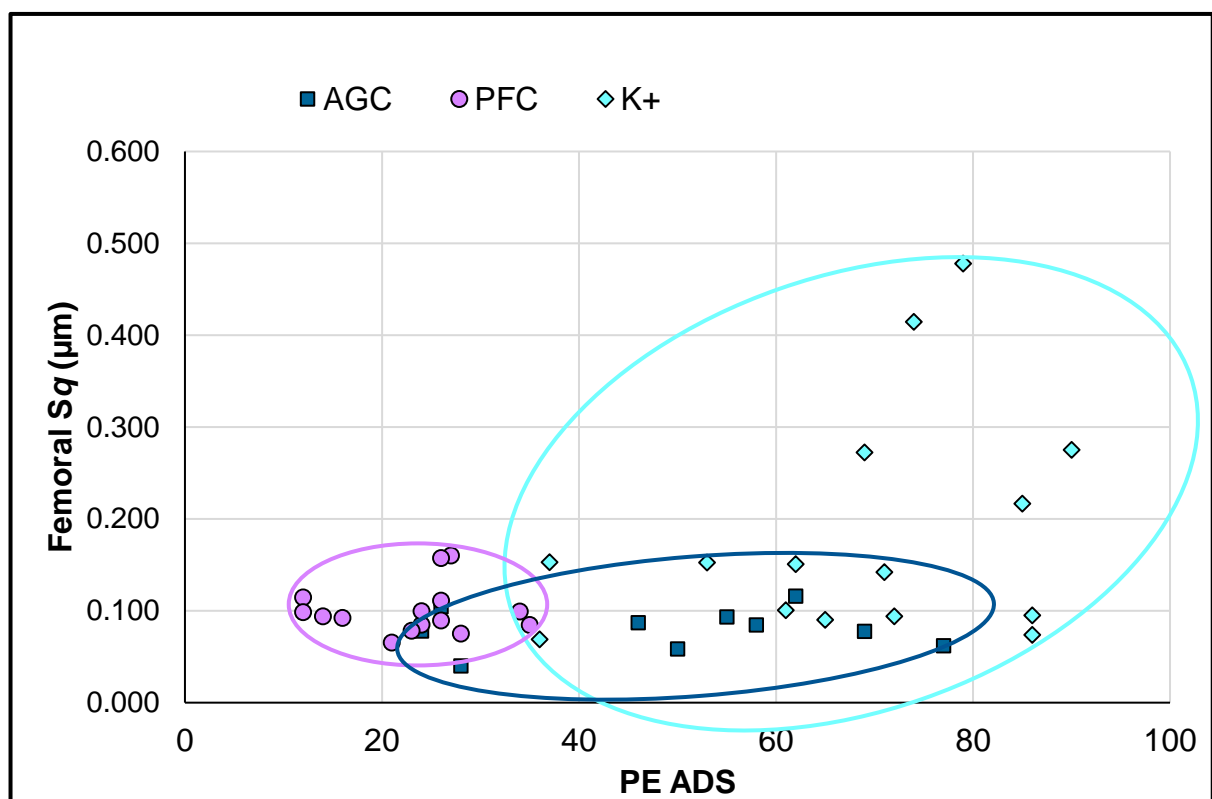


Figure 4.36 Retrieved femoral component  $S_q$  against PE ADS

The surface roughness parameters measured on the backside of the retrieved PE components do not correlate with the surface roughness parameters measured on

the retrieved tibial components. The comparison is shown in Figure 4.37 with the three groups, retrieved polished PFC tibial component, non-polished PFC tibial component and K+ tibial component identified.

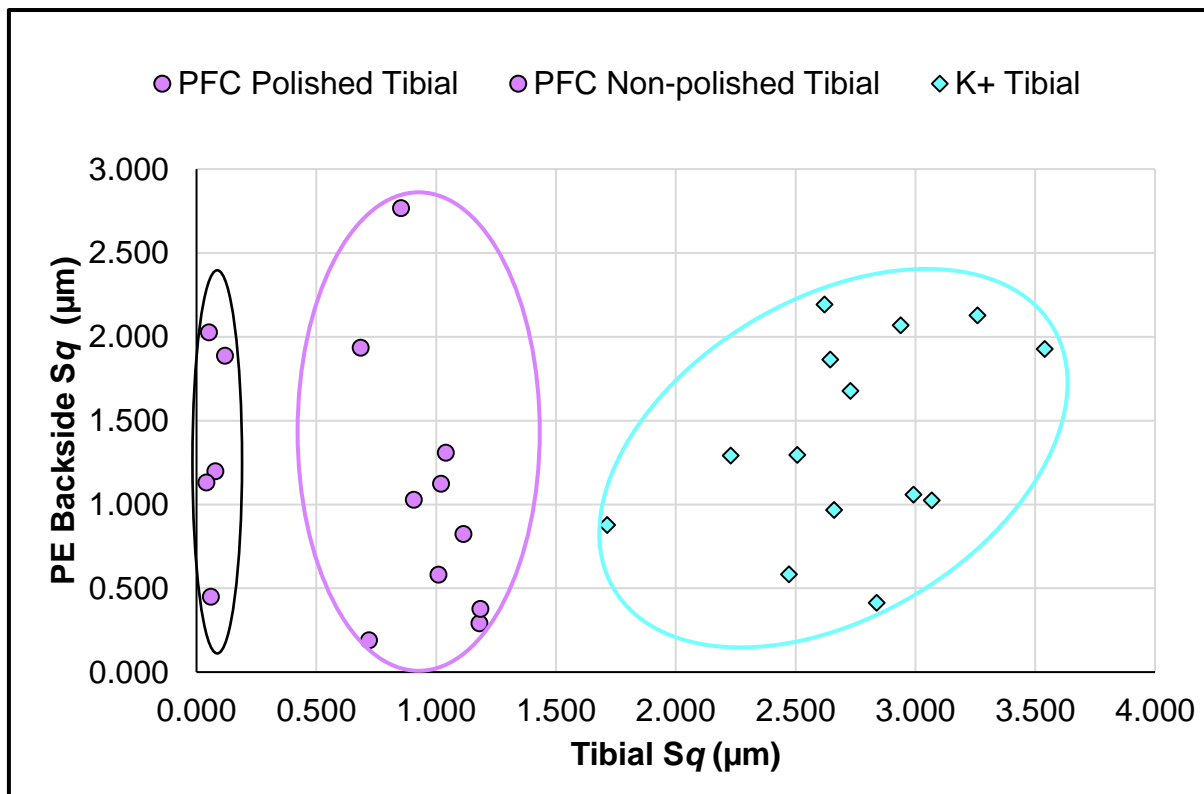


Figure 4.37 PE component backside surface  $S_q$  against tibial component  $S_q$

None of the surface roughness parameters measured on the retrieved tibial components correlate with the PE BDS. Figure 4.38 shows the retrieved tibial component  $S_q$  plotted against and PE BDS.



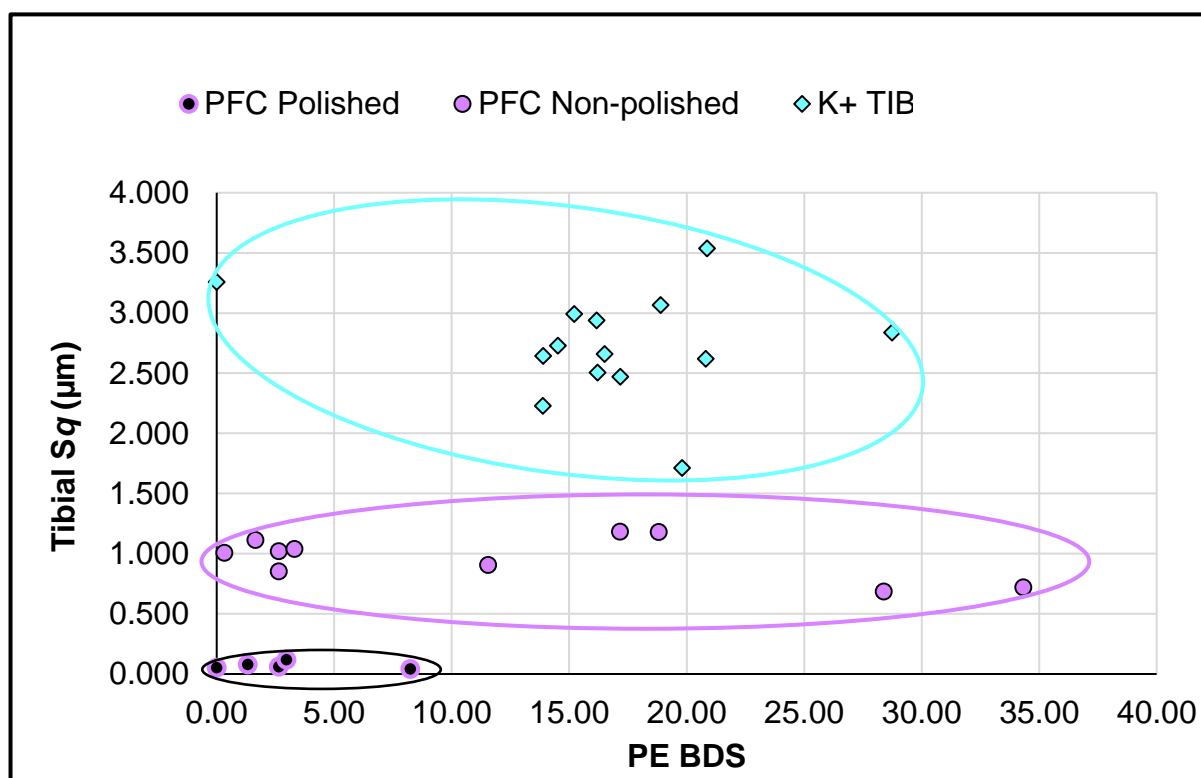


Figure 4.38 Tibial component surface  $S_q$  against PE component BDS

*Blank page*

## **Chapter 5 Surface Topographical Analysis of Explanted Unicondylar Knee Replacements with Cobalt Chromium Alloy Femoral Components**

This chapter presents the surface topographical analysis results of retrieved explanted Unicondylar Knee Replacement (UKRs) prostheses with cobalt chromium alloy (CoCr) femoral components using the methods described in Chapter 3 Materials and Methods. The literature review presented in Chapter 2 failed to identify any current published studies that provide an analysis of the surface roughness measurements specifically of retrieved UKR prostheses. Within this chapter the macroscopic observations, damage scoring results and surface roughness measurements for retrieved explanted UKRs are included. The damage scoring results and surface roughness measurements are correlated to enable the identification of relationships between the results. The retrieved explanted components shall hereby be known as “retrievals” or “retrieved components”.

### **5.1 Implant and Patient Variables**

Twenty-two UKR retrievals were identified within the Knee Explant Catalogue (Appendix B). This includes ten High Flexion Unicompartmental Knees (HFZ) (Zimmer Biomet, Warsaw, IN, US), eight Oxford ® UKRs (OB) (Zimmer Biomet, Warsaw, IN, US), two Oxinium Journey UKRs ® (JOxZr) (Smith & Nephew, London, UK), one Sled ® (SL) UKR (Link, Hamburg, Germany) and one other unidentified UKR (Oth). One of the retrieved OB UKRs was excluded from inclusion in this chapter as the retrieval only consisted of the PE component and a further two retrieved OB UKRs were excluded as there was no accompanying data with the prostheses and no means of identifying them. Seventeen retrieved UKRs, the ten HFZs, the five OBs, the SL and the one Oth, all had CoCr alloy femoral components. The two JOxZr UKRs had OxZr femoral components and the results from the analysis of these components shall be presented in Chapter 6. The HFZs, the SL and the JOxZrs UKRs were all fixed bearing designs whereas the OBs and the one Oth UKR were mobile bearing designs; all used cemented fixation.

As detailed in Chapter 3, there was only patient data available for four of the UKR retrievals (three OBs and the SL). For all these components the indication for primary surgery was osteoarthritis and the indications for revision included mechanical impingement of the tibial component on the patella tendon, pain and lack of extension, isolated pain and PE wear, aseptic loosening and metallosis. For these four components the length of time *in vivo* was 39, 125, 175 and 25 months. Figure 5.1 shows one of each of the models of retrieved UKR with CoCr femoral components.

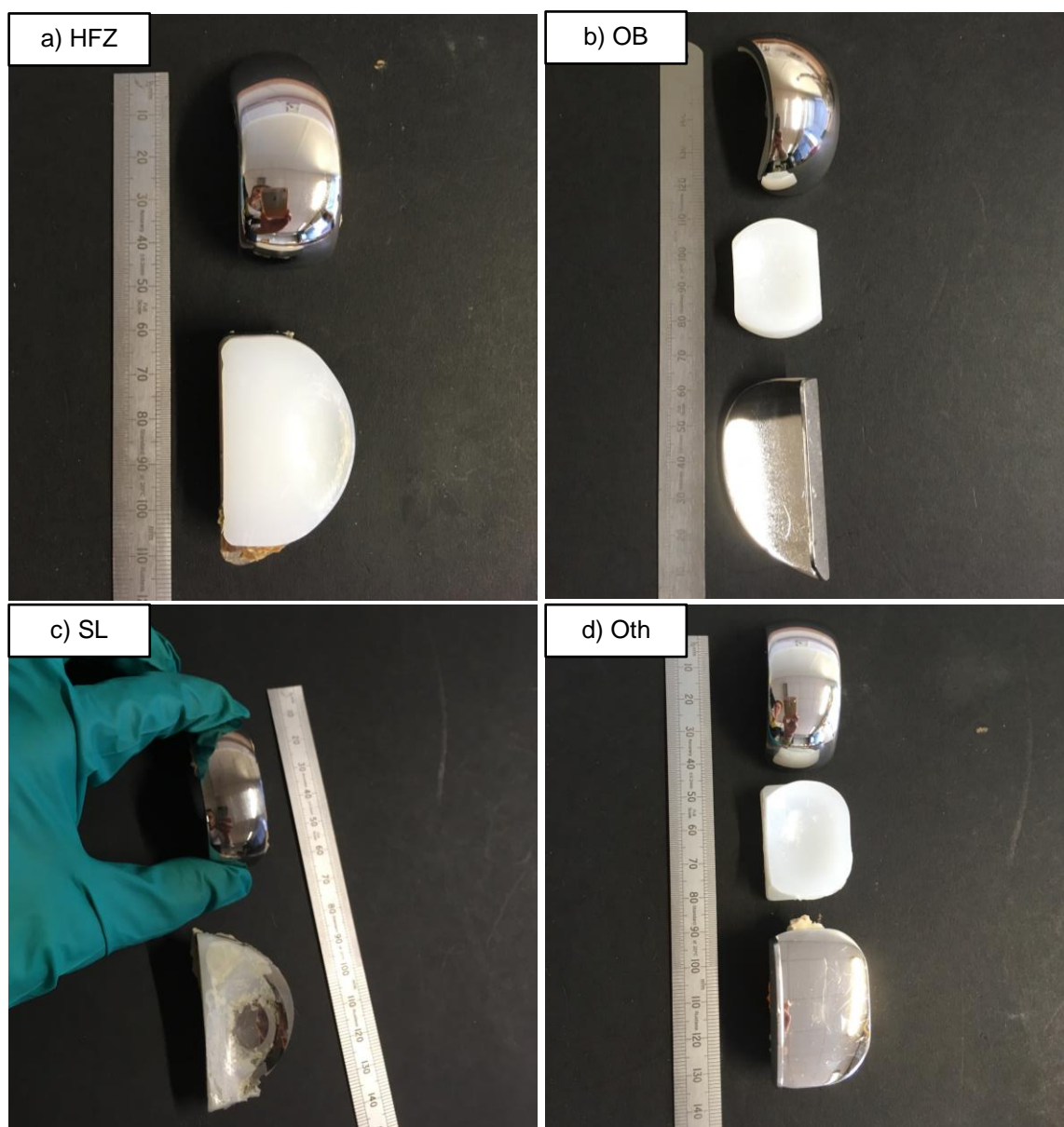


Figure 5.1 (a) Retrieved HFZ (b) OB (c) SL and (d) Oth UKR components

## 5.2 Macroscopic Visual Assessment and Semi-quantitative Damage Scoring

Macroscopic visual assessment of the surfaces of the femoral condyles and articulating and backside surfaces of the PE components and the tibial trays were performed. A summary of the assessments is given in the subsections below and the full assessments are tabulated in Table D1, Appendix D. Femoral component damage scoring, PE articular surface damage scoring and PE backside damage scoring was performed for the retrieved UKRs prostheses as per the methods described in Chapter 3. The results are summarised in Table 5.1 and the subsections below. As explained in previous chapters, the two decimal places of the FDS and PE BDS result have no bearing on the precision or accuracy of the data and are simple a product of using the arbitrary values 0.33 and 0.66 to represent the severity scores.

The femoral components of the ten retrieved HFZ UKRs were all observed to have some damage that was considered to be *in vivo* damage although very minimal damage (mean femoral damage score (FDS) = 3.22, range 0.66 -7.31), Four components were observed to have gouging, five showed light burnishing and eight showed light scratching or indentations. The PE components of the retrieved HFZ UKRs were characterised by the observation of a definite load area of approximately 10-15mm x 20-25mm. Within the load areas damage features burnishing (ten components), light pitting (nine components) and light scratching (nine components) were observed. The mean PE component articular damage score (ADS) was 18.40 (range 11 – 29). Only three of the retrieved HFZ PE components were separated from the tibial components, the other seven were unable to be separated without risking completely destroying the sample. The HFZ PE backside surfaces that were able to be macroscopically observed were characterised by very light burnishing (mean PE backside damage score (BDS) = 7.37, range 5.94 – 8.91).

The femoral components of the five retrieved OB UKRs were all observed to have burnished damage tracks and some light scratches and indentations. No gouging was observed. The mean FDS was 6.67 (range 3.96 -8.58). The articular surfaces of the PE components of the retrieved OB UKRs did not have definite load areas but were characterised by pitting (five components) and burnishing (four components)

over all the surface, one component was observed to have subsurface cracking which is considered to be pre-delamination fatigue damage. The mean PE ADS was 19 (range 12 – 33). The backside surfaces of the OB PE components were characterised by burnishing (five components), scratching (four components) and pitting (three components) and the mean PE BDS was 4.44 (range 1.32 – 9.97).

Table 5.1 FDS, PE ADS and PE BDS for Retrieved UKRs

	<b><u>Design</u></b>	<b><u>FDS</u></b>	<b><u>PE ADS</u></b>	<b><u>PE BDS</u></b>
<b>UKR1</b>	<b>HFZ</b>	0.66	15	-
<b>UKR2</b>	<b>HFZ</b>	7.31	29	-
<b>UKR3</b>	<b>HFZ</b>	0.66	19	7.26
<b>UKR4</b>	<b>HFZ</b>	2.98	20	-
<b>UKR5</b>	<b>HFZ</b>	1.00	14	-
<b>UKR6</b>	<b>HFZ</b>	1.33	23	5.94
<b>UKR7</b>	<b>HFZ</b>	3.30	13	-
<b>UKR8</b>	<b>HFZ</b>	6.00	22	-
<b>UKR9</b>	<b>HFZ</b>	4.95	18	8.91
<b>UKR10</b>	<b>HFZ</b>	3.99	11	-
<b>HFZ Mean (n=10)</b>		<b>3.22</b>	<b>18</b>	<b>7.37</b>
<b>HFZ Median (n=10)</b>		<b>3.14</b>	<b>18</b>	<b>7.26</b>
<b>UKR11</b>	<b>OB</b>	7.26	24	9.97
<b>UKR12</b>	<b>OB</b>	8.58	33	2.31
<b>UKR13</b>	<b>OB</b>	8.25	13	1.32
<b>UKR14</b>	<b>OB</b>	5.28	12	6.27
<b>UKR15</b>	<b>OB</b>	3.96	13	2.31
<b>OB Mean (n=5)</b>		<b>6.67</b>	<b>19</b>	<b>4.44</b>
<b>OB Median (n=5)</b>		<b>7.26</b>	<b>13</b>	<b>2.31</b>
<b>UKR HFZ &amp; OB Mean (n=15)</b>		<b>4.37</b>	<b>19</b>	<b>5.54</b>
<b>UKR HFZ &amp; OB Median (n=15)</b>		<b>3.99</b>	<b>18</b>	<b>6.11</b>
<b>UKR16</b>	<b>SL</b>	26.21*	22*	16.52*
<b>UKR17</b>	<b>Oth</b>	6.29	29	48.20 <sup>\$</sup>
<b>UKR CoCr Mean (n=17)</b>		<b>5.77</b>	<b>19</b>	<b>10.90</b>
<b>UKR CoCr Median (n=17)</b>		<b>4.95</b>	<b>19</b>	<b>6.77</b>

\*Complete PE wear through resulting in articulation of femoral and tibial components. <sup>\$</sup> Convex femoral and tibial components resulting in high PD BDS score. HFZ – High Flex Unicondylar Knee Zimmer; OB – Oxford Biomet; SL – Sled Link; Oth – Other design.

The FDS, PE ADS and PE BDS median, maximum, minimum and inter-quartile ranges for the retrieved HFZ and OB UKR prostheses are shown in Figure 5.2. (The median lines for the OB PE ADS and PE BDS data are not visible as the first quartile and median values are the same.) For the HFZ PE BDS there were only 3 components to analyse, these are shown as individual data points on the graph.

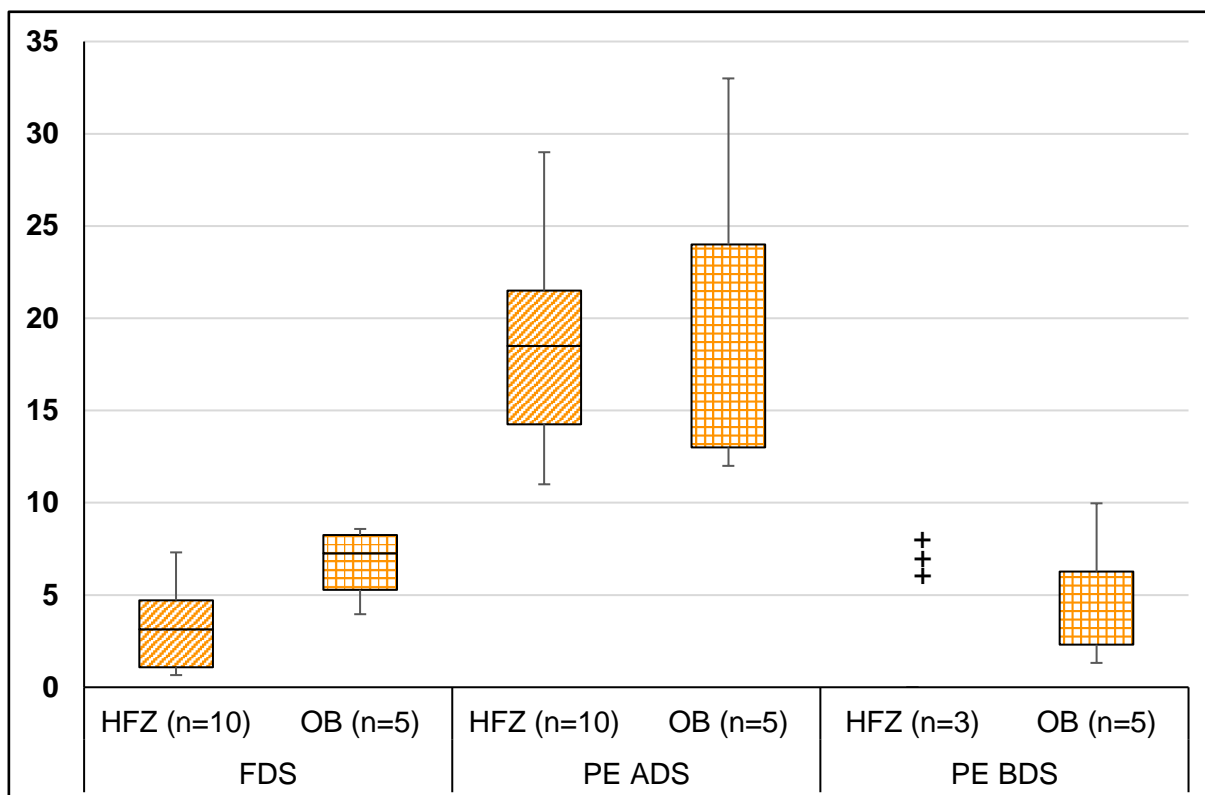


Figure 5.2 FDS, PE ADS and PE BDS for retrieved UKRs

The PE component of the SL UKR had completely worn through resulting in metal on metal articulation between the femoral component and the tibial tray, hence the exceptionally high FDS, PE ADS and PE BDS values. The Oth UKR was unusual in that the tibial tray was a convex geometry similar to the femoral component and the PE component was semi-constrained. Both the articular and backside surfaces were damaged in a similar fashion.

Figures 5.3 and 5.4 show the median, maximum, minimum and inter-quartile ranges of the FDS and DFS values, the PE ADS and DFS values and the PE BDS and DFS values respectively for the retrieved HFZ and OB UKR prostheses. The damaging

scoring results for the retrieved SL and Oth UKR prostheses are not shown graphically. Where there are less than four values a boxplot is not shown but the measurement points are given.

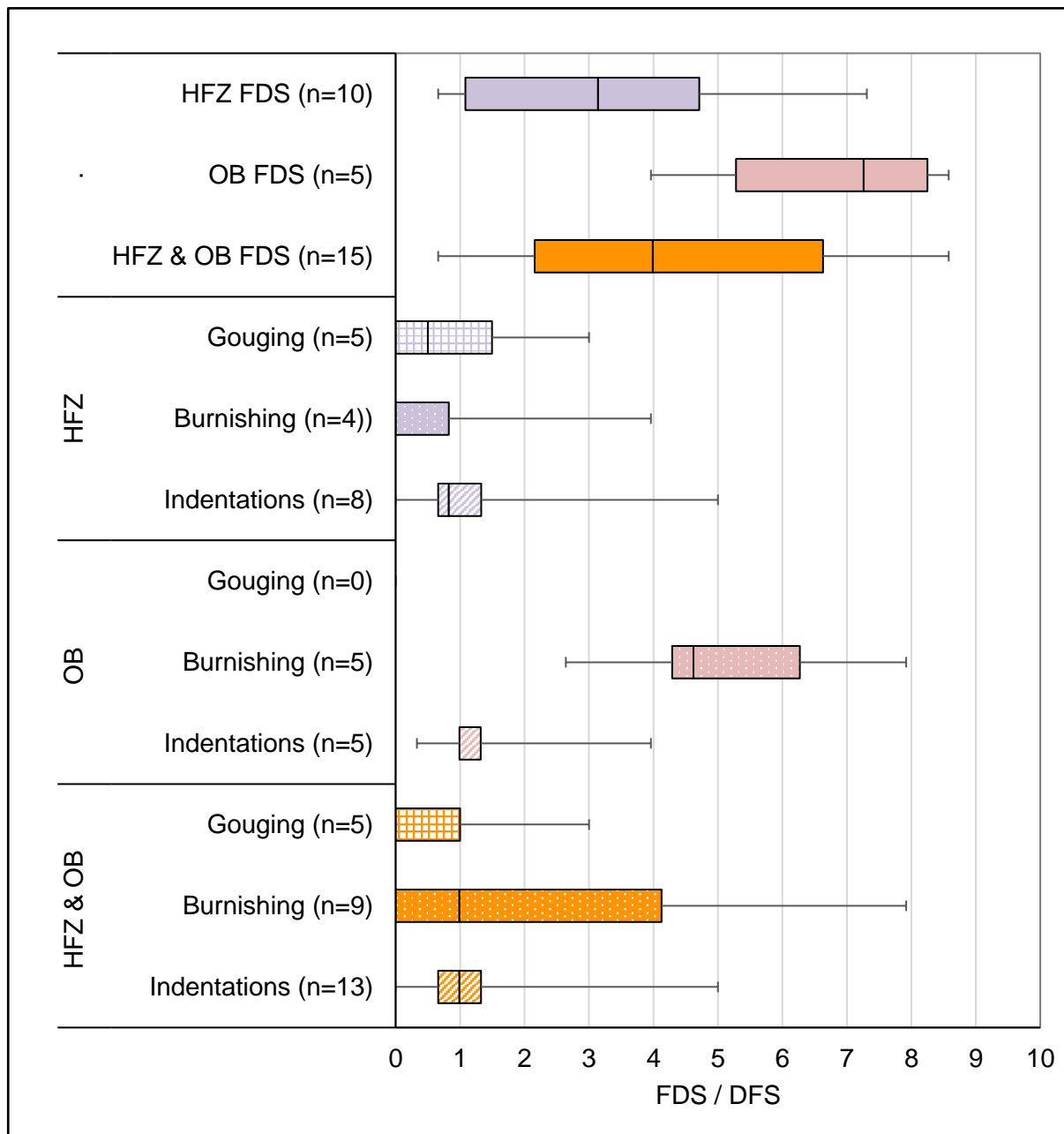


Figure 5.3 FDS and DFS values for retrieved HFZ and OB UKRs



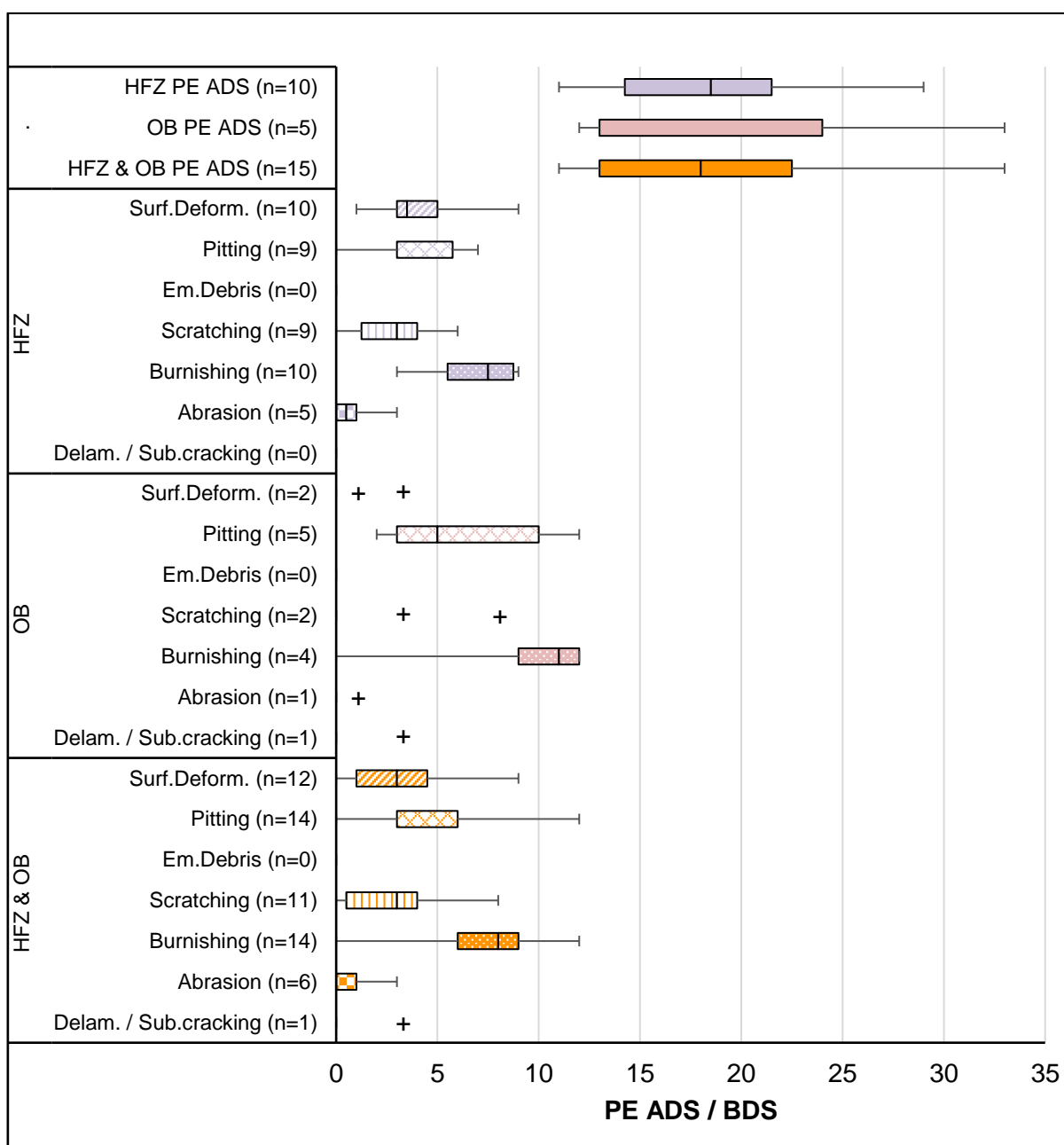


Figure 5.4 PE ADS and DFS values for retrieved HFZ and OB UKRs

### 5.3 Non-contacting Profilometry

The mean and standard errors of the surface roughness parameters measured on the femoral components of the retrieved UKR prostheses with CoCr femoral components (HFZ, OB, SL and Oth) are given in Table 5.2. The non-contacting profilometry results for the two retrieved UKR prostheses with OxZr femoral

components (JOxZr) are provided in Chapter 6. No reference UKR femoral component was available and so surface roughness parameters measured on the four reference TKR femoral components in Chapter 4 were combined to approximate a reference UKR femoral component surface (labelled “Reference” in Table 5.2 and Figure 5.5). The assumption was made that there is no difference between a reference TKR and reference UKR femoral component surface roughness. For each reference femoral component fifteen measurement points were taken on each condyle, giving a total of thirty measurements points per component. On the retrieved UKRs femoral components fifteen measurement points were taken per component. The ‘n’ value in the Table 5.2 are the number of components.

Table 5.2 UKR Femoral Component Surface Roughness Parameters

\*Mean value  $\pm$  standard error is given for each parameter except where n=1

	<b>Reference (n = 4)</b>	<b>HFZ (n = 10)</b>	<b>OB (n = 5)</b>
<b>S<sub>q</sub> (μm)</b>	0.055 ( $\pm$ 0.004)	0.073 ( $\pm$ 0.005)	0.077 ( $\pm$ 0.008)
<b>S<sub>p</sub> (μm)</b>	0.350 ( $\pm$ 0.031)	0.414 ( $\pm$ 0.016)	0.442 ( $\pm$ 0.063)
<b>S<sub>v</sub> (μm)</b>	-0.528 ( $\pm$ 0.071)	-0.597 ( $\pm$ 0.055)	-0.743 ( $\pm$ 0.110)
<b>PV (μm)</b>	0.877 ( $\pm$ 0.093)	1.010 ( $\pm$ 0.059)	1.185 ( $\pm$ 0.166)
<b>S<sub>z</sub> (μm)</b>	0.444 ( $\pm$ 0.033)	0.491 ( $\pm$ 0.021)	0.586 ( $\pm$ 0.082)
<b>S<sub>sk</sub> (-)</b>	-0.632 ( $\pm$ 0.272)	-0.381 ( $\pm$ 0.283)	-1.578 ( $\pm$ 0.546)
<b>S<sub>ku</sub> (-)</b>	27.667 ( $\pm$ 10.044)	14.778 ( $\pm$ 3.829)	19.856 ( $\pm$ 4.967)
	<b>SL (n = 1)</b>	<b>Oth (n = 1)</b>	<b>Retrieved UKR (n = 16)</b>
<b>S<sub>q</sub> (μm)</b>	0.307	0.070	0.074 ( $\pm$ 0.004)
<b>S<sub>p</sub> (μm)</b>	1.323	0.572	0.432 ( $\pm$ 0.023)
<b>S<sub>v</sub> (μm)</b>	-1.373	-0.746	-0.652 ( $\pm$ 0.050)
<b>PV (μm)</b>	2.696	1.318	1.084 ( $\pm$ 0.065)
<b>S<sub>z</sub> (μm)</b>	1.463	0.517	0.522 ( $\pm$ 0.029)
<b>S<sub>sk</sub> (-)</b>	-0.576	-2.995	-0.919 ( $\pm$ 0.307)
<b>S<sub>ku</sub> (-)</b>	7.561	38.099	17.822 ( $\pm$ 3.121)

The mean values of the surface roughness parameters measured on the retrieved UKR CoCr femoral components which includes ten HFZ, five OB and one Oth and excludes the SL femoral component are shown in Figure 5.5 (Retrieved UKR n = 16, Reference TKR n = 4). The SL UKR was observed to have complete PE wear through and severe damage to the femoral component unlike any of the other retrieved UKR CoCr femoral components and was therefore excluded from this analysis.

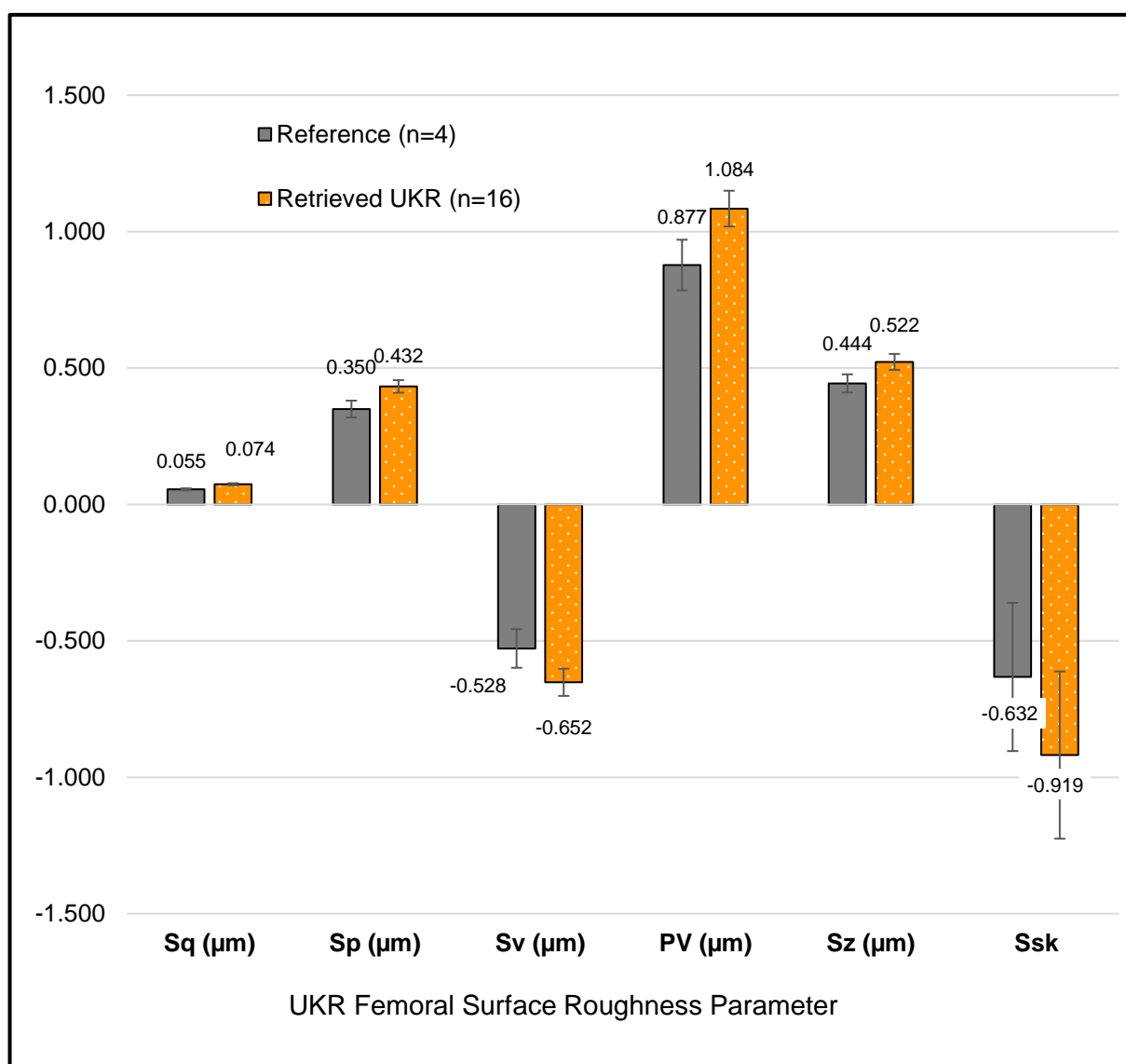


Figure 5.5 Retrieved vs reference UKR femoral component surface roughness parameters

The surface roughness parameters measured on the retrieved UKR femoral components were all greater ( $S_q$ ,  $S_p$ , PV and  $S_z$  more positive and  $S_v$  and  $S_{sk}$  more negative) than the surface roughness parameters measured on the reference components. The difference between the mean  $S_q$  value was shown to be significant ( $p=0.019$ ). None of the other differences were determined to be significant. The small sample sizes mean that any statistically significant differences identified may not be reliable and caution should be taken in the analysis of results.

Figures 5.6 – 5.9 show surface topography plots for measurement areas taken on the retrieved UKR CoCr femoral components for the HFZ, OB, SL and Oth.

All the surface topography plots show an oblique plot, an intensity map, a surface map and a surface profile for each measurement area. The RMS surface roughness,  $S_q$ , and the ten-point height average,  $S_z$ , values are detailed in the figure title.

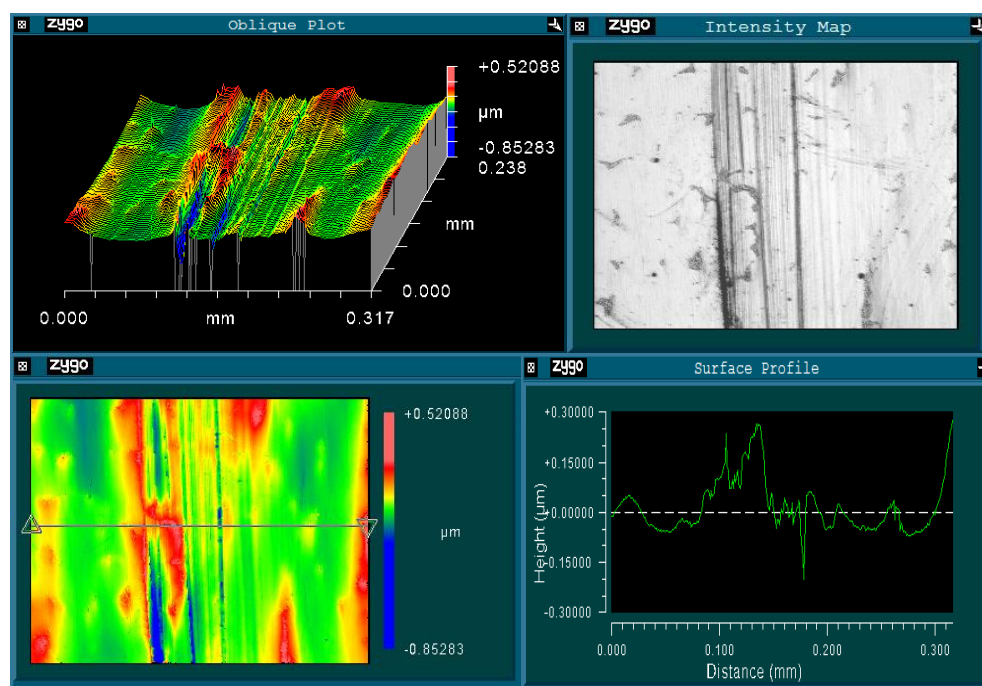


Figure 5.6 Surface topography plots for a measurement area on a retrieved HFZ femoral component  $S_q = 0.082\mu\text{m}$ ,  $S_z = 0.672\mu\text{m}$

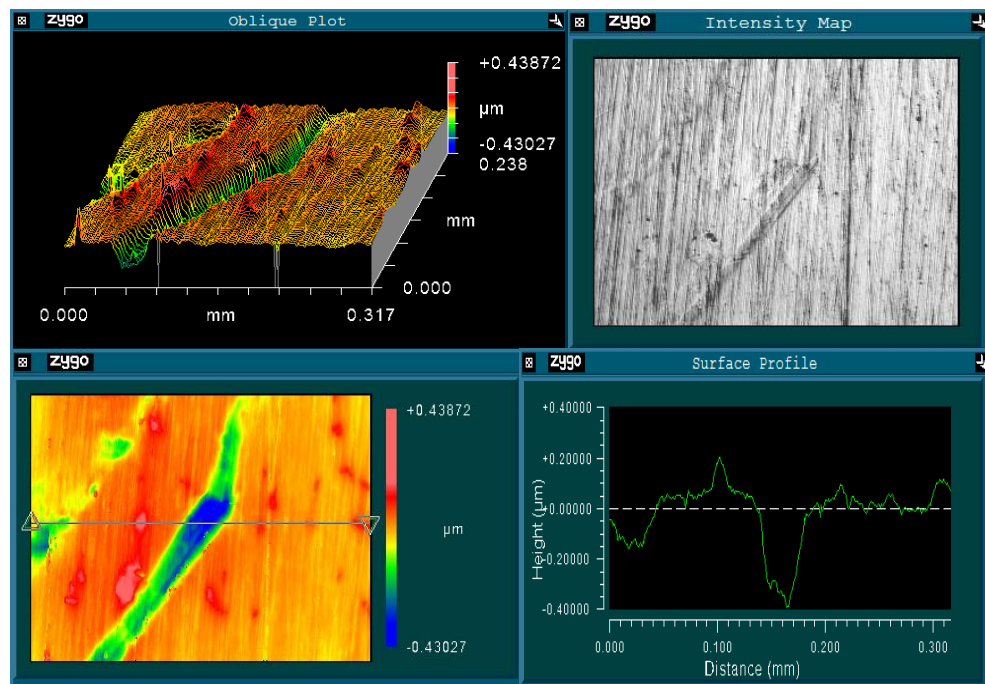


Figure 5.7 Surface topography plots for a measurement area on a retrieved OB femoral component  $S_q = 0.074\mu\text{m}$ ,  $S_z = 0.423\mu\text{m}$

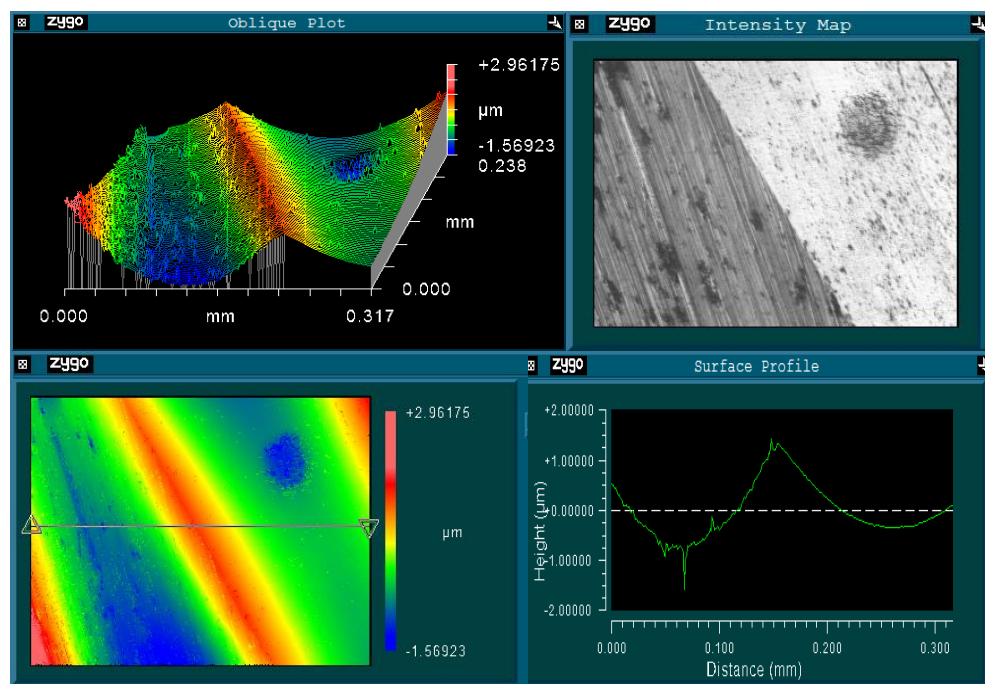


Figure 5.8 Surface topography plots for a measurement area on the retrieved SL femoral component  $S_q = 0.649\mu\text{m}$ ,  $S_z = 2.186\mu\text{m}$

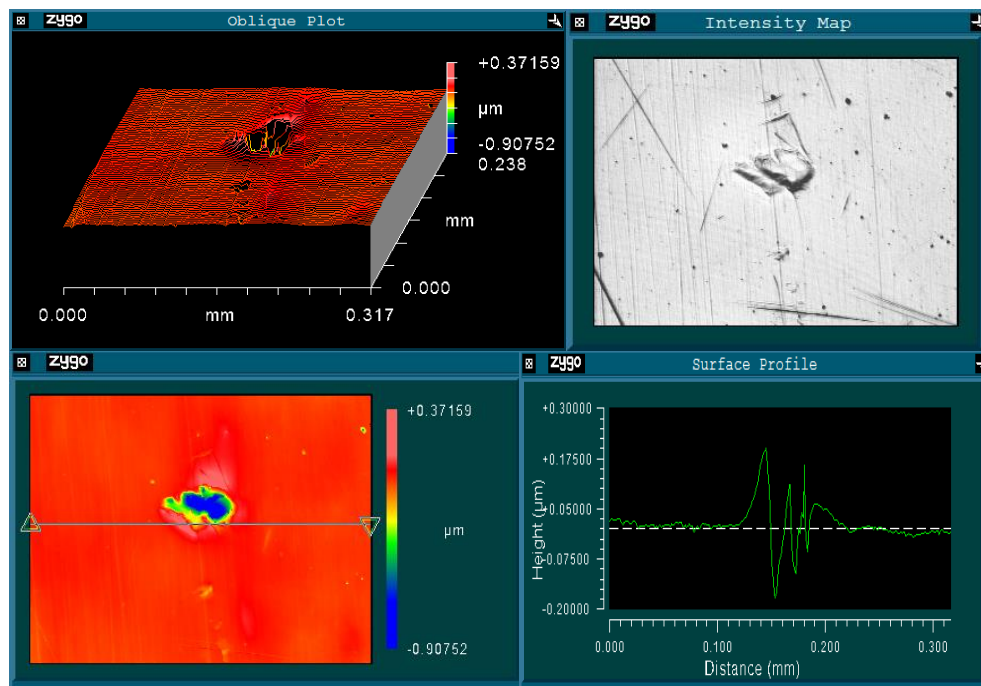


Figure 5.9 Surface topography plots for a measurement area on the retrieved Oth femoral component  $S_q = 0.073\mu\text{m}$ ,  $S_z = 0.483\mu\text{m}$

## 5.4 Results Summary

The FDS and PE ADS values for the retrieved UKRs with CoCr femoral components do not correlate (see Figure 5.10). Neither do the PE ADS and PE BDS values correlate. (see Figure 5.11). It is difficult with small sample numbers to determine correlations.

The data was analysed as a group of seventeen CoCr UKRs, as a group of fifteen HFZ and OB UKRs and also as separate groups of ten HFZ and five OB UKRs. There are no correlations between the FDS and PE ADS values and the surface roughness parameters within any of the groups.

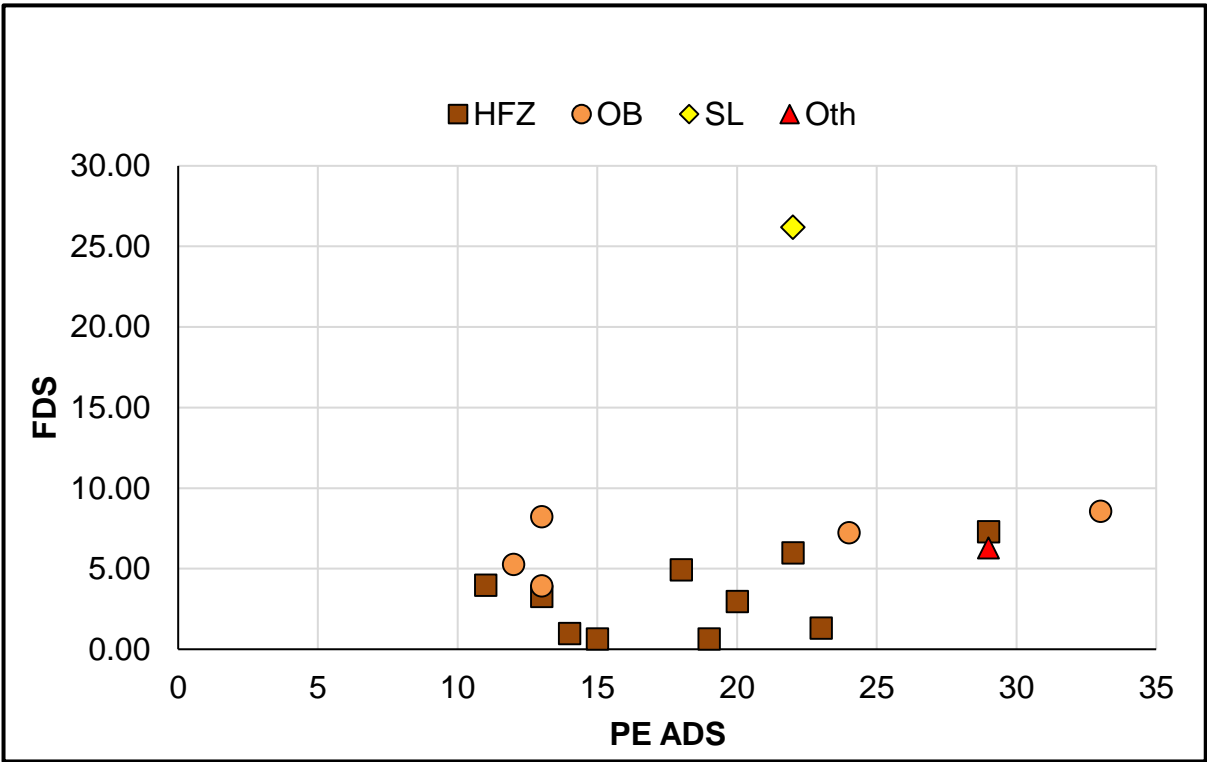


Figure 5.10 UKR FDS against PE ADS

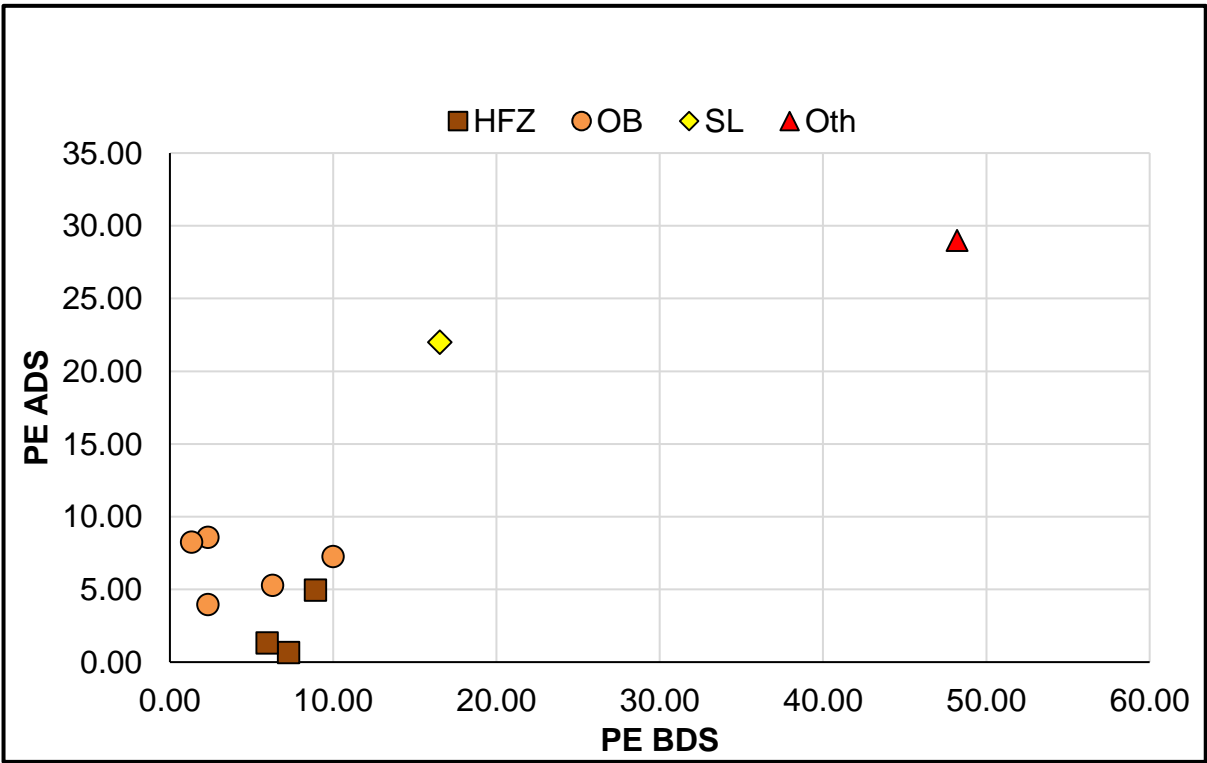


Figure 5.11 UKR PE ADS against PE BDS

*Blank page*



## **Chapter 6 Surface Topographical Analysis of Explanted Knee Replacement Prostheses with Oxidised Zirconium Femoral Components**

This chapter presents the surface topographical analysis results of retrieved explanted knee replacement prostheses (TKR and UKR) with oxidised zirconium (OxZr) femoral components using the methods described in Chapter 3 Materials and Methods. As described in the Literature Review in Chapter 2, there is limited understanding of the *in vivo* performance of knee replacement prostheses that utilise OxZr femoral components and of the surface topographic changes that occur to these components following time *in vivo*. There is no consensus within the literature that the surface roughness of retrieved OxZr femoral components increases following a period of time *in vivo*.

Within this chapter the surface topographical analysis results of retrieved explanted knee replacement prostheses with OxZr femoral components are compared with analysis results of retrieved explanted knee replacement prostheses with CoCr femoral components. The selection criteria of retrieved explanted knee replacement prostheses with CoCr femoral components used in comparison with the retrieved explanted knee replacement prostheses with OxZr femoral components is detailed.

Where available, the patient and implant variables of all the explanted prostheses analysed to provide the results within this chapter are provided. Macroscopic observations, damage scoring results and surface roughness measurements for the selected retrieved explanted components are included. A comparison between the surface roughness measurements of the retrieved explanted femoral components (OxZr and CoCr) and reference components is made. The retrieved explanted components shall hereby be known as “retrievals” or “retrieved components”.

### **6.1 Implant and Patient Variables**

Five retrieved knee replacement prostheses with OxZr femoral components were identified within the Knee Explant Catalogue (Appendix B). This includes three

Oxinium® (Smith & Nephew, Warsaw, London, UK) TKRs, two Genesis II and one Legion TKRs, and two Oxinium® Journey UKRs. These prostheses shall be identified as retrieved OxZr TKRs and retrieved OxZr UKRs.

Three retrieved PFC Sigma® (DePuy, Warsaw, IN, US) TKRs with CoCr femoral components were selected from the Knee Explant Catalogue to be used in comparison with the OxZr TKRs. These shall be identified as retrieved CoCr TKRs. The retrieved CoCr TKRs were selected to match the retrieved OxZr TKRs based on length of time *in vivo*. All retrieved TKRs were implanted with cemented fixation and with modular fixed PE bearings. The mean time *in vivo* for the retrieved OxZr TKRs was 58 ( $\pm 24.8$ ) months and 47 ( $\pm 14.3$ ) months for the retrieved CoCr TKRs. The mean BMI for the retrieved OxZr TKRs was 30.2 ( $\pm 3.3$ ) and 33.4 ( $\pm 5.4$ ) for the retrieved CoCr TKRs; the mean age at primary surgery was 51 ( $\pm 14.0$ ) years for the retrieved OxZr TKRs and 60 ( $\pm 8.5$ ) years for the retrieved CoCr TKRs. The patient and implant variables for the retrieved OxZr and CoCr TKRs are given in Table 6.1. Three new, unopened boxed femoral components, two PFC Sigma® and one Genesis II Oxinium® were available to be used as reference CoCr and OxZr components.

Limited patient and implant data were available for the retrieved OxZr UKRs and it was thought inappropriate to select just two retrieved UKRs with CoCr femoral components as a comparison. As such, all ten of the High Flexion Unicompartmental Knees (Zimmer Biomet, Warsaw, IN, US) were selected to be used as a comparison. All retrieved UKRs were implanted with cemented fixation and with modular fixed PE bearings. These shall be identified as retrieved OxZr UKRs and retrieved CoCr UKRs.

Figure 6.1 shows the retrieved OxZr TKRs and the retrieved OxZr UKRs.

Table 6.1 OxZr TKR and CoCr TKR Patient and Implant Variables

Implant	OxZr T1	OxZr T2	OxZr T3	CoCr T4	CoCr T5	CoCr T6
<b>Make &amp; Model of retrieved prosthesis</b>	S&N Genesis II Oxinium	S&N Genesis II Oxinium	S&N Legion Oxinium	DePuy PFC Sigma	DePuy PFC Sigma	DePuy PFC Sigma
<b>Gender</b>	Female	Male	Male	Female	Male	Female
<b>Side</b>	Right	Right	Left	Right	Left	Left
<b>BMI</b>	28.4	28.2	34	33	28.3	39
<b>Indication for primary surgery</b>	Osteoarthritis	First revision of primary TKR indicated for osteoarthritis.	Osteoarthritis	Osteoarthritis	Osteoarthritis	Osteoarthritis
<b>Indication for revision surgery</b>	Pain / Hypermobility	Instability	Chronic infection and instability / Pain	Component malalignment	Component malalignment	Instability / Pain
<b>Time <i>In Vivo</i> (Months)</b>	40 months	86 months	47 months	44 months	35 months	63 months
<b>Age at implantation of retrieved prosthesis</b>	37 years	51 years	65 years	50 years	66 years	63 years

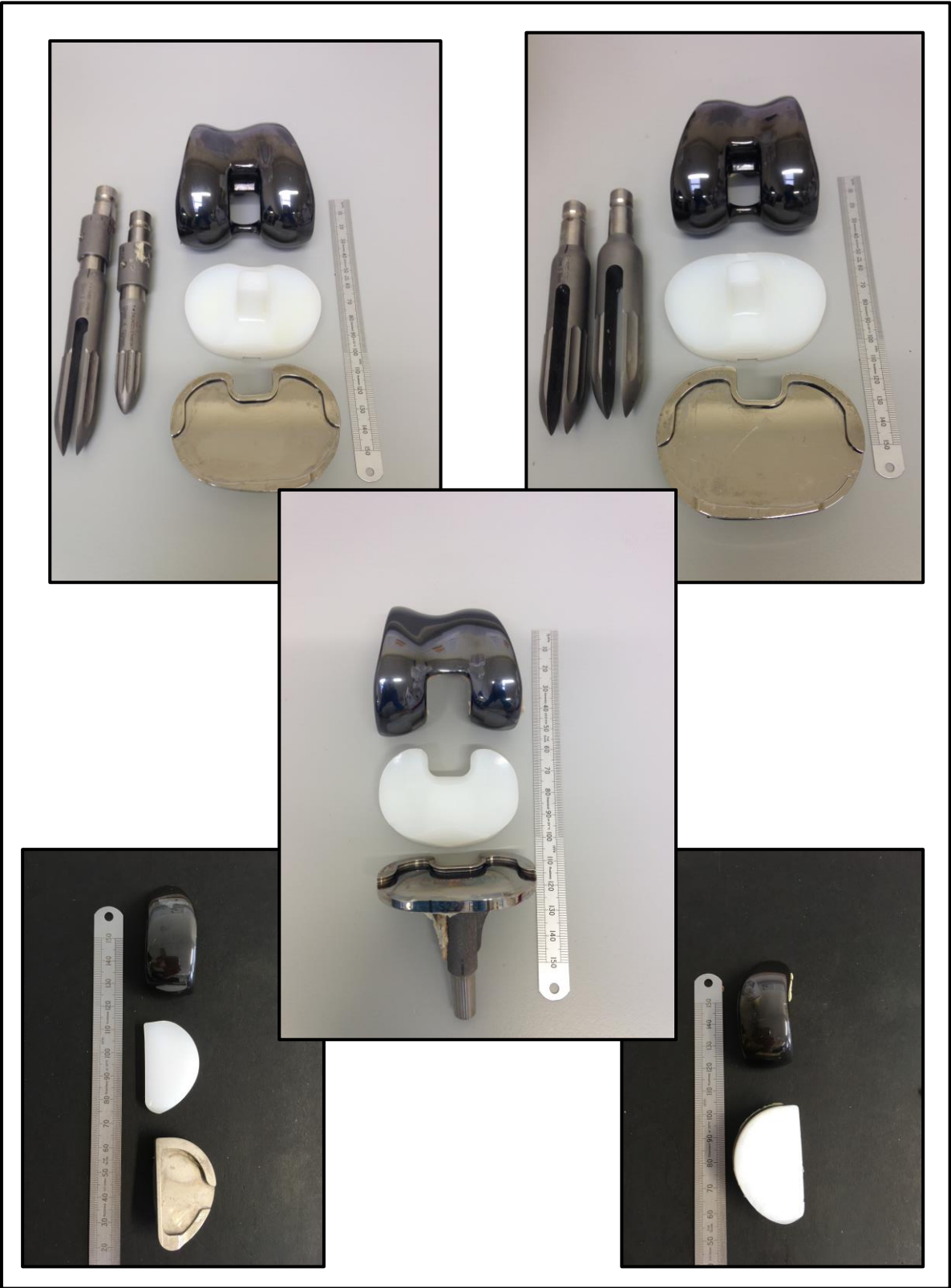


Figure 6.1 Retrieved OxZr TKRs and retrieved OxZr UKRs

## 6.2 Macroscopic Visual Assessment and Damage Scoring

Macroscopic visual assessments of the surfaces of the femoral condyles, the articulating and backside surfaces of the PE components and the distal surfaces of the tibial trays were performed. A summary of the assessments is given in the subsections below and the full assessments are tabulated in Table E1, Appendix E. Femoral component damage scoring, PE articular surface damage scoring and PE backside damage scoring where possible, was performed for all the retrieved OxZr and CoCr TKR and OxZr and CoCr UKR prostheses as per the methods described in Chapter 3. The results are summarised in Table 6.2. As detailed in preceding Chapters, the two decimal places of the FDS and PE BDS scores are not indicative of the level of accuracy or precision in the methods but are merely a result of using the numeric values 0.33 and 0.66 to represent differing levels of severity.

### 6.2.1 Femoral Components

Damage considered to have occurred *in vivo* was observed on all of the retrieved femoral components, OxZr and CoCr, TKR and UKR. Figure 6.2 shows the FDS and DFS values for the femoral components of the retrieved OxZr and CoCr TKRs and UKRs. The number of retrieved components observed to record an FDS or a DFS is indicated as the “n-value”. The mean FDS values for the CoCr femoral components (both TKR and UKR) are greater than those for the OxZr femoral components. (CoCr TKR mean FDS = 4.86, range 2.98 – 6.99, OxZr TKR mean FDS = 1.87, range 1.65 – 2.31, CoCr UKR mean FDS = 3.22, range 0.66 – 7.31 and OxZr UKR mean FDS = 2.83, range 2.32 and 3.33). All three retrieved CoCr TKR femoral components were observed to have burnished damage tracks and light scratching but no deeper scratches or gouging. Two of the retrieved OxZr TKR femoral components were observed to have deeper scratches and gouges, and two were observed to have small amount of burnishing. All three retrieved OxZr TKR femoral components were observed to have indentations or light scratches. On two of the retrieved OxZr TKR femoral components damage was observed posteriorly in high flexion on both condyles.

Both the retrieved OxZr UKR femoral components were observed to have gouging and indentations or light scratches but no burnishing. One of the retrieved OxZr UKR femoral components showed damage posteriorly in high flexion. In the larger group of retrieved CoCr UKR femoral components, eight were observed to have burnishing, five gouging or deeper scratches and four were observed to have indentations or light scratches.

Table 6.2 OxZr and CoCr TKR and UKR FDS, PE ADS and PE BDS Values

	<b><u>FDS</u></b>	<b><u>PE ADS</u></b>	<b><u>PE BDS</u></b>
<b>OxZr T1</b>	1.65	22	0.33
<b>OxZr T2</b>	1.65	35	1.32
<b>OxZr T3</b>	2.31	44	1.98
<b>OxZr TKR SUM (n=3)</b>	<b>5.61</b>	<b>101</b>	<b>3.63</b>
<b>OxZr TKR Mean (n=3)</b>	<b>1.87</b>	<b>34</b>	<b>1.21</b>
<b>CoCr T1</b>	2.98	25	1.32
<b>CoCr T2</b>	6.99	15	2.64
<b>CoCr T3</b>	4.62	33	8.25
<b>CoCr TKR SUM (n=3)</b>	<b>14.59</b>	<b>63</b>	<b>12.21</b>
<b>CoCr TKR Mean (n=3)</b>	<b>4.86</b>	<b>21</b>	<b>4.07</b>
<b>OxZr U1</b>	2.32	16	6.6
<b>OxZr U2</b>	3.33	17	6.27
<b>OxZr UKR Mean (n=2)</b>	<b>2.83</b>	<b>16.5</b>	<b>6.44</b>
<b>CoCr U1</b>	0.66	15	—
<b>CoCr U2</b>	7.31	29	—
<b>CoCr U3</b>	0.66	19	7.26
<b>CoCr U4</b>	2.98	20	—
<b>CoCr U5</b>	1.00	14	—
<b>CoCr U6</b>	1.33	23	5.94
<b>CoCr U7</b>	3.30	13	—
<b>CoCr U8</b>	6.00	22	—
<b>CoCr U9</b>	4.95	18	8.91
<b>CoCr U10</b>	3.99	11	—
<b>CoCr UKR Mean (n=10)</b>	<b>3.22</b>	<b>18</b>	<b>7.37</b>

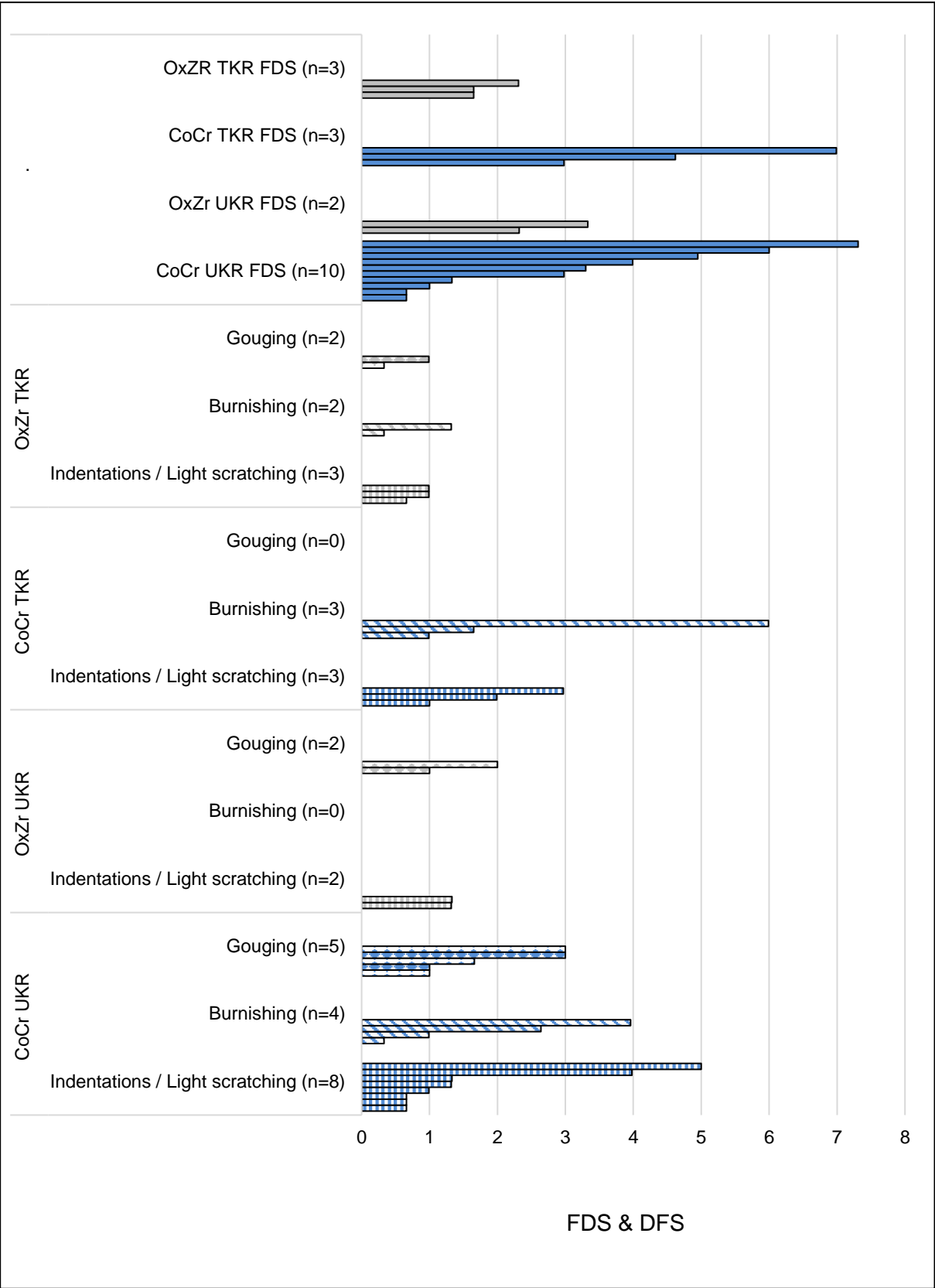


Figure 6.2 FDS and DFS values for retrieved OxZr and CoCr TKRs and UKRs

### **6.2.2 PE Components Articular Surface**

The articular surface of the PE components of the three retrieved CoCr TKRs were observed to have minimal damage with all three showing very light burnishing and scratching (CoCr TKR Mean PE ADS = 21, range 15 – 33). A small amount of light pitting and abrasion was observed on one of the retrieved CoCr TKR PE components. The mean PE ADS value for the retrieved OxZr TKRs was 34 (range 22 – 44). All three of the retrieved OxZr TKR PE components were observed to have damage to the articular surface which was characterised by burnishing (all three) and pitting and scratching (two of three components). Two components were observed to have a small amount of abrasion and deformations outside of the articulating condyles and also damage to the posterior stabilising post. All three retrieved OxZr TKR PE components showed damage that would be consistent with the femoral component pivoting and rotation about the lateral condyle with areas of damage outside of the PE articulating condyles.

The articular surfaces of the PE components of both retrieved OxZr UKRs were observed to have definite load areas of approximately 15mm x 20mm, one located posteriorly and the other located centrally. Burnishing was observed in the load areas and deep scratches were located all over the articular surface. Similarly, the articular surfaces of the PE component of the ten retrieved CoCr UKRs were characterised by a definite load area approximately 10-15mm x 20-25mm in size. Within the load areas damage features burnishing (ten components), light pitting (nine components) and light scratching (nine components) were observed. The mean PE ADS value for the retrieved CoCr UKRs (18.40 range 11 – 29) was similar to the PE ADS values for the two retrieved OxZr UKR PE components (16 and 17).

Figure 6.3 shows the PE ADS and DFS values for the articular surface of the PE components of the retrieved OxZr and CoCr TKRs and UKRs.



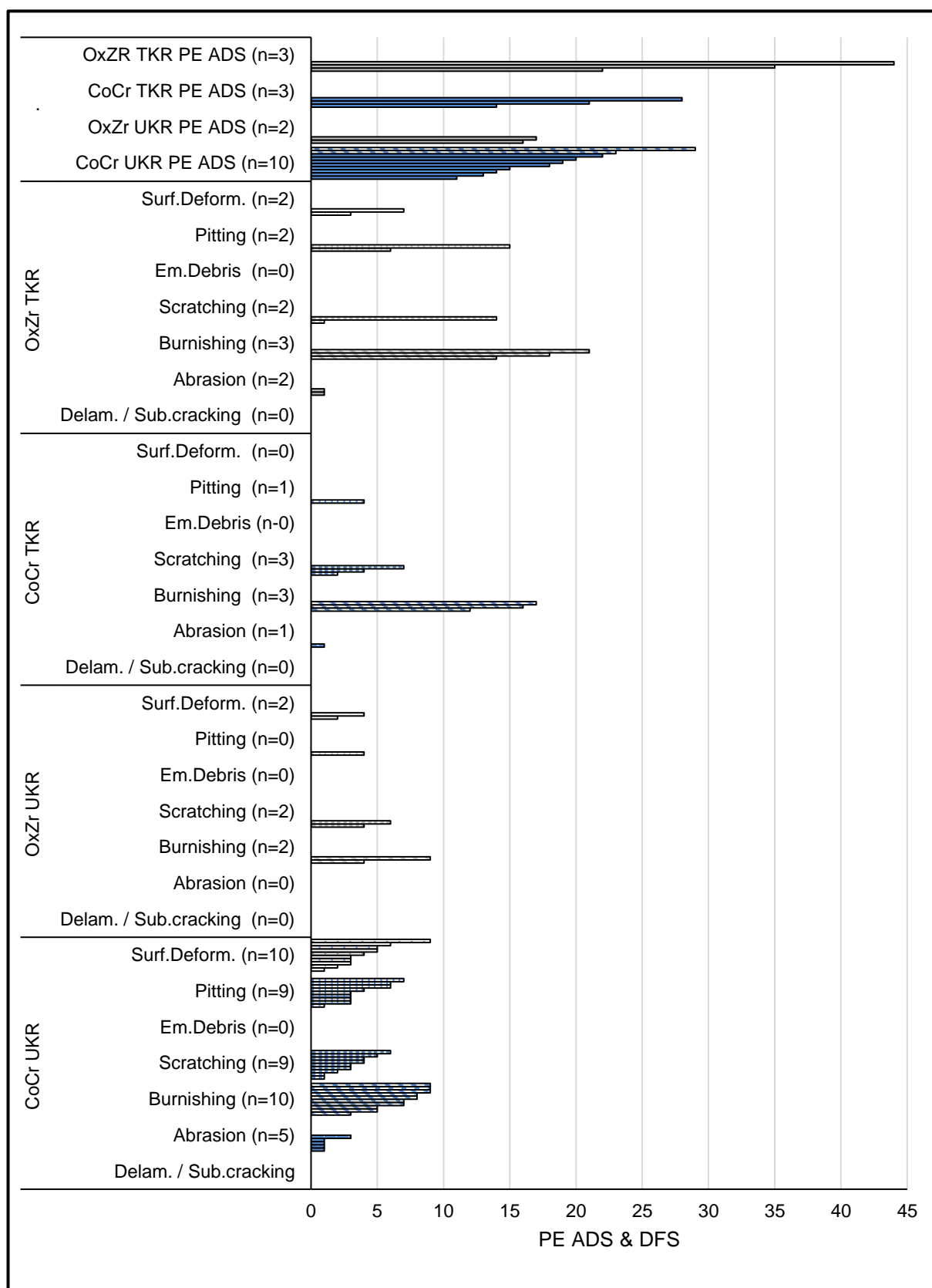


Figure 6.3 PE ADS and DFS for retrieved OxZr and CoCr TKRs and UKRs

### **6.2.3 PE Components Backside Surface and Tibial Trays**

The backside surfaces of the retrieved PE components, CoCr and OxZr, TKR and UKR, were all observed to have some, if only very minimal, *in vivo* damage or changes. None of the severity weightings assigned for any of the recorded damage features was greater than the minimum 0.33. The backside surfaces of the retrieved PE components of all three OxZr TKRs showed light burnishing and one showed pitting. The backside surfaces of the retrieved PE components of the three CoCr TKRs only were observed to have burnishing. The backside surfaces of the retrieved PE components of all three OxZr UKRs showed scratching and the backside surfaces of the retrieved PE components of the three CoCr UKRs all showed burnishing and one showed pitting. Typically, the burnishing was observed in an area corresponding to the load area observed on the articular surface of the PE component.

Despite just looking at four areas on the PE backside of the UKRs compared with six areas on the PE backside of the TKRs, the mean PE BDS values for the retrieved PE components of the UKRs were higher than the PE BDS values for the retrieved PE components of the TKRs. The retrieved tibial trays of the CoCr and OxZr TKRs all had polished distal tibial surfaces. No damage considered to be *in vivo* damage was observed on the retrieved tibial trays of the CoCr TKRs. On the retrieved tibial trays of one of the OxZr TKRs pits or small indentations were observed and on one other the imprint of the manufacturer's etching on the backside of the PE component was observed. The retrieved tibial trays of the CoCr and OxZr UKRs all had non-polished distal tibial surfaces. No notable damage was observed on the retrieved tibial tray of the OxZr UKRs. On one of the retrieved tibial trays of the CoCr UKRs burnishing and stippling was observed consistent with micromotion of the PE component within the tibial tray. On one other of the retrieved tibial trays of the CoCr UKRs pits were observed.

The PE BDS and DFS values for the backside surface of the PE component of the retrieved OxZr and CoCr TKRs and UKRs are shown in Figure 6.4.

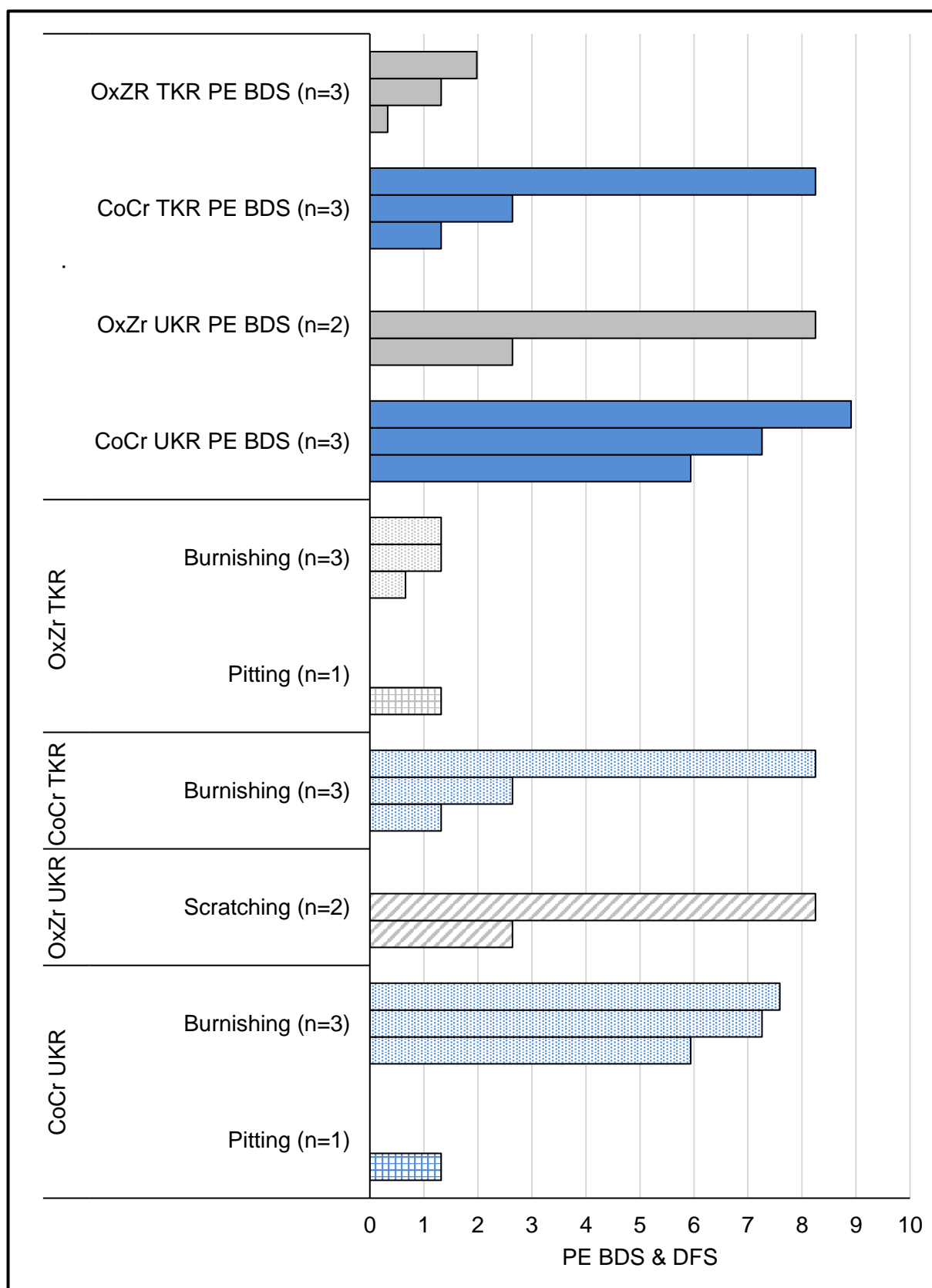


Figure 6.4 PE BDS and DFS for retrieved OxZr and CoCr TKRs and UKRs

### 6.3 Non-contacting Profilometry

The mean and standard errors of the surface roughness measurements for the reference and retrieved OxZr TKR and UKR femoral components are shown in Table 6.3. The mean and standard errors of the surface roughness measurements for the reference and retrieved CoCr TKR and UKR femoral components are shown in Table 6.4. As per previous non-contacting profilometry results 30 measurements were taken on each TKR femoral component and 15 measurements were taken on UKRs.

Table 6.3 OxZr TKR and UKR Surface Roughness Values

	Reference OxZr (n = 1)	OxZr U1	OxZr U2	OxZr UKR (n=2)
<b>S<sub>q</sub> (μm)</b>	<b>0.080</b>	0.102	0.111	<b>0.106 (± 0.005)</b>
<b>S<sub>p</sub> (μm)</b>	<b>0.426</b>	0.671	0.526	<b>0.599 (± 0.072)</b>
<b>S<sub>v</sub> (μm)</b>	<b>-0.589</b>	-0.737	-0.917	<b>-0.827 (± 0.090)</b>
<b>PV (μm)</b>	<b>1.015</b>	1.408	1.443	<b>1.426 (± 0.017)</b>
<b>S<sub>z</sub> (μm)</b>	<b>0.571</b>	0.677	0.846	<b>0.762 (± 0.085)</b>
<b>S<sub>sk</sub> (-)</b>	<b>0.315</b>	1.116	-0.812	<b>0.152 (± 0.964)</b>
<b>S<sub>ku</sub> (-)</b>	<b>13.070</b>	11.796	17.755	<b>14.776 (± 2.980)</b>
	OxZr T1	OxZr T2	OxZr T3	OxZr TKR (n=3)
<b>S<sub>q</sub> (μm)</b>	0.092	0.132	0.127	<b>0.117 (± 0.013)</b>
<b>S<sub>p</sub> (μm)</b>	0.444	0.555	0.761	<b>0.587 (± 0.093)</b>
<b>S<sub>v</sub> (μm)</b>	-0.913	-0.930	-1.008	<b>-0.950 (± 0.029)</b>
<b>PV (μm)</b>	1.356	1.486	1.769	<b>1.537 (± 0.122)</b>
<b>S<sub>z</sub> (μm)</b>	0.709	0.862	0.889	<b>0.820 (± 0.056)</b>
<b>S<sub>sk</sub> (-)</b>	-0.648	-0.696	0.296	<b>-0.349 (± 0.323)</b>
<b>S<sub>ku</sub> (-)</b>	9.720	14.798	16.646	<b>13.721 (± 2.071)</b>

Table 6.4 CoCr TKR and UKR Surface Roughness Values

	Ref CoCr 1	Ref CoCr 2	Reference CoCr (n = 2)	CoCr UKR (n=10)
<b>S<sub>q</sub> (μm)</b>	0.069	0.051	<b>0.060 (± 0.009)</b>	<b>0.073 (± 0.005)</b>
<b>S<sub>p</sub> (μm)</b>	0.294	0.269	<b>0.281 (± 0.013)</b>	<b>0.414 (± 0.016)</b>
<b>S<sub>v</sub> (μm)</b>	-0.497	-0.596	<b>-0.546 (± 0.050)</b>	<b>-0.597 (± 0.055)</b>
<b>PV (μm)</b>	0.790	0.865	<b>0.828 (± 0.037)</b>	<b>1.010 (± 0.059)</b>
<b>S<sub>z</sub> (μm)</b>	0.386	0.371	<b>0.379 (± 0.007)</b>	<b>0.491 (± 0.021)</b>
<b>S<sub>sk</sub> (-)</b>	-0.101	-1.189	<b>-0.645 (± 0.544)</b>	<b>-0.381 (± 0.283)</b>
<b>S<sub>ku</sub> (-)</b>	11.474	66.582	<b>39.028 (± 27.554)</b>	<b>14.778 (± 3.829)</b>
	CoCr T1	CoCr T2	CoCr T3	CoCr TKR (n=3)
<b>S<sub>q</sub> (μm)</b>	0.065	0.094	0.075	<b>0.078 (± 0.008)</b>
<b>S<sub>p</sub> (μm)</b>	0.334	0.394	0.343	<b>0.357 (± 0.019)</b>
<b>S<sub>v</sub> (μm)</b>	-0.451	-0.917	-0.488	<b>-0.618 (± 0.150)</b>
<b>PV (μm)</b>	0.785	1.311	0.831	<b>0.976 (± 0.168)</b>
<b>S<sub>z</sub> (μm)</b>	0.464	0.731	0.450	<b>0.548 (± 0.092)</b>
<b>S<sub>sk</sub> (-)</b>	-0.150	-1.946	-0.121	<b>-0.739 (± 0.603)</b>
<b>S<sub>ku</sub> (-)</b>	8.887	36.170	7.347	<b>17.468 (± 9.362)</b>

The surface roughness parameters S<sub>q</sub>, S<sub>p</sub>, PV and S<sub>z</sub> were greater and S<sub>v</sub> and S<sub>sk</sub> were more negative, for the retrieved OxZr TKR femoral components than for the reference OxZr femoral component (p<0.05). This was also seen for the surface roughness parameters for the retrieved OxZr UKR femoral components although significance was only seen when comparing the S<sub>q</sub> difference was found.

The surface roughness parameters  $S_q$ ,  $S_p$ , PV and  $S_z$  were greater and  $S_v$  and  $S_{sk}$  were more negative, for the retrieved CoCr TKR femoral components than for the reference CoCr femoral component although the difference was only significant when comparing the  $S_q$ ,  $S_p$  and  $S_z$  values. For the retrieved CoCr UKR femoral components, the surface roughness parameters  $S_q$ ,  $S_p$ , PV and  $S_z$  were greater and  $S_v$  more negative than for the reference CoCr femoral component however the  $S_{sk}$  was more positive. The differences were only significant when comparing the  $S_q$ ,  $S_p$  and  $S_z$  values.

The  $S_q$  and  $S_p$  were both significantly greater ( $p < 0.05$ ) for the reference OxZr femoral component than for the reference CoCr femoral components. While there was no significant difference between the  $S_q$ ,  $S_v$  and  $S_{sk}$  values measured on the retrieved OxZr TKRs compared with those measured on the retrieved CoCr TKRs, the  $S_p$ , PV and  $S_z$  were all seen to be significantly greater for the retrieved OxZr TKRs. There were no significant differences between any of the surface roughness parameters measured on the retrieved OxZr UKR femoral components compared to those measured on the retrieved CoCr UKR femoral components. The small sample sizes mean that the any statistically significant differences identified may not be reliable and caution should be taken in the analysis of results. There were no differences seen between the surface roughness parameters measured on the medial and lateral condyles of the retrieved OxZr and CoCr TKR femoral components.

The mean values of the surface roughness parameters  $S_q$ ,  $S_z$  and  $S_{sk}$  measured on the reference and retrieved OxZr and CoCr TKR and UKR femoral components are shown in Figure 6.5. The skewness  $S_{sk}$  uses a 3<sup>rd</sup> order differentiation in the defining equation and is considered less mathematically stable than the other surface roughness parameters. This could be an explanation for the higher errors in the calculation of the parameter as seen in Figure 6.5 [74]. The mean values of the surface roughness parameters  $S_p$ ,  $S_v$  and PV measured on the reference and retrieved OxZr and CoCr TKR and UKR femoral components are shown in Figure 6.6.

Figures 6.7 – 6.12 show surface topography plots for measurement areas taken on the reference and retrieved OxZr and CoCr TKR and UKR femoral components. All the surface topography plots show an oblique plot, an intensity map, a surface map and a surface profile for each measurement area. The RMS surface roughness,  $S_q$ , and the ten-point height average,  $S_z$ , values are detailed in the figure title.

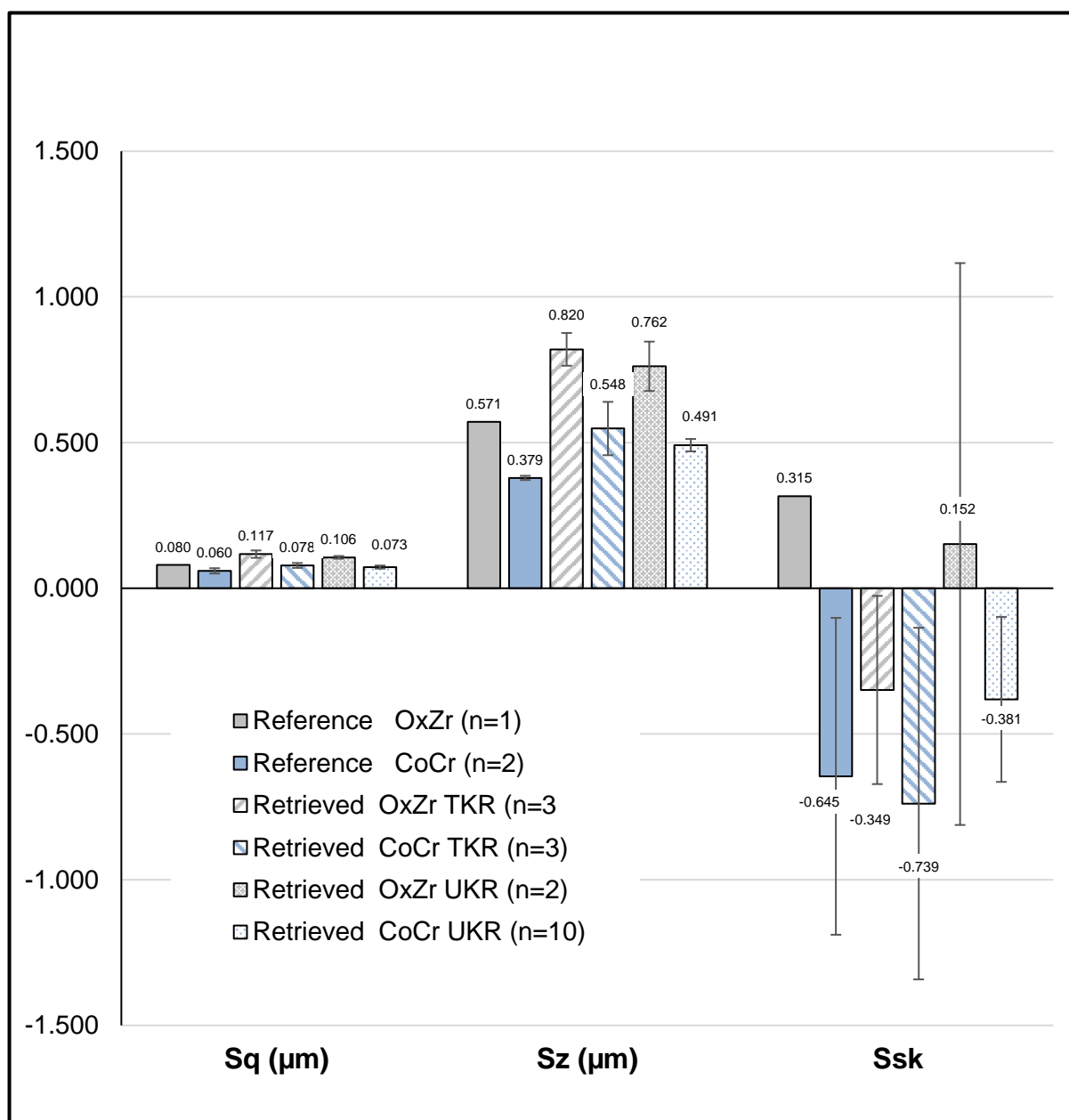


Figure 6.5 OxZr and CoCr retrieved and reference TKR and UKR femoral component surface roughness parameters  $S_q$ ,  $S_z$  and  $S_{sk}$

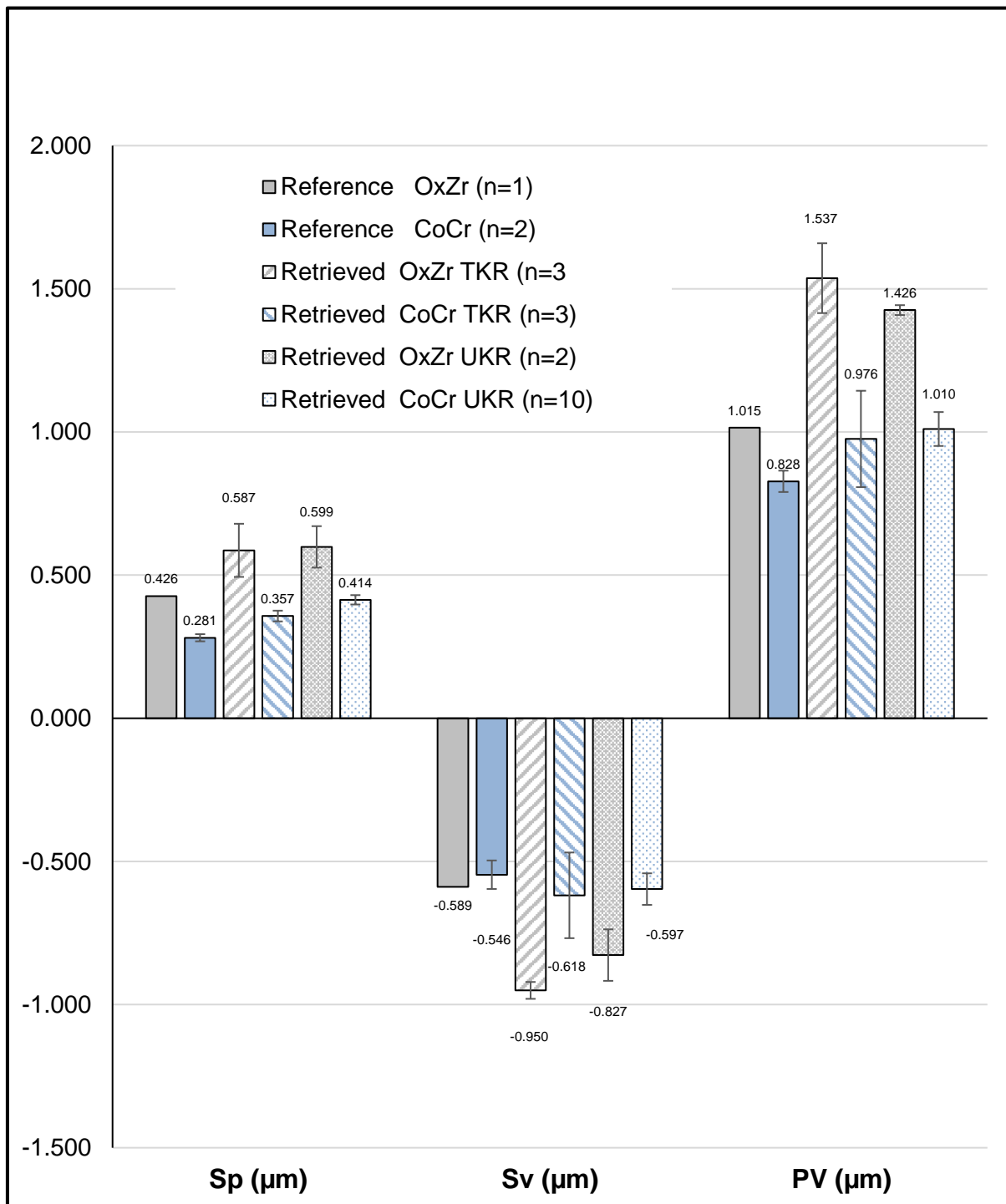


Figure 6.6 OxZr and CoCr retrieved and reference TKR and UKR femoral component surface roughness parameters  $S_p$ ,  $S_v$  and  $P$



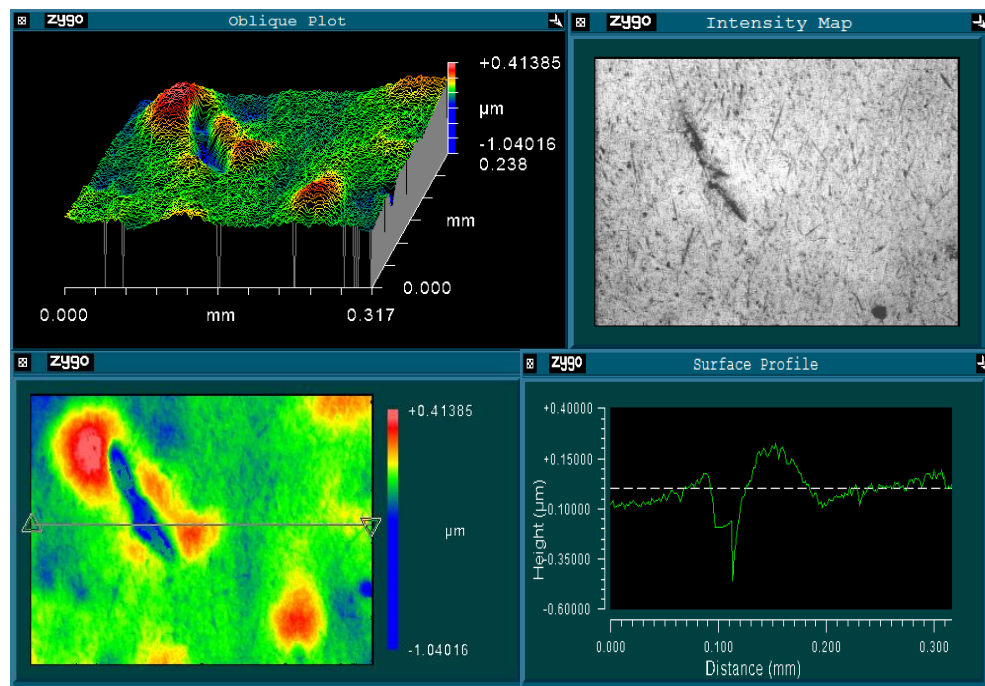


Figure 6.7 Surface topography plots for a measurement area on the reference OxZr femoral component  $S_q = 0.098\mu\text{m}$ ,  $S_z = 0.546\mu\text{m}$

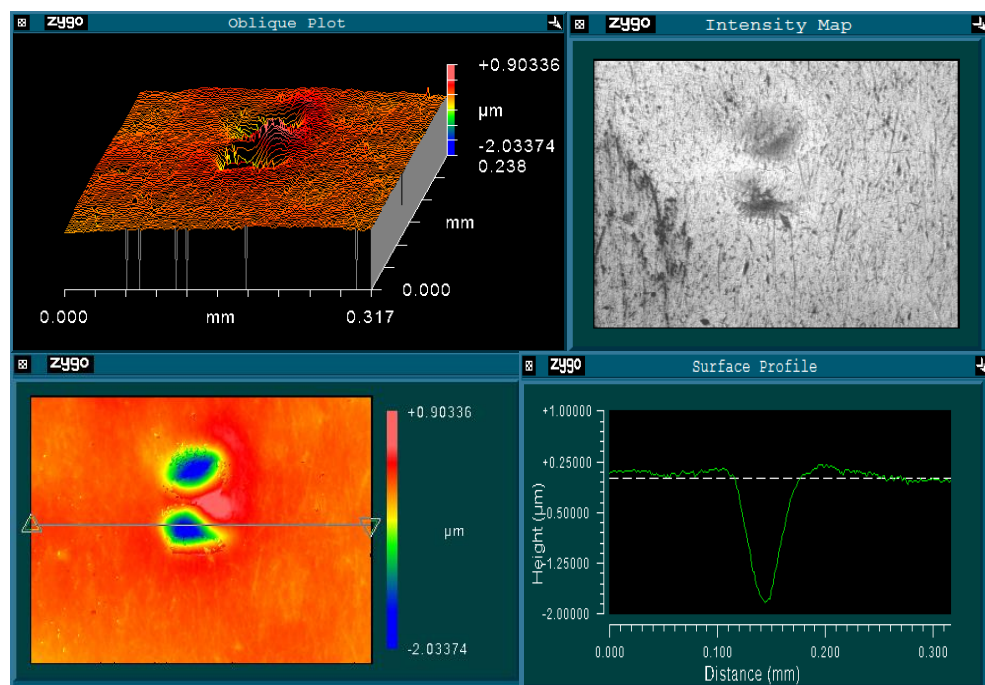


Figure 6.8 Surface topography plots for a measurement area on a retrieved OxZr TKR femoral component  $S_q = 0.236\mu\text{m}$ ,  $S_z = 1.392\mu\text{m}$

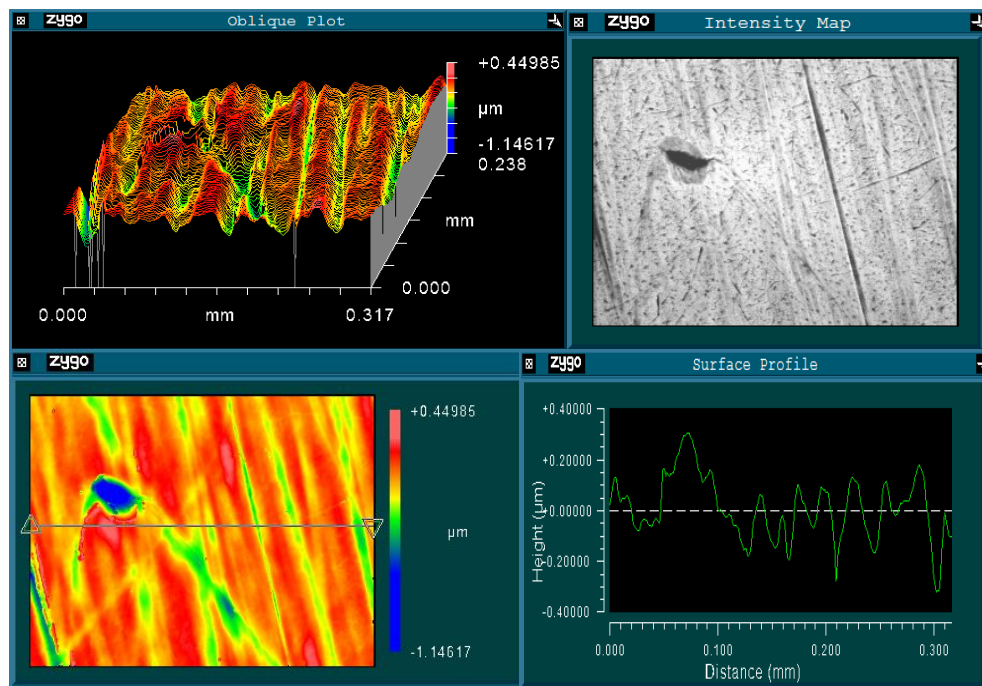


Figure 6.9 Surface topography plots for a measurement area on a retrieved OxZr UKR femoral component  $S_q = 0.134\mu\text{m}$ ,  $S_z = 0.854\mu\text{m}$

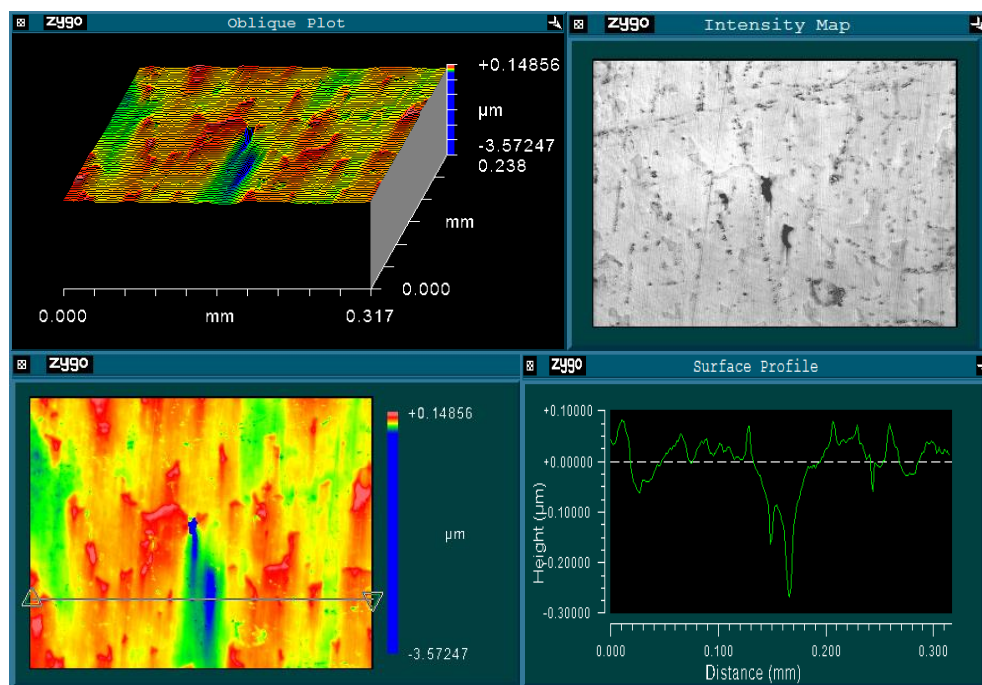


Figure 6.10 Surface topography plots for a measurement area on a reference CoCr femoral component  $S_q = 0.061\mu\text{m}$ ,  $S_z = 0.922\mu\text{m}$

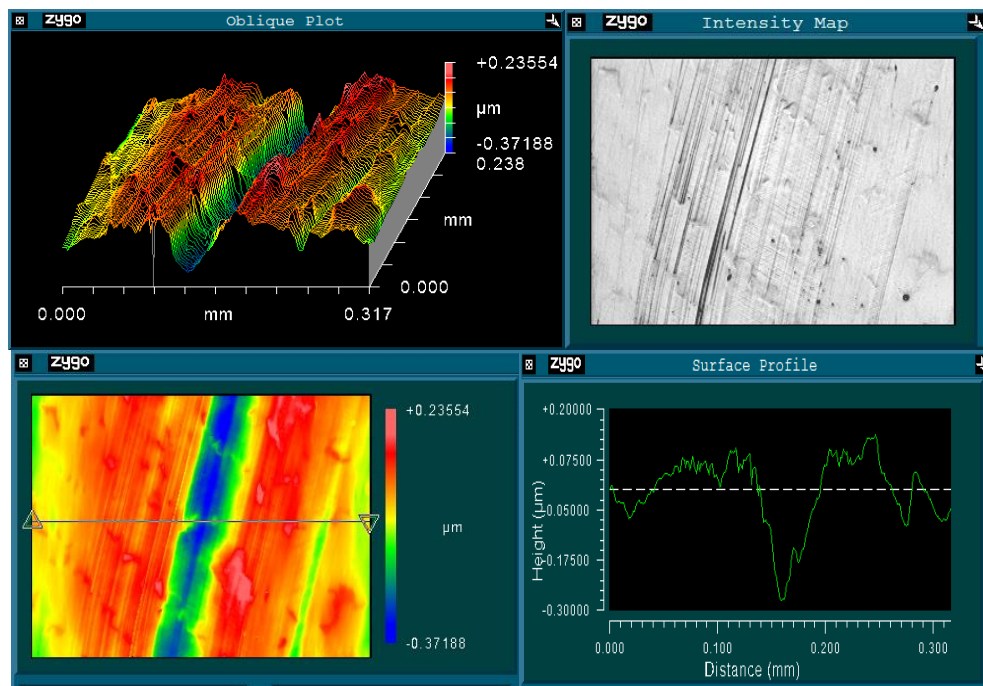


Figure 6.11 Surface topography plots for a measurement area on a retrieved CoCr TKR femoral component  $S_q = 0.099\mu\text{m}$ ,  $S_z = 0.267\mu\text{m}$

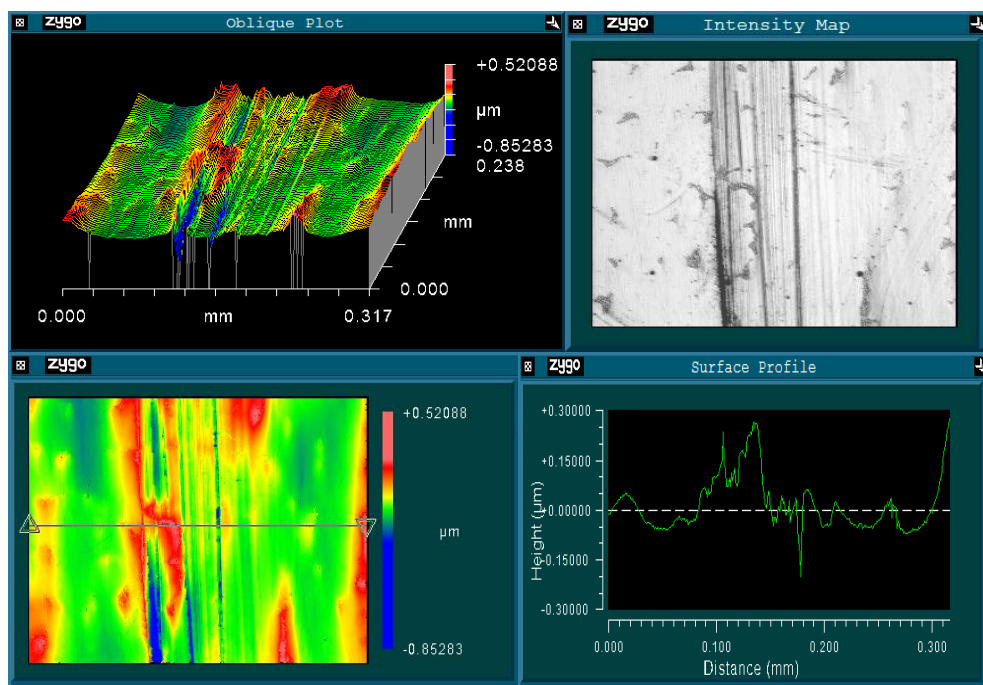


Figure 6.12 Surface topography plots for a measurement area on a retrieved CoCr UKR femoral component  $S_q = 0.082\mu\text{m}$ ,  $S_z = 0.672\mu\text{m}$

## 6.4 Results Summary

There is no correlation between the FDS values and the PE ADS and PE BDS values (see Figure 6.13). Neither is there a correlation between the PE ADS and the PE BDS values. There are no correlations between the femoral component surface roughness parameters and either the FDS or PE ADS values (see Figure 6.14). The small numbers of implants available for analysis will obviously influence the ability to identify correlations.

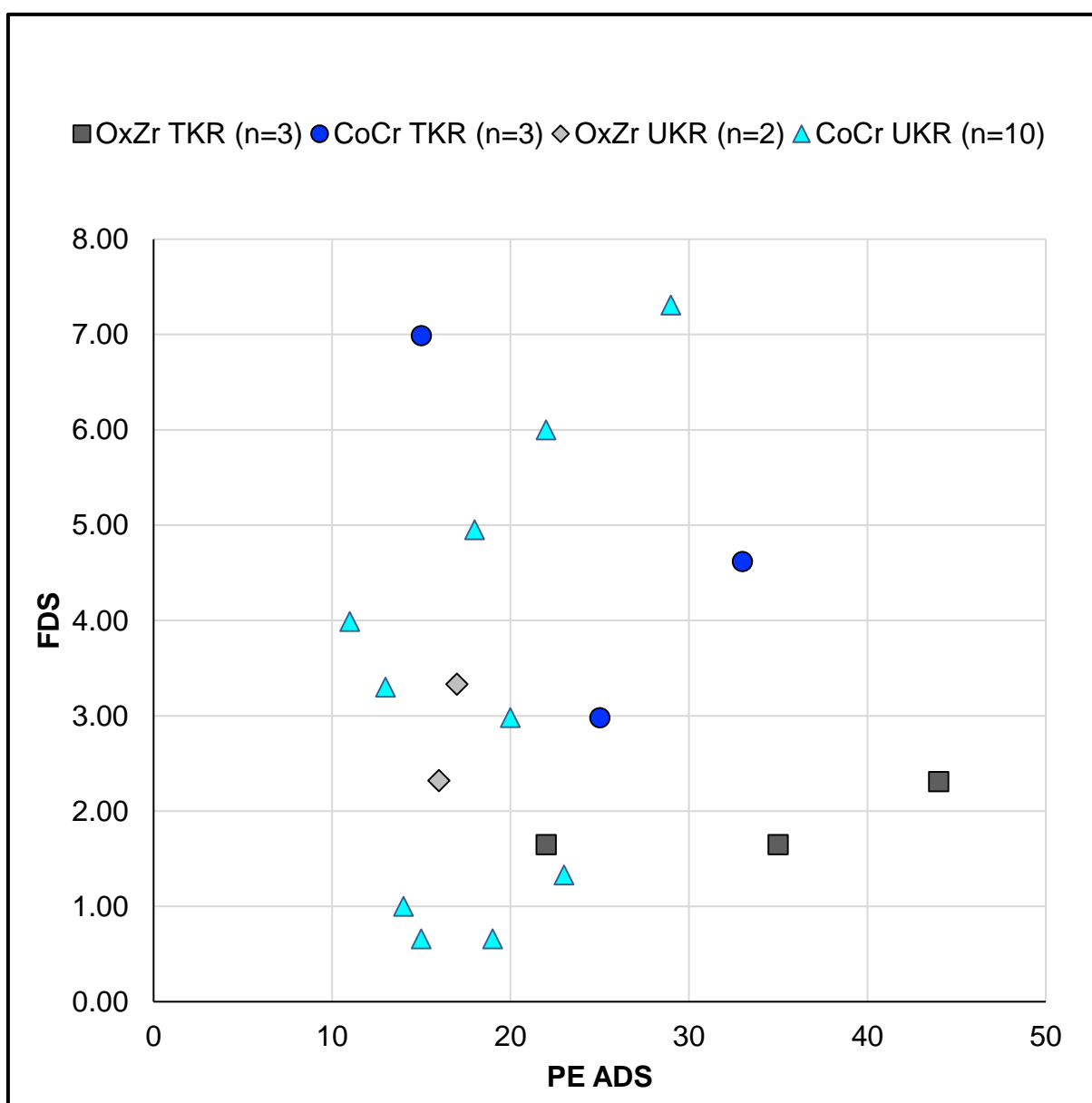


Figure 6.13 OxZr and CoCr TKR and UKR FDS against PE ADS values

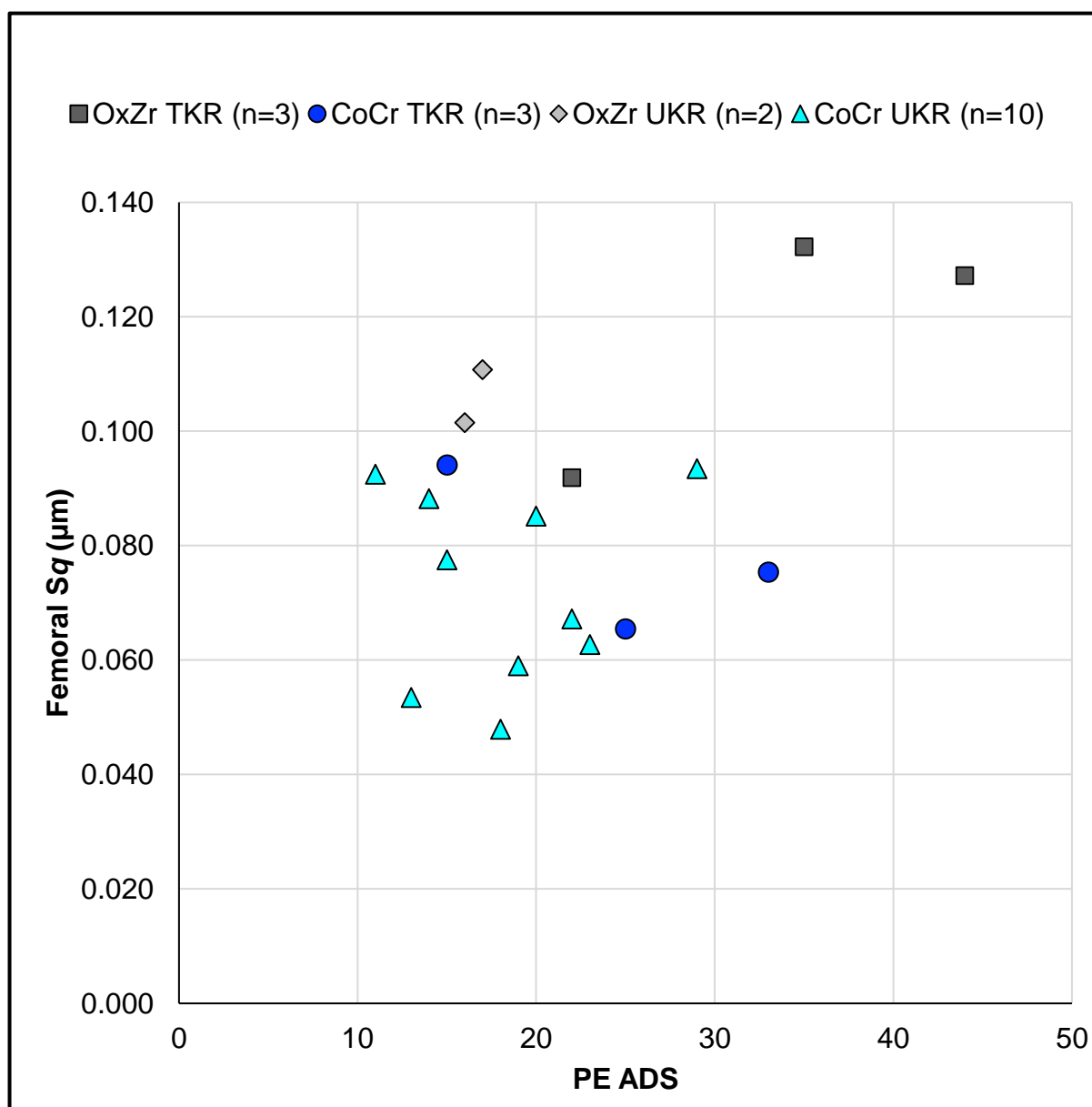


Figure 6.14 OxZr and CoCr TKR and UKR femoral component  $S_q$  against PE ADS values

*Blank page*

## Chapter 7 Discussion

Within the preceding chapters 4, 5 and 6, the results of the surface topographical analysis of retrieved knee replacement prostheses have been presented. Chapter 4 presented the results of the analysis of retrieved Total Knee Replacements (TKRs) with cobalt chromium alloy (CoCr) femoral components. Chapter 5 presented the results of the analysis of retrieved Unicondylar Knee Replacements (UKRs) with CoCr femoral components. Chapter 6 presented the results of the analysis of retrieved knee replacement prostheses with Oxidised Zirconium (OxZr) femoral components, including TKRs and UKRs, and compared these with the results of the analysis of with knee replacement prostheses with CoCr femoral components. The semi-quantitative damage scoring values and the measured surface roughness parameters of the selected groups of retrieved knee replacement prostheses have been compared. Correlations between the surface topographical analysis results and the patient and implant variables have been sought. This current chapter provides a discussion of all those results within the context of the published literature as summarised in Chapter 2. Consideration is given to the limitations and practical constraints of the methodologies employed within this study and the limitations of making comparisons with the published literature. At the end of this chapter, a discussion summary is provided. This collection of explanted knee replacement prostheses is the largest reported to date within the United Kingdom. The results presented in Chapter 5 are the first reported surface roughness measurements of retrieved UKR prostheses. The results presented in Chapter 6 concerned with the surface roughness measurement of knee replacement prostheses with OxZr femoral components have been published as an original research paper Kennard et al [14] and is included within Appendix G.

## **7.1 Surface Topographical Analysis of Explanted TKRs with CoCr Femoral Components**

The results of the surface topographical analysis of explanted TKRs with CoCr femoral components that were presented in Chapter 4 of this thesis are discussed within this subsection.

The selection of the explanted TKR prostheses to analyse was determined by the availability within the Knee Explant Catalogue, which in turn was determined by the revision surgeries performed by the orthopaedic surgeon team collaborating on this project. The discussion of the surface topographical results of the selected retrieved TKR prostheses must consider the design and implantation year and materials used and it must be accepted that this is not a homogeneous cohort of forty retrieved TKRs but three groups of different TKR prosthesis designs. As such, correlations may be influenced by the differences in the groups and a positive correlation does not necessarily indicate that one factor is the cause or result of the other. This is an inherent limitation of retrieval studies. The limitations of retrieval studies are discussed in more depth in section 7.4.

Kinemax Plus (K+) ® (Stryker Howmedica, Mahwah, NJ, US) TKRs were historically the main TKRs implanted at primary knee replacement surgery at the Freeman Hospital. In around 2008 a problem with early failure and gross delamination of the PE component of the K+ TKRs was identified and attributed to material defects of the PE [228]. The orthopaedic team at the Freeman Hospital switched from predominantly implanting K+ TKRs to implanting PFC Sigma ® (PFC) (DePuy, Warsaw, IN, US) TKRs at primary knee replacement surgery. None of the AGC ® (AGC) (Zimmer Biomet, Warsaw, IN, US) TKRs that were retrieved and included in the knee explant catalogue were implanted by the collaborating surgeon team at the Freeman Hospital. The AGC TKRs that are included in this knee explant catalogue were explanted from revisions referred to the Freeman Hospital from other centres.

There are no details available regarding the PE component material properties (i.e. the use of XLPE and stabilising additives) or the sterilisation and packaging processes of the PE component for any of the explanted prostheses. Given the dates



of implantation (K+ 1991 – 2005, AGC 1991 -2009 and PFC 2000 – 2014) and the damage modes observed on the articular surface of the PE component assumptions can be made however. It would be appropriate to assume that the K+ PE is not crosslinked and does not contain stabilising additives. It can also be assumed that the K+ PE components were sterilised by gamma irradiation in air. As mentioned previously, the PE of the K+ components were identified to have a material defect [228]. The PFC PE components were not seen to have any delamination or subsurface cracking and given the dates of implantation, most likely would have an element of cross-linking and/or contain stabilising additives. It can also be assumed given the dates of implantation, that the PFC PE components would have undergone a sterilisation and packaging process designed to prevent on the shelf or *in vivo* oxidation. Again, considering the dates of implantation it may be that the AGC PE components are not all the same in terms of material properties and may not all have undergone the same sterilisation and packaging process. These considerations are a major factor influencing the performance of the prostheses.

There was a noticeable difference in the macroscopic visual assessment of the femoral components of the three different designs of TKR. While all exhibited damage considered to have occurred *in vivo*, the damage modes exhibited were different for the three designs. Although the AGC femoral components had the highest mean femoral damage score (FDS) most of this was accounted for by a high burnishing score from the burnished damage tracks observed. In comparison, while the K+ femoral components had a similar mean FDS to the AGC femoral components, this value was due to damage seen on components where there had been complete PE wear through and articulation between the femoral and tibial components had occurred. There was also a noticeable difference in the macroscopic visual assessment of the articular surface of the PE components. The K+ PE components were observed to be the most severely macroscopically damaged with the highest PE ADS followed by the AGC PE components and then the PFC PE components.

As a full group, the FDS values were seen to correlate positively with the PE ADS values, however this correlation does not imply cause. A large FDS value may be an

attribute of a retrieved TKR that also exhibits a large PE ADS value, but a causality conclusion cannot be made. The same can be seen when considering the FDS and PE ADS and length of time *in vivo* and the the FDS and PE ADS and patient BMI. When separated into the individual designs, AGC, PFC and K+, no correlations were found between the FDS or PE ADS and the length of time *in vivo* for any of the three designs.

Although the PE ADS method was based directly on the Hood scoring system [194] with the specific intention of enabling comparisons with the published literature only one other group was found to have followed this methodology without any adaptations. Scholes & Kennard et al [15] (manuscript included in Appendix H) used a non-modified Hood scoring system and within a non-homogenous cohort of retrieved TKRs. Like the results presented in this thesis in Chapter 4, Scholes & Kennard et al [15] found no correlations between the PE Hood score and the patient BMI but did show relationships may exist between PE Hood score and the time *in vivo*. Comparisons with other published studies cannot reliably be made due to the differences in PE damage scoring methodologies used. This is discussed in more detail in section 7.4.

The FDS results reported in Brandt et al [180] are the closest approximation in terms of methodology used to the FDS results reported in this thesis. However, the numeric values of the FDS are not detailed in Brandt et al's publication and therefore a direct comparison cannot be made. Brandt et al show that within their cohort of twenty-six retrieved Smith & Nephew CoCr femoral components grooving was the highest damage feature score, followed by indentations and then gouging. It is not clear from the graphical representation within Brandt et al's publication as to whether the mean DFS (damage feature score) values for the group of twenty-six retrieved components or the total DFS values are reported. The FDS values reported in Fabry et al [17] are not comparable to those recorded in this thesis as they are calculated from the assessment of four different damage features as recorded on retrieved TiN coated femoral components.

The differences in methodologies and reporting of surface roughness data in the thesis and in the published literature makes direct comparisons between the absolute surface roughness results very difficult and unreliable. The limitations of the methodologies and the differences are discussed in more detail in the section 7.4 below.

In agreement with previous published studies, the results in Chapter 4 show that the surface roughness of the femoral components of retrieved TKRs increases after time *in vivo* [15, 17, 153, 180, 216, 220, 222]. On average the RMS surface roughness,  $S_q$  measured on the retrieved PFC, AGC and K+ femoral components increased by 67%, 100% and 263% respectively. In agreement with Fabry et al [17], the surface roughness parameters,  $S_q$ ,  $S_p$ ,  $S_v$ , PV and  $S_{sk}$  were seen to increase with the length of time *in vivo*. When separated by design, AGC, PFC and K+, there are no correlations between femoral component roughness and length of time *in vivo*. Furthermore, when the K+ components are removed and just the AGC and PFC components are considered there are still no correlations seen.

The femoral component surface roughness values do not correlate with the FDS for the retrieved TKR components or the PE ADS values. Scholes & Kennard et al [15] also found no correlation between the femoral component surface roughness parameters and the Hood scoring of the PE component. Retrieval studies of THRs have also failed to show clinical evidence of the correlation between PE damage and counterface femoral component surface roughness [181, 182]. It cannot be concluded from the results presented in Chapter 4 that a high quoted femoral surface roughness value will result directly in a high PE ADS value for all designs of TKR. When the retrieved K+ TKRs (with the most severely damaged femoral and PE components) are excluded from the analysis, it can be seen that there is no correlation between the femoral component roughness  $S_q$  or  $S_{sk}$  for the PFC and AGC components and the PE ADS values (see Figure 4.35, Chapter 4).

As per the results in Scholes & Kennard et al [15] and Que et al [220], no correlations were found between the femoral component surface roughness of the retrieved components and patient age at primary, BMI or side of implantation. No difference

was seen in the femoral component surface roughness of the medial condyle when compared to the lateral condyle of the retrieved components. This in agreement with Muratoglu et al [222] but in contrast to previous studies Scholes & Kennard et al [15] where the lateral condyle roughness was reported to be greater than the medial and Fabry et al [17] and Brandt et al [180] who reported the opposite. The results presented in Chapter 4 and in Que et al [220] show no difference in femoral component roughness was seen between male and female patients. This is in contrast to the results presented by Scholes & Kennard et al [15] where higher roughness values and more negative skewness values were seen with male patients.

The lack of consensus and the inconclusion within the results presented in Chapter 4 from the surface topographical analysis of explanted TKRs with CoCr femoral components and those in the published literature as to whether there are or are not, correlations between the surface roughness and the patient and implant variables was to be expected. For the retrieved prostheses analysed where there was no PE wear through and unintended articulation of the femoral condyles and the metallic tibial tray did not occur, the mechanism of femoral component damage can be attributed to discrete events of third body damage. The “third body” in these cases could be bone cement or metallic debris which enter into the joint space between the femoral condyles and the PE articular surface and which can lead to gouging and scratching of the femoral components as seen macroscopically and microscopically on the retrieved components. Figure 7.1 shows the surface topography plots for a measurement area where there was an indentation. Figure 7.2 shows the surface topography plots for a measurement area where there was defined scratch. The discrete event of third body damage can occur at any point during the time *in vivo* of the prosthesis and hence the lack of correlation between femoral component roughness and time *in vivo*.

The burnished areas were observed microscopically as areas of decreased reflectivity and fine scratches. These areas were recorded to have relatively low RMS surface roughness  $S_q$  values (see Figures 7.3 and 7.4). Figure 7.3 shows the surface topography plots for a measurement area on the edge of the burnished area and a defined scratch. Figure 7.4 shows the surface topography plots for a burnished area.

The influence of femoral component roughness on the wear of the PE component will be discussed in more detail in section 7.4 below.

Large wavelength deep scratches or gouging were identified microscopically as a waviness and these areas were measured to have relatively high  $S_q$  values. Figures 7.5 and 7.6 not only show the surface topography plots but also the lens camera view with the interference fringes for measurement areas as seen on the profilometer. In Figure 7.6 there is no obvious damage to the component other than the waviness.

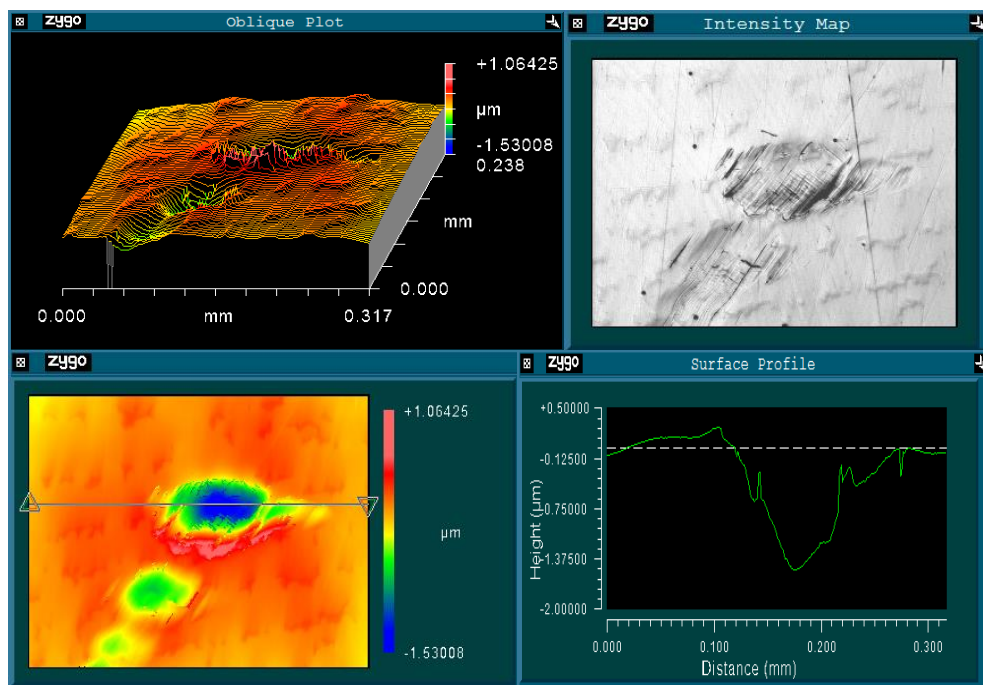


Figure 7.1 Surface topography plots for a measurement area on a retrieved CoCr femoral component showing an indentation,  $S_q = 0.250\mu\text{m}$ ,  $S_z = 0.957\mu\text{m}$

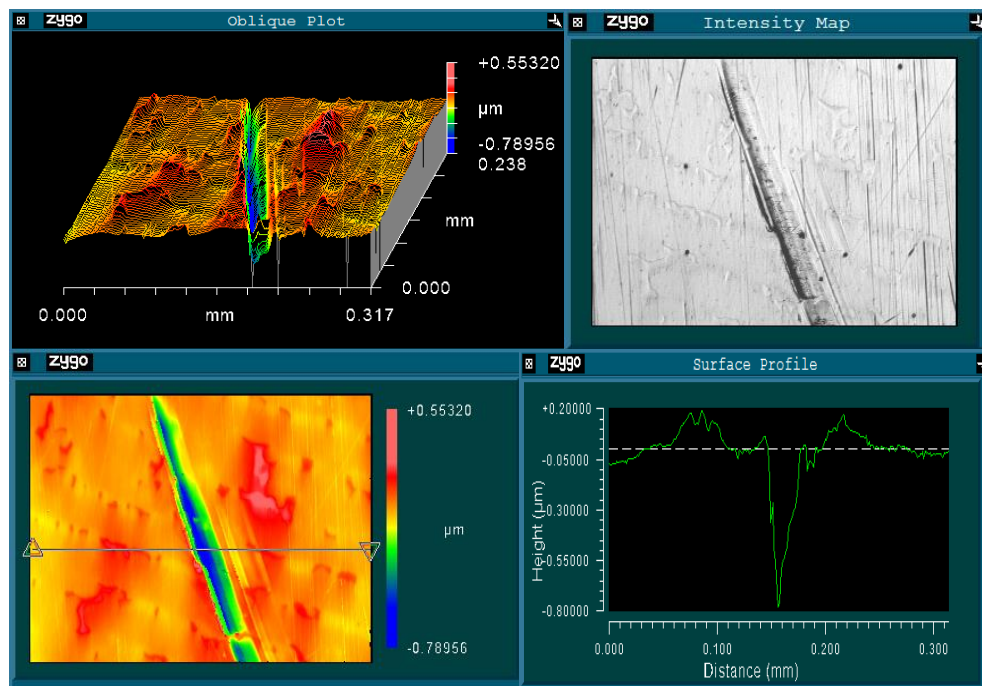


Figure 7.2 Surface topography plots for a measurement area on a retrieved CoCr femoral component showing defined scratching,  $S_q = 0.110\mu\text{m}$ ,  $S_z = 0.539\mu\text{m}$

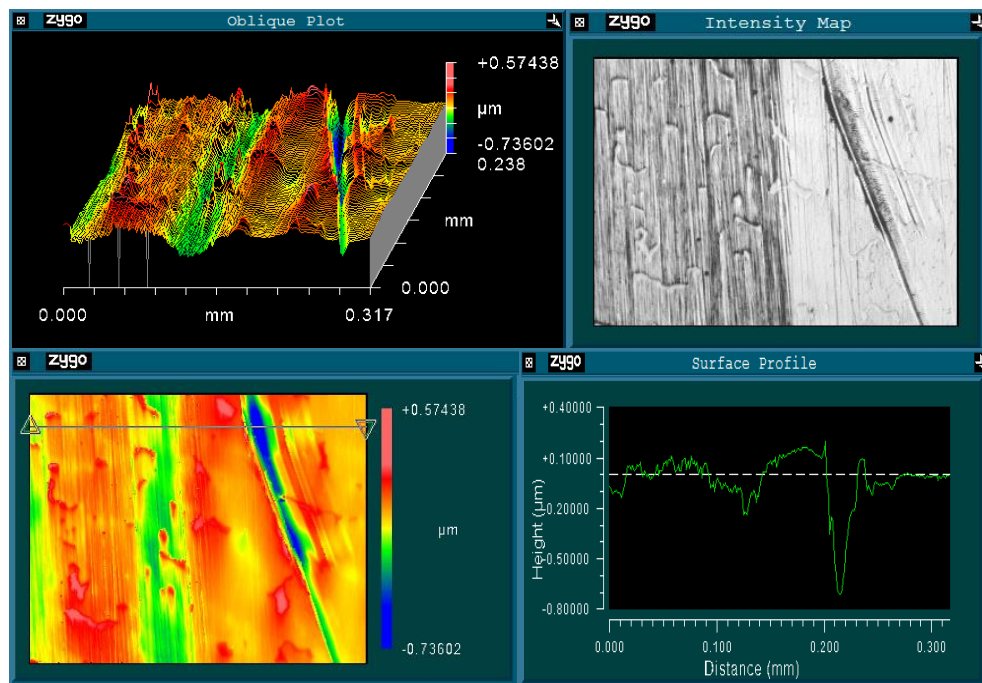


Figure 7.3 Surface topography plots for a measurement area on a retrieved CoCr femoral component showing the edge of a burnished area and a scratch,  $S_q = 0.120\mu\text{m}$ ,  $S_z = 0.725\mu\text{m}$

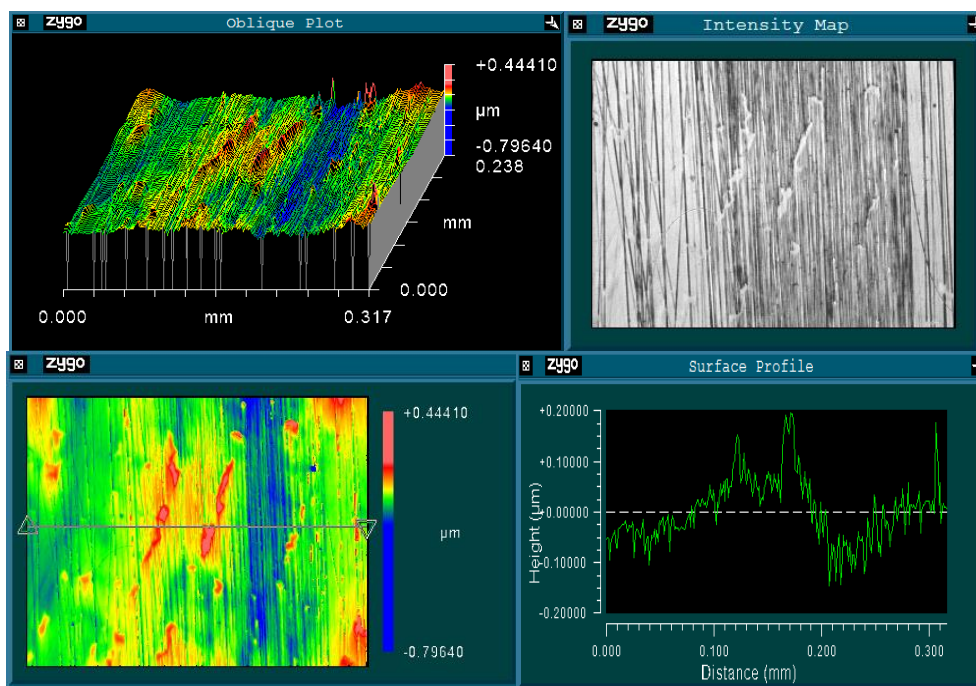


Figure 7.4 Surface topography plots for a measurement area on a retrieved CoCr femoral component showing a burnished area,  $S_q = 0.065\mu\text{m}$ ,  $S_z = 0.533\mu\text{m}$

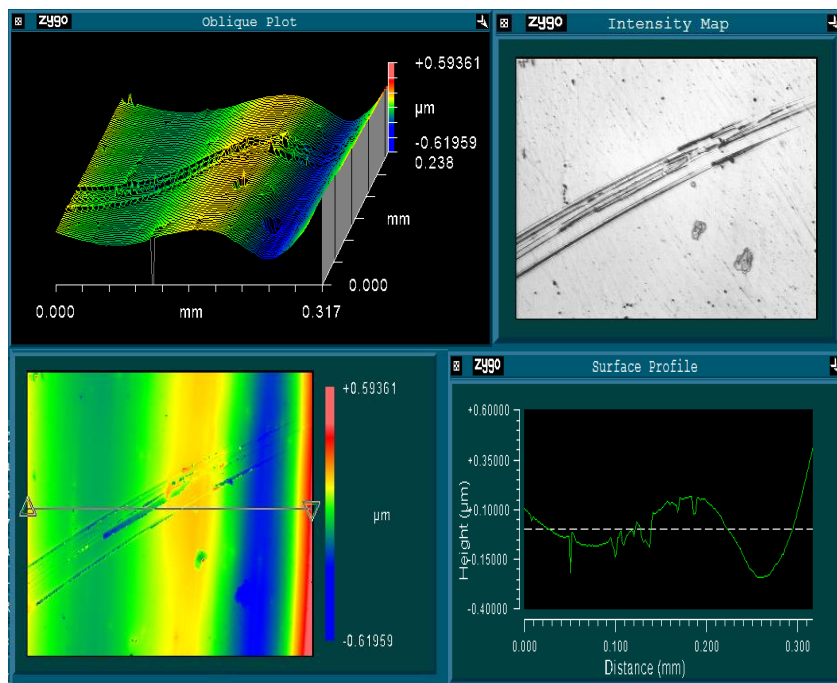


Figure 7.5 Surface topography plots and profilometer lens view for a measurement area on a retrieved CoCr femoral component showing waviness,  $S_q = 0.127\mu\text{m}$ ,  $S_z = 0.635\mu\text{m}$



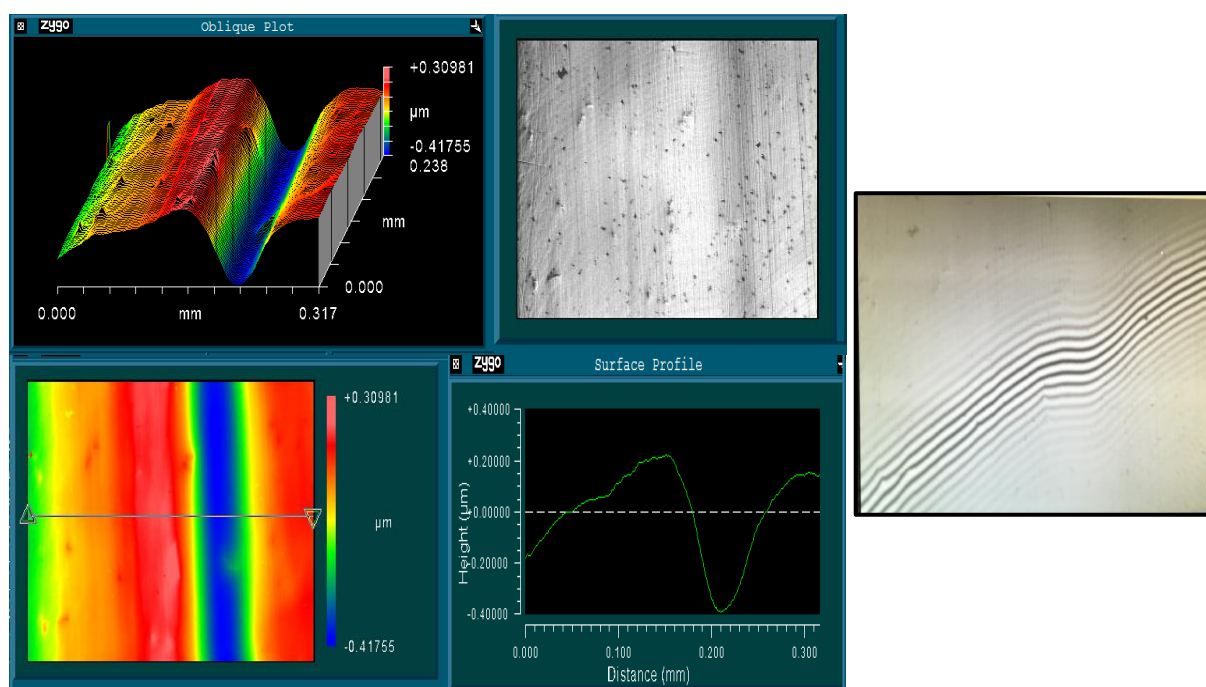


Figure 7.6 Surface topography plots and profilometer lens view for a measurement area on a retrieved CoCr femoral component showing waviness,  $S_q = 0.169\mu\text{m}$ , (there is not enough data to calculate  $S_z$ )

Considering the surface topography analysis results from the backside surface of the PE component and the tibial tray it was evident that retrieved TKRs with polished tibial trays had retrieved PE components with comparatively lower mean PE BDS values than the PE components of TKRs with non-polished tibial trays. This was expected and agrees with previous studies in the literature [163, 183, 184, 199]. Brandt et al 2012 [199] went further to report higher BDS values for PE components that had been gamma sterilised in air compared with those that had been sterilised in an inert environment. As previously discussed, the exact sterilisation processes are unknown for the retrieved components considered in Chapter 4. However, given the dates of implantation it could be assumed that the K+ PE components were sterilised by gamma irradiation in air whereas the PFC PE components would not have been. Based on this assumption, it could therefore be said that the results presented with this thesis repeat Brandt et al's findings.

The surface roughness measurements taken on the distal surface of the retrieved tibial trays, all with the exception of the skewness, correlated with the PE BDS.



However, as can be seen in Figure 4.31 in Chapter 4 there were no correlations when the results are grouped according to the prosthesis design. There was no correlation between the surface roughness parameters measured on the retrieved tibial tray component or the backside surface of the retrieved PE component and at the patient age at primary surgery or the patient BMI. There was no difference between the surface roughness parameters measured on the retrieved component that were implanted into the right or left side of the body or that had been implanted into male or female patients. This is in contrast to the findings by Brandt et al in 2012 who suggested that the male patients with a higher BMI in their study had a higher PE BDS [199].

## **7.2 Surface Topographical Analysis of Explanted UKRs with CoCr Femoral Components**

The results of the surface topographical analysis of explanted UKRs with CoCr femoral components that were presented in Chapter 5 of this thesis are discussed within this subsection.

As discussed in the review of the literature presented in Chapter 2, there are not many publications specifically on the surface topographical analysis of retrieved UKR prostheses and none were found within the literature review to report on the surface roughness. In 2017 Teeter et al [164] published the damage scoring results for the articular and backside surfaces of 16 retrieved mobile bearing Oxford UKRs. A wear rate for both surfaces was calculated using microCT scanning. Previously in 2010 Kendrick et al [202] published the damage scoring results of 47 mobile bearing Oxford UKRs along with a linear penetration calculated by measuring the PE thickness. As discussed in section 7.1 regarding the results presented in Chapter 4 for the surface topographical analysis of explanted TKRs with CoCr femoral components, it is difficult to make meaningful comparisons of damage scoring results due to the differences in the methodologies used. These limitations will be discussed in more depth in section 7.4. A further limitation of this particular aspect of this work is that no reference UKR prostheses were available for comparison. However, the reference TKR prostheses are considered to be the next best alternative as it can be

assumed that similar manufacturing and quality control procedures would be followed for UKRs as per TKRs.

The results presented in Chapter 5 show that damage occurred to all the retrieved UKR femoral and PE components but that there were no correlations to be found between the FDS and PE ADS or PE BDS values. The surface roughness parameters measured on the femoral components were all numerically greater for the retrieved components when compared to the reference components. These results were comparable with the results for the femoral condyles of the TKRs as presented in Chapter 4 and similar damage modes were observed. This gives further evidence to the conclusion that femoral component roughening is not correlated to, but indeed is independent from, the patient and implant variables.

There was a lack of patient and implant data for the retrieved UKR prostheses as detailed in Chapter 3 Materials and Methods. Only four of the retrieved UKR prostheses were from revisions performed by the collaborating surgeons. The remainder were loaned to this project via the Northern Retrieval Registry and were performed by other surgeons from hospitals that are outside the audit remit of this project and the collaborating surgeons. This meant that patient and implant data was unable to be accessed for the majority of the retrieved UKR prostheses. This is a limitation of this work. The limitations and practical constraints of retrieval studies are discussed in more depth in section 7.4 below.

### **7.3 Surface Topographical Analysis of Explanted Knee Prostheses with OxZr Femoral Components**

The results of the surface topographical analysis of explanted knee replacement prostheses (TKRs and UKRs) with OxZr femoral components that were presented in Chapter 6 of this thesis are discussed within this subsection.

The three retrieved TKRs with OxZr femoral components considered for analysis in Chapter 6 were not standard clinical cases. The age of the patients (37, 51 and 65 years) was considerably younger than the mean age for a primary TKR quoted in the

2018 NJR of 70 years [1] and the length of time *in vivo* was low at 40, 47 and 86 months. The indications for revision were pain, hypermobility, instability and chronic aseptic infection. One of the retrievals was a second revision. The three retrieved TKRs with CoCr femoral components were selected from the catalogue for comparison based the length of time *in vivo* (36, 44 and 63 months). Also included in Chapter 6 are the surface topographical analysis results for two retrieved UKR prostheses with OxZr femoral components. There was no patient or implant data with these two retrievals for the reasons previously explained. The ten retrieved UKRs with CoCr femoral components were used as a comparison not based on patient data but based on being a fixed-bearing, cemented design of UKRs similar to the Journey® Oxinium UKR.

Macroscopically the damage observed on the femoral components of the retrieved OxZr was different to that observed on the retrieved CoCr femoral components. All three of the retrieved CoCr TKR femoral components were observed to have burnished damage tracks in the anterior – posterior direction with light scratching but no deeper scratches or gouging. The retrieved CoCr UKR femoral components were observed to have burnishing, light scratches and also some deeper scratches. All of the five OxZr femoral components were observed to have light scratching or indentations and four were observed to have deeper scratches and gouges, there was only a small amount of burnishing on two of the retrieved OxZr TKR femoral components. Two of the OxZr TKR and one UKR were observed to damage posterior in high flexion on both condyles for the TKRs. This was unusual and initially considered to be retrieval damage. However corresponding damage was observed on the PE component which would suggest that this damage had been present *in vivo*. A review of the Smith & Nephew surgical techniques for the implantation of the Journey UKR system and the Genesis II TKR system showed that this damage may have been caused during implantation [229, 230]. Both surgical techniques instruct that the tibial baseplate is fixed into position first, then the femoral component is fixed and then the PE bearing is inserted. Figure 7.7 below shows images from the Smith & Nephew surgical techniques that illustrate this.

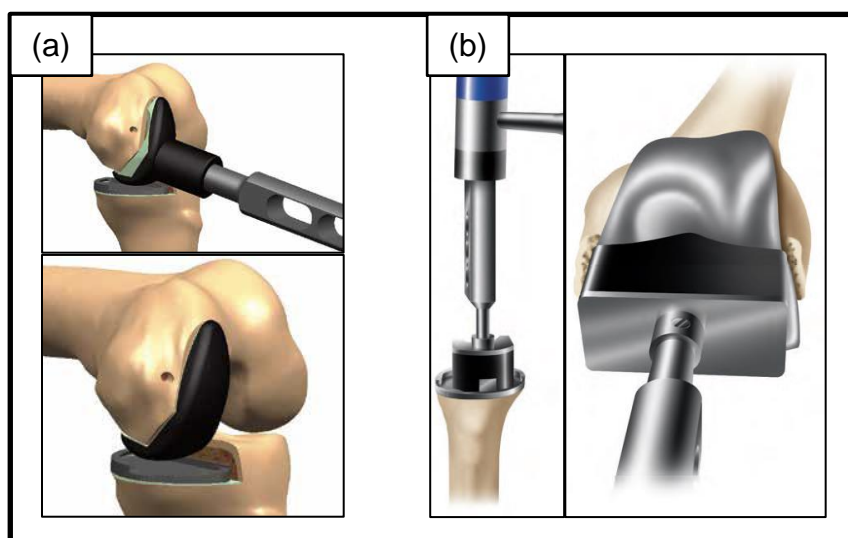


Figure 7.7 (a) Fixation of Journey UKR femoral component (b) Fixation of Gensis II TKR femoral component. (Images from Smith & Nephew surgical techniques) [229, 230]

A Smith & Nephew surgical technique for the Journey II TKR system, accessed in late 2018, does however include a “tibial baseplate cover” which is instructed to be placed over the tibial baseplate to provide protection while the femoral component is fixed into position. This stage may have been included in this latest version of that particular surgical technique to prevent the damage that was observed on 3 of the Smith & Nephew retrieved prostheses.

Comparisons between the absolute damage scoring results presented in Chapter 6 and results in the published literature are difficult due to the differences in methodologies. As discussed in section 7.1, Brandt et al [180] recorded grooving, indentations and gouging on the femoral components of retrieved OxZr TKRs but did not report the numeric values which makes comparisons challenging. There were minimal differences in the damage observed on the PE components of the retrieved PE components from the OxZr and CoCr TKR and UKRs.

The femoral component surface roughness results show that both OxZr and CoCr femoral components roughen *in vivo* which agrees with other reports of retrieved TKRs [15, 217]. Differences in methodology and parameters reported make absolute comparisons between the surface roughness results presented in Chapter 6 and

results in the published literature unreliable. However, the trends can still be discussed and compared.

The mean  $S_q$  and mean  $S_p$  were both significantly greater for the reference OxZr femoral component than for the reference CoCr femoral components. This result has been reported previously [180, 217]. In contrast to the data presented by Brandt et al [180] and Heyse et al [217], no differences were found between the  $S_q$ ,  $S_v$  and  $S_{sk}$  values for the retrieved OxZr femoral components and the retrieved CoCr femoral components. However, the  $S_p$ , PV and  $S_z$  values for the retrieved OxZr femoral components were found to be greater than for the retrieved CoCr femoral components. When reviewing these results, the differences in methodologies used must be considered. These will be discussed in section 7.4 along with the impact of changing the measurement and analysis parameters for the non-contacting optical profilometer on the absolute surface roughness parameter values. The selection of the sampling areas must also be considered; this also will be discussed later in section 7.4.

Regardless of the absolute values, it is clearly evident that the OxZr femoral component surfaces are different in surface texture than the CoCr femoral surfaces. The difference is characterised on the OxZr surface by a high frequency roughness with a high peak to valley or  $S_z$  parameter. This can be seen in the results presented in this thesis and also in the optical profilometry results presented by Heyse et al [217] and the contact profilometry results presented by Brandt et al [180]. Figures 7.8 – 7.10 illustrate this and comparing the profilometry results measured on OxZr and CoCr femoral components from this thesis, Heyse et al [217] and Brandt et al [180].

The results presented in Chapter 6 and this section of the discussion are included in the publication Kennard et al (manuscript included in Appendix F) [14]. While the discussion and conclusions are the same, there are some slight differences in the absolute numerical values due to differences in the methodology and the measurement and analysis controls used for the optical profilometry within this thesis compared to within the publication. This is discussed in more depth in section 7.4.

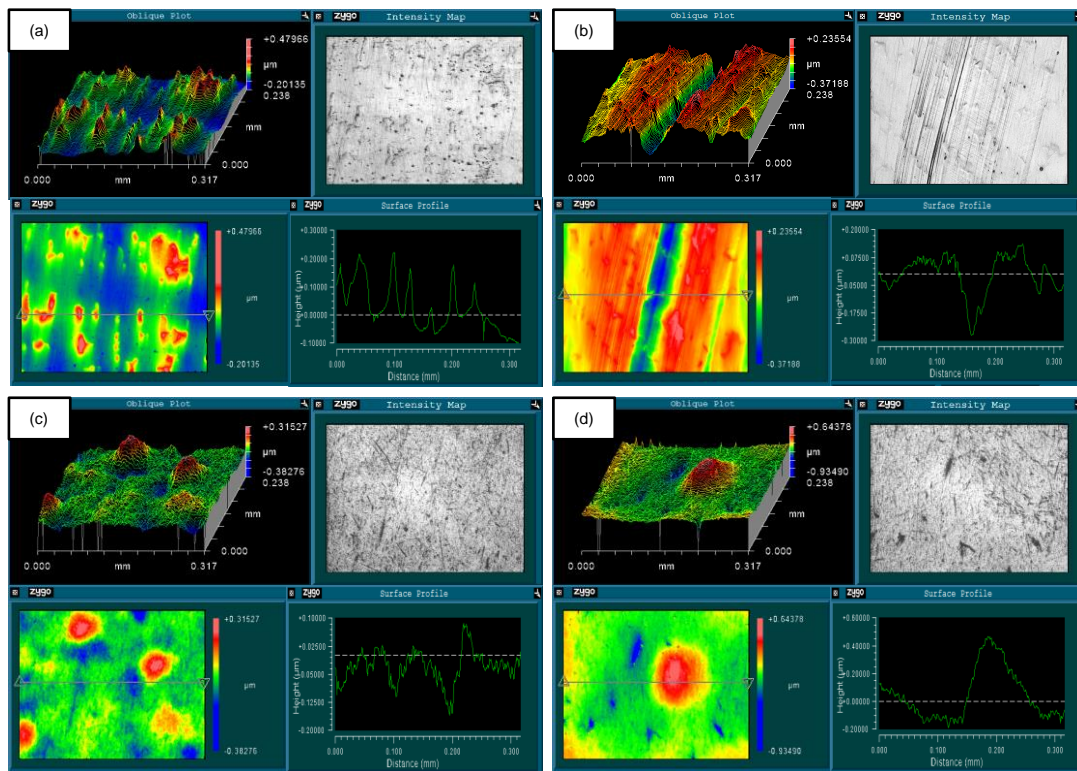


Figure 7.8 Surface topography plots from measurement areas on femoral components (a) CoCr reference ( $S_q = 0.063$ ,  $S_z = 0.403$ ) (b) CoCr retrieved ( $S_q = 0.099$ ,  $S_z = 0.267$ ) (c) OxZr reference ( $S_q = 0.099$ ,  $S_z = 0.433$ ) and (d) OxZr retrieved ( $S_q = 0.123$ ,  $S_z = 0.799$ )

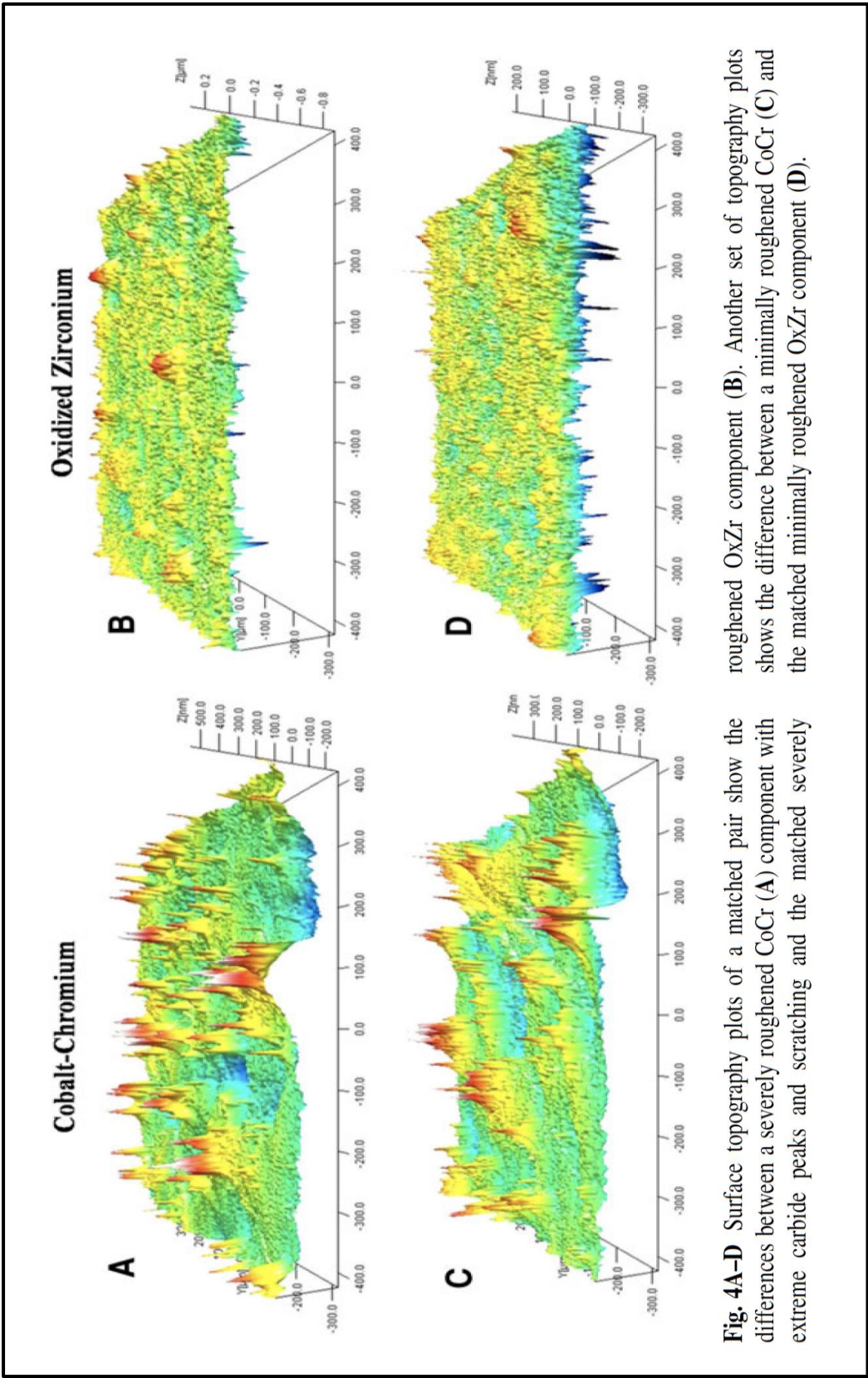


Figure 7.9 Images from Heyse et al [217]



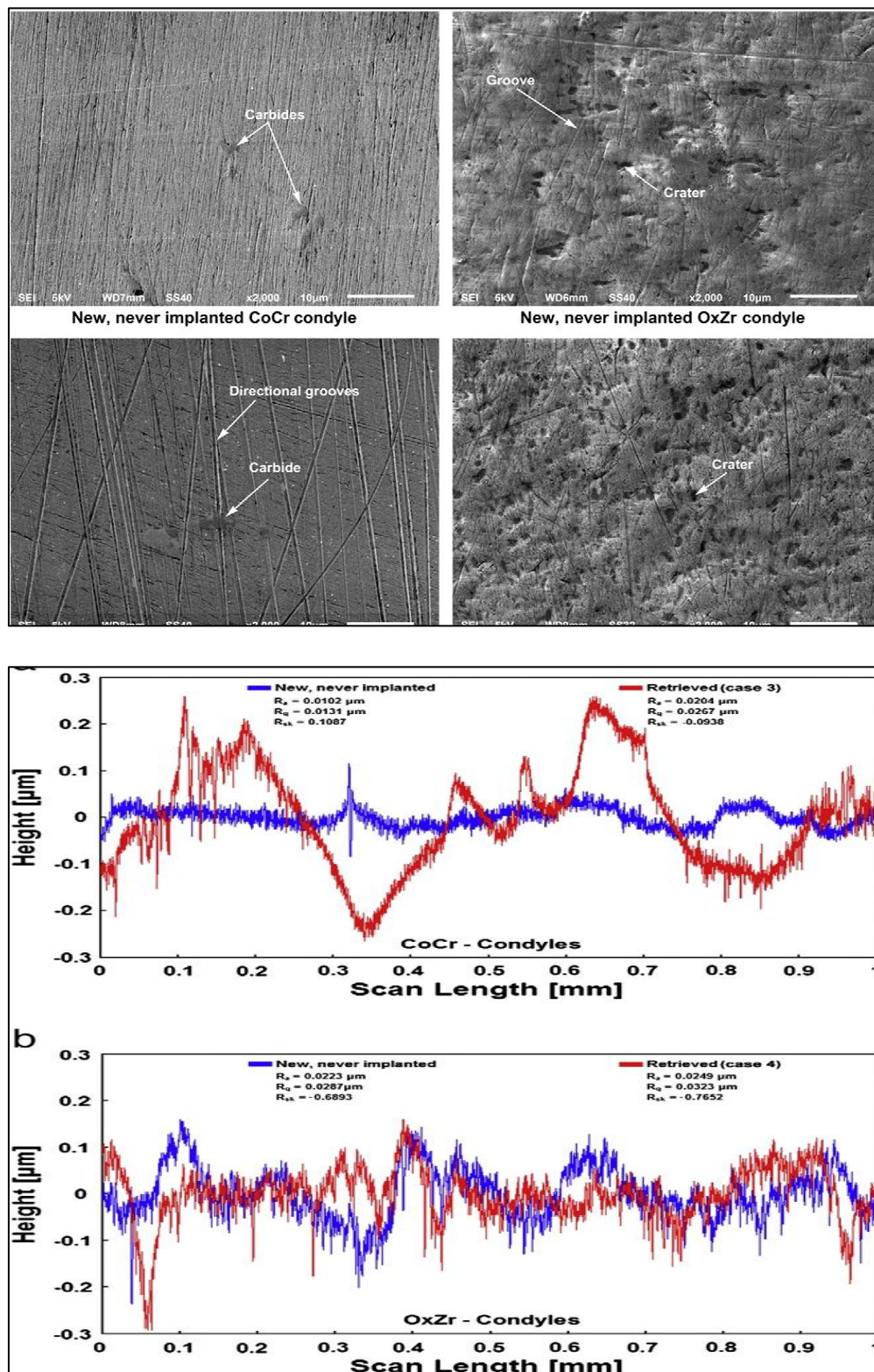


Figure 7.10 Images taken from Brandt et al [180] On the left are SEM images showing new (top) and retrieved (bottom) CoCr (left) and OxZr (right). On the right are contact profilometry plots for CoCr (top) and OxZr (bottom)



## 7.4 Limitations and Practical Constraints

This thesis has presented a thorough investigation into the surface topographical analysis of explanted knee replacement prostheses. There are however, many limitations and practical constraints that must be acknowledged when considering the results of the analyses. One of the main limitations associated with all studies of prostheses retrieved from revision surgery is that the analysis of “failed” prostheses may not accurately represent the *in vivo* performance of well-functioning prostheses. Furthermore, when studying retrieved prostheses, it is challenging to accurately approximate the pre-implantation surface topography of the retrieved components. Even when using new unused components as references, potential differences in manufacturing batches and design tolerances and also potential design changes over time can lead to inaccurate representation of the pre-implantation surface [214]. This can be seen in the variation of surface roughness measurement results of the reference components presented in Chapters 4, 5 and 6 and which are discussed in more detail below in section 7.4.2.

There are also limitations associated with the analysis of data collected from a newly established and relatively small Knee Explant Catalogue. The number of prostheses suitable for comparative analysis are low once exclusions have been made. While the numbers may be considered lower than the much larger retrieval catalogues reported typically within the United States [180, 217], the work and time involved to establish the physical collection of the retrievals must be acknowledged. This is the largest collection of explanted knee replacements prostheses within the United Kingdom. Within the UK the collection and management of patient data is rightly strictly regulated by ethics and data protection protocols. In the case of the UKR retrieved prostheses analysed within this thesis there was limited patient and implant data that was able to be accessed. A large number of the UKRs were retrieved from revisions collected as part of the Northern Retrieval Registry and not under the audit jurisdiction of the orthopaedic surgeon team collaborating on this project and that is why a lot of the patient and implant data was unavailable. For the TKR retrieved prostheses once exclusions had been made for the various reasons detailed in the selection criteria, there were just forty-six retrieved TKR prostheses suitable for

comparative analysis. The smallest group number was the three OxZr TKRs and the largest groups were the fifteen PFC and fifteen K+ TKRs. These relatively small numbers mean that there may be sample size induced errors in reported correlations and the interpretation of the practical significance of the analysis of results must be done with caution.

#### **7.4.1 Patient and Implant Variables**

The clinical data collected for the retrieved prostheses within the Knee Explant Catalogue can be compared with the data published in the 15<sup>th</sup> Annual Report for the National Joint Registry (NJR) for England, Wales, Northern Ireland and the Isle of Man [1]. Across all primary knee replacement procedures recorded in the NJR osteoarthritis is the main indication for 98% but within the Knee Explant Catalogue used in this thesis this is lower at 86% being indicated for osteoarthritis. There is no data within the NJR that details the primary indication of the revised knee replacement prostheses. Within the NJR the most common clinical reasons for revision cited for TKR were aseptic loosening, pain, infection and other and for UKR the revision indications were pain, aseptic loosening and other. Although aseptic loosening was the main indication for revision of the TKRs recorded in the Knee Explant Catalogue the next most prevalent reason was instability, followed by PE component wear, infection and then pain. From the limited data available for the UKR revisions within the Knee Explant Catalogue, pain was recorded as the main reason for revision of a UKR. The gender split within the catalogue of slightly more male revision patients than females agrees with the increased risk of revision for male patients reported in the NJR. The lower median age at primary surgery of 61 years for the revised TKRs and 62 years for the revised UKRs also agrees with the increased risk of revision for younger patients published in the NJR.

When reviewing the patient and implant demographics of the revisions included in the Knee Explant Catalogue and comparing them to the data in the NJR it is important to consider the clinical history of the prostheses within the catalogue. All the explanted prostheses (TKR and UKR) with patient and implant data were retrieved from revisions performed at the Freeman Hospital, Newcastle. These

revision patients are made up of patients who had their primary knee replacements performed by the collaborating surgeons as well as patients who have been referred. The split of TKRs vs UKRs is skewed by the fact that the collaborating surgeons who provided the revision prostheses for the Knee Explant Catalogue typically do not perform a large number of primary UKRs within their orthopaedic practice and hence they do not perform a large number of UKR revisions. The distribution of different designs of TKRs included in the Knee Explant Catalogue is influenced by the TKR prostheses the collaborating surgeons use for primary TKRs as discussed earlier in section 7.1. The collaborating surgeons do not routinely use Oxinium® (Smith & Nephew) prostheses hence the low numbers of these included in the Knee Explant Catalogue. In addition, it must be considered that revision procedures referred to the collaborating surgeon team are often complicated cases, and some are second revisions of a failed first revision.

#### **7.4.2 Damage Scoring**

Femoral component damage scoring provides a numeric value to quantifiably describe the damage observed on the femoral components of the retrieved prostheses. Damage scoring enables graphical representation of the results and allows comparisons and correlations to be made. However, it is not entirely appropriate to compare the femoral damage score (FDS) values reported in this thesis with those published by other groups in the literature due to the subtle differences in methodology used. Brandt et al [180] assessed grooving, indentations and gouging for CoCr and OxZr femoral components and Fabry et al [17] assessed at scratching, coating breakthrough, indentations and notches for TiN femoral components. The results presented in this thesis assess gouging, burnishing and indentations and scratches as that was what was considered appropriate for the retrieved femoral components included in the analysis. It was deemed more important to be able to accurately assess the damage features observed than compare directly with the literature.

The PE articular surface damage scoring method used in this thesis was a non-modified version of the original Hood scoring system [194]. It was chosen as it was a

semi-quantitative method of providing a measure of the damage on the PE component. However most of the recent published literature with the exception of Scholes & Kennard et al [15] use non-comparable modified versions of the Hood scoring system. Some of the published methodologies include an additional severity weighting and there are variations in the number of sections included in the analyses and the damage features recorded. This makes direct absolute comparisons meaningless. The same is applicable for the PE backside damage scoring.

Inherent within any semi-quantitative damage scoring system are inter- and intra-user errors. This was examined in depth in the publication by Harman et al [206] where it was shown that through the use of clear descriptions and a pictographic atlas the inter- and intra- observer errors may be reduced. Practically, given the resources available it was not feasible to have multiple users score the PE articular surface, PE backside surface and the femoral component for all the retrieved prostheses analysed within this thesis. However, it was considered acceptable to clearly define the damage features using images and written descriptions.

Even with clear written descriptions and images to help define the damage modes, the assessment of the area covered by a particular damage feature is user subjective with inter- and intra- user variations. Within the Hood damage scoring method [194] this a numerical value of 0 – 3 depending on an estimated area coverage of a damage feature. Within the FDS and PE BDS calculation this is an estimation of not only the area covered but also the severity [17, 180, 200].

With all of the damage scoring methods for retrieved components there is also a user judgement as to what is *in vivo* damage and what is retrieval and post-retrieval damage. To attempt to make the appropriate judgement the retrieved components cannot be analysed in isolation but must be where possible, considered as a complete prosthesis to assess whether the damage on the components is comparable.

Within the published literature, the PE articular damage scoring method has been shown to be a poor approximation of the volumetric PE wear [195]. Once the influences of the implant design have been considered, the results presented within

this thesis show that neither the femoral component damage scoring or the PE articular surface damage scoring are considered to correlate to the surface roughness data or the patient and implant variables.

Despite the limitations of damage scoring of retrieved prostheses, the methodology can provide a quantitative method of assessing damage to allow comparisons within the groups analysed. And while comparisons of absolute values are often not achievable, there can be some level of qualitative comparison of results with the published literature.

#### **7.4.3 *Surface Roughness Measurement***

The work done within this thesis presents a thorough investigation into the surface roughness analysis of explanted knee prostheses. This work also highlights the challenges and inconsistencies of using non-contacting profilometry to provide a numeric analysis of explanted knee prostheses. Due to these challenges and inconsistencies in methodologies, attempting comparisons between the published literature reporting surface roughness results of the analysis of retrieved knee replacement prostheses is very difficult. Not only do the cohorts of retrieved prostheses differ as discussed above, but there are a wide range of methodologies used and parameters reported. This all makes direct absolute comparisons very difficult and at high risk of being meaningless. This can be seen in the summary presented in Table 2.4, Chapter 2 Literature Review. There are contacting profilometry methods [17, 28, 153, 154, 180, 218, 219, 224] and non-contacting profilometry methods [15, 29, 169, 198, 216, 217, 220, 225]. There are differences in the parameters reported with some publications actually reporting linear profile parameters when non-contacting areal methods are used [29, 220, 225]. There are differences in the number of measurements taken and the areas considered for analysis with some publications considering “worn” areas [15], some considering measurements at a particular tibiofemoral flexion extension angle [180] and some considering measurements within a defined location [14, 217]. These differences all have an impact on the descriptive statistics (mean, median, standard deviation etc) of the surface roughness measurement values reported and can be described as a

sampling error. The major assumption driving this sampling error is that the entire surface topography of the component is assumed to be the same as the small sample areas that are measured. This is a wholly unrealistic assumption for a damaged component. One way to reduce the sampling error and provide an approximation of the overall surface roughness of the entire component would be to map the entire surface through digital stitching of measurement results.

Unfortunately, digital stitching of the surface topography measurement results was not possible with the technology available for use within this project.

Another way of reducing the sampling error would be to take a very large number of measurement areas as per the suggestion in Que et al [225] where two hundred measurements were taken in a 20mm x 10mm grid. However, with the equipment available for use within this project, to take a single surface roughness measurement on a retrieved knee prosthesis involves manual positioning of the component so that the surface is perpendicular to the light source, manual focusing of the objective lens and setting the light intensity levels. Due to the geometry of the knee replacement components analysed this is often not a simple process and is labour intensive and time consuming. The surface topography results presented within this thesis come from over two thousand optical profilometry measurements taken using the Zygo NewView 5000 following this component positioning protocol. Increasing the number of measurements taken would not have been practically achievable given the time constraints of completing this project. Arguably, unless the number of measurements were increased so much so that the entire component surface was measured, there would be minimal benefit to taking more surface roughness measurements.

To attempt to reduce the sampling error for the results presented in Chapters 4, 5 and 6 and to enable a practical interpretation of the results and their clinical impact, the methodology was clearly defined as thirty measurements taken on each femoral component of the most damage that was able to be measured given the constraints of the optical profilometer. This method then incurs a further user error as it is dependent on the user's assessment as to what is considered to be *in vivo* damage and what is considered to be retrieval or revision surgery handling damage. To

reduce this error, the femoral components were considered alongside the corresponding PE components to assess whether damage observed was concurrent.

As well as the surface roughness results from the optical profilometry being dependent on the location and number of measurement areas considered, the optical zoom has an impact on the absolute values recorded. Table 7.1 shows the camera lens view from the Zygo NewView 5000 for the same location on a CoCr femoral component but at different optical zooms (x0.5, x1.0 x2.0). The measurement area is given. And the surface topography plots are also shown. Table 7.2 shows the same for a location on an OxZr femoral component. The results presented in Chapters 4, 5 and 6 are all from optical profilometry using a 10Xobjective lens and a x 2 optical zoom which gives an area of view of 317 x 238  $\mu\text{m}$  as per previously published work [15, 32, 198, 226, 227]. Other publications have varied between 1.3mm x 0.9mm [29], 600 x 800 $\mu\text{m}$  [217], 632 x 475 $\mu\text{m}$  [169].

The optical zoom was used in order to identify the most damaged areas on the femoral components in Chapters 4, 5 and 6. This means that the component was observed at x 0.5 zoom, the most damaged areas were visually identified and then the component was positioned to zoom into that area and the measurement taken.

As well as the measurement controls of the zoom (and ultimately the area of measurement) having an impact on the surface roughness parameters recorded, the positioning of the component also influences the results. The femoral components are typically designed with multiple radii in two planes and vary according to design and can vary even within a particular design according to size. As highlighted in Chapter 2, curved surfaces do not modulate well during optical profilometry and can result in high signal to noise ratio as the instrumentation is unable to detect changes in wave modulation reflected from curved surfaces [85-87]. Filters do not resolve this as it is a measurement characteristic making the results sensitive to the curvature and tilt of the sample. The tilting table and a simple small custom-made positioning block were used to try to position the component parallel to the objective lens to attempt to overcome this problem (see Figure 7.11).

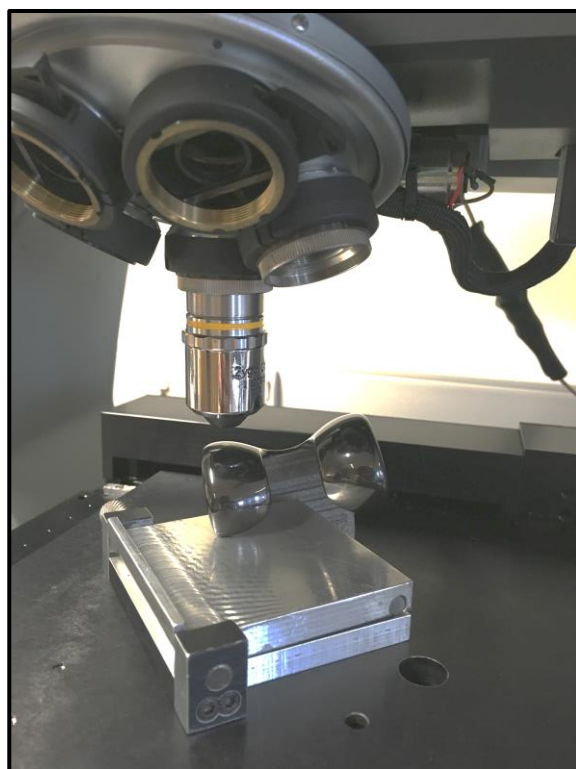


Figure 7.11 Positioning of an OxZr TKR femoral component for measurement utilising a positioning block

This process of component positioning and re-positioning for each individual measurement is time-consuming and limiting. There were occasions where a suitable measurement of a damaged area observed on a femoral component was just not possible due to being unable to position the component parallel to the objective lens. The surface topography measurements from the OxZr TKRs and UKRs were particularly sensitive to positioning of the component and the reason for this may be the combination of the optical properties of the OxZr surface and the geometry of the prostheses. As discussed in the literature review in Chapter 2, errors in surface roughness measurement can be introduced when attempting to analyse a surface with a different reflectivity to the reference surface in an optical profilometer.



Table 7.1 Surface roughness measurement results for the same location on a CoCr femoral component at different optical zooms

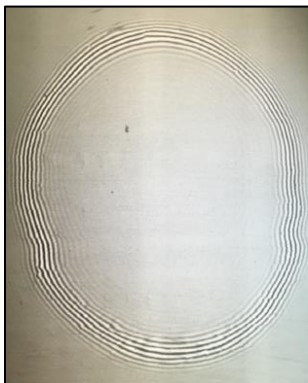
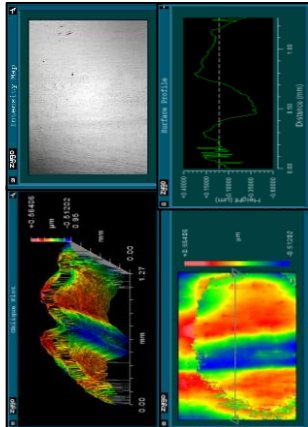

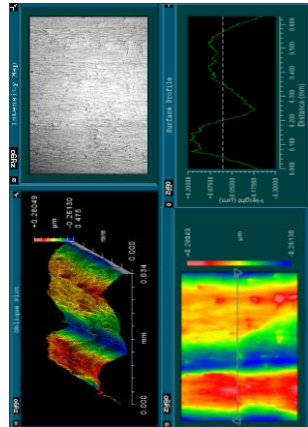

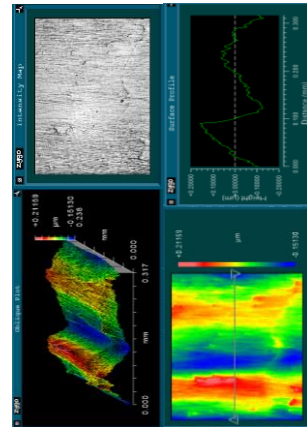
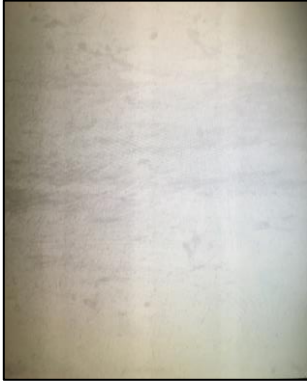
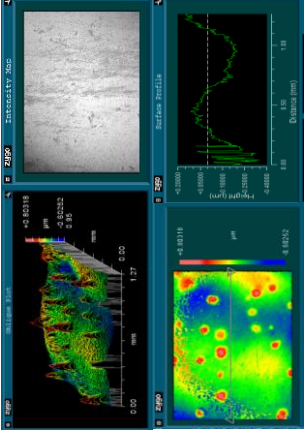

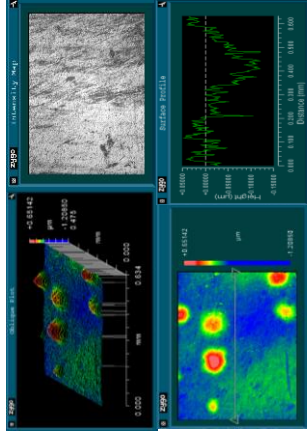

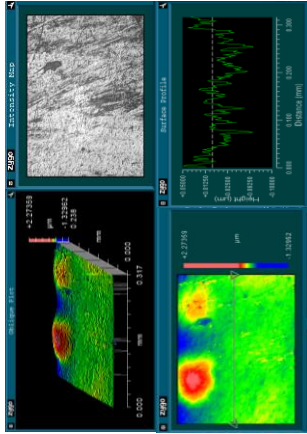
Optical Zoom	Measurement Area	Surface roughness values							Camera view	Surface topography plots
X 0.5	1.27mm x 0.95mm	$S_q$ (mm)	0.194							
		$S_z$ (mm)	0.797							
		PV (mm)	1.076							
		$S_p$ (mm)	0.564							
		$S_v$ (mm)	-0.512							
		$S_{sk}$ (-)	-0.429							
X 1.0	0.634mm x 0.475mm	$S_q$ (mm)	0.112							
		$S_z$ (mm)	0.29							
		PV (mm)	0.542							
		$S_p$ (mm)	0.28							
		$S_v$ (mm)	-0.261							
		$S_{sk}$ (-)	-0.298							
X 2.0	0.317mm x 0.238mm	$S_q$ (mm)	0.065							
		$S_z$ (mm)	0.182							
		PV (mm)	0.363							
		$S_p$ (mm)	0.212							
		$S_v$ (mm)	-0.151							
		$S_{sk}$ (-)	0.111							

Table 7.2 Surface roughness measurement results for the same location on an OxZr femoral component at different optical zooms (\*Interference fringes not shown on camera view)

Optical Zoom	Measurement Area	Surface roughness values						Camera view	Surface topography plots
		$S_q$ (mm)	$S_z$ (mm)	PV (mm)	$S_p$ (mm)	$S_v$ (mm)	$S_{sk}(-)$		
X 0.5	1.27mm x 0.95mm	0.156	1.135	1.406	0.803	-0.603	0.614		
X 1.0	0.634mm x 0.475mm	0.100	0.885	1.860	0.651	-1.209	2.468		
X 2.0	0.317mm x 0.238mm	0.101	1.811	3.603	2.274	-1.330	0.711		

As identified in the literature review of Chapter 2, the application of filters during the analysis of the surface topography results was deemed necessary to attempt to achieve appropriate surface roughness characterisation. A ‘remove cylinder’ form filter (the exact equation for which is embedded within the MetroPro software) was applied for the calculation of the surface roughness parameters on the femoral components. In addition, a “remove spikes” filter and a data fill filter were also applied. Table 7.3 provides a comparison of the surface roughness results from a reference CoCr femoral component and a reference OxZr femoral component analysed with and without the “Remove spikes” and “Data fill” filters applied.

Table 7.3 Surface roughness parameters variation dependent on analysis control remove spikes and data fill filters

	Reference CoCr (n = 30 measurement areas)		Reference OxZr (n = 30 measurement areas)	
	No filters	“Remove Spikes” and “Data Fill” filters	No filters	“Remove Spikes” and “Data Fill” filters
<b>S<sub>q</sub> (μm)</b>	0.070 (±0.008)	0.069 (±0.009)	0.086 (±0.002)	0.080 (±0.002)
<b>S<sub>z</sub> (μm)</b>	1.374 (±0.163)	0.386 (±0.042)	1.035 (±0.067)	0.571 (±0.073)
<b>PV (μm)</b>	0.856 (±0.058)	0.790 (±0.122)	1.451 (±0.081)	1.015 (±0.097)
<b>S<sub>p</sub> (μm)</b>	0.571 (±0.035)	0.294 (±0.017)	0.645 (±0.048)	0.426 (±0.050)
<b>S<sub>v</sub> (μm)</b>	-0.802 (±0.147)	-0.497 (±0.110)	-0.806 (±0.057)	-0.589 (±0.074)
<b>S<sub>sk</sub> (-)</b>	-0.371 (±0.447)	-0.101 (±0.399)	0.375 (±0.292)	-0.315 (±0.296)

The OxZr surfaces specifically do not modulate well giving high frequency oblique plots. However, the OxZr surface roughness measurements were not filtered further with a low pass frequency filter as the high frequency roughness was not considered to be optical noise (see Figure 7.8 and surface topography plots included in Table 7.2). This decision was based on comparison to Brandt et al's [180] contact

profilometry results for OxZr which also showed high frequency roughness but because of the methodology used could not be attributed to optical noise. Using the same logic, the minimum modulation frequency (effectively another form of low pass frequency filter) was not changed for the measurement of OxZr surfaces. A point to note regarding all the surface roughness measurement results presented in Chapters 4, 5 and 6 is that although the results for the surface roughness kurtosis have been recorded, they have not been included in any of the analyses or discussion. As a fourth order differential it is mathematically unstable, and this is reflected by the wide variations seen in the numeric values in the results. As such the interpretation of the results was nonsensical and have not been included.

#### **7.4.4 *Approximation of a Reference Surface***

A further limitation of retrieval studies lies with the approximation of the original surface. For the results presented in this thesis, new, un-opened components were used as the reference components and surface roughness measurements were taken on these components. For the PFC, K+ and OxZr femoral components the comparison was made between equivalent designs but for the AGC femoral components and the UKR components no new un-opened components of these designs were available for measurement.

The results in Chapter 4 Surface Topographical Analysis of Explanted Total Knee Replacements with Cobalt Chromium Alloy Femoral Components, showed that the surface roughness measurements of two different reference CoCr femoral components of the same design and size but not the same manufacturing lots varied in absolute values, although no statistically significant differences could reliably be determined. This has been reported before by Teeter et al with respect to PE tibial inserts [214]. What has not been recorded previously is the observation of peaks and also pits on new, un-opened femoral components (see section 4.3.1 and Figures 4.10 – 12). The BS ISO standard 7202-2 [106] requirement is for a  $R_a$  *max* value  $\leq 0.1\mu\text{m}$  measured in accordance with ISO 4288 [107]. It is important to note that this is a profile measurement not a surface areal measurement. What is unknown with

regards to the reference components is the design tolerances within the design manufacturing and quality control process of the implant manufacturers.

## 7.5 Summary

Considering all the limitations and practical constraints, the results presented in this thesis have provided evidence to demonstrate that a measured *in vivo* increase in femoral component surface roughness does not correlate to either the quantified damage observed on the PE component or the length of time *in vivo* of the prostheses. Furthermore, the increased femoral component surface roughness does not show conclusive correlations with the patient and implant variables.

The fundamental tribological studies and the laboratory simulations show that an increased counterface surface roughness leads to accelerated PE wear.

Theoretically, a surface with an increased peak height will ultimately lead to gouging and scratching of the bearing surface. In addition, a counterface surface with more asperities (described topographically by a positive skewness) may lead to more asperity contact and therefore potentially increased micro-adhesion and burnishing wear of the PE bearing. No evidence could be seen to conclusively say that the retrieved components had experienced PE wear due to increased femoral component roughening. In the *in vivo* environment there are multiple influencing surgeon, implant and patient factors that impact on the mechanisms of damage and wear of the PE component and increasing the femoral component surface roughness is just one of these factors. Trying to extrapolate out the influence of the individual factors is not simple.

Femoral component roughening in the form of gouging and indentations and light scratches is the result of a discrete third body damage event. These damage modes are observed on retrieved femoral components. They are considered to possibly be the result of either bone cement debris or metallic debris within the joint space. This third body damage could occur at any point during the length of the time *in vivo* from directly after, or even during as described above, implantation right up until just before revision. Considering these modes of femoral component roughening, the lack

of a relationship between the femoral component roughness and the patient and implant variables is reasonable to accept.

The burnished damage tracks observed macroscopically on some of the femoral components were also analysed microscopically. These areas did not result in high surface roughness measurements. It would appear that this damage mode is not the result of a discrete event but a progression over time. It has been suggested that within orthopaedic metallic and ceramic components articulating with PE bearings, material transfer may occur resulting in a transferred material layer [150, 231, 232]. Without testing the material composition on the burnished damage track it could not be determined for certain if this had occurred. This would be an interesting area for future studies.

Even though no correlations could be found for the increased femoral component surface roughness and the PE damage scoring, femoral component counterface roughness is still an important consideration for the tribological performance of knee replacement prostheses. From the results of the backside analysis it can be seen tibial trays with a high pre-implantation surface roughness (i.e. non-polished) can result in more PE damage than polished tibial trays.

However, it is not just the surface roughness of the material that is important as is evident from the results present in Chapter 6 for the OxZr reference components. OxZr components have resulted in lower PE wear rates in laboratory simulations [171, 187]. Interestingly, the reference OxZr components results presented in this thesis showed significantly greater mean  $S_q$  and mean  $S_p$  than for the reference CoCr femoral components. This result has been reported previously by Brandt et al and Heyse et al [180, 217]. This goes against the theory that surfaces with higher roughness values specifically higher peak values lead to increased PE bearing wear. Further investigation into surface texture and the ductility and wettability of the OxZr and CoCr materials is needed to further understand this material and the clinical implications of its use [232]. Such investigations were outside the scope of this thesis and would be an interesting direction for future work. It is also important to acknowledge that the clinical follow up results for OxZr knee replacement prostheses

are not superior than those for CoCr knee replacement prostheses [188, 192]. The discrepancy from the clinical and retrieved component results and the laboratory simulations warrant further investigation. A rough estimation is that OxZr knee replacement prostheses are typically double the cost of similar CoCr knee replacement prostheses. Without the clinical and retrieval study evidence it can be hard to see the justification of the higher costs. Only time will be able to tell whether there are any noticeable *in vivo* differences from the more expensive OxZr knee replacement prostheses. On this same topic, the longer clinical and retrieval study follow up of newer generation prostheses that utilise cross-linked polyethylene that includes stabilising additives is necessary.

An important consideration within this PhD is the sheer volume of work and time required to collect the data presented in the results sections. The physical collection and processing of explanted knee prostheses is a time-consuming laborious process and at the start of this PhD there were no systems in place to do this. When this PhD was started there was no laboratory facilities available at Newcastle University for the processing of the explants and there were many barriers to being able to set up a physical collection of explanted knee prostheses. Once those hurdles were overcome and the explanted components were collected and processed for ready for analysis, the subsequent surface roughness analysis of the components was not simple. The size and profiles of the knee prosthesis components make analysis using the available Zygo NewView non-contacting profilometer a laborious and time-consuming process. To enable a single surface roughness measurement to be taken the component would have to be positioned and focused for each measurement.

Despite the identified limitations and the practical constraints discussed above the study of retrieved components is of great importance as these prostheses have undergone the truest test of all through their time *in vivo*. It is only through the analysis of retrieved components that an understanding of how the components have actually changed during their time *in vivo* can be achieved. Recent orthopaedic history has shown the value and importance of analysing retrieved prostheses and reporting of the results [233] and this is the contribution that this thesis makes to the literature within this area.

*Blank Page*



## Chapter 8 Conclusions

The aim of this research was to use engineering techniques to quantify the surface topography of retrieved explanted knee prostheses to provide further understanding of *in vivo* topographical changes observed on the components. This aim has been realised through the presentation of the results and subsequent discussion in the preceding chapters of this thesis. The work contained within this thesis has provide a thorough investigation into the analysis of *in vivo* surface topographic changes of knee replacement prostheses and has investigated relationship between *in vivo* surface topographical changes and patient and implant demographics. This work has contributed to the body of knowledge within the field of orthopaedic knee replacements and knee prosthesis retrieval studies through the publication of two original research articles, Kennard et al [14] and Scholes & Kennard et al [15].

This chapter includes the conclusions that can be drawn from this research. Specific outcomes are detailed with respect to the specific objectives set in the Chapter 1 Introduction, areas for future work are identified and the defined contributions are listed.

### 8.1 Summary

The analysis of retrieved prostheses that have undergone the truest test of all through time *in vivo* is an extremely valuable contribution to the body of knowledge concerning orthopaedic replacements. The work presented in this thesis has shown that the semi-quantitative damage scoring of components provides a simple and effective method of recording and comparing *in vivo* damage observed on retrieved prostheses. Damage scoring provides a numeric result that can be correlated with patient and implant factors. The work presented in this thesis has shown that surface roughness measurement can provide information regarding the mechanisms of *in vivo* wear.

The Knee Explant Catalogue and the surface topographical analysis results presented within this thesis is the largest study of its kind to have been performed

within the United Kingdom to date. This is the first time that the surface roughness analysis of retrieved UKR prostheses has been presented. The analysis of the explanted knee prostheses with OxZr femoral components adds to the limited body of knowledge within this area and the results are published in Kennard et al [14] (Appendix G).

Three questions were posed in Chapter 1 Introduction and the research work presented in this thesis has provided the following answers:

**Q1** - *Do the quantified in vivo surface topographical changes correlate with patient and implant variables?*

No correlations between the surface topographical changes observed and measured on retrieved knee replacement prostheses and the patient and implant factors of age, BMI, gender or length of time *in vivo* were determined even once the influences of the differences within the cohorts studied had been considered.

**Q2** - *Are there any correlations between the femoral component in vivo topographical changes and the PE articular surface in vivo topographical changes?* There was no reliable determination of any correlation between the femoral component *in vivo* topographical changes and the PE articular surface *in vivo* topographical changes.

**Q3** - *Are there any correlations between the PE backside surface in vivo topographical changes and the tibial tray in vivo topographical changes?* There was no correlation between the PE backside surface and the tibial tray *in vivo* surface roughness measurements recorded on the retrieved prostheses. There was a positive correlation seen between the PE backside damage score on the retrieved PE component and the tibial tray surface roughness measurements. Polished tibial trays were seen to result in less damaged PE component backside surfaces.

Six specific objectives were set in Chapter 1 and these have been realised in the following outcomes (OC):

**OC1:** A protocol for the collection, cataloguing and analysis of retrieved explanted knee replacement prostheses was developed and is presented in Appendix A.

**OC2:** A physical collection of retrieved explanted knee replacement prostheses was established and is available at Newcastle University for future research work. A knee prosthesis explant catalogue including patient and implant data where available, was developed and is presented in Appendix B.

**OC3:** Surface topographical measurement techniques were utilised to investigate *in vivo* surface changes of retrieved knee replacement components and the results are presented in Chapters 4, 5 and 6.

**OC4:** Surface topographical analysis results were correlated with patient and implant variables and the analyses are presented in Chapters 4, 5 and 6.

**OC5:** The limitations and constraints and significance of the results have been discussed in Chapter 7.

**OC6:** Suggestions for future avenues of work are provided below in section 8.2.

The following conclusions are made:

- **C1:** Femoral component surface roughness for TKRs and UKRs with both CoCr and OxZr femoral components increases during time *in vivo* but this increase in surface roughness is not correlated to patient gender, implantation side, patient BMI and time *in vivo*.
- **C2:** Differences in the surface topography of OxZr and CoCr femoral components cannot reliably be determined through the measurement of the surface roughness parameters that were recorded in this thesis. Further analysis of retrieved OxZr knee replacement prostheses is highly recommended for the continued monitoring of knee replacements using OxZr femoral components.

- **C3:** Femoral component roughening can be classified as either third body abrasion resulting in an increased surface roughness or as adhesion and micro-abrasion. Adhesion and micro-abrasion results in an observed macroscopic burnished damaged area but this does not result in an increase in surface roughness.
- **C4:** Femoral component surface roughness is not correlated to the PE component damage score. Neither surface roughness nor damage scoring can provide an approximation of volumetric PE wear.
- **C5:** A polished tibial tray is observed to result in reduced PE bearing backside damage when compared with a non-polished tibial tray and prosthesis designs should consider this result.
- **C6:** The work has identified a definite need for the improved standardisation of the surface roughness measurement of components used for orthopaedic implants. The standards need to include surface roughness parameters for optical areal profilometry and not just contact linear profilometry.
- **C7:** The appropriate selection of measurement and analysis controls (specifically optical zoom and filters) in optical profilometry is essential. The controls detailed in the methodology of this thesis are suggested for future work in this area.
- **C8:** Surface roughness measurements of knee replacement prostheses are highly influenced by sample errors due to the large variations across the surfaces. Any future studies need to consider this limitation.

## 8.2 Future Work

This research has provided a thorough investigation in to the surface topographical of explanted knee replacement prostheses. A physical collection of explants and an associated catalogue of retrieved knee prostheses and patient and implant data have been established and these can be used for future research studies at Newcastle University. The methodology described within this thesis has provided a protocol (including a set of measurement and analysis control parameters) for optical

profilometry to enable the surface roughness measurement of knee replacement prostheses that can be employed in future surface roughness studies.

Despite the valuable contribution that this work has made to further the understanding of the surface topography of retrieved knee prostheses, there is more work that can be done. In the first instance, the measurement of reference UKR prostheses would be desirable to provide a more suitable comparison with the results of the retrieved UKR prostheses. Ideally as-manufactured, unopened boxed Zimmer Biomet® HighFlex Unicondylar, a Zimmer Biomet® Oxford Unicondylar and a Smith & Nephew Journey® OxZr Unicondylar prostheses should be used as reference components. Unfortunately, none of these prostheses were available for use within this project.

Within the design and development of knee replacement prostheses there is a desire for the quantification of wear of the retrieved prosthesis components to enable the performance of the prostheses to be assessed, surface topographical analysis utilising profilometry has not been shown to be able to provide this. Future analysis of retrieved prostheses could benefit from using laser scanning, microCT scanning or methodologies utilising CMMs, to provide a quantitative measure of volumetric *in vivo* PE wear. However, these techniques are not without limitations. They require specialist equipment which can be costly and are time consuming to employ. Furthermore, these techniques still all require the definition of an original reference surface which can prove challenging with knee replacement prostheses. The PE and femoral components of knee replacement prostheses can have complex geometries with multiple radii in both the anterior posterior and medial lateral direction and also multiple centres of rotation. The geometries not only differ within design but also within implant sizes of the same design. The geometric designs and tolerancing of the components are proprietary to the implant manufacturers and therefore not readily available. In addition, there can also be variances in geometry of new unused components of different manufacturing lots. This may be due to the manufacturing tolerance dimensions on the design drawings but could also be due to concessions that can be made within the manufacturing process. All of these issues mean that

establishing reference surfaces for use in the analysis of non-homogeneous groups of retrieved knee prostheses is not easily achieved.

Regardless of the analysis methodology employed to assess the *in vivo* performance of prostheses, studies of retrieved prostheses will always be constrained by the associated limitations as detailed in the discussion in Chapter 7. However, these constraints and limitations should never be allowed to detract from the extremely valuable information that studies of retrieved prostheses can provide. The collection and analysis of retrieved prostheses is a critical success factor within the continued progression of the development of orthopaedic joint replacement. Further retrieval studies can play an important role in determining the safety and efficacy of medical devices. It is only through the on-going analysis of failed components that problems and patterns can be identified and rectified and systems can strive for continuous improvement, to the ultimate benefit to the patient.

The collection and interdisciplinary evaluation of explanted knee replacement prostheses must continue in the future. Special interest must be given to the further analysis of greater numbers of explanted knee replacement prostheses with OxZr femoral components to enable the benefits and limitations of this material to become clearer. Ultimately the aim of the analysis of explanted prostheses is to lead to future improvements in knee replacements and a concomitant reduction of failures.

### **8.3 Contribution to the Literature**

The work done towards realising the aim and objectives of this thesis has resulted in the following publications and podium and poster presentations at conferences. The manuscripts of the publications are included in Appendices F, G and H. As noted in Chapter 1 Introduction, this thesis is submitted in my legal married name Emma Ritchie, however all my authored publications and presentations are in my maiden name Emma Kennard.

***Publications:***

Smith S. L., **Kennard E.** and Joyce T.J. *Shoulder simulator wear test of five contemporary total shoulder prostheses with three axes of rotation and sliding motion* Biotribology, 2018 (13): 36-41 [32] (manuscript included in Appendix F).

**Kennard E.**, Scholes S.C., Sidaginamale, R., Gangadharan, R., Weir, D.J., Holland J., Deehan D. and Joyce T.J. *A comparative surface topographical analysis of explanted Total Knee Replacement prostheses: Oxidised zirconium vs cobalt chromium femoral components* Medical Engineering and Physics, 2017 (50): 59-64 [14] (manuscript included in Appendix G).

Scholes S.C., **Kennard E.**, Gangadharan R., Weir D.J., Holland J., Deehan D and Joyce T.J. *Topographical analysis of the femoral components of ex vivo total knee replacements* Journal of Material Science: Material in Medicine, 2013 (24): 547-554 [15] (manuscript included in Appendix H).

***Podium and poster presentations:***

**Kennard et al** Podium presentation. Institute for Mechanical Engineers “Engineering the Knee” Conference 2018 London, UK. *A Surface Topographical Analysis of Retrieved Knee Replacement Prostheses.*

**Kennard et al** Poster presentation. British Association of Surgery of the Knee (BASK) 2016 Liverpool, UK. *Surface Topographical Analysis of Retrieved Oxidised Zirconium Femoral Components.*

**Kennard et al** Podium presentation. Bath Biomechanics Symposium 2015 Bath, UK. *Oxidised Zirconium – an innovative femoral component material: a case study of a retrieved total knee replacement.*

**Kennard et al** Podium presentation. Newcastle Institute of Ageing Annual Conference 2015 Newcastle, UK. *Ex-Vivo Analysis of Retrieved Total Knee Replacement Prostheses.*

**Kennard et al** Podium presentation. World Tribology Congress 2013 Turin, Italy.  
*Surface wear analysis of the polyethylene component of ex vivo knee prostheses.*

**Kennard et al** Poster presentation. SET for Britain 2013 London, UK. *Surface wear analysis of failed total knee replacements.*

**Kennard et al** Poster presentation. International Society for Technology in Arthroplasty (ISTA) 2011 Belgium. *Analysis of ex vivo knee prostheses.*



## Chapter 9 References

1. National Joint Registry for England, W., Northern Ireland, and the Isle of Man,, *15th Annual Report* 2018.
2. De Steiger, R.N., Muratoglu, O., Lorimer, M., Cuthbert, A.R. and Graves, S.E., *Lower prosthesis-specific 10-year revision rate with crosslinked than with non-crosslinked polyethylene in primary total knee arthroplasty*. *Acta Orthopaedica*, 2015. **86**(6): p. 721-7.
3. Jauregui, J.J., Cherian, J.J., Pierce, T.P., Beaver, W.B., Issa, K. and Mont, M.A., *Long-Term Survivorship and Clinical Outcomes Following Total Knee Arthroplasty*. *Journal of Arthroplasty*, 2015. **30**(12): p. 2164-6.
4. Kim, Y.H., Park, J.W., Kim, J.S., Kulkarni, S.S. and Kim, Y.H., *Long-term clinical outcomes and survivorship of press-fit condylar sigma fixed-bearing and mobile-bearing total knee prostheses in the same patients*. *Journal of Bone & Joint Surgery - American Volume*, 2014. **96**(19): p. e168(1-7).
5. Argenson, J.N., Boisgard, S., Parratte, S., Descamps, S., Bercovy, M., Bonnevalle, P., Briard, J.L., Brilhault, J., Chouteau, J., Nizard, R., Saragaglia, D. and Servien, E., *Survival analysis of total knee arthroplasty at a minimum 10 years' follow-up: a multicenter French nationwide study including 846 cases*. *Orthopaedics & Traumatology Surgery & Research*, 2013. **99**(4): p. 385-90.
6. Bae, D.K., Song, S.J., Park, M.J., Eoh, J.H., Song, J.H. and Park, C.H., *Twenty-year survival analysis in total knee arthroplasty by a single surgeon*. *Journal of Arthroplasty*, 2012. **27**(7): p. 1297-1304.
7. Robertsson, O., Bizjajeva, S., Fenstad, A.M., Furnes, O., Lidgren, L., Mehnert, F., Odgaard, A., Pedersen, A. B. and Havelin, L. I., *Knee arthroplasty in Denmark, Norway and Sweden. A pilot study from the Nordic Arthroplasty Register Association*. *Acta Orthopaedica*, 2010. **81**(1): p. 82-89.
8. Kallala, R.F., Vanhegan, I.S., Ibrahim, M.S., Sarmah, S. and Haddad, F.S., *Financial analysis of revision knee surgery based on NHS tariffs and hospital costs*. *The Bone & Joint Journal* 2015. **97B**: p. 197-201.
9. British Orthopaedic Association, [www.boa.ac.uk](http://www.boa.ac.uk) 2018.
10. McEwen, H.M.J., Fisher, J., Goldsmith, A.A.J., Auger, D.D., Hardaker C and Stone, M.H., *Wear of fixed bearing and rotating platform mobile bearing knees subjected to high levels of internal and external tibial rotation*. *Journal of Materials Science: Materials in Medicine*, 2001. **12**(10-12): p. 1049-1052.

11. Saikko, V., Vuorinen, V. and Revitzer, H., *Effect of CoCr Counterface Roughness on the Wear of UHMWPE in the Noncyclic RandomPOD Simulation*. Journal of Tribology, 2017. **139**: p. 021606/1-6.
12. Saikko, V., Vuorinen, V. and Revitzer, H., *Analysis of UHMWPE wear particles produced in the simulation of hip and knee wear mechanisms with the RandomPOD system*. Biotribology, 2015. **1-2**: p. 30-34.
13. Teeter, M.G., Parikh, A., Taylor, M., Sprague, J. and Naudie, D.D., *Wear and creep behavior of total knee implants undergoing wear testing*. Journal of Arthroplasty, 2015. **30**(1): p. 130-4.
14. Kennard, E., Scholes, S.C., Sidaginamale, R., Gangadharan, R., Weir, D., Holland, J., Deehan, D. and Joyce, T.J., *A comparative surface topographical analysis of explanted Total Knee Replacement prostheses: Oxidised Zirconium vs Cobalt Chromium femoral components*. Medical Engineering & Physics, 2017. **50**: p. 59-64.
15. Scholes, S.C., Kennard, E., Gangadharan, R., Weir, D., Holland, J., Deehan, D. and Joyce, T.J., *Topographical analysis of the femoral components of ex vivo total knee replacements*. Journal of Materials Science: Materials in Medicine, 2013. **24**(2): p. 547-54.
16. Anderson, F.L., Koch, C.N., Elpers, M.E., Wright, T.M., Haas, S.B. and Heyse, T.J., *Oxidised zirconium versus cobalt alloy bearing surfaces in total knee arthroplasty 3D Laser Scanning of Retrieved PE inserts* The Bone & Joint Journal, 2017. **99B**(6): p. 793-798.
17. Fabry, C., Zietz, C., Baumann, A., Ehall, R. and Bader, R., *High wear resistance of femoral components coated with titanium nitride: a retrieval analysis*. Knee Surgery Sports Traumatology Arthroscopy, 2017. **26**: p. 2630(1-6).
18. Thiele, K., Perka, C., Matziolis, G., Mayr, H. O., Sostheim, M. and Hube, R., *Current failure mechanisms after knee arthroplasty have changed: polyethylene wear is less common in revision surgery*. Journal of Bone and Joint Surgery - American Volume, 2015. **97**: p. 715-20.
19. Lombardi, A.V., Berend, K.R. and Adams, J.B., *The Revision Knee Arthroplasty: Why knee replacements fail in 2013 Patient, Surgeon or Implant?* The Bone & Joint Journal, 2014. **96-B**(11SA): p. 101-4.
20. Dalury, D.F., Pomeroy, D.L., Gorab, R.S. and Adams, M.J., *Why are total knee arthroplasties being revised?* Journal of Arthroplasty, 2013. **28**(8S): p. 120-1.
21. Schroer, W.C., Berend, K.R., Lombardi, A.V., Barnes, C.L., Bolognesi, M.P., Berend, M.E., Ritter, M.A. and Nunley, R.M., *Why are total knees failing*

- today? *Etiology of total knee revision in 2010 and 2011*. Journal of Arthroplasty, 2013. **28**(8S): p. 116-9.
22. Arsoy, D., Pagnano, M.W., Lewallen, D.G., Hanssen, A.D. and Sierra, R.J., *Aseptic tibial debonding as a cause of early failure in a modern total knee arthroplasty design*. Clinical Orthopaedics & Related Research, 2013. **471**(1): p. 94-101.
  23. Hazelwood, K.J., O'Rourke, M., Stamos, V.P., McMillan, R.D., Beigler, D. and Robb, W.J., *Case series report: Early cement-implant interface fixation failure in total knee replacement*. Knee, 2015. **22**(5): p. 424-8.
  24. Pang, H.N., Razak, B.A., Rahmatullah, H., Jamiecson, P., Teeter, M.G., Naudie, D.D.R. and MacDonald, S.J., *Factors Affecting Wear of Constrained Polyethylene Tibial Inserts in Total Knee Arthroplasty*. Journal of Arthroplasty, 2016. **31**(6): p. 1340-5.
  25. Ngai, V., and Wimmer, M.A., *Variability of TKR knee kinematics and relationship with gait kinetics: implications for total knee wear*. Biomedical Research International, 2015. **2015**: p. 1-6.
  26. Gallo, J., Goodman, S.B., Kontinen, Y.T., Wimmer, M.A. and Holinkag, M., *Osteolysis around total knee arthroplasty: A review of pathogenetic mechanisms*. Acta Biomaterialia, 2013. **9**: p. 8046 - 8058.
  27. Collier, M.B., Engh, C.A., McAuley, J.P. and Engh, G.A., *Factors associated with the loss of thickness of polyethylene tibial bearings after knee arthroplasty*. Journal of Bone & Joint Surgery - American Volume, 2007. **89**(6): p. 1306-14.
  28. Muratoglu, O.K., Burroughs, B.R., Bragdon, C.R., Christensen, S., Lozynsky, A. and Harris, W.H., *Knee simulator wear of polyethylene tibias articulating against explanted rough femoral components*. Clinical Orthopaedics & Related Research, 2004. **428**: p. 108 - 113.
  29. Puloski, S.K., McCalden, R.W., MacDonald, S.J., Bourne, R.B. and Rorabeck, C.H., *Surface analysis of posterior stabilized femoral components used in total knee arthroplasty*. Journal of Arthroplasty, 2003. **18**(7): p. 822-826.
  30. Siddique, M.S., Rao, M.C., Deehan, D.J. and Pinder, I.M., *Role of abrasion of the femoral component in revision knee arthroplasty*. Journal of Bone & Joint Surgery - British Volume, 2003. **85**(3): p. 393-8.
  31. Dowson, D., Taheri, S. and Wallbridge, N.C., *The role of counterface imperfections in the wear of polyethylene*. Wear, 1987. **119**(3): p. 277-93.
  32. Smith, S.L., Kennard, E. and Joyce, T.J., *Shoulder Simulator Wear Test of Five Contemporary Total Shoulder Prostheses With Three Axes of Rotation and Sliding Motion*. Biotribology, 2018. **13**: p. 36-41.

33. Palastanga, N., and Soames, R., *Anatomy and Human Movement Structure and Function* 6th ed. 2011, Edinburgh Churchill Livingstone.
34. Drake, R., Vogl, A.W. and Mitchell, A.W.M., *Gray's Anatomy for Students*. 3rd ed. 2014: Churchill Livingstone.
35. Levangie, P.K., and Norkin, C.C., *Joint Structure and Function: A Comprehensive Analysis* Fifth ed. 2011: Davies
36. Lee, D.C., and Byun, S.J., *High tibial osteotomy*. Knee Surgery and Related Research, 2012. **24**(2): p. 61-9.
37. Iyer, K.M., *The Knee Joint*, in *Orthopedics of the Upper and Lower Limb*, K.M. Iyer, Editor. 2013, Springer. p. 85-119.
38. Fox, A.J.S., Bedi, A. and Rodeo, S.A., *The basic science of articular cartilage: structure, composition, and function*. Sports Health, 2009. **1**(6): p. 461-8.
39. Makris, E.A., Hadidi, P. and Athanasiou, K.A., *The knee meniscus: structure-function, pathophysiology, current repair techniques, and prospects for regeneration*. Biomaterials, 2011. **32**(30): p. 7411-31.
40. Fox, A.J., Wanivenhaus, F., Burge, A.J., Warren, R.F. and Rodeo, S.A., *The human meniscus: a review of anatomy, function, injury, and advances in treatment*. Clinical Anatomy, 2015. **28**(2): p. 269-87.
41. Dhaher, Y.Y., and Francis, M.J., *Determination of the abduction-adduction axis of rotation at the human knee: Helical axis representation*. Journal of Orthopaedic Surgical Research, 2006. **24**: p. 2187.
42. Iwaki, H., Pinskerova, V. and Freeman, M.A., *Tibifemoral movement 1: The shapes and relative movements of the femur and tibia in the unloaded cadaver knee*. Journal of Bone & Joint Surgery - British Volume, 2000. **82**: p. 1189.
43. Churchill, D.L., Incavo, S.J. and Johnson C.C., *The transepicondylar axis approximates that optimal flexion axis of the knee*. Clinical Orthopaedics & Related Research, 1998. **111**.
44. Dutton, M., *Dutton's Orthopaedic Examination, Evaluation, and Intervention*. 2016.
45. Kurtz, S., *09 The Clinical Performance of UHMWPE in Knee Replacements*, in *UHMWPE Biomaterials Handbook: Ultra high molecular weight polyethylene in total joint replacement and medical devices*. 2016, William Andrew Elsevier.
46. Kutzner, I., Heinlein, B., Graichen, F., Bender, A., Rohlmann, A., Halder, A., Beier, A. and Bergmann, G., *Loading of the knee joint during activities of daily living measured in vivo in five subjects*. Journal of Biomechanics 2010. **43**(11): p. 2164-73.

47. Morrison, J.B., *The mechanics of the knee joint in relation to normal walking*. Journal of Biomechanics, 1970. **3**(1): p. 51-61.
48. Harrington, I.J., *A bioengineering analysis of force actions at the knee in normal and pathological gait*. Journal of Biomedical Engineering, 1976. **11**(5): p. 167-72.
49. Reilly, D.T., and Martens, M., *Experimental Analysis of the Quadriceps Muscle Force and Patello-Femoral Joint Reaction Force for Various Activities*. Acta Orthopaedica, 1972. **43**(2): p. 126-137.
50. Dahlkvist, N.J., Mayo, P. and Seedhom, B.B., *Forces during squatting and rising from a deep squat*. Engineering in Medicine, 1982. **11**(2): p. 69-76.
51. Ellis, M.I., Seedhom, B.B and Wright, V., *Forces in the knee joint whilst rising from a seated position*. Journal of Biomedical Engineering, 1981. **14**(8 ): p. 513-25.
52. Kettlekamp, D.B., and Jacobs A.W., *Tibiofemoral contact area determination and implications* Journal of Bone & Joint Surgery - American Volume, 1972. **54A**
53. Masouros, S.D., A.M.J. Bull, and A.A. Amis, *(i) Biomechanics of the knee joint*. Orthopaedics and Trauma, 2010. **24**(2): p. 84-91.
54. *BS ISO 14243-3:2014 Implants for surgery — Wear of total knee-joint prostheses — Part 3: Loading and displacement parameters for wear-testing machines with displacement control and corresponding environmental conditions for test*. 2014.
55. Arthritis Research UK, <http://www.arthritisresearchuk.org>. 2018.
56. Cooper, C., and Arden, N.K., *Excess mortality in osteoarthritis*. British Medical Journal, 2011. **342**: p. d1407.
57. NICE Clinical Guideline, *Osteoarthritis Care and Management CG177*. 2017.
58. Australian Orthopaedic Association, *Joint Registry Report*. 2018.
59. British Orthopaedic Association, *Commisioning Guide: Painful Osteoarthritis of the knee*. 2017.
60. Collins, N.J., Misra, D., Felson, D.T., Crossley, K.M. and Roos, E.M., *Measures of knee function*. Arthritis Care Research 2011. **63**(11S): p. S208-28.
61. Berenbaum, F., *Osteoarthritis as an inflammatory disease (osteoarthritis is not osteoarthrosis!)*. Osteoarthritis Cartilage, 2013. **21**(1): p. 16-21.

- 
62. Arthritis Research UK, *Topical Review Osteoarthritis: pathogenesis and prospects for treatment*. 2011.
  63. Lespasio, M.J., Piuizzi, N.S., Husni, M.E., Muschler, G.F., Guarino, A.J. and Mont, M.A., *Knee Osteoarthritis: A Primer*. The Permanente Journal, 2017. **21**: p. 16-183.
  64. Wright, R.W., and the Mars Group,, *Osteoarthritis Classification Scales: Interobserver Reliability and Arthroscopic Correlation*. Journal of Bone & Joint Surgery - American Volume, 2014. **96**(14): p. 1145-1151.
  65. O'Connor, M.I., *Osteoarthritis of the hip and knee: sex and gender differences*. Orthopaedic Clinics of North America 2006. **37**(4): p. 559-68.
  66. Blagojevic, M., Jinks, C., Jeffery, A. and Jordan, K.P., *Risk factors for onset of osteoarthritis of the knee in older adults: a systematic review and meta-analysis*. Osteoarthritis Cartilage, 2010. **18**(1): p. 24-33.
  67. Hame, S.L., and Alexander, R.A., *Knee osteoarthritis in women*. Current Reviews in Musculoskeletal Medicine, 2013. **6**(2): p. 182-7.
  68. Kulkarni, K., Karssiens, T., Kumar, V. and Pandit, H., *Obesity and osteoarthritis*. Maturitas, 2016. **89**: p. 22–8
  69. *Oxford English Dictionary* 1989, Oxford Univerisity Press
  70. Hutchings, I.M., and Shipway, P., *Tribology: Friction and Wear of Engineering Materials* 2nd ed. 2017 Elsevier
  71. Dowson, D., *History of Tribology*. 2nd ed. 1998: Wiley.
  72. *BS ISO 14243-2: 2009 Implants for surgery — Wear of total knee-joint prostheses Part 2: Methods of measurement*. 2009.
  73. Le Goïc, G., Bigerelle, M., Samper, S., Favrelière, H. and Pillet, M., *Multiscale roughness analysis of engineering surfaces: A comparison of methods for the investigation of functional correlations*. Mechanical Systems and Signal Processing, 2016. **66-67**: p. 437-457.
  74. Leach, R., *Characterisation of areal surface texture*. 2013: Springer.
  75. *BS ISO 25178-2: 2012 Geometrical product specifications (GPS) - Surface texture: Areal Part 2: Terms, definitions and surface texture parameters*. 2012.
  76. ISO, B., *ISO 25178-3: 2012 Geometrical product specifications (GPS) — Surface texture: Areal Part 3: Specification operators*. 2017
  77. *BS ISO 25178-6: 2010 Geometrical product specifications (GPS) - Surface texture: Areal Part 6: Classification of methods for measuring surface texture* 2010.
-

- 
78. Leach, R., *National Physics Laboratory Good Practice Guide 37: The Measurement of Surface Texture Using Stylus Instruments*. 2001.
  79. De Groot, P., *31 Interference Microscopy for Surface Structure Analysis*, in *Handbook of Optical Metrology: Principles and Applications*, T. Yoshizawa, Editor. 2017, CRC Press Taylor & Francis Group.
  80. Lee, D.H., and Cho, N.G. , *Assessment of surface profile data acquired by a stylus profilometer*. *Measurement Science and Technology*, 2012. **23**(10): p. 105601(1-12).
  81. *BS ISO 25178-604: 2013 Geometrical product specifications (GPS) — Surface texture: Areal Part 604: Nominal characteristics of noncontact (coherence scanning interferometry) instruments*. 2013.
  82. Zygo, *SOP\_ZygoNewView600*. 2018.
  83. Leach, R., *Optical Measurement of Surface Topography*. 2011.
  84. Gao, F., Leach, R.K., Petzing, J. and Coupland, J.M., *Surface measurement errors using commercial scanning white light interferometers*. *Measurement Science and Technology*, 2008. **19**(1).
  85. Su, R., Wang, Y., Coupland, J. and Leach, R., *On tilt and curvature dependent errors and the calibration of coherence scanning interferometry*. *Optics Express*, 2017. **25**(4): p. 3297-3310.
  86. Do Vale, J.L., de Cerjat Beltrão, V., da Silva, C.H. and Pintaúde, G., *Evaluation of the error of the light beam incidence on concave surfaces in 3D roughness parameters using optical interferometry*. *Measurement*, 2018. **120**: p. 182-192.
  87. MetroPro, *MetroPro Reference Guide 0347\_M*. 2018.
  88. *BS ISO 16610-61: 2015 Geometrical product specification (GPS) — Filtration Part 61: Linear areal filters — Gaussian filters*. 2015.
  89. Marshall, J.A. *Measuring copper surface roughness for high speed applications*. IPC proceedings 2015; 1-6]. Available from: <https://pdfs.semanticscholar.org/0fcc/a30af0ca1e32f26d212e338d391c20beb5bc.pdf>.
  90. Bhushan, B., *Introduction to Tribology*. 2nd ed. 2013: Wiley.
  91. Jin, Z. and J. Fisher, *Chapter 2 Tribology in Joint Replacement in Joint Replacement Technology* P.A. Revell, Editor. 2014
  92. Dowson, D., *Biotribology*. *Faraday Discussions*, 2012. **156**: p. 9-30.
-

- 
93. Kurtz, S., *08 The origins and adaptations of UHMWPE for Knee Replacements*, in *UHMWPE Biomaterials Handbook: Ultra high molecular weight polyethylene in total joint replacement and medical devices*, S. Kurtz, Editor. 2016 William Andrews Elsevier.
  94. *BS ISO 7207-1: 2007 Implants for surgery — Components for partial and total knee joint prostheses Part 1: Classification, definitions and designation of dimensions*. 2007.
  95. American Academy of Orthopedic Surgeons. <https://orthoinfo.aaos.org> 2018
  96. Scott, C.E.H., Eaton, M.J., Nutton, R.W., Wade, F.A., Pankaj, P. and Evans, S.L., *Proximal tibial strain in medial unicompartmental knee replacements: A biomechanical study of implant design*. Journal of Bone & Joint Surgery - British Volume, 2013. **95-B**.
  97. Machhindra, M.V., Kang, J.Y., Kang, Y.G., Chowdhry, M. and Kim, T.K., *Functional Outcomes of a New Mobile-Bearing Ultra-Congruent TKA System: Comparison With the Posterior Stabilized System*. Journal of Arthroplasty, 2015. **30**(12): p. 2137-42.
  98. Panigrahi, P., Durig, N., Alvarez, E. and Harman, M.K., *Damage from unintentional metal–metal articulation of CoCrMo, TiAlV, and oxidized zirconium knee replacements following polyethylene insert failure*. Wear, 2015. **324-325**: p. 1-9.
  99. Rack, H.J., and Qazi, J.I., *Titanium alloys for biomedical applications*. Materials Science and Engineering: C, 2006. **26**(8): p. 1269-1277.
  100. Eichler, J., Eisele, U. and Rodel, J., *Mechanical Properties of Monoclinic Zirconia*. Journal of the American Ceramic Society, 2004. **87**: p. 1401–14.
  101. DePuy Synthes. *PFC® Sigma Value Brief* 2018; Available from: <https://www.depuysynthes.com/hcp/knee/products/qs/SIGMA-Total-Knee-System#tab2>.
  102. ZimmerBiomet. *NexGen® CR-Flex and LPS-Flex Knees Design Rationale* 2018 Available from: <https://www.zimmerbiomet.com/content/dam/zimmer-biomet/medical-professionals/knee/nexgen-complete-knee-solution-legacy-knee-posterior-stabilized/nexgen-cr-flex-and-lps-flex-knees-design-rationale.pdf>.
  103. Stryker. *Triathlon® Design Rationale*. 2018 Available from: <https://www.strykermeded.com/media/1166/triathlon-design-rationale.pdf>.
  104. ZimmerBiomet. *Vanguard® Complete Knee System Design Rationale*. 2018; Available from: <https://www.zimmerbiomet.com/content/dam/zimmer-biomet/medical-professionals/knee/vanguard-knee-system/vanguard-complete-knee-system-design-rationale.pdf>.
-



- 
105. Smith & Nephew. *Legion® Primary Knee System Design Rationale*. 2018; Available from: [http://www.smith-nephew.com/documents/education%20and%20evidence/literature/2015/03386\\_bonejointscience-legion-primary-knee-system.pdf](http://www.smith-nephew.com/documents/education%20and%20evidence/literature/2015/03386_bonejointscience-legion-primary-knee-system.pdf).
  106. *BS ISO 7207-2: 2011+A1: 2016 Implants for surgery — Components for partial and total knee joint prostheses Part 2: Articulating surfaces made of metal, ceramic and plastics materials*. 2016.
  107. *BS EN ISO 4288: 1998 Geometric Product Specification (GPS) — Surface texture — Profile method: Rules and procedures for the assessment of surface texture*. 1998.
  108. Laskin, R.S., *An oxidized zirconium ceramic surfaced femoral component for total knee arthroplasty*. *Clinical Orthopaedics & Related Research*, 2003. **416**: p. 191-6.
  109. Schuttler, K.F., Efe, T., Heyse, T.J. and Haas, S.B., *Oxidized Zirconium Bearing Surfaces in Total Knee Arthroplasty: Lessons Learned*. *The Journal of Knee Surgery*, 2015. **28**(5): p. 376 - 381.
  110. Wright, T.M., *Polyethylene in knee arthroplasty: what is the future?* *Clinical Orthopaedics & Related Research*, 2005. **440**: p. 141-8.
  111. *BS ISO 5834-1: 2005 Implants for surgery- Ultra-highmolecular-weight-polyethylene —Part 1: Powder form*. 2005.
  112. Kurtz, S., *02 From Ethylene Gas to UHMWPE*, in *UHMWPE Biomaterials Handbook: Ultra high molecular weight polyethylene in total joint replacement and medical devices*, S. Kurtz, Editor. 2016, William Andrew Elsevier.
  113. Kurtz, S., *03 Packaging and Sterilization of UHMWPE*, in *UHMWPE Biomaterials Handbook: Ultra high molecular weight polyethylene in total joint replacement and medical devices*, S. Kurtz, Editor. 2016, William Andrew Elsevier.
  114. Costa, L., Bracco, P., Brach del Prever, E.M., Kurtz, S.M., and Gallinaro, P., *Oxidation and oxidation potential in contemporary packaging for polyethylene total joint replacement components*. *Journal of Biomedical Materials Research Part B: Applied Biomaterials*, 2006. **78**(1): p. 20-6.
  115. Kurtz, S.M., Hozack, W.J., Purtill, J.J., Marcolongo, M., Kraay, M.J., Goldberg, V.M., Sharkey, P.F., Parvizi, J., Rimnac, C.M. and Edidin, A.A., *2006 Otto Aufranc Award Paper: significance of in vivo degradation for polyethylene in total hip arthroplasty*. *Clinical Orthopaedics & Related Research*, 2006. **453**: p. 47-57.
  116. Kurtz, S., *10 Contemporary Total Knee Arthroplasty- Alternative Bearings*, in *UHMWPE Biomaterials Handbook: Ultra high molecular weight polyethylene in*
-

- total joint replacement and medical devices*, S. Kurtz, Editor. 2016, William Andrew Elsevier.
117. Brockett, C.L., Jennings, L.M., Hardaker, C. and Fisher, J., *Wear of moderately cross-linked polyethylene in fixed-bearing total knee replacements*. Proceedings of the Institution of Mechanical Engineers, Part H: Journal of Engineering in Medicine 2012. **226**(7): p. 529-35.
118. Stoller, A.P., Johnson, T.S., Popoola, O.O., Humphrey, S.M. and Blanchard, C.R., *Highly crosslinked polyethylene in posterior-stabilized total knee arthroplasty: in vitro performance evaluation of wear, delamination, and tibial post durability*. Journal of Arthroplasty, 2011. **26**(3): p. 483-91.
119. Utzschneider, S., Harrasser, N., Schroeder, C., Mazoochian, F. and Jansson, V., *Wear of contemporary total knee replacements--a knee simulator study of six current designs*. Clinical Biomechanics 2009. **24**(7): p. 583-8.
120. Lachiewicz, P.F.a.S., E.S., *Is There a Benefit to Highly Crosslinked Polyethylene in Posterior-stabilized Total Knee Arthroplasty? A Randomized Trial*. Clinical Orthopaedics & Related Research, 2016. **474**(1): p. 88-95.
121. Atwood, S.A., Van Citters, D.W., Patten, E.W., Furmanski, J., Ries, M.D. and Pruitt, L.A., *Tradeoffs amongst fatigue, wear, and oxidation resistance of cross-linked ultra-high molecular weight polyethylene*. Journal of Mechanical Behavior of Biomedical Materials, 2011. **4**(7): p. 1033-45.
122. Pruitt, L.A., Ansari, F., Kury, M., Mehdizah, A., Patten, E.W., Huddlestein, J., Mickelson, D., Chang, J., Hubert, K. and Ries, M.D., *Clinical trade-offs in cross-linked ultrahigh-molecular-weight polyethylene used in total joint arthroplasty*. Journal of Biomedical Materials Research Part B: Applied Biomaterials 2013. **101**(3): p. 476-84.
123. Dyrhovden, G.S., Lygre, S.H.L., Badawy, M., Gothesen, O. and Furnes, O., *Have the Causes of Revision for Total and Unicompartmental Knee Arthroplasties Changed During the Past Two Decades?* Clinical Orthopaedics & Related Research, 2017. **475**(7): p. 1874-1886.
124. Inacio, M.C.S., Paxton, E.W., Graves, S.E., Namba, R.S. and Nemes, S., *Projected increase in total knee arthroplasty in the United States - an alternative projection model*. Osteoarthritis Cartilage, 2017. **25**(11): p. 1797-1803.
125. Inacio, M.C.S., Graves, S.E., Pratt, N.L., Roughead, E.E. and Nemes, S., *Increase in Total Joint Arthroplasty Projected from 2014 to 2046 in Australia: A Conservative Local Model With International Implications*. Clinical Orthopaedics & Related Research, 2017. **475**(8): p. 2130-2137.

- 
126. Nemes, S., Rolfson, O.W., Dahl A., Garellick, G., Sundberg, M., Karrholm, J. and Robertsson, O., *Historical view and future demand for knee arthroplasty in Sweden*. Acta Orthopaedica, 2015. **86**(4): p. 426-31.
  127. Kurtz, S.M., Ong, K.L., Lau, E. and Bozic, K.J., *Impact of the economic downturn on total joint replacement demand in the United States: updated projections to 2021*. Journal of Bone & Joint Surgery - American Volume 2014. **96**(8): p. 624-30.
  128. Culliford, D., Maskell, J., Judge, A., Cooper, C., Prieto-Alhambra, D. and Arden, N.K., *Future projections of total hip and knee arthroplasty in the UK: results from the UK Clinical Practice Research Datalink*. Osteoarthritis Cartilage, 2015. **23**(4): p. 594-600.
  129. Patel, A.M., Pavlou, G., Mújica-Mota, R.E. and Toms, A.D., *The epidemiology of revision total knee and hip arthroplasty in England and Wales. A comparative analysis with projections for the united states. A study using the National Joint Registry Dataset*. Journal of Bone & Joint Surgery - British Volume, 2015. **97-B**: p. 1076–1081.
  130. Losina, E., Thornhill, T.S., Rome, B.N., Wright, J. and Katz, J.N., *The Dramatic Increase in Total Knee Replacement Utilization Rates in the United States Cannot Be Fully Explained by Growth in Population Size and the Obesity Epidemic*. Journal of Bone & Joint Surgery - American Volume, 2012. **94**: p. 201-7.
  131. Losina, E., and Katz, J.N., *Total knee arthroplasty on the rise in younger patients: Are we sure that past performance will guarantee future success?* Arthritis & Rheumatism, 2012. **64**(2): p. 339-341.
  132. *Swedish Registry Report*. 2017.
  133. McCalden, R.W., Hart, G.P., MacDonald, S.J., Naudie, D.D., Howard, J.H. and Bourne, R.B., *Clinical Results and Survivorship of the GENESIS II Total Knee Arthroplasty at a Minimum of 15 Years*. Journal of Arthroplasty, 2017. **32**(7): p. 2161-2166.
  134. New Zealand Orthopaedic Association, *18th Joint Registry Report*. 2017.
  135. Greidanus, N.V., Peterson, R.C., Masri, B.A. and Garbuz, D.S., *Quality of life outcomes in revision versus primary total knee arthroplasty*. Journal of Arthroplasty, 2011. **26**(4): p. 615-20.
  136. Kurtz, S.M., Ong, K.L., Schmier, J., Mowat, F., Saleh, K., Dybvik, E., Karrholm, J., Garellick, G., Havelin, L.I., Furnes, O., Malchau, H. and Lau, E., *Future clinical and economic impact of revision total hip and knee arthroplasty*. Journal of Bone & Joint Surgery - American Volume, 2007. **89 Suppl 3**: p. 144-51.

- 
137. Gibon, E., Cordova, L.A., Lu, L., Lin, T.H., Yao, Z., Hamadouche, M. and Goodman, S.B., *The biological response to orthopaedic implants for joint replacement: Part II: Polyethylene, ceramics, PMMA, and the foreign body reaction*. Journal of Biomedical Materials Research Part B: Applied Biomaterials, 2017.
138. Goldvasser, D., Marchie, A., Bragdon, L.K., Bragdon, C.R., Weidenhielm, L. and Malchau, H., *Incidence of osteolysis in total knee arthroplasty: comparison between radiographic and retrieval analysis*. Journal of Arthroplasty, 2013. **28**(2): p. 201-6.
139. Ollivere, B., Wimbhurst, J.A., Clarke, I.M. and Donell, S.T., *Current concepts in osteolysis*. Journal of Bone & Joint Surgery - British Volume, 2012. **94B**(1): p. 10-15.
140. Jacobs, J.J., Roebuck, K.A., Archibeck, M., Hallab, N.J. and Glant, T.T., *Osteolysis: basic science*. Clinical Orthopaedics & Related Research, 2001. **393**: p. 71-77.
141. Schmalzried, T.P., Jasty, M. and Harris, W.H., *Periprosthetic bone loss in total hip arthroplasty. Polyethylene wear debris and the concept of the effective joint space*. Journal of Bone & Joint Surgery - American Volume, 1992. **74**(6).
142. Hall, R.M., Siney, P., Unsworth, A. and Wroblewski B.M., *The effect of surface topography of retrieved femoral heads on the wear of UHMWPE sockets*. Medical Engineering & Physics, 1997. **19**(8): p. 711-719.
143. Kobayashi, A., Bonfield, W., Kadoya, Y., Yamac, T., Freeman, M.A., Scott, G. and Revell, P. A., *The size and shape of particulate polyethylene wear debris in total joint replacements*. Proceedings of the Institution of Mechanical Engineers, Part H: Journal of Engineering in Medicine 1997. **211**(1): p. 11-5.
144. Collier, M.B., Engh, C.A. and Engh, G.A., *Shelf age of the polyethylene tibial component and outcome of unicondylar knee arthroplasty*. Journal of Bone & Joint Surgery - American Volume, 2004. **86-A**(4): p. 763-9.
145. Schmalzried, T.P., and Callaghan, J.J., *Wear in total hip and knee replacements*. Journal of Bone & Joint Surgery - American Volume, 1999. **81A**(1): p. 115-36.
146. Paxton, E.W., Inacio, M.C., Kurtz, S., Love, R., Cafri, G. and Namba, R.S., *Is there a difference in total knee arthroplasty risk of revision in highly crosslinked versus conventional polyethylene?* Clinical Orthopaedics & Related Research, 2015. **473**: p. 999–1008.
147. Sharkey, P.F., Lichstein, P.M., Shen, C., Tokarski, A.T. and Parvizi, J., *Why are total knee arthroplasties failing today--has anything changed after 10 years?* Journal of Arthroplasty, 2014. **29**(9): p. 1774-8.
-

- 
148. Calliess, T., Ettinger, M., Hulsmann, N., Ostermeier, S. and Windhagen, H., *Update on the etiology of revision TKA - Evident trends in a retrospective survey of 1449 cases*. Knee, 2015. **22**: p. 174 - 179.
149. Khan, M., Osman, K., Green, G. and Haddad, F.S., *The epidemiology of failure in total knee arthroplasty: Avoiding your next revision*. . Journal of Bone & Joint Surgery - British Volume, 2016. **98-B**(1 Suppl A): p. 105–12.
150. Sava, M.M., Munteanu, B., Renault, E., Berthier, Y. and Trunfio-Sfarghiu, A.M., *Tribological Analysis of UHMWPE Tibial Implants in Unicompartmental Knee Replacements: From Retrieved to In Vitro Studies*. Biotribology, 2018. **13**: p. 1-15.
151. Rand, J.A., Trousdale, R.T., Ilstrup, D.M. and Harmsen, W.S., *Factors affecting the durability of primary Total Knee Prostheses*. Journal of Bone & Joint Surgery - American Volume, 2003. **85**(2): p. 259–265.
152. Affatato, S., Grillini, L., Battaglia, S., Taddei, P., Modena, E. and Sudanese, A., *Does knee implant size affect wear variability?* Tribology International, 2013. **66**: p. 174-181.
153. Battaglia, S., Taddei, P., Tozzi, S., Sudanese, A. and Affatato, S., *Toward the interpretation of the combined effect of size and body weight on the tribological performance of total knee prostheses*. International Orthopaedica 2014. **38**(6): p. 1183-90.
154. Battaglia, S., Taddei, P., Castiello, E., Tozzi, S., Sudanese, A. and Affatato, S., *Combined effect of the body mass index and implant size on the wear of retrieved total knee prostheses*. Journal of Mechanical Behavior of Biomedical Materials 2014. **38**: p. 69-77.
155. Vandekerckhove, P.T.K., Teeter, M.G., Naudie, D.D.R., Howard, J.L., MacDonald, S.J. and Lanting, B.A., *The Impact of Coronal Plane Alignment on Polyethylene Wear and Damage in Total Knee Arthroplasty: A Retrieval Study*. Journal of Arthroplasty, 2017. **32**(6): p. 2012-2016.
156. Pang, H.N., Jamieson, P., Teeter, M.G., McCalden, R.W., Naudie, D.D.R. and MacDonald, S.J., *Retrieval analysis of posterior stabilized polyethylene tibial inserts and its clinical relevance*. Journal of Arthroplasty, 2014. **29**(2): p. 365-8.
157. Srivastava, A., Lee, G.Y., Steklov, N., Colwell, C.W., Ezzet, K.A. and D'Lima, D.D., *Effect of tibial component varus on wear in total knee arthroplasty*. Knee, 2012. **19**(5): p. 560-3.
158. Tsao, A., Mintz, L., McRae, C.R., Stulberg, S.D. and Wright, T., *Failure of the porous-coated anatomic prosthesis in total knee arthroplasty due to severe polyethylene wear*. Journal of Bone & Joint Surgery - American Volume, 1993. **75**(1): p. 19-26.
-

- 
159. Wasielewski, R.C., Galante, J.O., Leighty, R.M., Natarajan, R.N. and Rosenberg, A.G., *Wear patterns on retrieved polyethylene tibial inserts and their relationship to technical considerations during total knee arthroplasty*. Clinical Orthopaedics & Related Research, 1994(299): p. 31-43.
160. Wright, T.M., Rimnac, C.M., Stulberg, S.D., Mintz, L., Tsao, A.K., Klein, R.W. and McCrae, C., *Wear of polyethylene in total joint replacements. Observations from retrieved PCA knee implants*. Clinical Orthopaedics & Related Research, 1992(276): p. 126-34.
161. Ashraf, T., Newman, J.H., Desai, V.V., Beard, D. and Nevelos, J.E., *Polyethylene wear in a non-congruous unicompartmental knee replacement: a retrieval analysis*. Knee, 2004. **11**(3): p. 177-81.
162. Wimmer, M.A., Laurent, M.P., Haman, J.D., Jacobs, J.J. and Galante, J.O., *Surface damage versus tibial polyethylene insert conformity: a retrieval study*. Clinical Orthopaedics & Related Research, 2012. **470**(7): p. 1814-25.
163. Sisko, Z.W., Teeter, M.G., Lanting, B.A., Howard, J.L., McCalden, R.W., Naudie, D.D., MacDonald, S.J. and Vasarhelyi, E.M., *Current Total Knee Designs: Does Baseplate Roughness or Locking Mechanism Design Affect Polyethylene Backside Wear?* Clinical Orthopaedics and Related Research, 2017. **475**(12): p. 2970-2980.
164. Teeter, M.G., Howard, J.L., McCalden, R.W., and Naudie, D.D., *Comparison of articular and backside polyethylene wear in mobile bearing unicompartmental knee replacement*. Knee, 2017. **24**(2): p. 429-433.
165. Schwarzkopf, R., Scott, R.D., Carlson, E.M. and Currier, J.H., *Does increased topside conformity in modular total knee arthroplasty lead to increased backside wear?* Clinical Orthopaedics & Related Research, 2015. **473**(1): p. 220-5.
166. Stoner, K., Jerabek, S.A., Tow, S., Wright, T. M. and Padgett, D.E., *Rotating-platform has no surface damage advantage over fixed-bearing TKA*. Clinical Orthopaedics & Related Research, 2013. **471**(1): p. 76-85.
167. Neufeld, M.E., Albers, A., Greidanus, N.V., Garbuz, D.S. and Masri, B.A., *A Comparison of Mobile and Fixed-Bearing Unicompartmental Knee Arthroplasty at a Minimum 10-Year Follow-up*. Journal of Arthroplasty, 2018. **33**: p. 1713-1718.
168. Brockett, C.L., Carbone, S., Fisher, J. and Jennings, L.M., *Influence of conformity on the wear of total knee replacement: An experimental study*. Proceedings of the Institution of Mechanical Engineers, Part H: Journal of Engineering in Medicine, 2018. **232**(2): p. 127-134.
-

- 
169. Roy, M.E., Whiteside, L.A., Tilden, D.S. and Noel, O.F., *Reduced UHMWPE wear using magnesia-stabilized zirconia instead of CoCr femoral components in a knee simulator*. Journal of Arthroplasty, 2015. **30**: p. 468-474.
170. Saikko, V., Calonijs, O. and Keranen, J., *Effect of counterface roughness on the wear of conventional and crosslinked ultrahigh molecular weight polyethylene studied with a multi-directional motion pin-on-disk device*. Journal of Biomedical Materials Research Part B: Applied Biomaterials, 2001. **57**: p. 506-512.
171. DesJardins, J., Burnikel, B. and LaBerge, M., *UHMWPE wear against roughened oxidized zirconium and CoCr femoral knee components during force-controlled simulation*. Wear, 2008. **264**: p. 245–256.
172. Spector, B.M., Ries, M.D., Bourne, R.B., Sauer, W.S., Long, M. and Hunter, G., *Wear performance of ultra-high molecular weight polyethylene on oxidized zirconium total knee femoral components*. Journal of Bone & Joint Surgery - American Volume, 2001. **83A**(S2): p. 80–86.
173. Bowsher, J.G., and Shelton, J.C., *Hip simulator study of the influence of patient activity level on the wear of crosslinked polyethylene under smooth and roughened femoral conditions*. Wear, 2001. **250**: p. 167-79.
174. White, S.E., Whiteside, L.A., McCarthy, D.S., Anthony, M. and Poggie, R.A., *Simulated knee wear with cobalt chromium and oxidized zirconium knee femoral components*. Clinical Orthopaedics & Related Research, 1994. **309**: p. 176-84.
175. Fisher, J., Firkins, P., Reeves, E.A., Hailey, J.L. and Isaac, G.H., *The influence of scratches to metallic counterfaces on the wear of ultra-high molecular weight polyethylene*. Proceedings of the Institution of Mechanical Engineers, Part H: Journal of Engineering in Medicine 1995. **209**(4): p. 263-4.
176. Ito, H., Maloney, C.M., Crowninshield, R.D., Clohisy, J.C., McDonald, D.J. and Maloney, W.J., *In vivo femoral head damage and its effect on polyethylene wear*. Journal of Arthroplasty, 2010. **25**(2): p. 302-8.
177. Cooper, J.R., Dowson, D. and Fisher, J., *Macroscopic and microscopic wear mechanisms in ultra-high molecular weight polyethylene*. Wear, 1993. **162–164**: p. 378-384.
178. Fisher, J., *Surface damage to femoral head prostheses*. Journal of Bone & Joint Surgery - British Volume, 1994. **76-B**: p. 852-858.
179. Heyse, T.J., Chen, D.X., Kelly, N., Boettner, F., Wright, T.M. and Haas, S.B., *Matched-pair total knee arthroplasty retrieval analysis: oxidized zirconium vs. CoCrMo*. Knee, 2011. **18**(6): p. 448-52.
-

- 
180. Brandt, J.M., Guenther, L., O'Brien, S., Vecherya, A., Turgeon, T.R. and Bohm, E.R., *Performance assessment of femoral knee components made from cobalt-chromium alloy and oxidized zirconium*. Knee, 2013. **20**(6): p. 388-96.
181. Taddei, P., Tozzi, S., Carmignato, S. and Affatato, S., *May the surface roughness of the retrieved femoral head influence the wear behavior of the polyethylene liner?* Journal of Biomedical Materials Research Part B: Applied Biomaterials 2016. **104**(7): p. 1374-85.
182. Elfick, A., Hall, R.M., Pinder, I.M. and Unsworth, A., *The influence of femoral head surface roughness on the wear of ultrahigh molecular weight polyethylene sockets in cementless total hip replacement*. Journal of Biomedical Materials Research Part B: Applied Biomaterials 1999. **48**: p. 712–718.
183. Teeter, M.G., Lanting, B.A., Shrestha, K.R., Howard, J.L. and Vasarhelyi, E.M., *Contribution of Surface Polishing and Sterilization Method to Backside Wear in Total Knee Arthroplasty*. Journal of Arthroplasty, 2015. **30**(12): p. 2320-2.
184. Abdel, M.P., Gesell, M.W., Hoedt, C.W., Meyers, K.N., Wright, T.M. and S.B. and Haas, *Polished trays reduce backside wear independent of post location in posterior-stabilized TKAs*. Clinical Orthopaedics & Related Research, 2014. **472**(8): p. 2477-82.
185. Currier, B.H., Currier, J.H., Franklin, K.J., Mayor, M.B., Reinitz, S.D. and Van Citters, D.W., *Comparison of Wear and Oxidation in Retrieved Conventional and Highly Cross-Linked UHMWPE Tibial Inserts*. Journal of Arthroplasty, 2015. **30**(12): p. 2349-53.
186. Liu, T., Esposito, C., Elpers, M., Wright, T., *Surface Damage Is Not Reduced With Highly Crosslinked Polyethylene Tibial Inserts at Short-term*. Clinical Orthopaedics & Related Research, 2016. **474**(1): p. 107-16.
187. Ezzet, K.A., Hermida, J.C., Steklov, N. and D.D. and D'Lima, *Wear of polyethylene against oxidized zirconium femoral components effect of aggressive kinematic conditions and malalignment in total knee arthroplasty*. Journal of Arthroplasty, 2012. **27**(1): p. 116-21.
188. Gascoyne, T.C., Teeter, M.G., Guenther, L.E., Burnell, C.D., Bohm, E.R. and Naudie, D.R., *In Vivo Wear Performance of Cobalt-Chromium Versus Oxidized Zirconium Femoral Total Knee Replacements*. Journal of Arthroplasty, 2016. **31**(1): p. 137-41.
189. Hofer, J.K.a.E., K.A., *A minimum 5-year follow-up of an oxidized zirconium femoral prosthesis used for total knee arthroplasty*. Knee, 2014. **21**(1): p. 168-71.
-



- 
190. Innocenti, M., Matassi, F., Carulli, C., Nistri, L. and Civinini, R., *Oxidized zirconium femoral component for TKA: a follow-up note of a previous report at a minimum of 10 years*. Knee, 2014. **21**(4): p. 858-61.
191. Kim, Y.H., Kim, J. S., Huh, W. and Lee, K.H., *Weight of polyethylene wear particles is similar in TKAs with oxidized zirconium and cobalt-chrome prostheses*. Clinical Orthopaedics & Related Research, 2010. **468**(5): p. 1296-304.
192. Vertullo, C.J., Lewis, P.L., Graves, S., Kelly, L., Lorimer, M. and Myers, P., *Twelve-Year Outcomes of an Oxinium Total Knee Replacement Compared with the Same Cobalt-Chromium Design: An Analysis of 17,577 Prostheses from the Australian Orthopaedic Association National Joint Replacement Registry*. Journal of Bone & Joint Surgery - American Volume 2017. **99**(4): p. 275-283.
193. Zietz, C., Reinders, J., Schwiesau, J., Paulus, A., Kretzer, J.P., Grupp, T., Utzschneider, S. and Bader, R., *Experimental testing of total knee replacements with UHMW-PE inserts: impact of severe wear test conditions*. Journal of Materials Science: Materials in Medicine, 2015. **26**(3): p. 1-13.
194. Hood, R.W., Wright, T. and Burstein, A.H., *Retrieval analysis of total knee prostheses: A method and its application to 48 total condylar prostheses*. Journal of Biomedical Materials Research Part B: Applied Biomaterials, 1983. **17**: p. 829 - 842.
195. Daines, S.B., Koch, C.N., Haas, S.B., Westrich, G.H. and Wright, T.M., *Does Achieving High Flexion Increase Polyethylene Damage in Posterior-Stabilized Knees? A Retrieval Study*. Journal of Arthroplasty, 2017. **32**(1): p. 274-279.
196. Schnaser, E.A., Elpers, M.E., Koch, C.N., Haas, S.B., Westrich, G.H. and Wright, T.M., *Posterior Stabilized Polyethylene Inserts in Total Knee Arthroplasty: A Retrieval Study Comparing Conventional to High-Flexion Designs*. Journal of Arthroplasty, 2016. **31**(2): p. 495-500.
197. Bali, K., Naudie, D.D., Howard, J.L., McCalden, R.W., MacDonald, S.J. and Teeter, M.G., *Comparison of Tibial Insert Polyethylene Damage in Rotating Hinge and Highly Constrained Total Knee Arthroplasty: A Retrieval Analysis*. Journal of Arthroplasty, 2016. **31**(1): p. 290-4.
198. Holleyman, R.J., Scholes, S.C., Weir, D., Jameson, S.S., Holland, J., Joyce, T.J. and Deehan, D., *Changes in surface topography at the TKA backside articulation following in vivo service: a retrieval analysis*. Knee Surgery Sports Traumatology Arthroscopy, 2015. **23**: p. 3523-3531.
199. Brandt, J.M., MacDonald, S.J., and R.B.a.M. Bourne, J.B., *Retrieval analysis of modular total knee replacements: factors influencing backside surface damage*. Knee, 2012. **19**(4): p. 306-15.
-

- 
200. Brandt, J.M., Haydon, C.M., Harvey, E P., McCalden, R.W. and Medley, J.B., *Semi-quantitative assessment methods for backside polyethylene damage in modular total knee replacements*. Tribology International, 2012. **49**: p. 96-102.
201. Lu, Y.C., Huang, C.H., Chang, T.K., Ho, F.Y. and Cheng, C.K., *Wear-pattern analysis in retrieved tibial inserts of mobile-bearing and fixed-bearing total knee prostheses*. Journal of Bone & Joint Surgery - British Volume, 2010. **92**(4): p. 500-7.
202. Kendrick, B.J.L., Longino, D., Pandit, H., Svard, U., Gill, H.S., Dodd, C.A.F., Murray, D.W. and Price, A.J., *Polyethylene wear in Oxford unicompartmental knee replacement: a retrieval study of 47 bearings*. Journal of Bone & Joint Surgery - British Volume, 2010. **92**(3): p. 367-73.
203. Engh, G.A., Zimmerman, R.L., Parks, N.L. and Engh, C.A., *Analysis of wear in retrieved mobile and fixed bearing knee inserts*. Journal of Arthroplasty, 2009. **24**(6S): p. 28-32.
204. Lavernia, C.J., Sierra, R.J., Hungerford, D.S. and Krackow, K., *Activity level and wear in total knee arthroplasty: a study of autopsy retrieved specimens*. Journal of Arthroplasty, 2001. **16**(4): p. 446-53.
205. Lapaj, L., Mroz, A., Kokoszka, P., Markuszewski, J., Wendland, J., Halak-Lapaj, C. and Kruczynski, J., *Peripheral snap-fit locking mechanisms and smooth surface finish of tibial trays reduce backside wear in fixed-bearing total knee arthroplasty*. Acta Orthopaedica, 2017. **88**(1): p. 62-69.
206. Harman, M., Cristofolini, L., Erani, P., Stea, S. and Viceconti, M., *A pictographic atlas for classifying damage modes on polyethylene bearings*. Journal of Materials Science: Materials in Medicine, 2011. **22**(5): p. 1137-46.
207. Stoner, K.E., Nassif, N.A., Wright, T.M. and Padgett, D.E., *Laser scanning as a useful tool in implant retrieval analysis: a demonstration using rotating platform and fixed bearing tibial inserts*. Journal of Arthroplasty, 2013. **28**(8 Suppl): p. 152-6.
208. Teeter, M.G., Brandt, J.M., Naudie, D.D., Bohm, E.R., McCalden, R.W. and Holdsworth, D.W., *Measurements of Surface and Subsurface Damage in Retrieved Polyethylene Tibial Inserts of a Contemporary Design*. Journal of Long-Term Effects of Medical Implants, 2012. **22**(1): p. 21–31.
209. Teeter, M.G., Naudie, D.D., Milner, J.S. and Holdsworth, D.W., *Determination of reference geometry for polyethylene tibial insert wear analysis*. Journal of Arthroplasty, 2011. **26**(3): p. 497-503.
210. Teeter, M.G., Naudie, D.D., McErlain, D.D., Brandt, J.M., Yuan, X., Macdonald, S.J. and Holdsworth, D. W., *In vitro quantification of wear in tibial inserts using microcomputed tomography*. Clinical Orthopaedics & Related Research, 2011. **469**(1): p. 107-12.
-

- 
211. Blunt, L.A., Bills, P.J., Jiang, X.Q. and Chakrabarty, G., *Improvement in the assessment of wear of total knee replacements using coordinate-measuring machine techniques*. Proceedings of the Institution of Mechanical Engineers, Part H: Journal of Engineering in Medicine 2008. **222**(3): p. 309-18.
212. Kop, A.M., and Swarts, E., *Quantification of polyethylene degradation in mobile bearing knees: a retrieval analysis of the Anterior-Posterior-Glide (APG) and Rotating Platform (RP) Low Contact Stress (LCS) knee*. Acta Orthopaedica, 2007. **78**(3): p. 364-70.
213. Lord, J.K., Langton, D.J., Nargol, A.V., Meek, R.M. and Joyce, T.J., *The Tribology of Explanted Hip Resurfacings Following Early Fracture of the Femur*. Journal of Functional Biomaterials, 2015. **6**(4): p. 1021-35.
214. Teeter, M.G., Milner, J.S., MacDonald, S.J. and Naudie, D.D., *Manufacturing lot affects polyethylene tibial insert volume, thickness, and surface geometry*. Proceedings of the Institution of Mechanical Engineers, Part H: Journal of Engineering in Medicine 2013. **227**(8): p. 884-9.
215. Dion, N.T., Bragdon, C., Muratoglu, O. and Freiberg, A.A., *Durability of highly cross-linked polyethylene in total hip and total knee arthroplasty. [Review]*. The Orthopedic Clinics of North America, 2015. **46**(3): p. 321-327.
216. Matz, J., Howard, J.L., Sisko, Z.W., Teeter, M.G. and Lanting, B.A., *Differences in Trochlear Surface Damage and Wear Between Three Different Total Knee Arthroplasty Designs*. Journal of Arthroplasty, 2017. **32**: p. 3763-3770.
217. Heyse, T.J., Elpers, M.E., Nawabi, D.H., Wright, T.M. and Haas, S.B., *Oxidized zirconium versus cobalt-chromium in TKA: profilometry of retrieved femoral components*. Clinical Orthopaedics & Related Research, 2014. **472**(1): p. 277-83.
218. Burnell, C.D.C., Brandt, J.M., Petrak, M.J. and Bourne, R.B., *Posterior Condyle Surface Damage on Retrieved Femoral Knee Components*. Journal of Arthroplasty, 2011. **26**(8): p. 1460-1467.
219. Lakdawala, A., Todo, S. and Scott, G., *The significance of surface changes on retrieved femoral components after total knee replacement*. Journal of Bone & Joint Surgery - British Volume, 2005. **87**(6): p. 796-9.
220. Que, L., Topoleski, L.D. and Parks, N.L., *Surface roughness of retrieved CoCrMo alloy femoral components from PCA artificial total knee joints*. Journal of Biomedical Materials Research Part B: Applied Biomaterials, 2000. **53**(1): p. 111-8.
221. Jones, V.C., Williams, I.R., Auger, D.D., Walsh, W., Barton, D.C., Stone, M.H. and Fisher, J., *Quantification of third body damage to the tibial counterface in*
-

- mobile bearing knees*. Proceedings of the Institution of Mechanical Engineers, Part H: Journal of Engineering in Medicine 2001. **215**(2): p. 171-9.
222. Muratoglu, O.K., Bragdon, C.R., Jasty, M., O'Connor, D.O., Von Knoch, R.S. and Harris, W.H., *Knee-simulator testing of conventional and cross-linked polyethylene tibial inserts*. Journal of Arthroplasty, 2004. **19**(7): p. 887-897.
223. Lancaster, J.G., Dowson, D., Isaac, G.H. and Fisher, J., *The wear of ultra-high molecular weight polyethylene sliding on metallic and ceramic counterfaces representative of current femoral surfaces in joint replacement*. Proceedings of the Institution of Mechanical Engineers, Part H: Journal of Engineering in Medicine 1997. **211**(1): p. 17-24.
224. Chapman-Sheath, P., Cain, S., Bruce, W.J.M., Chung, W.K. and Walsh, W.R., *Surface roughness of the proximal and distal bearing surface of mobile bearing total knee prostheses*. Journal of Arthroplasty, 2002. **17**(6): p. 713-717.
225. Que, L.a.T., L.D., *Surface roughness quantification of CoCrMo implant alloys*. Journal of Biomedical Materials Research Part B: Applied Biomaterials, 1999. **48**(5): p. 705-11.
226. Joyce, T.J., Langton, D.J., Jameson, S.S. and Nargol, A V.F., *Tribological analysis of failed resurfacing hip prostheses and comparison with clinical data*. Proceedings of the Institution of Mechanical Engineers, Part H: Journal of Engineering in Medicine 2009. **223**(3): p. 317-323.
227. Naylor, A., Talwalkar, S.C., Trail, I.A. and Joyce, T.J., *Evaluating the Surface Topography of Pyrolytic Carbon Finger Prostheses through Measurement of Various Roughness Parameters*. Journal of Functional Biomaterials 2016. **7**(2).
228. Reay, E., Wu, J., Holland, J. and Deehan, D., *Premature failure of Kinemax Plus total knee replacements*. Journal of Bone & Joint Surgery - British Volume, 2009. **91**(5): p. 604-11.
229. Smith & Nephew. *Genesis II® TKR Surgical Technique*. 2018; Available from: [http://www.smith-nephew.com/global/surgicaltechniques/recon/genesisii\\_acf\\_40420114\\_us.pdf](http://www.smith-nephew.com/global/surgicaltechniques/recon/genesisii_acf_40420114_us.pdf).
230. Smith & Nephew. *Journey® UKR Surgical Technique*. 2018; Available from: <https://www.smith-nephew.com/documents/nl-journey-uni-surgicaltechnique.pdf>.
231. Serro, A.P., Gispert, M.P., Martins, M.C., Brogueira, P., Colaco, R. and Saramago, B., *Adsorption of albumin on prosthetic materials: implication for tribological behavior*. Journal of Biomedical Materials Research Part B: Applied Biomaterials, 2006. **78**(3): p. 581-9.

232. Galetz, M.C., Seiferth, S.H., Thiele, B. and Glatzel, U., *Potential for adhesive wear in friction couples of UHMWPE running against oxidized zirconium, titanium nitride coatings, and cobalt-chromium alloys*. Journal of Biomedical Materials Research Part B: Applied Biomaterials, 2010. **93B**(2): p. 468-475.
233. Langton, D.J., Jameson, S.S., Joyce, T.J., Gandhi, J.N., Sidaginamale, R., Mereddy, P., Lord, J.K. and Nargol, A.V., *Accelerating failure rate of the ASR total hip replacement*. Journal of Bone & Joint Surgery - British Volume, 2011. **93B**(9): p. 1011 - 1016.
234. Smith, S.L., et al., *In vitro wear testing of a contemporary design of reverse shoulder prosthesis*. Journal of Biomechanics, 2015. **48**(12): p. 3072-3079.

*Blank page*

## **Appendix A: Knee Explant Retrieval Protocol**

The Knee Explant Retrieval Protocol shall be provided in this Appendix. This protocol was written by Emma Kennard Ritchie to enable the data necessary for this PhD to be collected. It is intended to provide consistency in methodology and future transfer of knowledge within the Bioengineering Group, School of Engineering, Newcastle University.

*Blank page*



# **Knee Explant Retrieval Protocol**

**Written by Emma Kennard Ritchie**

**Bioengineering Research Group**

**School of Engineering**

**Newcastle University**

## **Contents**

### **1. Introduction**

### **2. Prosthesis Preparation and Storage**

### **3. Data Collection, Recording and Storage**

#### 3.1 Knee Prosthesis Catalogue

#### 3.2 Digital Images

#### 3.3 Damage Scoring

##### 3.3.1 *Femoral Damage Scoring (FDS)*

##### 3.3.2 *PE Articular Surface Damage Scoring (PE ADS)*

##### 3.3.3 *PE Backside Damage Scoring (PE BDS)*

#### 3.4 Surface roughness measurement

##### 3.4.1 *Measurement Controls*

##### 3.4.2 *Roughness Parameters*

##### 3.4.3 *Analysis Controls*

*Blank page*

## **1. Introduction**

This protocol details the collection, analysis and storage of retrieved knee prostheses and the associated data by the Bioengineering Research Group, School of Mechanical and Systems Engineering, Newcastle University.

## **2. Prosthesis Preparation and Storage**

Prostheses shall be immersed in formaldehyde solution immediately following surgery and will be left for a minimum of 48 hours after collection by the representative from the Bioengineering Group, School of Engineering before being cleaned and stored.

Using a fume cupboard such as the one in the CB1 Lab, Mezzanine Level, Stephenson Building, School of Engineering, each component will be removed from the formaldehyde solution, shall be rinsed in water and left to drain. The formalin is collected in a clear plastic bottle and clearly labelled "Used Formalin."

All explanted knee prosthesis components shall be individually wrapped in tissue paper and stored in a plastic container. Knee prosthesis components from the same revision shall be stored in the same plastic container where possible. The containers shall be labelled with the knee joint number KXXX. The containers shall be kept in the storage cupboard in the inner Bioengineering Lab of CB1 Mezzanine Level, School of Engineering, Stephenson Building.

## **3. Data Collection, Recording and Storage**

### **3.1 Knee Prosthesis Catalogue**

Each knee retrieval will be labelled KXXX starting at K001 and continuing to K999 chronologically as they are received. This labelling is for all the components from each revision not for each individual component so that the components can be linked to a revision surgery and a patient.

### 3.2 Digital Images

Digital images of all prosthesis components will be taken. Images will be taken with an engineer's rule to indicate scale and images of the articulating and backside and fixation surfaces will be taken where possible.

### 3.3 Qualitative and Semi-quantitative Damage Assessment

A macroscopic visual assessment of damage was performed for each component and the location and extent of any macroscopically visible damage was recorded in a written description.

#### 3.3.1 Femoral Damage Scoring (FDS)

Damage scoring shall be performed for the femoral components of retrieved TKRs and UKRs to calculate femoral damage scores (FDS). The femoral components will be visually divided into eight sections for TKRs and four sections for UKRs (sections 1-4) as in Figure 1.

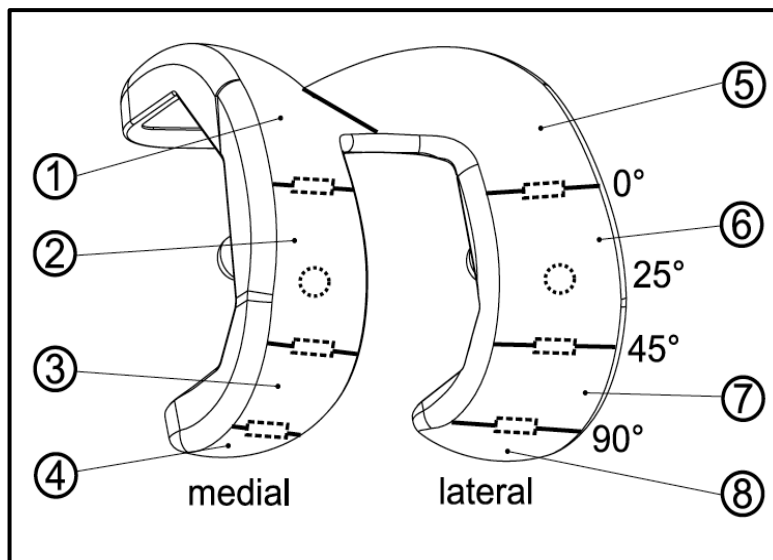


Figure 1. Damage areas on a cruciate retaining TKR femoral component

For each section, three damage features, gouging, burnishing and indentations are to be assessed and three Damage Feature Scores (DFS) are calculated. Gouging is

defined as deep scratches caused by third-body wear. Burnishing is defined as an area in the anterior-posterior direction of fine scratches and is identified by a macroscopically visible change in reflectivity. These areas can also be described as “damage tracks” in the macroscopic visual assessment. Burnishing is also used to describe the areas of damage from unintended metal on metal articulation of the femoral component with the tibial component resulting from PE wear through. Indentations or small pits caused by third body debris and light scratching also caused by third body debris are classed together as the same Damage Feature.

The DFS is calculated as the product of an area score and a severity score. The area score is a numeric 0 – 10 assigned based on the percentage area within the section that the damage feature covers. The area scores are 0 for no coverage, 1 for under 10% coverage, 2 for above 10% and up to 20%, 3 is for above 20% and up to 30% so on until 10 is above 90% and up to 100%. The severity score is also a numerical value assigned based on how visible the damage feature is. If the damage feature is not visible the severity score of 0 is assigned, if it is just visible the severity score assigned is 0.33, clearly visible and a severity score of 0.66 is assigned and severe damage visible is assigned a severity score of 1.

The total FDS is the sum of the three DFS in each of the eight areas. The maximum FDS for a TKR femoral component is 240 (i.e.  $10 \times 3 \times 8$ ) and for a UKR femoral component is 120 (i.e.  $10 \times 3 \times 4$ ).

### **3.3.2 PE Articular Surface Damage Scoring (PE ADS)**

The semi-quantitative damage scoring method [1] is to be applied to the articulating surface of the PE component to determine a PE Articular Surface Damage Score (PE ADS).

The articulating surface of a TKR PE component shall be visually divided into ten sections as shown in Figure 2. For UKR PE components the articulating surface shall be divided into just four sections (sections 0 – 3 as shown in Figure 2). Within each section, for each of seven damage features (deformation, pitting, embedded debris, scratching, burnishing, abrasion and delamination/subsurface cracking), a Damage

Feature Score (DFS) of 0, 1, 2 or 3 is assigned corresponding to the percentage area of the section the damage feature covers. The definitions of the damage features are detailed in table 1.

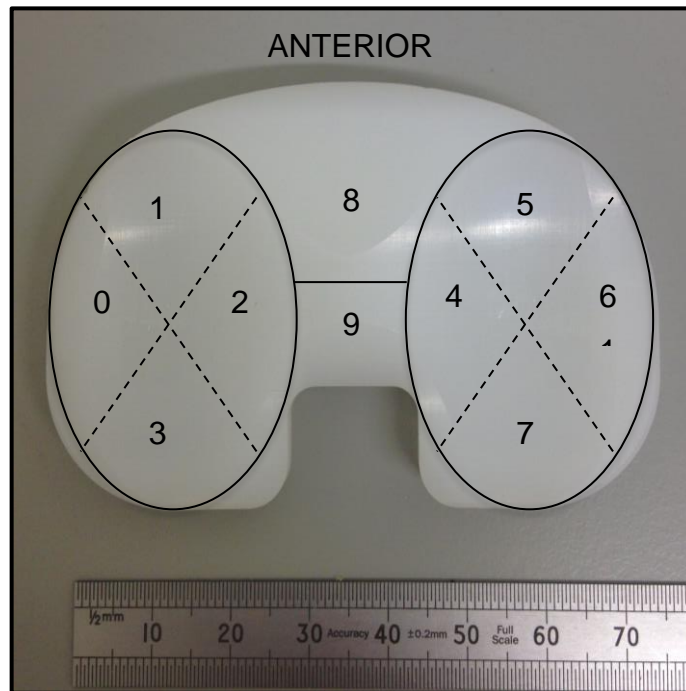


Figure 2. Damage areas on the articular surface of a cruciate retaining TKR PE component

If the damage feature is estimated to cover less than 10% of the section a damage feature score (DFS) of 1 is recorded, if the damage feature is estimated to cover between 10 and 50% of the section a DFS of 2 is recorded and if more than 50% of the section is covered by the identified damage feature a DFS of 3 is recorded. The sum of the grades for each damage feature in each section gives the PE ADS. For TKR PE components the maximum possible PE ADS would be 210 and for UKR PE component the maximum possible PE ADS would be 84.

### 3.3.3 PE Backside Damage Scoring (PE BDS)

A PE Backside Damage Score (PE BDS) is calculated for the distal surface of the PE component. The backside surface of the PE component is visually divided into six sections for TKR PE components and four sections for UKR PE (see Figure 3).

Within each section, six damage features, burnishing, scratching, indentations, surface deformation, pitting and stippling, are assessed and six Damage Feature Scores (DFS) are calculated. The definitions of the damage features are given in Table 1.

As for the femoral damage scoring method described above, a DFS is calculated as the product of an area score and a severity score. The area score is a numeric 0 – 10 assigned based on the percentage area within the section that the damage feature covers. The area scores are 0 for no coverage, 1 for under 10% coverage, 2 for above 10% and up to 20%, 2 is for above 20% and up to 30% so on until 10 is above 90% and up to 100%. The severity score is also a numerical value assigned based on how visible the damage feature is. If the damage feature is not visible the severity score is 0, if it is just visible, the severity score is 0.33, clearly visible is assigned 0.66 and severe damage visible is assigned a severity score of 1.

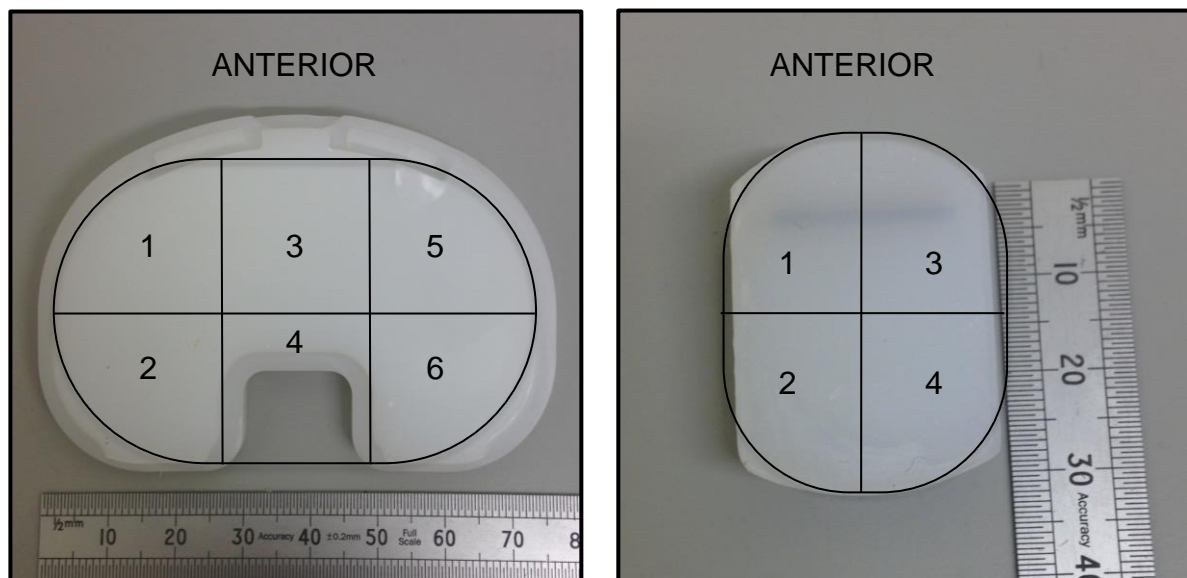
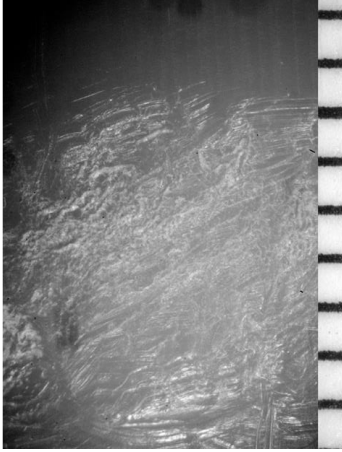
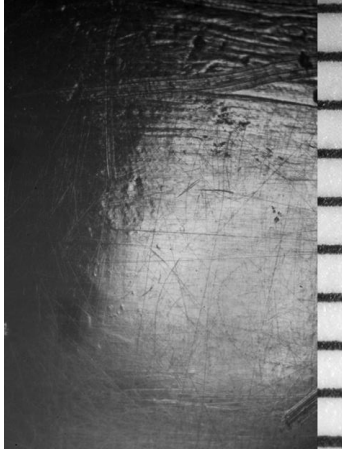
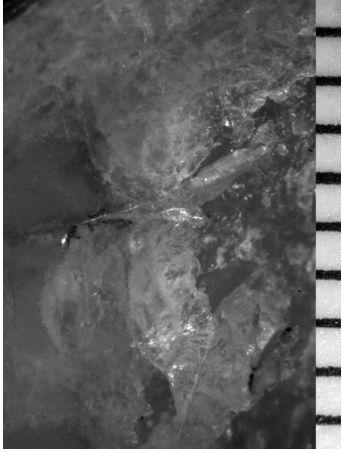


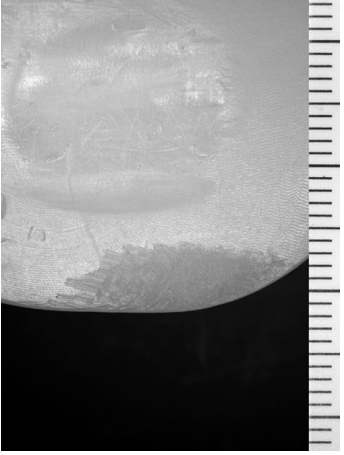
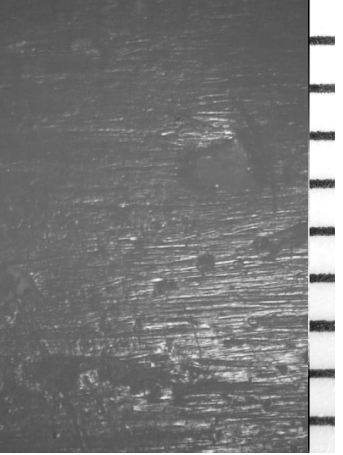
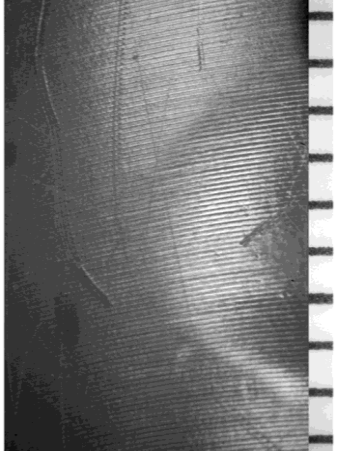
Figure 3. Damage areas on the backside surface of a TKR and UKR PE component

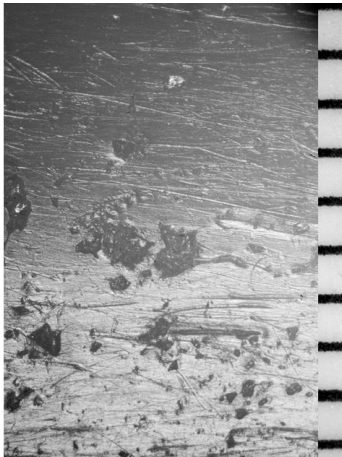
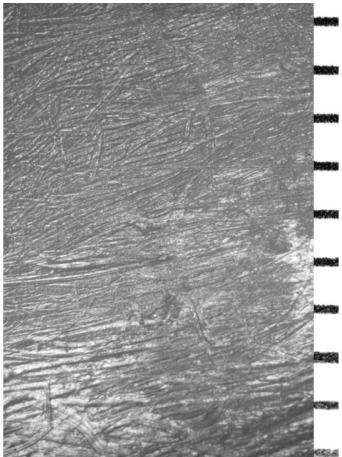
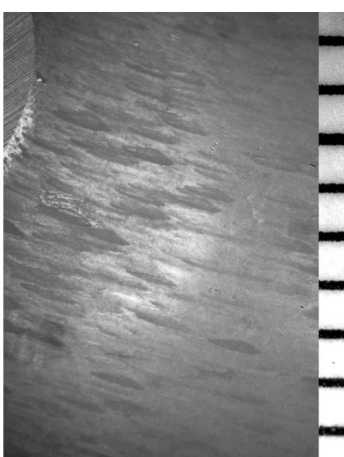
The total PE BDS is the sum of the six DFS values in each of the six areas for TKRs and four areas for UKRs. The maximum PE BDS for a TKR PE component is 360 (i.e. 10 x 6 x 6) and for a UKR femoral component is 240 (i.e. 10 x 6 x 4).

Table 1. PE articular surface and backside surface damage mode descriptions and identification. Images showing 1mm scale.

Damage Mode	Description	Identification
<u><b>Abrasion</b></u>	Abrasion is identified as areas where the PE has a rough, shredded or tufted appearance with limited directionality and with a change in colour of the PE.	
<u><b>Burnishing</b></u>	Burnishing is characterised by the observation of highly polished areas with a visibly increased reflectivity in comparison to the surrounding PE material.	
<u><b>Delamination / Subsurface cracking</b></u>	Delamination is observed where layers of PE material are separated and removed from the original surface, leaving an exposed surface. It may appear as a peeling of the PE. Subsurface cracking is where fatigue occurs to the PE below the original surface and is observed as a change in colour of the PE. Subsurface cracking often precedes delamination.	



Damage Mode (cont.)	Description (cont.)	Identification (cont.)
<p><b><u>Deformation</u></b></p>	<p>Surface deformation is observed as permanent deformation resulting in a change in the surface geometry. It is sometimes referred to as “ plastic deformation” or “ creep” . There is no material removal just a change in geometry. It is observed macroscopically and not typically associated with a change in colour of the PE. On the PE backside surface this can be the impression of screw holes from the tibial tray.</p>	
<p><b><u>Embedded Debris</u></b></p>	<p>Embedded debris are identified by areas that differ in colour and / or relative texture to the surrounding PE surface consistent with embedded third-body particles of suspected bone, cement or possibly metal.</p>	
<p><b><u>Indentations</u></b></p>	<p>Indentations are defined as non-uniform more pronounced scratches suspected to be the result of trapped third-body abrasions. Identified on the distal PE backside surface. Subsurface cracking often precedes delamination.</p>	

Damage Mode (cont.)	Description (cont.)	Identification (cont.)
<u>Pitting</u>	Pitting is visualised as depressions in the PE surface. Typically, the pits are between 1-2 mm in diameter, but they may be much larger with 20-30mm diameters. Within the pits the surface of the PE is burnished and very reflective.	
<u>Scratching</u>	Scratching is identified as thin indented lines which may be either ordered in the anterior / posterior direction or may be irregular in direction.	
<u>Stippling</u>	Stippling is uniquely identified on the distal PE backside surface and is visualised as short (approximately 1-2mm) unidirectional scratches often in a circumferential pattern.	

### 3.4 Surface Roughness Measurement

Surface roughness measurements are to be taken using a NewView 5000 (ZYGO, Middlefield, Connecticut, USA) non-contacting white light interferometric profilometer

Measurements are to be taken on the femoral condyles, proximal tibial tray surface, and the distal backside surface of the PE components of retrieved prostheses.

On each retrieved femoral condyle fifteen measurements are to be taken on the most macroscopically visually damaged areas that are considered to have been *in vivo* damage. This results in thirty measurements taken per component for TKRs and fifteen measurements per component for UKRs. The femoral components are to be macroscopically assessed with the corresponding PE components to determine whether damage is considered *in vivo* damage or retrieval damage.

On retrieved tibial tray components where the proximal surface is able to be accessed, six measurements are to be taken per retrieved component. The measurements are to be taken in the areas that corresponded to the sections defined in the PE backside damage scoring method described above.

#### 3.4.1. Roughness Parameters

The following roughness parameters are to be recorded from the MetroPro Software Version 8.0.3:

Root-mean-square surface roughness  $S_q$ ; maximum peak height  $S_p$ ; maximum valley depth  $S_v$ ; peak to valley height PV; 10-point height average  $S_z$ ; surface kurtosis  $S_{ku}$ ; and surface skewness  $S_{sk}$ .

#### 3.4.2. Measurement Controls

For all profilometry measurements a 10X objective lens with a x2 optical zoom is to be used to give an area of view of 317 x 238 mm. A scan length of 100  $\mu\text{m}$  is to be used for the CoCr femoral components and the tibial trays while for the PE components a scan length of 150  $\mu\text{m}$  is to be selected. For the measurement of CoCr and OxZr femoral components and polished tibial trays, a minimum modulation percentage

(Min Mod%) of 15% is to be selected. However, this may be reduced to 4% when measuring non-polished tibial trays and as low as 2% when measuring the PE component surfaces.

### **3.4.3 Analysis Controls**

For the curved surfaces of the femoral condyles a form filter of “remove cylinder” is to be applied to filter the effects of the curvature of the sample. For the measurement of the proximal surface of the tibial tray components and the distal backside surface of the PE components that were non-curved, a “remove plane” form filter is to be applied

Additional filters are to be applied including a “remove spike” filter and a “data fill filter” as considered appropriate by the operator.

The femoral component should be positioned, if possible, so that either the superior aspect of the component is at the top of the image screen or so that the superior aspect of the component is to the right of the image screen.

## **Appendix B: Knee Explant Catalogue**

The Knee Explant Catalogue is included within this Appendix.

*Blank Page*

**Knee Explant Catalogue****E. Ritchie, Bioengineering Research Group, School of Engineering, Newcastle University.****November 2018**

x – no data; CR – Cruciate retaining; PS – Posterior stabilised; H'd – Hinged; PF – Patellafemoral; MB – Mobile bearing; FB – Fixed bearing; C- Cemented; U – Uncemented; H – Hybrid fixation; M – Male; F – Female; L – Left; R – Right; med – medial; lat – lateral; OA – Osteoarthritis; AS – Ankylosing Spondylitis; SD – Still's Disease; PA – Psoriatic Arthritis; RA – Rheumatoid Arthritis; Fx – fracture; SA – Septic arthritis;

<u>Knee catalogue code</u>	<u>Retrieved components</u>	<u>Design</u>	<u>Fixation of retrieved components</u>	<u>Gender</u>	<u>Side</u>	<u>BMI</u>	<u>Indication for primary surgery</u>	<u>Indication for revision</u>	<u>Date of primary surgery</u>	<u>Date of Revision Surgery</u>	<u>Time in vivo - months</u>	<u>Patient Date of Birth</u>	<u>Age at Primary</u>	<u>Age at Revision</u>
K001	TKR Stryker Kinemax	CR	U	M	R	27.5	OA	Aseptic loosening	1990	09/11/2010	239 - 250	20/09/1929	60 - 61 years	81 years 2 months
K003	TKR Stryker Kinemax	CR	H	M	R	21.5	OA	Infection	08/01/1999	16/02/2011	145	25/03/1938	60 years 10 months	72 years 11 months

K005	TKR Stryker Kinemax	CR	C	M	R	28.5	OA	Aseptic loosening	2004 and 17.03.2010	07/03/2011	75 - 86	12/03/1954	49 - 50 years	57 years
K007	TKR Stryker Kinemax (single piece PE component)	CR	C	M	R	26	AS	Infection	1989	04/04/2011	256 - 267	26/06/1955	33 - 34 years	55 years 10 months
K014	TKR Stryker Kinemax	CR	C	M	L	26	OA	Aseptic loosening and PE component wear	1991	28/06/2011	234 - 245	29/05/1929	63 - 64 years	82 years 1 month
K018	TKR Stryker Kinemax	CR	C	M	L	33	OA	Aseptic loosening	14/08/1997	08/08/2011	168	05/09/1931	65 years 11 months	79 years 11 months
K020	TKR Stryker Kinemax (no PE component)	CR	C	M	R	x	OA	PE component wear	22/03/1997	07/09/2011	174	07/03/1936	61 years	75 years 6 months
K022	TKR Stryker Kinemax	CR	H	F	L	32	OA	PE component wear	07/07/1998	04/10/2011	159	01/06/1944	54 years 1 month	67 years 4 months

Appendix B: B256



K026	TKR Stryker Kinemax (no tibial component)	CR	C	F	L	31.8	OA	Pain and instability	18/01/2005	27/03/2014	110	08/05/1946	58 years 8 months	67 years 10 months
K042 / F04	TKR Stryker Kinemax	CR	C	M	L	22.3	SD	Pain and wear of lateral PE component	15/03/1995	27/02/2012	203	11/09/1957	37 years 6 months	54 years 5 months
K046 / F08	TKR Stryker Kinemax	CR	C	F	R	37	PA	PE component wear	1997	19/10/2011	166 - 177	11/12/1957	39 - 40 years	53 years 10 months
K048 / F10	TKR Stryker Kinemax	CR	H	M	R	32	OA	Aseptic loosening	1993	28/02/2012	218 - 229	19/01/1945	48 - 49 years	67 years 1 month
K071	TKR Stryker Kinemax	CR	C	F	L	24.6	OA	Instability, PE component wear, aseptic loosening	24/02/2001	14/07/2014	161	15/01/1948	53 years 1 month	66 years 6 months
K081	TKR Stryker Kinemax	CR	H	F	R	30.2	RA	PE component wear and instability	01/11/1997	16/05/2014	198	21/04/1949	48 years 7 months	64 years 11 months

Appendix B: B257

K084	TKR Stryker Kinemax	CR	C	M	L	22.5	AS	PE component wear and instability	08/12/1999	17/09/2014	177	19/06/1930	69 years 6 months	84 years 3 months
K106b	TKR Stryker Kinemax	CR	C	M	R	23.8	PA	PE component wear	03/04/1998	18/11/2015	211	26/11/1943	54 years 5 months	72 years
K107b	TKR Stryker Kinemax	CR	C	F	R	34.9	RA	PE component wear	Nov / Dec 1997	14/09/2015	213 - 224	02/08/1930	66 - 67 years	85 years 1 month
K108b	TKR Stryker Kinemax	CR	C	M	R	41.1	OA	PE component wear	2003	23/11/2015	143 - 154	25/02/1941	61 - 62 years	74 years 9 months
K122	TKR Stryker Kinemax	CR	C	M	R	22.1	OA	PE component wear and instability	19/09/2000	29/09/2015	180	15/11/1929	70 years 10 months	85 years 10 months
K019	TKR DePuy PFC	CR	C	F	R	x	OA	Infection	2004	17/08/2011	80 - 91	18/08/1932	71 - 72 years	79 years

K023	TKR DePuy PFC	CR	C	M	R	38	OA	Fixed flexion, tight anterior compartment	06/01/2009	31/08/2011	31	10/01/1944	65 years	67 years 6mths
K043 / F05	TKR DePuy PFC (older design)	CR	C	F	L	22.3	x	x	1997	08/03/2012	171 - 182	x	x	x
K047 / F09	TKR DePuy PFC (older design)	PS	C	x	x	x	x	x	x	x	x	x	x	x
K063	TKR DePuy PFC	CR	C	F	L	41.1	OA	Aseptic loosening of tibial implant	30/11/2000	10/06/2014	163	25/08/1939	61 years 3 months	74 years 10 months
K064	TKR DePuy PFC	CR	C	F	R	33.8	OA	Arthrofibrosis	14/11/2011	28/06/2014	31	14/10/1933	78 years 1 month	80 years 8 months
K065	TKR DePuy PFC	CR	C	F	R	33	OA	Component malalignment	04/10/2010	30/06/2014	44	22/05/1960	50 years 5 months	54 years 1 month
K085	TKR DePuy PFC	CR	C	M	L	33	RA	Infection	09/07/2012	22/09/2014	26	26/10/1950	61 years 9 months	63 years 11 months
K086	TKR DePuy PFC	CR	C	M	L	43.6	OA	Pain and instability	24/08/2004	05/09/2014	121	29/07/1936	68 years 1 month	78 years 2 months

Appendix B: B259

K087	TKR DePuy PFC	CR	C	M	L	28.3	OA	Component malalignment	07/10/2011	01/09/2014	35	30/01/1946	65 years 9 months	68 years 8 months
K093	TKR DePuy PFC	CR	C	F	R	33.5	OA	Component malalignment	08/08/2012	10/11/2014	27	25/08/1954	58 years	60 years 3 months
K098	TKR DePuy PFC	CR	C	M	L	36	OA	Arthrofibrosis	04/02/2014	26/01/2015	11	30/08/1958	55 years 6 months	56 years 5 months
K099	TKR DePuy PFC	CR	C	M	L	27.5	OA	Aseptic Loosening	09/06/2002	30/01/2015	151	19/03/1933	69 years 3 months	81 years 10 months
K107a	TKR DePuy PFC	CR	C	F	R	28.1	Trauma Osteoporotic Fx	Instability	04/12/2012	16/11/2015	35	12/10/1930	82 years 2 months	85 years 1 month
K108a	TKR DePuy PFC	CR	C	F	R	31.9	OA	Instability	18/11/2013	09/11/2015	24	03/05/1938	75 years 11 months	77 years 11 months
K112	TKR DePuy PFC	CR	C	M	R	28	OA	PE Wear, aseptic loosening of the tibial component	23/01/2001	21/04/2014	159	08/03/1940	60 years 10 months	74 years 1 month
K119	TKR DePuy PFC	CR	C	F	L	39	OA	Pain and instability	25/06/2010	18/09/2015	63	26/07/1947	62 years 11 months	68 years 2 months

Appendix B: B260

K008	TKR Biomet AGC (V2 HPPS interlok tibial component)	PS	C	F	L	24	OA	Aseptic loosening	01/12/2009	04/04/2011	16	06/07/1930	79 years 5 months	80 years 9 months
K013	TKR Biomet AGC	PS	C	F	R	x	OA	Aseptic loosening	1991	01/07/2011	235 - 246	06/09/1936	54 years 4 months - 55 years 3 months	74 years 10 months
K028	TKR Biomet AGC	PS	H	F	R	x	OA	Aseptic loosening & instability	1997	31/03/2014	195 - 206	09/08/1937	59 years 7 months - 60 years 6 months	76 years 7 months
K029	TKR Biomet AGC	CR	C	F	R	x	OA	Aseptic loosening & instability	2004	31/03/2014	111 - 122	18/10/1954	49 years 3 months - 50 years 2 months	59 years 5 months
K045 / F07	TKR Biomet AGC (Older design - Install Bursal 2)	PS	C	M	L	24.2	OA	Aseptic loosening & pain	1995	07/02/2012	194 - 205	06/01/1931	62 years 11 months - 64 years	81 years 1 month

K062	TKR Biomet AGC (Older design - Install Bursal 2)	PS	H	M	R	x	OA	Aseptic loosening	1992	20/06/2014	258 - 269	04/09/1928	63 years 4 months and 64 years 3 months	85 years 9 months
K068	TKR Biomet AGC	CR	C	F	L	x	OA	Pain and instability	2005	06/06/2014	102 - 113	25/05/1938	67 years 8 months - 68 years 7 months	76 years 1 month
K083	TKR Biomet AGC	CR	C	M	L	x	OA	Aseptic loosening	2000	11/08/2014	164 - 175	01/06/1946	53 years 7 months - 54 years 6 months	68 years 2 months
K091	TKR Biomet AGC	CR	C	M	R	x	OA	Pain and instability	2008	12/09/2014	69 - 80	05/05/1958	49 years 8 months - 50 years 7 months	56 years 4 months
K109	TKR Biomet AGC	CR	C	M	R	x	OA	Aseptic loosening	1998	24/07/2015	199 - 210	01/06/1946	51 years 7 months - 52 years 6 months	69 years 1 month
K114	TKR Biomet AGC	CR	C	M	R	x	OA	Aseptic loosening & pain	2002	04/03/2015	147 - 156	25/03/1941	60 years 10 months - 61 years 9 months	74 years

Appendix B: B262

K115	TKR Biomet AGC	CR	C	M	L	x	OA	Pain and instability	2009	04/09/2015	69 - 80	05/05/1958	50 years 8 months - 51 years 7 months	57 years 4 months
K027	TKR S&N Genesis (II) OxZr	CR	C	F	R	28.4	OA	Pain / Hypermobility	17/11/2010	60 years	40	29/08/1973	37 years 3 months	40 yrs 7 months
K104	TKR S&N Genesis (II) OxZr	PS	C	M	R	28.2	OA (2006) / Pain (2008)	Instability (2015) Pain (2008)	06/2006 & 2008	11/09/2015	81 - 92	14/09/1957	50 years 4 months - 51 years 3 months	58yrs
K105	TKR S&N Legion OxZr	PS	C	M	L	34	OA	Chronic infection and instability / Pain	08/03/2011	23/02/2015	47	15/04/1946	64 years 11 months	68 years 10 months
K016	UKR Biomet Oxford	MB	C	M	L Md	26.5	OA	Mechanical impingement of tibial component over the patella tendon	2009	22/07/2011	19 - 30	25/06/1949	59 years 7 months - 60 years 6 months	62 years 1 month
K037	UKR Biomet Oxford	MB	C	x	x	x	x	x	x	x	x	x	x	x

Appendix B: B263

K038	UKR Biomet Oxford	MB	C	x	x	x	x	x	x	Collected March 2012	x	x	x	x
K077	UKR Biomet Oxford (PE component only)	MB	x	F	L	x	OA	Collapse of Tibial shelf. Pain.	2002	07/04/2014	138 - 149	15/07/1939	61 years 6 months - 62 years 5 months	74 years 9 months
K100	UKR Link Sled	FB	C	M	L Md	x	OA	PE wear. Metallosis. Aseptic loosening	1999	22/01/2015	169 - 180	12/05/1950	48 years 8 months - 49 years 7 months	54 years 8 months
K117	UKR Biomet Oxford	MB	C	M	R Md	x	OA	Pain	2005	12/11/2015	119 - 130	27/12/1933	71 years 1 month - 72 years	81 years 11 months
K125	UKR Biomet Oxford	MB	C	F	R Md	x	x	x	x	20/05/2014	x	25/08/1962	x	51 years 9 months
K126	UKR Biomet Oxford	MB	C	F	R Md OR L Lt?	x	x	x	x		x	10/01/1952	x	
K127	UKR Zimmer High Flex	FB	C	M	L Md	x	x	x	x	12/11/2014	x	25/03/1954	x	60 years 8 months
K128	UKR Zimmer High Flex	FB	C	F	L Md	x	x	x	x	14/06/2014	x	05/01/1957	x	57 years 5 months

Appendix B: B264



K129	UKR Zimmer High Flex	FB	C	F	R Lt OR L Md?	x	x	x	x		x	09/10/1955	x	
K130	UKR Zimmer High Flex	FB	C	M	R Lt OR L Md?	x	x	x	x	20/04/2014	x	17/03/1953	x	61 years 1 month
K131	UKR Zimmer High Flex	FB	C	F	R Md	x	x	x	x	20/01/2016	x	09/03/1943	x	62 years 10 months
K132	UKR Zimmer High Flex	FB	C	F	L Md	x	x	x	x	04/11/2016	x	08/12/1946	x	69 years 11 months
K133	UKR Zimmer High Flex	FB	C	M	R Md	x	x	x	x	13/01/2016	x	19/03/1965	x	50 years 10 months
K134	UKR Smith& Nephew OxZr	FB	C	F	R Md	x	x	x	x	22/11/2016	x	12/03/1951	x	65 years 8 months
K135	UKR Smith& Nephew OxZr	FB	C	M	R Lt OR L Md	x	x	x	x	13/12/2016	x	17/06/1961	x	55 years 6 months
K136	UKR Zimmer High Flex	FB	C	F	R Md	x	x	x	x	26/10/2015	x	20/08/1957	x	58 years 2 months
K137	UKR Zimmer High Flex	FB	C	F	R Lt OR L Md	x	x	x	x	19/05/2016	x	15/05/1953	x	63 years
K138	UKR Zimmer High Flex	FB	C	M	R Md OR L Lt	x	x	x	x	15/01/2015	x	21/06/1950	x	49 years 7 months
K139	UKR Other	MB	C	M	x	x	x	x	x	28/11/2014	x	12/04/1957	x	57 years 7 months

Appendix B: B265

K140	UKR Biomet Oxford	MB	C	F	R Md	x	OA	Pain and lack of extension	2013	27/09/2016	33 - 44	19/12/1939	73 years 1 month - 74 years	76 and 9 months
K069	S&N Oxinium Patella Femoral	PF	C	F	R	x	x	x	x	04/08/2014	x	28/08/1969	x	x
K080	S&N Oxinium Patella Femoral (only the patella component)	PF	C	F	L	x	OA	Pain in the knee	2012	24/03/2014	x	07/12/1973	x	x
K094	S&N Oxinium Patella Femoral	PF	C	F	X	x	x	x	x	13/10/2014	x	14/06/1960	x	x
K110	S&N Oxinium Patella Femoral	PF	C	F	X	x	OA	Pain	x	11/09/2015	x	07/09/1946	x	x

K002	TKR Other - S&N Genesis	CR	H	M	R	29.5	OA	Wear of the PE component visible on the pre-revision radiograph and a periprosthetic fracture	14/10/1992	11/02/2011	220	02/09/1938	57 years 1 month	75 years 5 months
K004	TKR Other - Plus Orthopaedics TC Plus	CR	H	F	R	29.5	OA	Wear of the PE component	x	18/02/2011	68	08/10/1938	x	72
K006	TKR Other - Biomet Maxim	CR	C	F	L	27	OA	Instability	2004	01/04/2011	76 - 87	14/04/1920	83 years 9 months - 84 years 8 months	91
K089	TKR Other - S&N Genesis	CR	C	F	L	x	x	x	x	15/08/2014	x	04/05/1937	x	x
K123	TKR Other - S&N Triathlon	CR	C	M	R	x	OA	Infection	21/08/2014	09/06/2015	10	10/07/1932	82 years 1 month	82 years 11 months
K090	TKR Other - Zimmer	CR	C	F	R	x	x	x	x	06/10/2014	x	04/04/1961	x	x
K120	TKR Other - DePuy TC3	CR	C	F	R	x	x	x	x	05/03/2015	x	11/11/1945	x	x

Appendix B: B267

K030	TKR Other - Unidentified	CR	U	X	X	x	x	x	x	01/11/2011	x		x	x
K066	TKR Other - Unidentified	CR	C	F	R	x	x	x	x	03/12/2015	x	11/10/1935	x	X
K092	TKR Other - Unidentified	CR	C	M	L	x	x	x	x	27/10/2014	x	29/11/1958	x	X
K009	TKR Other - Biomet Dual Articular 2000	PS	C	M	L	41.7	OA	Infection. This was a second stage revision surgery.	Primary surgery date not known. First stage revision date 2005 (exact first stage revision date not known)	15/04/2011	64 - 75	07/09/1937	67 years 4 months - 68 years 3 months	73 years 7 months
K024	TKR Other - Exactech Optrak	PS	C	F	L	33.5	OA	Infection, tibial component loosening	x	12/09/2011	x	09/04/1962	x	X

K034	TKR Other - DePuy TC3	PS	C	F	L	32	SA	Infection	x	30.04.2012 . (then this was also revised on 10/05/2013 2nd 24/06/2013 to a TC3 mobile bearing.)	x	15/03/1964	x	X
K034b	TKR Other - DePuy TC3	PS	C	F	L	32	x	Infection	30.04.2012	1st 10/05/2013 2nd 24/06/2013	14	15/03/1964	48 years 1 month	49 years 3 months
K074	TKR Other - DePuy	PS	C	M	R	x	x	x	x		x	10/04/1963	x	X
K088	TKR Other - DePuy Srom	PS	C	F	L	x	x	x	x	05/09/2014	x	15/01/1948	x	x
K035	TKR Other - unidentified	PS	U	X	X	x	x	x	x	23/03/2013	x	x	x	x
K036	TKR Other - unidentified	PS	C	X	X	x	x	x	x	13/2/12 or 11/1/12	x	x	x	x
K070	TKR Other - unidentified	PS	C	M	R	x	x	x	x	08/08/2014	x	01/04/1937	x	x

Appendix B: B269

K073	TKR Other - unidentified	PS	C	M	R	x	x	x	x	11/07/2014	x	15/04/1946	x	x
K102	TKR Other - unidentified	PS	C	M	R	x	x	x	x	15/12/2014	x	19/09/1944	x	x
K025	TKR Other - DePuy Noles S-Rom	H'd	C	M	L	x	OA; Pain and instability indication for 1st revision	Infection	Primary Surgery - PFC 1997; First stage revision 18/04/2008 due to pain and instability	17/04/2014	72	x	x	x
K075	TKR Other Hinged - DePuy Srom (no femoral)	H'd	C	M	X	x	x	x	x	01/08/2014	x	23/08/1943	x	x
K095	TKR Other - DePuy TC3	H'd	C	M	X	x	x	x	x	03/11/2014	x	20/10/1964	x	x
K101	TKR Other - DePuy TC3	H'd	C	F	R	x	x	x	x	26/01/2015	x	13/07/1943	x	x
K082	TKR Other - Endolink	H'd	H	F	L	x	Fx	Loose Implant	10/10/2008	12/05/2014	67	07/10/1937	71 years	76 years 7 months
K096	TKR Other - Zimmer	H'd	C	F	X	x	x	x	x	14/11/2014	x	25/03/1939	x	x

Appendix B: B270

K072	TKR Other - Unidentified (no tibial)	H'd	C	M	X	x	x	x	x	x	x	13/12/1930	x	x
K097	TKR Other - Unidentified	H'd	C	M	X	x	x	x	x	x	x	28/09/1953	x	x
K103	TKR Other - Unidentified	H'd	C	M	L	x	x	x	x	05/01/2015	x	18/05/1935	x	x
K106a	TKR Other - Unidentified	H'd	C	X	X	x	x	x	x	17/07/2015	x	x	x	x
K111	TKR Other - Unidentified	H'd	C	M	X	x	x	x	x	11/05/2015	x	23/08/1943	x	x
K113	TKR Other - Unidentified	H'd	C	F	X	x	OA	Infection	2013	07/09/2015	21 - 32	22/09/1955	57 years 4 months - 58 years 3 months	60 years
K118	TKR Other - Unidentified	H'd	C	M	R	x	x	x	x	23/10/2015	x	10/04/1963	x	x
K124	TKR Other - Unidentified	H'd	x	x	L	x	x	x	x	29/09/2015	x	19/09/1947	x	x
K011	Steam Sterilised TKR Other - DePuy Noiles S-Rom	H'd	C	M	R	25	Indication for first stage revision: loosening of primary components	Infection	27/03/2009	24/06/2011	27	24/05/1933	75 years 10 months	78 years 1 month

Appendix B: B271

K012	Steam Sterilised TKR DePuy PFC	CR	C	M	R	31.5	OA	Infection	1997	27/06/2011	162 - 173	27/04/1932	64 years 9 months - 65 years 8 months	79 years 2 months
K052	Steam Sterilised TKR Other Unidentified	PS	x	x	X	x	x	x	x	x	x	x	x	x
K060	Steam Sterilised TKR Other - Unidentified	H'd	x	x	X	x	x	x	x	x	x	x	x	x
K078	Steam Sterilised TKR Other Unidentified	PS	x	F	X	x	OA	Arthrofibrosis / Oversized implants ROM 20-80	2011	14/04/2014	28 - 39	26/07/1950	60 years 6 months - 61 years 5 months	63 years 9 months
K010	Steam Sterilised TKR Stryker Kinemax	CR	C	F	L	30	OA	Suspected wear of the PE component of the prosthesis	1998	25/05/2011	149 - 160	22/05/1937	60 years 8 month - 61 years 7 months	74
K031	No Data TKR Other Unidentified	CR	x	x	X	x	x	x	x	x	x	x	x	x
K039 / F01	No Data TKR DePuy PFC	CR	C	x	X	x	x	x	x	x	x	x	x	x

Appendix B: B272



K040 / F02	No Data TKR Other Unidentified	CR	H	x	X	x	x	x	x	x	x	x	x	x
K041 / F03	No Data TKR Other Unidentified	PS	x	x	X	x	x	x	x	x	x	x	x	x
K044 / F06	No Data TKR DePuy PFC	CR	x	x	X	x	x	x	x	x	x	x	x	x
K079	No Data TKR Other Unidentified	CR	x	M	X	x	OA	Loosening	1994, 1984	27/03/2014	240	29/09/1933	60 years 4 months - 61 years 3 months	83 years 6 months
K121	No Data TKR Other Unidentified ? AGC	CR	x	x	X	x	x	x	x	x	x	x	x	x
K032	TKR Biomet AGC	CR	C	x	X	x	x	x	x	25/11/2011	x	x	x	x
K033	TKR Biomet AGC	CR	H	F	X	x	x	x	x	12/12/2011	x	26/08/1948	x	63 years 4 months
K017	Unidentified - PE component only. All PE tibial component.	PS	C	F	L	33.5	x	Septic loosening	1997	29/07/2011	162 - 173	09/04/1962	34 years 9 months - 35 years 8 months	48 years 3 months

Appendix B: B273

K053	Unidentified - Femoral component only	PS	C	x	X	x	x	x	x	31/03/2014	x	18/10/1954	x	x
K061	Unidentified - no femoral component	PS	C	F	R	x	x	x	x	27/05/2014	x	05/05/1946	x	x
K067	Unidentified - PE component only	CR	x	F	L	38.6	OA	Pain	2013	19/05/2014	5-16	14/03/1956	56 years 10 months - 57 years 9 months	58 years 2 months
K076	Unidentified - PE component only	PS	x	F	x	x	x	x	x	x	x	09/05/1959	x	x
K116	Unidentified - no femoral component	PS	C	F	L	x	x	Instability	2006 / 2008	24/04/2015	76 - 87	24/05/1948	59 years 8 months - 60 years 7 months	67 years 1 month
K015	Unidentified - 2 part PE component	CR	C	M	x	x	x	x	x	18/07/2011	x	15/03/1926	x	x
K021	TKR DePuy PFC (PE component only)	CR	C	M	L	29	OA	Anterior knee pain (excision of osteophyte and exchange of PE)	2008	03/10/2011	34 - 45	20/06/1938	69 - 70 years	73 years 4 months

Appendix B: B274

**Additional clinical notes to the Knee Explant Catalogue:**

<b>Knee catalogue code</b>	<b>Retrieved components</b>	<b>Additional Clinical Notes</b>
K001	TKR Stryker Kinemax	Complicated case. Aseptic loosening (metallosis was noted). A fracture of the distal shaft of femur was sustained in 2002; this was treated with open reduction and internal fixation with a dynamic compression plate. The patient had non-union of the fracture with failure of the dynamic compression plate, resulting in varus deformity of the distal femur. The plate was removed and a new LISS (Less Invasive Skeletal Stabilisation) plate was applied with allogenic bone graft, along with a single stage revision with a rotating hinge knee system.
K005	TKR Stryker Kinemax	An isolated PE insert exchange was performed with a patellar resurfacing on 17.03.2010. The retrieved PE does not have the same time in vivo as the retrieved femoral
K042 / F04	TKR Stryker Kinemax	Destruction of PE component anteriorly, both components soundly attached to bone during revision procedure
K008	TKR Biomet AGC (V2 HPPS interlok tibial component)	Aseptic loosening of the femoral and tibial components with a periprosthetic fracture. Complex revision. 17/01/2011 had an internal fixation for an insufficiency fracture of the left tibia

K013	TKR Biomet AGC	Loose Biomet to TC3 mobile bearing with medial condylar plate and cable. Loss of joint height assessed in pre-op clinic
K028	TKR Biomet AGC	Aseptic loosening & mechanical failure. Revision right knee replacement combined 1st and 2nd stage. Mechanically unstable right knee drifting into valgus position. Pain especially under the patella-femoral joint. Revised to a TC3 semi constrained implant. Unstable right knee
K029	TKR Biomet AGC	Gross osteolysis and instability. Tibial and femoral bone loss.
K045 / F07	TKR Biomet AGC (Older design - Install Bursal 2)	Showed signs of wear and is causing pain. July 2011 Femoral component and tibial component loose and removed easily.
K062	TKR Biomet AGC (Older design - Install Bursal 2)	Single stage revision right knee replacement using endo-link system. Laxity of the medial collateral ligament. Indicated for loosening. The tibial and femoral surfaces were so loose that they were moving around while just trying to take the locking pin out. The whole of joint lining was black and looked very metallotic. Indicated for pain initially

K068	TKR Biomet AGC	Bilateral TKR. Left is painful. Aspirations performed showed some infections. Pain in both knees, gross instability, pain with weight bearing. Findings were of well-fixed implants with minimal wear. Mal-positioning of components. Both removed with difficulty. Revised to TC3.
K083	TKR Biomet AGC	Bilateral TKRs, left worse than right knee pain. Underwent sequential staged knee replacement 14 and 16 years ago. The left knee is now swollen and painful and patient feels it unstable. Left complete loss of PE and early osteolysis. "pain and instability". Revised to a NEXGEN hinge. Massive synovitis found
K091	TKR Biomet AGC	Bilateral knee replacements. Right 2008 and left 2009. Both painful in 17/09/2013. Revision Right knee AGC to MBTC3. Gross mediolateral and anteroposterior laxity with a reverse tibial slope on lateral x ray. No infection. Implants removed easily. "Pain and instability."
K109	TKR Biomet AGC	Bilateral TKRs, left worse than right knee pain. Underwent sequential staged knee replacement 14 and 16 years ago. The left knee is now swollen and painful and patient feels it unstable. Left complete loss of PE and early osteolysis. "pain and instability". Revised to a NEXGEN hinge. Massive synovitis found
K114	TKR Biomet AGC	Bilateral TKR IN 2002. Knee pain with possible early loosening of tibial. Pain predominately on Right side. Case notes: brown colour staining of the synovium. Femoral component was loose and fell out with a gentle tap. The tibial implant which was a monoblock was cleared at periphery. Replaced with TC3.

K115	TKR Biomet AGC	Bilateral knee replacements. Right 2008 and left 2009. Both painful in 17/09/2013. Revision Right knee AGC to MBTC3. Gross mediolateral and anteroposterior laxity with a reverse tibial slope on lateral x ray. No infection. Implants removed easily. "Pain and instability."
K104	TKR S&N Genesis (II) OxZr	The retrieval was of a revision component which was revised for pain. The primary was indicated for osteoarthritis and the 1st revision was performed in June 2006 for pain
K105	TKR S&N Legion OxZr	This retrieval was a 1st revision after a primary in 2008. Revised in 2011 for chronic infection.
K016	UKR Biomet	Mechanical impingement of tibial component over the patellar tendon. Revision of left uni to PFC.
K077	UKR (PE component only)	Collapse of Tibial shelf. Pain. Revised to TC3 TKR

K100	UKR Biomet	Marked metallosis of the synovium. The plastic fixed bearing surface had worn through leading to metal on metal wear. Both femoral and tibial components were loose. Revised to Triathlon TKR
K117	UKR Biomet	Pain. Revision of right uni to Triathlon TKR
K140	UKR Other	Remains in constant discomfort with inability to fully extend knee.

*Blank page*



## **Appendix C: Surface Topographical Analysis of Explanted TKRs Results**

The following table is included in this Appendix:

Table C1: Macroscopic Visual Assessment of Explanted TKRs

*Blank page*

**Table C1: Macroscopic Visual Assessment of Explanted TKRs**

	Femoral component	PE component - Proximal articular surface	Tibial component	PE component - Distal backside surface
<b>AGC1</b>	Definite damage tracks observed. Definite scratching corresponding to the PE component damage. The articulating surfaces of both femoral condyles had light unidirectional scratches in the anterior / posterior direction of sliding.	This is a posterior stabilised component. Severe pitting and heavy scratching observed all over both condyles. An area of abrasion on the lateral posterior edge that is approximately 10mm x 7mm was observed. Post not grossly damaged. Macroscopically, the articulating surface of the PE component was damaged on both medial and lateral condyles with pitting being the most prevalent damage mode observed.	*The PE component of the AGC is moulded onto the tibial tray and therefore the proximal tibial surfaces and the distal backside surfaces of the PE components are not able to be assessed visually without destroying the samples.	*The PE component of the AGC is moulded onto the tibial tray and therefore the proximal tibial surfaces and the distal backside surfaces of the PE components are not able to be assessed visually without destroying the samples.
<b>AGC2</b>	Definite damage tracks observed. An area on the lateral condyle of retrieval damage observed.	This is a partially stabilised component. Medial gross damage to edge was observed. Delamination and subsurface cracking and pitting were also recorded	x	x
<b>AGC3</b>	Although the PE component is severely damaged, and the femoral component has some	Severe damage all over the component and in sections 8 and 9 was observed. Subsurface	x	x

	damage tracks there are no big areas of scratching or damage.	cracking, delamination and pitting across component however there was not much scratching.		
<b>AGC4</b>	The femoral component is not macroscopically severely damaged. There are light damage tracks on both condyles and small indentations on the media condyle.	The PE component is delaminated on the medial condyle anteriorly through sections 0, 1 and into 2. There is very minimal damage in section 3. Laterally there is subsurface cracking and delamination centrally and through to the edges and posteriorly. Inside the area where the delamination has occurred there is abrasion and pitting.	x	x
<b>AGC5</b>	Damage tracks on both condyles are observed. Scratches medially are possibly retrieval damage not <i>in vivo</i> damage. There are macroscopically visible “wavy” scratches on lateral condyle	Pitting burnishing subsurface cracking are all observed. Evidence is seen on the medial side of the femoral component deforming the posterior aspect during high flexion. Scratches on lateral condyle are thought to be retrieval damage. Damage in section 8 is also thought to be retrieval damage although it corresponds to femoral component damage.	x	x

<b>AGC6</b>	Damage tracks on both condyles observed. Scratches that appear “wavy” are visible macroscopically.	Delamination on both condyles giving an exposed pitted surface. Both condyles have severe subsurface cracking preceding delamination posteriorly. Lateral condyle is abraded and pitted. Medial condyle is pitted.	x	x
<b>AGC7</b>	Damage tracks on both condyles. Medial condyle has some scratches but doesn't look drastically different to lateral. On the lateral condyle in the ligament space scratches that may be retrieval damage do actually match up with the damage seen on the PE component in section 4 and 5. This may be from medial condyle pivoting. Would appear to be a very loose joint. This corresponds with the patient notes.	Medial condyle showed more damage on the anterior and edges and severe abrasion not seen before in this group posteriorly in two areas. Scratching, subsurface cracking and surface deformation were observed. Lateral condyle shows much less damage. Burnishing scratching and very light pitting.	x	x
<b>AGC8</b>	Macroscopically damaged and “wavy” scratches observed on the lateral condyle. Light damage tracks and light scratches observed on both condyles.	Severely damaged component. Medial more so than laterally. Severe delamination on both condyles. Pitting and abrasion. Subsurface cracking.	x	x

<b>AGC9</b>	Very light damage tracks observed. Medial scratch that is believed to be from the in vivo damage.	Very stained component. Pitting medially. Damage track laterally.	x	x
<b>AGC10</b>	Very light damage track. Some scratches found microscopically but thought to be retrieval damage not in vivo damage.	Very light damage. No massive delamination. However, there is a big scratch thought to be a retrieval scratch. And there is subsurface crack that has not developed.	x	x
<b>PFC1</b>	On the medial condyle there is an area of high damage on the femoral component that initially was considered retrieval damage. However, considering the PE component there is a corresponding area that is discoloured, and it may be that there has been a large third body that has gotten in between the two. Further round the medial femoral condyle is another area of damage. Laterally there is damage. There are pits and scratches on the PE.	Pitting on both condyles and scratches. Medial there is an area of discolouration that corresponds to the damage on the femoral component. There will have been third body debris in this joint to cause this damage.	Non-polished component. Debris still inside the tray.	Stippling in a circular pattern possible evidence of micromotion. Light deformation from the screw hole on tibial tray.

<b>PFC2</b>	Area of severe damage on lateral condyle which looks like retrieval damage as the PE component is not damaged. Medial / lateral scratches which look like retrieval damage too. Both condyles showed definite damage tracks.	Minimal damage observed. Two small areas (approx. 20 x 10 mm) centrally on each condyle of burnishing. Slightly different style PE that is more congruent than the rest in this group.	Non-polished tray with no damage observed.	No real evidence of any damage. Two small areas that may have the beginnings of burnishing underneath the condyles.
<b>PFC3</b>	On a macroscopic level the femoral component has very light damage tracks on both condyles. However, on both medial and lateral femoral condyles are two areas that were initially considered retrieval damage. However, on looking at the femoral and the PE together it would appear that this femoral damage corresponds to the two areas on the PE of subsurface cracking and discolouration. It would seem plausible that a 3rd body got into the space and damaged the femoral component, or the femoral component was possibly even damaged during implantation and this is an area of high contact stress and has subsequently damaged the PE.	Two areas (one on each condyle) of a change in colour of the PE and possible subsurface cracking and the initiation of pitting or delamination. These areas are approx. 3mm x 5-6mm in size. There is burnishing and scratching central to the condyles and pits on both condyles.	Non-polished tray. Stippling marks observed in a circular pattern. There is a small area that initially looks like retrieval damage however there is a corresponding area of damage on the PE backside surface.	Stippling in a circular pattern giving evidence of micromotion. Indentation of screw hole

<b>PFC4</b>	Definite macroscopically visible damage tracks on both femoral components in the anterior posterior direction. Some obvious retrieval scratches on the lateral condyle. Suspected material transfer onto the femoral component.	Burnishing and scratching. Light pitting and scratching and a defined damage track. Material machining marks have been removed.	Non-polished tray. Debris is observed in the fixation mechanism and damage on the medial condyle. No stippling or polishing is observed.	Large scratches assumed to be from retrieval were observed. Very small area of light burnishing in section 5 observed. .
<b>PFC5</b>	Very little damage observed. Very light central damage tracks on both condyles macroscopically visible more medially than laterally. However, on the lateral condyle on the edge is a small set of scratches that correspond to the scratching on the PE component. Also, on the medial condyle at the very posterior aspect during full flexion there is a small area of damage which corresponds to a small area of damage on the PE.	On the lateral condyle heavy scratching on the anterior edge corresponding to damage on the femoral component is observed. Damage track lightly defined on both condyles. Burnishing observed. Medially the component is lightly burnished however on the very posterior aspect there is an area of damage corresponding to the damage on the femoral component. Very slight subsurface cracking and slight deformation observed.	Polished tray. There are scratches observed that are assumed to be from retrieval.	Two very slight areas of burnishing underneath the condyles observed.
<b>PFC6</b>	Definite if narrow damage track visible on lateral condyle in high flexion. Lateral PE has heavy scratching and an element of	PE component slightly more congruent to others in this group. Very minimal damage visible. Lateral PE has heavy scratching and burnishing anteriorly. There is	Non-polished tray. No macroscopically visible damage	Very minimal damage observed. Machine marks still visible. Between 5-10 very small pits on the lateral condyle.



	burnishing anteriorly. Definite damage track on medial condyle.	a definite scratch large and deep on the medial condyle.		
<b>PFC7</b>	Large scratch on the medial condyle. Definite damage tracks and a scratched area on the lateral condyle.	Medial condyle macroscopic observation of a deep indentation into PE either from loss of material or cold forming. Significant burnished damage track. Lateral condyle not so deformed. Definite scratching pits and burnishing anteriorly.	Non-polished tray. Debris in the fixation mechanism and burnishing under both condyles. Large scratches assumed to be retrieval damage on the medial condyle. Light stippling observed corresponding to PE backside damage recorded.	Damage assumed to be retrieval damage on the anterior perimeter observed. Stippling in a circular pattern which may indicate micromotion observed. Deformation from tibial tray screw hole observed.
<b>PFC8</b>	Lateral condyle shows heavy AP scratches. Medial condyle shows light AP scratches. Heavy scratching on lateral condyle assumed to be retrieval damage. Some further damage on medial condyle that is considered to be in vivo damage	Very minimal damage. Some scratches on the lateral perimeter assumed to be from retrieval damage. On lateral condyle distinct damage scar central AP and slightly more anterior of the midline consisting of burnishing and very light scratching. Medial condyle damage scar central AP and slightly more posterior of the midline consisting of burnishing only.	Polished tray. Some scratches assumed to be retrieval damage observed. Also, areas of damage or possibly a film of material visible.	Lots of damage observed anteriorly assumed to be from removal of PE from tibial tray fixation. Condyles still observed to have machining marks. Only burnishing observed on the medial side.
<b>PFC9</b>	Lateral condyle moderate to heavy AP scratches more posteriorly. Lateral condyle AP scratches and one deep scratch which is assumed to be from retrieval	Very minimal damage observed. No clearly defined damage track on the lateral condyle. And only a small amount of burnishing in section 1 on the medial condyle.	Non-polished tray. Debris in the fixation mechanism around the perimeter. Scratches assumed to	Very minimal damage observed. Two scratches assumed to be from retrieval were observed. Posteriorly a small area of

	damage. Definite damage tracks and scratching that corresponds to the scratching on PE.	Some deep scratches though and small pits which could account for the femoral component scratching.	be from retrieval damage observed.	burnishing was observed, and light pitting was observed.
<b>PFC10</b>	Light scratching on lateral condyle. Medial condyle shows heavy scratching which initially was assumed to be retrieval damage but actually corresponds to one of the indentations on the PE component. There is a definite damage track on the femoral component medial condyle	Very minimal gross damage with a light burnished damage track observed on each condyle with light scratches. Not pits but indentations that correspond to the scratches on the femoral component.	Polished tray. Scratches assumed to be from retrieval.	Damage assumed to be retrieval damage on the anterior perimeter observed. No damage that was thought to have occurred <i>in vivo</i> was observed.
<b>PFC11</b>	Scratching and damage tracks on both condyles. Heavier scratching on the outside of the lateral condyle which corresponds to the PE damage observed. The scratching is considered to be in vivo damage. On the lateral PE condyle there is obvious evidence of 3rd body wear.	Medial damage track anteriorly with burnishing and a small amount of abrasion and scratching. Lateral condyle damage track central but slightly more anterior. Burnishing scratching and indentations. Looks like there has been third body wear.	Non-polished tray. A small amount of debris visible in fixation locking mechanism rim. Some small areas that have been burnished observed. Scratches assumed to be retrieval damage observed,	Scratches assumed to be retrieval damage observed. Burnishing observed on both condyles. .
<b>PFC12</b>	Definite damage tracks on both condyles and light scratches. In high flexion on medial condyle heavy damage. This corresponds to the medial PE observed damage. The heavy damage may	Pits, scratches and burnishing observed. Obviously, there has been third body damage here. Light damage more on the medial	Non-polished tray. Scratches assumed to be retrieval damage observed but no other damage.	Minimal amount of burnishing observed on both condyles

#### Appendix C: C290

	happen when there is low contact areas and high stress.	condyle than the lateral. Mainly burnishing.		
<b>PFC13</b>	Large scratch central along patella femoral articulation.	Much more macroscopically obvious damage than the rest of the group. Scratching and abrasion observed. Obvious third body damage. Would expect the femoral component to be damaged as well but it is not actually as severe as expected.	Polished tray. Debris observed in locking mechanism. Retrieval scratches observed.	Very minimal damage observed with light pitting in all sections.
<b>PFC14</b>	Very little damage at all. No obvious damage tracks.	Definite damage track on lateral condyle - burnishing pitting and scratching. A large scratch assumed to be retrieval damage on lateral condyle. Medial condyle definite damage track with burnishing and not exactly scratching or stippling but not burnishing.	Non-polished tray. Some stippling marks observed possibly from micromotion.	Stippling observed in a circular pattern.
<b>PFC15</b>	Damage tracks and light scratches observed. On the medial condyle there is a light scratch that corresponds to the PE damage. Although this is macroscopically visible it is not very deep. Lateral condyle shows damage tracks and retrieval damage scratches. This	More macroscopically visible damage particularly to the medial condyle. Some of the damage assumed to be from the retrieval process. Medial condyle pitting and burnishing. Abrasion to the edge of the medial condyle. Posterior deformation to the	Polished tray. A small area of damage observed on the tray by the screw hole assumed to be retrieval damage.	Two areas of burnishing observed on the outsides of both condyles

	component may have had lateral lift off and medial pivoting.	medial condyle. There may have been lateral component lift off and medial pivoting that has meant that the back edge of the femoral component has deformed the PE on the posterior of the medial condyle. Lateral condyle has an area centrally that has burnishing and also that strange not scratching nor stippling.		
<b>K+1</b>	Definite damage tracks on both condyles that correspond to the macroscopic PE damage. Light multidirectional scratching. Damage considered to be <i>in vivo</i> damage as the PE component is severely damaged with pits and gross material loss.	Medial condyle fully damaged with material loss around perimeter; pitting most severe in section 2. Lateral condyle area close to section 8 not damaged. Lateral condyle damage and material loss around posterior perimeter; area of no damage in section 4/5. Damage track would appear to indicate more a/p translation of the medial condyle.	Non-polished tray. Scratching and stripling and surface changes around the screws observed. On the lateral posterior aspect, a very small burnished area is observed that corresponds to the damage on the PE component backside. It would appear that 3rd body debris may have been in between the tibial and PE components.	Stippling was observed over the whole component. Deformation resulting from the tibial screw holes was observed in sections 2 and 6. Pitting and scratching were observed in section 6 and burnishing in section 1.
<b>K+2</b>	Definite damage tracks on both condyles. Light multidirectional scratching centrally on lateral and medial condyles. Not cemented. Heavy scratching in central	Severe damage anteriorly. Gross loss of material in sections 8 and 9. Area posteriorly where there is no damage at all. Lateral condyle has a big gouge and there is	Non-polished tray. A damage area of burnishing was observed where the femoral component had articulated with the tibial tray due	Stippling observed over the entire surface. A small deformation observed.

	ligament space where the PE completely wore through and there was articulation between the femoral and tibial component.	pitting and subsurface cracking and burnishing. Medial condyle has pitting, embedded debris, subsurface cracking and abrasion. Wear through to tibial tray meant articulation between femoral component and tibia.	to wear through of the PE. Slight stippling observed.	
<b>K+3</b>	A big scratch medial to correspond with embedded debris visible.	Severe damage on both medial and lateral condyles and in section 9. Pitting and delamination and abrasion all over component. Medial edge completely gouged away. Large embedded debris on medial condyle in section 7.	Non-polished tray. No evidence of damage observed.	Stippling observed over the entire component except section 4. Pitting observed in section 4. Deformation observed in sections 2 and 6 resulting from the tibial screw holes.
<b>K+4</b>	Area approx. 20mm x 5-10mm of damage where the medial condyle has articulated with the posterior edge of the tibial component due to PE wear through. Other moderate anterior posterior scratches visible on both condyles. Assumed retrieval damage on posterior lateral condyle.	Severe damage observed. Lateral condyle damage in central area. Medial condyle damage toward the posterior perimeter and PE wear through on posterior edge. Sections 8 undamaged. Section 4 / 5 medial anterior undamaged.	Non-polished tray. Burnishing observed on the medial posterior edge where the femoral component had articulated with the tibial tray due to wear through of the PE. A crack in the tibial tray was observed in this area.	Stippling observed over the entire component and burnishing observed posteriorly on both condyles in sections 2 and 6. Deformation observed in sections 2 and 6 where there was PE wear through.
<b>K+5</b>	Light AP scratching observed.	Not severely damaged but moderately damaged. Lateral condyle has the beginning signs of delamination but no gross material	Component not available for analysis.	Light stippling observed under both condyles, pitting observed in the central sections and

		loss. Medial condyle posteriorly has subsurface cracking.		deformation observed from the tibial screws.
<b>K+6</b>	On both condyles one single large scratch initially thought to be retrieval damage, but these scratches correspond with the areas of severe damage on the PE component.	Very large pit in section 1 matches with scratches on femoral component. Not severe damage all over the component. Lateral condyle posterior shows no or very little evidence of wear and machine marks on PE still visible. Section 2 and 1 large area of subsurface cracking and delamination with gross material loss. Possibly a large pit. Burnishing in section 1. Medial condyle anteriorly damaged with subsurface cracking delamination pitting and gross material loss. Embedded debris seen in section 5	Non-polished tray. Tibial component is not the same as the others. Looks possibly like it has been cast. No obvious damage observed.	Stippling observed in all but section 4. Deformation from screw holes only observed on lateral side. Burnishing observed posteriorly and laterally in section 6.
<b>K+7</b>	Medial condyle has two areas of large damage approx. 20 -25mm x 5-10mm where the femoral component has articulated with the tibial tray due to PE wear through. Also, light - moderate anterior posterior scratches with a thickness of approx. 1mm. Lateral	Severe damage and material loss from delamination and pitting all over the component with the exception of an area in section 8. Medial condyle has gross material loss and wear through of the PE in the posterior section 3 and 0. Section 9 severely damaged.	Non-polished tray. Heavy burnishing damage to the medial posterior edges from femoral component articulation due to PE wear through. Two areas highly burnished (one approx. 10mm x 2-3mm and one on the locking mechanism). The medial posterior	Severe damage observed with a quarter of section 2 and 5 missing and half of section 6 missing. On the surfaces that were present stippling was observed and deformations from the screw holes in the tibial component.

	condyle has heavy scratches with a thickness of approx. 1-2mm.	Lateral condyle posterior PE loss and just damaged.	locking flange has fractured and is not present.	
<b>K+8</b>	Light AP scratches observed on the lateral condyle (some deeper and larger scratches also observed). Area of scratching on posterior medial condyle. PE is damaged and worn away and there is a large pit on the medial condyle which corresponds with these observed femoral scratches.	Component not fully or severely damaged. Two damage tracks on each condyle. Medial condyle damage track is on the anterior and medial edge with section 3 and most of section 2 only showing very light burnishing damage. Pitting, burnishing and subsurface cracking are visible on in section 0 and 1. On the lateral condyle the damage track is towards the centre line and posteriorly (i.e. sections 4 and 7 and the lateral aspect of 9). Pitting, burnishing and subsurface cracking and delamination are visible on the lateral condyle. Section 5 shows burnishing and the start of pitting.	Non-polished tray. Different type of tibial component to the others in this group. Light burnishing observed over both condyles except an area approx. 7-8mm x 20mm that appears less damaged on lateral condyle.	Stippling observed in all sections.
<b>K+9</b>	Deep AP scratches causing a “wavy” appearance on the medial side.	On the lateral condyle the damage is all over the condyle but more on the posterior central sections (i.e. 3 and 2). On the medial condyle the damage is on the outer perimeter and across the AP line. There is pitting abrasion	Non-polished tray. No apparent damage.	Stippling observed in all sections apart from section 4 where pitting was observed. Deep deformations from the screw holes observed. Deformation observed on the lateral perimeter where the PE has over hung the tibial tray.

		burnishing and subsurface cracking and delamination.		Burnishing observed posteriorly and medially.
<b>K+10</b>	Very light scratching on both condyles. Definite damage tracks. Some deeper scratches may have been discounted because they were initially thought to be retrieval damage and however, they could be <i>in vivo</i> damage.	Lateral condyle relatively undamaged. A large (approx. 3-4mm diameter) pit and posteriorly some subsurface cracking which would lead to delamination. Medial condyle more grossly damaged specifically posteriorly. Delamination has occurred, and the underneath surface is pitted and abraded.	Non-polished tray. No apparent damage.	Stippling observed on both condyles. Burnishing observed posteriorly in sections 2 and 6 and deformation observed from the screws on the tibial tray. On the medial condyle a crack was observed.
<b>K+11</b>	Lots of deep long AP scratches making the condyles appear "wavy". Visibly damaged.	Lots of embedded debris. Pitting and delamination and abrasion on both condyles. Sections 8 and 9 relatively undamaged.	Non-polished tray. Light burnishing in a rotational direction observed.	Macroscopically more severely damaged than others in the group. Medial edge deformation observed where the PE has overhung the tibial tray. Area of burnishing posteriorly. Deformation from screw holes observed. Stippling observed over entire surface.
<b>K+12</b>	Light scratching on lateral condyle. Gross damage on medial condyle. Large damage scar from articulation of the medial condyle with the tibial tray due to PE wear through.	Missing half of section 0 and 2 and the whole of section 3. Hood score will not be accurate. Severely damaged in every other section. Area on the lateral condyle	Non-polished tray. On the medial condyle a burnished damage scar (approx. 6mm in diameter) observed resulting from articulation of the femoral component and the tibial component due to PE wear	Section 6 missing. Stippling observed over the other 5 sections. Deformation from the screw hole observed in section 2 and an area of burnishing observed. Lateral condyle observed to have an area of no



		appears undamaged. Sections 8 and 9 are also severely damaged.	through. Burnishing and cracking of the medial posterior flange observed.	damage and the manufacturing machine marks are still visible.
<b>K+13</b>	Light femoral scratches. No severe damage at all. Very light damage tracks	Minimal damage. Lateral condyle surface deformation wear scar. Medial condyle very light damage.	Non-polished tray. No apparent damage	Light stippling observed on both condyles. Burnishing observed posteriorly on both condyles. Deformations from tibial screw holes observed.
<b>K+14</b>	Light AP scratches and then on the lateral condyle multidirectional scratches that are possibly removal damage but then there are a lot of scratches on the PE component on the lateral PE condyle too	Not severe gross material loss but interesting damage pattern. On the medial condyle on the medial perimeter the damage is burnishing and subsurface cracking leading to some delamination. The lateral condyle has definite AP scratches unlike any seen in this group. On the lateral condyle perimeter there is an area of subsurface cracking	Non-polished tray. No apparent damage	Light stippling observed on both condyles. Deformations from tibial screw holes observed.
<b>K+15</b>	Light AP scratches and two areas one on each condyle of burnishing from the femoral component articulating with the tibial tray posteriorly due to PE wear through.	Severely damaged on both condyles with loss of material due to delamination. On the medial condyle the damage track is all over and on the lateral, it is concentrated posteriorly	Non-polished tray. Burnishing of the posterior flange on the lateral side and the beginnings of burnishing on the medial flange in the same area observed. This burnishing is from the femoral component articulating with the	Stippling observed and burnishing observed anteriorly laterally and posteriorly medially. Severe deformation observed on the lateral posterior condyle unlike any other in the group. Deformation from the screw holes of the tibial

			tibial component due to wear through of the PE.	component observed. Loss of PE material on both condyles.

**Appendix D: Surface Topographical Analysis of Explanted UKRs  
Results**

The following table is included in this Appendix:

Table D1: Macroscopic Visual Assessment of Explanted UKRs

*Blank page*

**Table D1: Macroscopic Visual Assessment of Explanted UKRs**

	Femoral component	PE component - Proximal articular surface	Tibial component	PE component - Distal backside surface
UKR 1 Left Medial	<b><u>Zimmer Uni-compartmental High Flex Knee.</u></b> CoCr alloy femoral component. Femoral component showed little very macroscopically visible damage. No burnished damage tracks observed only a very few light scratches and tiny indentations. Cemented	Fixed PE component. Defined load area anteriorly (approx. 25mm x 15mm) with surface deformation, burnishing, some scratching and very tiny (<1mm) pits observed within. Two small (5mm x 10mm) areas of the beginning of abrasion observed posteriorly. Some light scratches observed. No subsurface cracking or delamination observed. Some retrieval damage observed.	Fixed PE and tibial component. Flange design of fixation. Cemented.	x
UKR 2 Left Medial	<b><u>Zimmer Uni-compartmental High Flex Knee.</u></b> CoCr alloy femoral component. Femoral component showed indentations and light scratching anteriorly and proximally which will have been from articulation with a patella either replacement or natural. Moderate scratching was also observed in sections 2 and 3. Posteriorly and distally there was a	Fixed PE component. Defined load area (approx. 15mm x 25mm) centrally with surface deformation, burnishing, scratching and pitting within. Scratching was observed all over the component. No subsurface cracking or delamination was observed.	Fixed PE and tibial component. Flange design of fixation. Cemented.	x

	small amount of gouging. Cemented.			
<b>UKR 3</b> <b>Right</b> <b>Lateral or</b> <b>Left Medial</b>	<b><u>Zimmer Uni-compartmental High Flex Knee.</u></b> CoCr alloy femoral component. Femoral component very minimally damaged with only a few light scratches. Some deeper scratches were observed but these were assumed to be retrieval damage. No burnished damage tracks. Cemented.	Fixed PE component but retrieval separated. Definite load area (approx. 18mm x 23mm) more anteriorly with very light scratching and burnishing observed within. Two larger deeper scratches assumed to be retrieval damage observed. A small area of abrasion on the anterior edge observed. No subsurface cracking or delamination observed.	Fixed PE and tibial component but retrieval separated. Non-polished tibial tray. Burnishing observed giving evidence of micromotion. Flange design of fixation. Cemented.	PE component backside showed lightly burnished area posteriorly nothing anteriorly and a tiny amount of burnishing posteriorly.
<b>UKR 4</b> <b>Right</b> <b>Lateral or</b> <b>Left Medial</b>	<b><u>Zimmer Uni-compartmental High Flex Knee.</u></b> CoCr alloy femoral component. Femoral component showed some light scratches. Two large deeper scratches correspond to PE damage were observed. Cemented.	Fixed PE component. Two large damage areas (3-4mm x 2mm) observed that correspond to femoral component damage observed. Definite load area (approx. 30mm x 20mm) observed on outside of component with pitting, burnishing and scratching observed within. A small area (approx. 6/7mm x 5mm) of surface deformation and burnishing observed anteriorly to the inside edge. No subsurface cracking or delamination observed.	Fixed PE and tibial component. Flange design of fixation. Cemented.	x

<b>UKR 5</b>  <b>Right</b> <b>Medial</b>	<b><u>Zimmer Uni-compartmental High Flex Knee.</u></b> CoCr alloy femoral component. Femoral component showed an area of damage on the proximal section 1 which was assumed to be retrieval damage. Minimal macroscopic damage observed centrally. Small area of gouging observed in section 4 considered in vivo damage as it corresponds to scratches observed on the PE component. Cemented.	Fixed PE bearing. Load area (approx. 15mm x 25mm) observed posteriorly and centrally with burnishing and scratching observed within the load area. No subsurface cracking or delamination observed.	Fixed PE bearing. Tibial component fixation using three pegs. Cemented.	x
<b>UKR 6</b>  <b>Left Medial</b>	<b><u>Zimmer Uni-compartmental High Flex Knee.</u></b> CoCr alloy femoral component. Femoral component showed assumed retrieval damage in section 1. Very minimal <i>in vivo</i> damage was observed except in section 3 there was a light scratch and three indentations clearly defined. Cemented.	Fixed PE bearing but retrieval separated. Load area (approx. 15mm x 25mm) observed anteriorly and towards the outside edge of the component. Burnishing and pitting were observed within this load area. Burnishing was also observed over the posterior half of the component. Posteriorly an area (10mm x 10mm) of abrasion was observed. No subsurface cracking or delamination was observed. Retrieval damage was also observed.	Fixed PE and tibial component but retrieval separated. Non-polished tibial tray. Retrieval damage observed. Flange design of fixation. Cemented.	PE component backside showed area of light burnishing that is underneath the defined load area on the articular surface.

<b>UKR 7</b> <b>Right</b> <b>Medial</b>	<b><u>Zimmer Uni-compartmental High Flex Knee.</u></b> CoCr alloy femoral component. Femoral component showed definite burnished damage track. Gouging damage observed in section 4 assumed to be retrieval damage as no corresponding damage to the PE component. Cemented.	Fixed PE bearing. Load area (approx. 15mm x 25mm) observed posteriorly and centrally. Burnishing and very light scratching observed in the load area. Other observed scratches assumed to be retrieval damage. No surface deformation or delamination observed.	Fixed PE bearing. Tibial component fixation using three pegs. Cemented.	x
<b>UKR 8</b> <b>Right</b> <b>Medial</b>	<b><u>Zimmer Uni-compartmental High Flex Knee.</u></b> CoCr alloy femoral component. Femoral component showed light anterior posterior scratching centrally in sections 2, 3 and posteriorly in high flexion in section 4. Gouging damage observed in section 4 that corresponds to an area of damage on the PE component. It may be that the femoral component tracked over the anterior edge of the PE to cause this damage. Cemented.	Fixed PE bearing. Load area (approx. 15mm x 25mm) observed centrally. Burnishing, scratching and pitting observed within the load area. Area anteriorly that corresponds to damage on femoral component and surface deformation, scratching and burnishing is observed in this small area. It would seem that this knee was loaded centrally and then anteriorly in full flexion.	Fixed PE bearing. Tibial component fixation using three pegs. Cemented.	x
<b>UKR 9</b> <b>Right</b> <b>Lateral or</b> <b>Left Medial</b>	<b><u>Zimmer Uni-compartmental High Flex Knee.</u></b> CoCr alloy femoral component. Femoral component showed lightly burnished damage	Fixed PE bearing. Load area (approx. 15mm x 25mm) observed anteriorly and towards the outside edge. Burnishing and a small amount of light pitting observed in	Fixed PE and tibial component but retrieval separated. Non-polished tibial tray. Pits observed that correspond to damage observed on PE component backside.	PE component backside showed area of light burnishing that is underneath the defined load area on the articular surface. Pitting was also observed in the location



	tracks and light anterior posterior scratching. Cemented.	the load area. Some retrieval damage scratches observed. No subsurface cracking or delamination observed.	Retrieval damage observed. Tibial component fixation using three pegs Cemented.	corresponding to the observed pits on the tibial component.
<b>UKR 10</b> <b>Right Medial or Left Lateral</b>	<b><u>Zimmer Uni-compartmental High Flex Knee.</u></b> CoCr alloy femoral component. Femoral component showed retrieval damage in section 1. A burnished damage track was observed on the inside edge of the femoral component in sections 2 and 3. An indentation (approx. 1mm in length) was observed in section 4 corresponding to a pit observed in the PE component. Cemented.	Fixed PE bearing. Load area (approx. 15mm x 25mm) centrally but on the very outside edge of the component. Burnishing, pitting and deformation were observed in the load area. A pit was observed anteriorly of the load area (approx. 2mm in length). No subsurface cracking or delamination observed.	Fixed PE bearing. Tibial component fixation using three pegs. Cemented.	x
<b>UKR 11</b> <b>Left Medial</b>	<b><u>Oxford Biomet.</u></b> CoCr alloy femoral component. Definite damage tracks (burnished) and one or two larger scratches (gouging) that appear to have been from embedded debris in the PE. Cemented.	Mobile PE component. Large pits approx. 1-2-3mm across, some scratching and burnishing over the whole surface. No evidence of subsurface cracking / delamination or surface deformation.	Polished tibial component with damage tracks visible. Some retrieval scratches. Cemented.	Backside has an area of damage posteriorly and medially where there has been definite removal of material. There is also some pitting.
<b>UKR 12</b> <b>Right Medial</b>	<b><u>Oxford Biomet.</u></b> CoCr alloy femoral component. Femoral component has burnished wear tracks and lots of light	Mobile PE component. Damage to the anterior edge of the component. There is material loss across the front edge, but it is unclear as to the mechanism of	Polished tibial component. Light scratching posteriorly. Pitting observed on the anterior edge. Cemented.	Backside has very light scratching and a tiny deformation from overhanging the tibial component

	multidirectional scratches in section 4. Cemented.	<p>the damage. It does not appear to be retrieval damage but there is no corresponding femoral component damage. It may be that the femoral component slipped off the PE bearing during flexion as the component may not have covered the entire natural femoral condyle.</p> <p>Over the PE AS there are large pits approx. 1-2mm across. Scratching, burnishing and surface deformation were observed.</p>		anteriorly. Minimal damage comparatively.
<b>UKR 13</b> <b>Right</b> <b>Medial</b>	<b><u>Oxford Biomet.</u></b> CoCr alloy femoral component. Femoral component has light burnished damage track and some light scratching. Cemented.	Mobile PE component. Up to about 10 large pits (2mm diameter x 1). Anterior and posterior subsurface cracking on edge no deamination. Large pit visible centrally and abrasion on the edge to the central ligament space. Surface deformation to the edge.	Polished tibial component. Very light burnished damage tracks and scratching. A large (1mm diameter) pit anteriorly. Cemented.	Minimal area of abrasion to central edge. Three small pits less than 1mm diameter and one larger (1mm length) pit. Surface deformation to posterior edge.
<b>UKR 14</b> <b>Right</b> <b>Medial or</b> <b>Left</b> <b>Lateral</b>	<b><u>Oxford Biomet.</u></b> CoCr alloy femoral component. Femoral component very light burnished damage tracks and light scratches. Cemented.	Mobile PE component. Very minimal damage. Burnishing observed approx. 80% of the surface and approx. 20 small (less than 1mm diameter) pits and 1 larger pit (approx. 1mm x 0.5mm) recorded. No surface deformation,	Large polished cemented tibial component. Light AP scratching observed over the whole component. Some assumed retrieval damage observed. Cemented.	Light scratching all over the component and a few areas of abrasion which can only be recorded in the backside damage as burnishing. One pit approx. 1mm diameter observed anteriorly.

		subsurface cracking or delamination.		
<b>UKR 15</b> <b>Right</b> <b>Medial</b>	<b>Oxford Biomet.</b> CoCr alloy femoral component. Femoral component showed very light burnished damage track and very light scratching. Cemented	Mobile PE component. Minimal burnishing and pits observed. No subsurface cracking, delamination or surface deformation observed.	Polished tibial tray. Light scratches observed considered to be retrieval damage. Flange fixation. Cemented.	Very light area of light scratching and slight burnishing observed anteriorly and on the inside edge posteriorly.
<b>UKR 16</b> <b>Left Medial</b>	<b>“Sled” Link.</b> CoCr alloy femoral component with two fixation pegs. Complete wear through of the PE led to articulation of the femoral component with the underlying tibial component. Macroscopically visible damage to femoral component. No gouging from third body debris but areas of metal on metal recorded as gouging. Also, areas of burnishing anteriorly. Cemented. Femoral component roughness did not cause the PE damage. The roughness is a result of the PE damage and wear through. Cemented.	Fixed PE. Complete wear through of the PE (Delamination and subsurface cracking. Abrasion and surface deformation).	Non-polished component. Evidence of material loss from tibial component centrally and posteriorly. Large (15mm x 10mm) area of burnished tibial tray and crescent shaped burnishing (5mm x 35mm) where the femoral component articulated after PE wear through. Cemented.	Majority of PE component missing. Areas of stippling visible on remaining section.
<b>UKR 17</b> <b>Unknown</b>	<b>Other UKR.</b> No identifying details available. Very minimal damage observed. Very light burnished	Mobile PE bearing with conforming concave articular and backside geometries. Burnished, pitted and scratched all over. Surface deformation observed anteriorly	Polished convex component. Flange fixation. Pits and scratches observed that correspond to the	Mobile PE bearing with conforming concave geometry. Damage observed to the backside similar to damage observed to the PE articular surface. Burnishing, pits

	damage tracks and light scratching.	where it would appear that the femoral component has overridden the PE component in full flexion.	PE component backside damage observed. Cemented.	and scratches observed all over the surface. Posteriorly two areas of abrasion (which were recorded as burnishing in the PE BDS) where the PE component had articulated with the cement mantle.

## **Appendix E: Surface Topographical Analysis of Explanted Knee Prostheses with OxZr femoral components**

The following table is included in this Appendix:

Table E1: Macroscopic Visual Assessment of Explanted Knee Prostheses with OxZr and CoCr femoral components

*Blank page*

**Table E1: Macroscopic Visual Assessment of Explanted TKRs and UKRs with OxZr and CoCr femoral components**

	Femoral component	PE component - Proximal articular surface	Tibial component	PE component - Distal backside surface
<b>OxZr T1 TKR RIGHT</b>	Cruciate retaining design OxZr femoral component. Minimal damage was observed on the femoral component. A very slight burnished damage track on the medial condyle and a few indentations were observed. On the medial edge of the ligament space, gouging was observed, and it would appear that the OxZr layer had been removed as there was a colour change. Cemented.	Fixed PE component, cruciate retaining design. Very minimal damage observed. Burnishing observed centrally and anteriorly in the lateral condyle. Light burnishing observed centrally on the medial condyle. An area of burnishing observed in section 8 and an area of abrasion observed in the central corner of the posterior lateral condyle. These two damage observations are consistent with the damage seen on the femoral condyle. It is plausible to suggest that this TKR was rotation unsymmetrically leading to rotation about the lateral condyle and unintended articulation of the lateral femoral condyle on the posterior aspect of the PE and the medial condyle on the central ligament area of the PE.	Polished tibial tray. Imprints of the manufacturer's markings from the PE observed. Cemented.	Fixed PE component. Minimal damage observed only a very small amount of pitting on the edges in sections 1 and 5.

<b>OxZr T2 TKR RIGHT</b>	Posterior stabilised design OxZr femoral component. This is a revision component with a long femoral stem. Very little damage observed apart from a small area of gouging on the medial edge of the ligament space and a few small indentations and light scratches. The deep scratches posteriorly were not considered to be <i>in vivo</i> damage but considered to be retrieval damage. Cemented.	Fixed PE component, posterior stabilised design. Burnishing observed on the lateral condyle (approx. 20mm x 30mm). More severe burnishing observed in the medial condyle centrally and also anteriorly toward the section 8. From the damage tracks it is plausible to suggest that the femoral component was pivoting and rotation about the lateral condyle. Damage was observed to the posterior post; pitting to the anterior base of the post, burnishing to the posterior top of the post and surface deformation behind the post.	Polished tibial tray. A few (<5) small pits or indentations observed. Revision component with long tibial stem. Cemented.	Minimal damage observed on the fixed PE component backside surface. Very light burnishing in sections t 2 5 and 6 not even enough to remove the machine marks.
<b>OxZr T3 TKR LEFT</b>	Posterior stability design OxZr femoral component. This is a revision component with a long femoral stem. Some scratches observed on the lateral condyle of the femoral component. Gouging damage to the posterior was observed in sections 4 and 8. This is thought to be retrieval damage given that the PE component is not severely damaged. Cemented.	Fixed PE component, posterior stabilised design. Burnishing, pitting and scratching observed over both condyles, posteriorly more than anteriorly. The scratching was in a circular pattern indicating rotation about the post. There was a small amount of burnishing and deformation to the posterior edge of the post.	Polished tibial tray. No <i>in vivo</i> damage recorded, or retrieval scratches observed. Revision component with long tibial stem. Cemented.	Ever so light pitting around the edges in section 3 and 5. Very light burnishing in 2 4 and 6 - the machine marks have not even been removed.



<b>CoCr T1 TKR RIGHT</b>	Very little damage observed. Very light central damage tracks on both condyles macroscopically visible more medially than laterally. However, on the lateral condyle on the edge is a small set of scratches that correspond to the scratching on the PE component. Also, on the medial condyle at the very posterior aspect during full flexion there is a small area of damage which corresponds to a small area of damage on the PE.	On the lateral condyle heavy scratching on the anterior edge corresponding to damage on the femoral component is observed. Damage track lightly defined on both condyles. Burnishing observed. Medially the component is lightly burnished however on the very posterior aspect there is an area of damage corresponding to the damage on the femoral component. Very slight subsurface cracking and slight deformation observed.	Polished tray. There are scratches observed that are assumed to be from retrieval.	Two very slight areas of burnishing underneath the condyles observed.
<b>CoCr T2 TKR LEFT</b>	Lateral condyle shows heavy AP scratches. Medial condyle shows light AP scratches. Heavy scratching on lateral condyle assumed to be retrieval damage. Some further damage on medial condyle that is considered to be in vivo damage	Very minimal damage. Some scratches on the lateral perimeter assumed to be from retrieval damage. On lateral condyle distinct damage scar central AP and slightly more anterior of the midline consisting of burnishing and very light scratching. Medial condyle damage scar central AP and slightly more posterior of the midline consisting of burnishing only.	Polished tray. Some scratches assumed to be retrieval damage observed. Also, areas of damage or possibly a film of material visible.	Lots of damage observed anteriorly assumed to be from removal of PE from tibial tray fixation. Condyles still observed to have machining marks. Only burnishing observed on the medial side.

<b>CoCr T3 TKR LEFT</b>	Damage tracks and light scratches observed. On the medial condyle there is a light scratch that corresponds to the PE damage. Although this is macroscopically visible it is not very deep. Lateral condyle shows damage tracks and retrieval damage scratches. This component may have had lateral lift off and medial pivoting.	More macroscopically visible damage particularly to the medial condyle. Some of the damage assumed to be from the retrieval process. Medial condyle pitting and burnishing. Abrasion to the edge of the medial condyle. Posterior deformation to the medial condyle. There may have been lateral component lift off and medial pivoting that has meant that the back edge of the femoral component has deformed the PE on the posterior of the medial condyle. Lateral condyle has an area centrally that has burnishing and also that strange not scratching nor stippling.	Polished tray. A small area of damage observed on the tray by the screw hole assumed to be retrieval damage.	Two areas of burnishing observed on the outsides of both condyles
<b>OxZr U1 UKR Right Medial</b>	OxZr Femoral component. There are light single scratches observed that are considered to be retrieval damage. In section 4 in high flexion there is an area that is thought to be either <i>in vivo</i> damage or possibly damage that occurred during implantation. This area of damage corresponds with the PE damage and therefore is	Fixed PE bearing. Load area (approx. 15mm x 20mm) observed posteriorly with burnishing and heavy scratching within. Retrieval damage scratches are observed. It is possible that the femoral component was damaged during implantation and resulted in this damage pattern on the PE component.	Fixed PE bearing separated at revision from tibial tray. Area of burnishing observed posteriorly. Cemented.	Area of burnishing observed posteriorly under load area and corresponding to damage observed on tibial tray.

	not considered to be retrieval damage. Cemented.			
<b>OxZr U2 UKR Right Lateral or Left Medial</b>	OxZr Femoral component. Heavy scratching observed in sections 2 and 3. Some gouging in section 3. Cemented.	Fixed PE bearing. Central load area (approx. 15mm x 20mm) observed with burnishing within the load area. Anterior to the load are is an area (approx. 15mm x 8mm) of heavy deep scratching observed that corresponds to the scratching seen on the femoral component.	Fixed PE bearing separated at revision from tibial tray. Cemented.	Area of burnishing observed posteriorly under load area and corresponding to damage observed on tibial tray.
<b>CoCr U1 UKR Left Medial</b>	CoCr alloy femoral component. Femoral component showed little very macroscopically visible damage. No burnished damage tracks observed only a very few light scratches and tiny indentations. Cemented	Fixed PE component. Defined load area anteriorly (approx. 25mm x 15mm) with surface deformation, burnishing, some scratching and very tiny (<1mm) pits observed within. Two small (5mm x 10mm) areas of the beginning of abrasion observed posteriorly. Some light scratches observed. No subsurface cracking or delamination observed. Some retrieval damage observed.	Fixed PE and tibial component. Flange design of fixation. Cemented.	x
<b>CoCr U2 UKR Left Medial</b>	CoCr alloy femoral component. Femoral component showed indentations and light scratching anteriorly and proximally which will have been from articulation with a	Fixed PE component. Defined load area (approx. 15mm x 25mm) centrally with surface deformation, burnishing, scratching and pitting within. Scratching was observed	Fixed PE and tibial component. Flange design of fixation. Cemented.	x

	patella either replacement or natural. Moderate scratching was also observed in sections 2 and 3. Posteriorly and distally there was a small amount of gouging. Cemented.	all over the component. No subsurface cracking or delamination was observed.		
<b>CoCr U3 UKR Right Lateral or Left Medial</b>	CoCr alloy femoral component. Femoral component very minimally damaged with only a few light scratches. Some deeper scratches were observed but these were assumed to be retrieval damage. No burnished damage tracks. Cemented.	Fixed PE component but retrieval separated. Definite load area (approx. 18mm x 23mm) more anteriorly with very light scratching and burnishing observed within. Two larger deeper scratches assumed to be retrieval damage observed. A small area of abrasion on the anterior edge observed. No subsurface cracking or delamination observed.	Fixed PE and tibial component but retrieval separated. Non-polished tibial tray. Burnishing observed giving evidence of micromotion. Flange design of fixation. Cemented.	PE component backside showed lightly burnished area posteriorly nothing anteriorly and a tiny amount of burnishing posteriorly.
<b>CoCr U4 UKR Right Lateral or Left Medial</b>	CoCr alloy femoral component. Femoral component showed some light scratches. Two large deeper scratches correspond to PE damage were observed. Cemented.	Fixed PE component. Two large damage areas (3-4mm x 2mm) observed that correspond to femoral component damage observed. Definite load area (approx. 30mm x 20mm) observed on outside of component with pitting, burnishing and scratching observed within. A small area (approx. 6/7mm x 5mm) of surface deformation and burnishing observed anteriorly to the inside	Fixed PE and tibial component. Flange design of fixation. Cemented.	x

		edge. No subsurface cracking or delamination observed.		
<b>CoCr U5 UKR Right Medial</b>	CoCr alloy femoral component. Femoral component showed an area of damage on the proximal section 1 which was assumed to be retrieval damage. Minimal macroscopic damage observed centrally. Small area of gouging observed in section 4 considered in vivo damage as it corresponds to scratches observed on the PE component. Cemented.	Fixed PE bearing. Load area (approx. 15mm x 25mm) observed posteriorly and centrally with burnishing and scratching observed within the load area. No subsurface cracking or delamination observed.	Fixed PE bearing. Tibial component fixation using three pegs. Cemented.	x
<b>CoCr U6 UKR Left Medial</b>	CoCr alloy femoral component. Femoral component showed assumed retrieval damage in section 1. Very minimal <i>in vivo</i> damage was observed except in section 3 there was a light scratch and three indentations clearly defined. Cemented.	Fixed PE bearing but retrieval separated. Load area (approx. 15mm x 25mm) observed anteriorly and towards the outside edge of the component. Burnishing and pitting were observed within this load area. Burnishing was also observed over the posterior half of the component. Posteriorly an area (10mm x 10mm) of abrasion was observed. No subsurface cracking or delamination was observed. Retrieval damage was also observed.	Fixed PE and tibial component but retrieval separated. Non-polished tibial tray. Retrieval damage observed. Flange design of fixation. Cemented.	PE component backside showed area of light burnishing that is underneath the defined load area on the articular surface.

<b>CoCr U7 UKR Right Medial</b>	CoCr alloy femoral component. Femoral component showed definite burnished damage track. Gouging damage observed in section 4 assumed to be retrieval damage as no corresponding damage to the PE component. Cemented.	Fixed PE bearing. Load area (approx. 15mm x 25mm) observed posteriorly and centrally. Burnishing and very light scratching observed in the load area. Other observed scratches assumed to be retrieval damage. No surface deformation or delamination observed.	Fixed PE bearing. Tibial component fixation using three pegs. Cemented.	x
<b>CoCr U8 UKR Right Medial</b>	CoCr alloy femoral component. Femoral component showed light anterior posterior scratching centrally in sections 2, 3 and posteriorly in high flexion in section 4. Gouging damage observed in section 4 that corresponds to an area of damage on the PE component. It may be that the femoral component tracked over the anterior edge of the PE to cause this damage. Cemented.	Fixed PE bearing. Load area (approx. 15mm x 25mm) observed centrally. Burnishing, scratching and pitting observed within the load area. Area anteriorly that corresponds to damage on femoral component and surface deformation, scratching and burnishing is observed in this small area. It would seem that this knee was loaded centrally and then anteriorly in full flexion.	Fixed PE bearing. Tibial component fixation using three pegs. Cemented.	x
<b>CoCr U9 UKR Right Lateral or Left Medial</b>	CoCr alloy femoral component. Femoral component showed lightly burnished damage tracks and light anterior posterior scratching. Cemented.	Fixed PE bearing. Load area (approx. 15mm x 25mm) observed anteriorly and towards the outside edge. Burnishing and a small amount of light pitting observed in the load area. Some retrieval damage scratches observed. No	Fixed PE and tibial component but retrieval separated. Non-polished tibial tray. Pits observed that correspond to damage observed on PE component backside. Retrieval damage observed. Tibial	PE component backside showed area of light burnishing that is underneath the defined load area on the articular surface. Pitting was also observed in the location corresponding to the observed pits on the tibial component.

		subsurface cracking or delamination observed.	component fixation using three peps Cemented.	
<b>CoCr U10 UKR Right Medial or Left Lateral</b>	CoCr alloy femoral component. Femoral component showed retrieval damage in section 1. A burnished damage track was observed on the inside edge of the femoral component in sections 2 and 3. An indentation (approx. 1mm in length) was observed in section 4 corresponding to a pit observed in the PE component. Cemented.	Fixed PE bearing. Load area (approx. 15mm x 25mm) centrally but on the very outside edge of the component. Burnishing, pitting and deformation were observed in the load area. A pit was observed anteriorly of the load area (approx. 2mm in length). No subsurface cracking or delamination observed.	Fixed PE bearing. Tibial component fixation using three peps. Cemented.	x

*Blank page*



## **Appendix F: Smith, S., Kennard E. and Joyce T.J. Biotribology 2018**

Within this appendix is included the manuscript for the publication:

Smith S. L., **Kennard E.** and Joyce T.J. *Shoulder Simulator Wear Test of Five Contemporary Total Shoulder Prostheses with Three Axes of Rotation and Sliding Motion* Biotribology, 2018 (13): 36-41 [32] (manuscript included in Appendix F)

As noted on page 5 of Chapter 1 Introduction, this thesis is submitted in my legal married name Emma Ritchie, however my authored publications are in my maiden name Emma Kennard.

*Blank page*

**TITLE:** Shoulder Simulator Wear Test of Five Contemporary Total Shoulder Prostheses with Three Axes of Rotation and Sliding Motion

**AUTHORS:** Simon L. Smith\*, Emma Kennard\*, Thomas J. Joyce\*

\*Bioengineering Group, School of Engineering, Newcastle University, Stephenson Building, Newcastle upon Tyne, NE1 7RU, England, United Kingdom.

## **ABSTRACT**

Shoulder joint replacement generally utilizes ultra-high molecular weight polyethylene (UHMWPE) as a bearing surface. Long term survival of such implants is recognized to be limited by wear of the UHMWPE. Commercially available JRI 42mm diameter VAIOS Total shoulders were wear tested in diluted bovine serum for five million cycles in a unique Shoulder Wear Simulator. Five Total shoulders were subject to rotational and translational motion, and loading, to replicate the “Mug to Mouth” activity of daily living. A sixth Total shoulder was subject to loading only in a control station. Wear was measured gravimetrically, and surface roughness was measured with a non-contacting profilometer. Mean wear rate of the UHMWPE components was  $21.5 \pm 5.4 \text{ mm}^3/\text{million cycles}$ . The humeral heads roughened, from  $19 \pm 3 \text{ nm Sa}$  to  $43 \pm 13 \text{ nm Sa}$  over the five million cycles of the test, while the UHMWPE glenoid components became smoother, from  $959 \pm 230 \text{ nm Sa}$  to  $77 \pm 17 \text{ nm Sa}$ . This is the first reported wear test of multiple samples of a commercially available Total shoulder in a dedicated shoulder simulator.

**KEYWORDS:** Shoulder simulator; Total shoulder prostheses; Wear test; Polyethylene.

## 1. INTRODUCTION

Shoulder joint replacement (SJR) is the third most common orthopaedic joint replacement after hip and knee joint replacement in England and Wales [1], and data suggests that primary SJR is growing exponentially [2,3]. There are two main types of SJR. Total shoulders are anatomically correct and typically have differing humeral and glenoid component spherical diameters allowing both rotation and sliding of the joint. Reverse shoulders are anatomically inverted and have similar humeral and glenoid diameters giving a conforming geometry, akin to ball and socket joints, and are intended to operate with a largely rotational motion. Most SJRs generally employ a Cobalt Chromium (CoCr) component rubbing against ultra-high molecular weight polyethylene (UHMWPE) as an articulation.

It is recognized that implants using UHMWPE are limited in their longevity by wear of the UHMWPE and the body's reaction to UHMWPE wear debris [4]. Wear of the polyethylene glenoid component elicits an osteolytic response to the wear particles, leading to aseptic loosening of the joint. This has been established through numerous studies of Total shoulders, spanning many years. A study in 1999 [5] examined the membranes surrounding Total SJR revised for aseptic loosening associated with osteolysis and found UHMWPE wear particles. A subsequent study in 2001 of 39 Total shoulder glenoid components found that 97.2% were loose [6]. A review published in 2008 recognized that glenoid component failure was the most common complication in Total SJR [7].

To investigate SJR wear in vitro, the Newcastle Shoulder Wear Simulator was designed, commissioned and validated [8,9]. It is the first multi-station shoulder simulator capable of applying physiological motion in three axes with physiological loading. It is fully programmable allowing it to reproduce shoulder activities of daily living (ADLs). For example, lifting an object to head height, or drinking from a mug [10].

In a previous study, the Newcastle Shoulder Wear Simulator was used to wear test commercially available JRI Orthopaedics 42mm diameter Reverse VAIOS shoulders using three axes of physiological motion with physiological loading [9]. The loads and motions associated with the “mug to mouth” activity of daily living were applied and a

wear rate of 14.3mm<sup>3</sup>/million cycles was measured [9]. However, total shoulders are designed to allow the translational motion seen in the natural glenohumeral joint [11]. In the current study, in addition to applying the loads and motions associated with “mug to mouth”, a translational sliding motion was therefore added to the simulator to wear test commercially available JRI Orthopaedics 42mm diameter Total VAIOS shoulders (see Fig. 1).



Figure 1. JRI Orthopaedics Total VAIOS shoulder Joint Replacement. To the upper left is the UHMWPE glenoid component with its titanium backing. To the right is the humeral component, with the CoCr head atop a titanium stem

Previous shoulder simulators [12–16] offered limited statistical value having been single station machines. Other Total shoulder implant wear tests have employed knee simulators [17,18] with limited ranges of motion compared to those available at the human glenohumeral joint. Nevertheless, it is worth considering the results of previous Total shoulder wear tests.

A single station test machine was used to apply motion in the abduction- adduction axis alone [13]. Such simplification of motion to one axis [19], or application of a linear wear path [20], has been shown to produce negligible wear levels in UHMWPE hip joints and therefore give non-clinically relevant results. This same single station test machine was also used in a later study [15] and the results were inconsistent between the studies. Geary et al. [14] used a different single station machine with

two axes of motion to wear test Total shoulders. However, the joints were mounted in Sawbone which prevented gravimetric wear measurement.

Dieckmann et al. [16] used a single station simulator to wear test a 54mm diameter commercially available (Capica, Implantcast) Titanium Nitride (TiN) coated titanium humeral head against an UHMWPE glenoid. The simulator featured two axes of applied motion, dynamic loading, and a third axis which allowed longitudinal motion resisted by a spring. The maximum translational displacement was given as 'about $\pm 0.7$ ' without units. After 5 million cycles, average wear of the glenoid was 9.9mm<sup>3</sup>/million cycles when converted to a mean volumetric wear rate. An AMTI knee simulator was used to test 48mm diameter CoCr humeral components against UHMWPE glenoid components with 'abduction-adduction rotation', sliding translation and a constant load of 756 N [17].

Wirth et al. also tested three 48mm diameter CoCr humeral components against cross-linked polyethylene (XLPE) [17]. Using a density of 930 kg/m<sup>3</sup> for XLPE [21] to convert the gravimetric results to volumetric results, the study measured a wear rate of 7.5mm<sup>3</sup>/million cycles compared with 49.4mm<sup>3</sup>/million cycles for UHMWPE. That XLPE should give a lower wear rate compared with UHMWPE is to be expected [22]. In a separate study, six XLPE glenoid components were articulated against 44mm diameter CoCr humeral components with both rotation and translation in an MTS knee simulator [18].

## **2. METHODS**

The Newcastle Shoulder Wear Simulator [8,9] has five articulating stations and one static control station. Axial loading to each implant is applied using a pneumatic cylinder, the compressed air to these six cylinders being supplied equally from a proportional valve via a manifold. Three other pneumatic cylinders with integral position encoders move five glenohumeral prostheses simultaneously in the flexion-extension, abduction-adduction, and internal-external rotation axes. A mechanism with a rotational centre eccentric to the internal external axis, and driven by the internal-external motion, was built into the components between the loading cylinder and lubricant bath to provide translational sliding motion to each test station. The

simulator is programmed in LabView and National Instrument controllers are used to control the pneumatics.

“Mug to Mouth” was chosen as the ADL to use in this wear test as this was used in a previous wear test of reverse shoulders [9] and thus allowed a direct comparison. Rotational motion ranges per cycle were  $-16^{\circ}$  to  $+11^{\circ}$  in flexion-extension,  $-18^{\circ}$  to  $-6^{\circ}$  in abduction-adduction, and  $-42^{\circ}$  to  $-17^{\circ}$  in internal-external rotation. Joint rotations and loads mimicked those in the previous test of Reverse shoulders [9]. A cadaveric study of glenohumeral mechanics [11] measured a mean range of translation of  $3.5 \pm 1.0$  mm. Hence, 3.4mm of translational sliding was applied each cycle in the shoulder simulator, in an arc approximately in the abduction-adduction direction. The offset of the centre of rotation was 9 mm. The various motions applied in the simulator test are shown in Fig. 2. Dynamic loads applied over each cycle ranged between approximately 180 N to 250 N [9]. These are shown in Fig. 3.

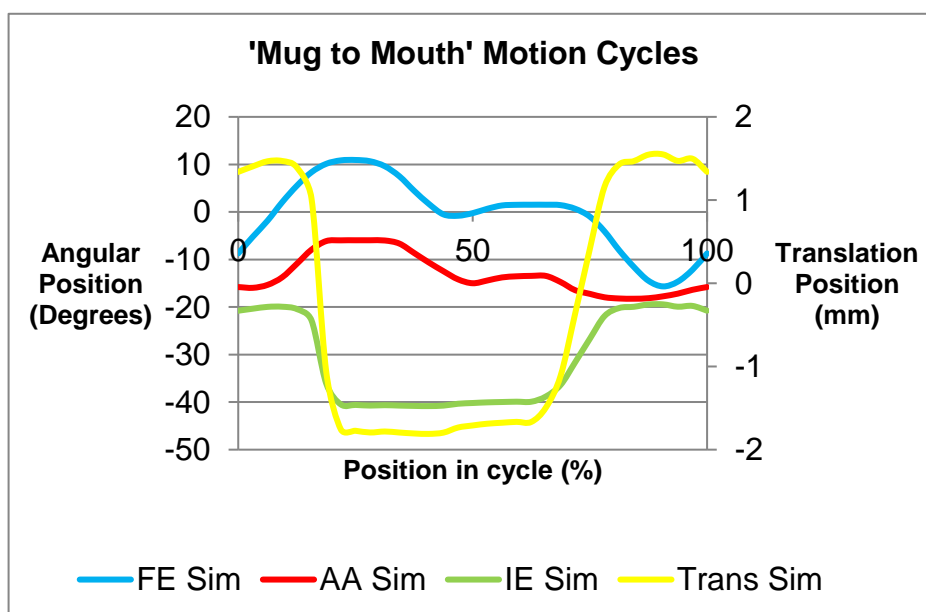


Figure 2. Motions applied in the shoulder simulator for testing Total shoulder prostheses. FE=flexion/extension; AA=abduction/adduction; IE=internal-external rotation; Trans=translational.

A 5 million cycle wear test was performed with JRI Orthopaedics Total VAIOS shoulders. These consist of a CoCr humeral head articulating against an UHMWPE glenoid component. Five 42mm diameter Total shoulders were wear tested and a sixth was subject to dynamic loading in the ‘control’ station. The lubricant employed

was newborn calf serum diluted to give a protein content of 26 g/l, maintained at ambient temperature. 26 g/l was chosen to match previous test work using the shoulder simulator [9]. Moreover, it fits well with other guidance which has been summarised elsewhere and suggests: above 20 g/l; in the range 20–35 g/l; and ‘about 30 g/l’ [23]. In regard to ambient temperature, it has been seen that protein precipitation, which reduces wear, occurs at higher temperatures [24]. In addition, temperatures around ambient produced clinically valid wear [25]. Gravimetric measurements (Denver Instruments TB-215D, sensitivity 10 µg) were used to determine the weight change and thus the wear of components. At regular intervals the simulator was stopped, lubricant was decanted, test components were carefully removed, cleaned and weighed to a consistent protocol. The gravimetric method was based on ISO 14242-2 for testing hip prostheses [26], in the absence of a similar ISO protocol for shoulder prostheses. Using a density of 938 kg/m<sup>3</sup> for the UHMWPE, volumetric wear was then calculated from weight losses, which were compensated by any weight changes of the control. Roughness measurements of the articulating surfaces of the prostheses were obtained using a ZYGO NewView 5000 non-contacting profilometer [27]. Ten measurements were taken per component and the mean roughness average (Sa) calculated.

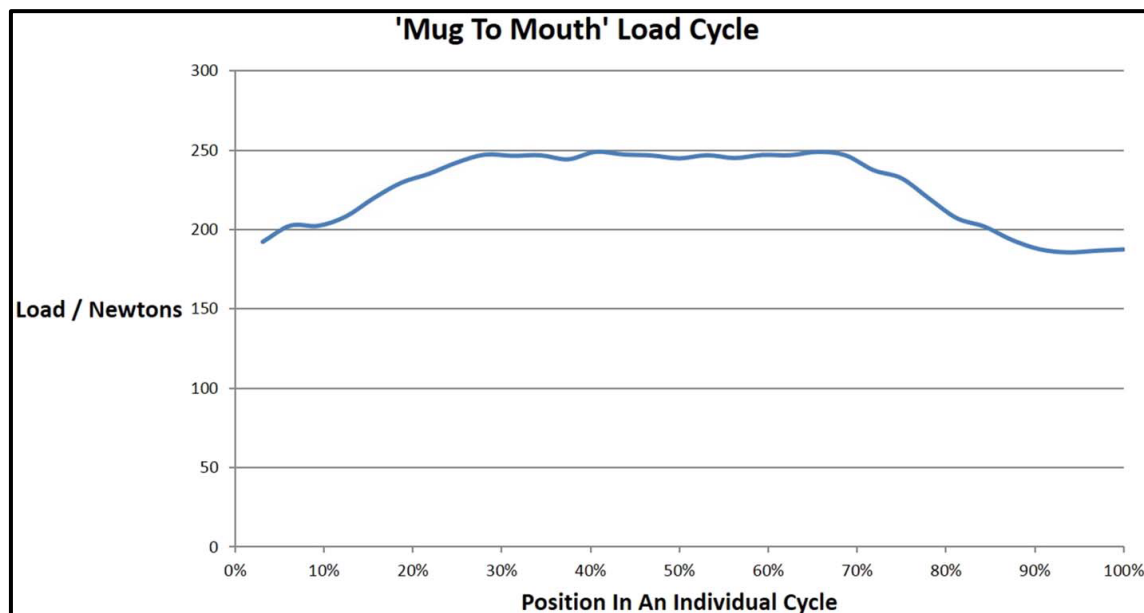


Figure 3. Loading applied in the shoulder simulator during “mug to mouth”.



### 3. METHODS

The mean wear results for the UHMWPE components of the Total shoulders are shown in Fig. 4. As can be seen, the results were linear over the 5 million cycles of testing. A mean  $\pm$  S.D. wear rate of  $21.5 \pm 5.4 \text{ mm}^3/\text{million cycles}$  was measured.

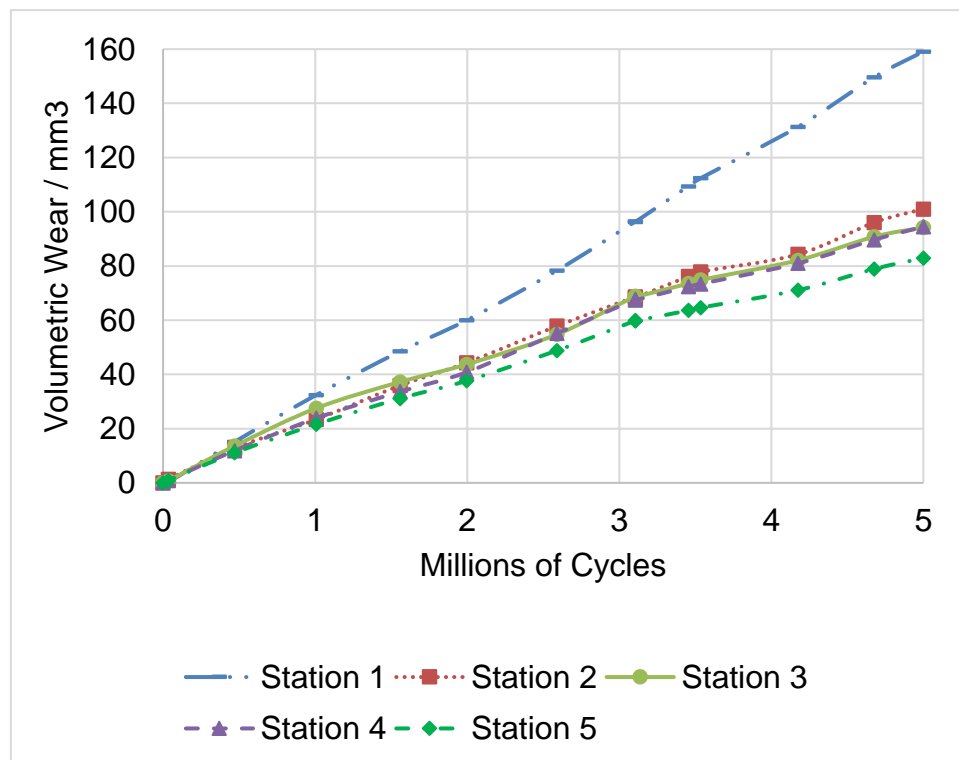


Figure 4. Wear results for the five JRI VAIOS Total shoulders.

In Table 1, the surface roughness measurements,  $S_a$ , of all the CoCr humeral heads and UHMWPE glenoid cups are given at zero cycles, prior to testing, and at 5.0 million cycles after wear testing. The mean  $\pm$  S.D. values are also given. The CoCr humeral heads roughened, from  $19 \pm 3 \text{ nm } S_a$  to  $43 \pm 13 \text{ nm } S_a$  over the duration of the test, which was statistically significant ( $p=0.013$ ). The UHMWPE glenoid components became smoother, from  $959 \pm 230 \text{ nm } S_a$  to  $77 \pm 17 \text{ nm } S_a$  over the duration of the test, and this was also statistically significant ( $p=0.001$ ).

An image of the surface of the unworn humeral head from station 3 taken prior to testing using the Zygo profilometer is shown in Fig. 5.

This contrasts with Fig. 6 for the same component taken after 5 million cycles of testing, where numerous irregular scratches can be seen.

Fig. 7 is an image of the paired glenoid component prior to testing, with regular, parallel machining marks in the UHMWPE.

The surface of the same glenoid component is shown in Fig. 8 after 5 million cycles of wear testing. The machining marks are no longer evident and the surface is an order of magnitude smoother than prior to testing.

Table 1: Surface Roughness measurements of the five CoCr humeral heads and five UHMWPE glenoid cups at zero cycles prior to testing and after 5,000,000 cycles of wear testing.

Station	CoCr Humeral head zero cycles Sa (nm)	CoCr Humeral head 5,000,000 cycles Sa (nm)	UHMWPE Glenoid cup zero cycles Sa (nm)	UHMWPE Glenoid cup 5,000,000 cycles Sa (nm)
1	13	56	1064	73
2	22	32	1288	51
3	20	59	954	74
4	20	31	779	92
5	19	37	712	93
<b>Mean <math>\pm</math> S.D.</b>	<b>19 <math>\pm</math> 3</b>	<b>43 <math>\pm</math> 13</b>	<b>959 <math>\pm</math> 230</b>	<b>77 <math>\pm</math> 17</b>

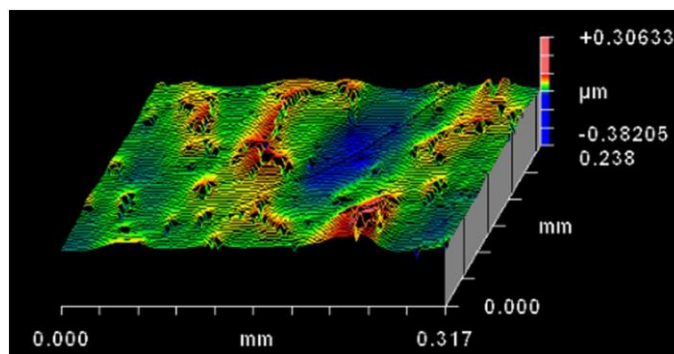


Fig. 5. An image of the surface of the unworn humeral head from station 3, Sa=20 nm, taken prior to testing using the Zygo profilometer.

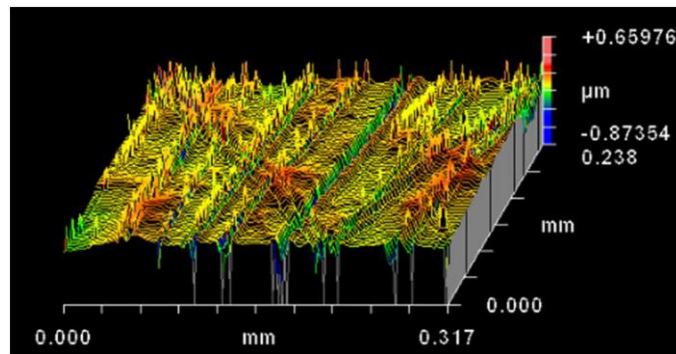


Fig. 6. An image from the Zygo profilometer of the surface of the same humeral head from station 3,  $S_a=59$  nm, taken after 5 million cycles of testing. Note numerous irregular scratches.

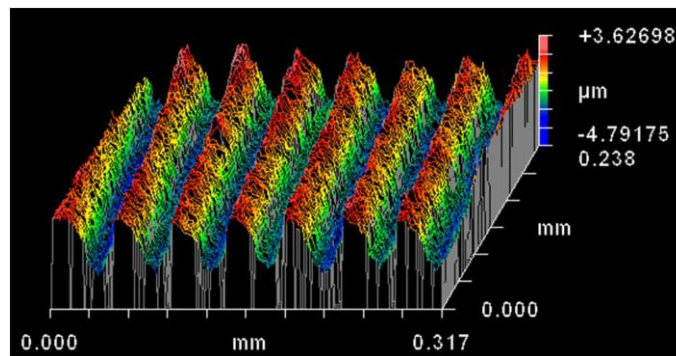


Fig. 7. An image taken on the Zygo profilometer prior to testing of the glenoid component from station 3,  $S_a=954$  nm. Note the regular, parallel machining marks in the UHMWPE.

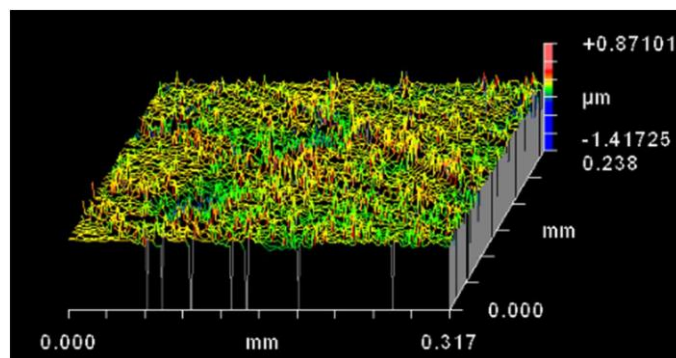


Fig. 8. The surface of the same glenoid component from station 3 after 5 million cycles of testing. The machining marks are no longer evident and the surface roughness is an order of magnitude smoother than prior to testing,  $S_a=74$  nm.

#### 4. DISCUSSION

Our hypothesis was that, due to the additional translational motion, wear rates would be increased compared with a previous Reverse shoulder test where only rotations were applied [9]. The wear rate of Reverse VAIOS shoulders over 4.5 million cycles was  $14.3 \pm 1.6 \text{ mm}^3 / 106 \text{ cycles}$ . The Total VAIOS shoulders, tested with the addition of translational motion, exhibited a 50% larger wear rate ( $21.5 \pm 5.4 \text{ mm}^3 / 106 \text{ cycles}$ ) compared with the Reverse shoulders. An explanation for the increase in wear rate of Total shoulder joints over Reverse shoulder joints is likely the application of translational sliding, resulting in more complicated motion paths in the Total shoulder wear test. Further work may validate this explanation or give reason to consider other explanations. Due mainly to the sample size, the difference in wear results is not quite statistically significant at 95% ( $p=0.068$ ). From Fig. 4 it is clear that the UHMWPE test component in station 1 showed higher wear than in the other stations. All components were of the same size and made to the same specification, so there were no differences in this regard. In terms of CoCr component roughness, the component in station 1 did not show the highest roughness so again this does not provide an explanation. While no final explanation is currently available, it should be noted that such differences in wear rates between stations have been seen in simulator studies of metal on polymer bearings [28,29]. A comparison of the wear results at the end of this study of Total shoulders and the previous study of Reverse shoulders is given in Table 2.

Table 2: Comparison of results and final measurements from this study of Total shoulders with rotation and sliding motion and a previous study of Reverse shoulders with rotation only (Smith et al, 2015)[234]

	Total shoulders with sliding	Reverse shoulders without sliding
Wear rate ( $\text{mm}^3/\text{million cycles}$ )	$21.5 \pm 5.4$	$14.3 \pm 1.6$
CoCr roughness, Sa (nm)	$43 \pm 12$	$36 \pm 12$
UHMWPE roughness, Sa (nm)	$77 \pm 17$	$258 \pm 74$
UHMWPE median particle diameter (nm)	$177 \pm 22$	$167 \pm 32$

As can be seen from Table 2, surface roughness values for the CoCr components show good agreement across the Total and Reverse tests. The surface roughness for the UHMWPE components both before and after testing were different. However, both sets of UHMWPE components had become smoother over the course of testing. This smoothing is expected if comparison is drawn with UHMWPE surface roughness changes in knee simulator testing [30] for the Total shoulders due to the similar combination of rotational and translational sliding motion. Similarly, comparison with smoothing of UHMWPE in the Reverse shoulders may be drawn with hip simulator testing [31] as both are subject only to rotational motion.

From testing the Total shoulders, the CoCr humeral heads roughened significantly ( $p=0.026$ ) over the course of the wear test,  $S_a$  increasing from 19 to 43 nm. The wear rates of the UHMWPE glenoid cups were linear over the course of the wear test, suggesting that this roughening did not impact on the wear rate of the UHMWPE. Comparison cannot be drawn with the other reported Total shoulder studies, as only Dieckmann et al. [16] reported roughness data. However, the latter study did not use a CoCr humeral head and therefore comparison with those measurements is inappropriate. The authors are unaware of any studies reporting clinical surface roughness measurements of explanted Total shoulders. Replacement knee joints are subject to both rotational and translational motion and hence might be used to draw comparison with Total shoulders. Explanted and new CoCr knee replacements have been measured [21,32] and surface roughness is greater with explanted prostheses, being 130 nm  $S_q$  (root mean square surface roughness) compared with 30 nm  $S_q$  for unworn [21]. This increase in roughness fits with the increase in  $S_a$  which we measured. Roughening of CoCr femoral knee components articulating against UHMWPE has also been reported in a simulator study [30]. Hence, the roughening of the CoCr humeral heads over the course of the wear test in this study might be expected.

Smoothing of the UHMWPE glenoid components in this study shows broad agreement with other studies. The UHMWPE glenoid cups became significantly ( $p=0.001$ ) smoother over the wear test,  $S_a$  reducing from 959 to 77 nm. The single specimen Total shoulder simulator study by Dieckmann et al. [16] reported smoothing of the UHMWPE glenoid from 250 nm to 30 nm. Again, the authors are

unaware of clinical studies of shoulders which have measured similar surface roughness parameters. Similarly, the authors are unaware of published clinical studies for the articulating surface of UHMWPE tibial trays from knee prostheses. However, unpublished data of such measurements by one of the authors (EK) found polished regions of ex-vivo tibial trays to be smoother than those of new prostheses. Smoothing of UHMWPE tibial trays has also been observed in a knee simulator study [30].

Table 3. Simulator wear studies of Total shoulders

Author	Simulator	Load	Motion	Prostheses	Results mm <sup>3</sup> /10 <sup>6</sup> cycles
This study	Newcastle Shoulder Wear Simulator	Physiological 180 to 250N	Flexion-extension -16° to +12° Abduction- adduction +18° to -5° Internal-external rotation -42° to - 17° Sliding translation 4 mm	5 x 42mm Total VAIOS CoCr v UHMWPE	21.5 ± 5.4
Dieckmann et al, 2013	'test control unit'	Max 500N Min 100N	Flexion-extension +10° to -10° Abduction- adduction +35° to -35° Spring limited translation 'about±0.7' no units	1 x 54mm Total Capica TiAlVa coated with TiN v UHMWPE	9.9
Wirth et al, 2009	AMTI knee simulator	Constant 756N	Abduction- adduction ±8° Sliding translation ±2mm Elevation 0° to 8°	3 x 48mm Humeral with 6mm Glenoid mismatch CoCr v UHMWPE	49.4
Wirth et al, 2009	AMTI knee simulator	Constant 756N	Abduction- adduction ±8° Sliding translation ±2mm Elevation 0° to 8°	3 x 48mm Humeral with 6mm Glenoid mismatch CoCr v XLPE	7.5
Mummert et al, 2016	MTS knee simulator	Constant 756N	Abduction- adduction Sliding translation Forward elevation	6 x 48mm Global Advantage Total Shoulders CoCr v XLPE	3.5 ± 0.9

A summary of this study and the various multiple station Total shoulder wear tests discussed in the Introduction are shown in Table 3. This and the other studies all report linear relationships between wear volume and number of cycles, and therefore offer one strong area of comparison.

The results of this study bear good comparison with the various studies when accounting for load, joint diameter and material. For example, the 21.5mm<sup>3</sup>/million cycles measured in this study does not initially appear to show good agreement with the 49.4mm<sup>3</sup>/million cycles reported by Wirth et al. [17], with the latter being 2.3 times greater. However, CoCr joints articulating against UHMWPE operate in a mixed lubrication regime [33,34]. The mixed lubrication regime between CoCr and UHMWPE is one where the majority of the load across the joint is carried by asperity contact. When the majority of the load is carried by asperity contact, wear of the joint is typical of a boundary lubrication regime. For joints operating in a boundary lubrication regime, the Lancaster [35] wear equation is applicable

$$V = kPx$$

where V, the volume of material removed by wear, is proportional to the product of wear factor, k, applied load, P, and sliding distance, x. Therefore, as load increases, wear should increase proportionally. Similarly, as sliding distance increases, wear should increase, and sliding distance increases with increasing joint diameter. Detailed wear path analysis is beyond the scope of this work, however, simple comparison of loads and joint size with other studies is appropriate. The Wirth et al. study [17] used larger (48 mm) diameter joints, than the 42mm diameter in this study. The load was also larger, 756 N versus 250 N. Adjusting the wear rate of 21.5mm<sup>3</sup>/million cycles by a factor of 48mm over 42mm for joint size, and a factor of 756 N over 250 N for load, gives an adjusted wear rate of 72.8mm<sup>3</sup>/million cycles. Comparison of this adjusted wear rate with the 49.4mm<sup>3</sup>/million cycles from the Wirth et al. study shows reasonable agreement in the absence of more detailed analysis of the differing wear paths. Equally however, this calculation could indicate that the Newcastle shoulder simulator, under the complex motions that it is capable of applying, gave the greatest wear compared with other tests of Total shoulders undertaken in simulators. Once such data becomes available, validation against wear

volumes of shoulder explants will probably give the definitive answer to what is the 'true' wear of an artificial shoulder joint. Until then, we caution that the complex motions applied by the Newcastle shoulder simulator may more accurately predict wear and that the simplified motions and loadings used in other, non-shoulder simulators could underestimate wear. Certainly, recent orthopaedic history, namely the debacle of metal-on-metal hip joints, has shown that wear and its devastating impact on the human body should never be underestimated [36–38].

While this study advanced our understanding of rotational and translational loading regimes applied to TSR, it is not without limitations. A limitation of this study may be the apparently low applied loads replicated in the "Mug to Mouth" ADL. However, by using the "Mug to Mouth" ADL, direct comparison with the previous Newcastle Shoulder Wear Simulator testing of Reverse shoulders was possible. Having completed wear studies on Total and Reverse shoulders with the 'Mug to Mouth' ADL, future wear studies will include other ADLs with higher loads, for example, 'lift shopping bag' [39]. The sample size of five may be considered small but this is actually a greater number than any other tests of Total shoulder joints aside from the six reported recently in a conference paper by Mummert et al. [18]. That a single size of implant was tested may be considered a limitation. However, as can be seen from Table 3, this is typical of artificial joint testing. Moreover, as metal-on-polyethylene implants generally work under boundary or mixed lubrication, it is relatively straightforward to extrapolate wear results from one size to other sizes. Indeed, this computational wear analysis has been done for artificial shoulder joints [40,41]. Another limitation is that we have assumed that all the wear is from UHMWPE, rather than UHMWPE and CoCr. However, this assumption is based on the common finding in biotribological studies that there is no discernible wear of the hard metal component compared with the softer polyethylene [22,42].

A wear test of Total shoulders was completed with both rotational and sliding motions. The wear rate and linear relationship of wear volume with increasing cycles shows good agreement with other studies of Total shoulders tested in knee simulators. Surface roughness measurements showed that the CoCr humeral heads roughened over the course of the wear test. This showed agreement for ex-vivo and simulator knee studies, which likely give the closest approximations given the lack of



data specifically related to Total shoulders. The UHMWPE glenoid components in this study became smoother over the course of the wear tests, showing agreement with shoulder and knee simulator studies.

### **Conflict of interest statement**

None

### **Acknowledgements**

The authors would like to acknowledge and thank the following Newcastle University students for their help with this study: Amr Alkhaznadar, Andy Williams, Chris Freeburn, Ed Blackwell, Jonny Bew and Ollie Francis.

### **References**

- [1] National Joint Registry for England, Wales, Northern Ireland And The Isle Of Man. 13th Annual Report, (2016) (Accessed 1 October 2016).
- [2] National Joint Registry for England, Wales And Northern Ireland. 11th Annual Report, (2014) (Accessed 22 October 2014).
- [3] National Joint Registry for England, Wales, Northern Ireland And The Isle Of Man. 12th Annual Report, (2015) (Accessed 1 February 2016).
- [4] R.L. Ilgen li, L.M. Bauer, B.T. Hotujec, S.E. Kolpin, A. Bakhtiar, T.M. Forsythe, Highly crosslinked vs conventional polyethylene particles: relative in vivo inflammatory response, *J. Arthroplast.* 24 (2009) 117–124.
- [5] M.A. Wirth, C.M. Agrawal, J.D. Mabrey, et al., Isolation and characterization of polyethylene wear debris associated with osteolysis following total shoulder arthroplasty, *J. Bone Joint Surg. Am.* 81 (1999) 29–37.
- [6] M.M. Scarlat, F.A. Matsen, Observations on retrieved polyethylene glenoid components *J. Arthroplast.* 16 (2001) 795–801.
- [7] F.A. Matsen III, J. Clinton, J. Lynch, A. Bertelsen, M.L. Richardson, Glenoid component failure in total shoulder arthroplasty, *JBJS* 90 (2008) 885–896.

- [8] S.L. Smith, L. Li, T.J. Joyce, Engineering of a multi-station shoulder simulator, *Proc. Inst. Mech. Eng. H J. Eng. Med.* 230 (2016) 470–480.
- [9] S.L. Smith, B.L. Li, A. Buniya, et al., In vitro wear testing of a contemporary design of reverse shoulder prosthesis, *J. Biomech.* 48 (2015) 3072–3079.
- [10] I.A. Murray, G.R. Johnson, A study of the external forces and moments at the shoulder and elbow while performing every day tasks, *Clin. Biomech.* 19 (2004) 586–594.
- [11] R. Kelkar, V.M. Wang, E.L. Flatow, et al., Glenohumeral mechanics: a study of articular geometry, contact, and kinematics, *J. Shoulder Elb. Surg.* 10 (2001) 73–84.
- [12] D. Muller, A. Marti, P. Herzig, Evaluation Of Peek For Shoulder Endoprosthetics In A Screening And A Simulated Physiological Wear Test. 47th Annual Meeting, Orthopaedic Research Society, San Francisco, California, 2001 P. 0782.
- [13] A.J. Pijl, W. Swieszkowski, H.E.N Bersee, Technical application series. Design of a wear simulator for in vitro shoulder prostheses testing, *Exp. Tech.* 28 (2004) 45–48.
- [14] C. Geary, G.E. O'Donnell, E. Jones, D. Fitzpatrick, C. Birkinshaw, Automated invitro testing of orthopaedic implants: a case study in shoulder joint replacement, *Proc. Inst. Mech. Eng. H J. Eng. Med.* 224 (2010) 1297–1309.
- [15] W. Swieszkowski, H.E.N. Bersee, K.J. Kurzydowski, Effect of the design parameters on the in vitro wear performance of total shoulder arthroplasties, *Mater. Sci. Eng. C* 31 (2011) 313–319.
- [16] R. Dieckmann, D. Liem, G. Gosheger, et al., Evaluation of a reconstruction reverse shoulder for tumour surgery and tribological comparison with an anatomical shoulder arthroplasty, *Int. Orthop.* 37 (2013) 451–456.
- [17] M.A. Wirth, C. Klotz, D.L. Deffenbaugh, D. McNulty, L. Richards, J.L. Tipper, Crosslinked glenoid prosthesis: a wear comparison to conventional glenoid prosthesis with wear particulate analysis, *J. Shoulder Elb. Surg.* 18 (2009) 130–137.

- [18] J. Mummert, L. Rodriguez, S. Ghosh, S. Bombosch, Rim Loading Wear For Total Shoulder Applications, Orthopedic Research Society, 2016, p. 1179.
- [19] S.L. Smith, A. Unsworth, Simplified motion and loading compared to physiological motion and loading in a hip joint simulator, J. Eng. Med. 214 (2000) 233–238.
- [20] C.R. Bragdon, D.O. O'Connor, J.D. Lowenstein, W.D. Synivta, The importance of multidirectional motion on the wear of polyethylene, J. Eng. Med. 210 (1996) 157–165.
- [21] S. Scholes, E. Kennard, R. Gangadharan, et al., Topographical analysis of the femoral components of ex vivo total knee replacements, J. Mater. Sci. Mater. Med. 24 (2013) 547–554.
- [22] A.P. Harsha, T.J. Joyce, Comparative wear tests of ultra-high molecular weight polyethylene and cross-linked polyethylene, Proc. Inst. Mech. Eng. H J. Eng. Med. 227 (2013) 600–608.
- [23] A.P. Harsha, T.J. Joyce, Challenges associated with using bovine serum in wear testing orthopaedic biopolymers, Proc. Inst. Mech. Eng. H J. Eng. Med. 225 (2011) 948–958.
- [24] Y.S. Liao, H.A. Mckellop, Z. Lu, P. Campbell, P. Benya, The effect of frictional heating and forced cooling on the serum lubricant and wear of Uhmw polyethylene cups against cobalt-chromium and zirconia balls, Biomaterials 24 (2003) 3047–3059.
- [25] V. Saikko, A hip wear simulator with 100 test stations, Proc. Inst. Mech. Eng. H J. Eng. Med. 219 (2005) 309–318.
- [26] ISO14242-2, Implants For Surgery - Wear Of Total Hip Joint Prostheses, Part 2. Methods Of Measurement, ISO, Geneva, 2016.
- [27] T.J. Joyce, D.J. Langton, S.S. Jameson, A.V.F. Nargol, Tribological analysis of failed resurfacing hip prostheses and comparison with clinical data, J. Eng. Tribol. 223 (2009) 317–323.

- [28] S.L. Smith, I.C. Burgess, A. Unsworth, Evaluation of a hip joint simulator, *J. Eng. Med.* 213 (1999) 469–473.
- [29] S.L. Smith, A. Unsworth, A five-station hip joint simulator, *J. Eng. Med.* 215 (2001) 61–64.
- [30] P.I. Barnett, H.M.J. Mcewen, D.D. Auger, M.H. Stone, E. Ingham, J. Fisher, Investigation of wear of knee prostheses in a new displacement/force-controlled simulator, *J. Eng. Med.* 216 (2002) 51–61.
- [31] S.L. Smith, Design, Development and Applications of Hip Joint Simulators, University Of Durham, 1999, <http://Etheses.Dur.Ac.Uk/1132/>.
- [32] E. Kennard, S.C. Scholes, R. Sidaginamale, et al., A comparative surface topographical analysis of explanted total knee replacement prostheses: oxidised zirconium vs cobalt chromium femoral components, *Med. Eng. Phys.* 50 (2017) 59–64.
- [33] J.O. Kelly, A. Unsworth, D. Dowson, V. Wright, An experimental study of friction and lubrication in hip prostheses, *Eng. Med.* 8 (1979) 153–159.
- [34] A. Unsworth, S.C. Scholes, S.L. Smith, A.P.D. Elfick, H.A. Ash, Tribology of replacement hip joints, *Tribol. Interface Eng. Ser.* (2000) 195–202.
- [35] J.K. Lancaster, Dry bearings: a survey of materials and factors affecting their performance, *Tribology* 6 (1973) 219–251.
- [36] D. Cohen, Out of joint: the story of the Asr, *BMJ* 342 (2011).
- [37] M. Wienroth, P. McCormack, T. Joyce, Precaution, governance and the failure of medical implants: the Asr(Tm) hip in the UK, *Life Sci. Soc. Pol.* 10 (2014) 19.
- [38] D.J. Langton, S.S. Jameson, T.J. Joyce, N.J. Hallab, S. Natsu, A.V.F. Nargol, Early failure of metal-on-metal bearings in hip resurfacing and large-diameter total hip replacement: a consequence of excess wear, *J. Bone Joint Surg. (Br.)* 92-B (2010) 38–46.

- [39] M. Masjedi, G.R. Johnson, Glenohumeral contact forces in reversed anatomy shoulder replacement, *J. Biomech.* 43 (2010) 2493–2500.
- [40] L. Mattei, F. Di Puccio, T.J. Joyce, E. Ciulli, Numerical and experimental investigations for the evaluation of the wear coefficient of reverse total shoulder prostheses, *J. Mech. Behav. Biomed. Mater.* 55 (2015) 53–66.
- [41] L. Mattei, F. Di Puccio, T.J. Joyce, E. Ciulli, Effect of size and dimensional tolerance of reverse total shoulder arthroplasty on wear: an in-silico study, *J. Mech. Behav. Biomed. Mater.* 61 (2016) 455–463.
- [42] B. Hunt, T. Joyce, A tribological assessment of ultra high molecular weight polyethylene types Gur 1020 and Gur 1050 for orthopedic applications, *Lubricants* 4 (2016) 25

*Blank page*

## **Appendix G: Kennard et al MEP 2018**

Within this appendix is included the manuscript for the publication:

**Kennard, E**, Scholes SC, Sidaginamale R, Gangadaharan R, Weir DJ, Holland J, Deehan D and Joyce TJ. *A comparative surface topographical analysis of explanted total knee replacement prostheses: Oxidised zirconium vs cobalt chromium femoral components*. Medical Engineering and Physics. 2017; 50:59-64 [14]

As noted on page 5 of Chapter 1 Introduction, this thesis is submitted in my legal married name Emma Ritchie, however my authored publications are in my maiden name Emma Kennard.

*Blank page*



**TITLE:** A comparative surface topographical analysis of explanted Total Knee Replacement prostheses: Oxidised Zirconium vs Cobalt Chromium femoral components

**AUTHORS:** Emma Kennard<sup>a</sup>, Susan C. Scholes<sup>a</sup>, Raghavendra Sidaginamale<sup>a</sup>, Rajkumar Gangadharan<sup>b</sup>, David J. Weir<sup>b</sup>, James Holland<sup>b</sup>, David Deehan<sup>b</sup> and Thomas J. Joyce<sup>a</sup>.

<sup>a</sup> Bioengineering Group, School of Engineering, Newcastle University, Stephenson Building, Newcastle upon Tyne, NE1 7RU, England, United Kingdom.

<sup>b</sup> Freeman Hospital, Newcastle upon Tyne, NE1 7DN, England, United Kingdom.

## **ABSTRACT**

It has been proposed that an increased surface roughness of the femoral components of Total Knee Replacements (TKRs) may be a contributing factor to the accelerated wear of the polyethylene (PE) bearing and ultimately prosthesis failure. Oxidised Zirconium was introduced to the orthopaedic market in an attempt to reduce PE wear associated failures and increase the longevity of the prosthesis.

In this study, non-contacting profilometry was used to measure the surface roughness of the femoral components of 6 retrieved TKRs (3 Oxidised Zirconium (OxZr) and 3 Cobalt Chromium alloy (CoCr) femoral components) and 2 as-manufactured femoral components (1 OxZr and 1 CoCr). A semi-quantitative method was used to analyse the damage on the retrieved PE components.

The  $S_a$  values for the retrieved OxZr femoral components ( $S_a = 0.093\mu\text{m} \pm 0.014$ ) and for the retrieved CoCr femoral components ( $S_a = 0.065\mu\text{m} \pm 0.005$ ) were significantly greater ( $p < 0.05$ ) than the roughness values for the as-manufactured femoral components (OxZr  $S_a = 0.061\mu\text{m} \pm 0.004$  and CoCr  $S_a = 0.042\mu\text{m} \pm 0.003$ ). No significant difference was seen between the surface roughness parameters of the retrieved OxZr and retrieved CoCr femoral components. There was no difference between the PE component damage scores for the retrieved OxZr TKRs compared to the retrieved CoCr TKRs.

These results agree with other studies that both OxZr and CoCr femoral components roughen during time *in vivo* but the lack of difference between the surface roughness measurements of the two materials is in contrast to previous topographical reports. Further analysis of retrieved OxZr TKRs is recommended so that a fuller appreciation of their benefits and limitations be obtained.

**KEYWORDS:** Total Knee Replacement; retrieval; Oxidised Zirconium (OxZr); surface roughness; profilometry.

## 1. INTRODUCTION

Total Knee Replacement (TKR<sup>2</sup>) offers improved mobility and pain relief for many people suffering with the debilitating disease of osteoarthritis [1-4]. In the longer-term, wear of the polyethylene (PE) component and PE wear-debris associated problems continue to limit TKR longevity. The 2016 Australian Orthopaedic Association National Joint Replacement Registry (AOANJRR) [1] and the National Joint Registry (NJR) Annual Report for England, Wales, Northern Ireland and the Isle of Man [3] both cite aseptic loosening as the main reason for TKR revision at 10 years and beyond. Whilst there are many factors that influence PE wear within TKR, an increased surface roughness of the counter-face femoral component has been reported as one of the causative mechanisms of accelerated PE wear [5-10].

In 2004, Oxidised Zirconium (OxZr) (a surface-modified metal comprising a uniform ceramic surface with a gradual transition from ceramic oxide to substrate metal alloy) was introduced for TKR femoral components in an attempt to reduce PE wear associated failures [11, 12]. With a greater surface hardness and wettability than cobalt-chromium alloy (CoCr) [13], OxZr femoral components should theoretically lead to the reduction of PE wear. While *in-vitro* wear testing of OxZr TKRs has shown significant wear reduction when compared to CoCr TKRs [13-15], the 10-year clinical

---

<sup>2</sup> List of Abbreviations: Total Knee Replacement (TKR); polyethylene (PE); Australian Orthopaedic Association National Joint Replacement Registry (AOANJRR); National Joint Registry (NJR) Oxidised Zirconium (OxZr); Cobalt Chromium (CoCr); Body Mass Index (BMI); Anterior – posterior (AP).

follow-up reviews reported no difference in survivorship or patient-reported outcome measures [16-19]. Further, the revision rates reported in both the NJR and the AOANJRR for Genesis II Oxinium are higher at 12 years than that of the standard CoCr Genesis II [1, 3]. Vertullo et al [20] analysed data presented in the 2016 AOANJR report [1] and concluded that OxZr femoral components did not reduce revision rates compared with the same CoCr femoral components across all age groups.

While laboratory simulation can provide important data, the analysis of retrieved TKR components provides invaluable insights into the *in-vivo* tribological performance of the prostheses. Two previous retrieval studies [21, 22] reported on the measurement of roughness parameters of as-manufactured and retrieved OxZr and CoCr femoral components. Using contact profilometry, Brandt et al [21] analysed the surface damage of 26 pairs of retrieved OxZr and CoCr TKRs. All roughness parameters were found to be significantly lower on an as-manufactured CoCr femoral component when compared to retrieved CoCr femoral components but no significant difference was found between the roughness parameters measured on an as-manufactured OxZr femoral component compared to retrieved OxZr femoral components. The surface roughness parameters for the as-manufactured CoCr femoral component were significantly lower than for the as-manufactured OxZr femoral component, however there was no significant difference between the results for the retrieved CoCr femoral components and the retrieved OxZr femoral components.

Non-contacting profilometry is a preferable method of surface roughness measurement as it is not limited by errors induced by the physical profile of the stylus and potential damage to the sample as the stylus drags across the surface [23]. Heyse et al [22] used non-contacting profilometry to compare the roughness measurements of as-manufactured OxZr and CoCr femoral components and 10 retrieved OxZr and CoCr femoral components. The overall roughness for the retrieved CoCr implants was 83% greater than that of the retrieved OxZr implants and, in agreement with Brandt et al [21], the as-manufactured CoCr femoral component had a lower surface roughness than the as-manufactured OxZr femoral component. In contrast to Brandt et al, the retrieved OxZr components measured by

Heyse et al had a significantly greater surface roughness than the as-manufactured OxZr component.

Gascoyne et al [16] used observer damage scoring and microcomputed tomography to quantify the damage observed on the articular surface of the PE inserts from the same cohort used by Brandt et al [21]. No significant difference was found between the PE damage of the two groups.

The purpose of this study was to use non-contacting profilometry to investigate the *in vivo* changes in surface roughness of OxZr TKRs and CoCr TKRs in order to add to the limited literature available on this topic. It was hypothesised that both OxZr and CoCr femoral components will roughen *in vivo* when comparing retrieved to as-manufactured prostheses; further, the extent of the roughening would be greater on retrieved CoCr femoral components compared with retrieved OxZr femoral components.

## **2. MATERIALS & METHODS**

Ethical approval was obtained for the retrieval of 6 explanted TKRs (3 with OxZr and 3 with CoCr femoral components) from the Freeman Hospital, Newcastle upon Tyne, UK. All prostheses were implanted with cemented fixation with modular fixed PE bearings. The 3 retrieved CoCr TKRs (DePuy PFC Sigma Bicondylar) were selected to match the OxZr TKRs (3 Smith & Nephew Oxinium TKRs – 2 Genesis II; 1 Legion) based on time *in vivo*. The mean time *in vivo* for the OxZr retrievals was 58 ( $\pm 24.8$ ) months and 47 ( $\pm 14.3$ ) months for the CoCr retrievals. The mean BMI for the OxZr retrievals was 30.2 ( $\pm 3.3$ ) and 33.4 ( $\pm 5.4$ ) for the CoCr retrievals; the mean age at primary surgery was 51 ( $\pm 14.0$ ) years for the OxZr prostheses and 60 ( $\pm 8.5$ ) years for the CoCr prostheses. The patient and implant variables are shown in Table 1.

An as-manufactured Smith & Nephew Genesis II Oxinium femoral component and an as-manufactured DePuy PFC Sigma Bicondylar femoral component were available for analysis. Before the commencement of any analyses, all retrieved explanted

components were sterilised in formaldehyde solution for at least 48 hours, rinsed with water and air-dried.

## **2.1 Qualitative and Semi-quantitative Damage Assessment**

A macroscopic visual assessment of damage was performed for each retrieved femoral component. A Mitutoyo QuickScope vision measuring system with a x25 magnification (x50 lens and x0.5 zoom) was used to perform the semi-quantitative Hood analysis technique [24] and a surface damage score was calculated for the articulating surface of each PE component. The articulating surface of the PE component was divided into sections and a grade assigned for each section corresponding to the estimated percentage area covered by 7 damage modes (surface deformation, pitting, embedded debris, scratching, burnishing, abrasion and delamination). The sum of the grades for each damage mode in each section gives the PE damage score with the maximum possible being 210.

## **2.2 Non-contacting Profilometry**

Surface roughness measurements for the retrieved and the as-manufactured femoral components were performed on a Zygo NewView 5000 non-contacting white light interferometric profilometer as used in previous explant studies [25-27]. The 10Xlens was used with a x2 zoom, giving an area of view of 317 x 238  $\mu\text{m}$ . The Zygo has a vertical resolution of greater than 1 nm. Measurements were taken of mean surface roughness  $S_a$  (the mean of the variation in peaks and valleys from the centreline of the sampling area), root-mean-square surface roughness  $S_q$  (the root-mean-square of the variation in peaks and valleys from the centreline of the sampling area), maximum peak height  $S_p$ , maximum valley depth  $S_v$ , peak to valley  $S_z$  (sum of the maximum peak height and the maximum valley depth of the sampling area) and surface skewness  $S_{sk}$  (the symmetry of the profile about the mean line) [28]. Fifteen measurements were taken at approximately 30° flexion on each femoral condyle (see Figure 1).



Figure 1. Profilometer measurements were taken at approximately 30° flexion in the boxed areas as shown on this femoral component

### **2.3 Statistical Analysis**

Statistical software programme Minitab® 17 was used to perform two-sample Student's t-tests to compare the roughness measurement results. A p-value of <0.05 was considered to show significant difference. Sample sizes for the roughness values were n=30 and n=90 for the as-manufactured and retrieved components respectively. Normality was not checked as the sample sizes were great enough for the tests to be accurate for non-normal data.

## **3. RESULTS**

Macroscopic visual assessment showed the damage to the retrieved OxZr femoral components to be minimal but there were obvious scratches in the anterior –posterior (AP) direction; the retrieved CoCr femoral components showed light to moderate scratching also in the AP direction.

The roughness parameters,  $S_a$ ,  $S_q$ ,  $S_z$  and  $S_p$  were greater, and  $S_v$  and  $S_{sk}$  were more negative, for the retrieved than for the as-manufactured for both OxZr and CoCr femoral components. There were no significant differences between any of the surface roughness parameters measured on the retrieved OxZr femoral components compared to those measured on the retrieved CoCr femoral components (see Table 2 and Figures 2 and 3). The  $S_a$  and  $S_q$  were both significantly greater ( $p<0.001$ ) for the as-manufactured OxZr femoral component than for the as-manufactured CoCr femoral component.

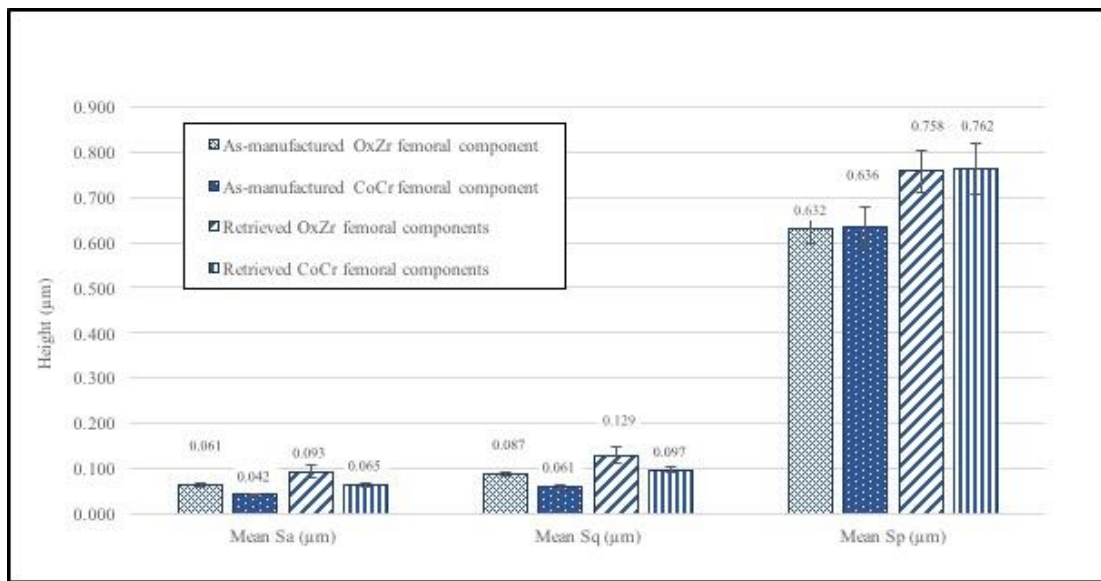


Figure 2: Surface roughness parameters  $S_a$ ,  $S_q$  and  $S_p$  measured on as-manufactured OxZr and CoCr femoral components and retrieved OxZr and CoCr femoral components.

All six of the retrieved PE components displayed *in vivo* damage with burnishing being the most prevalent damage mode observed; there was no embedded debris or delamination detected. Figure 4 shows a retrieved PE component with an area of burnishing and a pit approximately 1mm in size. The Hood damage scores are given in Table 1.

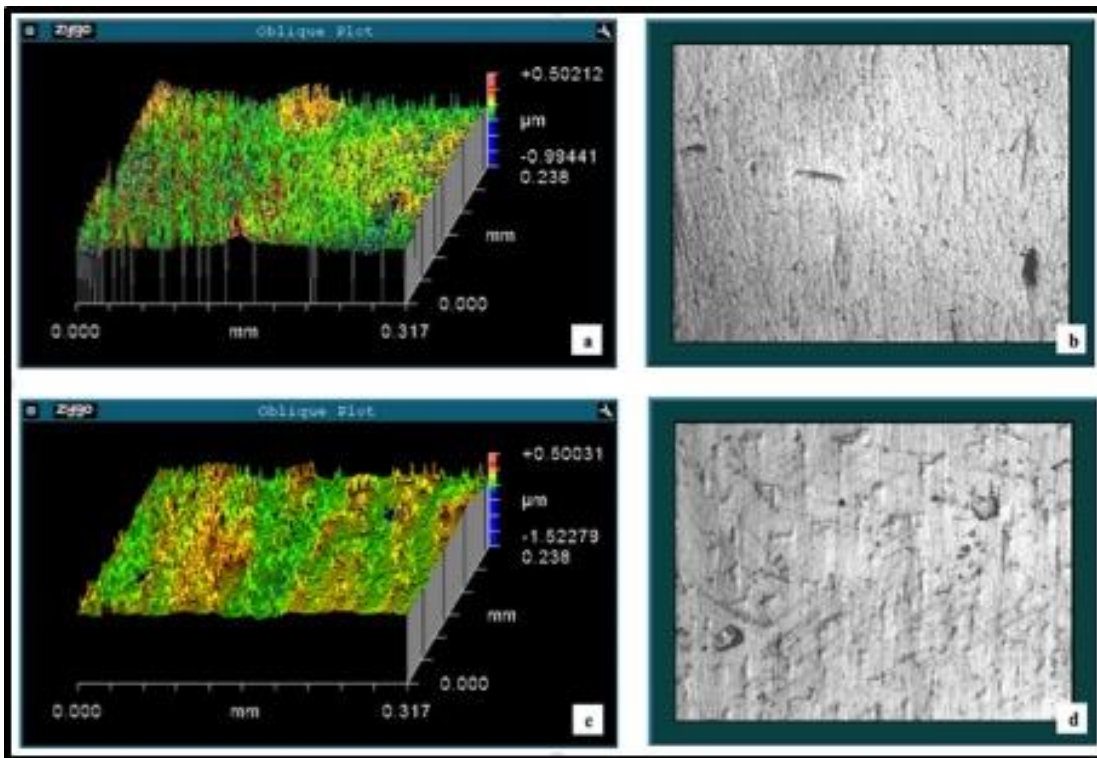


Figure 3: Surface roughness parameters  $S_v$ ,  $S_z$  and  $S_{sk}$  measured on as-manufactured OxZr and CoCr femoral components and retrieved OxZr and CoCr femoral components.

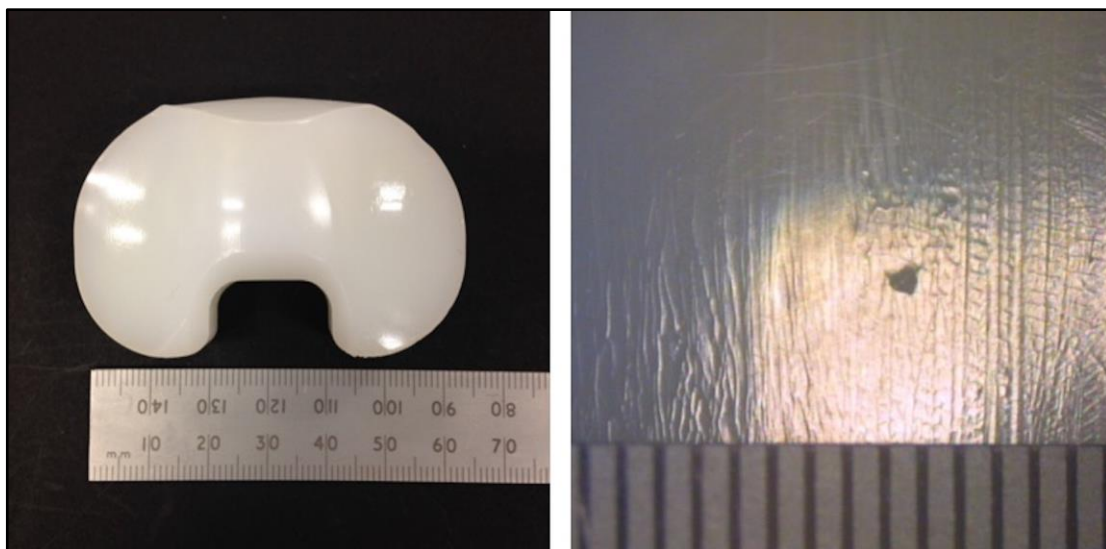


Figure 4: A retrieved PE component from an OxZr TKR



#### 4. DISCUSSION

The results show that both OxZr and CoCr femoral components roughen *in vivo* which is in agreement with other reports of retrieved TKRs components [22, 27]. Further, in agreement with Scholes et al [27], femoral component roughening does not appear to be correlated to length of time *in vivo*.

The mean  $S_a$  values for the as-manufactured OxZr femoral component ( $S_a = 0.061\mu\text{m} \pm 0.004$ ), the as-manufactured CoCr component ( $S_a = 0.042\mu\text{m} \pm 0.003$ ) and the retrieved OxZr femoral components ( $S_a = 0.093\mu\text{m} \pm 0.014$ ) are comparable to the mean  $S_a$  values reported by Heyse et al [22] for an as-manufactured OxZr femoral component ( $S_a = 0.05\mu\text{m} \pm 0.00$ ), an as-manufactured CoCr femoral component ( $S_a = 0.04\mu\text{m} \pm 0.01$ ) and retrieved OxZr femoral components ( $S_a = 0.15\mu\text{m} \pm 0.39$ ). However, the mean  $S_a$  value for the retrieved CoCr femoral components ( $S_a = 0.065\mu\text{m} \pm 0.005$ ) is much lower than that reported by Heyse et al ( $S_a = 0.21\mu\text{m} \pm 0.21$ ). In contrast to the data presented by both Brandt et al [21] and Heyse et al [22], no difference was found between the surface roughness measurements for the retrieved OxZr femoral components and the retrieved CoCr femoral components. When reviewing these results, it must be considered that the as-manufactured and retrieved CoCr femoral components used in this study are a different design to those reported on by Brandt et al and Heyse et al which may go towards explaining the differences seen.

The mean  $S_a$  and  $S_q$  were significantly less for the as-manufactured CoCr femoral component than for the as-manufactured OxZr femoral component which has been reported previously [21, 22]. Simulator studies report that the PE wear rate increases with increasing counter-face surface roughness [5, 13, 14] and so it would be expected that the rougher as-manufactured OxZr component would result in a greater PE wear rate than the as-manufactured CoCr component. However, the results from this study show that both OxZr and CoCr femoral components roughen after time *in vivo* (minimum time *in vivo* in this study is 35 months) and that there is no difference between the surface roughness parameters of the retrieved OxZr and CoCr femoral components. Kim et al [19] reported that the PE wear particles from CoCr TKRs were not different in weight, size or shape than those from OxZr TKRs

which would be expected if the femoral components of both materials roughened to the same extent after a period of time *in vivo*. The results in this study and in Kim et al [19] support the findings that report no clinical difference between TKRs with OxZr femoral components and TKRs with CoCr femoral components at the 10 year follow up period [12, 17, 18].

All the retrieved PE components were observed to have undergone *in vivo* damage but there was no noticeable difference between the damage observed on the OxZr TKRs compared with the CoCr TKRs. There was no relationship found between the Hood scoring system of the PE component damage and the femoral component roughness measurements. These results match those presented in a recent study [16].

In TKR, PE wear and failure due to debris related aseptic loosening and osteolysis is influenced by multiple contributing factors that are a combination of surgeon, patient and implant variables [29, 30]. Surface roughness of the femoral component is just one of these factors and differentiating out individual effects continues to be challenging. Data from retrieval studies can add to the long-term clinical follow-up studies and *in vitro* wear analyses to help provide a clearer understanding of the interdependencies influencing wear *in vivo*.

It is acknowledged that this study is limited by the small number of retrieved OxZr TKRs that were available for analysis. However, there is a limited literature on retrieved OxZr TKRs and the recent history of orthopedics has shown the vital role that explant analysis can provide in understanding why some implants fail [31]. There are inherent limitations associated with the analysis of 'failed' prostheses as opposed to those which are still *in vivo* and may be functioning 'well'. However, such 'failed' implants have arguably undergone the truest test of all in the human body, and this unique data should be shared. The surface roughness data of this retrieval study contributes to the current literature within this area [16, 20-22, 27]. In time, with longer clinical follow-up periods reported in arthroplasty registries and the further analysis of more explanted samples, the benefits and limitations of OxZr femoral components may become clearer. Ultimately the aim of the interdisciplinary

evaluation of retrieved prostheses is to lead to future improvements in TKRs and a concomitant reduction of failures.

## **5. CONCLUSIONS**

Both OxZr and CoCr femoral components show increased surface roughness parameters following time *in vivo*. No significant difference was seen between the surface roughness parameters of the retrieved OxZr and CoCr femoral components. Further analysis of retrieved OxZr TKRs is recommended so that a fuller appreciation of their benefits and limitations be obtained.

## **ACKNOWLEDGMENTS**

We thank Smith & Nephew and DePuy Synthes for providing as-manufactured femoral components.

## **COMPETING INTERESTS**

Author, DJW has received monies from Stryker with regards to lecturing not related to this work; author JH has received monies from Zimmer Biomet and Stryker for education not related to this work; and, author TJJ has received monies paid to Newcastle University for expert testimony not related to this work. All other authors certify that she or he has no commercial associations (e.g consultancies, stock ownership, equity interest, patent/licensing arrangements, etc.) that might pose a conflict of interest in connection with the submitted article.

## **FUNDING**

Work was performed at Newcastle University, Newcastle-upon-Tyne, England, UK. This research did not receive any specific grant from funding agencies in the public, commercial, or not-for-profit sectors.

## **ETHICAL COMMITTEE REVIEW STATEMENT**

This study is approved by Ethical Committee Review REC 09/H0906/72.

## REFERENCES

- [1] Australian Orthopaedic Association National Joint Replacement Registry. *Annual Report. 2016.*
- [2] Bae DK, Song SJ, Park MJ, Eoh JH, Song JH, Park CH. Twenty-year survival analysis in total knee arthroplasty by a single surgeon. *Journal of Arthroplasty. 2012; 27(7): 1297-304*
- [3] National Joint Registry for England, Wales and Northern Ireland. *The 13<sup>th</sup> Annual Report. 2016.*
- [4] Swedish Knee Arthroplasty Register. *Annual Report. 2015.*
- [5] Muratoglu OK, Burroughs BR, Bragdon CR, Christensen S, Lozynsky A, Harris WH. Knee simulator wear of polyethylene tibias articulating against explanted rough femoral components. *Clinical Orthopaedics & Related Research. 2004; 428: 108-13.*
- [6] Puloski SK, McCalden RW, MacDonald SJ, Bourne RB, Rorabeck CH. Surface analysis of posterior stabilized femoral components used in total knee arthroplasty. *Journal of Arthroplasty. 2003; 18(7): 822-6.*
- [7] Puloski SK, McCalden RW, MacDonald SJ, Rorabeck CH, Bourne RB. Tibial post wear in posterior stabilized total knee arthroplasty. An unrecognized source of polyethylene debris. *Journal of Bone & Joint Surgery - American Volume. 2001; 83-A(3): 390-7*
- [8] Que L, Topoleski LD, Parks NL. Surface roughness of retrieved CoCrMo alloy femoral components from PCA artificial total knee joints. *Journal of Biomedical Materials Research. 2000; 53(1): 111-8.*
- [9] Siddique MS, Rao MC, Deehan DJ, Pinder IM. Role of abrasion of the femoral component in revision knee arthroplasty. *Journal of Bone & Joint Surgery - British Volume. 2003; 85(3): 393-8*

- [10] Saikko V, Vuorinen V, Revitzer H. Effect of CoCr Counterface Roughness on the Wear of UHMWPE in the Noncyclic RandomPOD Simulation. *Journal of Tribology*. 2016; 139(2):
- [11] Laskin RS. An oxidized Zr ceramic surfaced femoral component for total knee arthroplasty. *Clinical Orthopaedics & Related Research*. 2003; 416:191-6.
- [12] Schuttler KF, Turgay E, Heyse TJ, Haas SB. Oxidized Zirconium Bearing Surfaces in Total Knee Arthroplasty: Lessons Learned. *Journal of Knee Surgery*. 2015; 28(5): 376-381
- [13] Spector BM, Ries MD, Bourne RB, Sauer WS, Long M, Hunter G. Wear performance of ultra-high molecular weight polyethylene on oxidized zirconium total knee femoral components. *Journal of Bone and Joint Surgery-American Volume*. 2001; 83-A: 80–86
- [14] DesJardins JD, Burnikel B, LaBerge M. UHMWPE wear against roughened oxidized zirconium and CoCr femoral knee components during force-controlled simulation, *Wear*, 2008; 264: 245–56
- [15] Ezzet KA, Hermida JC, Colwell CW, D’Lima DD. Oxidized zirconium femoral components reduce polyethylene wear in a knee wear simulator. *Clinical Orthopaedics & Related Research*. 2004; 428: 120-24.
- [16] Gascoyne TC, Teeter MG, Guenther LE, Burnell CD, Bohm ER, Naudie DR. In vivo wear performance of cobalt-chromium versus oxidized zirconium femoral total knee replacements. *Journal of Arthroplasty*. 2016; 31(1): 137-41.
- [17] Hofer JK, Ezzet KA. A minimum 5-year follow-up of an oxidized zirconium femoral prosthesis used for total knee arthroplasty. *Knee*. 2014; 21(1): 168-71.
- [18] Innocenti M, Matassi F, Carulli C, Nistri L, Civinini R. Oxidized zirconium femoral component for TKA: a follow-up note of a previous report at a minimum of 10 years. *Knee*. 2014; 21(4): 858-61.
- [19] Kim YH, Park JW, Kim JS. Comparison of the Genesis II total knee replacement with oxidised zirconium and cobalt-chromium femoral components in the same patients: a

prospective, double-blind, randomized controlled study. *J Bone Joint Surg Br.* 2012; 94(9): 1221-7.

- [20] Vertullo CJ, Lewis PL, Graves S, Kelly L, Lorimer M, Myers P. Twelve-Year Outcomes of an Oxinium Total Knee Replacement Compared with the Same Cobalt-Chromium Design. *J Bone Joint Surg Am* 2017; 99: 275-83.
- [21] Brandt JM, Guenther L, O'Brien S, Vecherya A, Turgeon TR, Bohm ER. Performance assessment of femoral knee components made from cobalt-chromium alloy and oxidized zirconium. *Knee.* 2013; 20(6): 388-96.
- [22] Heyse TJ, Elpers ME, Nawabi DH, Wright TM, Haas SB. Oxidized zirconium versus cobalt-chromium in TKA: profilometry of retrieved femoral components. *Clinical Orthopaedics & Related Research.* 2014; 472(1): 277-83.
- [23] Hutchings IM. *Tribology: Friction and Wear of Engineering Materials.* 1<sup>st</sup> ed. Butterworth-Heinemann; 1992
- [24] Hood RW, Wright TM, Burstein AH. Retrieval analysis of total knee prostheses: A method and its application to 48 total condylar prostheses. *Journal of Biomedical Materials Research.* 1983; 17(5): 829-42.
- [25] Holleyman RJ, Scholes SC, Weir D, Jameson SS, Holland J, Joyce TJ, Deehan DJ. Changes in surface topography at the TKA backside articulation following in vivo service: a retrieval analysis. *Knee Surgery Sports Traumatology Arthroscopy.* 2015; 23(12): 3523-31.
- [26] Joyce TJ, Langton DJ, Jameson SS, Nargol AV. Tribological analysis of failed resurfacing hip prostheses and comparison with clinical data. *Proceedings of the Institution of Mechanical Engineers Part J Journal of Engineering Tribology.* 2009; 223(3): 317-323.
- [27] Scholes SC, Kennard E, Gangadharan R, Weir D, Holland J, Deehan D, Joyce TJ. Topographical analysis of the femoral components of ex vivo total knee replacements. *Journal of Materials Science-Materials in Medicine.* 2012; 24(2): 547-54

- [28] ISO 4287, Geometric Product Specification (GPS). Surface texture: Profile method – terms, definitions and surface texture parameters. 2009.
- [29] Gallo J, Goodman SB, Konttinen YT, Wimmer MA, Holinka M. Osteolysis around total knee arthroplasty: A review of pathogenetic mechanisms. *Acta Biomaterialia* 2013; 9: 8046-8058.
- [30] Vandekerckhove PTK, Teeter MG, Naudie DDR, Howard JL, MacDonald SJ, Lanting BA. The Impact of Coronal Plane Alignment on Polyethylene Wear and Damage in Total Knee Arthroplasty: A Retrieval Study. *Journal of Arthroplasty* 2017; 32: 2012-2016.
- [31] Langton DJ, Jameson SS, Joyce TJ, Gandhi JN, Sidaginamale R, Mereddy P, Lord J, Nargol AVF. Accelerating failure rate of the ASR total hip replacement. *JBJS(Br)* 2011; 93-B(8): 1011-1016

Implant No.	1	2	3	4	5	6
<b>Make &amp; Model of retrieved prosthesis</b>	S&N Genesis II Oxinium	S&N Genesis II Oxinium	S&N Legion Oxinium	DePuy PFC Sigma	DePuy PFC Sigma	DePuy PFC Sigma
<b>Gender</b>	Female	Male	Male	Female	Male	Female
<b>Side</b>	Right	Right	Left	Right	Left	Left
<b>BMI</b>	28.4	28.2	34	33	28.3	39
<b>Indication for primary surgery</b>	Osteoarthritis	First revision of primary TKR indicated	Osteoarthritis	Osteoarthritis	Osteoarthritis	Osteoarthritis
<b>Indication for Revision</b>	Pain / Hypermobility	Instability	Chronic infection and instability / Pain	Component malalignment	Component malalignment	Instability / Pain
<b>Time <i>In Vivo</i> (Months)</b>	40 months	86 months	47 months	44 months	35 months	63 months
<b>Age at implantation of retrieved prosthesis</b>	37 years	51 years	65 years	50 years	66 years	63 years
<b>PE Articular Surface Hood Damage Score</b>	22	35	44	25	15	33

Table 1. Patient and Implant Variables



	As-manufactured OxZr femoral component (n = 30, 1 component x 30 areas)	Retrieved OxZr femoral components (n = 90, 3 components x 30 areas per component)	As-manufactured CoCr femoral component (n = 30, 1 component x 30 areas)	Retrieved CoCr femoral components (n = 90, 3 components x 30 areas per component)	p-value 1 OxZr As-manufactured vs Retrieved	p-value 2 CoCr As-manufactured vs Retrieved	p-value 3 Retrieved OxZr vs Retrieved CoCr	p-value 4 As-manufactured OxZr vs As-manufactured CoCr
Mean $S_a$ ( $\mu\text{m}$ )	0.061 ( $\pm 0.004$ )	0.093 ( $\pm 0.014$ )	0.042 ( $\pm 0.003$ )	0.065 ( $\pm 0.005$ )	0.033	<0.001	0.059	<0.001
Mean $S_q$ ( $\mu\text{m}$ )	0.087 ( $\pm 0.005$ )	0.129 ( $\pm 0.017$ )	0.061 ( $\pm 0.004$ )	0.097 ( $\pm 0.006$ )	0.021	<0.001	0.079	<0.001
Mean $S_p$ ( $\mu\text{m}$ )	0.632 ( $\pm 0.035$ )	0.758 ( $\pm 0.045$ )	0.636 ( $\pm 0.042$ )	0.762 ( $\pm 0.056$ )	0.029	0.075	0.960	0.937
Mean $S_v$ ( $\mu\text{m}$ )	-0.613 ( $\pm 0.028$ )	-1.000 ( $\pm 0.078$ )	-0.831 ( $\pm 0.211$ )	-1.145 ( $\pm 0.087$ )	<0.001	0.178	0.218	0.314
Mean $S_z$ ( $\mu\text{m}$ )	1.245 ( $\pm 0.053$ )	1.758 ( $\pm 0.115$ )	1.467 ( $\pm 0.222$ )	1.918 ( $\pm 0.112$ )	<0.001	0.077	0.322	0.337
Mean $S_{sk}$	0.6194 ( $\pm 0.105$ )	0.118 ( $\pm 0.129$ )	0.806 ( $\pm 0.515$ )	-0.466 ( $\pm 0.345$ )	0.003	0.045	0.116	0.725

Table 2. Femoral component surface roughness measurements

\* The mean value  $\pm$  standard error is given for each surface roughness parameter. P-value 1 corresponds to the difference between the results for the retrieved OxZr femoral components compared to those for the as-manufactured OxZr femoral component. P-value 2 corresponds to the difference between the results for the retrieved CoCr femoral components and the as-manufactured CoCr femoral component. P-value 3 corresponds to the difference between the results for retrieved OxZr femoral components compared to those for retrieved CoCr femoral components. P-value 4 corresponds to the difference between the results for the as-manufactured OxZr femoral component and the as-manufactured CoCr femoral component

*Blank page*

## **Appendix H: Scholes et al JMatSci:MatMed 2018**

Within this appendix is included the manuscript for the publication:

Scholes S.C., **Kennard E.**, Gangadharan R., Weir D.J., Holland J., Deehan D and Joyce T.J. *Topographical analysis of the femoral components of ex vivo total knee replacements* Journal of Material Science: Material in Medicine, 2013 (24): 547-554 [15]

As noted on page 5 of Chapter 1 Introduction, this thesis is submitted in my legal married name Emma Ritchie, however my authored publications are in my maiden name Emma Kennard.

*Blank page*

**TITLE:** Topographical analysis of the femoral components of ex vivo total knee replacements

**AUTHORS:** Susan C. Scholes <sup>a</sup>, Emma Kennard <sup>a</sup>, Rajkumar Gangadharan <sup>b</sup>, David J. Weir <sup>b</sup>, James Holland <sup>b</sup>, David Deehan <sup>b</sup> and Thomas J. Joyce <sup>a</sup>.

<sup>a</sup> Bioengineering Group, School of Engineering, Newcastle University, Stephenson Building, Newcastle upon Tyne, NE1 7RU, England, United Kingdom.

<sup>b</sup> Freeman Hospital, Newcastle upon Tyne, NE1 7DN, England, United Kingdom.

## **ABSTRACT**

With greater numbers of primary knee replacements now performed in younger patients there is a demand for improved performance. Surface roughness of the femoral component has been proposed as a causative mechanism for premature prosthesis failure. Nineteen retrieved total knee replacements were analysed using a non-contacting profilometer to measure the femoral component surface roughness. The Hood technique was used to analyse the wear and surface damage of the matching ultra-high molecular weight polyethylene (UHMWPE) tibial components. All femoral components were shown to be up to 119 rougher after their time in vivo while 95 % showed a change in skewness, further indicating wear. This increase in roughness occurred relatively soon after implantation (within 1 year) and remained unchanged thereafter. Mostly, this roughness was more apparent on the lateral condyle than the medial. This increased femoral surface roughness likely led to damage of the UHMWPE tibial component and increased Hood scores.

**Keywords:** Explanted knee joint; surface topography; femoral component wear; UHMWPE surface damage; failure.

## 1. INTRODUCTION

Successful total knee replacement (TKR) surgery offers the relief of debilitating issues such as the pain and reduced mobility suffered by those with arthritic diseases. Over the past 10 years there has been an upward trend in the numbers of TKRs performed each year [1, 2]. This increase is highest in the younger population (patients under 65) [2]. It is well known that failure of these knee implants occurs and, as stated by Losina and Katz (2012) [3], “the greater risk of implant failure in younger patients, coupled with longer remaining life expectancy in this age group, will combine to produce even higher rate of revision”.

Kurtz *et al* (2005) [4] stated that over 30,000 revision TKRs are performed in the United States each year. It is clear from the National Joint Registry for England and Wales [1] that knee joint replacement in these countries is now more common than replacement of the hip joint. There were 81,979 knee replacement procedures recorded in this registry [1] in 2010. Of these, 5,109 were revision procedures and this revision burden has been seen to increase year by year. On top of patient discomfort and disability, this has a growing financial burden [5].

The majority of failures to TKRs in the longer-term are due to wear particle induced osteolysis [6]. It is important to investigate not only the damage caused to the ultra-high molecular weight polyethylene (UHMWPE) surface but that suffered by the harder femoral component also. Damage to the articulating surface of the femoral component is likely to cause further damage to the softer UHMWPE tibial bearing surface and increased wear particle production leading to osteolysis and failure [7]. Our knowledge of the clinical importance of femoral component surface roughness of the revised knee prostheses and the correlation between patient factors and roughness values [8-11] remains limited. The principal barrier to advancement of our understanding has been the small numbers of explants examined and the use of simple contacting stylus profilometers. Many of these profilometers are limited in their accuracy of measurement depending on the degree of roughness and, also, the surface profile that is being measured. Furthermore, contact profilometers use a diamond stylus to trace over the surface; which in itself may lead to surface damage. Only one of the papers referenced above used a non-contacting profilometer [8]. The machine used by Que

*et al* (2000) [8] (Zygo NewView 100 non-contacting profilometer) has a vertical resolution of better than 1nm and has been shown to provide reliable surface topography measurements. This non-contacting profilometer measures the surface with different magnifications giving different areas of view whereas the contacting machines used by others [9-11] can only provide line profiles. Therefore, the non-contacting profilometer allows a detailed assessment of the surface roughness to be performed in 3D rather than 2D. Unlike in the work by Que *et al* (2000) we sought to compare femoral and tibial wear, and also to correlate these changes over time. Moreover, we did not limit our study to a single design of TKR.

In this study, preliminary work has been undertaken, and is discussed, assessing an experimental technique used to analyse the surfaces of explanted knee prostheses. The surface roughness of the femoral components of 19 retrieved TKRs was assessed on a Zygo NewView 5000 non-contacting profilometer. The Hood analysis [12] was then performed on the 19 matching UHMWPE tibial components to provide a wear and surface damage score. The apparent relationships between surface characteristics and patient/component variables in this small sample set were then determined.

## **2 MATERIALS AND METHODS**

Ethical approval was obtained to allow the provision of 19 retrieved TKRs (11 males and 8 females) by Freeman Hospital, Newcastle upon Tyne, UK. Details of these 19 knee prostheses are given in Table 1. These joints were all cobalt chromium molybdenum (CoCrMo)-on-UHMWPE prostheses. The duration of implantation ranged from 1 to 22 years (mean: 11 years; median: 12 years). Patient age at time of revision surgery ranged from 49 to 90 years (mean: 73 years; median: 73 years). Body mass index (BMI) was available for 17 of the 19 patients and this ranged from 21.5 to 41.7 (mean: 29.6; median: 29.5). There were various designs of TKR including Biomet AGC, Biomet Dual Articular 2000, DePuy PFC Sigma, Stryker Kinematic, and Stryker Kinemax. This knee replacement surgery was performed on the right knee for 11 patients and on the left for 8 patients. Two of the joints were uncemented and the other 17 were cemented. Failure of all but one of the prostheses was due to infection, instability, wear, component loosening or aseptic loosening. Periprosthetic fracture

was seen in two of these cases; one at the distal shaft of the femur (joint 2) and the other at the junction of the metaphyseal and diaphyseal region of the tibia (joint 8). One component was revised because of fixed flexion with a tight anterior compartment.

Before the commencement of measurements, both the femoral and tibial components were sterilised in formaldehyde solution for at least 48 hours, rinsed with water and the femoral components were wiped with acetone. Each femoral and tibial component was then photographed with an 18 megapixel Canon EOS 600D camera using an 18-55 mm zoom lens.

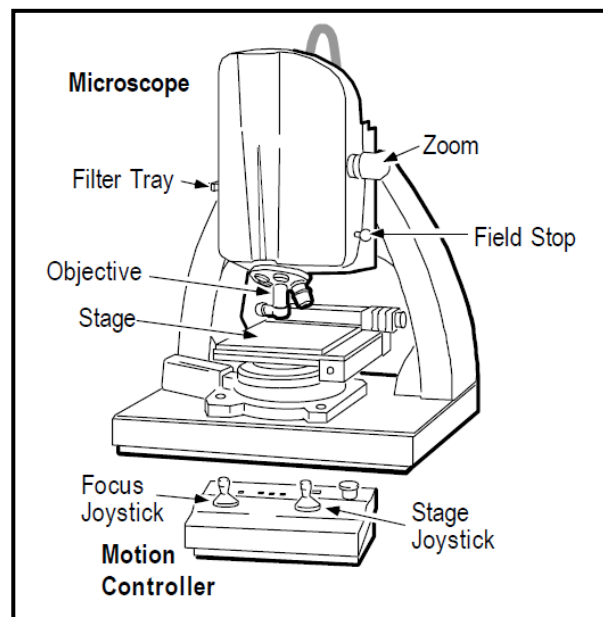


Figure 1. Zygo NewView 5000 profilometer (taken with permission from Lambda Photometrics from the operating manual)

The surface roughness analyses of the femoral components were performed on a Zygo NewView 5000 non-contacting white light interferometric profilometer (see Figure 1). The x10 lens was used with a x2 zoom, giving an area of view of 317 x 238  $\mu\text{m}$ . The Zygo had a vertical resolution of better than 1 nm and a 0.99  $\mu\text{m}$  lateral (x, y) resolution for the magnification used. Measurements of  $S_q$  (root mean square surface roughness) and  $S_{sk}$  (surface skewness) were taken. The skewness of a surface is a measure of symmetry of the profile about the mean line. A positively skewed surface has a predominance of peaks and a negatively skewed surface has more pronounced valleys. When new, components tend to have a positive skewness and as they become worn the skewness becomes negative. Ten measurements were performed



on the unworn area (five on the medial side and five on the lateral) to provide an approximation of the surface roughness and skewness at implantation time. Twenty measurements were taken on the worn area (10 on the medial side and 10 on the lateral) to show how roughness and skewness varied with time *in vivo*.

Surface analyses on the UHMWPE tibial component were performed using a Mitutoyo Quick Scope (non-contact vision measuring machine) with a x50 lens and x0.5 zoom resulting in a x25 magnification. The analysis reported by Hood *et al* (1983) [12] was used to determine a damage score for the UHMWPE component. The Hood technique is a well-known, well referenced 'industry standard' [13]. In this technique, the UHMWPE tibial components are assessed to determine the degree of damage to the surfaces in relation to seven different damage modes: surface deformation, pitting, embedded debris, scratching, burnishing, abrasion and delamination. The gradings range from zero to three for each of the types of surface damage and the bearing surface is divided into 10 sections (as described by Hood [12]) resulting in a total, maximum damage score of 210.

### 3 RESULTS

The macroscopic surface damage on the femoral and tibial components of an example prosthesis (joint 1) is shown in Figure 2.

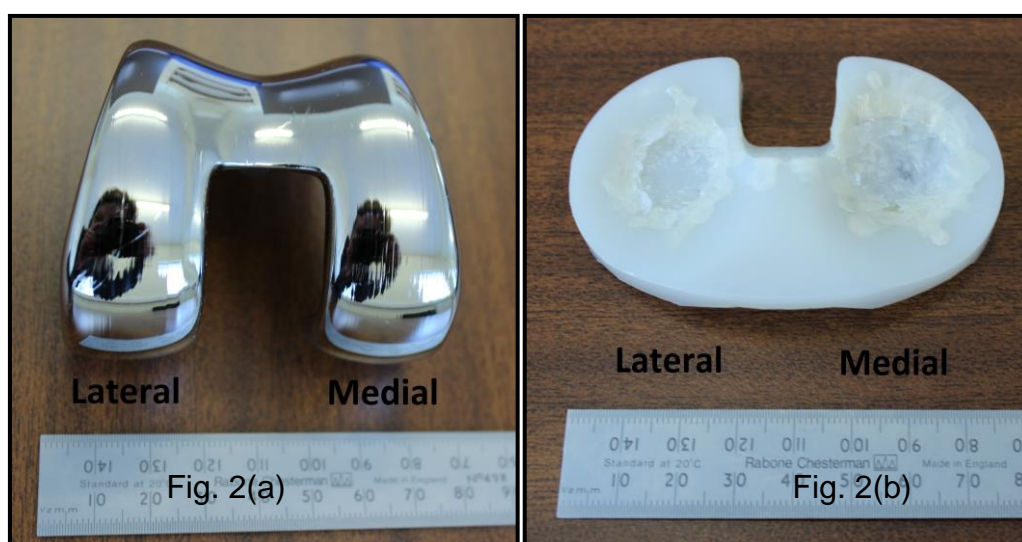


Figure 2. (a) Femoral component (b) Tibial component (grey marks within wear area show ink residue from Hood analysis)

Figure 3 shows an example of an image acquired by the non-contacting profilometer on the un-worn (a) and worn (b) regions of the femoral component. The average unworn and worn surface roughness values ( $S_q$  and  $S_{sk}$ ) for all the femoral components are shown in Table 2 and Figure 4. The roughness order of the worn femoral components is shown in Figure 5 (average combined  $S_q$  value of the medial and lateral sides). The related Hood wear score for the UHMWPE components for these joints is also shown in Figure 5.

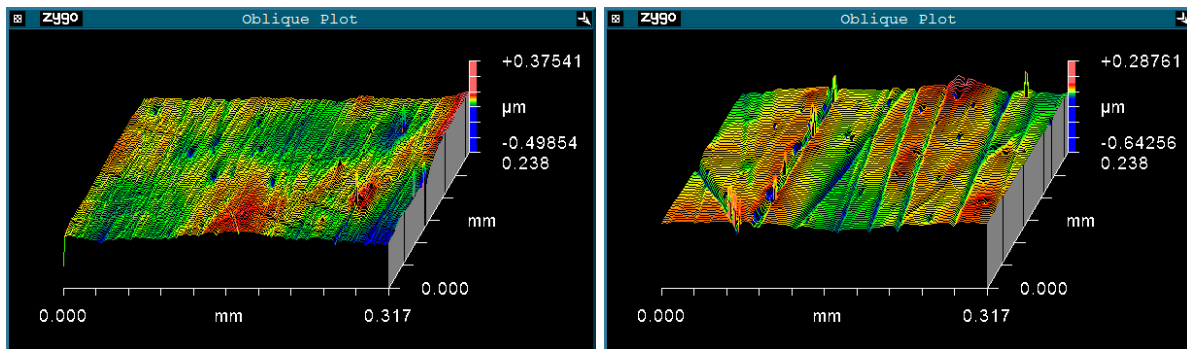


Figure 3. Surface topography images of a femoral component (a) un-worn (b) worn

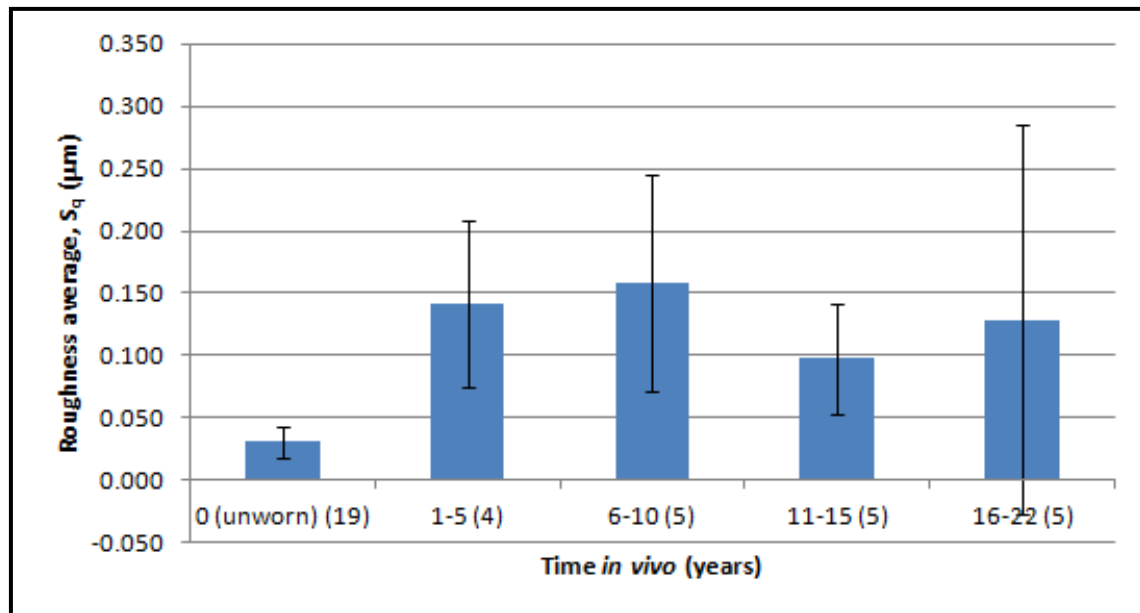


Figure 4.  $S_q$  roughness values (mean and standard deviations) with time *in vivo* (number of data points shown in brackets)

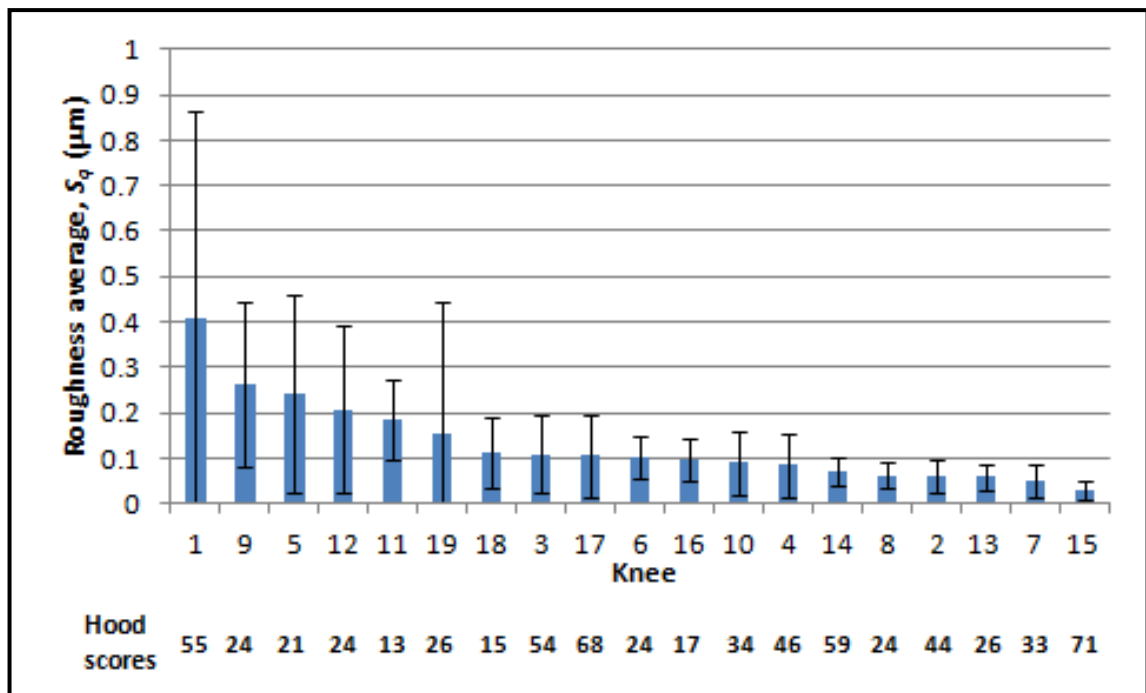


Figure 5.  $S_q$  roughness values (mean and standard deviations) with Hood scores for all joints in order of roughness

The surface roughness had increased on all of the retrieved femoral components with a move to a more negative skewness (see Table 2 and Figures 4 and 6). The average unworn  $S_q$  was  $0.031 \mu\text{m}$  (range:  $0.014 - 0.060 \mu\text{m}$ ), the average worn medial  $S_q$  was  $0.110 \mu\text{m}$  (range:  $0.023 - 0.281 \mu\text{m}$ ) and the average worn lateral  $S_q$  was  $0.151 \mu\text{m}$  (range:  $0.037 - 0.535 \mu\text{m}$ ). The majority of these wear marks were unidirectional scratches in the anterior-posterior direction. The average skewness values changed from being  $0.431$  for the unworn surface to  $-0.929$  for the worn medials and  $-0.566$  for the worn lateral condyles.

There was no correlation between roughness of the femoral component and time *in vivo* or patient age (see Figures 4 and 7). Patient age was separated into younger ( $<65$ ) and older patients ( $\geq 65$ ) as stated by Losina *et al* (2012) [2]. There was also no apparent correlation between roughness and BMI or roughness and Hood score. In addition to this, there was no obvious relationship between Hood score and BMI or the time *in vivo* and BMI. Also there was no relationship between whether the implant was positioned on the left or right hand side of the patient and the time *in vivo*. There was no relationship between the positioning of the implant (left or right-hand side) and the

roughness of the medial and lateral femoral condyles. Figure 8 shows that there was also no apparent correlation between time *in vivo* and either gender or age.

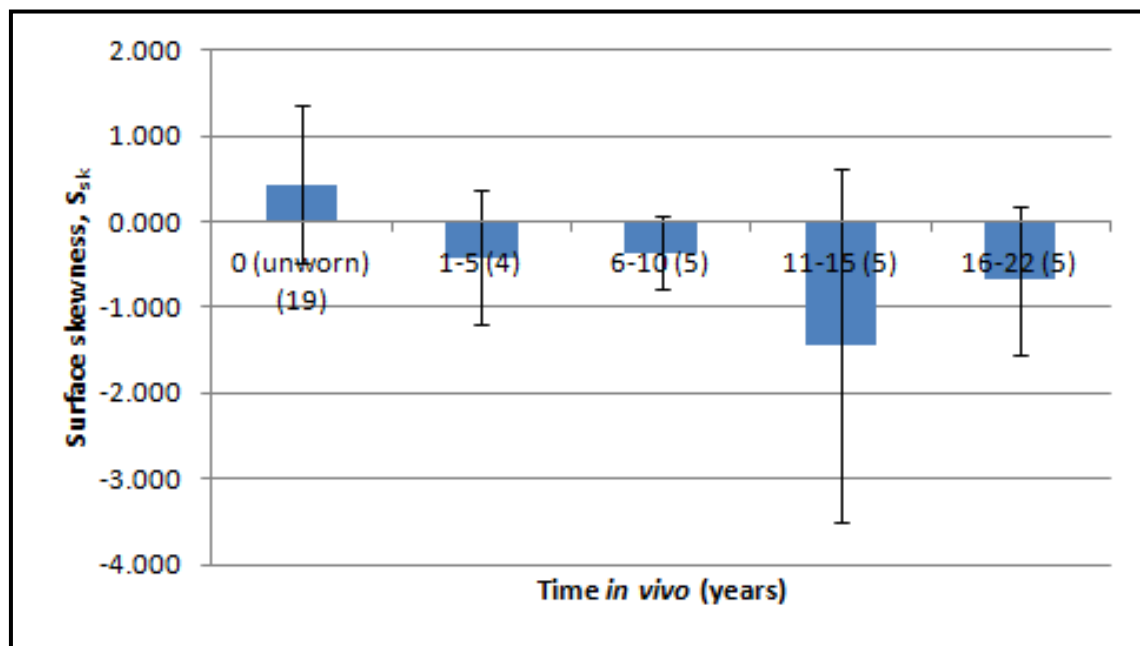


Figure 6. Surface skewness values (mean and standard deviations) with time *in vivo* (number of data points shown in brackets)

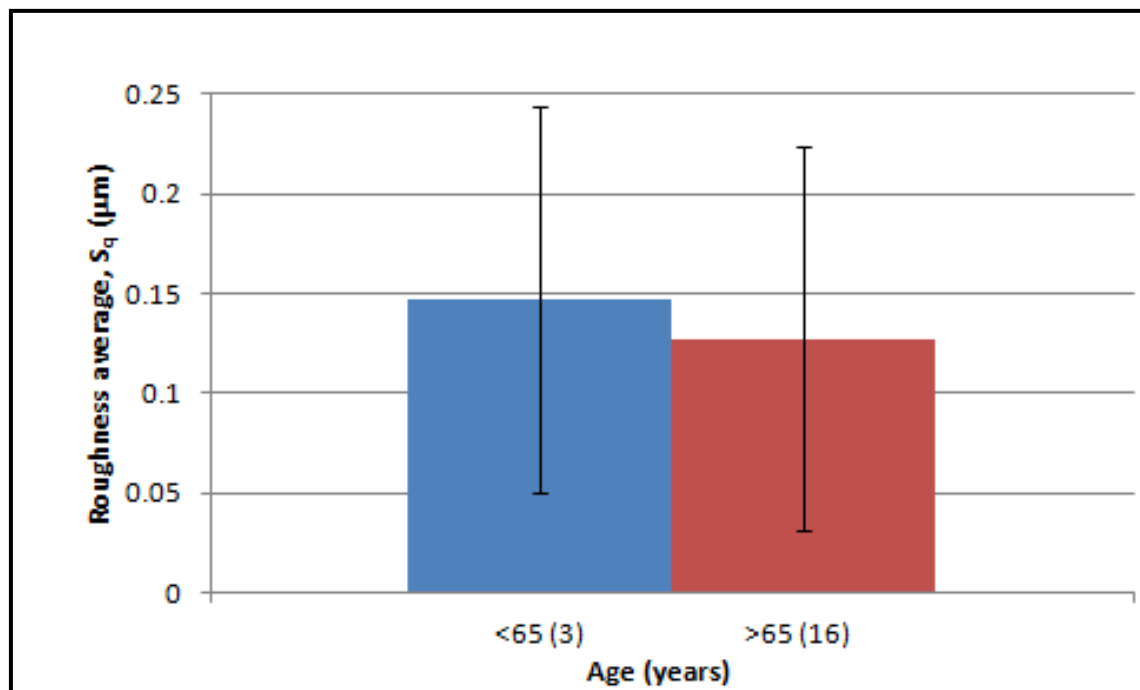


Figure 7.  $S_q$  roughness values (mean and standard deviations) with age at revision surgery (number of data points shown in brackets)

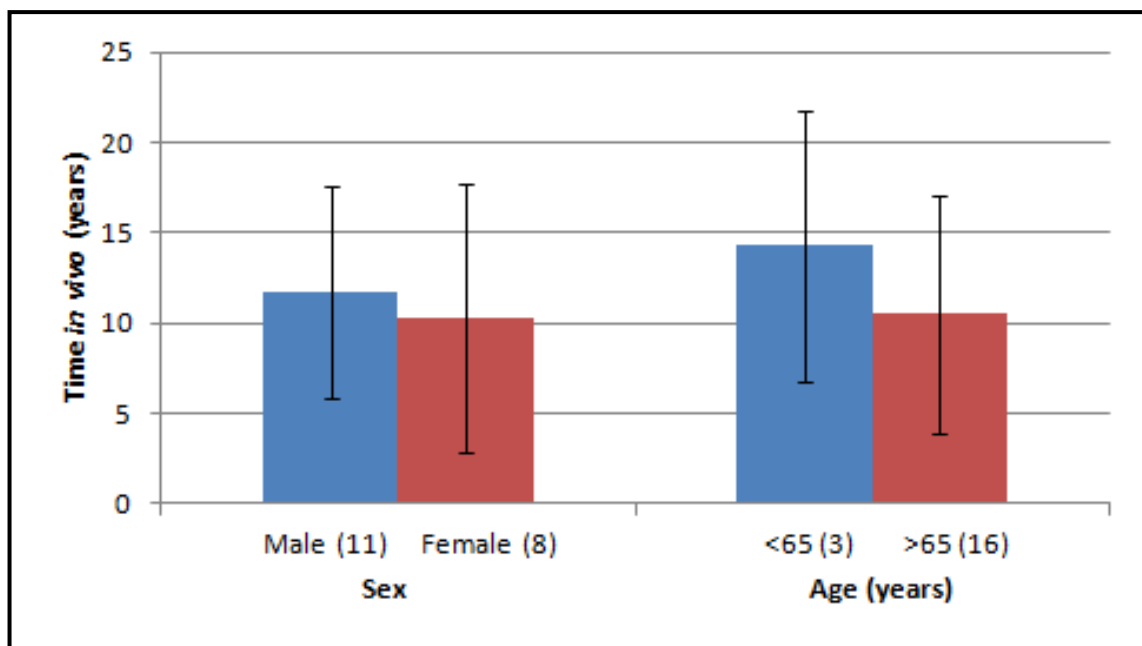


Figure 8. Time *in vivo* (mean and standard deviations) with gender and age at revision surgery (number of data points shown in brackets)

There did, however, appear to be a correlation between surface roughness and gender of the patient. Higher surface roughness values were found with male patients than with females. This is shown in Figure 9.

Figure 10 shows that 10 of the femoral components were rougher on the lateral side, 4 were rougher on the medial and 5 had similar roughness values on both the medial and lateral sides (within 10 nm). From this figure it can be seen that more joints were rougher on the lateral side than the medial.

Trends may also exist between time *in vivo* and Hood score (see Figure 11) along with Hood score and age at revision surgery, this is shown in Figure 12. In addition to this, it was found that the indication for revision surgery may be related to the duration of implantation. All but one implant revisions after 13 years *in vivo* were performed at this later stage due to aseptic loosening or wear of the implant.

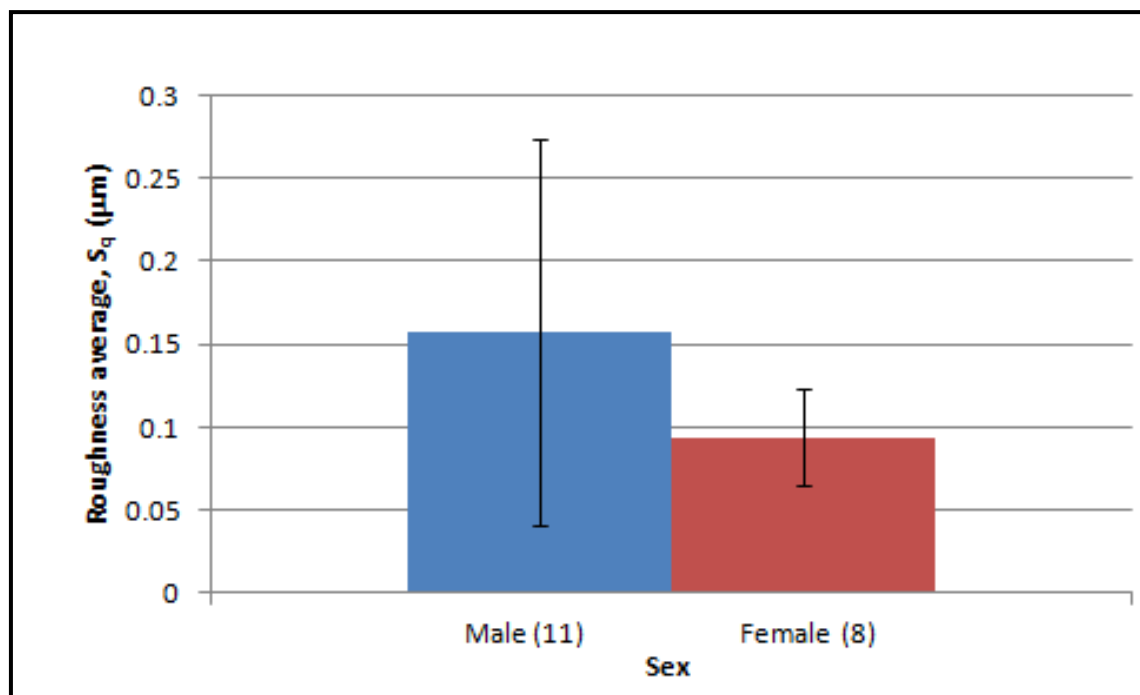


Figure 9.  $S_q$  roughness values (mean and standard deviations) with gender (number of data points shown in brackets)

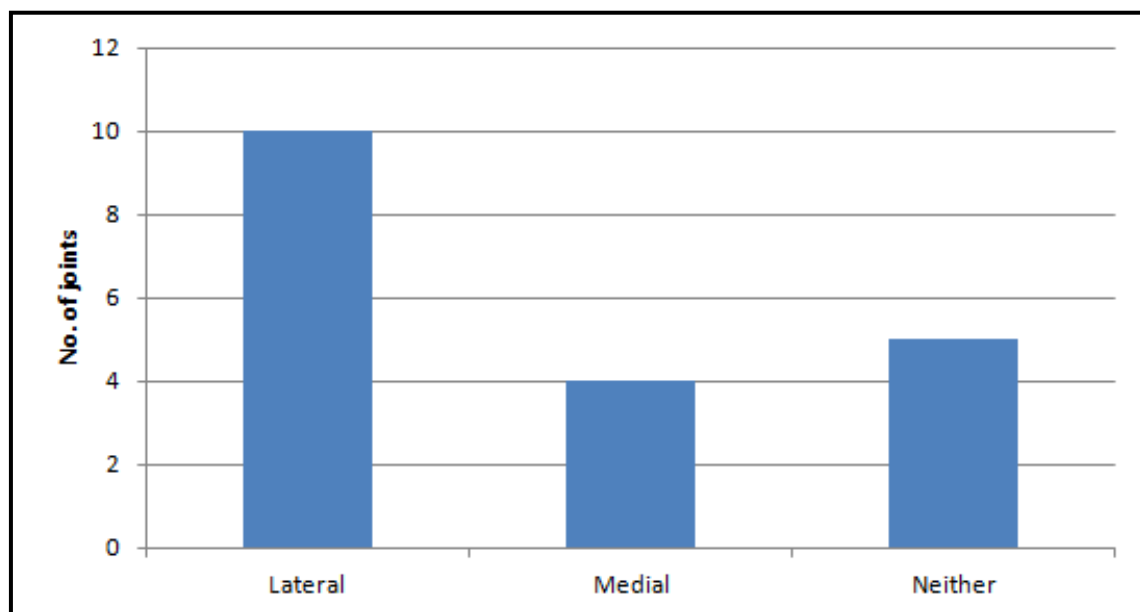


Figure 10. Number of femoral condyles showing the greatest roughness

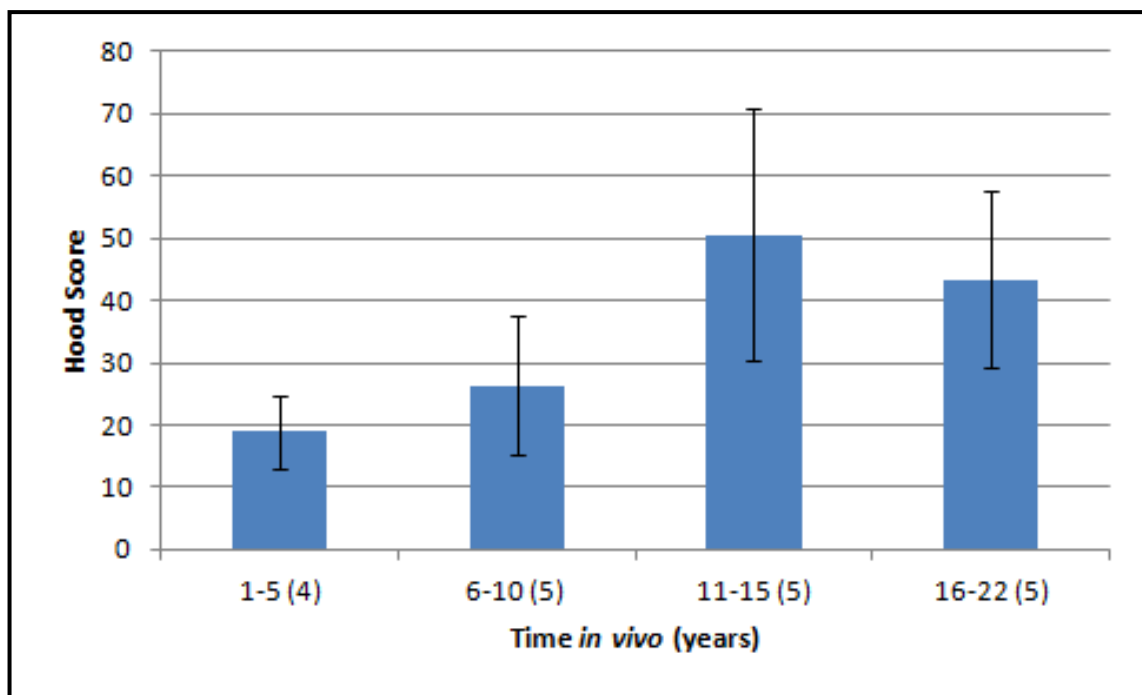


Figure 11. Time *in vivo* (mean and standard deviations) and Hood score (number of data points shown in brackets)

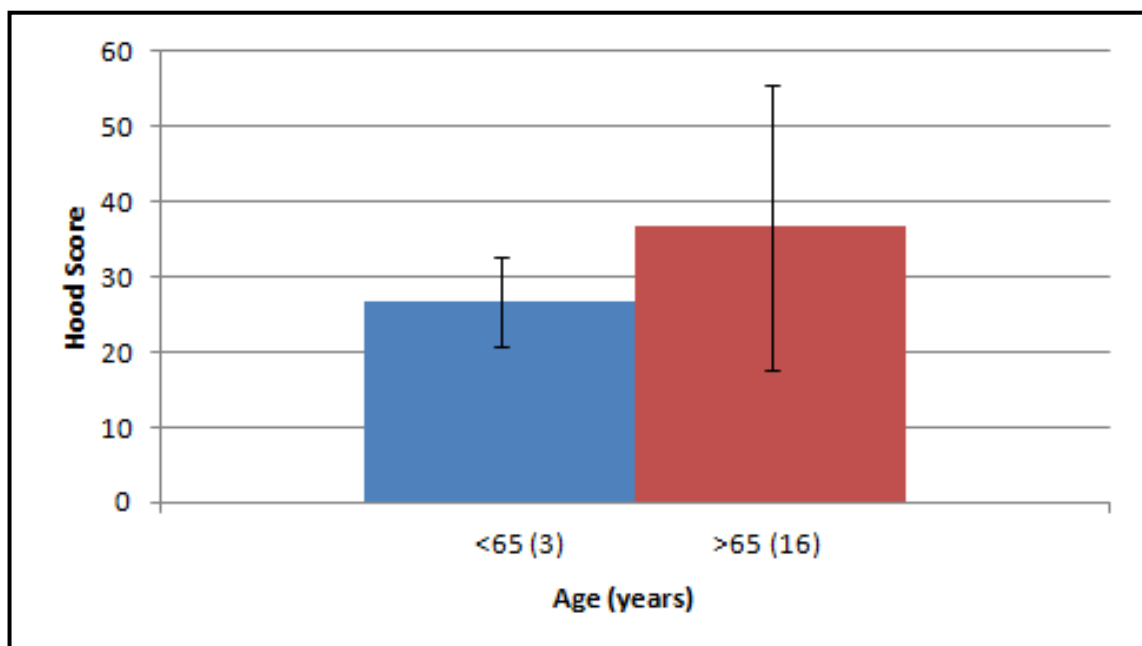


Figure 12. Relationships between Hood score (mean and standard deviations) and age at revision surgery (number of data points shown in brackets)

## 4.0 DISCUSSION

The surface roughness measurements of the worn areas of all of the femoral components were found to be between x2 and x11 rougher than the unworn sections of the surfaces. Siddique *et al* (2003) [7] noted that macroscopic abrasion marks were evident on the femoral components of retrieved porous coated anatomical (PCA) knees. These authors speculated that these marks on the femoral components may have led to early wear of the UHMWPE tibial components and recommended that, if this surface damage was evident at revision, the femoral component should be revised also [7]. During fundamental tribological studies, UHMWPE wear has been found to be increased with a rougher counterface [14-16]. Also within the laboratory, femoral component surface roughness has been found to increase UHMWPE wear [17, 18]. Such an increase in wear *in vivo* may lead to increased numbers of TKR failures. In this study, there was a clear increase in roughness between the worn and unworn regions of the surfaces even after only 1 year *in vivo*. The increase in roughness, shown in Figure 4, seemed to occur relatively soon after implantation (within the first year) for all joint designs. After this the roughness remained relatively unchanged and, therefore, surface roughness was not found to be related to time *in vivo*. This can be seen for both the  $S_q$  and  $S_{sk}$  values shown in Figures 4 and 6. To the authors' best knowledge this roughening soon after implantation and subsequent plateau has not previously been reported. No obvious relationship was found between femoral component surface roughness and patient age (see Figure 7) or BMI and no relationship was found between Hood score and BMI. In addition to this, the duration of implantation did not appear to be related to gender, age (see Figure 8) or BMI.

An apparent relationship was, however, found between the surface roughness of the femoral component and gender of the patient (Figure 9). A relationship was also found between the Hood score (describing the wear and surface damage of the UHMWPE component) and time *in vivo*. From Figure 11 it can be seen that this is a co-linear relationship; the Hood score increased in a linear manner with duration of implantation. This indicates that damage to the UHMWPE tibial components is a continuous process. A relationship was also found between the Hood score and age at revision surgery (see Figure 12).



In addition to this a relationship was found between time *in vivo* and indication for revision surgery. This is to be expected as it is well known that aseptic loosening is a longer-term diagnosis and the majority of infections happen at an earlier stage. The two cases that seem to negate this (joint 7 with failure due to infection after 22 years *in vivo* and joint 8 which failed with aseptic loosening after only one year) can be explained. The late failure due to infection, joint 7, was an extreme case. This patient, previous to the knee revision surgery, had chronic on-going infection in his right hip replacement which led to the need for removal of this hip. Long-term immunosuppressive medication for severe ankylosing spondylitis resulted in a grossly infected TKR and the need for this knee revision due to infection at such a late stage. The early failure due to aseptic loosening of joint 8 was due to malalignment of the tibial component at primary surgery (primary surgery was performed elsewhere, not Freeman hospital) resulting in instability and aseptic loosening which contributed to a fall and periprosthetic fracture.

Nine of the UHMWPE tibial components showed delamination wear. All of these joints had been implanted for 7 years or more and the sterilisation process is unknown. However, delamination wear has been found to be related to the sterilisation method used for UHMWPE components [19, 20]. For this reason, gamma irradiation in air is no longer used.

An interesting discovery from this study was that the majority of femoral components showed more surface damage on the lateral condyle than the medial. This supports the work of Cho *et al* (2010) [10] who examined the surface roughness ( $R_a$ ) of four retrieved femoral components. They found that the mean values of roughness were higher on the lateral side than the medial (0.180  $\mu\text{m}$  and 0.149  $\mu\text{m}$  compared with the mean values of  $S_q$  found in this study with a larger sample size ( $n=19$ ) of 0.151  $\mu\text{m}$  and 0.110  $\mu\text{m}$  for the lateral and medial components respectively). One of the four explanted femoral components investigated by Muratoglu *et al* (2004) [17] showed higher surface roughness on the lateral side (average  $R_a$  values were found to be 0.20  $\mu\text{m}$  for the lateral condyle and 0.12  $\mu\text{m}$  for the medial). The other three gave similar roughness values on the medial and lateral.

Few studies have taken surface roughness measurements of retrieved femoral components [8-11, 17] and only one of these discusses surface topography measurements taken using a non-contacting profilometer [8]. Que *et al* (2000) [8] measured the surface roughness of retrieved CoCrMo femoral components articulating against PCA tibial components using a non-contacting Zygo NewView 100 profilometer. They found that the worn areas of the explanted femorals were one order of magnitude greater in roughness than the unworn areas and the condyles showed unidirectional scratches in the anterior-posterior direction. As with this study, they found no correlation between roughness of the femoral component and the patient age, weight or total time of implantation. Using a contact stylus profilometer however, Lakdawala *et al* (2005) [9] showed no differences in surface roughness between the articulating surfaces of 22 joints and areas of the femoral component that were not in articulation with either the patella or tibia, defined as the control areas. The study reported here and that reported by Que *et al* (2000) have, however, found otherwise. From Table 2, it is clear that all of the femoral components in this study suffered different degrees of damage with increased surface roughness values. The non-contacting profilometer used for this research (and also that used by Que *et al* (2000)[8]) is capable of taking repeatable surface roughness measurements at high resolution (less than 1 nm) to allow reliable data capture. The contact stylus profilometer used by Lakdawala *et al* (2005) had a resolution of 0.01  $\mu\text{m}$  and a  $R_a$  maximum uncertainty of 5 nm and is, therefore, less precise than the non-contacting machine used in this study.

One limitation of the study reported here is the small sample size of 19. However, a key aim of this study was to set up a robust and reliable protocol which allowed measurement of femoral component roughness alongside use of a proven methodology for the assessment of damage to the polyethylene tibial component. The surface analysis of additional knee retrievals using this technique continues and will provide a larger sample set allowing stronger relationships to be determined between surface damage and failure (of both the femoral and tibial components) and patient/component variables. This information will be disseminated to clinicians and manufacturers in the hope that improvements to total knee arthroplasty can be made, for the long-term benefit of the millions of people likely to need these artificial joints.

## 5.0 CONCLUSIONS

In this study the increased roughness of the femoral components was found to take place relatively soon after implantation, after which the roughness appeared to remain relatively unchanged. Skewness changed from positive to negative in the majority of cases thus further indicating wear of the femoral components. Lateral femoral condyles tended to be rougher than medial condyles. No relationship was found between the increased surface roughness measured on the worn areas of the femoral surfaces and the age of the patient, BMI of the patient or time *in vivo* of the implant. In addition to this, the roughness of the femoral component did not relate to the damage score of the UHMWPE component. There was also no trend between time *in vivo* and gender, age or BMI. There was, however, a relationship between time *in vivo* and UHMWPE damage score along with Hood score and age at revision surgery. As expected, indication for revision surgery was associated with time *in vivo*.

This study has described a useful technique to analyse the surfaces of explanted knee joints and offer new insights into the pathogenesis of early failures. The work performed has also given preliminary results from the use of this technique to determine the relationships between surface characteristics and patient/component variables.

## ACKNOWLEDGMENTS

The funding for this work was provided by a Knowledge Transfer Account (KTA). This KTA came from an Engineering and Physical Sciences Research Council (EPSRC) award given to Newcastle and Durham Universities. None of the authors hold any professional or financial affiliations that may be perceived to have biased the presentation.

## REFERENCES

1. National Joint Registry for England and Wales. 8th Annual Report. 2011.

2. Losina E, Thornhill TS, Rome BN, Wright J, Katz JN. The dramatic increase in total knee replacement utilization rates in the United States cannot be fully explained by growth in population size and the obesity epidemic. *J Bone Joint Surg-Am Vol.* 2012;94(3):201-7.
3. Losina E, Katz JN. Total knee arthroplasty on the rise in younger patients: Are we sure that past performance will guarantee future success? *Arthritis Rheum.* 2012;64(2):339-41. doi:10.1002/art.33371.
4. Kurtz S, Mowat F, Ong K, Chan N, Lau E, Halpern M. Prevalence of primary and revision total hip and knee arthroplasty in the United States from 1990 through 2002. *J Bone Joint Surg-Am Vol.* 2005;87A(7):1487-97. doi:10.2106/jbjs.d.02441.
5. Lavernia C, Lee DJ, Hernandez VH. The Increasing Financial Burden of Knee Revision Surgery in the United States. *Clin Orthop Rel Res.* 2006; 446:221-6  
10.1097/01.blo.0000214424.67453.9a.
6. Gioe TJ, Killeen KK, Grimm K, Mehle S, Scheltema K. Why are total knee replacements revised? Analysis of early revision in a community knee implant registry. *Clin Orthop Rel Res.* 2004(428):100-6.
7. Siddique MS, Rao MC, Deehan DJ, Pinder IM. Role of abrasion of the femoral component in revision knee arthroplasty. *J Bone Joint Surg-Br Vol.* 2003;85B(3):393-8. doi:10.1302/0301-620x.85b3.13041.
8. Que L, Topoleski LDT, Parks NL. Surface roughness of retrieved CoCrMo alloy femoral components from PCA artificial total knee joints. *J Biomed Mater Res.* 2000;53(1):111-8. doi:10.1002/(sici)1097-4636(2000)53:1<111::aid-jbm15>3.0.co;2-y.
9. Lakdawala A, Todo S, Scott G. The significance of surface changes on retrieved femoral components after total knee replacement. *J Bone Joint Surg-Br Vol.* 2005;87B(6):796-9. doi:10.1302/0301-620x.87b6.15776.
10. Cho CH, Murakami T, Sawae Y. Influence of microscopic surface asperities on the wear of ultra-high molecular weight polyethylene in a knee prosthesis. *Proc. Inst.*

Mech. Eng. Part H-J Eng. Med. 2010;224(H4):515-29.

doi:10.1243/09544119jeim690.

11. Burnell CDC, Brandt JM, Petrak MJ, Bourne RB. Posterior Condyle Surface Damage on Retrieved Femoral Knee Components. J Arthroplast. 2011;26(8):1460-7.

doi:10.1016/j.arth.2011.03.011.

12. Hood RW, Wright TM, Burstein AH. Retrieval analysis of total knee prostheses - a method and its application to 48 total condylar prostheses. J Biomed Mater Res. 1983;17(5):829-42.

doi:10.1002/jbm.820170510.

13. Kurtz SM. The UHMWPE Biomaterials Handbook: Ultra-High Molecular Weight Polyethylene in Total Joint Replacement and Medical Devices (2nd Edition).

Burlington, MA: Academy Press; 2009.

14. Dowson D, Taheri S, Wallbridge NC. The role of counterface imperfections in the wear of polyethylene. Wear. 1987;119(3):277-93.

doi:10.1016/0043-1648(87)90036-6.

15. Fisher J, Firkins P, Reeves EA, Hailey JL, Isaac GH. The influence of scratches to metallic counterfaces on the wear of ultra-high molecular weight polyethylene.

Proc. Inst. Mech. Eng. Part H-J Eng. Med. 1995;209(4):263-4.

doi:10.1243/pime\_proc\_1995\_209\_353\_02.

16. Bowsher JG, Shelton JC. Hip simulator study of the influence of patient activity level on the wear of crosslinked polyethylene under smooth and roughened femoral conditions. Wear. 2001;250:167-79.

doi:10.1016/s0043-1648(01)00619-6.

17. Muratoglu OK, Burroughs BR, Bragdon CR, Christensen S, Lozynsky A, Harris WH. Knee simulator wear of polyethylene tibias articulating against explanted rough femoral components. Clin Orthop Rel Res. 2004(428):108-13.

doi:10.1097/01.blo.0000143801.41885.8b.

18. DesJardins JD, Burnikel B, LaBerge M. UHMWPE wear against roughened oxidized zirconium and CoCr femoral knee components during force-controlled simulation. Wear. 2008;264(3-4):245-56.

doi:10.1016/j.wear.2007.03.020.

19. Collier JP, Sperling DK, Currier JH, Sutula LC, Saum KA, Mayor MB. Impact of gamma sterilization on clinical performance of polyethylene in the knee. *J Arthroplast.* 1996;11(4):377-89. doi:10.1016/s0883-5403(96)80026-x.
20. Kennedy FE, Currier JH, Plumet S, Duda JL, Gestwick DP, Collier JP et al. Contact fatigue failure of ultra-high molecular weight polyethylene bearing components of knee prostheses. *Journal of Tribology-Transactions of the Asme.* 2000;122(1):332-9. doi:10.1115/1.555364.

Table 1. Clinical data for the retrieved knee prostheses (NK: Not Known)

Knee	Age at Revision	BMI	Sex	Right or Left	Time <i>in vivo</i> (years)	Cemented (C) or uncemented (U)	Knee Type	Indication for revision
1	81	27.5	M	R	20	U	Stryker Kinematic	Aseptic loosening
2	72	29.5	M	R	19	C	Smith and Nephew Genesis	Wear of UHMWPE, periprosthetic fracture
3	72	21.5	M	R	12	C	Stryker Kinemax	Infection
4	72	29.5	F	R	7	C	Plus Orthopaedics TC Plus	Wear of UHMWPE
5	56	28.5	M	R	7	C	Stryker Kinemax	Loosening
6	90	27	F	L	7	C	Biomet Maxim	Instability
7	55	26	M	R	22	C	Stryker Kinemax Plus	Infection
8	80	24	F	L	1	C	Biomet AGC V2 HPPS	Instability, aseptic loosening, periprosthetic fracture
9	73	41.7	M	L	6	C	Biomet Dual Articular 2000	Infection
10	73	30	F	L	13	C	Stryker Kinemax	Wear of UHMWPE
11	77	25	M	R	2	C	DePuy Noiles S-ROM rotating hinge	Infection
12	79	31.5	M	R	5	C	DePuy PFC Sigma	Infection
13	85	NK	F	R	20	C	Biomet AGC V2 HPPS	Tibial loosening
14	82	25	M	L	19	C	Stryker Kinematic	Aseptic loosening and wear
15	79	32.7	M	L	14	C	Stryker Kinemax	Aseptic loosening
16	79	NK	F	R	7	C	DePuy PFC Sigma	Infection
17	67	32	F	L	13	C	Stryker Kinemax	Wear of UHMWPE
18	67	38	M	R	3	C	DePuy PFC Sigma	Fixed flexion, tight anterior compartment
19	49	33	F	L	14	U	Exactech Optetrak	Tibial loosening

Table 2: Surface roughness values of each femoral component

Knee	Unworn		Worn Medial		Worn Lateral	
	$S_q$ ( $\mu\text{m}$ )	$S_{sk}$	$S_q$ ( $\mu\text{m}$ )	$S_{sk}$	$S_q$ ( $\mu\text{m}$ )	$S_{sk}$
1	0.036	0.176	0.281	-0.342	0.535	-0.289
2	0.021	-0.444	0.055	-1.104	0.065	-0.816
3	0.047	0.474	0.131	-1.210	0.086	-1.513
4	0.014	-0.331	0.031	-0.655	0.138	-0.276
5	0.023	0.566	0.109	0.16	0.375	-0.276
6	0.060	0.449	0.119	0.152	0.087	-0.431
7	0.022	-1.157	0.053	-2.52	0.044	0.010
8	0.035	0.623	0.059	-0.458	0.067	1.203
9	0.029	1.093	0.199	-0.024	0.326	-0.322
10	0.031	-0.320	0.066	-6.681	0.116	-0.684
11	0.045	2.300	0.127	-0.140	0.243	-1.019
12	0.024	0.268	0.260	-1.407	0.153	-0.908
13	0.021	-0.038	0.046	0.507	0.070	-1.466
14	0.022	0.866	0.073	-0.653	0.065	-0.145
15	0.015	-0.894	0.023	-1.468	0.037	0.700
16	0.040	0.696	0.084	-1.282	0.109	-0.652
17	0.025	0.266	0.150	-0.562	0.062	-1.324
18	0.047	1.198	0.113	-0.509	0.106	-0.070
19	0.027	2.404	0.109	0.553	0.194	-2.280



